INTERNATIONAL SOIL AND WATER CONSERVATION RESEARCH (ISWCR)

Volume 9, No. 3, September 2021

CONTENTS

International Soil and Water Conservation Research (ISWCR) Vol. 9 (2021) 305–484

ISSN 2095-6339
CN 10-1107/P

International Soil and Water Conservation Research

Volume 9, No. 3, September 2021

国际水土保持研究

United Nations Educational, Scientific and Cultural Organization
International Research and Training Center on Erosion and Sedimentation
CHINA WATER & POWER PRESS
IWHR

ISSN 2095-6339

The *International Soil and Water Conservation Research (ISWCR)* is the official journal of World Association of Soil and Water Conservation (WASWAC), which is a non-governmental, non-profit organization. The mission of WASWAC is to promote the wise use of management practices, to improve and safeguard the quality of land and water resources. The Journal is co-owned by the International Research and Training Center on Erosion and Sedimentation, China Water & Power Press, and China Institute of Water Resources and Hydropower Research.

United Nations Educational, Scientific and Cultural Organization

International Research and Training Center on Erosion and Sedimentation

20 Chegongzhuang West Road
IRTCES Building 401-514
Beijing 100048, China
+86 10 68766413
irtces@iwhr.com
www.irtces.org

The International Research and Training Center on Erosion and Sedimentation (IRTCES) was jointly set up by the Government of China and UNESCO. It aims at the promotion of international exchange of knowledge and cooperation in the studies of erosion and sedimentation.

CHINA WATER & POWER PRESS

Building D, No. 1, South Yuyuantan Road,
Beijing 100038, China
+86 10 68545912
zt@waterpub.com.cn
http://www.waterpub.com.cn

China Water & Power Press (CWPP) is affiliated to the Ministry of Water Resources of China, which takes leadership of science and technology publishing in China.

A-1 Fuxing Road,
Beijing100038, China
+86 10 68781650
dic@iwhr.com
http://www.iwhr.com

China Institute of Water Resources and Hydropower Research is the largest and most comprehensive research institute in the field of water resources and hydropower in China.

Publishing services provided by Elsevier B.V. on behalf of KeAi

International Soil and Water Conservation Research (ISWCR)

Editorial Board

International Soil and Water Conservation Research (ISWCR)

Volume 9, Number 3, September 2021

International Research and Training Center on Erosion and Sedimentation and China Water and Power Press

AIMS AND SCOPE

The ***International Soil and Water Conservation Research*** (*ISWCR*), *the official journal of World Association of Soil and Water Conservation* (*WASWAC*) *www.waswac.org*, is a multidisciplinary journal of soil and water conservation research, practice, policy, and perspectives. It aims to disseminate new knowledge and promote the practice of **soil and water conservation.**

The scope of ***International Soil and Water Conservation Research*** includes research, strategies, and technologies for prediction, prevention, and protection of soil and water resources. It deals with identif cation, characterization, and modeling; dynamic monitoring and evaluation; assessment and management of conservation practice and creation and implementation of quality standards.

Examples of appropriate topical areas include (but are not limited to):

- ∑ Soil erosion and its control
- ∑ Watershed management
- ∑ Water resources assessment and management
- ∑ Nonpoint-source pollution
- ∑ Conservation models, tools, and technologies
- ∑ Conservation agricultural
- ∑ Soil health resources, indicators, assessment, and management
- ∑ Land degradation
- ∑ Sedimentation
- ∑ Sustainable development
- ∑ Literature review on topics related soil and water conservation research

Peer review under responsibility of IRTCES and CWPP.

INTERNATIONAL SOIL AND WATER CONSERVATION RESEARCH (ISWCR)

Volume 9, No. 3, September 2021

CONTENTS

International Soil and Water Conservation Research 9 (2021) 305–318

Contents lists available at ScienceDirect

International Soil and Water Conservation Research

journal homepage: www.elsevier.com/locate/iswcr

Review Paper

Recent advances in assessment of soil erosion vulnerability in a watershed

Shachi Pandey [a, *], Parmanand Kumar [b], Miodrag Zlatic [c], Raman Nautiyal [d], Vijender Pal Panwar [b]

[a] Forest Ecology and Climate Change Division, Forest Research Institute, Dehradun, India
[b] Forest Ecology and Climate Change Division, Forest Research Institute, Dehradun, India
[c] Faculty of Forestry, Belgrade University, Belgrade, Serbia
[d] Indian Council of Forestry Research and Education, India

ARTICLE INFO

Article history:
Received 10 October 2020
Received in revised form
3 March 2021
Accepted 4 March 2021
Available online 11 March 2021

Keywords:
Soil erosion vulnerability
RUSLE
MCDM

ABSTRACT

Soil erosion is one of the most critical hazards adversely affecting both environment and economy. Assessment of the annual soil erosion rate provides information on soil erosion risk zones indicating the areas with high, severe and low risks. Modelling and prediction of soil erosion has a long history of more than seven decades. It becomes imperative to be familiar with the quantum of studies conducted and methods employed across the world to assess vulnerability of ecosystems to soil erosion to plan strategies for their conservation. There are several methods based on various factors like land use, soil quality, topography etc. available to assess the susceptibility of a region to soil loss. With time the gap in understanding of such models and their use around the world has increased. Numerous models for assessing soil erosion exist but there is a lack of knowledge on spatial distribution of the methods being used. Academic papers related to assessment of soil erosion vulnerability published during the past three decades (1991–2019) were reviewed. Total 160 studies were reviewed to understand advances in the methods used to assess soil erosion vulnerability worldwide, identification of the most popular methods and proportion of studies conducted in the fragile region of Himalayas. The results show that 18 different methods have mainly been used to assess soil erosion risk in different regions. These methods include statistical, physical, process based and empirical models. The use of few physical methods like ANSWERS and SHE has decreased with time while that of physical and process methods like RUSLE, SWAT, WEPP and PESERA has increased with time. The review highlighted that various models being used worldwide are based on their suitability to the region. It also brings to attention that few models like PESERA, EUROSEM and WEPP are mostly being used concentrated in a particular region. Models like PESERA and EPM are mostly used in European region and may be encouraged to estimate soil erosion in Himalayan region. The review also highlights lack of studies with inclusion of water quality as an important parameter while assessing soil erosion vulnerability in the region. The review suggests that in case of lack of data, various statistical methods like PCA, CF, FUZZY etc. can be preferred for qualitative assessment over quantitative assessment. Considering availability of accurate input, researchers need to attempt more methods and perform comparative studies to attain accurate results for assessing soil erosion vulnerability leading to strategizing soil conservation in fragile regions.

Contents

* Corresponding author. Forest Ecology and Climate Change Division, Forest Research Institute, Dehradun.
E-mail address: shachi0213@gmail.com (S. Pandey).

https://doi.org/10.1016/j.iswcr.2021.03.001

1. Introduction

Soil, one of the most essential resources of humankind, is under a threat of erosion (Alewell et al., 2019). It depends on combination of factors such as steepness of slope, climate, land use & land cover and ecological disasters like forest fires (Parveen et al., 2012). Soil erosion has both on-site and off-site detrimental impacts and is one of the most critical environmental hazards as it adversely affects both environment and economy. Erosivity, erodibility and land use management practices play key role in defining status of soil. Topography controls soil movement in a watershed and areas mostly covered by high fraction vegetation are at a lower risk of soil erosion (Prasannakumar et al., 2011). Reduction of protective effect of land cover leads to demotion of vulnerability categories (Stathopoulos et al., 2017). The eroded materials carried down to the lower reaches of the rivers make rivers incompatible to carry excess amount of water and sediment load especially during monsoons thus making water quality a strong indicator of soil erosion (Ghosh et al., 2013). Vulnerability assessment of a watershed to soil erosion plays a key role in identifying extent of fragility and making appropriate plans for its conservation. To understand soil conservation and ecosystem management in a watershed, it is important to evaluate the soil erosion and map the susceptible area to soil loss (Gelagay & Minale, 2016). Assessment of the annual soil erosion rate and developing a soil erosion map provides spatial patterns of classified soil erosion risk zones indicating the areas with high, severe and low erosion risk area (Zhou et al., 2014). Soil erosion processes and modelling approaches have socioeconomic importance and helps in understanding ecosystem dynamics and stability (Alewell et al., 2019).

There are several methods available to assess the susceptibility of a region to soil loss, which use various factors like land use, soil quality and topography etc. Modelling and prediction of soil erosion has a long history of more than seven decades (Alewell et al., 2019; Bennett, 1939). Advancements in climatic datasets, remote sensing technologies, earth observations data and increased big datasets are promising factors for modelling approaches in present and future (Alewell et al., 2019). Study of soil erosion in various regions has increased in the past decade. A wide variety of methods including physical models, empirical models, statistical models and process based models have been used by many researchers to predict soil erosion worldwide (Dimotta, 2019). There is a gap in understanding of such models with time and their use around the world. Himalayan region is one of the most fragile ecosystems because of its steep slope, unstable soil and heavy monsoon rains making it important to study its fragility. With this view, it becomes necessary to be familiar with the frequency of previous studies conducted in this region and the methods employed globally to assess such ecosystems to plan future strategies. Numerous soil erosion assessment models exists but there is a lack of knowledge on spatial distribution of methods being used. Therefore, compilation of soil erosion models is crucial for both large and small spatial scales for planning, management and policy measures. The objective of this paper is to **a)** understand advances in the methods used to assess soil erosion vulnerability worldwide **b)** identify most popular methods to assess soil erosion vulnerability, in the past three decades **c)** know the proportion of studies conducted in the fragile region of Himalayas in research related to assessment of soil erosion vulnerability. The study do not claim to make an attempt to review all existing methods rather it focusing on the most used methods with their strength and limitation in last three decades (1991–2019).

2. Advances in various approaches for assessing soil erosion vulnerability

2.1. Methodology for the review

Academic papers related to assessing soil erosion vulnerability that were published during the past three decades (1991–2019) were selected using the Google scholar and publishers' websites using the primary key words are soil erosion vulnerability assessment, Himalayan region, RUSLE in three different sets and combinations. The papers including any qualitative or quantitative method to assess soil erosion vulnerability were selected from journals published worldwide to cover the work done across the globe. These studies were further filtered on the basis of decade and were classified into three sets, each spanning a decade, namely, 1991–2000, 2001–2010 and 2011–2019. The papers obtained from both the searches were compared and repetitions were removed. Among the top searches which were directly related to the subject, 160 research papers were selected to review the various methods used to assess soil erosion vulnerability in past three decades (1991–2019) and distribution of the studies conducted in Himalayan and Non- Himalayan region. Further, each study was categorised according to the methods to identify the most popular methods in the past three decades.

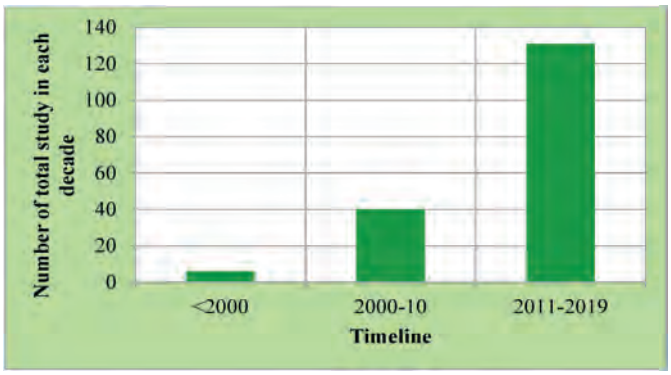

Fig. 1. Year wise increase in research on soil erosion vulnerability (Source: Author).

2.2. Results

The results showed that various physical, process based and empirical models such as Water Erosion Prediction Project (WEPP), Revised Universal Soil Loss Equation (RUSLE), Soil & Water Assessment Tool (SWAT), Erosion Potential Method (EPM), and Pan-European Soil Erosion Risk Assessment (PESERA) etc. have been used for quantitative estimation of soil erosion vulnerability for soil erosion. Statistical methods such as Principal Component Analysis (PCA) and Multi Criteria Decision Method (MCDM) based methods such as Technique for Order of Preference by Similarity to Ideal Solution (TOPSIS), Compound Factor (CF), Više Kriterijumska Optimizacija i Kompromisno Rešenje (VIKOR) were used for qualitative assessment of the soil erosion vulnerability status of the region. The results showed that RUSLE is the most popular model having been used in 42.7 percent of the selected studies (Fig. 4) for quantitative estimation while Compound Factor is the most used statistical method for qualitative estimation accounting for 7.9% of the papers reviewed. PESERA is the most used physical model used by 7.3% of the papers considered. Studies related to soil erosion vulnerability using different methods (Fig. 1) have increased in each decade since 2000. Along the years, number of studies more than tripled in 2011–2019 (131) as compared to 2000–2010 (40) (Fig. 1). Eighteen methods were used so far among which ten provide qualitative status (Fig. 3) and eight models (RUSLE, SWAT, EPM, Areal Nonpoint Source Watershed Environment Response Simulation (ANSWERS), PESERA, The European Soil Erosion Model (EUROSEM), Systeme Hydrologique Europeen (SHE) and WEPP) provide quantitative estimation of soil erosion. Both qualitative and quantitative method involves various parameters like topography, land use, soil quality, runoff, sediment yield etc. whereas water quality parameters as indicators were not considered. Methods used to assess soil erosion have been discussed briefly in the following section.

2.2.1. Process based models

2.2.1.1. Revised Universal Soil Loss Equation (RUSLE). ***General Description:*** The Revised Universal Soil Loss Equation (RUSLE) is a straightforward and an empirical model capable of predicting long term average annual rate of soil erosion on slopes using data on rainfall, soil type, topography, crop system and management practices (Mondal et al., 2016; Prasannakumar et al., 2011). RUSLE has the following structure (Renard et al., 1997) in Eq. (1):

$$\boldsymbol{A = R \times K \times LS \times C \times P} \quad (1)$$

where,

A = soil loss (t ha^{-1} yr^{-1}), R = rainfall erosivity (MJ mm ha^{-1} h^{-1} yr^{-1}), K = soil erodibility (t h MJ^{-1} mm^{-1}), LS = topographic factor (dimensionless), C = soil use and management factor (dimensionless), P = soil conservation practice factor (dimensionless)

Although empirical, it not only predicts erosion rates of ungauged watersheds using knowledge of the watershed characteristics and local hydro climatic conditions, but also presents the spatial heterogeneity of soil erosion that is feasible with reasonable costs and better accuracy in larger areas (Angima et al., 2003). It has been widely used to predict the average annual soil loss by introducing improved means of computing the soil erosion factors in both agricultural and forest watersheds (Renard et al., 1997; Wischmeier & Smith, 1978). Digital Elevation Model (DEM) along with remote sensing data and GIS can be successfully integrated in the model to enable rapid as well as detailed assessment of erosion hazards (Jain et al., 2001; Kouli et al., 2009). In order to estimate soil erosion and to develop optimal soil erosion management plans RUSLE has been widely applied worldwide to predict soil loss because of its convenience in application and compatibility with GIS (Dabral et al., 2008; Jain et al., 2001; Jasrotia & Singh, 2006; Millward & Mersey, 1999; Pandey et al., 2009; Shivhare et al., 2018; Zhou et al., 2014). The estimated soil loss in the watershed can further be categorised into soil erosion vulnerability classes on the basis of annual soil loss (tonne ha^{-1} yr^{-1}).

In addition to the studies reviewed by Benavidez et al. (2018), the equations for determining the factors of the model have been modified by various researchers while retaining their basic structure. Though being widely used, the factors may not be universally applicable to all environmental contexts worldwide, thus caution must be exercised when used in different parts of the world (Phinzi & Ngetar, 2019). Modifications of each factor have been discussed below.

Rainfall Erosivity (R): This factor quantifies the potential of rain to cause erosion of soil particles in an exposed and unprotected soil surface. R is defined as the product of rainfall kinetic energy and the maximum rainfall intensity in consecutive 30-min intensity (EI_{30}). The basic equation to determine R, *viz.* $R = 1.753 \times 10((1.5\log\Sigma(Pi_2)/P) - 0.8188)$ was given by Wischmeier and Smith (1978) and also used by Tahiri et al. (2016) in Morrocco. Various researchers have developed equations consistent with local conditions for determining R value. Rainfall data is one key input parameter in all the equations. The data is commonly obtained from meteorological gauge stations, TRMM etc. For example, $R = 79 + 0.363X$ by Bhat et al. (2017); Parveen et al. (2012); Kumar and Kushwaha (2013); Ghosh et al. (2013); Mahapatra et al. (2018) in India, $R = 0.0483 \times X1.610$ by Uddin et al. (2016) in Nepal, $R = -8.12+(0.562 \times X)$ by Gelagay and Minale (2016) in Ethiopia, $R = 0.562P - 8.12$ by Haregeweyn et al. (2017) in Egypt, etc. Wherever mentioned, X is average annual rainfall in mm, P is monthly precipitation in mm and P_2 is the annual precipitation.

Soil erodibility factor (K): K measures the erodibility of soil and relates it to the rate at which different soils erode. The factor is rated on a scale from 0 to 0.7, with zero indicating the least vulnerability and 0.7 as most vulnerable soils to erosion. K has also been determined following different methods like equations or literature. The basic equation to determine R, *viz.* $100K = 2.1 \times 10^{-4} M^{1.14}(12\text{-}a)+3.25*(b\text{-}2)+2.5(c\text{-}3)$ given by Wischmeier and Smith (1978). Some examples are $K = 2.8 \times 10^{-7} M^{1.14}(12\text{-}a)+4.3 \times 10^{-3}(b\text{-}2)+3.3 \times 10^{-3}(c\text{-}3)$ (Renard et al., 1997; Kumar & Kushwaha, 2013; Mahapatra et al., 2018; Gaubi et al., 2016). Where ever mentioned, **K** = soil erodibility factor, t ha^{-1} MJ^{-1} mm^{-1}, **M** = particle size parameter (per cent silt + per cent very fine sand) × (100−per cent clay), **a** = organic matter content (per cent), **b** = soil structure code (very fine granular 1; fine granular 2; medium or coarse granular 3; blocky, platy or massive 4) **c** = soil permeability class(rapid 1; moderate to rapid 2; moderate 3; slow to moderate 4; slow 5; very slow 6). In Ethiopia, Gelagay and Minale (2016) assigned the values to K based on soil colour. Black, brown, red and yellow coloured soil were i.e. 0.15, 0.20, 0.25 and 0.30 respectively. In India, the K values were assigned, based on textural class and organic matter content (Parveen et al., 2012). The value of K for sandy soil with organic matter content less than 0.5 percent varied from 0.12 to 0.44, whereas it varied from 0.10 to 0.38 and 0.08 to 0.30 in soil with organic matter 2 percent and 4 percent respectively. In case of Loam with organic matter content less than 0.5 percent varied from 0.27 to 0.48, whereas it varied from 0.24 to 0.41 and 0.19 to 0.33 in soil with organic matter 2 percent and 4 percent respectively. In Clay, with organic matter content less than 0.5 percent, K was 0.25, whereas it was 0.23 and 0.19 with organic matter 2 percent and 4 percent respectively.

Topographic factor (LS): The assessment of vulnerability of soils to erosion on a large scale, like those in basins, can be carried out with the RUSLE model by reformulating its topographic factor thereby improving its representation in the basin's scale (Adediji, 2010;

Oliveira et al., 2014; Ozsoy et al., 2012; Prasannakumar et al., 2011; Yuksel et al., 2008). LS is a factor determined by slope length (L) and slope gradient (S). The DEM can be used to obtain the accumulated flow and slope map. The basic equation to determine LS, *viz.* LS= $(\lambda/22.13)^{m}\cdot(65.4\sin^2\beta + 4.5\sin\beta + 0.0654)$ was given by Wischmeier and Smith (1978). Various researchers have used different modifications to determine LS factor such as LS=((Flow accumulation × cell size)/22.13)$^{0.6}$ × [Sine(Slope)/0.0896]$^{1.3}$ by Bhat et al. (2017) in India and Gelagay and Minale (2016) in Ethiopia. Another equation, L= $(\lambda/22.13)^{m}$; S = (0.43 + 0.30S + 0.043 S2)/6.613 by Mahapatra et al. (2018) in India and by Uddin et al. (2016) in Nepal. In Morocco, Tahiri et al. (2016) used LS = (sl 22.13)$^{m}\cdot(0.065 + 0.045\cdot S + 0.065\cdot S2)$ while LS=(A/22.13)$^{0.6}$ × [SineB/0.0896]$^{1.3}$ was used by Parveen et al. (2012) in India. Another equation, $LS® = (m + 1)\,[A®/22.13]^{m}\,[\sin\beta®/0.09]^{n}$ was used by Gaubi et al. (2016) in Tunisia and Kumar and Kushwaha, 2013 in India. Wherever mentioned, λ is the field slope length (m) with a value between 0.2 and 0.5, sl is slope length of the site (in meters) and S is the slope factor, A is the upslope contributing factor, B is the slope angle, β ® is the land surface slope in degrees, m and n constants equal to 0.6 and 1.3, A® is up-slope contributing area per unit width of cell spacing ($m^2\ m^{-1}$).

Crop Cover Management Factor (C): Crop cover management factor is the ratio of soil loss from land with specific vegetation to the corresponding soil loss from a continuous fallow land (Wischmeier & Smith, 1978). The C- factor is one important erosion factor that can most easily be influenced by humans to reduce erosion (Phinzi & Ngetar, 2019). Remote sensing based techniques like land use/land cover (LULC) classification, spectral indices like Normalized Difference Vegetation Index (NDVI), an indicator of the vegetation vigor and health, are now preferred over conventional techniques owing to their low costs, rapid and relative accurate data analysis (Phinzi & Ngetar, 2019). Upon deriving LULC classes from remotely sensed imagery, corresponding values of C-factor are obtained from USLE guide tables (Wischmeier & Smith, 1978). The value of C for built up land is 0.20, for scrub forest is 0.020 and wasteland with scrub & without scrub are 0.95 & 0.80 respectively. The value of C for waterbody is 0. In Morocco, the assigned value to C was 0.014 for shrub land, and 0.05, 0.024, 0.6 & 0.04 for grazing land, built up land, barren land, forest land respectively (Gelagay & Minale, 2016). In India, Kumar and Kushwaha (2013) assigned the values 0.5, 0.004, 0.008, 0.08, 0.4, 0.02, 0.1, 0.05, 0.6 for built up land, very dense forest, dense forest, moderately dense forest, open forest, forest plantation, orchard, dense scrub, and wasteland with scrub respectively. C for water was assigned 0 value by both. Mahapatra et al. (2018) used the values of 0.58, 0.01, 0.14, 0.5 and 1 for agriculture land, forest and grasslands, degraded forest/wastelands, degraded lands and fallow lands respectively. The equations to derive the crop factor in Morocco by Uddin et al. (2016) and India by Parveen et al. (2012) are based on imagery by using equation C = 0.431–0.805 × NDVI. In India, Bhat et al. (2017) also used equation C = exp[-α {NDVI/(β-NDVI)}]. Where ever mentioned α and β are unitless parameters that determine the shape of the curve relating to NDVI and the C-factor.

Conservation Practices Factor (P): P represents the ratio of soil loss with specific support practice to the corresponding soil loss with up-slope and down-slope cultivation. The value of P has been assigned by various researcher based on slope and maximum length of the region. Based on slope (%) and maximum length (Wischmeier & Smith, 1978), the value assigned to P were such that if slope varied from 1 to 8% and maximum length varied from 122 to 61m, the value assigned was 0.5, 0.6 for slope varying from 9 to 12% and maximum length of 36m, 0.7 for slope varying from 13 to 16% and maximum length of 24m, 0.8 for slope varying from 17 to 20% and maximum length of 18m, 0.9 for slope varied from 21 to 25% and maximum length of 15m. Renard et al. (1997) assigned the values to P based on slope (%) only such that if slope ranges from 0 to 1, 1–3, 3–5, 5–10, 10–15 and 15–35 percent the values assigned to P were 0.6, 0.6, 0.5, 0.5, 0.7 and 1 respectively. Values to P can also be assigned empirically in large catchments as proposed by Wener, 1981 referred by Lufafa et al. (2003) according to which P = 0.2 + 0.03 × S, where S is the slope. In India, Naqvi et al. (2012) used values based on land use type where dense vegetation, sparse vegetation, built-up, water bodies, scrub land, agricultural cropland, fallow land, bare soil/barren land were assigned the values 1, 0.8, 1, 1, 1, 0.5, 0.9 and1 respectively. In Morocco, the value of P was based on land use type and slope (%) for agricultural land by Gelagay and Minale (2016) was 0.1 if slope varied from 0 to 5 percent and 0.12, 0.14, 0.19, 0.25 and 0.33 for slope varying from 5 to 10, 10–20, 20–30, 30–50, 50–100 percent respectively. For all other lands, the value was 1 regardless of the slope. In Europe, Panagos et al. (2015) also assigned P values based on slope with slope varying from 9 to 12, 13–16, 17–20, 21–25 and > 25 percent being assigned the values 0.6, 0.7, 0.8, 0.9 and 0.95 respectively.

Categories of soil erosion vulnerability are defined by various researchers in literature such as Beskow et al. (2009) in Brazil, Parveen et al. (2012) and Mahapatra et al. (2018) in India and Haregeweyn et al. (2017) in Egypt and are given in Table 1:

Status: It was observed that the use of this model has consistently increased from 2000 to 2019 (Fig. 3) and with 42.7 percent study based on it, is the most popular one among all the 18 methods (Fig. 4).

Limitations: The model has limitations too. Comparisons show that it predicted higher erosion rates (127.6 t ha^{-1} yr^{-1}) than PESERA when compared to the measured sediment yield (106.1 t ha^{-1} yr^{-1}), resulting higher prediction of mean erosion rates for different land uses/covers, particularly for those with steep slopes (Li et al., 2019). Models like EUROSEM and WEPP are superior over RUSLE because they give attention to runoff in determining the erosive stresses being applied to the land surface (Khaleghpanah et al., 2016).

2.2.1.2. Water Erosion Prediction Project (WEPP). ***General Description:*** WEPP are process-based models for runoff and soil erosion prediction (Laflen et al., 1997). Similar to the empirical models such as RUSLE, the models have been widely used to model soil erosion in agricultural land (Renard et al., 1997). WEPP has also been used to predict soil loss in a range of environments, e.g. rangeland and forest. WEPP model is capable of simulating runoff and sediment yield from the untreated watershed with good accuracy. It is based on single rainfall-event and can be applied to slopes and small catchments up to 50ha (Obeta & Adewumi, 2013). The model is based on the continuity equation (2) (Nearing et al., 1989):

$$\frac{dG}{dx} = Dr + Di \tag{2}$$

where,s

G = sediment load (kg·s-1· m-1)
x = distance down slope (m)
Dr = rill erosion rate (+for detachment, - for deposition)
Di = interrill sediment delivery ($kg\cdot s^{-1}\cdot m^{-2}$).

It helps in formulating structure based management strategies of watersheds to control soil loss and runoff. The WEPP software includes an erosion prediction model, a climate generator program and a Windows interface (Flanagan et al., 2007). Data required for this model are climate files, soil input and practices and management scenarios. This model requires the parameters amount and duration of rainfall, maximum and minimum temperature, solar

Table 1
Categories of soil erosion vulnerability (Source: Author).

Soil Loss (Tons ha^{-1} yr^{-1})	Beskow et al. (2009)	Parveen et al. (2012)	Haregeweyn et al. (2017)	Mahapatra et al. (2018)
0–2.5	Slight	Very Slight	Slight	Very Slight
2.5–5	Slight to Moderate			
5–10	Moderate	Slight	Moderate	Slight
10–15	Moderate to High		High	Moderate
15–20	High	Moderate		Moderately Severe
20–25			Very High	Severe
25–30				
30–40		Severe		
40–50			Severe	Very Severe
50–60	Very High	Very Severe		
60–70				
70–80				
80–100			Very Severe	
>100	Extremely High			

Table 2
Summary of the review for Himalayan Region (Source: Author).

Methods	Himalayan Region
CF	(Singh & Singh, 2018) (Altaf et al., 2014) (Vijith et al., 2012) (Rawat et al., 2011) **India**
LULC	(Altaf et al., 2014) (Malik & Bhat, 2014) (Rawat et al., 2013) (B et al., 2014) **India**
Morphometric	(Pareta et al., 2019) (Malik & Bhat, 2014) (Altaf et al., 2014) (Singh et al., 2008) **India**
RUSLE	(Mahapatra et al., 2018) (Sharda & Mandal, 2018) (Bhat et al., 2017) (Singh & Panda, 2017) (Kalambukattu & Kumar, 2017) (Kumar et al., 2014) (Kumar & Kushwaha, 2013) (Sharda et al., 2013) (Ghosh et al., 2013) (Naqvi et al., 2012) (Mandal & Sharda, 2011) (Sheikh et al., 2011) (Pandey et al., 2009) (Dabral et al., 2008) (Jain et al., 2001) (Rawat et al., 2013) **India**; (Uddin et al., 2016) **Nepal**; (Hui et al., 2010) **China**
SWAT	(Kushwaha & Jain, 2013) **India**
WEPP	(Singh et al., 2012) **India**

radiation, organic carbon, texture and land use management practices in the watershed.

Status: It model has been increasingly used from 2011 to 2019 (Fig. 3) with few studies available in the preceding decade (2000–2010). This method has been used only in 2.2% studies reviewed (Figs. 3 and 4).

Limitations: The model may be of limited use because of its non-GIS interface and specific data requirements related to sediment yield and runoff generation. This model is good for estimating sediment yield but other models like PESERA where the mean predicted value of annual soil losses was 22.0 Mg ha^{-1} close to the measured value i.e. 20.1 Mg ha^{-1} and EPM are more competent in providing soil erosion estimates (Fernández & Vega, 2016).

2.2.2. Statistical methods

2.2.2.1. Technique for Order of Preference by similarity to Ideal Solution (TOPSIS). ***General Description:*** This method was first introduced by Hwang and Yoon in 1981 and Ameri et al. (2018) used it to study the soil erosion susceptibility in a watershed (Table 2&3). This method shares 0.6% of the total studies reviewed being among the least used MCDM method so far (Fig. 3). It is a distance - based method and the main source of calculation is based on Positive Ideal Solution (PIS) and Negative Ideal Solution (NIS) for identifying decision making alternatives. In the model, the preferred alternative is the one that has the least distance from PIS and a higher distance from NIS. The results of the two distances are expressed in the form of closeness coefficient (C). The method is based on equation (3)(Ameri et al., 2018):

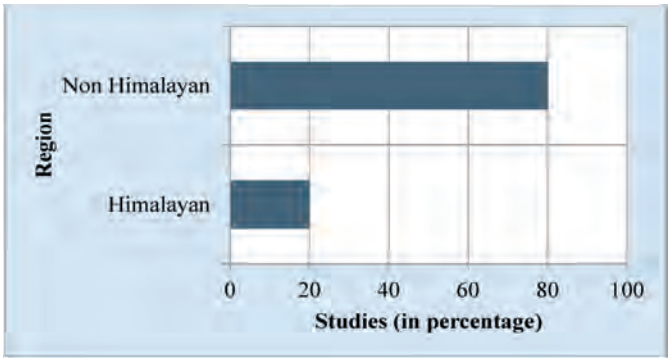

Fig. 2. Region wise studies conducted on soil erosion vulnerability assessment. (Source: Author).

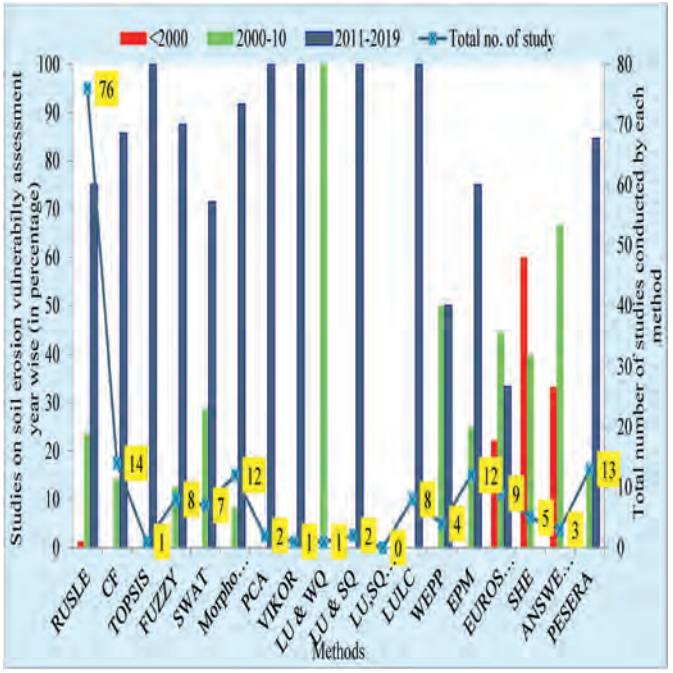

Fig. 3. Various methods used along the years (1991–2019) Source: Author.

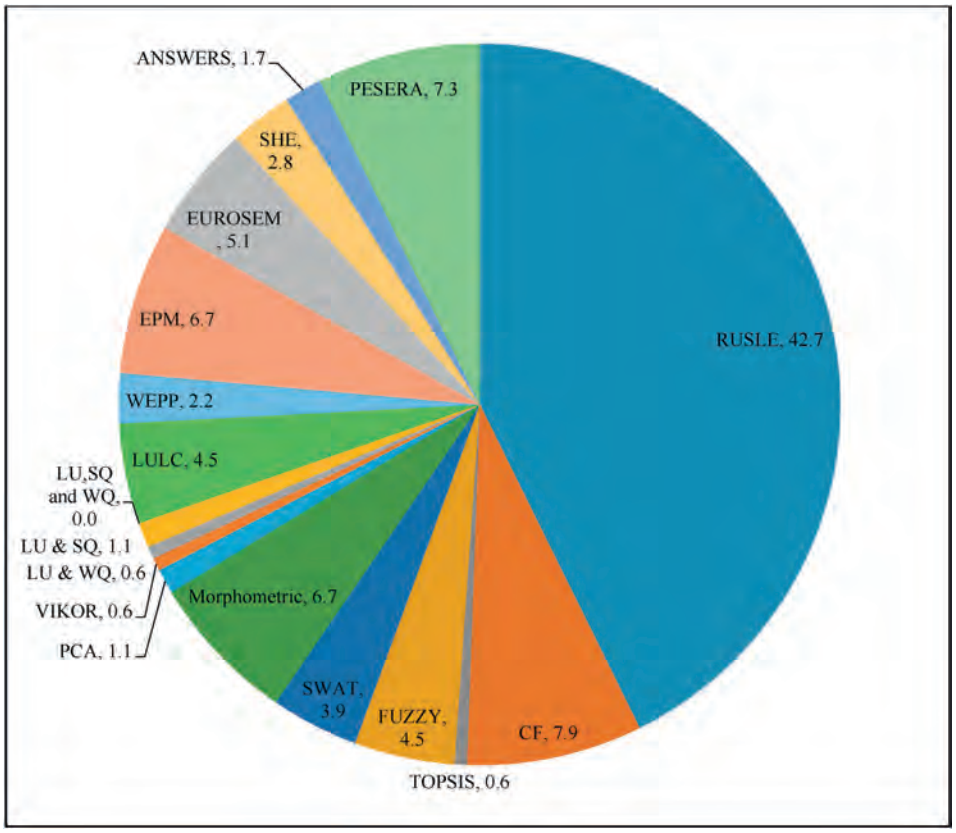

Fig. 4. Percentage of models used for assessing soil erosion vulnerability in various researches (n = 160) Source: Author.

$$C = \frac{PIS}{PIS - NIS};\ 0 \le C \le 1 \tag{3}$$

The highest closeness coefficient indicates the most preferred alternative (Kannan et al., 2009; Liou & Wang, 1992). In this method, different parameters like morphology, geology, slope, soil quality and land use can be taken depending upon the data availability and behaviour of the parameter.

Status: It was observed that this method has been used during 2011–2019 and is a useful method for qualitatively ranking of watersheds with respect to soil erosion (Figs. 2 and 3). This method has been used in very few studies (0.6%) to rank the watersheds (Figs. 2 and 3).

Limitations: Among the statistical method this is least popular probably due to the difficulty in selecting the most preferred alternatives. Lesser the number of parameter used, less accurate results are obtained making selection of relevant parameters crucial. It provides a subjective ranking of the watersheds and gives qualitative results.

2.2.2.2. Više Kriterijumska Optimizacija i Kompromisno Rešenje (VIKOR). VIKOR, first introduced by (Opricovic & Tzeng, 2004) is a very well known MCDM technique which emphasizes on selection and ranking of alternative set of conflicting criteria. The method is less used in assessing and ranking of sub watersheds (Tables 2 and 3). In this method, normalized decision matrix based on criteria and their behaviour towards the alternatives and weighted decision matrix is computed. The advantage of this method is that the evaluation of all the criteria does not require expert review; raw data can also be used for assigning weights to the criteria. Methods like AHP (Analytical Hierarchy Process) may be used for assigning weights. S_i (Utility Index) and R_i (Regret Index) are calculated based on best and worst value of each function. Q index is then calculated and highest ranked alternative based on Q index is taken as best alternative. This method is suggested as best among other MCDM methods by Ameri et al. (2018) and is based on equation (4).

$$Q = V(S_i - S^-|S^+ - S^-) + (1 - V)(R_i - R^-|R^+ - R^-) \tag{4}$$

where, $S^- = \min S_i$, $S^+ = \max Si$, $R^- = \min R_i$, $R^+ = \max R_i$, and V is introduced as a weight of the strategy of the maximum group utility or the majority of criteria.

Status: It was observed that the model has been used from 2011 to 2019 (Fig. 3) and making it only 0.6% of the total number of study (Figs. 3 and 4).

Limitations: The method provides qualitative results and accuracy generally depends upon the number of parameters used. Selection of parameters is crucial to provide accurate results. Assigning the weights in this methods is important which needs extensive raw data which might be challenging in few cases.

2.2.2.3. Compound Factor (CF). ***General Description:*** This is the most commonly used MCDM method and provides a comparative estimation driven by scientific knowledge and understanding of a qualitative phenomenon (Todorovski & Džeroski, 2006). The ranks are assigned based on the number of samples/options available. The method is based on equation (5) (Ameri et al., 2018) in:

$$CF = \frac{1}{n}\sum_{i=1}^{n} R \tag{5}$$

where CF is Compound value, R is rank of options, and n is number

of parameters. The average of the ranks of all the parameters is designated as compound value and represents the collective impact of all the parameters (Altaf et al., 2014). This method is flexible with number of parameters selected for the study and, if required, weights assignment can be assigned based on expert review.

Status: It was observed that the use of this method for assessing vulnerability to soil erosion increased from preceding decade to 2019 from 14 to 85 percent (Fig. 3) although very few studies were conducted in preceding decade (2000–2010). This method has been widely used worldwide making it the most frequently used (7.9%) qualitative method (Figs. 3 and 4). In the method, land use and land cover, morphometric parameters, soil quality, and combinations of these have been used to study soil erosion vulnerability. It is evident from the results reviewed that no study among 160 studies has incorporated all three parameters i.e. soil quality, water quality and land use together to study the soil erosion vulnerability

Limitations: The method has limited utility because of its qualitative and subjective nature.

It also has no provision for normalization of variables of different scale and sizes and, in case of same values, equal ranks can lead to over or underestimation of the state.

2.2.2.4. Principal Component Analysis (PCA). ***General Description:*** PCA is a powerful multivariate statistical technique to segregate parameters contributing to observed criteria and can be used to assess soil erosion vulnerability in a sub-watershed (Khaledian et al., 2016). It may be employed to explore most influential parameters of different criteria like morphometry, soil and land use, etc., based on the parameters which are highly correlated with important components. Further this can be used to rank sub-watersheds to assess the soil erosion vulnerability. This method is flexible for criteria selection but requires large number of parameters and sample size.

Status: It was observed that this model has been in use from 2011 onwards (Fig. 3). This method has been used in (1.1%) studies reviewed making it the third most used qualitative method (Figs. 3 and 4).

Limitations: The usage of this model is limited because of the requirement of large number of parameters and dataset. This method provides a qualitative outlay of the watershed which is subjective to the region.

2.2.2.5. FUZZY. ***General Description:*** Fuzzy method can provide optimum solution when there are uncertainties associated with evaluating criteria. The prioritization of watersheds according to their vulnerability to soil erosion based various related criteria like morphometric, land use etc., or even single criterion with different parameters can be performed using fuzzy analysis technique. According to Chang's extent analysis Fuzzy AHP method (Chang, 1996), each criterion can be evaluated through formation of pair wise comparison matrix based on the fuzzy linguistic scale and weightage obtained through normalization of fuzzy measures. Prioritization of each sub watershed can be carried out on the basis of FAHP analysis score where the first rank will be assigned to the sub watershed having the highest analysis value which will indicate the most vulnerable zone. Fuzzy techniques are mostly useful for carrying out ranking with overlapping parameters and there is a lot of scope for application of this method for ranking of sub watersheds (Table 3).

Status: It was observed that the use of this method has increased from 2011 to 2019 (Fig. 3) and very few studies were conducted n preceding decade (2000–2010). This method has been widely used in European continent making it second (4.5%) most used qualitative method (Figs. 3 and 4).

Limitations: The model suffers from the limitation of requiring a large number of parameters and expertise for selection of the accurate representative parameters. In addition, this method provides qualitative results in form of rank.

2.2.3. Physical models

2.2.3.1. Systeme Hydrologique Europeen (SHE). ***General Description:*** SHE was one of the most advanced system available during 1990–2000 (Abbott et al., 1986) to provide sound scientific basis for tackling problems arising in the hydrological cycle due to adverse human interference. The formulation of the model was initiated in 1976, as its structure and process are represented in Abbott et al. (1986). The SHE is a generalized mathematical modelling system capable of describing the entire land phase of the hydrological cycle in a basin in any geographical area (Refsgaard et al., 1992). It was developed jointly by Danish Hydraulic Institute (DHI), the Institute of Hydrology (UK) and SOGREAH (France). According to Bathurst and Cooley (1996), this model has a particular advantage for the studying the effects of changes in land use on soil erosion and can be used with sparse datasets. At present, two codes of SHE exist to assess contaminant and sediment transport based on the original SHE concept: the MIKE SHE code developed by DHI, Denmark and the SHETRAN code developed by University of Newcastle, UK (Refsgaard et al., 2010). Development of SHE arose from the need for a new modelling approach for use in assessing environmental impacts of river basin development. SHE have been applied on various spatial scales ranging from 30 m^2 to 5000 km^2. The datasets required for this model vary between catchment but all variation can be accommodated in the model software without modification. The parameters required for the model have a physical meaning (e.g. soil conductivity, channel dimensions and sediment size distribution) and can be measured in the field. This model has the ability to furnish the soil pore water pressure and ground water conditions needed to determine slope and gully wall stability.

Status: As results indicate (Fig. 3) SHE was used by many researchers in two decades from 1991 to 2010 while its inclusion in research has decreased in last decade. A study conducted by Golmohammadi et al. (2014) suggested MIKE-SHE model to be better and SWAT model at predicting the overall variation in stream flow. It was indicated by monthly calibration and validation i.e. R^2 was 0.80 and 0.64 and 0.74 and 0.64 for MIKE-SHE and SWAT respectively.

Limitations: The less usage of the SHE models can be attributed to its complex nature with very high demand of modelling team in terms of scientific training, modelling experience and multi-disciplinary knowledge covering hydrogeology, soil science and surface water hydraulics (Refsgaard et al., 2010). In addition, MIKE-SHE and SHETRAN are private and University based when it comes to organisation developing code. SHETRAN is not very user friendly and may require experts and trained team with ability of coding (Refsgaard et al., 2010).

2.2.3.2. Areal Nonpoint Source Watershed Environment Response Simulation (ANSWERS). ***General Description:*** The ANSWERS hydrologic model was developed primarily for agricultural watersheds originally by Huggins and Monke (1966). This is a distributed parameter, physical, and event based model developed that simulates hydrologic behaviour, sediment yield and sediment concentration of agricultural watersheds (Beasley et al., 1980). The model is based on Yalin's equation (6) (Ahmadi et al., 2006):

$$T_f = \frac{1}{4} P_s \times S_g \times P_w \times D \times V^* g \tag{6}$$

where: T_f is the sediment transport capacity in kg s^{-1}; P_S is the

Table 3
Summary of the review non Himalayan Region (Source: Author).

Methods	Non Himalayan Region
ANSWERS	(Ahmadi et al., 2006) **Iran**; (Singh et al., 2006) **India**; (Bouraoui & Dillaha, 1996); **USA**
CF	(Halefom et al., 2019) (Amsalu & Mengaw, 2014) (Setegn et al., 2009) **Ethiopia**; (Ameri et al., 2018) **Iran**; (Gaikwad & Bhagat, 2018) (Pal, 2016) (Chowdary et al., 2013) (Aher et al., 2013) **India**; (Stathopoulos et al., 2017) **Greece**; (Rahman et al., 2009) **China**
EPM	(Lense et al., 2019) **Brazil**; (Kostadinov et al., 2018) **Serbia**; (Lovric & Tosic, 2018) **Bosnia and Herzegovina**; (Dragičević et al., 2018) **Croatia**; (Spalevic et al., 2016) (Spalevic et al., 2015) **Montenegro**; (Yousefi et al., 2014) **Iran**; (Blinkov et al., 2013) **Macedonia, Serbia and Bulgaria**; (Amini et al., 2010) (Haghizadeh et al., 2009) (Sadoddin et al., 2008) **Iran**
EUROSEM	(Khaleghpanah et al., 2016) **Iran**; (Obeta & Adewumi, 2013) **Nigeria**; (Smets et al., 2011) **Belgium**; (Centeri et al., 2009) **Hungary**; (Cai et al., 2005) **China**; (Rosenmund et al., 2005) **Italy**; (Veihe et al., 2001) **Mexico**; (Folly et al., 1999) **Netherlands**; (Quinton, 1997) **United Kingdom**
FUZZY	(Haidara et al., 2019) **Morocco**; (Makaya et al., 2019) **South Africa**; (Richardson & Amankwatia, 2019) **Mexico**; (Shahabi et al., 2015) **Iran**; (Aher et al., 2013) **India**; (Li et al., 2009) **China**; (Campos Pinto et al., 2016) **Brazil**; (Quiroz Londoño et al., 2016) **Argentina**
LU & WQ	(Hart, 2006) **USA**
LU & SQ	(Campos Pinto et al., 2016) **Brazil**; (Quiroz Londoño et al., 2016) **Argentina**
LULC	(Baloshi et al., 2019) **Albania**; (Tadesse et al., 2017) **Ethiopia**; (Khaledian et al., 2016) **Iran**; (Bagyaraj et al., 2014) **India**
TOPSIS	(Ameri et al., 2018) **Iran**
SHE	(Zhou et al., 2013) (Bathurst & Cooley, 1996) (Wicks & Bathurst, 1996) **USA**; (Golmohammadi et al., 2014) **Canada**; (Refsgaard et al., 1992) **India**
Morphome–ric	(Hembram et al., 2019) (Said et al., 2018) (Bagyaraj et al., 2014) (Kinthada et al., 2013) (Aher et al., 2013)**India**; (Ameri et al., 2018) **Iran**; (Farhan & Anaba, 2016) **Jordan**
VIKOR	(Ameri et al., 2018) **Iran**
PCA	(Farhan et al., 2017) **Jordan**; (Khaledian et al., 2016) **Iran**
PESERA	(Li et al., 2019) **China**; (Vieira et al., 2018) **Portugal**; (Ahmet Cilek, 2017) (Cilek et al., 2015) **Turkey**; (Fernández & Vega, 2016) (Vente et al., 2008) **Spain**; (Pásztor et al., 2016) **Hungary**; (Djuma et al., 2016) **Cyprus**; (Karamesouti et al., 2016) (Karamesouti et al., 2015) (Tsara et al., 2005) **Greece**; (Vanmaercke et al., 2012) (Podmanicky et al., 2011) **Europe**
RUSLE	(Yacine et al., 2019) (Jazouli et al., 2018) (Tahiri et al., 2016) (Lahlaoi et al., 2015) **Morocco**; (Mustefa et al., 2019) (Haregeweyn et al., 2017) (Gelagay & Minale, 2016) (Bewket & Teferi, 2009) **Ethiopia**; (Mihi et al., 2019) Algeria; (Obiora-Okeke, 2019) **Nigeria**; (Karan et al., 2019) (Markose & Jayappa, 2016) (Balasubramani et al., 2015) (Biswas & Pani, 2015) (Dutta et al., 2015) (Ganasri & Ramesh, 2015) (Abdul Rahaman et al., 2015) (Pancholi et al., 2015) (Patil et al., 2015) (Tirkey et al., 2013) (Chatterjee et al., 2014) (Parveen et al., 2012) (Prasannakumar et al., 2012) (Prasannakumar et al., 2011) (Shinde et al., 2011) (Vemu & Pinnamaneni, 2011) (Jain & Das, 2010) **India**; (Phan et al., 2019) **Vietnam**; (Xavier et al., 2016) **Brazil**; (Gaubi et al., 2016) (Kefi et al., 2011) **Tunisia**; (Bhandari et al., 2015) **Nepal**; (Farhan & Nawaiseh, 2015) (Farhan et al., 2013) **Jordan**; (Panagos et al., 2015) **Europe**; (Yue-qing et al., 2014) (Guo et al., 2013) **China**; (Patil & Sharma, 2013) **Malaysia**; (Borrelli et al., 2014) **Italy**; (Ashiagbor et al., 2013) **Ghana**; (Rozos et al., 2013) **Greece**; (Manyiwa & Dikinya, 2013) **Botswana**; (Demirci & Karaburun, 2012) (Fistikoglu & Harmancioglu, 2002) **Turkey**; (Owusu, 2012) **Ghana**; (Karaburun, 2010) **Istanbul**; (Beskow et al., 2009) **Brazil**; (Zhang et al., 2009) **USA**; (Claessens et al., 2008) (Mutua & Klik, 2004) (Angima et al., 2003) **Kenya**; (Efe et al., 2008) (Erdogan et al., 2007) **Turkey**; (Bhattarai & Dutta, 2007) **Thailand**; (Fu et al., 2005) **China**; (Lee, 2003) **Korea**; (Millward & Mersey, 1999) **Mexico**
SWAT	(Ahn & Kim, 2017) **South Korea**; (Panagopoulos et al., 2019) **Greece**; (B et al., 2014) **India**; (Oeurng et al., 2011) **France**; (Nunes et al., 2008) **Portugal**; (Setegn et al., 2009) **Ethiopia**
WEPP	(Albaradeyia et al., 2011) **Palestinian Territories**; (Landi et al., 2011) **Iran**; (Greer et al., 2006) **USA**

number of particles in transport; S_g is the particle specific gravity in gml^{-1}; P_w is the density of water in kg m^{-3}; V* is the shear velocity in ms^{-1}; g is the acceleration due to gravity in m s^{-2}; D is the mean diameter of particle in m, generally as D_{50}, where D_{50} represents the particle diameter such that

50% of the material by dry weight is of a smaller diameter. The model defines areas contributing severe erosion and evaluates the effects of different land treatments within the watershed (Beasley et al., 1980). The model is in a pyramid setup where one output serves as input for next parameter. The integration of GIS with distributed parameters reduces time needed for generating different inputs required for the model (Singh et al., 2006). The overall model structure consists of three different model i.e. a hydrologic model, routing components necessary to describe overland and sub-surface flow and sediment detachment and transport model. The model consist of many parameters such as Potential Interception Volume (PIT) in mm; Percentage of Vegetative Cover (PER); Roughness Coefficient (RC); Maximum roughness height (HU) in mm, and Relative erosiveness parameter (C_0). The inputs required are soil textural class, slope, land cover, sediment yield, and continuous measurements of rainfall (intensity, duration and amount) runoff and peak flow which may be integrated on GIS platform. The model operates on a grid system in which each cell is hydrologically homogeneous and behaves independently. The inflow and outflow of the cell is solved using continuity equation. The model handles the overland flow, channel flow, subsurface drainage and sediment detachment and transport in a unique way.

Status: This model is capable of simulating runoff, peak flow and sediment yield from a watershed with acceptable level of deviation (S_d <20%) (Singh et al., 2006). The review revealed that the model was practiced more before 2010 and the use has decreased gradually in the last decade (2011–19) (Fig. 3). Among all the models used in the study, this model shares 1.7 percent (Fig. 4) of the total studies.

Limitations: Presumptions such as no detachment in the channel bed in the model have caused underestimation of sediment concentration (Ahmadi et al., 2006). Singh et al. (2006) suggested that the model ignores the reattachment of the soil particles to the soil surface leading to higher concentration in sediment yield. The model becomes cumbersome when it comes to data collection and without long term physical data of rainfall this model may not provide accurate results. Its focus on runoff estimation and a different interface could be a reason of its less popularity among the recently used models.

2.2.3.3. Pan-European Soil Erosion Risk Assessment (PESERA).
General Description: PESERA model is a process-based erosion model developed for estimating rill and inter-rill erosion with focus on Europe-wide input data availability for applications to large areas (Pásztor et al., 2016; Kirkby et al., 2008). The purpose of this model is to provide a state of art soil erosion risk assessment at European scale (Kirkby, 2003). The model can be disaggregated into runoff generation and a sediment transport component. The model further breaks up precipitation into overland flow, evapotranspiration and soil moisture. The parameters required for the model include transpiration, land use, soil erodibility, slope and overland flow (Kirkby et al., 2008). The model can accommodate 128 data layers which comprise of 6 soil layer, 96 climate parameters, 25 land use and land cover and 1 topographic layer. Daily rainfall is required to calculate runoff. Sediment transport is calculated based on erodibility and runoff discharge and slope gradient (Kirkby, 2003). Soil erosion in this model is calculated using equation (7) (Cilek et al., 2015):

$$E = k\Delta\Omega \text{ in } \left(\text{E; t ha}^{-1}\text{ yr}^{-1}\right) \quad (7)$$

where, k = erodibility, Δ = topographic potential, Ω = runoff and soil erosion potential

The requirement for the above mentioned factors are land use, soil parameters and vegetation cover, gridded climatic data, water balance and plant growth model. The model has potential in estimating on-site erosion on a regional scale and can also be used to assess sensitivity to altered conditions as climate and land use are explicit drivers in the model. The model performs well in predicting post-fire erosion loss as this model considers sediment transport processes only (Fernández & Vega, 2016).

Status: It was observed that the usage of this model has increased from 2011 to 2019 (Fig. 3) although the field validation of the model is still scarce (Fernández & Vega, 2016). Also, among all the models used in the study, this model features in 7.6 percent (Fig. 4) of the studies reviewed.

Limitations: The model provides less accurate sediment yield when compared to other models like RUSLE although providing better estimates for mean erosion rate. This model needs further improvement on steep slopes to better account for soil erosion processes (Li et al., 2019; Pásztor et al., 2016). As opposed to the USLE, it is a process-based model, and has a significantly higher demand for input data (Fernández & Vega, 2016). PESERA performed reasonably well in predicting soil losses, but needs a better characterization of soil burn severity in the soil inputs (crusting and erodibility) because of the high sensitivity of the model to these parameters. The model does not consider gully, channel erosion, channel delivery processes and routing and is explicitly based on sediment delivered to the hillside (Cilek et al., 2015).

2.2.3.4. The European Soil Erosion Model (EUROSEM). ***General Description:*** EUROSEM is a process based model for simulating erosion on an event basis for fields and small catchments (Cai et al., 2005). The model requires accurate estimation of sediment concentration in runoff to simulate the rate of soil loss satisfactorily. This is an event based model which is a peculiar feature to this model when compared to other empirical models such as USLE (Wischmeier & Smith, 1978) and RUSLE (Renard et al., 1997), and process-based models, such as WEPP (Nearing et al., 1989) and ANSWERS (Beasley et al., 1980). This model uses description of physical parameters and simulates erosion on an event on a minute to minute basis. The model computes runoff and soil loss based on dynamic mass balance equation (Morgan et al., 1998). The model deals with volume and kinetic energy of the rainfall reaching the ground surface as direct throughfall and leaf drainage (the interception of rainfall by the plant cover) volume of stemflow, volume of surface depression storage, detachment of soil particles by raindrop impact and runoff, sediment deposition, and transport capacity of the runoff. The algorithm of the model deals with soils and stoniness. Revised version of the model is EUROSEM-10 which predicts well the total runoff volumes and soil loss from bare and covered soil surfaces (Smets et al., 2011).

Status: It use of this model has increased from 2000 to 2010 (Fig. 3) and decreased in the following decade (2011–2019). Among all the models used in the studies reviewed, this model shares 5.1 percent coverage (Fig. 4).

Limitation: This model gives attention to runoff in determining the erosive stresses which require exhaustive real time data and gauging which limits its utility in ungauged conditions (Khaleghpanah et al., 2016). This model does not perform as good as WEPP for bare and cultivated soils (Obeta & Adewumi, 2013) as on the bare interill only soil detachment is assumed not the deposition of the sediment (Smets et al., 2011).

2.2.4. Empirical models

2.2.4.1. Soil and Water Assessment Tool (SWAT). ***General Description:*** The Soil and Water Assessment Tool (SWAT) is a river basin model developed by the United States (US) Department of Agriculture in collaboration with Texas A&M University. SWAT version 2012 has been released in combination with ArcGIS (version 10.4) and ArcSWAT interface. Within the Geographic Information Systems (GIS) environment, SWAT is a distributed modelling as a watershed is delineated into sub-basins and subsequently into hydrologic response units (HRUs), which represent homogeneous combinations of land use, soil types, and slope classes in each sub basin. The physical processes associated with water and sediment movement, crop growth, and nutrient cycling are modelled at the HRU scale to assess the runoff generated from the streams (Tables 2 and 3). SWAT provides two methods for estimating surface runoff. The first one is based on the Soil Conservation Service curve number and the second one estimates runoff height using the Green and Ampt infiltration method. SWAT calculates the surface erosion caused by rainfall and runoff within each HRUs with the help of Modified Universal Soil Loss Equation (MUSLE) (Williams, 1975). SWAT uses equation (8) to calculate sediment yield:

$$\text{sed} = 11.8 \times (\text{Qsurf} \times \text{qpeak} \times \text{areahru})^{0.56} \times K_{USLE} \times C_{USLE} \times P_{USLE} \times LS_{USLE} \times C_{FRG} \quad (8)$$

Where: sed is the sediment yield on a given day (metric tons); Qsurf is the surface runoff volume (mm H_2O ha^{-1}); qpeak is the peak runoff rate (m^3 s^{-1}); areahru is the area of the HRU (ha); K_{USLE} is the USLE soil erodibility factor; C_{USLE} is the USLE cover and management factor; P_{USLE} is the USLE support practice factor; LS_{USLE} is the USLE topographic factor, and C_{FRG} is the coarse fragment factor.

This model simulates hypothetical, real and future scenarios and is proven to be an effective method to evaluating alternative land use effects on runoff, sediment and pollutant losses.

Status: Although very few studies used this model initially (2000–2010), its use saw an increase from 2011 to 2019 (Fig. 3). This method has been widely used around the world covering 3.9% of the total studies reviewed (Figs. 3 and 4).

Limitations: Owing to the model being based on runoff generation in the catchment which requires extensive data collection, the model has a limited use.

2.2.4.2. Erosion Potential Method (EPM). ***General Description:*** The Gavrilović method (Erosion Potential Method, EPM) is an empirical, semi-quantitative model which has been extensively applied to erosion and torrent-related problems in the Balkan countries. The method encompasses erosion mapping, sediment quantity estimation, and torrent classification. The method does not explore physics of erosion processes and it is difficult to predict them efficiently with minimal data and lack of previous research on erosion (Kostadinov et al., 2014). Equations (9)–(11) are used in this method (Gavrilovic et al., 2005). Total annual erosion in m^3/year (W) is determined by equation (9):

$$W = T \times H \times F \times \pi\sqrt{Z^3} \quad (9)$$

where, T is the temperature coefficient, H is the mean annual precipitation (mm), Z is the erosion coefficient, and F is the basin area (km^2). The temperature coefficient (T) is calculated by Equation (10):

$$T = \sqrt{\frac{t}{10}} + 0.1 \quad (10)$$

The soil erosion coefficient (Z) is calculated from equation (11):

$$Z = Y \times X\left(\phi + \sqrt{I_{av}}\right) \quad (11)$$

where, X is the soil protection coefficient which reflect type of land use, Y is the coefficient of soil resistance depends on soil and geology, ϕ is erosion and stream network developed coefficient that includes type and extent of erosion, I is the average slope (%) of the watershed. This model requires total 18 parameters and it is advantageous for areas with minimal data availability or a lack of previous research (Dragičević et al., 2018). The outputs of this model is based on parameters such as average annual temperature, average slope of the study area, and drainage density etc. T, H, F and Z are classified as very high-sensitivity parameter while ϕ, I_{av}, X and Y may have medium to high sensitivity.

Status: It was observed that the use of this model has increased from 2011 to 2019 (Fig. 3) and very few studies were conducted in preceding decade (2000–2010). This method has been widely used in European continent making it third (6.7%) most used quantitative method (Figs. 3 and 4).

Limitations: The use of this model is limited to European continent perhaps because of its detailed and comprehensive data collection requirements and independent interface which demands expertise.

Apart from above mentioned, researchers have used single components and a combination of components such as morphometry, land use, water quality and soil quality of watersheds to estimate their vulnerability to soil erosion. Above mentioned has been used to prioritise watersheds using combined component i.e. land use and water quality (0.6%); land use and soil quality (1.1%) and few studies have estimated it based on only one component such as morphometry (6.7%) and land use and land cover (4.5%) (Fig. 4) (Tables 2 and 3). The decadal trends and regional comparison are given below.

2.2.5. Status in Himalayan region

In the past three decades, 80 percent of the studies reviewed were distributed mainly in the non-Himalayan region while the Himalayan region, which is one of the most fragile ecosystems was addressed by only 20 percent of the total studies reviewed (Fig. 2). The studies conducted in Himalayan region either used qualitative estimation using statistical methods or used models such as WEPP, RUSLE and SWAT. Models like PESERA, EPM, SHE and EUROSEM which were primarily made for Europe and American continents were not used by researchers for estimating soil erosion in Himalayan region (Tables 2 and 3). Perhaps because of the complex data requirement by these models.

3. Conclusion

This review focuses on describing methods used worldwide to estimate soil erosion losses in the last 30 years. The results shows that 18 different methods have mainly been used to assess soil erosion risk in different regions. These methods include statistical, empirical and process based methods. The use of few physical methods like ANSWERS and SHE usage has decreased with time while that of physical and process methods like PESERA, SWAT, WEPP and RUSLE has increased with time. RUSLE, with no independent interface and with few limitations, has been most popular in last three decades because of its flexibility and compatibility with ArcGIS although great care is required for selection of input values for rainfall (Kouli et al., 2009) and soil erodibility (Morgan et al., 1998) factors. While using this method, it should also be kept in mind that this equation cannot provide information on the sediment once eroded. The review has highlighted that various models are being used worldwide based on their suitability to the region. It also brings to attention that few models like PESERA, EUROSEM and WEPP have superiority over RUSLE but are being used by limited researchers mostly concentrated in a particular region. Models like PESERA and EPM are mostly used in European region and may be encouraged to estimate soil erosion in Himalayan region. The EPM method is the most appropriate for hilly-mountain and mountain region (Blinkov & Kostadinov, 2010) but has not been attempted in the Himalayan region so far. The only constraints with using such models over RUSLE is higher demand of input data and most of them are based on sediment yield and runoff.

This paper also suggests that in case of lack of data, qualitative assessment can be preferred over quantitative assessment using various statistical methods like PCA, CF, FUZZY etc. The review brings to light that statistical methods have been used worldwide and CF is the most used method so far. The review also highlights lack of studies with inclusion of water quality as an important parameter while assessing soil erosion vulnerability in the region. Determination of such relationships is suggested as an advance approach to provide adequate information about characteristics of a watershed. The review also highlights that from the selected studies very few focus on the Himalayan region. Thus, there is a greater scope of conducting soil erosion vulnerability assessment with help of more robust methods like EPM and PESERA. There is also a need of increasing frequency of studies in the fragile region of Himalayas. In order to protect fragile regions, researchers need to attempt more methods and compare them to attain more accurate results. However, while doing this, requirement and availability of accurate input should be considered.

Declaration of competing interest

The authors declare that they have no known competing financial interests or personal relationships that could have appeared to influence the work reported in this paper.

Appendix A. Supplementary data

Supplementary data to this article can be found online at https://doi.org/10.1016/j.iswcr.2021.03.001.

References

Abbott, M. B., Bathurst, J. C., Cunge, J. A., O'Connell, P. E., & Rasmussen, J. (1986). An introduction to the European Hydrological System - Systeme Hydrologique Europeen, "SHE", 1: History and philosophy of a physically-based, distributed modelling system. *Journal of Hydrology, 87*(1–2), 45–59. https://doi.org/10.1016/0022-1694(86)90114-9

Abdul Rahaman, S., Aruchamy, S., Jegankumar, R., & Abdul Ajeez, S. (2015). Estimation of annual average soil loss, based on RUSLE model in Kallar watershed, Bhavani Basin, Tamil Nadu, India. *ISPRS Annals of the Photogrammetry, Remote Sensing and Spatial Information Sciences, 2*(2W2), 207–214. https://doi.org/10.5194/isprsannals-II-2-W2-207-2015

Adediji, A. (2010). Assessment of revised universal soil loss equation (RUSLE) in Katsina area, Katsina state of Nigeria using remote sensing (RS) and geographic information system (GIS). *Iranian Journal of Energy and Environment; Previously Called: Iranica Journal of Energy and Environment, 1*(3), 255–264.

Aher, P. D., Adinarayana, J., & Gorantiwar, S. D. (2013). Prioritization of watersheds using multi-criteria evaluation through fuzzy analytical hierarchy process. *Agricultural Engineering International: CIGR Journal, 15*(1), 11–18.

Ahmadi, S. H., Amin, S., Reza Keshavarzi, A., & Mirzamostafa, N. (2006). Simulating watershed outlet sediment concentration using the ANSWERS model by applying two sediment transport capacity equations. *Biosystems Engineering, 94*(4), 615–626. https://doi.org/10.1016/j.biosystemseng.2006.04.015

Ahn, S. R., & Kim, S. J. (2017). Assessment of watershed health, vulnerability and resilience for determining protection and restoration priorities. *Environmental*

Modelling & Software, 1–19. https://doi.org/10.1016/j.envsoft.2017.03.014
Albaradeyia, I., Hani, A., & Shahrour, I. (2011). WEPP and ANN models for simulating soil loss and runoff in a semi-arid Mediterranean region. *Environmental Monitoring and Assessment, 180*(1–4), 537–556. https://doi.org/10.1007/s10661-010-1804-x
Alewell, C., Borrelli, P., Meusburger, K., & Panagos, P. (2019). Using the USLE: Chances, challenges and limitations of soil erosion modelling. *International Soil and Water Conservation Research, 7*(3), 203–225. https://doi.org/10.1016/j.iswcr.2019.05.004
Altaf, S., Meraj, G., & Romshoo, S. A. (2014). Morphometry and land cover based multi-criteria analysis for assessing the soil erosion susceptibility of the western Himalayan watershed. *Environmental Monitoring and Assessment, 186*(12), 8391–8412. https://doi.org/10.1007/s10661-014-4012-2
Ameri, A. A., Pourghasemi, H. R., & Cerda, A. (2018). Erodibility prioritization of subwatersheds using morphometric parameters analysis and its mapping: A comparison among TOPSIS, VIKOR, saw, and CF multi-criteria decision making models. *The Science of the Total Environment, 613–614*, 1385–1400. https://doi.org/10.1016/j.scitotenv.2017.09.210
Amini, S., Rafiei, B., Khodabakhsh, S., & Heydari, M. (2010). Estimation of erosion and sediment yield of Ekbatan Dam drainage basin with EPM, using GIS. *Iranian Journal of Earth Sciences, 2*, 173–180.
Amsalu, T., & Mengaw, A. (2014). GIS based soil loss estimation using RUSLE Model: The case of Jabi Tehinan Woreda, ANRS, Ethiopia. *Natural Resources, 5*, 616–626. https://doi.org/10.4236/nr.2014.511054
Angima, S. D., Stott, D. E., O'Neill, M. K., Ong, C. K., & Weesies, G. A. (2003). Soil erosion prediction using RUSLE for central Kenyan highland conditions. *Agriculture, Ecosystems & Environment, 97*(1–3), 295–308. https://doi.org/10.1016/S0167-8809(03)00011-2
Ashiagbor, G., Forkuo, E. K., Laari, P., & Aabeyir, R. (2013). Modeling soil erosion using RUSLE and GIS tools. *International Journal of Remote Sensing and Geoscience, 2*(4), 7–17.
Bagyaraj, M., Ramkumar, T., Venkatramanan, S., Chung, S. Y., & Gurugnanam, B. (2014). Assessment of soil erosion probability in Kodaikanal, India using GIS and remote sensing. *Disaster Advances, 7*(2), 36–49.
Balasubramani, K., Veena, M., Kumaraswamy, K., & Saravanabavan, V. (2015). Estimation of soil erosion in a semi-arid watershed of Tamil Nadu (India) using revised universal soil loss equation (RUSLE) model through GIS. *Modeling Earth Systems and Environment, 1*(10), 1–17. https://doi.org/10.1007/s40808-015-0015-4
Baloshi, V., Gjoka, F., & Toromani, E. (2019). Determination of soil loss by erosion in different land covers categories and slope classes in Bovilla. *International Journal of Environmental and Ecological Engineering, 13*(2), 57–61.
Bathurst, J. C., & Cooley, K. R. (1996). Use of the SHE hydrological modelling system to investigate basin response to snowmelt at Reynolds Creek, Idaho. *Journal of Hydrology, 175*(1–4), 181–211. https://doi.org/10.1016/S0022-1694(96)80011-4
Beasley, D. B., Huggins, L. F., & Monke, E. J. (1980). Answers: A model for watershed planning. *Transactions of the American Society of Agricultural Engineers, 23*(4), 938–944. https://doi.org/10.13031/2013.34692
Benavidez, R., Jackson, B., Maxwell, D., & Norton, K. (2018). A review of the (Revised) Universal Soil Loss Equation ((R)USLE): With a view to increasing its global applicability and improving soil loss estimates. *Hydrology and Earth System Sciences, 22*(11), 6059–6086. https://doi.org/10.5194/hess-22-6059-2018
Bennett, H. H. (1939). A permanent loss to New England: Soil erosion resulting from the Hurricane. Wiley. *American Geographical Society, 29*(2), 196–204.
Beskow, S., Mello, C. R., Norton, L. D., Curi, N., Viola, M. R., & Avanzi, J. C. (2009). Soil erosion prediction in the Grande River Basin, Brazil using distributed modeling. *Catena, 79*(1), 49–59. https://doi.org/10.1016/j.catena.2009.05.010
Bewket, W., & Teferi, E. (2009). Assessment of soil erosion hazard and prioritization for treatment at the watershed level: Case study in the Chemoga Watershed, Blue Nile Basin, Ethiopia. *Land Degradation & Development, 20*, 609–622. https://doi.org/10.1002/ldr
Bhandari, K. P., Aryal, J., & Darnsawasdi, R. (2015). A geospatial approach to assessing soil erosion in a watershed by integrating socio-economic determinants and the RUSLE model. *Natural Hazards, 75*(1), 321–342. https://doi.org/10.1007/s11069-014-1321-2
Bhat, S. A., Hamid, I., Dar, M. U. D., Rasool, D., Pandit, B. A., & Khan, S. (2017). Soil erosion modeling using RUSLE & GIS on micro watershed of J&K. *Journal of Pharmacognosy and Phytochemistry, 6*(65), 838–842.
Bhattarai, R., & Dutta, D. (2007). Estimation of soil erosion and sediment yield using GIS at catchment scale. *Water Resources Management, 21*(10), 1635–1647. https://doi.org/10.1007/s11269-006-9118-z
Biswas, S. S., & Pani, P. (2015). Estimation of soil erosion using RUSLE and GIS techniques: A case study of Barakar river basin, Jharkhand, India. *Modeling Earth Systems and Environment, 1*(4), 1–13. https://doi.org/10.1007/s40808-015-0040-3
Blinkov, I., & Kostadinov, S. (2010). Applicability of various erosion risk assessment methods for engineering purposes. *Balwois, 2010*, 1–13. May.
Blinkov, I., Kostadinov, S., & Marinov, I. T. (2013). Comparison of erosion and erosion control works in Macedonia, Serbia and Bulgaria. *International Soil and Water Conservation Research, 1*(3), 15–28. https://doi.org/10.1016/S2095-6339(15)30027-7
Borrelli, P., Märker, M., Panagos, P., & Schütt, B. (2014). Modeling soil erosion and river sediment yield for an intermountain drainage basin of the Central Apennines, Italy. *Catena, 114*, 45–58. https://doi.org/10.1016/j.catena.2013.10.007
Bouraoui, F., & Dillaha, T. A. (1996). ANSWERS-2000: Runoff and sediment transport model. *Journal of Environmental Engineering, 122*(June), 493–502.
B, H. K., Sai, R., Sampath, O., & Nagendher, T. (2014). A Review- Impact of land use land cover change and best management practices in a watershed by using swat model. *International Journal of Pure & Applied Bioscience, 2*(1), 276–285.
Cai, Q. G., Wang, H., Curtin, D., & Zhu, Y. (2005). Evaluation of the EUROSEM model with single event data on Steeplands in the three Gorges reservoir areas, China. *Catena, 59*(1), 19–33. https://doi.org/10.1016/j.catena.2004.05.008
Campos Pinto, L., de Mello, C. R., Norton, L. D., Owens, P. R., & Curi, N. (2016). Spatial prediction of soil-water transmissivity based on fuzzy logic in a Brazilian headwater watershed. *Catena, 143*, 26–34. https://doi.org/10.1016/j.catena.2016.03.033
Centeri, C., Barta, K., Jakab, G., Szalai, Z., & Bíró, Z. (2009). Comparison of EUROSEM, WEPP, and MEDRUSH model calculations with measured runoff and soil-loss data from rainfall simulations in Hungary. *Journal of Plant Nutrition and Soil Science, 172*(6), 789–797. https://doi.org/10.1002/jpln.200900009
Chang, D. Y. (1996). Applications of the extent analysis method on fuzzy AHP. *European Journal of Operational Research, 95*(3), 649–655. https://doi.org/10.1016/0377-2217(95)00300-2
Chatterjee, S., Krishna, A. P., & Sharma, A. P. (2014). Geospatial assessment of soil erosion vulnerability at watershed level in some sections of the Upper Subarnarekha river basin, Jharkhand, India. *Environmental Earth Sciences, 71*(1), 357–374. https://doi.org/10.1007/s12665-013-2439-3
Chowdary, V. M., Chakraborthy, D., Jeyaram, A., Murthy, Y. V. N. K., Sharma, J. R., & Dadhwal, V. K. (2013). Multi-Criteria Decision making approach for watershed prioritization using Analytic Hierarchy Process technique and GIS. *Water Resources Management, 27*(10), 3555–3571. https://doi.org/10.1007/s11269-013-0364-6
Cilek, A. (2017). Soil organic carbon losses by water erosion in a Mediterranean watershed. *Soil Research, 55*(4), 363–375. https://doi.org/10.1071/SR16053
Cilek, A., Berberoglu, S., Kirkby, M., Irvine, B., Donmez, C., & Erdogan, M. A. (2015). Erosion modelling in a Mediterranean Subcatchment under climate change scenarios using pan-European soil erosion risk assessment (PESERA). *International Archives of the Photogrammetry. Remote Sensing and Spatial Information Sciences - ISPRS Archives, 40*(7W3), 359–365. https://doi.org/10.5194/isprsarchives-XL-7-W3-359-2015
Claessens, L., Breuge, P. V., Notenbaert, A., Herrero, M., & Steeg, J. V. (2008). *Mapping potential soil erosion in east Africa using the universal soil loss equation and secondary data* (Vol. 325, pp. 398–407). IAHS-AISH Publication.
Dabral, P. P., Baithuri, N., & Pandey, A. (2008). Soil erosion assessment in a hilly catchment of North Eastern India using USLE, GIS and remote sensing. *Water Resources Management, 22*(12), 1783–1798. https://doi.org/10.1007/s11269-008-9253-9
Demirci, A., & Karaburun, A. (2012). Estimation of soil erosion using RUSLE in a GIS framework: A case study in the Buyukcekmece lake watershed, northwest Turkey. *Environmental Earth Sciences, 66*(3), 903–913. https://doi.org/10.1007/s12665-011-1300-9
Dimotta, A. (2019). *Soil erosion interdiscplinary overview: Modelling approaches, ecosystem services assessment and soil quality Restoration. Applications and analyses in the Basilicata region (Italy)*. Dublin, Ireland: Earth- & Eco-Systems Expertise for Environmental Modeling & Restoration.
Djuma, H., Bruggeman, A., Camera, C., & Zoumides, C. (2016). Combining qualitative and quantitative methods for soil erosion assessments: An application in a sloping Mediterranean Watershed, Cyprus. *Land Degradation & Development, 28*(1), 243–254. https://doi.org/10.1002/ldr.2571
Dragičević, N., Karleuša, B., & Ožanić, N. (2018). Modification of erosion potential method using climate and land cover parameters. *Geomatics, Natural Hazards and Risk, 9*(1), 1085–1105. https://doi.org/10.1080/19475705.2018.1496483
Dutta, D., Das, S., Kundu, A., & Taj, A. (2015). Soil erosion risk assessment in Sanjal watershed, Jharkhand (India) using geo-informatics, RUSLE model and TRMM data. *Modeling Earth Systems and Environment, 1*(4), 1–9. https://doi.org/10.1007/s40808-015-0034-1
Efe, R., Ekinci, D., & Curebal, I. (2008). Erosion analysis of Fındıklı Creek catchment (Northwest of Turkey) using GIS based on RUSLE (3D) method. *Fresenius Environmental Bulletin, 17*, 568–576.
Erdogan, E. H., Erpul, G., & Bayramin, I. (2007). Use of USLE/GIS methodology for predicting soil loss in a semiarid agricultural watershed. *Environmental Monitoring and Assessment, 131*(1–3), 153–161. https://doi.org/10.1007/s10661-006-9464-6
Farhan, Y., & Anaba, O. (2016). A remote sensing and GIS approach for prioritization of Wadi Shueib Mini-Watersheds (Central Jordan) based on morphometric and soil erosion susceptibility analysis. *Journal of Geographic Information System*, 1–19. https://doi.org/10.4236/jgis.2016.81001, 08(01).
Farhan, Y., Anbar, A., Al-Shaikh, N., & Mousa, R. (2017). Prioritization of semi-arid agricultural watershed using morphometric and Principal Component Analysis, remote sensing, and GIS techniques, the Zerqa River Watershed, Northern Jordan. *Agricultural Sciences*, 113–148. https://doi.org/10.4236/as.2017.81009, 08(01).
Farhan, Y., & Nawaiseh, S. (2015). Spatial assessment of soil erosion risk using RUSLE and GIS techniques. *Environmental Earth Sciences, 74*(6), 4649–4669. https://doi.org/10.1007/s12665-015-4430-7
Farhan, Y., Zregat, D., & Farhan, I. (2013). Spatial estimation of soil erosion risk using RUSLE approach, RS, and GIS techniques: A case study of Kufranja watershed, Northern Jordan. *Journal of Water Resource and Protection*, 1247–1261. https://doi.org/10.4236/jwarp.2013.512134, 05(12).

Fernández, C., & Vega, J. A. (2016). Evaluation of RUSLE and PESERA models for predicting soil erosion losses in the first year after wildfire in NW Spain. *Geoderma, 273*, 64–72. https://doi.org/10.1016/j.geoderma.2016.03.016

Fistikoglu, O., & Harmancioglu, N. B. (2002). Integration of GIS with USLE in assessment of soil erosion. *Water Resources Management, 16*(6), 447–467. https://doi.org/10.1023/A:1022282125760

Flanagan, D., Gilley, J., & Franti, T. (2007). Water erosion prediction project (Wepp). *Transactions of the ASABE, 50*(5), 1603–1612.

Folly, A., Quinton, J. N., & Smith, R. E. (1999). Evaluation of the EUROSEM model using data from the Catsop watershed, The Netherlands. *Catena, 37*(3–4), 507–519. https://doi.org/10.1016/S0341-8162(99)00036-3

Fu, B. J., Zhao, W. W., Chen, L. D., Zhang, Q. J., Lü, Y. H., Gulinck, H., & Poesen, J. (2005). Assessment of soil erosion at large watershed scale using RUSLE and GIS: A case study in the loess plateau of China. *Land Degradation & Development, 16*(1), 73–85. https://doi.org/10.1002/ldr.646

Gaikwad, R., & Bhagat, V. (2018). Multi-criteria watershed prioritization of Kas basin in Maharashtra India: AHP and influence approaches. *Hydrospatial Analysis, 1*(1), 41–61. https://doi.org/10.21523/gcj3.17010105

Ganasri, B. P., & Ramesh, H. (2015). Assessment of soil erosion by RUSLE model using remote sensing and GIS - a case study of Nethravathi Basin. *Geoscience Frontiers, 7*(6), 953–961. https://doi.org/10.1016/j.gsf.2015.10.007

Gaubi, I., Chaabani, A., Ben Mammou, A., & Hamza, M. H. (2016). A GIS-based soil erosion prediction using the revised universal soil loss equation (RUSLE) (Lebna watershed, Cap Bon, Tunisia). *Natural Hazards, 86*(1), 219–239. https://doi.org/10.1007/s11069-016-2684-3

Gavrilovic, Z., Stefanovic, M., Milojevic, M., & Cotric, J. (2005). Erosion Potential Method " an important support for integrated water resource management. *Balwois, 2006*, 1–14.

Gelagay, H. S., & Minale, A. S. (2016). Soil loss estimation using GIS and remote sensing techniques: A case of Koga watershed, Northwestern Ethiopia. *International Soil and Water Conservation Research, 4*(2), 126–136. https://doi.org/10.1016/j.iswcr.2016.01.002

Ghosh, K., Kumar De, S., Bandyopadhyay, S., & Saha, S. (2013). Assessment of soil loss of the Dhalai river basin, Tripura, India using USLE. *International Journal of Geosciences*, 11–23. https://doi.org/10.4236/ijg.2013.41002, 04(01).

Golmohammadi, G., Prasher, S., Madani, A., & Rudra, R. (2014). Evaluating three hydrological distributed watershed models: MIKE-SHE, apex, SWAT. *Hydrology, 1*(1), 20–39. https://doi.org/10.3390/hydrology1010020

Greer, R. C., Wu, J. Q., Singh, P., & McCool, D. K. (2006). WEPP simulation of observed winter runoff and erosion in the U.S. Pacific Northwest. *Vadose Zone Journal, 5*(1), 261. https://doi.org/10.2136/vzj2005.0055

Guo, J., Niu, T., Rahimy, P., Wang, F., Zhao, H., & Zhang, J. (2013). Assessment of soil erosion susceptibility using empirical modeling. *Acta Meteorologica Sinica, 27*(1), 98–109. https://doi.org/10.1007/s13351-013-0110-2

Haghizadeh, A., Shui, L. T., & Godarzi, E. (2009). Forecasting sediment with Erosion Potential Method with emphasis on land use changes at basin. *Electronic Journal of Geotechnical Engineering, 14*, 1–12.

Haidara, I., Tahri, M., Maanan, M., & Hakdaoui, M. (2019). Efficiency of fuzzy analytic hierarchy process to detect soil erosion vulnerability. *Geoderma, 354*(113853), 1–15. https://doi.org/10.1016/j.geoderma.2019.07.011

Halefom, A., Teshome, A., & Sisay, E. (2019). GIS-based MCDA model to assess erosion sensitivity in Gumara watershed, Blue Nile, Basin Ethiopia. *Asian Journal of Applied Sciences, 12*(2), 61–70. https://doi.org/10.3923/ajaps.2019.61.70

Haregeweyn, N., Tsunekawa, A., Poesen, J., Tsubo, M., Meshesha, D. T., Fenta, A. A., Nyssen, J., & Adgo, E. (2017). Comprehensive assessment of soil erosion risk for better land use planning in river basins: Case study of the Upper Blue Nile River. *The Science of the Total Environment, 574*, 95–108. https://doi.org/10.1016/j.scitotenv.2016.09.019

Hart, H. M. (2006). *Effect of land Use on total suspended solids and Turbidity in the little river watershed, Blount County, Tennessee*. Knoxville: University of Tennessee. https://trace.tennessee.edu/utk_gradthes/1569.

Hembram, T. K., Paul, G. C., & Saha, S. (2019). Comparative analysis between morphometry and geo-environmental factor based soil erosion risk assessment using weight of evidence model: A study on Jainti river basin, eastern India. *Environmental Processes, 6*(4), 883–913. https://doi.org/10.1007/s40710-019-00388-5

Huggins, L., & Monke, E. (1966). The mathematical simulation of the hydrology of small watersheds. In *IWRRC Technical Reports*. Purdue University.

Hui, L., Xiaoling, C., Lim, K. J., Xiaobin, C., & Sagong, M. (2010). Assessment of soil erosion and sediment yield in Liao watershed, Jiangxi Province, China, Using USLE, GIS, and RS. *Journal of Earth Sciences, 21*(6), 941–953. https://doi.org/10.1007/s12583-010-0147-4

Jain, M. K., & Das, D. (2010). Estimation of sediment yield and areas of soil erosion and deposition for watershed prioritization using GIS and remote sensing. *Water Resources Management, 24*(10), 2091–2112. https://doi.org/10.1007/s11269-009-9540-0

Jain, S. K., Kumar, S., & Varghese, J. (2001). Estimation of soil erosion for a himalayan watershed using GIS technique. *Water Resources Management, 15*, 41–54.

Jasrotia, A. S., & Singh, R. (2006). Modeling runoff and soil erosion in a catchment area using the GIS in the Himalayan region, India. *Environmental Geology, 51*(1), 29–37. https://doi.org/10.1007/s00254-006-0301-6

Jazouli, A. El, Barakat, A., Khellouk, R., Rais, J., & Baghdadi, M. El (2018). Remote sensing and GIS techniques for prediction of land use land cover change effects on soil erosion in the high basin of the Oum Er Rbia River (Morocco). *Remote Sensing Applications: Society and Environment, 13*, 361–374. https://doi.org/10.1016/j.rsase.2018.12.004

Kalambukattu, J., & Kumar, S. (2017). Modelling soil erosion risk in a mountainous watershed of Mid-Himalaya by integrating RUSLE model with GIS. *Eurasian Journal of Soil Science, 6*(2). https://doi.org/10.18393/ejss.286442, 92–92.

Kannan, G., Pokharel, S., & Kumar, P. S. (2009). A hybrid approach using ISM and fuzzy TOPSIS for the selection of reverse logistics provider. *Resources, Conservation and Recycling, 54*(1), 28–36. https://doi.org/10.1016/j.resconrec.2009.06.004

Karaburun, A. (2010). Estimation of C factor for soil erosion modeling using NDVI in Buyukcekmece watershed. *Ozean Journal of Applied Sciences, 3*(1), 77–85.

Karamesouti, M., Detsis, V., Kounalaki, A., Vasiliou, P., Salvati, L., & Kosmas, C. (2015). Land-use and land degradation processes affecting soil resources: Evidence from a traditional Mediterranean cropland (Greece). *Catena, 132*, 45–55. https://doi.org/10.1016/j.catena.2015.04.010

Karamesouti, M., Petropoulos, G. P., Papanikolaou, I. D., Kairis, O., & Kosmas, K. (2016). Erosion rate predictions from PESERA and RUSLE at a Mediterranean site before and after a wildfire: Comparison & implications. *Geoderma, 261*, 44–58. https://doi.org/10.1016/j.geoderma.2015.06.025

Karan, S. K., Ghosh, S., & Samadder, S. R. (2019). Identification of spatially distributed hotspots for soil loss and erosion potential in mining areas of Upper Damodar Basin – India. *Catena, 182*, 1–9. https://doi.org/10.1016/j.catena.2019.104144

Kefi, M., Yoshino, K., Setiawan, Y., Zayani, K., & Boufaroua, M. (2011). Assessment of the effects of vegetation on soil erosion risk by water: A case of study of the Batta watershed in Tunisia. *Environmental Earth Sciences, 64*(3), 707–719. https://doi.org/10.1007/s12665-010-0891-x

Khaledian, Y., Kiani, F., Ebrahimi, S., Brevik, E. C., & Aitkenhead-Peterson, J. (2016). Assessment and monitoring of soil degradation during land use change using Multivariate Analysis. *Land Degradation & Development, 28*(1), 128–141. https://doi.org/10.1002/ldr.2541

Khaleghpanah, N., Shorafa, M., Asadi, H., Gorji, M., & Davari, M. (2016). Modeling soil loss at plot scale with EUROSEM and RUSLE2 at stony soils of Khamesan watershed, Iran. *Catena, 147*, 773–788. https://doi.org/10.1016/j.catena.2016.08.039

Kinthada, N. R., Gurram, M. K., Eedara, A., & Velaga, V. R. (2013). Remote sensing and GIS in the geomorphometric analysis of micro- watersheds for hydrological Scenario assessment and characterization - a study on Sarada river basin , Visakhapatnam district , India. *International Journal of Geomatics and Geosciences, 4*(1), 195–212.

Kirkby, M. (2003). Modelling erosion- the PESERA project. In *Soil conservation and protection for Europe (SCAPE), European Commission*. Energy, Environment and Sustainable Development (EESD).

Kirkby, M. J., Irvine, B. J., Jones, R. J. A., Govers, G., Boer, M., Cerdan, O., Daroussin, J., Gobin, A., Grimm, M., Bissonnais, Y., Kosmas, C., Mantel, S., Puigdefabregas, J., & Lynden, G. V. (2008). The PESERA coarse scale erosion model for Europe. I. - model rationale and implementation. *European Journal of Soil Science, 59*(6), 1293–1306. https://doi.org/10.1111/j.1365-2389.2008.01072.x

Kostadinov, S., Braunović, S., Dragićević, S., Zlatić, M., Dragović, N., & Rakonjac, N. (2018). Effects of erosion control works: Case study- Grdelica Gorge, the South Morava river (Serbia). *Water, 10*(8), 1–19. https://doi.org/10.3390/w10081094

Kostadinov, S., Miodrag, Z., Dragovic, N., & Gavrilovic, Z. (2014). Serbia and Montenegro. In J. Boardman, & J. Poesen (Eds.), *Soil erosion in Europe* (pp. 271–277). John Wiley & Sons. https://doi.org/10.1177/002070200305800207.

Kouli, M., Soupios, P., & Vallianatos, F. (2009). Soil erosion prediction using the revised universal soil loss equation (RUSLE) in a GIS framework, Chania, Northwestern Crete, Greece. *Environmental Geology, 57*(3), 483–497. https://doi.org/10.1007/s00254-008-1318-9

Kumar, A., Devi, M., & Deshmukh, B. (2014). Integrated remote sensing and geographic information system based RUSLE Modelling for estimation of soil loss in Western Himalaya, India. *Water Resources Management, 28*(10), 3307–3317. https://doi.org/10.1007/s11269-014-0680-5

Kumar, S., & Kushwaha, S. P. S. (2013). Modelling soil erosion risk based on RUSLE-3D using GIS in a Shivalik sub-watershed. *Journal of Earth System Science, 122*(2), 389–398. https://doi.org/10.1007/s12040-013-0276-0

Kushwaha, A., & Jain, M. K. (2013). Hydrological Simulation in a forest dominated watershed in Himalayan region using SWAT Model. *Water Resources Management, 27*(8), 3005–3023. https://doi.org/10.1007/s11269-013-0329-9

Laflen, J. M., Elliot, W. J., Flanagan, D. C., Meyer, C. R., & Nearing, M. A. (1997). WEPP-Predicting water erosion using a process-based model. *Journal of Soil and Water Conservation*, 96–102.

Lahlaoi, H., Rhinane, H., Hilali, A., Lahssini, S., & Khalile, L. (2015). Potential erosion risk calculation using remote sensing and GIS in Oued El Maleh Watershed, Morocco. *Journal of Geographic Information System*, 128–139. https://doi.org/10.4236/jgis.2015.72012, 07(02).

Landi, A., Barzegar, A. R., Sayadi, J., & Khademalrasoul, A. (2011). Assessment of soil loss using WEPP Model and geographic information system. *Journal of Spatial Hydrology, 11*(1), 40–51.

Lee, S. (2003). Soil erosion assessment and its verification using the universal soil loss equation and geographic information system: A case study at Boun, Korea. *Environmental Geology, 45*(4), 457–465. https://doi.org/10.1007/s00254-003-0897-8

Lense, G. H. E., Parreiras, T. C., Moreira, R. S., Avanzi, J. C., & Mincato, R. L. (2019). Estimates of soil losses by the erosion potential method in tropical latosols. *Ciencia E Agrotecnologia, 43*. https://doi.org/10.1590/1413-7054201943012719

Liou, T. S., & Wang, M. J. J. (1992). Fuzzy weighted average: An improved algorithm. *Fuzzy Sets and Systems, 49*(3), 307–315. https://doi.org/10.1016/0165-0114(92)90282-9

Li, L., Shi, Z. H., Yin, W., Zhu, D., Ng, S. L., Cai, C. F., & Lei, A. L. (2009). A fuzzy analytic hierarchy process (FAHP) approach to eco-environmental vulnerability assessment for the danjiangkou reservoir area, China. *Ecological Modelling, 220*(23), 3439–3447. https://doi.org/10.1016/j.ecolmodel.2009.09.005

Li, P., Zang, Y., Ma, D., Yao, W., Holden, J., Irvine, B., & Zhao, G. (2019). Soil erosion rates assessed by RUSLE and PESERA for a Chinese Loess Plateau catchment under land-cover changes. *Earth Surface Processes and Landforms, 45*(3), 707–722. https://doi.org/10.1002/esp.4767

Lovric, N., & Tosic, R. (2018). Assessment of soil erosion and sediment yield using erosion potential method: Case study- Vrbas River Basin (B&H). *Bulletin of the Serbian Geographical Society, 98*(1), 1–14.

Lufafa, A., Tenywa, M. M., Isabirye, M., Majaliwa, M. J. G., & Woomer, P. L. (2003). Prediction of soil erosion in a Lake Victoria basin catchment using a GIS-based Universal Soil Loss model. *Agricultural Systems, 76*(3), 883–894. https://doi.org/10.1016/S0308-521X(02)00012-4

Mahapatra, S. K., Obi Reddy, G. P., Nagdev, R., Yadav, R. P., Singh, S. K., & Sharda, V. N. (2018). Assessment of soil erosion in the fragile Himalayan ecosystem of Uttarakhand, India using USLE and GIS for sustainable productivity. *Current Science, 115*(1), 108–121. https://doi.org/10.18520/cs/v115/i1/108-121

Makaya, N., Dube, T., Seutloali, K., Shoko, C., Mutanga, O., & Masocha, M. (2019). Geospatial assessment of soil erosion vulnerability in the upper uMgeni catchment in KwaZulu Natal, South Africa. *Physics and Chemistry of the Earth, 112*, 50–57. https://doi.org/10.1016/j.pce.2019.02.012

Malik, M. I., & Bhat, M. S. (2014). Integrated approach for prioritizing watersheds for management: A study of Lidder catchment of Kashmir Himalayas. *Environmental Management, 54*(6), 1267–1287. https://doi.org/10.1007/s00267-014-0361-4

Mandal, D., & Sharda, V. N. (2011). Appraisal of soil erosion risk in the eastern himalayan region of India for soil conservation planning. *Land Degradation & Development, 24*(5), 430–437. https://doi.org/10.1002/ldr.1139

Manyiwa, T., & Dikinya, O. (2013). Using universal soil loss equation and soil erodibility factor to assess soil erosion in Tshesebe village , north east Botswana. *African Journal of Agricultural Research, 8*(30), 4170–4178. https://doi.org/10.5897/AJAR2013.7081

Markose, V. J., & Jayappa, K. S. (2016). Soil loss estimation and prioritization of sub-watersheds of Kali river basin, Karnataka, India, using RUSLE and GIS. *Environmental Monitoring and Assessment, 188*(4), 224–240. https://doi.org/10.1007/s10661-016-5218-2

Mihi, A., Benarfa, N., & Arar, A. (2019). Assessing and mapping water erosion-prone areas in northeastern Algeria using analytic hierarchy process, USLE/RUSLE equation, GIS, and remote sensing. *Applied Geomatics, 12*(2), 179–191. https://doi.org/10.1007/s12518-019-00289-0

Millward, A. A., & Mersey, J. E. (1999). Adapting the RUSLE to model soil erosion potential in a mountainous tropical watershed. *Catena, 38*(2), 109–129. https://doi.org/10.1016/S0341-8162(99)00067-3

Mondal, A., Khare, D., & Kundu, S. (2016). A comparative study of soil erosion modelling by MMF, USLE and RUSLE. *Geocarto International, 33*(1), 89–103. https://doi.org/10.1080/10106049.2016.1232313

Morgan, R. P. C., Quinton, J. N., Smith, R. E., Govers, G., Poesen, J. W. A., Auerswald, K., Chisci, G., Torri, D., & Styczen, M. E. (1998). The European soil erosion model (EUROSEM): A dynamic approach for predicting sediment transport from fields and small catchments. *Earth Surface Processes and Landforms, 23*(6), 527–544.

Mustefa, M., Fufa, F., & Takala, W. (2019). GIS estimation of annual average soil loss rate from hangar river watershed using rusle. *Journal of Water and Climate Change, 11*(2), 529–539. https://doi.org/10.2166/wcc.2019.181

Mutua, B. M., & Klik, A. (2004). Soil erosion management at a large catchment scale using the RUSLE-GIS : The case of Masinga catchment , Kenya. *Management Information Systems*, 287–297.

Naqvi, H. R., Mallick, J., Devi, L. M., & Siddiqui, M. A. (2012). Multi-temporal annual soil loss risk mapping employing revised universal soil loss equation (RUSLE) model in Nun Nadi watershed, Uttrakhand (India). *Arabian Journal of Geosciences, 6*(10), 4045–4056. https://doi.org/10.1007/s12517-012-0661-z

Nearing, M. A., Foster, G. R., Lane, L. J., & Finkner, S. C. (1989). Process-based soil erosion model for USDA-water erosion prediction project technology. *Transactions of the American Society of Agricultural Engineers, 32*(5), 1587–1593. https://doi.org/10.13031/2013.31195

Nunes, J. P., Seixas, J., & Pacheco, N. R. (2008). Vulnerability of water resources, vegetation productivity and soil erosion to climate change in Mediterranean watersheds. *Hydrological Processes, 22*, 3115–3134. https://doi.org/10.1002/hyp.6897

Obeta, I. N., & Adewumi, J. K. (2013). Soil loss in Samaru Zaria Nigeria: A comparison of WEPP and EUROSEM models. *Nigerian Journal of Technology, 32*(2), 197–202.

Obiora-Okeke, O. A. (2019). Erosion mapping using revised universal soil loss equation model and geographic information system: A case study of Okitipupa, Nigeria. *European Journal of Engineering and Technology, 7*(4), 73–80.

Oeurng, C., Sauvage, S., & Sánchez-Pérez, J. M. (2011). Assessment of hydrology, sediment and particulate organic carbon yield in a large agricultural catchment using the SWAT Model. *Journal of Hydrology, 401*, 145–153. https://doi.org/10.1016/j.jhydrol.2011.02.017

Oliveira, V. A., Mello, C. R., Durães, M. F., & Silva, A. M. (2014). Vulnerabilidade dos Solos a ' Erosão Hídrica Na Bacia Hidrográfca do Rio Verde, Sul De Minas Gerais. *Ciencia E Agrotecnologia, 38*(3), 262–269. https://doi.org/10.1590/S1413-70542014000300006

Opricovic, S., & Tzeng, G. H. (2004). Compromise solution by MCDM methods: A comparative analysis of VIKOR and TOPSIS. *European Journal of Operational Research, 156*(2), 445–455. https://doi.org/10.1016/S0377-2217(03)00020-1

Owusu, G. (2012). A GIS-based estimation of soil loss in the Densu basin in Ghana. *West African Journal of Applied Ecology, 20*(2), 41–51.

Ozsoy, G., Aksoy, E., Dirim, M. S., & Tumsavas, Z. (2012). Determination of soil erosion risk in the Mustafakemalpasa river basin, Turkey, using the revised universal soil loss equation, geographic information system, and remote sensing. *Environmental Management, 50*(4), 679–694. https://doi.org/10.1007/s00267-012-9904-8

Pal, S. (2016). Identification of soil erosion vulnerable areas in Chandrabhaga river basin: A multi-criteria decision approach. *Modeling Earth Systems and Environment, 2*(1), 1–11. https://doi.org/10.1007/s40808-015-0052-z

Panagopoulos, Y., Dimitriou, E., & Skoulikidis, N. (2019). Vulnerability of a Northeast Mediterranean Island to soil loss. Can grazing management Mitigate erosion? *Water, 11*, 1–20. https://doi.org/10.3390/w11071491

Panagos, P., Borrelli, P., Poesen, J., Ballabio, C., Lugato, E., Meusburger, K., Montanarella, L., & Alewell, C. (2015). The new assessment of soil loss by water erosion in Europe. *Environmental Science & Policy, 54*, 438–447. https://doi.org/10.1016/j.envsci.2015.08.012

Pancholi, V. H., Lodha, P. P., & Prakash, I. (2015). Estimation of soil erosion for Vishwamitri River Watershed using universal soil loss equation and GIS. *International Journal for Scientific Research & Development, 3*, 444–449. https://doi.org/10.11648/j.ajwse.20150102.11 (03/2015/111).

Pandey, A., Mathur, A., Mishra, S. K., & Mal, B. C. (2009). Soil erosion modeling of a Himalayan watershed using RS and GIS. *Environmental Earth Sciences, 59*(2), 399–410. https://doi.org/10.1007/s12665-009-0038-0

Pareta, K., Jakobsen, F., & Joshi, M. (2019). Morphological characteristics and vulnerability assessment of Alaknanda , Bhagirathi , Mandakini and Kali rivers, Uttarakhand (India). *American Journal of Geophysics, Geochemistry and Geosystems, 5*(2), 49–68.

Parveen, R., Kumar, U., & Singh, V. K. (2012). Geomorphometric characterization of upper South Koel basin, Jharkhand: A remote sensing & GIS approach. *Journal of Water Resource and Protection, 4*, 1042–1050. https://doi.org/10.4236/jwarp.2012.412120

Pásztor, L., Waltner, I., Centeri, C., Belényesi, M., & Takács, K. (2016). Soil erosion of Hungary assessed by spatially explicit modelling. *Journal of Maps, 12*, 407–414. https://doi.org/10.1080/17445647.2016.1233913

Patil, R. J., & Sharma, S. K. (2013). Remote Sensing and GIS based modeling of crop/cover management factor (C) of USLE in Shakker river watershed. In *International Conference on Chemical, agricultural and Medical sciences (CAMS-2013)* (pp. 1–4). https://doi.org/10.15242/IICBE.C1213023

Patil, R. J., Sharma, S. K., & Tignath, S. (2015). Remote Sensing and GIS based soil erosion assessment from an agricultural watershed. *Arabian Journal of Geosciences, 8*(9), 6967–6984. https://doi.org/10.1007/s12517-014-1718-y

Phan, B. H., Nguyen, Q. V., Pham, A. H., Le, X. T., Le, S. C., & Nguyen, X. H. (2019). Integrated geographical information system (GIS) and remote sensing for soil erosion assessment by using universal soil loss equation (USLE): Case study in Son La province. *VNU Journal of Science: Earth and Environmental Sciences, 35*(1), 42–52. https://doi.org/10.25073/2588-1094/vnuees.4350

Phinzi, K., & Ngetar, N. S. (2019). The assessment of water-borne erosion at catchment level using GIS-based RUSLE and remote sensing: A review. *International Soil and Water Conservation Research, 7*(1), 27–46. https://doi.org/10.1016/j.iswcr.2018.12.002

Podmanicky, L., Balázs, K., Belényesi, M., Centeri, C., Kristóf, D., & Kohlheb, N. (2011). Modelling soil quality changes in Europe. An impact assessment of land use change on soil quality in Europe. *Ecological Indicators, 11*(1), 4–15. https://doi.org/10.1016/j.ecolind.2009.08.002

Prasannakumar, V., Shiny, R., Geetha, N., & Vijith, H. (2011). Spatial prediction of soil erosion risk by remote sensing, GIS and RUSLE approach: A case study of Siruvani river watershed in Attapady valley, Kerala, India. *Environmental Earth Sciences, 64*(4), 965–972. https://doi.org/10.1007/s12665-011-0913-3

Prasannakumar, V., Vijith, H., Abinod, S., & Geetha, N. (2012). Estimation of soil erosion risk within a small mountainous sub-watershed in Kerala, India, using Revised Universal Soil Loss Equation (RUSLE) and geo-information technology. *Geoscience Frontiers, 3*(2), 209–215. https://doi.org/10.1016/j.gsf.2011.11.003

Quinton, J. N. (1997). Reducing predictive uncertainty in model simulations: A comparison of two methods using the European soil erosion model (EUROSEM). *Catena, 30*(2–3), 101–117. https://doi.org/10.1016/S0341-8162(97)00022-2

Quiroz Londoño, O. M., Romanelli, A., Lima, M. L., Massone, H. E., & Martínez, D. E. (2016). Fuzzy logic-based assessment for mapping potential infiltration areas in low-gradient watersheds. *Journal of Environmental Management, 176*, 101–111. https://doi.org/10.1016/j.jenvman.2016.03.038

Rahman, M. R., Shi, Z. H., & Chongfa, C. (2009). Soil erosion hazard evaluation-An integrated use of remote sensing, GIS and statistical approaches with biophysical parameters towards management strategies. *Ecological Modelling, 220*(13–14), 1724–1734. https://doi.org/10.1016/j.ecolmodel.2009.04.004

Rawat, J. S., Joshi, R. C., & Mesia, M. (2013). Estimation of erosivity index and soil loss under different land uses in the tropical foothills of Eastern Himalaya (India). *Tropical Ecology, 54*(1), 47–58.

Rawat, P. K., Tiwari, P. C., Pant, C. C., Sharama, A. K., & Pant, P. D. (2011). Modelling of stream run-off and sediment output for erosion hazard assessment in lesser Himalaya: Need for sustainable land use plan using remote sensing and GIS: A case study. *Natural Hazards, 59*(3), 1277–1297. https://doi.org/10.1007/s11069-011-9833-5

Refsgaard, J. C., Seth, S. M., Bathurst, J. C., Erlich, M., Storm, B., Jrgensen, G. H., & Chandra, S. (1992). Application of the SHE to catchments in India Part 1. General results. *Journal of Hydrology, 140*(1–4), 1–23. https://doi.org/10.1016/0022-1694(92)90232-K

Refsgaard, J. C., Storm, B., & Clausen, T. (2010). Système Hydrologique Européen (SHE): Review and perspectives after 30 years development in distributed physically-based hydrological modelling. *Hydrology Research, 41*(5), 355–377. https://doi.org/10.2166/nh.2010.009

Renard, K. G., Foster, G. R., Weesies, G. A., McCool, D. K., & Yoder, D. C. (1997). *Predicting soil erosion by water: A guide to conservation planning with the Revised universal soil loss equation (RUSLE)*. United States Department of Agriculture.

Richardson, C. P., & Amankwatia, K. (2019). Assessing watershed vulnerability in Bernalillo County, New Mexico using GIS-based fuzzy Inference. *Journal of Water Resource and Protection, 11*, 99–121. https://doi.org/10.4236/jwarp.2019.112007, 02.

Rosenmund, A., Confalonieri, R., Roggero, P., Toderi, M., & Acutis, M. (2005). Evaluation of the EUROSEM Model for Simulating erosion in hilly areas of Central Italy. *Italian Journal of Agrometeorology, 10*(2), 15–23.

Rozos, D., Skilodimou, H. D., Loupasakis, C., & Bathrellos, G. D. (2013). Application of the revised universal soil loss equation model on landslide prevention. An example from N. Euboea (Evia) Island, Greece. *Environmental Earth Sciences, 70*(7), 3255–3266. https://doi.org/10.1007/s12665-013-2390-3

Sadoddin, A., Sheikh, V., Mostafazade, R., & Halili, M. G. (2008). Multiple-criteria decision making for integrated watershed management in the Ramian watershed, Golestan, Iran. *International Congress on Environmental Modelling and Software, 17*, 662–669.

Said, S., Siddique, R., & Shakeel, M. (2018). Morphometric analysis and sub-watersheds prioritization of Nagmati river watershed, Kutch district, Gujarat using GIS based approach. *Journal of Water and Land Development, 39*(1), 131–139. https://doi.org/10.2478/jwld-2018-0068

Setegn, S. G., Srinivasan, R., Dargahi, B., & Melesse, A. M. (2009). Spatial delineation of soil erosion vulnerability in the lake Tana basin, Ethiopia Shimelis. *Hydrological Processes, 23*, 3738–3750. https://doi.org/10.1002/hyp

Shahabi, H., Hashim, M., & Ahmad, B. B. (2015). Remote sensing and GIS-based landslide susceptibility mapping using frequency ratio, logistic regression, and fuzzy logic methods at the central Zab basin, Iran. *Environmental Earth Sciences, 73*(12), 8647–8668. https://doi.org/10.1007/s12665-015-4028-0

Sharda, V. N., & Mandal, D. (2018). Prioritization and field validation of erosion risk areas for combating land degradation in North Western Himalayas. *Catena, 164*, 71–78. https://doi.org/10.1016/j.catena.2017.12.037

Sharda, V. N., Mandal, D., & Ojasvi, P. R. (2013). Identification of soil erosion risk areas for conservation planning in different states of India. *Journal of Environmental Biology, 34*(2), 219–226.

Sheikh, A. H., Palria, S., & Alam, A. (2011). Integration of GIS and universal soil loss equation (USLE) for soil loss estimation in a himalayan watershed. *Recent Research in Science and Technology, 3*(3), 51–57.

Shinde, V., Sharma, A., Tiwari, K. N., & Singh, M. (2011). Quantitative determination of soil erosion and prioritization of micro-watersheds using Remote Sensing and GIS. *Journal of the Indian Society of Remote Sensing, 39*(2), 181–192. https://doi.org/10.1007/s12524-011-0064-8

Shivhare, N., Dikshit, P. K. S., & Dwivedi, S. B. (2018). A Comparison of SWAT Model calibration techniques for hydrological modeling in the Ganga river watershed. *Engineering, 4*(5), 643–652. https://doi.org/10.1016/j.eng.2018.08.012

Singh, G., & Panda, R. K. (2017). Grid-cell based assessment of soil erosion potential for identification of critical erosion prone areas using USLE, GIS and remote sensing: A case study in the Kapgari watershed, India. *International Soil and Water Conservation Research, 5*(3), 202–211. https://doi.org/10.1016/j.iswcr.2017.05.006

Singh, R. K., Panda, R. K., Satapathy, K. K., & Ngachan, S. V. (2012). Runoff and sediment yield modelling for a treated hilly watershed in eastern Himalaya using the water erosion prediction project model. *Water Resources Management, 26*(3), 643–665. https://doi.org/10.1007/s11269-011-9937-4

Singh, O., Sarangi, A., & Sharma, M. C. (2008). Hypsometric integral estimation methods and its relevance on erosion status of North-Western Lesser Himalayan watersheds. *Water Resources Management, 22*(11), 1545–1560. https://doi.org/10.1007/s11269-008-9242-z

Singh, O., & Singh, J. (2018). Soil erosion susceptibility assessment of the lower Himachal Himalayan watershed. *Journal of the Geological Society of India, 92*(2), 157–165. https://doi.org/10.1007/s12594-018-0975-x

Singh, R., Tiwari, K. N., & Mal, B. C. (2006). Hydrological studies for small watershed in India using the ANSWERS model. *Journal of Hydrology, 318*, 184–199. https://doi.org/10.1016/j.jhydrol.2005.06.011

Smets, T., Borselli, L., Poesen, J., & Torri, D. (2011). Evaluation of the EUROSEM model for predicting the effects of erosion-control blankets on runoff and interrill soil erosion by water. *Geotextiles and Geomembranes, 29*(3), 285–297. https://doi.org/10.1016/j.geotexmem.2011.01.012

Spalevic, V., Barovic, G., Mitrovic, M., Hodzic, R., & Mihajlovic, G. (2015). Assessment of sediment yield using the erosion potential method (EPM) in the Karlicica watershed of Montenegro. *International Conference on Soil, 1–9*.

Spalevic, V., Vujacic, D., Barovic, G., Simunic, I., Moteva, M., & Tanaskovikj, V. (2016). Soil erosion evaluation in the Rastocki Potok watershed of Montenegro using the erosion potential method. *Journal of Agricultural, Food and Environmental Sciences, 69*, 32–40.

Stathopoulos, N., Lykoudi, E., Vasileiou, E., Rozos, D., & Dimitrakopoulos, D. (2017). Erosion vulnerability assessment of Sperchios river basin, in east Central Greece—a GIS based analysis. *Open Journal of Geology*, 621–646. https://doi.org/10.4236/ojg.2017.75043, 07.

Tadesse, L., Suryabhagavan, K. V., Sridhar, G., & Legesse, G. (2017). Land use and land cover changes and soil erosion in Yezat watershed, north western Ethiopia. *International Soil and Water Conservation Research, 5*(2), 85–94. https://doi.org/10.1016/j.iswcr.2017.05.004

Tahiri, M., Tabyaoui, H., Tahiri, A., Hadi, H. El, Hammichi, F. El, & Achab, M. (2016). Modelling soil erosion and sedimentation in the oued Haricha sub-basin (Tahaddart watershed, western Rif, Morocco): Risk assessment. *Journal of Geoscience and Environment Protection*, 107–119. https://doi.org/10.4236/gep.2016.41013, 04.

Tirkey, A. S., Pandey, A. C., & Nathawat, M. S. (2013). Use of satellite data, GIS and RUSLE for estimation of average annual soil loss in Daltonganj watershed of Jharkhand (India). *Journal of Remote Sensing Technology, 1*(1), 20–30. https://doi.org/10.18005/jrst0101004

Todorovski, L., & Džeroski, S. (2006). Integrating knowledge-driven and data-driven approaches to modeling. *Ecological Modelling, 194*, 3–13. https://doi.org/10.1016/j.ecolmodel.2005.10.001

Tsara, M., Kosmas, C., Kirkby, M. J., Kosma, D., & Yassoglou, N. (2005). An evaluation of the pesera soil erosion model and its application to a case study in Zakynthos, Greece. *Soil Use & Management, 21*(4), 377–385. https://doi.org/10.1079/sum2005322

Uddin, K., Murthy, M. S. R., Wahid, S. M., & Matin, M. A. (2016). Estimation of soil erosion dynamics in the Koshi basin using GIS and Remote Sensing to assess priority areas for conservation. *PloS One, 11*(3), 1–19. https://doi.org/10.1371/journal.pone.0150494

Vanmaercke, M., Maetens, W., Poesen, J., Jankauskas, B., Jankauskiene, G., Verstraeten, G., & de Vente, J. (2012). A comparison of measured catchment sediment yields with measured and predicted hillslope erosion rates in Europe. *Journal of Soils and Sediments, 12*(4), 586–602. https://doi.org/10.1007/s11368-012-0479-z

Veihe, A., Rey, J., Quinton, J. N., Strauss, P., Sancho, F. M., & Somarriba, M. (2001). Modelling of event-based soil erosion in Costa Rica, Nicaragua and Mexico: Evaluation of the EUROSEM model. *Catena, 44*, 187–203. https://doi.org/10.1016/S0341-8162(00)00158-2

Vemu, S., & Pinnamaneni, U. B. (2011). Estimation of spatial patterns of soil erosion using remote sensing and GIS: A case study of Indravati catchment. *Natural Hazards, 59*, 1299–1315. https://doi.org/10.1007/s11069-011-9832-6

Vente, J., Poesen, J., Verstraeten, G., Rompaey, A. V., & Govers, G. (2008). Spatially distributed modelling of soil erosion and sediment yield at regional scales in Spain. *Global and Planetary Change, 60*(3–4), 393–415. https://doi.org/10.1016/j.gloplacha.2007.05.002

Vieira, D. C. S., Serpa, D., Nunes, J. P. C., Prats, S. A., Neves, R., & Keizer, J. J. (2018). Predicting the effectiveness of different mulching techniques in reducing post-fire runoff and erosion at plot scale with the RUSLE, MMF and PESERA models. *Environmental Research, 165*, 365–378. https://doi.org/10.1016/j.envres.2018.04.029

Vijith, H., Suma, M., Rekha, V. B., Shiju, C., & Rejith, P. G. (2012). An assessment of soil erosion probability and erosion rate in a tropical mountainous watershed using remote sensing and GIS. *Arabian Journal of Geosciences, 5*, 797–805. https://doi.org/10.1007/s12517-010-0265-4

Wicks, J. M., & Bathurst, J. C. (1996). Shesed: A physically based, distributed erosion and sediment yield component for the SHE hydrological modelling system. *Journal of Hydrology, 175*, 213–238. https://doi.org/10.1016/S0022-1694(96)80012-6

Williams, J. R. (1975). Predicting sediment yield frequency for rural basins to determine man's effect on long-term sedimentation. In *Present and Prospective Technology for predicting sediment yield and sources* (pp. 244–252). Washington DC: United State Department of Agriculture, Agriculture Research Service.

Wischmeier, W. H., & Smith, D. D. (1978). Predicting rainfall erosion losses. In *Agriculture Handbook, science and Education Administration* (pp. 1–51). United State Department of Agriculture.

Xavier, A. P. C., Silva, R. M., Silva, A. M., & Santos, C. A. G. (2016). *Mapping soil erosion vulnerability using remote sensing and GIS: A case study of Mamuaba watershed, Paraiba state* (pp. 1677–1688). Revista Brasileira de Cartografia.

Yacine, E. A., Essahlaoui, A., Oudija, F., Mimich, K., & Nassiri, L. (2019). Assessment of soil erosion by (RUSLE) using remote sensing and GIS case of watershed of Beht in upstream of Ouljat Sultan dam (Morocco). *ARPN Journal of Engineering and Applied Sciences, 14*(9), 1765–1776.

Yousefi, S., Kivarz, N., Ramezani, B., Rasoolzadeh, N., Naderi, N., & Mirzaee, S. (2014). An estimation of sediment by using erosion potential method and geographic information systems in Chamgardalan watershed: A case study of Ilam province, Iran. *Geodynamics Research International Bulletin, 2*, 34–41, 02.

Yue-qing, X., Jian, P., & Xiao-mei, S. (2014). Assessment of soil erosion using RUSLE and GIS: A case study of the Maotiao river watershed, Guizhou province, China. *Environmental Earth Sciences, 56*, 1643–1652. https://doi.org/10.1007/s12665-014-3436-x

Yuksel, A., Gundogan, R., & Akay, A. E. (2008). Using the remote sensing and GIS technology for erosion risk mapping of Kartalkaya Dam watershed in Kahramanmaras, Turkey. *Sensors, 8*, 4851–4865. https://doi.org/10.3390/s8084851

Zhang, Y., Degroote, J., Wolter, C., & Sugumaran, R. (2009). Integration of Modified Universal Soil loss equation (MUSLE) into a GIS framework to assess soil erosion risk. *Land Degradation & Development, 20*, 84–91. https://doi.org/10.1002/ldr.893

Zhou, X., Helmers, M., & Qi, Z. (2013). Modeling of subsurface tile drainage using MIKE SHE. *Applied Engineering in Agriculture, 29*(6), 865–873. https://doi.org/10.13031/aea.29.9568

Zhou, Q., Yang, S., Zhao, C., Cai, M., & Ya, L. (2014). A soil erosion assessment of the upper mekong river in yunnan province, China. *Mountain Research and Development, 34*(1), 36–47. https://doi.org/10.1659/MRD-JOURNAL-D-13-00027.1

International Soil and Water Conservation Research 9 (2021) 319–332

Contents lists available at ScienceDirect

International Soil and Water Conservation Research

journal homepage: www.elsevier.com/locate/iswcr

Original Research Article

A hillslope version of the revised Morgan, Morgan and Finney water erosion model

Geert Sterk

Department of Physical Geography, Utrecht University, PO Box 80.115, NL-3508 TC, Utrecht, the Netherlands

ARTICLE INFO

Article history:
Received 4 October 2020
Received in revised form
14 January 2021
Accepted 19 January 2021
Available online 30 January 2021

Keywords:
Water erosion modelling
Morgan-morgan-finney model
Hillslope
Surface runoff
Sediment transport
Soil loss
Soil and water conservation

ABSTRACT

The revised Morgan, Morgan and Finney (rMMF) water erosion model calculates annual surface runoff and soil loss from field-sized areas. The original version of the rMMF is neither suited to calculate water erosion along irregular hillslopes, nor capable to allow infiltration of once generated surface runoff at places where the runoff speed slows down, and infiltration could occur under natural conditions. The aim of this article is to describe a new hillslope version of the rMMF model that allows infiltration of surface runoff, and to show examples of soil erosion modelling along real and hypothetical hillslopes. The new hillslope version (hMMF) splits the entire hillslope into a number of sections that have individual properties, such as slope angle, slope length, soil properties and vegetation characteristics. The surface runoff along the slope is calculated by summing the volume of surface runoff generated in a particular section with the surface runoff coming from the immediate upslope section. The related sediment transport is calculated for each section using the calculated detachment for the section, the sediment coming from the upslope section and the transport capacity. A new variable is introduced to account for infiltration of surface runoff and allows simulating the effects of soil and water conservation structures on water erosion. The model was tested using measured data from plots in Africa, Asia, the US and Europe, as well as for a surveyed hillslope in Tunisia (Barbara watershed). Overall, the performance of the hMMF was reasonable for surface runoff and poor for soil loss when recommended input variable values are used. Calibration of the model resulted in a good performance, which shows the capability of the hMMF model to reproduce measured surface runoff and erosion amounts. In addition, realistic water erosion patterns on hillslopes with soil and water conservation can be simulated.

1. Introduction

Water erosion is globally the most widespread soil degradation problem (Oldeman et al., 1991), with 15.4% of the total land area being affected by moderate to very high erosion rates (Borrelli et al., 2017). Scientific efforts to better understand erosion processes and develop control techniques started already in the 1930's (Bennett, 1939). The first equations to quantify amounts of erosion as a function of terrain characteristics are from the 1940's (Zingg, 1940; Musgrave, 1947), which eventually culminated in the Universal Soil Loss Equation (USLE) (Wischmeier & Smith, 1978). The USLE is a fully empirical soil erosion model that calculates annual soil losses by multiplying six factors: the rainfall erosivity factor (R), the soil erodibility factor (K), the slope length factor (L), the slope steepness factor (S), the crop management factor (C) and the erosion-control practice factor (P) (Wischmeier & Smith, 1978).

The empiricism of the USLE and its specific database from which it was developed has generated criticism. Morgan (2005) and others argued that the USLE is not universal at all, and that the multiplication of six factors cannot adequately describe water erosion. Many water erosion models have been developed since the publication of the USLE. These models vary from deterministic, e.g. the Water Erosion Prediction Project (WEPP) model (Nearing et al., 1989; Flanagan & Nearing, 1995), to fully empirical, e.g. Revised Universal Soil Loss Equation (RUSLE) (Renard et al., 1997) and AGricultural Non-Point Source Pollution Model (AGNPS) (Young et al., 1989). An intermediate water erosion model is the Morgan, Morgan and Finney model (Morgan et al., 1984), which can be classified as a semi-empirical model. It retained the simplicity of the USLE but has a stronger physical base. The model was revised by

E-mail address: g.sterk@uu.nl.

https://doi.org/10.1016/j.iswcr.2021.01.004

Morgan (2001) and since then is known as the revised Morgan, Morgan and Finney (rMMF) model.

The rMMF model separates the water erosion processes in a water phase and a sediment phase. The water phase calculates the amount of rainfall energy and the surface runoff volume. The sediment phase calculates the amounts of splash detachment, the surface runoff detachment, and the transport capacity of the surface runoff. The final outcome of the model is an annual soil loss from a field sized area on a hillslope (Morgan, 2005). It only accounts for splash erosion, interrill erosion and rill erosion processes; gully erosion is not part of the model. The rMMF model uses 12 equations and requires 15 input variables. Three input variables are rainfall related, five are soil related, six are land cover related and one variable accounts for the slope angle. Morgan (2001) tested the rMMF by comparing model predictions with measured amounts of surface runoff and soil loss on 67 sites. The rMMF model performed reasonably well, but the surface runoff predictions were poor for situations where erosion control measures were implemented. Several other studies reported satisfactory results in different countries. For instance, the model was successfully used in Hungary (Hudek et al., 2014), Kenya (Vigiak et al., 2005) and Spain (Fernandez et al., 2010; Lopez-Vicente et al., 2008).

The rMMF model has at least two limitations that reduce its applicability. First, the model was developed for uniform areas with a linear slope. But hillslopes often have irregular slope profiles and also spatially variable soil and vegetation characteristics. These spatial heterogeneities influence water erosion processes, but the rMMF is not able to capture this. The second issue is infiltration of once generated surface runoff, which can occur on a natural hillslope. For instance, for a concave slope, the slope steepness towards the end of the slope is decreasing. This smaller slope angle will slow down the speed of the surface runoff, and water gets more time to infiltrate (Van de Giesen et al., 2000). The surface runoff infiltration process should not be ignored in the simulation of hillslope hydrology (Vigiak et al., 2006). Indeed, measurements of hillslope surface runoff generally have shown a tendency of decreasing runoff coefficients with increasing slope length (Sheridan et al., 2014). One of the main reasons for this decrease in runoff coefficients with slope length is due to infiltration of surface runoff in areas downslope (Langhans et al., 2014). Moreover, when soil and water conservation measures are present in the field, the original rMMF can only incorporate the effects of such measures through the USLE *P* factor. Actual simulations of the influence of the measures on surface runoff and sediment transport are not possible, because the original model does not allow infiltration of once generated surface runoff. But when grass strips, bench terraces or other soil and water conservation (SWC) measures are implemented on a hillslope, these structures will cause infiltration of surface runoff and reduce its transport capacity. This will result in deposition of sediment, which is also not accounted for in the original rMMF.

Since its publication by Morgan in 2001, several modifications to the original rMMF have been published. These modifications of the rMMF model have usually introduced a number of new variables and equations. For instance, Morgan and Duzant (2008) made changes to the original rMMF model to incorporate effects of vegetation characteristics and soil texture on erosion and deposition processes. The changes comprised 41 new equations and 11 new variables. Likewise, Choi et al. (2017) modified further the Morgan and Duzant (2008) rMMF version to make it applicable at daily time scale. They developed 45 new equations and 18 new variables to make the model suitable for areas with seasonal climates and complex surface configurations. Finally, Shrestha and Jetten (2018) also developed a model version that enables daily-based simulation of soil erosion. They introduced 16 new equations and an equal number of new variables to better account for vegetation dynamics and extreme rain storms in soil erosion processes.

This article presents a new hillslope version of the rMMF model, the hMMF model, that 1) can simulate erosion processes along an irregular hillslope profile, and 2) allows infiltration of surface runoff. The adaptations to the rMMF model are mainly changes of the original field scale rMMF equations, while only two new variables are introduced. It was attempted to retain the simplicity of the rMMF as much as possible. The spatial scale of the hMMF model is the hillslope, and the temporal scale is annual. The aim of this article is to describe the new equations and calculation scheme for the hMMF model, evaluate the model against measured values, and show examples of soil erosion modelling along hillslopes with and without SWC measures.

2. Model description

2.1. The field-scale rMMF model

The following summarizes the main rMMF equations used to calculate annual soil erosion at field-scale as described by Morgan (2001; 2005).

The rainfall kinetic energy (*KE*; J m^{-2}) is a function of the effective rainfall (P_e; mm), i.e. the fraction of mean annual rainfall (*P*; mm) that is not intercepted by the vegetation canopy (*A*; fraction between 0 and 1):

$$\boldsymbol{P_e} = \boldsymbol{P}(1 - \boldsymbol{A}) \tag{1}$$

The effective rainfall is split into direct throughfall (*DT*; mm), which directly reaches the soil, and leaf drainage (*LD*; mm), which is intercepted by the canopy and reaches the surface by stem flow or dripping from leaves. *LD* is a function of the canopy cover (*CC*; fraction between 0 and 1):

$$\boldsymbol{LD} = \boldsymbol{P_e CC} \tag{2}$$

And the remaining part of the effective rainfall is thus direct throughfall:

$$\boldsymbol{DT} = \boldsymbol{P_e} - \boldsymbol{LD} \tag{3}$$

The kinetic energy of the direct throughfall (*KE* (*DT*); J m^{-2}) is determined as a function of rainfall intensity (*I*; mm h^{-1}), using a typical value for the erosive rain of the climatic region. In Table 1 examples of equations for different regions with specific rainfall characteristics are given, which can be used to calculate *KE* (*DT*).

The kinetic energy of the leaf drainage (*KE* (*LD*); J m^{-2}) is a function of plant canopy height (*PH*; m) as proposed by Brandt (1990):

$$\boldsymbol{KE}(\boldsymbol{LD}) = \left[\left(15.80\boldsymbol{PH}^{0.5}\right) - 5.875\right]\boldsymbol{LD} \tag{5}$$

The total energy of the effective rainfall (*KE*; J m^{-2}) is the sum of the two energy components:

$$\boldsymbol{KE} = \boldsymbol{KE}(\boldsymbol{DT}) + \boldsymbol{KE}(\boldsymbol{LD}) \tag{6}$$

The annual surface runoff (*SR*; mm) is obtained from:

$$SR = Pexp\left(-\frac{S_c}{P_o}\right) \tag{7}$$

where P_o = the mean rain per rain day (mm) (i.e., mean annual rainfall *P* divided by the number of rainy days per year) and S_c = the soil moisture storage capacity (mm) and estimated as:

Table 1
Examples of equations for the calculation of rainfall kinetic energy (Morgan, 2001).

Kinetic energy equation[a]	Eq.	Suitability region	Reference
$KE(DT) = 11.87 + 8.73^{10}logI$	(4a)	North America, east of Rocky Mountains	Wischmeier and Smith (1978)
$KE(DT) = 8.95 + 8.44^{10}logI$	(4b)	Northwest Europe and similar climate zones	Brandt (1990)
$KE(DT) = 9.81 + 11.25^{10}logI$	(4c)	Regions with a Mediterranean climate	Zanchi and Torri (1980)
$KE(DT) = 35.9(1 - 0.56e^{-0.034I})$	(4d)	West Mediterranean	Coutinho and Tomás (1995)
$KE(DT) = 29.8 - (127.5/I)$	(4e)	Regions with tropical climates	Hudson (1965)
$KE(DT) = 9.81 + 10.60^{10}logI$	(4f)	East Asia	Onaga, Shirai, and Yoshinaga (1988)
$KE(DT) = 29.0(1 - 0.6e^{-0.04I})$	(4g)	Temperate southern hemisphere climates	Rosewell (1986)

[a] $KE\ (DT)$ = *kinetic energy in J m^{-2} mm^{-1}; I = rainfall intensity in mm h^{-1}.*

$$\boldsymbol{S_c} = 1000\ \boldsymbol{MS\ BD\ EHD}\left(\frac{\boldsymbol{Et}}{\boldsymbol{Eo}}\right)^{0.5} \quad (8)$$

where MS = the gravimetric soil moisture content at field capacity (kg kg^{-1}), BD = the dry bulk density of the soil (Mg m^{-3}), EHD = the effective hydrological depth of the soil (m), and Et/Eo = the ratio of actual crop evapo-transpiration to maximum crop evapo-transpiration (mm mm^{-1}). The EHD indicates the depth of soil within which the moisture storage capacity controls generation of surface runoff. It is a function of plant cover, which influences the depth and density of roots, and, in some instances, the effective soil depth, for example on soils shallower than 0.1 m or where a surface seal or crust has formed (Morgan, 2001). There are some guide values of EHD for use with the rMMF model. Values range from 0.05 for bare and shallow soils on steep slopes, to 0.20 for forest soils (Morgan, 2005). The larger the EHD, the more water can be stored in the soil, and less surface runoff is produced. Typical values for MS and BD are provided by Morgan (2005). Generally, BD varies from 1.1 for a clay soil to 1.5 for a sand soil, and MS varies from 0.08 for a sand soil to 0.45 for a clay soil.

Soil particle detachment by raindrop (F; kg m^{-2}) is a function of total KE and soil erodibility:

$$\boldsymbol{F} = 10^{-3}\boldsymbol{K\ KE} \quad (9)$$

where K = soil detachability index (g J^{-1}), defined as the weight of soil detached from the soil mass per unit of rainfall energy. Soil particle detachment by surface runoff (H; kg m^{-2}) is estimated as:

$$\boldsymbol{H} = 10^{-3}(0.5\boldsymbol{COH})^{-1}\boldsymbol{SR}^{1.5}\boldsymbol{sin}(\boldsymbol{S})(1 - \boldsymbol{GC}) \quad (10)$$

where COH = cohesion of the soil surface (kPa), S = slope (°) and GC = fraction of vegetation ground cover (0–1). The equation assumes that soil particle detachment by surface runoff occurs only where the soil is not fully protected by ground cover. As a first approximation, this seems reasonable since a dense ground cover will dissipate most shear stress from surface runoff, leaving less shear stress for particle detachment. Values of K and COH for different soil textures are provided by Morgan (2005). K values vary from 0.05 for clay to 1.2 for sand, while values of COH vary from 2 for sand, loamy sand and sandy loam to 12 for clay.

The transport capacity is the maximum amount of sediment that a given volume of surface runoff can carry. The transport capacity of surface runoff (TC; kg m^{-2}) is calculated as:

$$\boldsymbol{TC} = 10^{-3}\boldsymbol{C\ SR}^2\boldsymbol{sin}(\boldsymbol{S}) \quad (11)$$

where C = crop or plant cover factor, which is an index (0.1–1) of soil loss at a given vegetation cover compared with the soil loss at bare soil. The C factor can be adjusted to take account of different tillage practices and levels of crop residue retention.

Eventually, the estimates of soil particle detachment by raindrop impact and by surface runoff are added together to give a total annual detachment rate. This is then compared with the annual transport capacity of the surface runoff and the lesser of the two values is the annual erosion rate E (kg m^{-2}):

$$\boldsymbol{E} = \boldsymbol{min}[(\boldsymbol{F} + \boldsymbol{H}), \boldsymbol{TC}] \quad (12)$$

2.2. Hillslope-scale rMMF model: the hMMF model

The field scale version of the rMMF model cannot be used to accurately calculate erosion on a natural hillslope with variations in slope steepness, soil properties, and vegetation cover. For such complex hillslopes, the hMMF model can calculate surface runoff volume and sediment transport using the following approach.

2.2.1. Hillslope properties

The hillslope is divided into $i = 1, \ldots, n$ sections of variable lengths and slope steepness. The first section starts at the top of the hillslope, and section n is the lowest section of the slope. A similar approach was used by Morgan and Duzant (2008), but their approach results in different and sometimes unrealistic surface runoff amounts (see Appendix A). Each section has its own soil and vegetation characteristics, but it is assumed that the amount of annual rainfall is homogeneous over the entire hillslope. In this way, complicated slope profiles can be simulated.

2.2.2. Surface runoff

The surface runoff along the slope is calculated by summing the volume of surface runoff generated in a particular section with the surface runoff coming from the immediate upslope section. The annual surface runoff of the first (top) section is calculated according to eq. (7). This amount in mm is converted to a volume per meter width by multiplying SR_1 with the length of the slope section (L_1):

$$SR'_1 = 10^{-3}SR_1L_1 \quad (13)$$

where SR'_1 is in m^2. For the second section, the total volume of surface runoff is equal to the volume that is generated by the section itself plus the volume that is flowing in from the upper section:

$$SR'_2 = 10^{-3}SR_2L_2 + SR'_1 \quad (14)$$

where SR'_2 is again in m^2. For a hillslope consisting of $i = 1, \ldots, n$ sections, eq. (14) can be generalized to:

$$SR'_i = 10^{-3}SR_iL_i + SR'_{i-1} \quad (15)$$

The SR'_0 is the boundary condition and equal to zero, meaning that there is no inflow coming from above.

2.2.3. Surface runoff infiltration

In the original, field-scale rMMF version it is assumed that all surface runoff will flow down the field, and there is no infiltration of surface runoff possible. For natural hillslopes this is unrealistic as infiltration of surface runoff may occur. However, simulating infiltration of surface runoff in a (semi-)empirical model is difficult, as there is no physically-based infiltration sub-model and generally few data are available on surface runoff infiltration along hillslopes. In the hMMF version it simply has been solved by introducing a new variable, SR_i^{inf}, which accounts for the fraction (0–1) of surface runoff infiltrating in a particular section. The new surface runoff calculation that accounts for surface runoff infiltration becomes then:

$$SR_i'' = \left(SR_i' + SR_{i-1}''\right)\left(1 - SR_i^{inf}\right) \tag{16}$$

2.2.4. Sediment transport

The actual sediment transport along the hillslope depends on the calculated amounts of detachment and the transport capacity of the surface runoff. In the rMMF model, the amount of surface runoff in mm (SR) was used in eq. (10) and eq. (11). But, in the case of a continuous hillslope, the amount of surface runoff in mm can be already very high at the first section, while the actual volume of surface runoff is low. This may lead to unrealistic values for H and TC. Therefore, in the new calculations of detachment by surface runoff and transport capacity, the SR_i'' values (in m^2) are used for each slope section. Two new equations have been developed based on literature (Aksoy & Kavvas, 2005; Julien & Simons, 1985; Prosser & Rustomji, 2000; Zhang et al., 2011), while retaining the simplicity of eq. (10) and eq. (11). The annual detachment by overland flow is calculated by:

$$H_i' = (0.5COH_i)^{-1}\left(SR_i''\right)^{2.5} S_i'(1 - GC_i) \tag{17}$$

where S_i' is slope gradient (m m^{-1}). The annual transport capacity equation becomes:

$$TC_i' = C_i\left(SR_i''\right)^{\beta} S_i' \tag{18}$$

where TC_i' is now in kg m^{-1}. The coefficient β is a variable that can be used to calibrate the soil erosion in case quantitative data are available. If no data is available, a value of 1.5 is recommended (Prosser & Rustomji, 2000).

The actual amount of sediment transport in a certain section (ST in kg m^{-1}) is dependent on the amount that is generated by that section (the total detachment) and the amount of sediment already in transport. First the sediment transport deficit (ST_i^{def} in kg m^{-1}) for section i is calculated by withdrawing the incoming sediment transport from above from the transport capacity of the section:

$$ST_i^{def} = TC_i' - ST_{i-1} \tag{19}$$

ST_0 is the boundary condition and equal to zero, meaning that no sediment is entering from above. Depending on the value of ST_i^{def} the following rules apply:

- If $ST_i^{def} < 0 \rightarrow ST_i = TC_i'$ (deposition in section)
- If $ST_i^{def} = 0 \rightarrow ST_i = TC_i'$ (transport only; no soil loss or deposition)
- If $ST_i^{def} > 0$ then ST_i depends on the total detachment of the section:
  - o If $(F_i + H_i')L_i \geq TC_i' \rightarrow ST_i = TC_i'$ (detachment exceeds transport capacity)
  - o If $(F_i + H_i')L_i < TC_i' \rightarrow ST_i = ST_{i-1} + (F_i + H_i')L_i$ (transport capacity exceeds detachment)

3. hMMF model application

The hMMF model was tested using several datasets. First, the hMMF was compared with the rMMF model using the same surface runoff and erosion data as used by Morgan (2001) to test the rMMF. Those data were derived from a large number of published studies from different countries and described by Morgan and Finney (1982). The results of the model comparison are provided in Appendix B. Further hMMF model testing was done by using original USLE plot data, an experimental hillslope in Hungary, a surveyed hillslope in NW Tunisia, and some hypothetical hillslope situations to show its potential for simulation of surface runoff, sediment transport and the impacts of SWC measures on surface hydrology and erosion. The first application is using data from USLE plots at Beemerville, New Jersey, USA. The second application is based on the experimental plot data of Hudek and Rey (2009), which were also used by Hudek et al. (2014) to run the field scale rMMF erosion model. The third application is the modelling of a long (1711 m) hillslope from NW Tunisia on which an erosion survey was conducted by Sterk (2009). Hypothetical hillslope runs were based on the same hillslope of Hudek and Rey (2009). Two different aspects were tested: 1. The effect of infiltration of surface runoff on sediment transport; 2. The possibility of simulation of SWC measure impacts on surface runoff and sediment transport.

3.1. hMMF testing using beemerville USLE erosion data

The United States Department of Agriculture (USDA) has made available some of the original data that were measured on erosion plots (https://www.ars.usda.gov/midwest-area/west-lafayette-in/national-soil-erosion-research/docs/usle-database/usle-data/), and used for the development of the USLE. Here the available data of rainfall, surface runoff, soil loss, and crop management from the six plots at Beemerville were used to test the hMMF model. This dataset comprises the years 1938–1940, which have complete records. All plots were 21.4 × 4.3 m in size, the slope was 9.4°, and the soil texture type was loam. Three cropping systems were used:

- Maize crop planted up/down (plots 1 & 3)
- Maize planted along contour (plots 2 & 4)
- Mixed grass and legumes (plots 5 & 6)

The rainfall, surface runoff and soil loss data were averaged for the three years of measurement, and for the three cropping systems (Table 2). Then the hMMF was first run using recommended variable values (Morgan, 2005, Table 3). The results of the hMMF calculations are in Table 2 and show that the model consistently underestimates the amount of surface runoff by 6 mm (plots 5 & 6), by 17 mm (plots 2 & 4) to 26 mm (plots 1 & 3). The modelled values of soil loss are reasonably good in two cases (plots 2 & 4; plots 5 & 6), but for plot 1 & 2 the soil loss is 83.2% lower than the measured value. This is due to the relatively small amount of surface runoff which leads to a relatively low annual transport capacity. The underestimation of surface runoff by using recommended input variable values is similar to the results of the rMMF and hMMF comparison in Appendix B. In general, the recommended values of

Table 2
Characteristics and average measured rain, surface runoff and erosion values of the Beemerville erosion plots during the years 1938–1940.

Plots	Land use	Rain	Rain days	Surface runoff		Soil loss	
				measured	modelled	measured	modelled
		mm	no.	mm	mm	kg m^{-2}	kg m^{-2}
1 & 3	Maize (up-down)	1177	111	131	105	1.73	0.29
2 & 4	Maize (contour)	1177	111	103	86	0.29	0.22
5 & 6	Grass + herbs	1177	111	61	55	0.01	0.11

Table 3
Recommended variable values used for the hMMF modelling of the Beemerville erosion plots for the years 1938–1940.

Plots	*A*	*CC*	*I*	*PH*	*MS*	*BD*	*EHD*	*Et/Eo*	*K*	*COH*	*GC*	*C*	*β*
	–	–	mm h^{-1}	m	wt.%	Mg m^{-3}	m	–	g J^{-1}	kPa	–	–	–
1&3	0.15	0.45	10	0.82	0.2	1.3	0.12	0.68	0.80	3	0.10	0.20	1.5
2&4	0.15	0.45	10	0.82	0.2	1.3	0.13	0.68	0.80	3	0.10	0.20	1.5
5&6	0.30	0.90	10	0.10	0.2	1.3	0.14	0.80	0.80	3	0.80	0.20	1.5

EHD (Morgan, 2005) result in an underestimation of the surface runoff amounts.

It is fairly easy to match the hMMF values of surface runoff by changing the *EHD* variable, while the β variable can be changed to modify the sediment transport capacity and thus the soil loss. By changing the *EHD* into 0.109 and the β into 2.88 gives the exact same surface runoff and soil loss values as measured on plots 1 & 3. For plots 2 & 4 changing *EHD* into 0.121 and β into 1.51 gives exact matches with the measured values, and for plots 5 & 6 this is achieved by changing *EHD* into 0.135 and β into 1.00.

3.2. hMMF application at 30-m hillslope in Hungary

Hudek and Rey (2009) measured surface runoff and soil loss from erosion plots at Szentendre in the north of Hungary. All plots were 30 m long and had a linear slope of 8°. The plots had different treatments. One plot was bare (=control), while the other plots had a cover of *M. aquifolium* shrubs of different ages (4, 12, 20, 25 years). Here only the data from the bare plot and the 4-year old *M. aquifolium* plot were used. Erosion measurements were conducted for one full year (June 2007–May 2008). Details about the plots and the measured amounts of surface runoff and soil loss are in Table 4. The same variable values as used by Hudek et al. (2014) for the field scale rMMF application were used here for the hMMF model (Table 5). Eq. (4b) was used for the calculation of the rainfall kinetic energy. The hillslope was represented in the model by ten equal sections of 3 m each.

Fig. 1 shows the hMMF results of annual surface runoff and sediment transport along the 30 m slope for bare soil (Fig. 1a) and the 4-year *M. aquifolium* cover (Fig. 1b). The surface runoff shows a linear increase because the soil and vegetation variables are kept constant along the slope, and no surface runoff infiltration was allowed ($SR_i^{inf} = 0$). The sediment transport profile shows a realistic pattern. It is near zero at the top of the slope and remains small till approximately 6 m on the bare plot, and about 15 m on the *M. aquifolium* plot. From those points downward the sediment transport rapidly increases due to the increase in transport capacity of the surface runoff. The sediment transport on the bare soil is transport capacity limited up to 12 m and from there on becomes detachment limited to the end of the slope. For the *M. Aquifolium* plot, sediment transport is limited by the transport capacity on the upper part of the slope, but changes to detachment limited transport from 18 m to the end of the slope.

For the bare soil (Fig. 1a) the modelled annual surface runoff from the slope is 383.5 mm and the corresponding soil loss equal to 2.21 kg m^{-2}, which exactly matches the measured amounts of Hudek and Rey (2009). For the situation with vegetation cover, the modelled surface runoff is 116.7 mm and the soil loss equal to 0.56 kg m^{-2}. Again, these results match closely the observed surface runoff and soil loss values of Hudek and Rey (2009) (Table 4). The close match between measured and modelled surface runoff is because of the calibrated *EHD* values by Hudek et al. (2014). To obtain the correct soil losses with the hMMF version, the value β in eq. (18) was calibrated at 2.52 for the bare soil and 4.85 for the plot with *M. aquifolium* cover. When the recommended values for *EHD* (0.05 for control; 0.10 for *M. aquifolium*) are used the calculated surface runoff is 5.7% (control) and 40.7% (*M. aquifolium*) lower than the measured values. Using the recommended value for β (= 1.5) for both plots, the calculated soil loss is 92.3% lower in the control plot and no erosion is calculated in the *M. aquifolium* plot. This example shows the need for soil erosion measurements to allow model calibration, as in this case the recommended values result in a strong underestimation of the measured erosion values.

3.3. hMMF application at a 1711-m hillslope in Tunisia

Sterk (2009) conducted an erosion survey at the Barbara watershed in Tunisia as part of a WorldBank project on sustainable land use. Actual measurements of surface runoff and sediment transport were not available. Instead, detailed erosion descriptions were made along two hillslopes draining into the Barbara river. One

Table 4
Characteristics and measured surface runoff and soil losses of two erosion plots at Szentendre, Hungary (Hudek & Rey, 2009).

Plot	Soil texture	Length	Slope	Slope type	Rain	Rain days	Surface runoff	Soil loss
		m	°		mm	no.	mm	kg m^{-2}
Bare	Clay loam	30	8	Linear	551.5	86	383.0	2.20
M. aquif.	Clay loam	30	8	Linear	551.5	86	118.2	0.56

Table 5
Variable values used for the hMMF modelling of two erosion plots at Szentendre, Hungary (Hudek et al., 2014). No surface runoff infiltration was allowed ($SR_i^{inf} = 0$).

Plot	*A*	*CC*	*I*	*PH*	*MS*	*BD*	*EHD*	*Et/Eo*	*K*	*COH*	*GC*	*C*
	_	–	mm h^{-1}	m	wt.%	Mg m^{-3}	m	–	g J^{-1}	kPa	–	–
Bare	0	0	10	0	0.24	1.01	0.043	0.05	0.25	10	0	1.00
M. aquif.	0.11	0.31	10	0.22	0.24	1.01	0.075	0.30	0.25	10	0.42	0.30

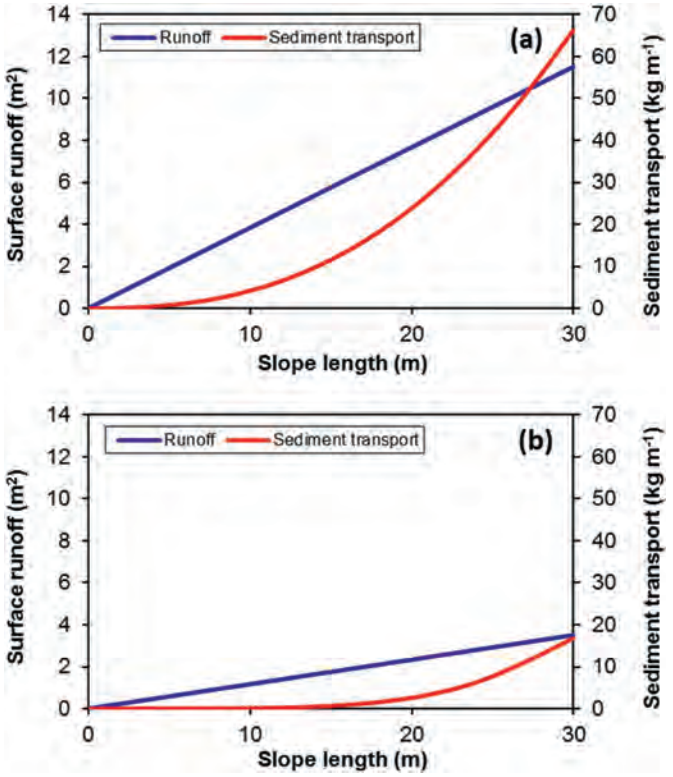

Fig. 1. Surface runoff and sediment transport modelled with the hMMF hillslope erosion model along a 30 m linear slope at Szetendre, Hungary. (a) for bare soil conditions; (b) for a 4 year *M. aquifolium* vegetation cover.

of these transects was used here to illustrate the possibility of simulating erosion and deposition along an irregular hillslope with the hMMF model.

The Barbara watershed is located in Northwest Tunisia, near to the town Aïn Draham. The dam of the Barbara reservoir is at 36° 44′ 2.28″ N; 8° 31′ 54.30″ E, and the watershed stretches in Southwestern direction from there. A small part of the watershed (17 km^2) is located in Northeast Algeria. The size of the watershed upstream of the dam is 177 km^2. Altitude in the watershed ranges from 180 to 1200 m. Climate in the region is of the Mediterranean type, with dry summers and wet winters. The average annual rainfall is approximately 800 mm, with frequently high intensity rainstorms.

The Barbara watershed is composed of a complex topography with slopes varying from flat to very steep (>25°). Soils have textures varying from sandy loam to clay, with moderate rock content, and a generally good soil structure. Land use in the watershed consists mainly of cropland (39.2%), grassland (3.0%), forest (24.9%), agroforestry (13.9), scrubland (4.0%) and natural vegetation (8.2%). The entire watershed was under a low to moderate vegetation cover varying between 10% and 50%. The major crops in the watershed are olives, cereals and beans (Sterk, 2009).

The transect used for the modelling has a length of 1711 m and runs from SSE towards the NNW. It drains into a tributary of the Barbara river. The elevation of this transect goes from 442 m to 198 m. Land use varies from a natural vegetation or grass cover on the highest part to arable cropland in the middle part, and arable cropland combined with acacia tree agroforestry in the lower part of the hillslope. The transect was divided into 18 sections of approximately 95 m length for which the average slope, soil type (texture), the land use, and erosion severity was determined. The transect starts with a steep slope on the upper part, decreasing towards the middle, but then increasing again until an almost flat part in the lower middle part of the hillslope. From there the slope angle increases, but before reaching the Barbara river it decreases again.

The hMMF modelling was based on the same 18 slope sections measured in the survey. The main model variables, except slope degree, were grouped into three categories based on the land use along the hillslope (Table 6). The annual amount of rainfall and number of rain days used was based on the measured data at the Barbara dam and equal to 812 mm and 62 days. Eq. (4c) was used to calculate the rainfall kinetic energy. The hMMF variable values per slope category are provided in Table 7. No surface runoff infiltration was allowed ($SR_i^{inf} = 0$).

The hMMF model calculated 145 mm of surface runoff and a soil loss of 0.22 kg m^{-2} for the entire slope. The modelled sediment transport and related mass balance values were plotted along the hillslope profile using SURFER 8.05 (Golden Software). Sediment transport is low at the upper part of the hillslope (Fig. 2a) due to the good vegetation cover. Here the erosion process is transport capacity limited. In the middle part the amount of surface runoff strongly increases (not shown here) but the erosion process remains transport capacity limited all the way down to the end of the slope. In the middle part, first the slope steepness increases and the sediment transport increases strongly, leading to a negative mass balance (Fig. 2b; between 1200 and 1000 m). Below this zone, the slope angle decreases again, resulting in a lower sediment transport. Much of the eroded sediment is deposited in this section (Fig. 2b; between 1000 and 850 m). The same pattern is repeated further downslope, with a strong increase in erosion and sediment transport between 400 and 200 m. Again below the steep zone there is much deposition (Fig. 2b; between 200 and 30 m) due to the smaller slope angle and the actual soil loss from the entire slope is low. Fig. 3 shows an example of actual sediment deposition on a part of the hillslope (at ~900 m) with a small slope angle.

3.4. hMMF application at 30-m hillslope in Hungary: surface runoff infiltration

For this application the 30-m bare soil slope of Hudek and Rey (2009) was used. The simulation of surface runoff and sediment transport along the hillslope with and without any surface runoff infiltration is provided in Appendix C. The inclusion of surface runoff infiltration was achieved by modifying the SR_i^{inf} value along the slope. The results (Figure C1) show that the surface runoff

Table 6
Characteristics a hillslope transect in the Barbara watershed, Tunisia (Sterk, 2009).

Part	Length	Slope	Slope type	Soil texture	Land use	Erosion severity
	M	°				
Upper	678	11.6	Concave	Loam	Natural vegetation/grass	Negligible
Middle	563	5.9	Concave	Loam	Crop land	Moderate rill erosion
Lower	470	5.5	S-shape	Sandy loam	Crop land/agro-forestry	Severe rill erosion

Table 7
Variable values used for the hMMF modelling of a hillslope in the Barbara watershed, Tunisia (Sterk, 2009). No surface runoff infiltration was allowed ($SR_i^{inf} = 0$).

Part	*A*	*CC*	*I*	*PH*	*MS*	*BD*	*EHD*	*Et/Eo*	*K*	*COH*	*GC*	*C*	*β*
	_	–	mm h^{-1}	m	wt.%	Mg m^{-3}	m	–	g J^{-1}	kPa	–	–	–
Upper	0.10	0.2	30	0.2	0.28	1.2	0.08	0.8	0.7	2	0.20	0.01	1.90
Middle	0.10	0.3	30	0.5	0.20	1.3	0.10	0.6	0.8	3	0.25	0.20	1.90
Lower	0.15	0.4	30	1.0	0.20	1.3	0.11	0.7	0.8	3	0.30	0.15	1.90

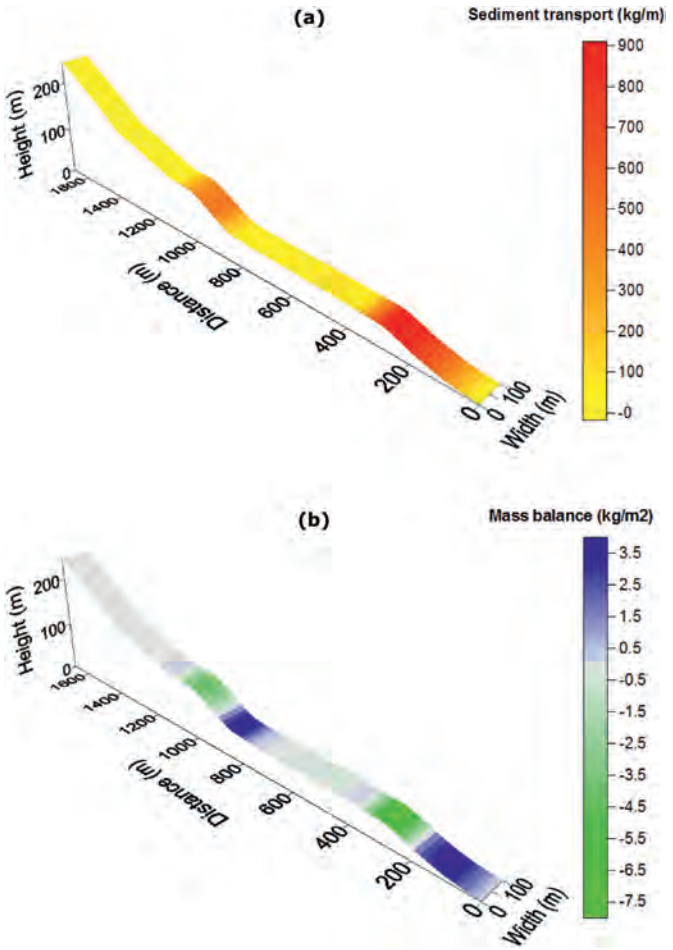

Fig. 2. Erosion modelled with the hMMF model along a hillslope in the Barabara watershed, NW Tunisia. (a) sediment transport profile along the slope; (b) mass balance profile showing erosion (green) and deposition (blue) zones.

profiles become curved and result in less surface runoff from the slope. The obtained profiles (Figures C1c-d) are realistic for natural hillslopes (Sheridan et al., 2014), but it remains uncertain what appropriate values of the SR_i^{inf} variable are, as data of surface runoff infiltration along hillslopes are scarce, if available at all. The lower surface runoff amounts obviously lead to lower sediment transport and soil losses (Figure C1).

3.5. hMMF application at 30-m hillslope in Hungary: SWC measures

The advantage of the hillslope version of the hMMF model is that it can directly incorporate SWC measures such as grass strips and bench terraces. Such structures stimulate surface runoff infiltration at the grass strip or on the near level bench terrace surface, which can be simulated through the SR_i^{inf} variable.

Fig. 4 shows simulations of grass strips on the 30-m bare soil plot at Szentendre, Hungary (Hudek & Rey, 2009). Fig. 4a and b shows respectively the impacts of a single, 1-m wide grass strip at the middle and at the end of the plot. The surface runoff infiltration was set at 25% ($SR_i^{inf} = 0.25$) for the grass strip. This reduces surface runoff from the slope with the grass strip in the middle from 383 mm to 327 mm, compared to the situation without a grass strip (Fig. 1a). Erosion is subsequently reduced by 0.73 kg m^{-2} (from 2.21 to 1.48 kg m^{-2}), mainly due to the deposition of eroded sediment at the grass strip. A grass strip at the end of the plot (Fig. 4b) results in even more reduction. Surface runoff is reduced to 282 mm and soil loss to 0.51 kg m^{-2}. These results nicely show the effects of a grass strip at the end of a slope: part of the surface runoff is passing through, but the bulk of sediments is filtered from the running water and deposited in the strip. Such grass strips are often termed Vegetative Filter Strips (e.g. Abu-Zreig et al., 2004). The third simulation (Fig. 4c) shows the effects of two grass strips, one in the middle and one at the end. In this case only 243 mm of surface runoff passes the lower strip and the hillslope soil loss is reduced to 0.35 kg m^{-2}.

The last example (Fig. 5) shows the simulation of three bench terraces of 10 m wide (Fig. 5a). An infiltration of surface runoff at the bench surface of 50% ($SR_i^{inf} = 0.5$) was assumed. The resulting surface runoff and soil loss are 68 mm and 0.29 kg m^{-2}. The hMMF model only calculates erosion along the risers of the terraces, and this sediment is deposited on the next bench terrace surface (Fig. 5b). Hence, the calculated soil loss for the entire field actually comes only from the lowest riser, which is consisting of bare soil in the calculation. If a grass cover on the risers is simulated, the surface runoff becomes 49 mm and the soil loss 0.09 kg m^{-2}.

4. Discussion

The comparison between the original rMMF and the hMMF simulation results (Appendix B) shows that the rMMF performed better than the hMMF when using recommended values for *EHD*

Fig. 3. Sediment deposition at a nearly flat area along a hillslope in the Barabara watershed, NW Tunisia.

and β. In general, the *EHD* values recommended by Morgan (2005) resulted in an underestimation of the amounts of measured surface runoff. This underestimation subsequently led to an underestimation in the soil loss values. By calibrating the variables *EHD* and β, the hMMF simulations exactly matched the measured surface runoff amounts, while the simulated soil losses were close to the measured values.

The applications of the hMMF model in the US, Hungary and Tunisia show that the model is capable of reproducing measured surface runoff and erosion rates from the erosion plots in Beemerville (Table 2) and Szentendre (Fig. 1), as well as erosion/deposition patterns along the hillslope in the Barbara watershed (Fig. 2). For the Beemerville plots the hMMF simulated surface runoff underestimated the measured values by 9.1%–19.8% when the recommended model variable values were used. For the Hungarian plots the underestimation of surface runoff was 5.7% for the bare plot and 40.7% for the *M. aquifolium* plot using recommended values. Except for the latter value, the overall performance for surface runoff can be considered reasonably good. Given the general underestimation of surface runoff when using recommended *EHD* values there is a need to re-analyse the *EHD* values for a wide range of soil erosion studies to improve the recommended values for different bio-physical conditions.

For soil losses the hMMF modelled values were very different from the measured values. Only on plots 2 & 4 at Beemerville a relatively low underestimation of 24.1% was obtained; all other simulation resulted in differences of 83.2% or more. However, by changing the *EHD* and β values, the model could be calibrated in such a way that the measured and modelled values of surface runoff and soil loss exactly match. It is however questionable if this exact match between measured and modelled values is really needed in most model studies. It is well known that most, if not all, plot-based erosion measurements are inherently variable, both in spatial and temporal sense (Nearing & Hairsine, 2016; Wendt et al., 1986). The uncertainty in the measured values of surface runoff and soil loss may subsequently lead to modelling efforts that try to reproduce a situation that is inherently variable. In addition, uncertainty in model equations as well as model input variable values further complicate the accuracy of the modelling process (Beven & Brazier, 2016). Hence, reproducing spatial patterns of erosion, like in the case illustrated in Figs. 2 and 3, could sometimes be more relevant than trying to reproduce actual measured erosion values.

In the hMMF model version two new variables are introduced: SR_i^{inf} and β. The SR_i^{inf} variable in eq. (16) accounts for infiltration of upslope generated surface runoff, and is especially useful for simulating the effects of SWC measures on soil erosion (Figs. 4 and 5). As shown in Appendix C, SR_i^{inf} can be used also to model infiltration along a hillslope without SWC measures, which naturally occurs in downslope areas (Langhans et al., 2014). The resulting profiles (Figs. C1c & C1d) compare well with experimentally determined profiles (Sheridan et al., 2014), but obtaining correct values for SR_i^{inf} along a certain hillslope remains challenging. This would require detailed measurements of surface runoff depths and infiltration amounts at different sections on a hillslope.

The value of β which has been introduced in the modified transport capacity equation (eq. (18)) actually regulates the annual sediment transport rate. In many cases the erosion process in the hMMF is transport capacity limited, so by increasing β to a higher value, the amount of sediment transport is enhanced. Likewise, a lower value of β decreases the sediment transport along the hillslope. Currently one single value of β is used for each section of the hillslope, but it would be possible to have separate values of β for each hillslope segment. However, obtaining the actual values of β along a complex hillslope is complicated as observations of sediment transport along a hillslope profile usually are unavailable. In case no sediment transport data from the hillslope are available, a value of 1.5 is recommended, which is based on the review of sediment transport capacity studies by Prosser and Rustomji (2000).

The hMMF model has an annual time step, which can be considered appropriate for the modelling of SWC measures. By

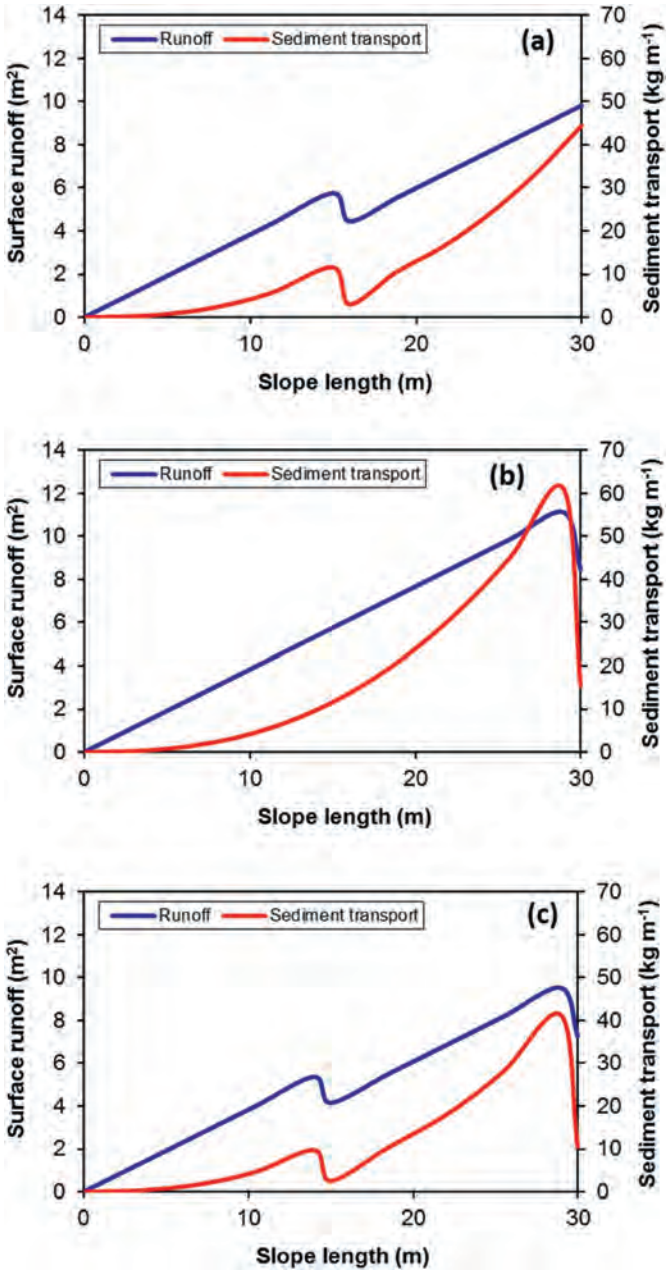

Fig. 4. The influence of grass strips on surface runoff and sediment transport along a 30-m hillslope at Szentendre, Hungary. (a) simulation of a 1-m wide grass strip at the middle of the plot; (b) simulation of a 1-m wide grass strip at the end of the plot; (c) simulation of two 1-m wide grass strips at the middle and end of the plot. In the simulations, a surface runoff infiltration of 25% (SR_i^{inf} = 0.25) was assumed, and no surface runoff infiltration in the rest of the plot.

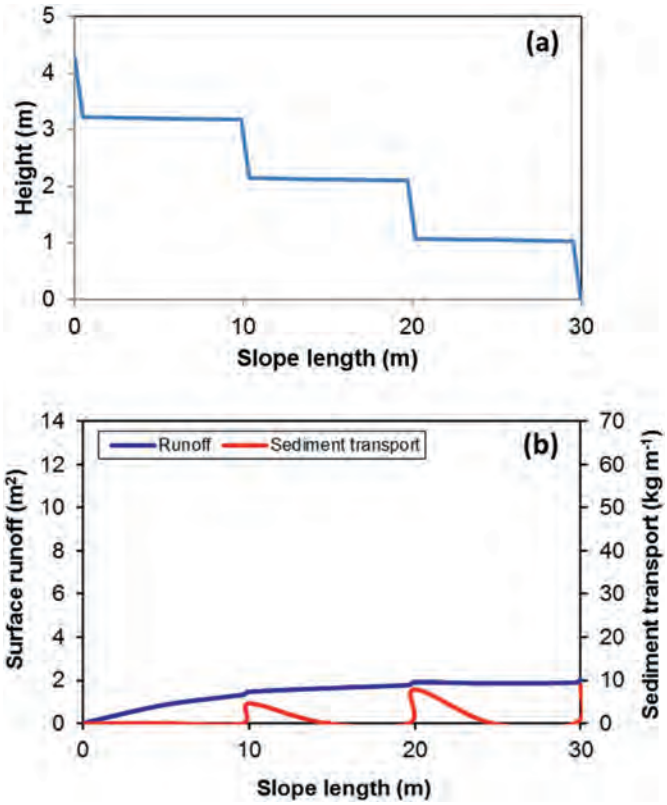

Fig. 5. hMMF simulation of bench terraces on a 30-m hillslope at Szentendre, Hungary. (a) The slope profile showing the terraces; (b) the simulated surface runoff and sediment transport along the bare slope. In the simulations of bench terraces a 50% (SR_i^{inf} = 0.50) surface runoff infiltration on the bench surface was assumed, and no surface runoff infiltration on the bare risers.

incorporating the SWC structures in the hMMF model the impacts they have on surface runoff and sediment transport can be simulated (Figs. 4 and 5). It is unlikely that a shorter time step (event, daily, monthly) would show different impacts of SWC structures. The only reason to have an event-based simulation could be that the effects of extreme events could be better captured, and actually may show a different response as compared to the annual based simulations. But, changing the model from its current annual time step to a daily or event time step is not trivial, and will require new equations and new model variables (e.g. Shrestha & Jetten, 2018).

Another problem with the simulations of SWC structures is the lack of knowledge about the amount of infiltration of surface runoff generated by the specific measures. For instance, the amount of surface runoff infiltration on the bed of a bench terrace can be assumed to be high, but not much information on this can be found in the SWC literature. The same holds for grass strips and how much surface runoff infiltration and sediment filtering those strips may cause. A few studies exist where the amounts of surface runoff infiltration and sediment trapping were measured in grass strips (e.g. Van Dijk et al., 1996) and by bench terraces (e.g. Tenge et al., 2011). The hMMF modelled reductions in soil losses varied from 33.0% for the case with a grass strip in the middle of the field (Fig. 4a), to 76.9% for the grass strip at the end of the field (Figs. 4b), and 84.2% for the case with two grass strips (Fig. 4c). The latter two reductions are in the same range as reported soil erosion reductions by grass strips in Van Dijk et al. (1996). Measured soil losses on fields with bench terraces in the West Usambara Mountains ranged from 0.15 to 0.37 kg m^{-2} (Tenge et al., 2011), which is similar to the amount modelled with hMMF in Fig. 5 (0.29 kg m^{-2}). Hence, the hMMF simulations of SWC measures led to similar reductions in erosion as reported in a few studies.

5. Conclusions

The semi-empirical rMMF soil erosion model is a relatively easy to apply, but good model for field-scale water erosion quantification. Two shortcomings of the rMMF are 1. The assumption of a

homogeneous and linear slope of the field, and 2. The incorporation of SWC measures through the USLE *P*-factor only. The new hMMF version is capable to simulate surface runoff and sediment transport along irregular hillslope profiles with or without SWC measures. By introducing a surface runoff infiltration factor (SR_i^{inf}) in the model equations the effects of SWC measures can be directly simulated, and the effectiveness of different measures can be quantified. Therefore, the hMMF allows designing appropriate SWC measures for specific hillslope conditions.

The model was tested against one hillslope erosion survey and quantitative datasets of surface runoff and soil loss values from experimental plots. The overall performance of hMMF simulation of surface runoff ranged from poor to reasonably good. The evaluation resulted in a general tendency of underestimation of measured amounts when the recommended model variable values were used. It is concluded that the *EHD* values recommended by Morgan (2005) are generally too large and result often in an underestimation of the surface runoff amounts. It is therefore needed to re-analyse those recommended *EHD* values and improve them for a wide range of bio-physical conditions. Simulation of soil losses using recommended values resulted in large errors. Hence calibration of model variable values is generally needed to obtain a good match between modelled and measured soil loss values. The examples from Beemerville, USA, and Szentendre, Hungary, show that with calibration of the model variables *EHD* and β it is possible to get nearly exact matches between measured and modelled values.

The modelling of grass strips (Fig. 4) and bench terraces (Fig. 5) shows the capability of the hMMF model to quantify the impacts of such SWC structures on surface runoff and soil erosion. The simulated patterns of surface runoff and sediment transport are realistic, but actual data on the amounts of surface runoff infiltration and sediment filtering are scarce. Comparisons with reported experimental values are in the same range as modelled in this study. Hence it can be concluded that the hMMF model is able to simulate SWC structures directly instead of using the USLE *P* factor, as it mostly done. Therefore, the hMMF provides a tool for design and testing of SWC conservation measures under variable bio-physical conditions, such as slope angle, soil type, rainfall characteristics, and vegetation cover.

Funding

This research did not receive any specific grant from funding agencies in the public, commercial, or not-for-profit sectors.

Declaration of competing interest

I herewith confirm that there is no conflict of interest whatsoever with the contents of the manuscript “A hillslope version of the revised Morgan, Morgan and Finney water erosion model”.

Appendix A

Comparison between the Morgan/Duzant rMMF and hMMF models

Morgan and Duzant (2008) modified the rMMF model by adding new equations and changing some of the existing equations to better quantify effects of vegetation on water erosion. One of the changes was a modification of the surface runoff equation (eq. (7)) to make it applicable for slope lengths longer than 10 m that are divided in sections:

$$SR = (P + SR_{up})\,exp\left(-\frac{S_c}{P_o}\right)\left(\frac{L}{10}\right)^{0.1} \quad \text{A.1}$$

where SR_{up} (mm) is the surface runoff coming from the upper section and L is the slope length (m). The last term on the right-hand side of eq. (A.1) is an empirical adjustment for slope length to correct for the sensitivity of the equation for the number of elements at which a long slope of maximum 50 m is divided.

A simple rMMF model was created for a 50 m linear slope, divided in five sections of 10 m each. Eq. (A.1) was used for the surface runoff calculation, and the results are compared here with the hMMF procedure for the same slope and model variables. The simulation is for a bare soil. The input values for both models are shown in Table A1. For the calculation of the kinetic energy of the direct throughfall (*KE* (*DT*)) eq. (4b) (Table 1) was used.

Table A.1
Input variable values used in hMMF and the rMMF modified model version of Morgan and Duzant (2008) for the simulation of a 50 m linear hillslope with a 5° slope angle and bare soil.

Variable	Value	Variable	Value
Rain (*P*)	600 mm	Bulk density (*BD*)	1.3 Mg m^{-3}
Rain days (P_o)	80 days	Effective hydraulic depth (*EHD*)	0.06 m
Interception (*A*)	0	Evapo-transpiration ratio (E_t/E_o)	0.05
Canopy cover (*CC*)	0	Soil particle detachment (*K*)	0.7 g J^{-1}
Plant height (*PH*)	0 m	Cohesion (*COH*)	10 kPa
Rainfall intensity (*I*)	10 mm h^{-1}	Ground cover (*GC*)	0
Soil moisture content (*MS*)	0.40 kg kg^{-1}	Crop cover factor (*C*)	1

The resulting patterns of hillslope surface runoff and sediment transport are shown in Figure A1. The hMMF calculates an annual surface runoff equal to 237 mm and a soil loss of 0.84 kg m^{-2}. The surface runoff increases linearly with slope length, while the sediment transport starts low at the upper slope and increases rapidly on the lower part of the slope, after approximately 25 m (Figure A1a).

The Morgan/Duzant rMMF model, using Eq. (A.1) for the surface runoff calculation, results in 507 mm of surface runoff and a soil loss of 7.35 kg m^{-2}. This is highly unrealistic, which can be easily seen from the slope profiles of surface runoff and sediment transport (Figure A1b). The high volume at the uppermost section immediately leads to unrealistically high sediment transport values. The problem with eq. (A.1) is that it sums the surface runoff

values in mm, while these should first be converted to a volume before summing them. Then the sediment transport calculation would also become more realistic.

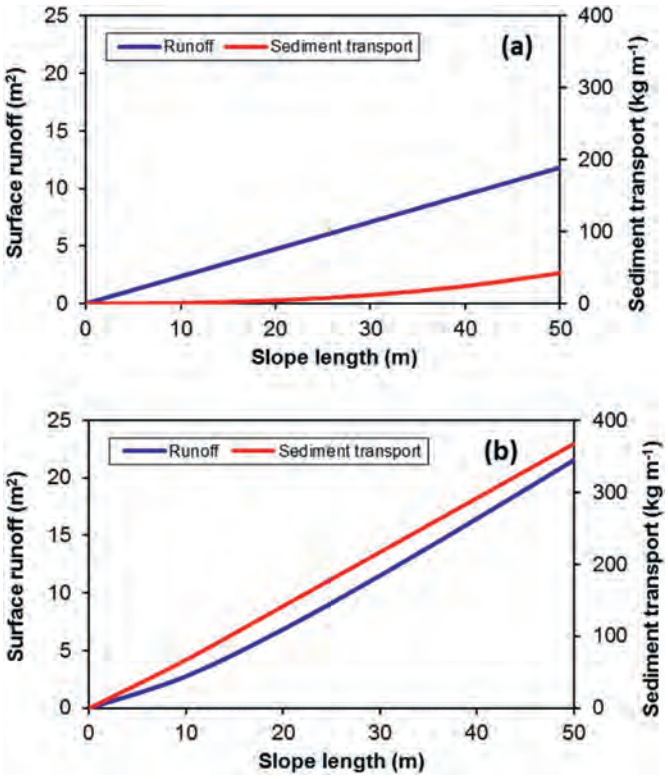

Fig. A.1. Simulated profiles of surface runoff and sediment transport with the hMMF model (a), and the rMMF model as modified by Morgan and Duzant (2008) (b).

Appendix B

Comparison of the hMMF with the rMMF model using measured soil erosion data

The hMMF and rMMF models were compared by simulating surface runoff and soil loss values from nine different locations. The data used were collected and described by Morgan and Finney (1982) to test the initial MMF model. Morgan (2001) used the same data to test the rMMF model, and here the same observations were used to calculate surface runoff and soil losses with the hMMF (Table B1). Not all data as used by Morgan (2001) could be used here, as for several sites details about soil type, crop type, slope steepness and rainfall were not provided by Morgan and Finney (1982). Another problem is the lack of information about the plot sizes that were used at the nine locations. The MMF and rMMF models are independent of slope length, but this is not the case for the hMMF. The surface runoff values calculated in mm's by the hMMF are independent of the slope length as long as $SR_i^{inf} = 0$, and will give exactly the same amounts as the rMMF, keeping all variables the same. For soil loss calculations this is not the case as the soil loss may increase with increasing slope length, depending on the slope shape. Unfortunately, also the information about the slope shape was not provided either, and in the hMMF calculations it was assumed that all slopes have a linear shape and a slope length of 22.1 m, similar to the length of the standard USLE erosion plot.

The hMMF calculations used the input variable values for P, P_o, A, I, MS, BD, S, Et/Eo, K and C as provided by Morgan and Finney (1982). Other input variables (CC, PH and GC) were estimated based on the provided crop types. No surface infiltration ($SR_i^{inf} = 0$) was assumed. Two types of hMMF simulations were made. In the first simulation, the recommended values (Morgan, 2005) for the input variables EHD and COH, and 1.5 for β were used. In the second simulation the values of EHD and β were calibrated to optimize the surface runoff and soil loss calculations.

The simulations results are provided in Table B1. Overall, the hMMF model with recommended values (hMMF rec.) performed less good as the rMMF model in Morgan (2001). The Nash-Sutcliffe Efficiency (NSE) for surface runoff is 0.55 for rMMF, while for the hMMF using recommended values it is 0.11. This is surprising as Morgan (2001) has used the same data, but his surface runoff amounts are closer to the measured values. If Morgan (2001) has used the same P, P_o, MS, BD, S and Et/Eo values as provided in Morgan and Finney (1982), it can only mean that Morgan (2001) has used different EHD values than the ones that are recommended by Morgan (2005). In many cases (e.g., Taiwan) the hMMF using the recommended EHD values largely underestimates the measured amounts. However, in a few cases (e.g., Lusotho, Tanzania) the calculated values of surface runoff match the measured values quite well.

For soil losses the hMMF using recommended values performed even less good than the rMMF. The NSE values are 0.56 for the rMMF and −0.06 for hMMF. There are several reasons for this poorer performance. The general underestimation of surface runoff results in low sediment transport amounts, and thus an underestimation of the soil losses as well. Moreover, the slope length used in the calculations (22.1 m) may not be correct for all sites which may introduce more errors.

During the second hMMF simulations (hMMF calib.) the EHD and β values were calibrated to match the measured surface runoff and soil loss values as good as possible. The NSE values are 1.00 for surface runoff and 0.73 for soil loss. This shows that the hMMF is well capable to simulate measured erosion values, but the recommended input variable values, especially EHD, may not be sufficiently accurate. In general the EHD values recommended by Morgan (2005) are too large and lead to underestimation of the surface runoff amounts. This underestimation subsequently results in often too low soil erosion amounts.

Table B.1
Comparison of measured, rMMF and hMMF modelled surface runoff and soil loss values.

Site	Surface runoff				Soil loss			
	Measured	rMMF	hMMF rec.	hMMF calib.	Measured	rMMF	hMMF rec.	hMMF calib.
	mm	mm	mm	mm	kg m^{-2}	kg m^{-2}	kg m^{-2}	kg m^{-2}
Lusotho, Tanzania								
Clay, maize/beans intercropped	0.2–1.0	12–19	0.3–0.7	0.2–1.0	0.001	0.005–0.014	0.000	0.000
Sandy Clay loam, evergreen forest	2.6–5.7	46–79	2.6–6.0	2.6–5.7	0.001–0.003	0.002–0.005	0.000	0.000
Sandy Clay loam, evergreen forest, steep slope	8.5–15	51–88	3.3–7.3	8.5–15	0.001–0.003	0.004–0.013	0.000	0.000
Clay, maize/beans intercropped, steep slope	0.4–0.8	1.1–12	0.3–0.7	0.4–0.8	0.001	0.000–0.012	0.000	0.000

(*continued on next page*)

Table B.1 (*continued*)

Site	Surface runoff				Soil loss			
	Measured	rMMF	hMMF rec.	hMMF calib.	Measured	rMMF	hMMF rec.	hMMF calib.
	mm	mm	mm	mm	kg m^{-2}	kg m^{-2}	kg m^{-2}	kg m^{-2}
Adiopodoume, Ivory Coast								
Sandy loam, secondary tropical forest	15	316	30	15	0.001–0.020	0.046	0.000	0.000
Sandy loam, bare soil	707–1415	1142	1337	1022	6.90–15.0	17.5	10.3	10.2
Sandy loam, oil palm	43–172	333	58	108	0.001–0.050	0.77	0.001	0.003
Sandy loam, banana with mulch	11–86	385	56	49	0.004–0.005	0.021	0.000	0.000
Sandy loam, maize	643–1608	617	248	1126	3.50–13.1	8.85	0.089	7.8
Sandy loam, groundnut	579–1565	731	332	1072	5.90–12.0	3.09	0.232	6.7
Sefa, Senegal								
Loam, secondary tropical forest	1.6–19	400	71	10	0.002–0.020	0.006	0.000	0.000
Loam, groundnut	130–699	723	276	415	0.29–1.63	2.43	0.042	1.1
Loam, cotton	15–699	646	429	357	0.05–1.85	4.17	0.126	0.619
Loam, maize	504	639	321	504	1.03	1.62	0.024	0.840
Loam, sorghum	390–683	660	341	537	0.33–1.24	3.48	0.057	0.610
Pong Khrai, Thailand								
Clay loam, upland rice	22–32	102	17	27	1.4–2.4	2.20	0.000	0.001
Clay loam, upland rice, bench terraces	16–53	84	12	35	1.1–1.3	0.63	0.000	0.001
Marchiazza Basin, Italy								
Loamy sand, bare soil with tufted grass	201–261	341	138	231	2.7–3.1	4.14	0.072	1.3
Loamy sand, Molinia moor grass	51–58	112	33	55	0.05–0.09	0.02	0.000	0.000
Loamy sand, chestnut and oak trees	36–38	92	2.8	37	0.009–0.018	0.005	0.000	0.000
Taiwan								
Clay loam, citrus, clean cultivation	1268	654	118	1268	15.6	16.34	0.043	15.5
Clay loam, citrus, bench terracing	344	543	94	344	0.50	8.25	0.041	0.48
Clay loam, citrus with mulch	109	360	59	109	0.094–0.28	0.07	0.000	0.003
Clay loam, banana, clean cultivation	1113–1449	346	1.5	1279	3.94–6.37	8.27	0.000	5.00
Clay loam, banana with mulch	189	257	1.0	190	0.009	0.015	0.000	0.009
Clay loam, banana with contour bunds	483–1029	346	1.0	757	0.11–0.39	0.22	0.000	0.28
Mpwapwa, Tanzania								
Sandy loam, bare soil	446	390	436	446	14.7	6.64	0.795	5.0
Sandy loam, sorghum and millet	80–259	141	2.1	170	5.5–9.0	0.61	0.000	0.114
Sandy loam, tufted grass	8–65	110	0.9	37	0.0–0.07	0.07	0.000	0.002
Sandy loam, savanna grass	3–4	59	0.2	4	0.0	0.002	0.000	0.000
Lyamungu, Tanzania								
Clay loam, coffee, clean cultivation	15–232	166	12	125	4.3	1.36	0.000	0.079
Clay loam, coffee, cover crops	10–98	54	2.0	54	0.4	0.015	0.000	0.001
Clay loam, coffee, contour ridges	36	170	8.3	36	0.3	0.09	0.000	0.000
Clay loam, coffee, cover crops, contour ridges	27	54	1.2	27	0.1	0.005	0.000	0.000
Henderson, Zimbabwe								
Clay, maize	8–61	78	13	35	0.2–0.3	0.106	0.000	0.000
Clay, grass	8–26	61	8.7	17	0.05–0.1	0.016	0.000	0.000

Appendix C

hMMF application at 30-m hillslope in Hungary: surface runoff infiltration

For this application, the 30-m bare soil slope of Hudek and Rey (2009) was used. The simulation of surface runoff and sediment transport along the hillslope without any surface runoff infiltration is shown in Fig. 1a, and copied here in Figure C1a. Figures C1b-d show the same hillslope simulation with different degrees of infiltration of surface runoff. The SR_i^{inf} values corresponding to Figures C1a-d are provided in Table C1. It was assumed that on top of the slope there is little surface runoff and thus also no or negligible infiltration. But as the layer of water builds up in downslope direction the hydraulic head increases, which may lead to increased infiltration of surface runoff (Langhans et al., 2014).

The surface runoff profiles of Figure C1 show that the profiles become curved and result in less surface runoff from the slope. The simulated values of surface runoff decrease from 383 mm in Figure C.1a to 198 mm in Figure C1d. The intermediate values are 330 mm and 269 mm in Figures C.1b and C.1c, respectively. Notwithstanding the difficulties in quantifying actual amounts of infiltration of surface runoff, the profiles presented in Figure C1c and C.1d show much similarity with experimental surface runoff profiles as presented in Sheridan et al. (2014). Inclusion of surface runoff infiltration leads therefore to a more realistic surface runoff profile, but the values of the SR_i^{inf} variable remain largely unknown for actual infiltration levels on a natural hillslope.

Inclusion of surface runoff infiltration in the hillslope hydrology leads to lower sediment transport and soil losses (Figure C1). The actual soil loss from the plot was 2.20 kg m^{-2} and the simulated value was 2.21 kg m^{-2} in the case without surface runoff infiltration (Figure C1a). With surface runoff infiltration the soil loss values drop to 1.51 kg m^{-2} (Figure C.1b), 0.90 kg m^{-2} (Figure C.1c) and 0.42 kg m^{-2} (Figure C1d). The sediment transport is transport capacity limited in all three cases with surface runoff infiltration.

Table C.1
Values of SR_i^{inf} variable used in hMMF model simulations of the bare soil plot at Szentendre, Hungary (Hudek & Rey, 2009).

Slope section	SR_i^{inf}			
m	Fig. C1a	Fig. C1b	Fig. C1c	Fig. C1d
0–3	0	0	0	0
3–6	0	0	0	0
6–9	0	0.01	0.03	0.03
9–12	0	0.01	0.03	0.06
12–15	0	0.02	0.05	0.09
15–18	0	0.02	0.05	0.12
18–21	0	0.03	0.07	0.13
21–24	0	0.03	0.07	0.14
24–27	0	0.04	0.09	0.15
27–30	0	0.04	0.09	0.16

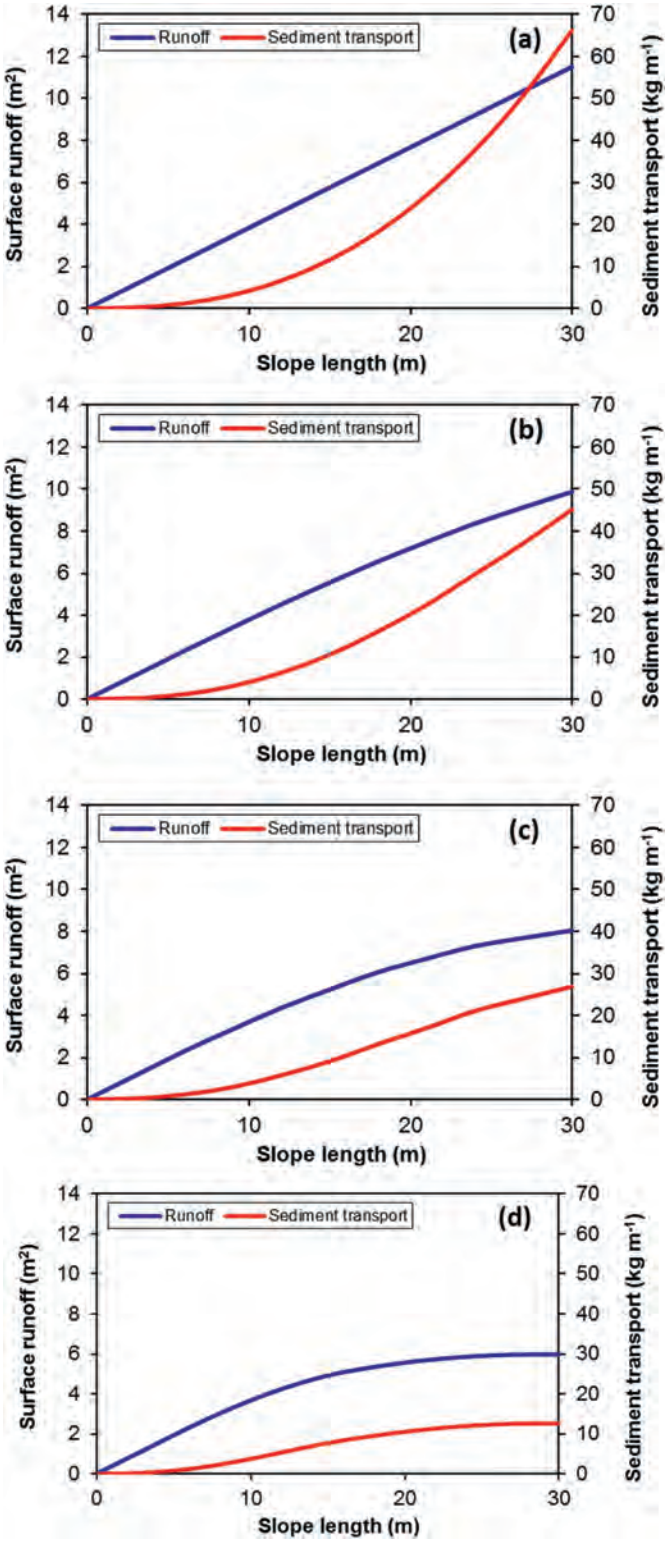

Fig. C.1. The influence of surface runoff infiltration on surface runoff amount and sediment transport along a 30-m hillslope at Szentendre, Hungary. Surface runoff infiltration has been accounted for with the SR_i^{inf} variable in the hMMF model. Values of SR_i^{inf} used in Figures (a), (b), (c) and (d) are provided in Table C1.

References

Abu-Zreig, M., Rudra, R. P., Lalonde, M. N., Whiteley, H. R., & Kaushik, N. K. (2004). Experimental investigation of runoff reduction and sediment removal by vegetated filter strips. *Hydrological Processes, 18*, 2029–2037.

Aksoy, H., & Kavvas, M. L. (2005). A review of hillslope and watershed scale erosion and sediment transport models. *Catena, 64*, 247–271.

Bennett, H. H. (1939). *Soil conservation*. New York, USA: McGraw-Hill.

Beven, K. J., & Brazier, R. E. (2016). Dealing with uncertainty in erosion model predictions. In R. P. C. Morgan, & M. A. Nearing (Eds.), *Handbook of erosion modelling* (pp. 52–79). Chichester, U.K: Wiley.

Borrelli, P., Robinson, D. A., Fleischer, L. R., Lugato, E., Ballabio, C., Alewell, … Panagos, P. (2017). An assessment of the global impact of 21st century land use change on soil erosion. *Nature Communications, 8*, 2013. https://doi.org/10.1038/s41467-017-02142-7

Brandt, C. J. (1990). Simulation of the size distribution and erosivity of raindrops and throughfall drops. *Earth Surface Processes and Landforms, 15*, 687–698.

Choi, K., Arnhold, S., Huwe, B., & Reineking, B. (2017). Daily based morgan–morgan–finney (dmmf) model: A spatially distributed conceptual soil erosion model to simulate complex oil surface configurations. *Water, 9*, 278. https://doi.org/10.3390/w9040278

Coutinho, M. A., & Tomás, P. (1995). Characterisation of raindrop size distributions at the vale formoso experimental erosion centre. *Catena, 25*, 187–197.

Fernandez, C., Vega, J. A., & Vieira, D. C. S. (2010). Assessing soil erosion after fire and rehabilitation treatments in NW Spain: Performance of RUSLE and revised Morgan-Morgan-Finney models. *Land Degradation & Development, 21*, 58–67.

Flanagan, D. C., & Nearing, M. A. (Eds.). (1995). *USDA Water Erosion Prediction Project hillslope and watershed model documentation*. USDA-ARS National Soil Erosion Research Laboratory. NSERL Report No. 10. West Lafayette, Ind.

Hudek, C., & Rey, F. (2009). Studying the effects of Mahonia aquifolium populations on small-scale mountain agro-ecosystems in Hungary with the view to minimise land degradation. *Land Degradation & Development, 20*, 252–260.

Hudek, C., Sterk, G., van Beek, R. L. P. H., & de Jong, S. M. (2014). Modelling soil erosion reduction by Mahonia aquifolium on hillslopes in Hungary: The impact of soil stabilization by roots. *Catena, 122*, 159–169.

Hudson, N. W. (1965). *The influence of rainfall on the mechanics of soil erosion with particular reference to Southern Rhodesia*. Town, Cape Town, South Africa: MSc Thesis, University of Cape.

Julien, P. Y., & Simons, D. B. (1985). Sediment capacity of overland flow. *Transactions of the ASAE, 28*, 755–762.

Langhans, C., Govers, G., Diels, J., Stone, J. J., & Nearing, M. A. (2014). Modeling scale-dependent runoff generation in a small semi-arid watershed accounting for rainfall intensity and water depth. *Advances in Water Resources, 69*, 65–78.

Lopez-Vicente, M., Navas, A., & Machın, J. (2008). Modelling soil detachment rates in rainfed agrosystems in the south-central Pyrenees. *Agricultural Water Management, 95*, 1079–1089.

Morgan, R. P. C. (2001). A simple approach to soil loss prediction: A revised morgan-morgan-finney model. *Catena, 44*, 305–322.

Morgan, R. P. C. (2005). *Soil erosion and conservation*. Oxford, UK: Blackwell Publishing.

Morgan, R. P. C., & Duzant, J. H. (2008). Modified MMF (Morgan–Morgan–Finney) model for evaluating effects of crops and vegetation cover on soil erosion. *Earth Surface Processes and Landforms, 32*, 90–106.

Morgan, R. P. C., & Finney, H. J. (1982). *Stability of agricultural ecosystems: Validation of a simple model for soil erosion assessment. Collaborative paper CP-82-76*. Laxenburg, Austria: International Institute for Applied Systems Analysis.

Morgan, R. P. C., Morgan, D. D. V., & Finney, H. J. (1984). A predictive model for assessment of erosion risk. *Journal of Agricultural Engineering Research, 30*, 245–253.

Musgrave, G. W. (1947). The quantitative evaluation of factors in water erosion: A first approximation. *Journal of Soil & Water Conservation, 2*, 133–138.

Nearing, M. A., Foster, G. R., Lane, L. J., & Finkner, S. C. (1989). A process-based soil erosion model for USDA Water Erosion Prediction Project technology. *Transactions of the ASAE, 32*, 1587-1593.

Nearing, M. A., & Hairsine, P. B. (2016). The future of soil erosion modelling. In R. P. C. Morgan, & M. A. Nearing (Eds.), *Handbook of erosion modelling* (pp. 389–397). Chichester, U.K: Wiley.

Oldeman, L. R., Hakkeling, R. T. A., & Sombroek, W. G. (1991). *World map of the status of human-induced soil degradation; an explanatory note*. Wageningen, The Netherlands: International Soil Reference and Information Centre.

Onaga, K., Shirai, K., & Yoshinaga, A. (1988). Rainfall erosion and how to control its effects on farmland in Okinawa. In S. Rimwanich (Ed.), *Land conservation for future generations* (pp. 627–639). Bangkok: Department of Land Development.

Prosser, I. P., & Rustomji, P. (2000). Sediment transport capacity relations for overland flow. *Progress in Physical Geography, 24*, 179–193.

Renard, K., Foster, G., Weesies, G., McCool, D., & Yoder, D. (1997). *Predicting soil erosion by water: A guide to conservation planning with the revised universal soil loss equation (RUSLE)*. Washington, DC: US Government Printing Office.

Rosewell, C. J. (1986). Rainfall kinetic energy in eastern Australia. *Journal of Climate and Applied Meteorology, 25*, 1695–1701.

Sheridan, G. J., Noske, P. J., Lane, P. N. J., Jones, O. D., & Sherwin, C. B. (2014). A simple two-parameter model for scaling hillslope surface runoff. *Earth Surface Processes and Landforms, 39*, 1049–1061.

Shrestha, D. P., & Jetten, V. G. (2018). Modelling erosion on a daily basis, an adaptation of the MMF approach. *International Journal of Applied Earth Observation and Geoinformation, 64*, 117–131.

Sterk, G. (2009). *Generating environmental benefits to improve watershed management in Tunisia; Watershed erosion and reservoir sedimentation assessment. Part 2: Erosion and sedimentation calculations*. Utrecht, The Netherlands: Department of Physical Geography, Utrecht University.

Tenge, A. J., Sterk, G., & Okoba, B. O. (2011). Farmers' preferences and physical effectiveness of soil and water conservation measures in the East African Highlands. *Journal of Social Sciences, 2*, 84–100. The University of Dodoma.
Van Dijk, P. M., Kwaad, F. J. P. M., & Klapwijk, M. (1996). Retention of water and sediment by grass strips. *Hydrological Processes, 10*, 1069–1080.
Van de Giesen, N. C., Stomph, T. J., & de Ridder, N. (2000). Scale effects of Hortonian overland flow and rainfall-runoff dynamics in a West African catena landscape. *Hydrological Processes, 14*, 165–175.
Vigiak, O., Okoba, B. O., Sterk, G., & Groenenberg, S. (2005). Modelling catchment-scale erosion patterns in the east african highlands. *Earth Surface Processes and Landforms, 30*, 183–196.
Vigiak, O., Romanowicz, R. J., van Loon, E. E., Sterk, G., & Beven, K. J. (2006). A disaggregating approach to describe overland flow occurrence within a catchment. *Journal of Hydrology, 323*, 22–40.
Wendt, R. C., Alberts, E. E., & Hjemfelt, A. T., Jr. (1986). Variability of runoff and soil loss from fallow experimental plots. *Soil Science Society of America Journal, 50*, 730–736.
Wischmeier, W. H., & Smith, D. D. (1978). *Predicting rainfall erosion losses: A guide to conservation planning*. Washington, D.C.: USDA. Agriculture Handbook No. 537.
Young, R. A., Onstad, C. A., Bosch, D. D., & Anderson, W. P. (1989). AgNPS: A non-point source pollution model for evaluating agricultural watersheds. *Journal of Soil & Water Conservation, 44*, 168–173.
Zanchi, C., & Torri, D. (1980). Evaluation of rainfall energy in central Italy. In M. De Boodt, & D. Gabriels (Eds.), *Assessment of erosion* (pp. 133–142). London: Wiley.
Zhang, G. H., Wang, L. L., Tang, K. M., Luo, R. T., & Zhang, X. C. (2011). Effect of sediment size on transport capacity of overland flow on steep slopes. *Hydrological Sciences Journal, 56*, 1289–1299.
Zingg, A. W. (1940). Degree and length of land slope as it affects soil loss in runoff. *Agricultural Engineering, 21*, 59–64.

International Soil and Water Conservation Research 9 (2021) 333–343

Contents lists available at ScienceDirect

International Soil and Water Conservation Research

journal homepage: www.elsevier.com/locate/iswcr

Original Research Article

Is the runoff coefficient increasing or decreasing after ecological restoration on China's Loess Plateau?

Haiyan Zheng, Chiyuan Miao*, Guanghui Zhang, Xiaoyan Li, Shuai Wang, Jingwen Wu, Jiaojiao Gou

State Key Laboratory of Earth Surface Processes and Resource Ecology, Faculty of Geographical Science, Beijing Normal University, Beijing, 100875, China

ARTICLE INFO

Article history:
Received 29 January 2021
Received in revised form
15 April 2021
Accepted 15 April 2021
Available online 22 April 2021

Keywords:
Loess Plateau
Precipitation
Runoff coefficient
Budyko-based elasticity method
Land use/cover change

ABSTRACT

The "Grain for Green" project (GGP) was launched in 1999 on China's Loess Plateau to reduce soil erosion, which had far-reaching impacts on the local eco-hydrological processes. In this study, we use monthly runoff depth and precipitation datasets spanning 1961 to 2015 for 16 primary basins of the plateau to reveal changes in runoff generation capacity before and after the GGP. We use a Budyko-based elasticity method to calculate the runoff depth (R_1) and runoff coefficient (C_1) exclusively attributable to land use/cover change. Results indicate that the mean annual runoff coefficients (C_0) decline by 26%–76% from the periods 1961–1999 to 2000–2015. The annual observed runoff depth (R_0) and C_0 for 75% of basins show significant downward trends during 1961–1999; after the implementation of the GGP, both annual R_0 and annual C_0 for over 50% of basins show upward trends. The study further finds that the increase of erosive rainfall during the period 2000–2015, whose mean increasing rate reaches 4.6 mm/year, is the main reason for the upward trends of R_0 and C_0. After removing the effect of precipitation variation during this period, we find that 11 out of 16 basins show decreased trends for C_1, with the downward rate between 2.4% and 6.0% per year. The reduction rate in semi-arid areas is about four times the rate in semi-humid areas. The results remind us to consider the carrying capacity of local water resources when implementing soil and water conservation measures across the Loess Plateau.

1. Introduction

Runoff is an important indicator of the local water cycle condition, as a measure of sustainable water availability (Milly et al., 2005). Surface runoff is generated from precipitation interacting with and redistributed by the ground surface. Understanding runoff generation processes and their variation is of great significance for basin water management efforts and predicting soil erosion. The runoff coefficient is the ratio of the direct runoff at a basin outlet to the total precipitation within this basin. It has been used in many studies as an index reflecting the runoff generation capacity for a basin (Chen et al., 2018; Merz et al., 2006; Velpuri and Senay, 2013).

Runoff generation processes in a watershed can generally be divided into soil infiltration processes, slope confluence processes and river network confluence processes. Changes in underlying conditions, namely, the implementation of soil conservation measures (including engineering and ecological measures), are expected to greatly influence these processes (Dwarakish et al., 2015). Engineering measures, such as check dams and reservoirs, mainly affect the river network confluence processes; ecological measures (e.g., afforestation) mostly affect evapotranspiration, soil infiltration and slope confluence processes. Reported results differ globally as to whether afforestation is expected to increase or decrease runoff outcomes (Filoso et al., 2017; Tuset et al., 2015). Filoso et al., 2017 reported that the change in water yield was closely correlated with geographic area and the spatial and temporal scale of the afforestation project. Even for the same study area, the results vary with the research methods and indicators used to characterize the water response (Tuset et al., 2015). In addition, previous researchers have shown that, in addition to changes in the land surface, climate change is also a nonnegligible factor influencing runoff generation capacity because of its effects on precipitation (Merz et al., 2006; Sun et al., 2019; Zhang et al., 2013), precipitation intensity (Almeida et al., 2020; Kim et al., 2019), and potential evapotranspiration (Liu & McVicar, 2012).

* Corresponding author.
E-mail address: miaocy@vip.sina.com (C. Miao).

https://doi.org/10.1016/j.iswcr.2021.04.009

The Loess Plateau, located in northern China and the middle reaches of the Yellow River, has attracted much attention due to soil erosion over the past several decades (Liu et al., 2020). From the 1970s to the 1990s, in order to prevent sediment from entering the Yellow River, erosion regulation measures had been implemented on many small watersheds on the Loess Plateau, such as building terraces, check dams and conducting reforestation (Li et al., 2016), even though land use change on the Loess Plateau had been relatively slight and mainly concentrated in steep areas of abandoned cultivated land. In 1999, China's famous ecological project known as the "Grain for Green" Project (GGP) was launched, with the goal of returning farmland on steep slopes to forest and grassland (Wang et al., 2015). And after 1999, the degree of land use/cover change (LUCC) was considerably higher (Zhou et al., 2019): cultivated land area decreased greatly, while woodland/shrub/grassland area and built-up land area increased greatly (Xu & Xu, 2017). In addition, the vegetation density on the Loess Plateau shows an obvious increasing trend (Kong et al., 2018; Miao et al., 2019; Yang, Wei, Chen, & Mo, 2012). Therefore, the runoff response on the plateau during the earlier period (the 1970s–1999) displays some spatio-temporal differences compared to the later period (2000–2015).

Mu et al. (1998) illustrated that the runoff depth in a small watershed on the Loess Plateau decreased significantly during the 1970s–1999 because of soil and water conservation engineering measures. Liu et al. (2014) revealed that the runoff coefficient over the loess area had decreased with the increase of vegetation recovery area from the 1970s to 2013—and the more arid the area, the greater the decrease. Then, Mu et al. (2019) reported that vegetation restoration has changed some of the soil physical properties on the Loess Plateau for the last few years; for example, both soil infiltration capacity and water storage capacity have become stronger, which would certainly affect runoff generation processes. A recent study shows that permanent surface water has increased over the Loess Plateau, which may be caused in part by large-scale afforestation (Zeng et al., 2020). However, Sun et al. (2020) concluded that afforestation is not likely to increase water yield across the Loess Plateau based on the theory of water balance. These discrepancies and gaps lead us to conclude that there is still a lack of systematic research on how and why the GGP project affects runoff generation capacity over the Loess Plateau.

Therefore, in this research, we analyze spatial and temporal changes in the runoff depth and runoff coefficient and, simultaneously, quantify the runoff coefficient after removing the effects of precipitation variation. This study aims to quantitatively answer the question of whether the runoff generation capacity has increased or decreased after the implementation of the GGP across the Loess Plateau. This information can provide a foundation for evaluating and prioritizing different soil and water conservation measures and provide guidance for future soil conservation policies on the Loess Plateau.

2. Study area and dataset

2.1. Study area

The Loess Plateau is one of four famous plateaus in China. It is famous for its deep loess layer, whose thickness often ranges from 30 to 200 m, even reaching 300 m in some places (Fu et al., 2017). This region is located at the edge of temperate monsoon area, and most belongs to the semi-arid and semi-humid climatic zones (Shi & Huang, 2021). In general, southeastern part of the plateau is in the semi-humid climatic zone and northwestern part of the plateau is in the semi-arid zone (the boundary line, displayed in Fig. 1, is identified by the differences in altitude and climate conditions). Annual precipitation often ranges from about 400 to 600 mm (Tang et al., 2018) and generally decreases from southeast to northwest (Miao et al., 2020). Even though annual precipitation is low, it is highly concentrated in the period from June to September, and the amount during these months accounts for 72% of annual precipitation (Zhang, Gao, Fu, Wang, & Li, 2020). Moreover, the average frequency of extreme precipitation is 1.0–2.1 days per year over the Loess Plateau, and mean annual extreme precipitation decreases spatially from southeast to northwest (Zhang, Gao et al., 2020).

Beginning in the 1950s, vigorous reclamation of sloping farmland (aiming to increase food production) caused serious soil erosion, resulting in the annual sediment load of the Yellow River reaching 1.6 billion tons (Liu, 2016). Fortunately, as a result of a large number of soil and water conservation projects in recent years, especially the GGP, the annual sediment load transported by the Yellow River has sharply dropped to 200–300 million tons (Liu, 2016; Zheng et al., 2019). The GGP includes two aspects: conversion of sloping farmland to forest/grassland and afforestation on barren lands. The total area involved in the GGP across the Loess Plateau had reached about 333,000 km^2 by 2019, accounting for 52% of the plateau area, and the vegetation coverage had increased to 63.6%, which was about double the vegetation area before 2000 (Shan & Xu, 2019). The GGP had effectively promoted natural vegetation coverage, and natural grassland had already made up about 40% of the total land area of the plateau by 2019 (Shan & Xu, 2019).

2.2. Datasets

Monthly runoff depth (mm) data were obtained from the Yellow River Conservancy Commission (YRCC), acquired at 16 hydrological stations over the period spanning 1961 to 2015 (Fig. 1). Observed daily precipitation (mm) data were obtained from the National Meteorological Information Center (https://data.cma.cn/). Precipitation in the watersheds was estimated by kriging interpolation. Table 1 shows the basic information for these 16 basins. Thirty-meter resolution land use/cover datasets for the years 1975, 2000 and 2015 were acquired from the Soil Type Database of China, a nationwide soil dataset based on the Second National Soil Survey. Actual evapotranspiration data from 1982 to 2015 with spatial resolution of 0.25° were obtained from the Global Land Evaporation Amsterdam Model (GLEAM) dataset, described in Martens et al. (2017) and Miralles et al. (2011) (https://www.gleam.eu/#downloads). Normalized difference vegetation index (NDVI) data spanning 1982 to 2015 with spatial resolution of 0.083°, were sourced from the GIMMS dataset (https://www.nasa.gov/nex/data). In addition, daily soil moisture data during the period spanning 1984–2015 with spatial resolution of 0.25° were downloaded from the European Space Agency (ESA) Climate Change Initiative (CCI) programme (https://www.esa-soilmoisture-cci.org).

2.3. Method

2.3.1. Calculating precipitation elasticity (ε_p) based on the Budyko hypothesis

The Budyko hypothesis (Budyko, 1974) states that the long-term water-balance equation for a specific watershed can be expressed as

$$P = R + E + \Delta u \tag{1}$$

where P is the precipitation (mm), R is the runoff depth (mm), E is the actual evapotranspiration (mm) and Δu is the change in water storage inside the watershed; Δu may be negligible over a long period (Gao et al., 2016; Jiang et al., 2015; Liang et al., 2014). Subsequently, the Budyko framework describes the hydrothermal

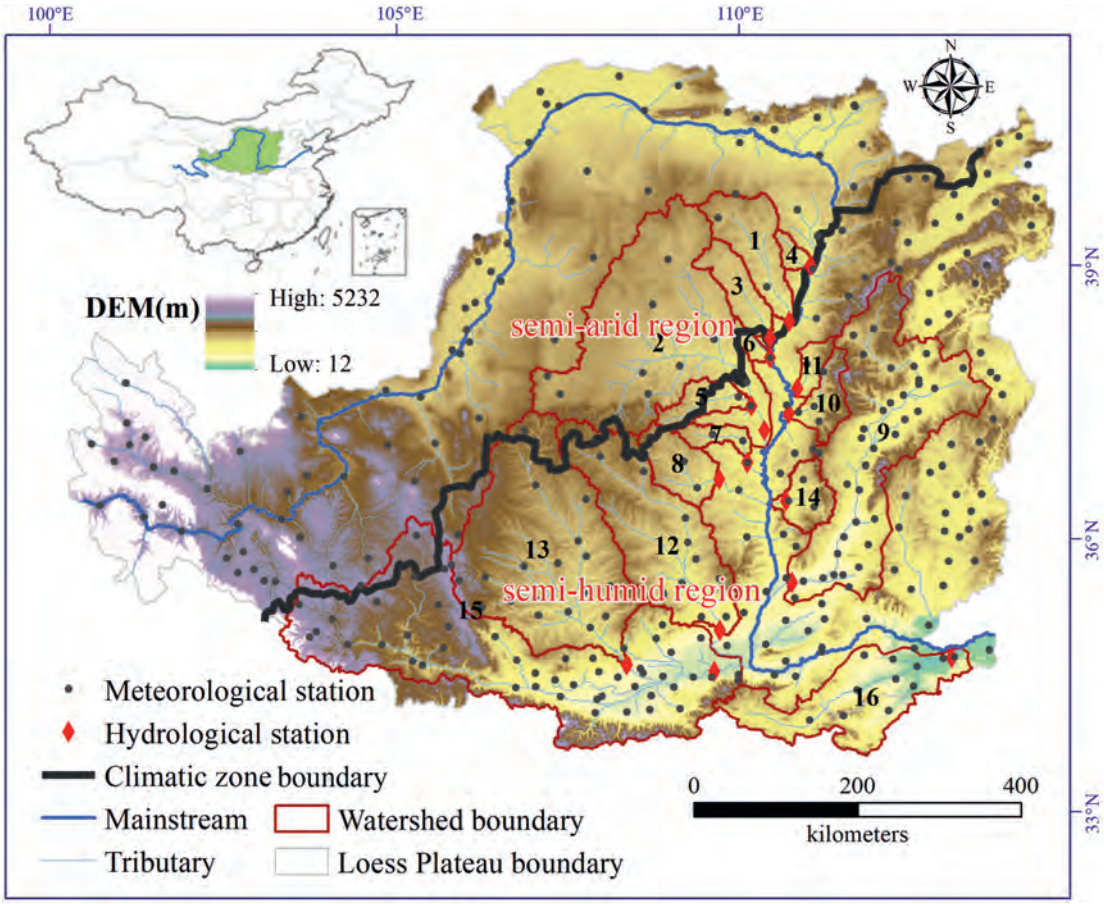

Fig. 1. Locations of meteorological stations and the control hydrological stations of 16 important basins on the Loess Plateau. Detailed information about these basins is in Table 1. The boundary between the climatic zones is sourced from Xiao et al. (2017).

Table 1
Information for 16 basins in Fig. 1.

ID	Basin name	Hydrological station	Latitude (°N)	Longitude (°E)	Control Area (km^2)	Climatic zone	Long-term average annual value		
							P (mm/yr)	E_0 (mm/yr)	*Tmean* (°C)
1	Kuye	Wenjiachuan	110.75	38.43	8621	Semi-arid	384	1015	7.45
2	Wuding	Baijiachuan	110.42	37.23	44,683	Semi-arid	397	1054	7.92
3	Tuwei	Gaojiachuan	110.48	38.25	4955	Semi-arid	416	1036	7.93
4	Gushan	Gaoshiya	111.05	39.05	1260	Semi-arid	418	1039	8.12
5	Dali	Suide	110.23	37.50	3861	Transitional zone	446	1051	7.96
6	Jialu	Shenjiawan	110.48	38.03	1138	Transitional zone	451	1068	8.64
7	Qingjian	Yanchuan	110.18	36.88	2095	Semi-humid	496	1075	8.57
8	Yan	Ganguyi	109.80	36.70	5857	Semi-humid	506	1078	8.24
9	Fen	Hejin	110.80	35.57	39,199	Semi-humid	510	1066	8.77
10	Sanchuan	Houdacheng	110.75	37.42	4027	Semi-humid	513	994	8.26
11	Qiushui	Linjiaping	110.87	37.70	2015	Semi-humid	518	1031	8.00
12	Beiluo	Zhuangtou	109.83	35.03	25,723	Semi-humid	531	1029	8.59
13	Jing	Zhangjiashan	108.60	34.63	43,106	Semi-humid	537	999	8.24
14	Xinshui	Daning	110.72	36.47	3992	Semi-humid	539	1003	8.44
15	Wei	Huaxian	109.77	34.58	106,103	Semi-humid	557	997	8.97
16	Yiluo	Heishiguan	112.93	34.72	18,707	Semi-humid	705	1069	12.60

Note: The order for basins is based on average annual precipitation. "Long term" for *P* (precipitation), E_0 (potential evapotranspiration) and *Tmean* (surface air temperature) refers to 1961 to 2015.

regime of a watershed, which is shown as

$$\frac{E}{P}=f\left(\frac{E_0}{P}\right)=f(\phi) \tag{2}$$

Here, E_0 is the potential evapotranspiration (mm), and ϕ ($=E_0/P$) is the multi-year average dryness index. Budyko (1974) illustrated that $\phi < 1$ reflects an energy-limited basin and $\phi > 1$ reflects a water-limited basin. Different detailed Budyko-type equations have been developed in recent years (Wu et al., 2017). The nonlinear mathematical equation used in this study was developed by Choudhury (1999), as follows:

$$f(\phi) = \frac{\phi}{[1 + (\phi)^n]^{1/n}} \tag{3}$$

where the parameter n reflects the basin characteristics such as soil properties, slope, vegetation cover and climate seasonality (Yang et al., 2008; Yang, Lu, Yang, & Hu, 2012). The n value of each year can be determined through Eqs. (1)–(3) with known P, R and E_0. Here, we assume that the Δu in Eq. (1) is negligible during a long period, which we consider to be 5 years in this research (Wu et al., 2017). The value of n is calculated with a 5-year sliding window. Taking a specific basin as an example, the n value in 1963 is calculated using annual P, R and E_0 values from 1961 to 1965. Fig. S1 displays the changes in n for 16 basins on the Loess Plateau, and larger n values have more distinctive changes in basin characteristics, especially land use. In addition, E_0 from 1961 to 2015 is calculated by the Hargreaves and Samani method (Hargreaves & Samani, 1985).

From Eqs. (1) and (2), the observed runoff depth (R) can be transformed as a function of P and ϕ:

$$R = P(1 - f(\phi)) \tag{4}$$

Then, we define the elasticity of R in response to P: $\varepsilon_p = \frac{\partial R/R}{\partial P/P}$. According to Eq. (4), the ε_p can be calculated as

$$\varepsilon_p = \frac{\partial R}{\partial P}\cdot\frac{P}{R} = 1 + \frac{\phi f'(\phi)}{1 - f(\phi)} \tag{5}$$

Finally, we use the detailed Budyko-Choudhury equation (Eq. (3)) to get specific expressions for ε_p:

$$\varepsilon_p = \frac{1 - \frac{1}{(1+\phi^{-n})^{1+\frac{1}{n}}}}{1 - \frac{1}{(1+\phi^{-n})^{\frac{1}{n}}}} \tag{6}$$

With the annual P, E_0 and n values from 1961 to 2015, we calculated ε_p in each year for every basin (see Fig. S2). Greater elasticity indicates more sensitivity of runoff depth to precipitation. Fig. 2 displays the relations between multiyear average elasticity (ε_p) and the dryness index (ϕ) for 16 basins on the Loess Plateau. It shows that all basins on the Loess Plateau belong to water-limited areas; the lower the annual precipitation, the higher the dryness index. Moreover, the mean elasticity across the southeastern region (basin IDs 7–15) is generally larger than that across the northwestern region (basin IDs 1–6).

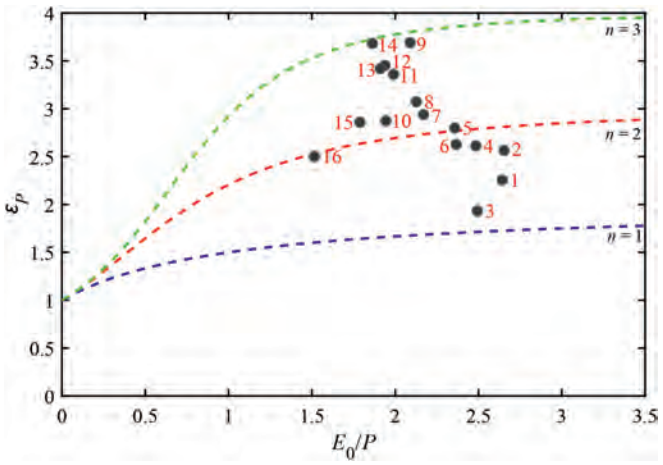

Fig. 2. Relationship between ε_p (the elasticity of runoff depth (R) in response to precipitation (P)) and ϕ (E_0/P) for 16 basins (numbered in red) on the Loess Plateau. Here the parameter n reflects the basin characteristics in the Budyko framework.

2.3.2. Calculating runoff coefficient exclusively attributable to land use/cover change (C_1)

For a closed basin, the changes in observed runoff depth (ΔR_0) are caused by the changes in actual evapotranspiration and precipitation. Here, we assume that domestic and industrial water consumption remains at the same level over a long-term period.

$$\Delta R_0 = \Delta R_1 + \Delta R_2 \tag{7}$$

ΔR_1 is the runoff depth change caused by actual evapotranspiration variation and ΔR_2 is that caused by precipitation variation. Actual evapotranspiration is closely related to precipitation, LUCC (in this research, NDVI is introduced to reflect the LUCC), and temperature changes across the Loess Plateau. Further, Fig. S3 and Table S1 illustrate that precipitation and especially NDVI are the vital driving factors affecting actual evapotranspiration in most regions of the plateau. In other words, temperature rising has the smallest effect on ΔR_1 out of these three factors. Since that precipitation changes directly affect runoff depth while temperature changes indirectly affect it through changing the evaporation and transpiration of the underlying surface, we regard the effects of temperature changes as the results of underlying surface changes in this study. Moreover, we also discuss the effects of domestic and industrial water consumption changes on the ΔR_1 in the supplementary information.

The ΔR_1 in each year can be calculated as follows:

$$\Delta R_1 = \Delta R_0 - \Delta R_2 \tag{8}$$

As mentioned above, $\varepsilon_p = \frac{\Delta R_2/R_0}{\Delta P/P}$, so

$$\Delta R_2 = R_0 \cdot \varepsilon_p \cdot \frac{\Delta P}{P} = R_0 \cdot \varepsilon_p \cdot \frac{P - \overline{P}}{\overline{P}} \tag{9}$$

where $\overline{P}$ is the mean annual precipitation (mm), P is annual precipitation (mm) and R_0 is annual observed runoff depth (mm).

To reflect the runoff generation capacity for a basin, we define

$$C_0 = R_0/P \tag{10}$$

and

$$C_1 = R_1/P \tag{11}$$

C_0 reflects the observed runoff generation capacity for a basin, and C_1 reflects the actual runoff generation capacity after removing the influence of changes in precipitation.

3. Results

3.1. Observed runoff (R_0) and runoff coefficient (C_0) before and after the GGP

The average runoff coefficients indeed become lower during the period 2000–2015 in comparison to the earlier period, 1961–1999 (Fig. 3). The C_0 for the 16 basins ranges from 0.08 to 0.14 (25^{th}–75^{th} percentile) during 1961–1999 and from 0.04 to 0.08 during 2000–2015. Runoff coefficients for all basins decline by 26%–76%, and for 5 basins, they decline by > 50%. C_0 values in the Kuye (ID 1) and Gushan (ID 4) Rivers show the greatest declines, both > 65%. In addition, basins in semi-arid areas generally show a greater decline than those in semi-humid areas, averaging 51% for basin IDs 1–6 and 40% for IDs 7–16.

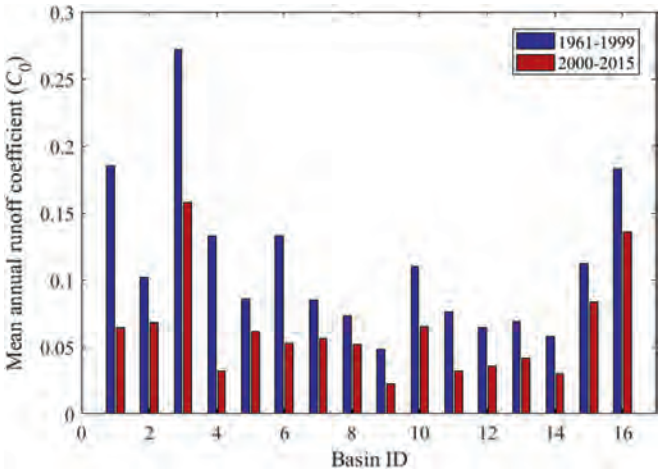

Fig. 3. Mean annual runoff coefficient (C_0) for 16 basins during 1961–1999 and 2000–2015.

Annual observed runoff depth (R_0) trends during the periods 1961–1999 and 2000–2015 are distinctly different (Fig. 4 and S4). Before 1999, both R_0 and C_0 show significant decreasing trends ($p < 0.05$) for 12 out of 16 basins. However, after 1999, the trends for R_0 and C_0 exhibit obvious spatial differences. The rates of change for R_0 range from −0.16 to 1.64 mm/year, with a mean value of 0.37 mm/year. Most values of C_0 throughout the northwestern plateau (basin IDs 1–7) show decreasing trends; most values throughout the southeast (IDs 8–16) show upward or stable trends. Overall, 9 out of 16 basins show an upward trend for C_0.

3.2. Change in precipitation and erosive rainfall

Precipitation has an extremely important impact on the runoff generation capacity for basins, reflected in not only spatial scales but also time scales. Fig. 5 shows annual precipitation trends have undergone a distinct shift between the two periods of 1961–1999 and 2000–2015: precipitation for most basins shows a clear downward trend from 1961 to 1999 (7 basins with significant declines), but then it shows a clear upward trend for 2000 to 2015. According to precipitation datasets for the two periods, the average annual precipitation for 8 basins increased by 10–44 mm. In addition, many previous studies have mentioned that heavy rainfall is the dominant form of precipitation on the Loess Plateau (Wu et al., 2018), which determines the most important pattern of runoff generation here: infiltration-excess runoff, which is when the precipitation intensity exceeds infiltration capacity. Results for erosive rainfall (daily precipitation > 12 mm/day; Xie et al., 2000), which is the dominant form that generates actual runoff, are exhibited in Fig. 6. It shows that the frequency of erosive rainfall for 83% of stations increased from 2000 to 2015. Moreover, the annual erosive precipitation for 81% of stations also increased, especially in the central and southern plateau. The rate of increase in erosive rainfall over these basins is 4.6 mm/year. Therefore, we find that the increasing annual precipitation after 2000 is mostly in the form of erosive rainfall, which would greatly affect the annual runoff coefficient (C_0).

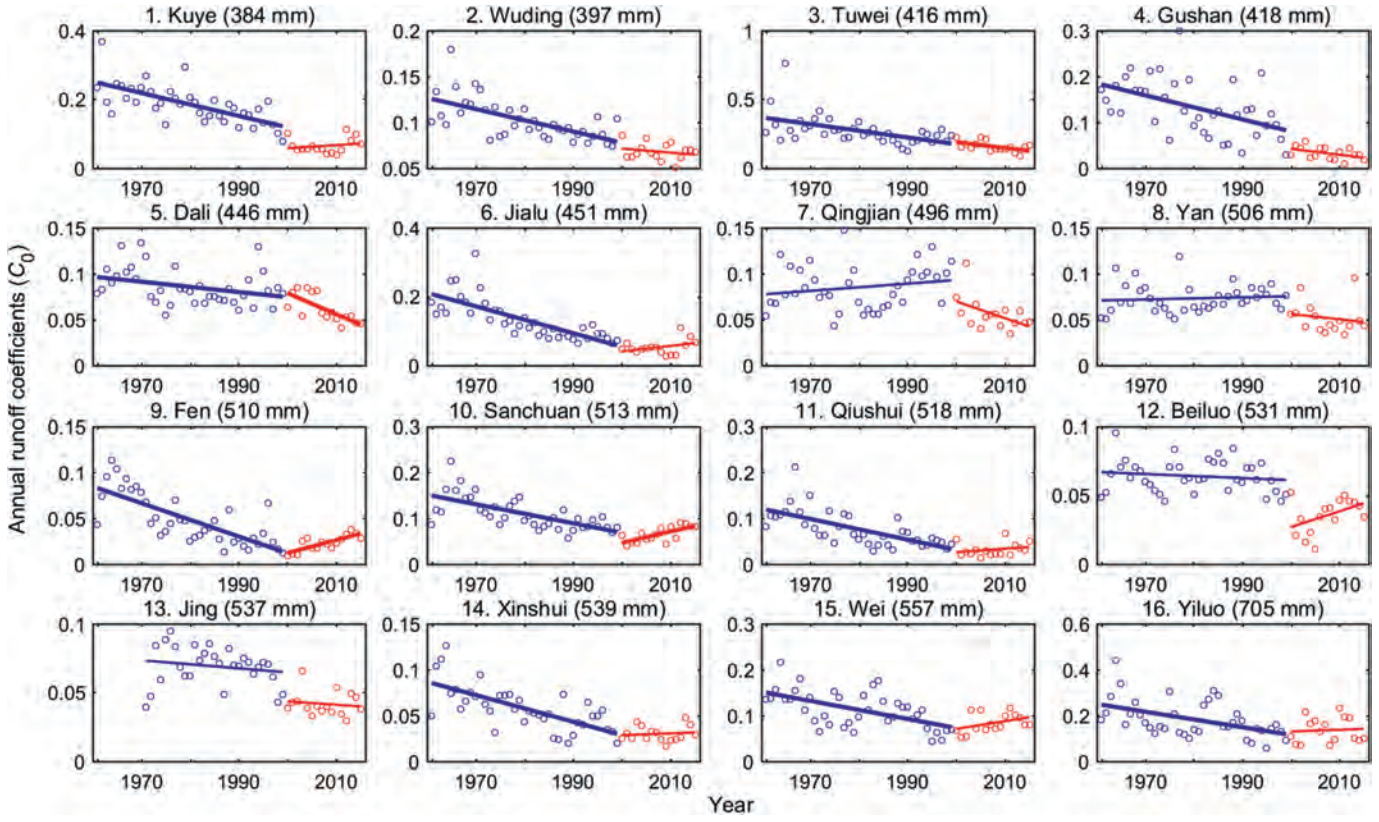

Fig. 4. Annual runoff coefficients (C_0) for 16 basins during 1961–1999 and 2000–2015. Blue and red lines show the trends for each period. Bold lines indicate trends that are significant at $p < 0.05$. The numbers in parentheses in the subtitles give the mean annual precipitation from 1961 to 2015 for that basin. The runoff depth data during 1961–1970 for basin ID 13 are missing.

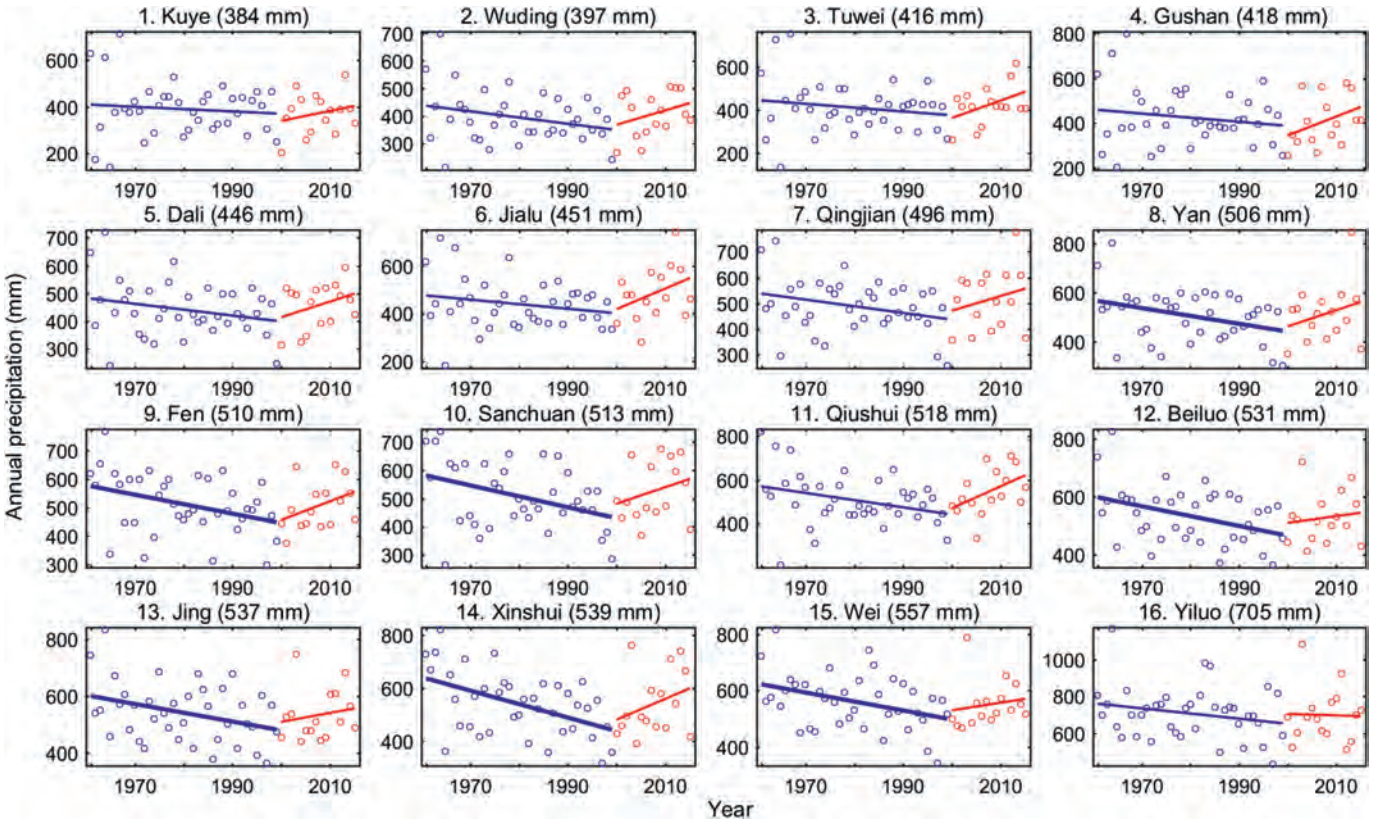

Fig. 5. Annual precipitation trends for 16 basins during 1961–1999 and 2000–2015. Blue and red lines show the trends for each period. Bold lines indicate trends that are significant at $p < 0.05$. The numbers in parentheses in the subtitles give the mean annual precipitation from 1961 to 2015 for each basin.

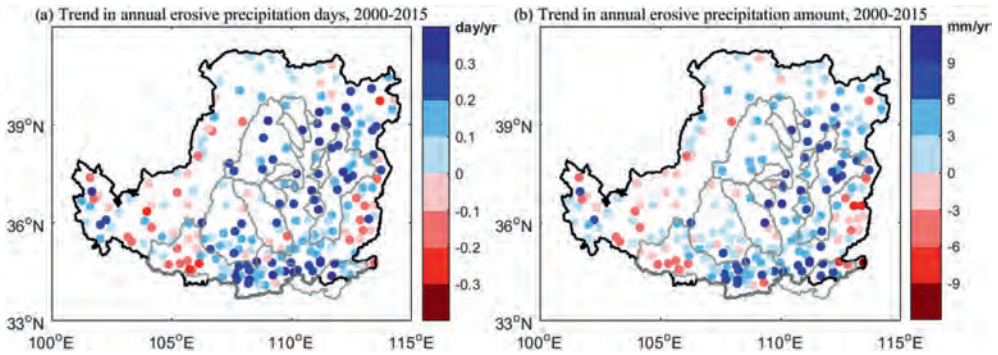

Fig. 6. (a) Trend in number of days with $P > 12$ mm and (b) trend in precipitation amount for the days with $P > 12$ mm during 2000 to 2015.

3.3. Runoff coefficient exclusive of precipitation variation (C_1) before and after the GGP

Since precipitation has a large impact on the runoff coefficient, we remove the part of runoff variation caused by annual precipitation variation through an elasticity method based on the Budyko framework (section 2.3) and calculate runoff depth (R_1) and runoff coefficient (C_1) exclusively attributable to land use/cover change; the results are shown in Fig. S6 and Fig. 7. The positive value of elasticity of runoff depth in response to precipitation (Fig. 2) offsets part of the trend of C_0 (or R_0). Differing from the trends in R_0 and C_0 in the period 1961–1999, both R_1 and C_1 show a stable trend for about half of the basins. After 1999, because of the persistent effects of the GGP, C_1 shows distinct spatial differences. For basin IDs 9, 10, 12 and 15, the trends in C_1 are slight. The upward rate of change for C_1 for basin ID 16 is 1.96% per year, and noteworthily, the downward rates of change for C_1 for the other 11 basins are between 2.4% and 6.0% per year. Overall, the rate of reduction of the runoff depth or the runoff coefficient in the semi-arid zone is about four times what it is in the semi-humid zone.

Compared with the period 1961–1999, the decrease in mean C_1 after the GGP for the 16 basins ranges from 34% to 52% (25^{th}–75^{th} percentile), with a mean decrease of 44%. Considering that the actual runoff generation capacity for specific basins does not show upward trends, we suggest the combined actions of the GGP and engineering measures (e.g., check dams, terraces, reservoirs, etc.) have a stronger capacity to decrease runoff than engineering measures alone. The greatest declines of C_1 are in the Gushan (ID 4) and Jialu (ID 6) River basins, both > 68% after the GGP compared with before the GGP, which probably is related to the relatively

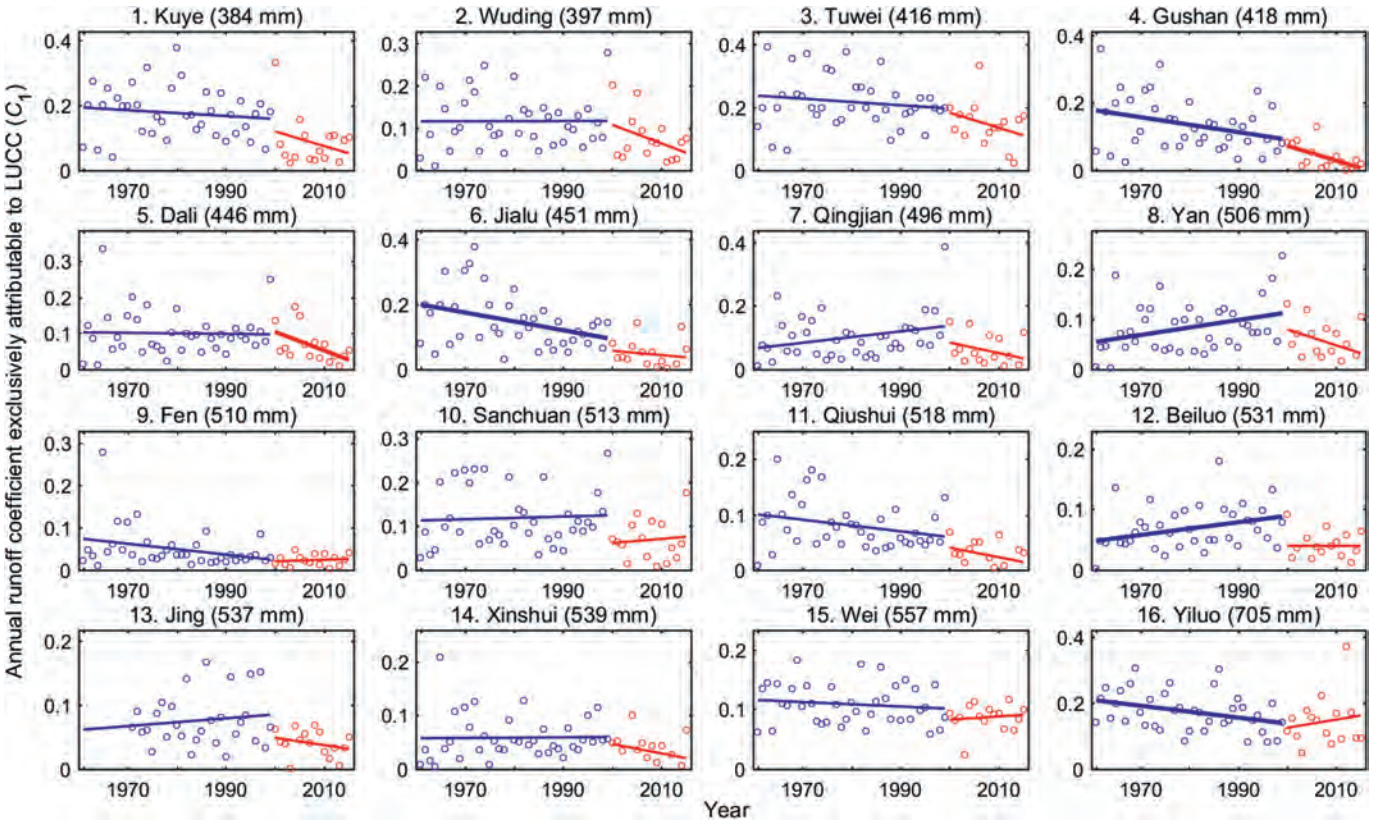

Fig. 7. Changes in the annual runoff coefficient exclusively attributable to land use/cover change (C_1) for 16 basins during 1961–1999 and 2000–2015. Blue and red lines show the trends in each period. Bold lines indicate trends that are significant at $p < 0.05$. The numbers in parentheses on the subtitles are the mean annual precipitation from 1961 to 2015. The runoff depth data during 1961–1970 for basin ID 13 are missing.

small areas of these basins, 1260 and 1138 km^2, respectively. The runoff generation capacity of small watersheds in the semi-arid or arid zone is more easily affected by external factors (Liu, 2016), such as a large degree of land use change of the whole basin. Moreover, the large decrease of C_1 in the Jialu basin may also be related to the great increase of forest land area (7%).

4. Discussion

Fig. 8 shows the drastic changes in land use after the GGP. The major transitions are from agricultural land to grassland (cyan color) and from grassland to forest (medium green color). The increases in forest land areas mainly appear in the Beiluo basin (ID 12), the lower reaches of the Jing basin (ID 13), and the middle and southern reaches of the Wei basin (ID 15), while grassland increased in most regions of the plateau. Table 2 shows the net percent change in land use area from 2000 to 2015. Agricultural land area for these 16 basins decreased by 18%–48%; grassland area in the northwestern region increased by 28%–47%; and forest land area increased by > 10% for most basins in the semi-humid area. Even though the construction of check dams during this period is also notable (Miao et al., 2020), Zhang et al. (2019) reported that reforestation after the GGP has had more important impacts on the runoff coefficient than check dams have had; this is because vegetation interception always takes place in the first step of runoff generation, and more importantly, the soil and water conservation measures areas (e.g., farmland returning to forest or grass; reforestation) on the sloped lands are much larger than the control areas of water conservation measures in the channels (e.g., check dams and reservoirs). Given that annual precipitation on the Loess Plateau increased visibly from 2000 to 2015 (Fig. 5), the combined and opposing effects of these influencing factors make the changes in the runoff coefficient seem more complicated than we might expect. But in general, the mean runoff generation capacity has declined after the GGP (Fig. 7), which is consistent with the conclusions of many previous researchers (Wang et al., 2011; Wu et al., 2020; Zhang, Shao, Zhao, & Wu, 2020).

Most regions across the Loess Plateau are water limited (precipitation < potential evapotranspiration), especially in the northwest. Here, the evapotranspiration (including transpiration, interception evaporation, and soil evaporation) is a key factor affecting the water discharge. The main factors affecting actual evapotranspiration include climatic conditions (dryness index), surface material composition (e.g., soil type, rocky content) and vegetation characteristics (including vegetation type, growth status, vegetation area, etc.). More generally, vegetation associated with check dam systems (Li et al., 2018) is more efficient for increasing infiltration and evapotranspiration. After the GGP, because of the absence of human interference, vegetation coverage has become more stable over time. Stems, leaves, vegetation litter and root systems play more stable roles in reducing runoff. Generally speaking, the larger the vegetation area, the stronger the evapotranspiration, assuming constant vegetation density (Ma et al., 2019). The dryness index also has a large impact on the evapotranspiration (Liu et al., 2014). As the dryness index increases from the southeast to the northwest on the Loess Plateau, the actual runoff generation capacity (C_1) in the northwestern region has dropped much more substantially than in the southeast following the initiation of the GGP (Fig. 7). By our calculation, the annual evapotranspiration increased at a mean rate of 5.8 mm/year from

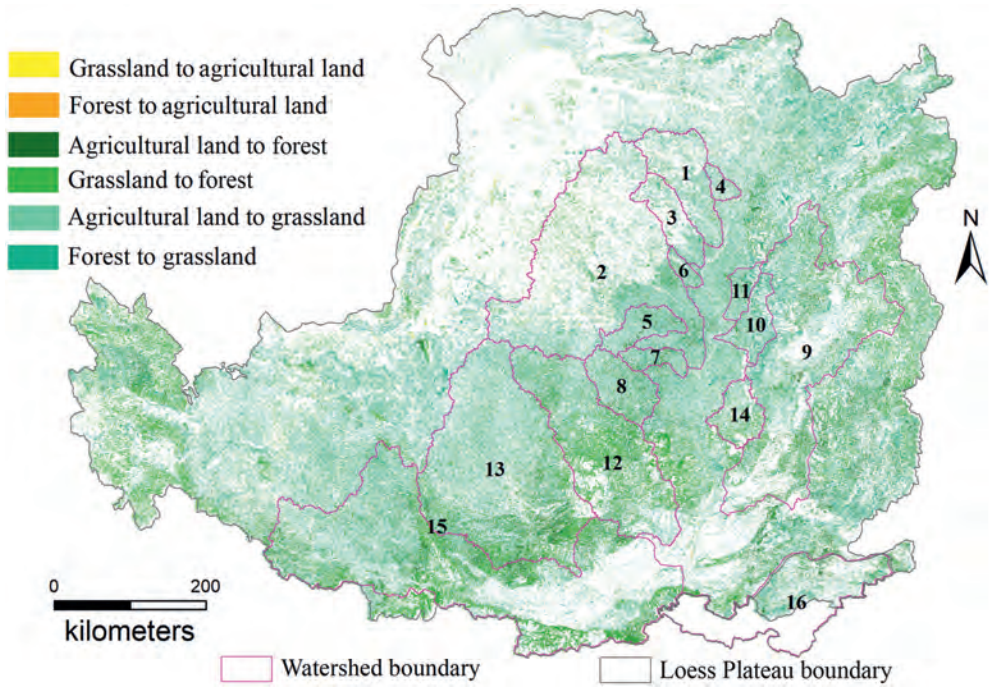

Fig. 8. Spatial transitions among grassland, forest and agricultural land from 2000 to 2015 on the Loess Plateau. White areas in this figure had no changes in land use, or they had other land use transitions not shown here.

Table 2
Net rate of change in land use area (forest/shrubland, grassland and agricultural land) from 1975 to 2000 and from 2000 to 2015 for 16 basins.

ID	Name	From 1975 to 2000			From 2000 to 2015		
		Forest/Shrubland	Grassland	Agricultural land	Forest/Shrubland	Grassland	Agricultural land
1	Kuye	< 1%	< 1%	< 1%	−4%	**28%**	**−20%**
2	Wuding	< 1%	< 1%	< 1%	< 1%	**30%**	**−18%**
3	Tuwei	< 1%	1%	< 1%	−2%	**45%**	**−19%**
4	Gushan	< 1%	< 1%	< 1%	−5%	**28%**	**−27%**
5	Dali	< 1%	< 1%	< 1%	−3%	**47%**	**−48%**
6	Jialu	< 1%	< 1%	< 1%	7%	**39%**	**−43%**
7	Qingjian	< 1%	< 1%	< 1%	−2%	**41%**	**−41%**
8	Yan	< 1%	< 1%	< 1%	9%	**27%**	**−38%**
9	Fen	3%	−3%	−1%	< 1%	13%	**−19%**
10	Sanchuan	< 1%	< 1%	< 1%	**−17%**	**37%**	**−23%**
11	Qiushui	< 1%	< 1%	< 1%	−4%	**38%**	**−35%**
12	Beiluo	< 1%	< 1%	< 1%	**16%**	1%	**−19%**
13	Jing	< 1%	< 1%	< 1%	11%	**16%**	**−28%**
14	Xinshui	2%	−2%	< 1%	8%	7%	**−18%**
15	Wei	< 1%	1%	−1%	12%	10%	**−25%**
16	Yiluo	1%	−1%	−1%	1%	12%	**−19%**

Bold means a change of >15%.

2000 to 2015 (Zhang, Shao et al., 2020; Zhou et al., 2019); Fig. 9 also shows, moreover, that both transpiration and interception loss from 2000 to 2015 have increasing trends on most regions of the plateau, especially in key GGP areas (i.e., the central plateau). Actual evapotranspiration increasing is the main direct reason for most of the C_1 decline. Understandably, if the increase in the rate of actual evapotranspiration is smaller than that of precipitation, observed runoff depth will show an increasing trend (Fig. S5). In other words, the increase in the observed runoff coefficient for some basins in recent years (Fig. 4) is mainly due to the increase in annual precipitation, not to a greater capacity for runoff generation.

Further, the characteristics of vegetation root systems (such as root length and density) can affect the soil water content and thus change water storage capacity (Gou et al., 2021). After returning farmland to forest, surface soil moisture increased in the southeast and decreased in most areas of the northwest (Fig. 10a). As for areas showing the opposite changes, we speculate that this may have a close correlation with geomorphology on the Loess Plateau (Fig. 10b). The figure shows that surface soil water storage capacity becomes stronger (soil moisture increases) in most of the southeastern plateau, where the geomorphology is mostly composed of rocky mountains and *Yuan* landforms (loess flat highland areas). Zheng et al. (2020) reported that soil water storage in forests and grasslands reaches 70–80% of total precipitation and is used for vegetation growth or evaporation, which means that less water discharges at watershed outlets. Moreover, the surface soil moisture depends strongly on the precipitation, whereas the deeper soil water content has actually declined in some areas due to the GGP during the past decade (Cheng et al., 2014; Gao et al., 2017; Liu et al., 2017).

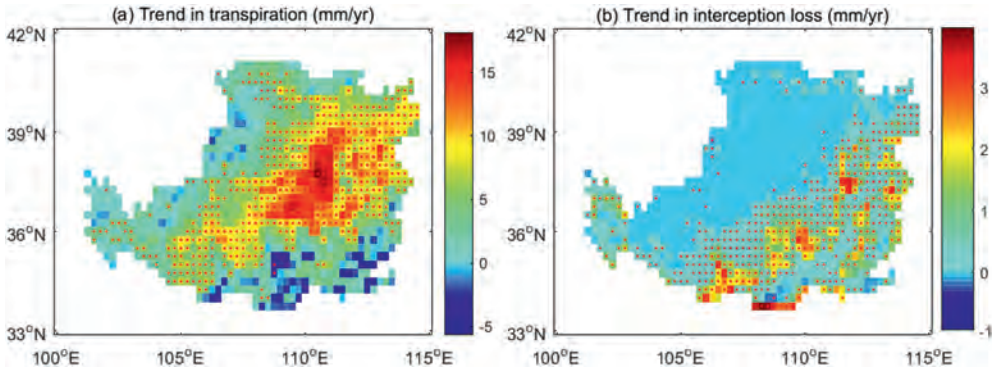

Fig. 9. Trends in (a) transpiration and (b) interception loss on the Loess Plateau from 2000 to 2015. Spatial resolution is 0.25°. The red dots represent significant trends at $p < 0.05$.

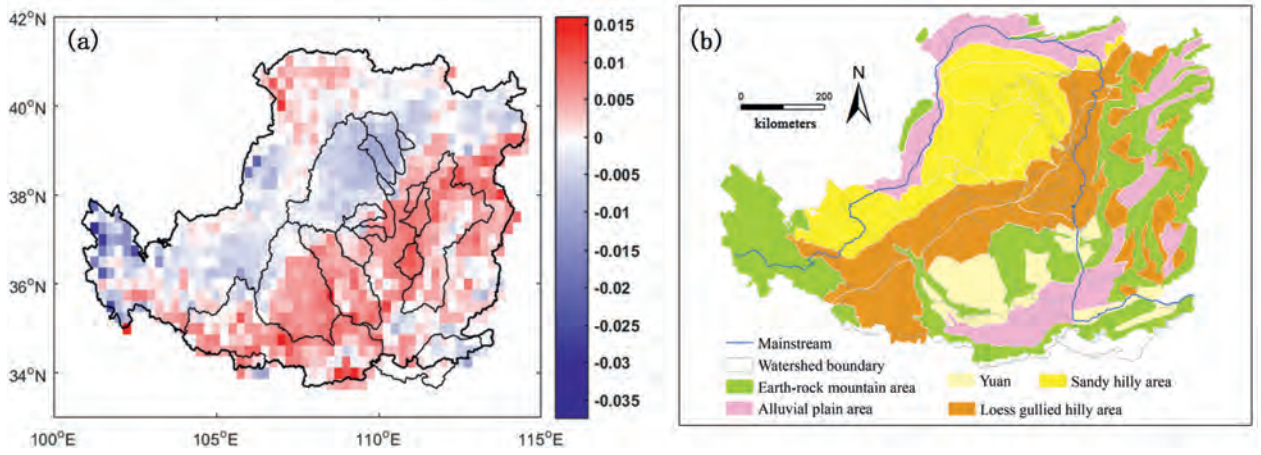

Fig. 10. (a) Differences in mean daily soil moisture (volumetric water content, m^3 water /m^3 soil) of top soil layer between 1984–1999 and 2000–2015. (b) The geomorphology of the Loess Plateau. There are five basic geomorphological types on the Loess Plateau: the earth-rock mountain area, the alluvial plain area, the loess flat highland area (*Yuan*), the sandy hilly area, and the loess gullied hilly area.

In addition, as for the Yiluo River basin (ID 16), the mean runoff coefficient is relatively larger than in most of the other basins during 2000–2015 (Fig. 3), and it shows a slight upward trend (Fig. 4 and Fig. 7), which is mostly determined by two key conditions: adequate precipitation and special geomorphic features (such as the relatively shallow soil layer and location of earth-rock mountain). In these areas, saturation-excess runoff (i.e., when the soil is saturated) is a major pattern generating runoff (Li et al., 2015), rather than infiltration-excess runoff (in which the precipitation intensity exceeds infiltration capacity), and the capacity of generating runoff tends to be enhanced with increased vegetation area.

5. Conclusions

To investigate the actual effect of the GGP on runoff generation capacity on the Loess Plateau, we utilize a Budyko-framework elasticity method to remove the effect of precipitation variation and to calculate the runoff depth (R_1) and runoff coefficient (C_1) exclusively attributable to LUCC. It is found that the mean annual runoff coefficients decline by 26%–76% during the period 1961–1999 when comparing with the period 2000–2015. We notice that the observed runoff coefficient (C_0) for 9 out of 16 basins shows an upward trend after GGP, which is mainly due to the increase of erosive rainfall from 2000 to 2015, and the rate of increase in erosive rainfall over 16 basins is 4.6 mm/year. After removing the effect of precipitation variation, we find that the R_1 values in 11 out 16 basins show decreasing trends following GGP with the rates ranging from −3.23 to −0.38 mm/year, and the corresponding downward rates of change in C_1 are between 2.4% and 6.0% per year. Compared to the earlier period, the decrease in C_1 ranges from 34% to 52% (25^{th}–75^{th} percentile), with a mean decrease of 44% in the later period. In addition, the reduction rate of the runoff coefficient in the semi-arid zone is about four times that in the semi-humid zone. We conclude that implementation of the GGP on a large scale has reduced the actual runoff generation capacity in water-limited areas, especially in the northwestern plateau (semi-arid zone), because of greater evapotranspiration.

Declaration of competing interest

The authors declare that they have no known competing financial interests or personal relationships that could have appeared to influence the work reported in this paper.

Acknowledgements

This research was supported by the National Natural Science Foundation of China (No. 41877155), and the National Key Research and Development Program of China (No. 2016YFC0501604). We are grateful to the Yellow River Conservancy Commission (YRCC) (http://www.yrcc.gov.cn) and the National Geographic Resource

Science SubCenter, National Earth System Science Data Center, National Science & Technology Infrastructure of China (http://gre.geodata.cn) for providing the observed water discharge and sediment load, and to China Meteorological Administration (CMA) (http://data.cma.cn/) for providing the precipitation data. We would like to thank the high-performance computing support from the Center for Geodata and Analysis, Faculty of Geographical Science, Beijing Normal University (https://gda.bnu.edu.cn/).

Appendix A. Supplementary data

Supplementary data to this article can be found online at https://doi.org/10.1016/j.iswcr.2021.04.009.

References

Almeida, W. S., Seitz, S., Oliveira, L., & Carvalho, D. F. (2020). Duration and intensity of rainfall events with the same erosivity change sediment yield and runoff rates. *International Soil and Water Conservation Research*. https://doi.org/10.1016/j.iswcr.2020.10.004

Budyko, M. I. (1974). *Climate and life*. New York, CA: Academic Press.

Cheng, L., Liu, W., & Li, Z. (2014). Soil water in deep layers under different land use patterns on the Loess Tableland. *Acta Geographica Sinica, 34*(8), 1975–1983 (*In Chinese*).

Chen, B., Krajewski, W. F., Helmers, M. J., & Zhang, Z. (2018). Spatial variability and temporal persistence of event runoff coefficients for cropland hillslopes. *Water Resources Research, 55*(2), 1583–1597.

Choudhury, B. J. (1999). Evaluation of an empirical equation for annual evaporation using field observations and results from a biophysical model. *Journal of Hydrology, 216*(1–2), 99–110.

Dwarakish, G. S., Ganasri, B. P., & De Stefano, L. (2015). Impact of land use change on hydrological systems: A review of current modeling approaches. *Cogent Geoscience, 1*(1), 1115691.

Filoso, S., Bezerra, M. O., Weiss, K. C. B., & Palmer, M. A. (2017). Impacts of forest restoration on water yield: A systematic review. *PLoS One, 12*(8), Article e0183210.

Fu, B., Wang, S., Liu, Y., Liu, J., Liang, W., & Miao, C. (2017). Hydrogeomorphic ecosystem responses to natural and anthropogenic changes in the Loess Plateau of China. *Annual Review of Earth and Planetary Sciences, 45*, 223–243.

Gao, G., Fu, B., Wang, S., Liang, W., & Jiang, X. (2016). Determining the hydrological responses to climate variability and land use/cover change in the Loess Plateau with the Budyko framework. *The Science of the Total Environment, 557–558*, 331–342.

Gao, H., Pang, G., Li, Z., & Ceng, S. (2017). Evaluating the potential of vegetation restoration in the Loess Plateau, 05 *Acta Geographica Sinica, 72*, 863–874 *(*In Chinese*)*.

Gou, J., Miao, C., Samaniego, L., Xiao, M., Wu, J., & Guo, X. (2021). CNRD v1.0: A high-quality natural runoff dataset for hydrological and climate studies in China. *Bulletin of the American Meteorological Society*. https://doi.org/10.1175/BAMS-D-20-0094.1

Hargreaves, G. H. A., & Samani, Z. (1985). Reference crop evapotranspiration from temperature. *Applied Engineering in Agriculture, 1*(2), 96–99.

Jiang, C., Xiong, L., Wang, D., Liu, P., Guo, S., & Xu, C. (2015). Separating the impacts of climate change and human activities on runoff using the Budyko-type equations with time-varying parameters. *Journal of Hydrology, 522*, 326–338.

Kim, J. B., Im, E. S., & Bae, D. H. (2019). Intensified hydroclimatic regime in Korean basins under 1.5 and 2 °c global warming. *International Journal of Climatology, 40*(1), 1965–1978.

Kong, D., Miao, C., Duan, Q., Lei, X., & Li, H. (2018). Vegetation-climate interactions on the Loess Plateau: A nonlinear granger causality analysis. *Journal of Geophysical Research Atmospheres*. https://doi.org/10.1029/2018JD029036

Liang, W., Bai, D., Wang, F., Fu, B., Yan, J., Wang, S., Yang, Y., Long, D., & Feng, M. (2014). Quantifying the impacts of climate change and ecological restoration on streamflow changes based on a Budyko hydrological model in China's Loess Plateau. *Water Resources Research, 51*(8), 6500–6519.

Li, Z., Huang, P., Zhang, Y., Yao, C., Yan, C., & Huo, W. (2015). Analyses on annual inhomogeneity characteristic of precipitation and its variation. *Yellow River, 37*(10), 1–6 *(*In Chinese).

Li, J., Liu, Q., Feng, X., Shi, W., Fu, B., Lü, Y., & Liu, Y. (2018). The synergistic effects of afforestation and the construction of check-dams on sediment trapping: Four decades of evolution on the Loess Plateau. *Land Degradation & Development, 30*(6), 622–635.

Li, E., Mu, X., Zhao, G., Gao, P., & Sun, W. (2016). Effects of check dams on runoff and sediment load in a semi-arid river basin of the Yellow River. *Stochastic Environmental Research and Risk Assessment, 31*, 1791–1803.

Liu, X. (2016). *Causes of decline in water discharge and sediment load of Yellow River's in recent years*. Beijing: Science Press *(*In Chinese).

Liu, X., Liu, C., Yang, S., Jin, S., Gao, Y., & Gao, Y. (2014). Influences of shrubs-herbs-arbor vegetation coverage on the runoff based on the remote sensing data in Loess Plateau. *Acta Geographica Sinica, 69*(11), 1595–1603 *(*In Chinese).

Liu, Q., & McVicar, T. R. (2012). Assessing climate change induced modification of Penman potential evaporation and runoff sensitivity in a large water-limited basin. *Journal of Hydrology, 464–465*, 352–362.

Liu, G., Shangguan, Z., Yao, W., Yang, Q., Zhao, M., Dang, X., Guo, M., Wang, G., & Wang, B. (2017). Ecological effects of soil conservation in Loess Plateau, 01 *Bulletin of Chinese Academy of Sciences, 32*, 11–19 *(*In Chinese*)*.

Liu, B., Xie, Y., Li, Z., et al. (2020). The assessment of soil loss by water erosion in China. *International Soil and Water Conservation Research, 8*, 430–439.

Martens, B., Miralles, D. G., Lievens, H., van der Schalie, R., de Jeu, R. A. M., Fernández-Prieto, D., Beck, H. E., Dorigo, W. A., & Verhoest, N. E. C. (2017). GLEAM v3: Satellite-based land evaporation and root-zone soil moisture. *Geoscientific Model Development, 10*, 1903–1925.

Ma, Z., Yan, N., Wu, B., Stein, A., Zhu, W., & Zeng, H. (2019). Variation in actual evapotranspiration following changes in climate and vegetation cover during an ecological restoration period (2000–2015) in the Loess Plateau, China. *The Science of the Total Environment, 689*, 534–545.

Merz, R., Blöschl, G., & Parajka, J. (2006). Spatio-temporal variability of event runoff coefficients. *Journal of Hydrology, 331*, 591–604.

Miao, C., Duan, Q., Sun, Q., Lei, X., & Li, H. (2019). Non-uniform changes in different categories of precipitation intensity across China and the associated large-scale circulations. *Environmental Research Letters, 14*, Article 025004.

Miao, C., Zheng, H., Jiao, J., Feng, X., Duan, Q., & Mpofu, E. (2020). The changing relationship between rainfall and surface runoff on the Loess Plateau, China. *Journal of Geophysical Research: Atmosphere, 125*, Article e2019JD032053.

Milly, P. C., Dunne, K. A., & Vecchia, A. V. (2005). Global pattern of trends in streamflow and water availability in a changing climate. *Nature, 438*, 347–350.

Miralles, D. G., Holmes, T. R. H., de Jeu, R. A. M., Gash, J. H., Meesters, A. G. C. A., & Dolman, A. J. (2011). Global land-surface evaporation estimated from satellite-based observations. *Hydrology and Earth System Sciences, 15*, 453–469.

Mu, X., Gu, C., Sun, W., Zhao, G., Gao, P., & Wang, S. (2019). Preliminary assessment effect of vegetation restoration on runoff generation pattern of the Loess Plateau. *Yellow River, 41*, 31–39 *(*In Chinese).

Mu, X., Xu, X., & Wang, W. (1998). The impact of high-level controlling of soil and water loss on watershed runoff in the Loess Plateau. *Journal of Arid Land Resources & Environment, 12*, 119–126 *(*In Chinese).

Shan, L., & Xu, B. (2019). Discussion on some issues about returning farmland to forest or grassland on Loess Plateau in new era. *Journal of Soil and Water Conservation, 39*(6), 295–297 (In Chinese).

Shi, W., & Huang, M. (2021). Predictions of soil and nutrient losses using a modified SWAT model in a large hillygully watershed of the Chinese Loess Plateau. *International Soil and Water Conservation Research*. https://doi.org/10.1016/j.iswcr.2020.12.002

Sun, G., Gao, H., & Hao, L. (2020). Comments on "large-scale afforestation significantly increases permanent surface water in China's vegetation restoration regions. In Y. Zeng, X. Yang, N. Fang, & Z. Shi (Eds.), *(2020). Agricultural and forest meteorology* (Vol. 290, p. 108001). Agricultural and Forest Meteorology, 296.

Sun, Q., Miao, C., Hanel, M., Borthwick, A. G. L., Duan, Q., Ji, D., & Li, H. (2019). Global heat stress on health, wildfires, and agricultural crops under different levels of climate warming. *Environment International, 128*, 125–136.

Tang, X., Miao, C., Xi, Y., Duan, Q., Lei, X., & Li, H. (2018). Analysis of precipitation characteristics on the loess plateau between 1965 and 2014, based on high-density gauge observations. *Atmospheric Research, 213*, 264–274.

Tuset, J., Vericat, D., & Batalla, R. J. (2015). Rainfall, runoff and sediment transport in a Mediterranean mountainous catchment. *The Science of the Total Environment, 540*, 114.

Velpuri, N. M., & Senay, G. B. (2013). Analysis of long-term trends (1950–2009) in precipitation, runoff and runoff coefficient in major urban watersheds in the United States. *Environmental Research Letters, 8*, Article 024020.

Wang, S., Fu, B., Piao, S., Lü, Y., Ciais, P., Feng, X., & Wang, Y. (2015). Reduced sediment transport in the Yellow River due to anthropogenic changes. *Nature Geoscience, 9*, 38–41.

Wang, Y., Yu, P., Feger, K. H., Wei, X., Sun, G., Bonell, M., Xiong, W., Zhang, S., & Xu, L. (2011). Annual runoff and evapotranspiration of forestlands and non-forestlands in selected basins of the Loess Plateau of China. *Ecohydrology, 4*, 277–287.

Wu, L., Jiang, J., Li, G., & Ma, X. (2018). Characteristics of pulsed runoff-erosion events under typical rainstorms in a small watershed on the Loess Plateau of China. *Scientific Reports, 8*(1), 3672.

Wu, J., Miao, C., Wang, Y., Duan, Q., & Zhang, X. (2017). Contribution analysis of the long-term changes in seasonal runoff on the Loess Plateau, China, using eight Budyko-based methods. *Journal of Hydrology, 545*, 263–275.

Wu, Q., Zhang, Z., Zhang, G., Jian, S., Zhang, L., Ran, G., Zhao, D., Lv, X., & Hu, C. (2020). Rainfall-runoff processes in the Loess Plateau, China: Temporal dynamics of event rainfall–runoff characteristics and diagnostic analysis of runoff generation patterns. *Hydrology and Earth System Sciences*. https://doi.org/10.5194/hess-2020-431

Xiao, B., Cui, B., Li, D., & Chang, X. (2017). Temporal and spatial variations of precipitation in different climatic regions of the Loess Plateau. *Science of Soil and Water Conservation, 15*, 51–61 (*In Chinese*).

Xie, Y., Liu, B., & Zhang, W. (2000). Study on standard of erorive rainfall. *Journal of Soil and Water Conservation, 14*(4), 6–11 (In Chinese).

Xu, X., & Xu, Y. (2017). Analysis of spatial-temporal variation of human activity intensity in Loess Plateau region. *Geographical Research, 36*, 661–672 (In Chinese).

Yang, H., Lu, H., Yang, D., & Hu, Q. (2012a). Seasonality of precipitation and potential

evaporation and its impact on catchment water-energy balance. *Journal of Hydroelectric Engineering, 31*(4), 54–59 (In Chinese).
Yang, L., Wei, W., Chen, L., & Mo, B. (2012b). Response of deep soil moisture to land use and afforestation in the semi-arid Loess Plateau, China. *Journal of Hydrology, 475*, 111–122.
Yang, H., Yang, D., Lei, Z., & Sun, F. (2008). New analytical derivation of the mean annual water-energy balance equation. *Water Resources Research, 44*(3), W03410.
Zeng, Y., Yang, X., Fang, N., & Shi, Z. (2020). Large-scale afforestation significantly increases permanent surface water in China's vegetation restoration regions. *Agricultural and Forest Meteorology, 290*, 108001.
Zhang, J., Gao, G., Fu, B., & Gupta, H. V. (2019). Formulating an elasticity approach to quantify the effects of climate variability and ecological restoration on sediment discharge change in the Loess Plateau, China. *Water Resourses Research, 55*(11), 9604–9622.
Zhang, J., Gao, G., Fu, B., Wang, C., & Li, R. (2020a). A universal multifractal approach to assessment of spatiotemporal extreme precipitation over the Loess Plateau of China. *Hydrology and Earth System Sciences, 24*(2), 809–826.
Zhang, Q., Li, H., Zhang, L., Yue, P., & Shi, J. (2013). Responses of the land-surface process and its parameters over the natural vegetation underlying surface of the middle of Gansu in loess plateau to precipitation fluctuation. *Acta Physica Sinica, 62*(1), Article 019201 (In Chinese).
Zhang, B., Shao, R., Zhao, X., & Wu, P. (2020b). Effects of large-scale vegetation restoration on eco-hydrological processes over the Loess Plateau, China. *Journal of Basic Science and Engineering, 28*, 594–606 (In Chinese).
Zheng, H., Miao, C., Wu, J., Lei, X., Liao, W., & Li, H. (2019). Temporal and spatial variations in water discharge and sediment load on the Loess Plateau, China: A high-density study. *The Science of the Total Environment, 666*, 875–886.
Zheng, F., Tan, J., Wang, X., Wei, T., Ma, Z., & Zhang, W. (2020). Progress of study on rainfall interception by water conservation forest in the Loess Plateau. *Yellow River, 42*(4), 89–93 (In Chinese).
Zhou, Z., Sun, W., Mu, X., Gao, P., Zhao, G., & Song, X. (2019). Temporal and spatial pattern of actual evapotranspiration in the Loess Plateau from 2001 to 2017. *Yellow River, 41*, 76–84 (In Chinese).

International Soil and Water Conservation Research 9 (2021) 344–359

Contents lists available at ScienceDirect

International Soil and Water Conservation Research

journal homepage: www.elsevier.com/locate/iswcr

Review Paper

Advantages and disadvantages of terracing: A comprehensive review

Chuxiong Deng [a], Guangye Zhang [a], Yaojun Liu [a], Xiaodong Nie [a], Zhongwu Li [a, b, *], Junyu Liu [a], Damei Zhu [a]

[a] College of Resources and Environmental Science, Hunan Normal University, Changsha, 410082, PR China
[b] College of Environmental Science and Engineering, Hunan University, Changsha, 410081, PR China

ARTICLE INFO

Article history:
Received 3 August 2020
Received in revised form
9 November 2020
Accepted 10 March 2021
Available online 17 March 2021

Keywords:
Ecosystem services
Terraces
Terrace abandonment
Terrace management
Soil and water loss

ABSTRACT

For thousands of years, terracing has been one of the most important systems for preventing soil erosion, conserving water, and increasing agricultural production. Despite having a long history, the wide-ranging effects and mechanisms of terracing are poorly understood owing to large-scale spatial and temporal distribution patterns and the challenges related to assessing the ecosystem services of terraced landscapes. Thus, our study aims to review comprehensively the effect of terraces by describing the mechanisms behind terraced systems. Terraces provide many ecosystem services, including the reduction of runoff and sediment by over 41.9% and 52%, respectively, and the improvement of grain yields and soil moisture content by 44.8% and 12.9%, respectively. In addition, terracing can also contribute toward the conservation of plant biodiversity on a local scale. However, as terraces age, a number of disadvantages gradually emerge, including interference with water circulation and the development of serious environmental problems caused by poorly designed or mismanaged terraces, where the average runoff and soil loss can be 1–5 times that of well-managed terraces. Although understanding the complexity and multifaceted effects of terracing is vital for terrace construction and management, the negative effects of terracing are often not considered, and existing studies have several shortcomings. Within this context, this paper aims to describe both the benefits and disadvantages of terracing, investigate the gaps in current research, as well as discuss preventive and remedial measures so as to negate the possible bad impacts of terracing.

Contents

* Corresponding author. College of Resources and Environmental Sciences, Hunan Normal University, Changsha, China.
E-mail address: lzw17002@hunnu.edu.cn (Z. Li).

https://doi.org/10.1016/j.iswcr.2021.03.002

1. Introduction

As one of the oldest techniques for conserving water and soil, terracing is common in hilly and mountainous regions that are subjected to substantial population pressure. Terraces are built along contour lines to increase the arable surface area and conserve water and soil on hillslopes (Cao et al., 2013). Terraced fields can be of different shapes and sizes, and consist of a flat section and a near vertical riser, protected by a wall of dry stones, soil, grass, or trees. The height of the riser or wall can be from several decimeters to a few meters, with a continuous or intermittent structure comprised of single walls or a complex series of walls (Arnáez et al., 2015). The flat surface created by terracing is generally used for cultivation (Cevasco et al., 2014) (Fig. 1). Terraced fields were constructed in Southeast Asia as early as 5000 years ago, after which the technique gradually spread to the northern and southern shores of the Mediterranean (Price & Nixon, 2005). The shortage of arable land together with technological progress and population growth resulted in the global distribution of terraces. Portugal, Switzerland, Italy, Nepal, Indonesia, the Philippines, Peru, China, Japan, and Ethiopia (Baryla & Pierzgalski, 2008), among others, have extensive terraced farmland areas. Other well-known examples include the Arab gardens in Spain and the agricultural terraces of Asia, as well as Central and South America (Kladnik et al., 2017).

Under ideal situations, terraced fields achieve a hydraulic equilibrium between geomorphic setting and anthropogenic use, resulting in reduced water and soil loss, stabilized hill slopes, and improved site conditions (Antle et al., 2006; Yang et al., 2009; Shao et al., 2013). Slope management by terracing has been found to be one of the most effective engineering measures, provided that terraces are well-designed, correctly built, and appropriately maintained (Morgan & Condon, 1986). The creation of terraces on sloping land can reduce slope steepness by dividing the slope into smaller, gently sloping sections (Li et al., 2006; Wang et al., 2011; Chen et al., 2012; Uchida et al., 2013), resulting in reduced soil and water loss. Terracing with correct field management can reduce both runoff and sediment loss, on average, by over 41.9% and 52%, respectively (Table 1). In the hilly, red-soil area of South China, the terracing of fields has reduced both runoff and sediment loss by up to 99.9% (Zuo & Li, 2004). Though terraces are considered as advisable conservation practices to avoid soil and water loss, the construction and management of terraces often disturb carbon flux between the atmosphere and soil via shifting land-use type and topography, which potentially alter soil organic carbon (SOC) dynamics (Zhang, Wang, & Li, 2015). Proper land use, examples of terraced reforestation and afforestation, could markedly crease SOC accumulation. According to Chen, Wei, and Chen (2020), for China's landscapes, terraces increased SOC sequestration by 32.4% compared to that of the sloping lands on average. Among the ecosystem services provided by terracing are the increase in crop productivity, expansion of land for cultivation and creation of aesthetically pleasing landscapes (Lee & Kim, 2011; Liu et al., 2011). While terracing is also associated with other ecosystem services, the sequestration of carbon, retention soil and water, and recreation has been a focal point of terrace-related research (Garcia-Franco et al., 2014; He, 2010).

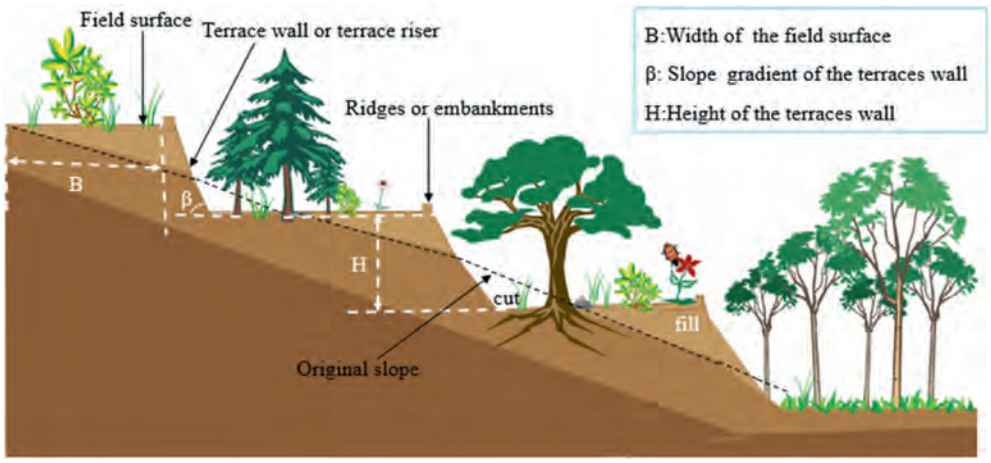

Fig. 1. Sectional drawing of a terrace. Terraces are formed by cut and fill areas. By filling areas, the arable land can be expanded, thus making it possible to grow crops on a large scale in hilly areas. The ridges or embankments play an important role in the interception of runoff and field water. But terraces are also at risk of collapse, and the higher the terraces wall, the greater the risk of collapse.

Table 1
The reduction of runoff and soil erosion on different terraced types.

Terraced type	Study area	Method	Climate	Runoff Reduction	Sediment reduction	References
Dryland terraces	Valley of Jinsha River Basin, Southwest China	Experiment	Annual rainfall:700–850 mm	Over 30%	Over 30%	Xiao et al. (2019)
Grass ridge t erraces	New Brunswick, Canada	SWAT model	Annual rainfall:768.9 mm		56%	Yang et al. (2009)
Grassed terraces	New Brunswick, Canada	Plot experiment	Annual rainfall: 768.9 mm	19.5%		Chow et al. (1999)
Bench terraces	West Java, Indonesia	Modelling/plots	Humid tropical climate	3.0–3.9% of rainfall	11–30 t ha^{-1} yr^{-1}	Van Dijk et al. (2005)
Broad embankment terraces	Chungju dam, South Korea	SWAT model	Annual rainfall: 1206.3 −1580.4 mm		75.4%	(Park et al., 2014)
Bench terraces	Dehradun, India	Plot experiments	Sub-humid climate	Over 80%	Over 90%	Sharda et al. (2002)
Paddy terraces	Tam Duong, Vietnam	Field measurements	Annual rainfall:1436 mm	75%	88%	Mai et al. (2013)
Agricultural terraces	Dhading, Nepal	Plots	Annual rainfall: about 1200 mm	11%	28%	Tiwari et al. (2009)
Stone wall terraces	Tigray, Ethiopia	Plots	Tropical, subhumid and subtropical		5.3 t ha^{-1} yr^{-1}	Nyssen et al. (2004)
Agricultural terraces	Buberuka, Rwanda	Plot experiment	Annual rainfall:1219 mm		16-42 t ha^{-1} yr^{-1}	Kagabo et al. (2013)
Level terraces	Loess Plateau, China	Plot experiment	Semi-arid continental monsoon climate	86.7%	87.7%	Wu et al. (2004)
Agricultural terraces	Zhuanglang county, China	Plot experiment	Annual precipitation of about 547 mm	4.6–8.3%	57–124.5 t ha^{-1} yr^{-1}	Liu et al. (2011)
Agricultural terraces	Jianyang County, Sichuan Basin, China	Plot experiment	Mean annual precipitation is 872.2 mm	21.5%	30.06%	Zhang et al. (2008)
Stone terraces	central Negev of southern Israel	Plot experiment	Mean annual precipitation:90 mm		42%	Stavi et al. (2018)
Broad-based terraces	Meridional Plateau, southern Brazil	Plot experiment	Average annual rainfall: 1677 mm	78%	0.28 t ha^{-1} yr^{-1}	Londero et al. (2018)
Stone-walled terracing	Ramallah District	Plot experiment	Mean annual rainfall of 580 mm	16%	3.343 t ha^{-1} yr^{-1}	Hammad et al. (2004)
Tilled contour bench terraces	El Gouazine hill reservoir, central Tunisia	Plot experiment	Annual rainfall (1993–2006): 366 mm	75%	47%	Al Ali et al. (2008)

Despite having a long history, mechanisms behind terracing and the overall effects of this technique are still poorly understood. Although terracing-related research has been conducted globally over the last few decades, at a site- or plot-scale, the conclusions from these small-scale studies are inconsistent (Chen et al., 2017). However, several relevant studies have described the drawbacks or possible negative effects of terracing. A number of researchers reported that abandoned and newly-built terraces may cause deterioration of soil conditions (e.g., stability, nutrient, erosion-resistence) (Calsamiglia et al., 2018; Gallart et al., 1994). The reasons for these findings are related to the specific structure, construction material, and vegetation cover of terraced fields, which may differ across ecosystems, resulting in a variation of ecosystem services (Wei et al., 2016). Especially terraced landscapes across the world have degraded significantly in recent decades, as a result of changes in economic and social activities (e.g., rural labor force and population transfer, urban expansion, slumps in agriculture and uncertainty regarding tenure) (Schoenbrodt-Stitt et al., 2013). These degraded landscapes may have negative effects on ecosystems and pose a threat to human wellbeing. In many regions, the abandonment of terraces due to socioeconomic development, has increased water and soil erosion as well as the risk of slope collapse. Thus, the effects of terracing on ecosystems and human welfare are highly complex and it is challenging to draw general conclusions about the effects of terraces while considering the variability in associated plant species, terrace age, spatiotemporal distribution, land use, and topography.

Although the focal point of terrace-related research is shifting, along with a continuous increase in understanding, previous studies of terracing have primarily focused only on either the advantages or disadvantages associated with this technique. We believe that the evaluation of both advantages and disadvantages of terracing is crucial for correct management decisions and should therefore, be investigated. Currently, only a few systematic and integrated studies have been conducted on the benefits and drawbacks of terracing, highlighting the need for further studies. Based on this, the purpose of this study is describing both the advantages and disadvantages of terracing, investigating the deficiencies of current research, as well as discussing preventive and remedial measures so as to negate the possible bad impacts of terraces and promote sustainable development of them.

2. Ecological benefits of terraces

2.1. Reduced runoff and water conservation

The core problem of the comprehensive treatment of small watersheds is the realization of scientific regulation and rational utilization of runoff. There are three primary ways that terracing reduces runoff and sediment loss. Firstly, terracing transforms steep slopes into an artificial sequence of relatively flat surfaces (Fashaho et al., 2020), thereby decreasing slope length and gradient, which significantly reduces sediment yield and runoff (Shi et al., 2004) (Fig. 2). Reshaped slopes change specific hydrological paths, decrease hydrological connectivity and enlarged catchment area, so they may intercept rainfall and mitigate flood peak discharge efficiently. Furthermore, the interception of surface runoff from terraced fields encourages infiltration, while the diverting of harvested rainwater to protected outlets at controlled velocities prevents soil erosion and water loss (Hazel, 2008;

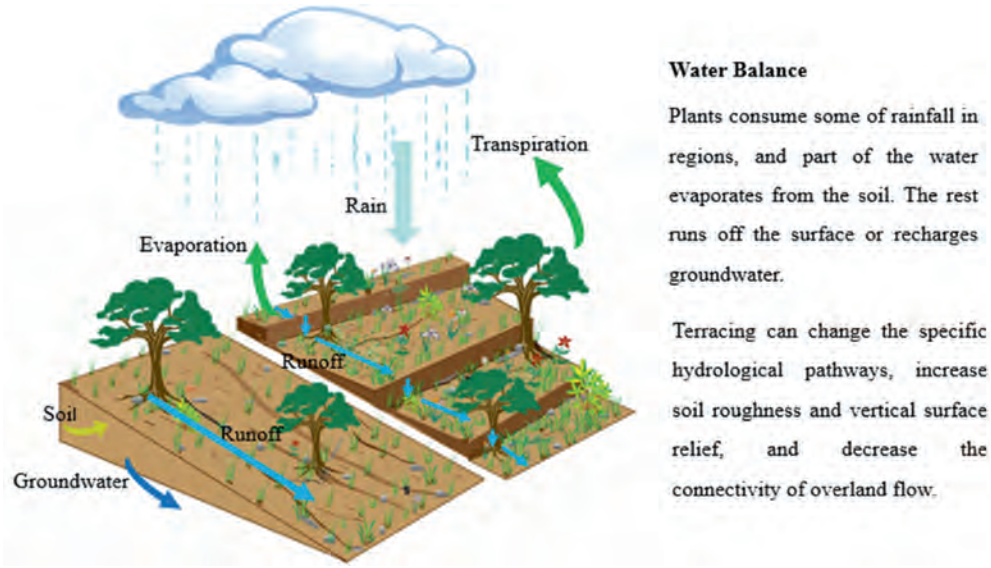

Fig. 2. Schematic diagram of runoff and sediment paths on terraced fields and natural slopes. Terraces reduce runoff and sediment through reforming topography and contributing to plant growth.

Meerkerk et al., 2009). By terracing, the runoff is reduced by over 41.9% averagely, when compared to that of the natural slope (Table 1). When slope length was increased by 40%–67%, for example, slopes at 14°40′ and 28°52′ (1.4 times that of the original slope), annual runoff increased by 2%–3%, excluding wash loads (Liu et al., 2011).

Secondly, terracing increases surface roughness and vertical surface relief. This, increases infiltration, soil moisture, and the soil water holding capacity (Wei et al., 2016). Terracing can increase soil moisture content by 4.24%–12.9% (5.0–6.2 times that of sloped land) (Chen, Wei, Daryanto & Tarolli, 2020; Feng et al., 2017; Mojeremane et al., 2010). Zhang, Min, et al. (2017) and Kosmowski (2018) also found that terraces can store water and thereby, allows for the restoration of vegetation in water-limited ecosystems (Fu et al., 2011; Posthumus et al., 2015; Yu et al., 2017).

Thirdly, terracing often includes the formation of ridges or embankments (Fig. 1) that was greatly beneficial in reducing runoff. Terraces with ridges, for example, have been shown to retain 18% more runoff than terraces without ridges (Jiao & Wang, 1999).

2.2. Erosion control and soil conservation

Soil erosion is closely related to runoff. During intense storms, a portion of rain infiltrates into the soil and the remainder becomes runoff. As runoff increases, its velocity, volume and erosivity also increase (Bai et al., 2019; Zuazo et al., 2011). Critical runoff velocity, at which soil particles are transported over the surface, depends on slope gradient and soil particle size (Johnson & Holly, 1992). Therefore, terraces are designed to accumulate and conserve overland runoff to ultimately reduce sediment yield. In some regions, it has been estimated that soil erosion could be reduced by 43%–70%, when the area of terraced land makes up of more than 40% of total mountain slope land (Al Ali et al., 2008; Gebrernichael et al., 2005; Shi et al., 2012). Research conducted in the Wangjiaqiao watershed in the Three Gorges Area indicates that terraces built from 1995 to 2005 significantly reduced sediment yield by reducing soil loss from 18.5 to 13.2 t ha $^{-1}$ y $^{-1}$, decreasing the sediment delivery ratio from 0.454 to 0.295 and increasing sediment deposition from 7.7 to 12.4 t ha $^{-1}$ y $^{-1}$ (Shi et al., 2012). Clear decreases in soil loss, from an average of 20 to less than 1 t ha^{-1}, have occurred through the transformation of sloping fields to terraces in combination with the development of grassed waterways (Chow et al., 1999). In addition, erosion rates on terraced fields are very low, usually not more than 1 t ha^{-1} y^{-1}, only if the slope tangent exceeds 0.1 (Quine et al., 1999).

Terracing increases erosion control efficiency in numerous ways. Firstly, terracing weakens erosive forces by reducing both the velocity and total amount of runoff (Chen, Chen, & Peng, 2013). Secondly, terraced fields that prevent soil erosion often contain the measurements like upslope contour hedgerows, vegetative filter strips, and grass barriers (Walle & Sims, 1999). Terracing also provides an environment for plant growth, promoting an increase in canopy cover, which was crucial in controlling soil erosion. Furthermore, an increase in surface roughness of the root and litter layer, leads to a decrease in soil erosion, with a specific decrease in splash, rill, and inter-rill erosion (Shimoda & Koyanagi, 2017). In addition, the terraces intercept not only the water and sediment they-produced, but also the sediment laden flow coming from the upslope. The effect of soil erosion control is especially significant when considering the effects of sediment reduction in terraced surface, the interception of upslope runoff, and the reduction of downhill gully sediment yield by reducing slope runoff (Chen et al., 2016).

2.3. Increase of crop yield

The recent global increase in terracing relates to increased population density in areas with limited arable land. By terrace building, a steep slope is converted into a relatively flat surface (Xu et al., 2018) that not only increases the area available for cultivation but also facilitates more intensive farming practices (Xu et al., 2011). In general, arable land can be increased by 20%–40% through the conversion of slope land into terraced fields, which is significant to increase grain yield (about 20%–40%) (Hu et al., 2005; Posthumus & De Graaff, 2005). Besides, farming practices, such as ploughing, help to form pedo-environments with their own characteristics, i.e., modified profiles with high percentages of organic materials and nutrients (Stanchi et al., 2012). That is why terraced soils usually have higher organic matter and nutrient contents compared with non-terraced agricultural plots. Furthermore,

terracing also increases the moisture by avoiding water loss, which effectively enhances crop endurance to droughts and consequently increases crop yield. Accordingly, terrace is especially important for the irrigation and fertilization of barren hillsides (Adgo et al., 2013; Damene et al., 2013; Fu et al., 2013; Shi et al., 2009). In a case study from Tanzania, the average yield of maize was 270% higher in fertile terraced fields than in bare slope fields (Wickama et al., 2014).

The benefits of terracing on soil conservation and fertility, as well as the consequent increase in agricultural productivity, are visible in a wide range of environments, thereby explaining how terracing can help fight famines and support food security. In mountainous areas with pressing environmental problems, terracing has been an important foundation for the modernization of agriculture.

2.4. Cultural landscape

Terracing creates a cultural landscape that reflects human wisdom in understanding the relationship between man and a specific environment, as well as the connection with a valuable natural ecosystem (Brunori et al., 2018; Momirski and Kladnik, 2009). Over the past decades, there has been an increase in research on terraced landscape within the fields of geography, landscape architecture, ethnology, rural sociology, and other spatial disciplines. Terraces have been identified as part of a "cultural landscape" heritage and play a key role in aesthetic appreciation and spiritual enrichment (Kladnik et al., 2017). Famous examples are the Arab gardens in Spain and the agricultural terraces in Central and South America and Asia. These terraces attract thousands of visitors each year due to their aesthetic value and productive, pleasing, neat, and sustainable landscapes (Hrdalo et al., 2019; Rodewald & Liechti, 2016). Thus, terraces create large income for local residents (Zhang, Wei, et al., 2017). At the Longji terraces in China, for example, income from tourism accounts for 70.8% of the total income for local families (Zhang et al., 2019). Across the globe, five well-known ancient terraced fields have been designated as globally important agricultural heritage systems (GIAHS) by the Food and Agriculture Organization (FAO) of the United Nations (Fig. 3).

2.5. Habitat and protects biodiversity protection

In many eroded or water-limited ecosystems, afforestation or reforestation programs are difficult to complete without other inputs, due to the poor condition of existing sites and harsh climatic conditions (Wen et al., 2009). The terracing of fields, as an additional measure, can increase regional landscape heterogeneity, thereby providing habitats, facilitating the symbiosis of organisms, and maintaining biodiversity by playing a vital role in the reconstruction and improvement of habitats (Arévalo et al., 2016; Merino et al., 2010).

There are two primary reasons for terracing for increasing biodiversity. Firstly, the increase in water and nutrients in terraced fields allows for improved plant growth (Shimoda & Koyanagi, 2017) and, secondly, terracing improves the growing conditions for different species, consequently helping to increase biodiversity. In Toho village, Japan, 189 plant species from 81 families were recorded in terraced fields (Uchida et al., 2015). Furthermore, the biomass of non-terraced fields has been shown to be 32%–70% lower than that of terraced lands under similar environmental conditions (Carlos et al., 2019; Havlova et al., 2017; Park et al., 2017).

3. Possible disadvantages of terraces

Except above benefits, a number of studies have recorded the negative effects associated with terraces. These bad impacts, usually caused by inadequate design, mismanagement, and agricultural abandonment, challenge the man-land relationship and threaten ecosystem stability (Fig. 4).

3.1. Disruption of water circulation

Terracing plays a clear role in the conservation of water and soil sources, and quantitative research prove the effects of terracing on the interception of runoff. However, effects of terracing on hydrological processes should be noted, especially in areas with water resources strain (Higson & Singer, 2015).

Precipitation that falls to the ground enters into both a small and large regional water cycle. The smaller cycle includes soil

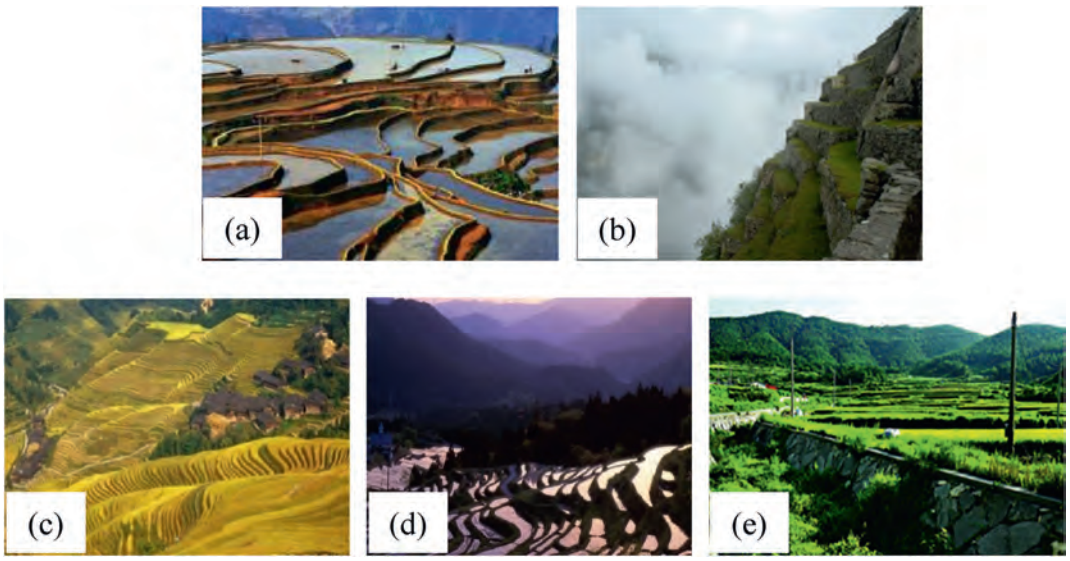

Fig. 3. Well-known ancient terraced landscapes from around the globe. (a) Hani terraces of China, (b) Machu Picchu terraces in Peru, (c) rice terraces of the Philippine Cordilleras, (d) Noto Peninsula terraces in Japan, and (e) Gudeuljangnon rice terraces in South Korea. The inscription dates of these terraces in the GIAHS are 2010, 2011, 2002, 2011, and 2014, respectively.

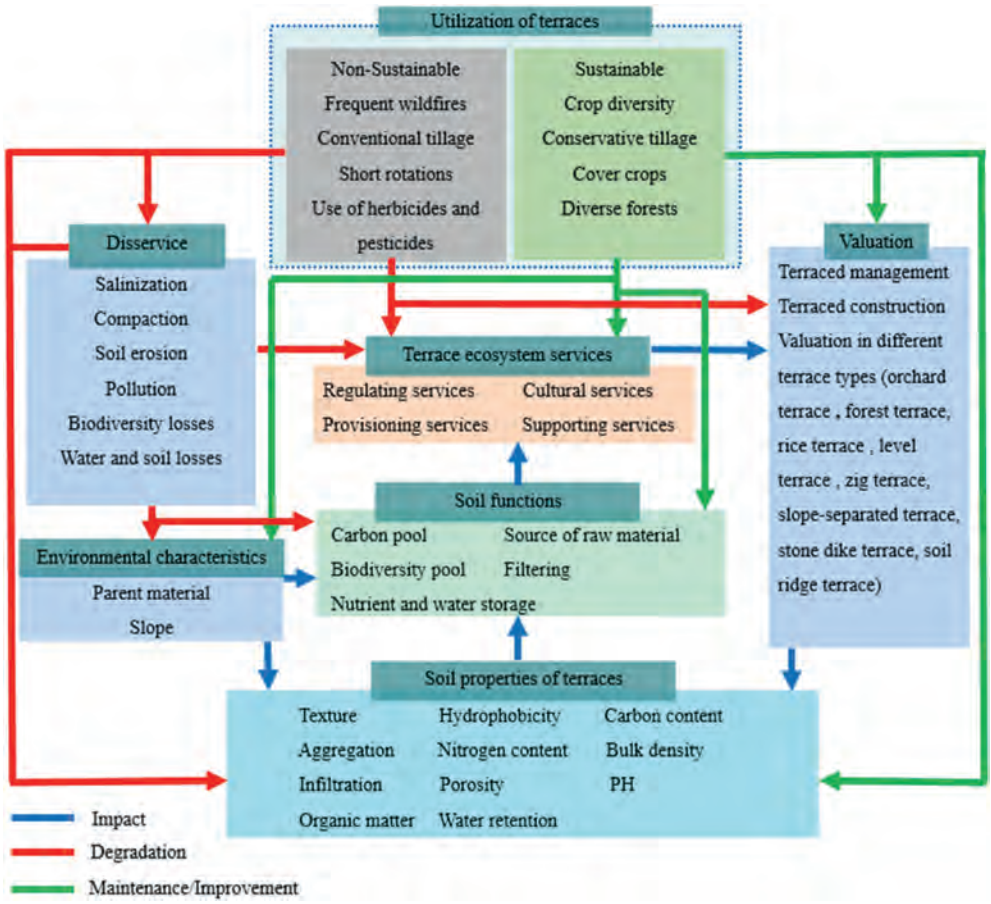

Fig. 4. The relationship between terrace utilization and soil quality.

infiltration and storage, rainwater collection, supplementary irrigation, and eventually evapotranspiration (Preti et al., 2018). The remainder of precipitation flows into watershed stream in the form of surface and underground runoff. Transforming slope lands into terraced fields may affect the small and large regional water cycle, thereby causing potential threats in the amount of available water for human activities.

Large area terracing increases water volume in the terraced field itself consequently reduces the outflow volume by intercepting runoff, altering the path of runoff and decreasing the hydrological connectivity so as to encourage it to infiltrate (Gibson et al., 2018; Schilling & Jacobson, 2016). Lesschen et al. (2009) modelled different scenarios for surface runoff and the result displayed that runoff could not connect the channel of a catchment if terraces were present.

Terracing encourages crop and vegetation to growth by improving soil conditions. Plant total water consumption and runoff reduction also increase with an increase in surface vegetation cover (Durán et al., 2019; Wang et al., 2019). The water demand of the newly-planted vegetation in the seasonally dry areas is of especial concern (Feng et al., 2016). Lu et al. (2009) suggest that one-third of the water in terraces is lost through evaporation in the semiarid northwest Loess Plateau. Because of the significant effects of storing and saving water of terraces, which consequently, increases local circulation of water between soil, vegetation, and atmosphere, affects downstream flow of Yellow River (Gao et al., 2015; Tang et al., 2008), and this result in a 56% reduction in available freshwater resources from 1961 to 2009 (Feng et al., 2016). Therefore, these both aspects affect the hydrological cycle from a water storage and water use perspective, with the result of a weakened large hydrological cycle and reduced river runoff (Gates et al., 2011). The reduction in runoff from crop planting and revegetation affects the dynamic balance of water resources between regions, so as to create potentially conflicting demands for water resources between different regions.

3.2. Erosion/mass movement due to poorly designed terraces

Although terraces are considered advisable and effective measure for soil and water conservation. Nevertheless, negative effects of poorly designed terrace are always concerned. Wei et al. (2016) pointed out that improperly designed terraced systems even than no terracing at all.

Improper terraces induce rill and gully erosion (Fig. 5a) can be explained by the following two reasons. On the one hand, terracing and contour ridges were always constructed on the steeper hillslopes, thus the terraced field surfaces are not completely level. Gully erosion on terraced fields was discovered to occur mainly as the terraces or contour ridges have a relatively inclination. These inclined terraces accelerate runoff concentration, which give rise to increased rill or gully erosion during heavy rainfall (Wen et al., 2020). If terrace-produced runoff is directed follow the poorly designed waterway to low sections of the terraces, which causing as to control of erosion of drainage channel more difficult. If runoff concentrates in the lowest spots of each terraced field because of without suitable waterways, the water finally ponds behind a shoulder bund or contour ridge and eventually, initial incision is caused as a mass of excess water overtop the terrace. This process

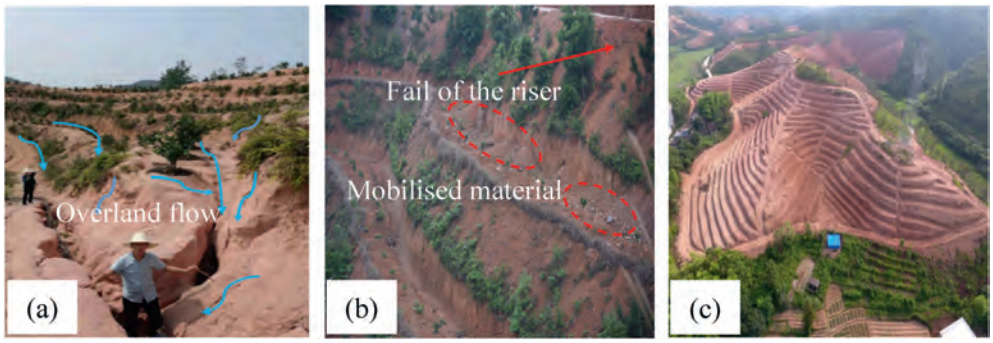

Fig. 5. Terrace-induced ecological problems in Ningdu county, Southern China. (a) Overland runoff flows along the inclined terraces and concentrates in the lower part of terraces, consequently causing severe gully erosion; (b) The mobilised material is accumulated in the lower section of the risers with low vegetation cover. (c) New mechanized terraces spread across the whole hillslope. A mass of topsoil was removed, and vegetation was completely destroyed.

can continue from the upper terrace down to the bottom of the slope. Moreover, gully erosion as a consequence of overland flow concentration in damaged risers. Finally, some farmers are inclined to plant fruit trees on the terraced beds and keep the surface bare to prevent weed-crop from competition for nutrients. Yet rill erosion became very common on the bare terraced beds and surface. In this case, the role of terraces is limited.

Followed by mass movement and landslides mainly caused by riser collapse (Fig. 5b). In the risers, landslides and mass movements caused by poorly designed terraces are frequent. Terrace risers are not protected by stone walls or natural vegetation (Peng & Wang, 2012; Zhang, Wang, Bai & Lv, 2015). Bare risers deteriorate soil conditions, including soil erodibility, infiltration capacity. When directly exposed to the raindrops, there would be a serious splash erosion on the steep bare risers. Furthermore, the concentrated flow on the steep bare risers promote the rill or gully erosion, when there is a gully, the soil loss increased exponentially (Verheijen et al., 2009). The stability of rill wall with large moisture content decreases under the action of water erosion. Collapse occur easily when the rill wall out of balance. Meanwhile, those geological hazards result in damages on the plants, training structures and field infrastructures. Another reason for riser collapse is that risers may become too high due to the terraces are constructed on very steep slope. In theory, terraced fields can be constructed on any slope but, in fact, the risers become too high on quite steep slopes and are difficult to management and maintenance (Ramos et al., 2007). Thereby the stability of terraced risers against mass movements is reduced, especially during heavy or prolonged rainfall.

3.3. Deterioration of soil quality

The degradation of soil quality on newly built terraced fields can be explained by the fertile topsoil is removed, soil structure is destroyed and nutrient loss due to soil and water loss (Liu, Dong, et al., 2013).

When constructing terraces, slopes must be reshaped, which has significant impact on soil and vegetation. Firstly, soil structure is primarily affected by disturbance from the reshaping of slope topography. The creation of terraces can lead to the removal of fertile topsoil and the upturning of subsoil. Those removed topsoil is then buried at terrace tips to enlarge flat areas (Liang et al., 2018). And upturned subsoil with poor soil structure and nutrient condition (Fig. 5c). Furthermore, local vegetation will be destroyed completely in the process of terracing, thereby exposing the ground and large amount of loose materials. These changes will bring the following adverse effects. Unstable slope structure and extremely sparse vegetation can easily lead to soil loss and erosion during rainstorm events at first (Stanchi et al., 2012). Similar to soil loss and erosion, when topsoil is removed by terrace construction, its SOC is likely to be deprived away. Such extensive soil redistribution and land leveling processes may also cause significant soil carbon perturbations (Ni & Zhang, 2007; Zhou et al., 2015; Trinugraheni et al., 2017). Furthermore, changes in nitrogen and carbon content of soil are similar, the nitrogen contents decrease with soil loss and vegetation reduction (Wang et al., 2011). The absence of an organic surface layer reduces the soil organic matter (SOM) accumulation in the soil that leads to very low amounts of total organic carbon and finally, a better remineralisation of the SOM to low carbon and nitrogen contents (Vogel & Conedera, 2020). Therefore, the nutrient content of newly built terraces is very low during initial years (Liu & Zhou, 2017; Qiu et al., 2014; Siriri et al., 2005). Notably, there is a lack of data indicating a significant increase in output in the first five to ten years after establishment of terraces (Mesfin et al., 2018).

Terracing not only brings benefits and hope to people, but also ecological risk. With the development of economy and society, terraces are no longer just for cultivating traditional crops, more large-scale terraces are used to develop economic forest and fruit tree for a higher economic benefit. For example, in the Priorat region of NE Spain with >27,000 ha of mechanized vineyards (Ramos et al., 2007). Citrus orchards systems occupy large parts of the mountain region in the Three-Gorges Area of China (Xu et al., 2012). Increased application, and particularly the irrational use of fertilizers and pesticides for economic benefits in mountain region orchard terraces production systems are quite common for a long time. More contamination are moving down and polluting deep soil and groundwater, because these terraces encourage surface flow infiltration and prolong the infiltration time. Coupled with the obviously soil conservation benefits of terraces, a large amount of foreign substances (e.g., Cu, As, Cr, Hg, Ni, and Zn) can be stored in the soil. Zhang, Wu, et al. (2017) stated that, in the Loess Plateau of China, the terrace farmland and terrace orchard land have greater Cr, Cu and Zn contents, compared with the slope farmland. Notably, the concentration of Cu in orchard terraces is higher than that in olive orchards and grassland, primarily due to the extensive use of copper-based fungicides (Miloš & Bensa, 2019). Previous research on orchard soils noted that pollutants concentrated and increased with tilled time and application rates of chemical fertilizers and pesticide (Gao et al., 2019; Guo et al., 2016). Thusly, groundwater and deep soil will be contaminated inevitably (Shao et al., 2019).

3.4. Soil erosion after terrace abandonment

Although many studies have been conducted on the positive

Table 2
Part of worldwide research cases of abandoned terraces.

Study area	Methods/scale/type	Research purpose	Major conclusions	References
Ifugo (Philippines)	Micro-plot/rice terrace	Quantifying the role of traditional terrace in water resources regulation	There is a positive feedback loop between terrace abandonment and decline of water resources. Terrace abandonment resulted in a reduction of about 30% in total groundwater recharge. Land-cover change induced by terrace abandonment was shown to lead to an overall decrease in water resource availability.	Soriano et al. (2018)
Yura Peninsula (Japan)	Statistical analysis/ Stone-walled terraces	To elucidate how the land-use legacy and site conditions have influenced revegetation processes after abandonment of mountain slopes used for terraced fields and wood production	Stone-walled terracing will influence the local populations of many fern species for decades or possibly longer after reforestation on abandoned fields.	Tokuoka and Hashigoe (2015)
Mula basin (Spain)	watershed/ Experimental analysis	To analyze factors contributing to piping process in abandoned terraces	The piping process appears to be linked to the low-sloped terrace beds with significant hydraulic gradient. The largest pipes are to be found in the currently abandoned cultivated terraces.	Díaz et al. (2007)
Camero Viejo	GIS/watershed/Stone-walled terraces	To evaluate the environmental change caused by land use and analyze the erosion process caused by terrace abandonment	The most important erosion process was the collapse of terrace walls as a consequence of massive soil movement. There was a significant and positive correlation between the volume of landslides and the height of the terrace wall.	Lasanta et al. (2001)
Mediterranean	regional/systematic review Stone-walled terraces	To Analyses the main environmental and human characteristics associated with soil erosion processes and the main factors influencing the extreme variability of soil erosion.	In the long run, terrace abandonment accelerates erosion of pipes, rills and gravity, and exacerbates marginal landslides.	García-Ruiz et al. (2013)
Liguria (Italy)	GIS/watershed/ farmland terrace	Investigating the land use transformations that occurred in a small coastal terraced basin from the early 1950s to 2011.	Terrace abandonment for a short time showed the highest landslide susceptibility. They are prone to collapse.	Pepe et al. (2019)
Italy	Stone-wall terraces	To analyzes the present situation of terrace landscape and its existing problems, and probes into possible solutions	Terraced landscapes subject to abandonment can progressively increase gully erosion and cause soil quality decline.	Tarolli et al. (2014)
Valtellina (Italian Alps)	Field observations/ Stone-wall terraces	To determine the processes and mechanisms that triggered landslides	Soil slips and soil slips debris flows are recurrent phenomena along terraced slopes. Poorly maintained terraces are more likely to cause large-scale movement.	Crosta et al. (2003)
Mediterranean	systematic review and meta-analysis/region/ agricultural terraces	To explore the main effects of land abandonment of Mediterranean agricultural terraces on local hydrological and geomorphological processes	The development of vegetation cover and degradation of terraced structures as the main factors controlling the hydrological behavior of abandoned terrace systems. Severe geomorphological problems, in the form of intense surface erosion, aggressive piping and gullying, occurred under special climatic, lithologic and structural conditions.	Moreno-de-las-Heras et al. (2019)
Negev (Israel)	Laboratory Analyses/ Stone terraces	Assessing the on-site impact of failure and the collapse of stone terraces on the geo-ecosystem functioning of ancient, terraced agricultural lands	Terrace abandonment will accelerates soil erosion and land degradation and adversely affects vegetation restoration.	Stavi et al. (2018)
Sa Font de la Vila catchment (Spain)	Watershed/Plot experiment/ agricultural terraces	To study the effects of land abandonment and wildfires on terraces' deterioration and its influence on catchment sensitivity	Land abandonment and wildfires were key factors causing major changes in the sensitivity of terraces. Wall failures promotes runoff concentration that in turn accelerates the hydraulic processes causing their collapse.	Calsamiglia et al. (2018)
Murcia (Spain)	Field plot、Sigma Plot 13.0、/agricultural terraces	To assess the effect of different lithologies and soil properties on the early stages of soil erosion by water in abandoned dry terraces	The highest soil loss (41.41 g m −2 in cultivated plots and 17.05 g m $^{-2}$ in the abandoned plots) and runoff (3.79 L m −2 in the abandoned plot) occurred on marl substrata (17.05m^{-2}).	Martínez-Hernández et al. (2017)
Serra de Rodes catchmen (Spain)	Field measurements、Statistical analysis、ANOVA/Watershed/ agricultural terraces	To evaluate the shallow soil properties of abandoned terraces and the relationship between soil erosion, rainfall and runoff	Terrace abandonment aggravates the erosion process and the vegetation restoration process is limited.	Pardini et al. (2017)

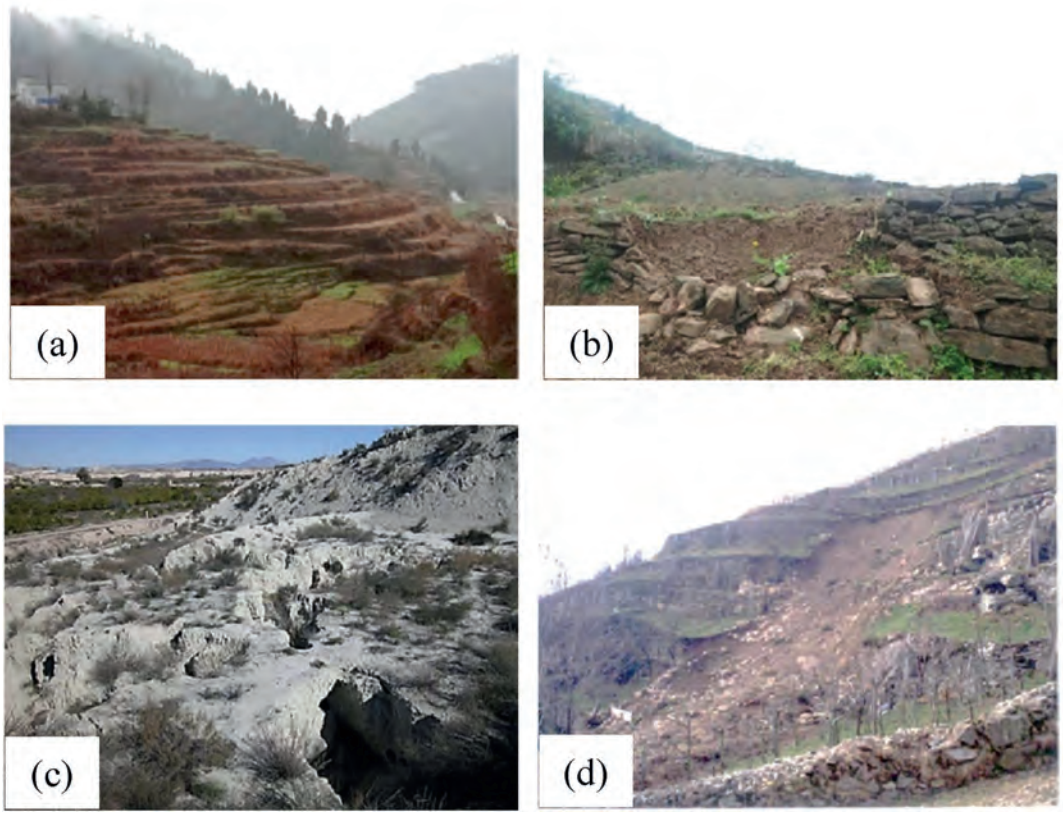

Fig. 6. Examples of terrace mismanagement. (a) terrace abandonment, (b) terrace collapse (These terraces were only abandoned for two years), (c) abandoned cultivated terraces affected by piping, and (d) landslides on abandoned terraces where soil slip progressed into a small debris flow along the terraced slope. All these lead to soil degradation with the gradual loss of vegetation and productivity. (Note: (c) and (d) by Díaz et al. (2007) and Crosta et al. (2003), respectively).

Fig. 7. Keyword cloud map of European terrace-related literature. Two words (i.e., "terrace" and "terracing") were used to search through existing European literature from Web of Science, resulting in 102 articles, from which key words (Top 100) were extracted.

effects of terracing on water conservation and soil maintenance (as described chapter 2), several studies have yielded opposite conclusions (Li & Lindstrom, 2001; van Dijk, 2004; Sang-Arun et al., 2006; Pietsch & Mabit, 2012; Calsamiglia et al., 2017; Romero Díaz et al., 2007) (Table 2), specifically regarding abandoned terraces (Fig. 6a). These studies indicate the runoff coefficient of abandoned terraced fields to be between 20% and 40%. Soil erosion at the foot of an abandoned terrace slope has been shown to be approximately 100 times higher than that of semi-natural hillslopes and 2–3 times higher than that before abandonment. Furthermore, runoff and soil loss of abandoned terraces is more than three and ten times greater than that of well-managed terraces, respectively (Agnoletti et al., 2019; Atta & Aref, 2010; Lesschen et al., 2008).

Firstly, the abandonment of terraced fields causes changes in the spatial pattern of hydrological connectivity, resulting in concentrated runoff, as well as increased soil erosion and degradation (Koulouri & Giourga, 2007; Schönbrodt-Stitt et al., 2013). Terrace abandonment has become common over the last decades. In particular, degraded terraced field landscapes have gradually become the most characteristic "abandoned landscapes" in the European mountains (Varotto & Lodatti, 2014) (Fig. 7). Numerous land-use change predictions indicate that this phenomenon will continue to increase in southern Europe (Olesen & Bindi, 2002). In the long-term, abandoned terraces may lead to the collapse of stone walls, mass soil movements, sheet wash erosion, and the formation of gullies, piping, and landslides on marginal slopes (Fig. 6 b, c, and d).

The restoration of vegetation is especially difficult in semi-arid environments. Large amounts of exposed land and heavy rain greatly increase the risk of terrace collapse, especially for abandoned terraces with bare and unprotected terrace risers (Londoño et al., 2017). Furthermore, abandoned land with marl soils is more easily eroded due to clay mineral dispersion, high expansion pressure, and spalling (Bryan & Yair, 1982).

Additionally, infiltration rates of terrace beds are high and as water begins to accumulate behind stone walls like underground runoff when it reaches the original soil of the hillside or a more impermeable substrate. This increases the weight and height of the terrace walls, leading to collapse and movement of soil (Zgaier, 2008). The abandonment of terraces at high altitudes is

Table 3
Soil erosion on different terraces by surface runoff.

Terraced type	Study area	Climate	Method	Hillslope gradient	Erosion (t $ha^{-1}yr^{-1}$)	References
Abandoned terraces	Costaviola-Reggio Calabria (Italy)	Mediterranean	USLE	29.65–81.8%	0.50–18.70	Bazzofi & Gardin (2011)
	Lesbos Islands (Greece)	Mediterranean	Gerlach plots	10–50%	0.04–0.05	Koulouri and Giourga (2007)
	Andean mountains (Perú)	Subtropical Monsoon	Experimental plots	50–60°	0.01	Inbar and Llerena (2000)
Fallow terraces	Spain	Mediterranean	USLE		0.53–2.22	Ruecker et al. (1998)
	North Taiwan (China)	Subtropical Monsoon	Plots, USLE	25°	0.74	Chen et al. (2012)
Grazing terraces	Cap Creus (Spain)	Mediterranean	Gerlach plots	18%	0.05	Pardini and Gispert (2012)
Forest terraces	Cap Creus (Spain)	Mediterranean	Gerlach plots	18%	0.01–0.35	Pardini and Gispert (2012)
	Cap Creus (Spain)	Mediterranean	Gerlach plots	15%	0.03	Pardini and Gispert (2012)
Rice terraces	Northern Vietnam	Tropical Monsoon	Plots	3–8°	0.16–1.77	Mai et al. (2013)
	North Taiwan (China)	Subtropical Monsoon	Plots, USLE	25°	0.77	Chen et al. (2012)
Mixed crops terrace	Yimeng Mountains (China)	Continental Monsoon	137Cs	12°	27.00	Zhang et al. (2014)
	Baiquan County (China)	Temperate Monsoon	137Cs	3–10°	25.04	Zhang and Li (2014)
	Lesbos Islands (Greece)	Mediterranean	Gerlach plots	10–50%	0.03	Koulouri and Giourga (2007)
	West Java (Indonesia)	Warm and humid	Models	15–20°	30.0–34.0	Van Dijk (2002)
	West Java (Indonesia)	Warm and humid	Models	15–20°	80.00	Van Dijk (2002)

extremely common, with Dick et al. (1994) reporting abandonment in 62% of terraced fields in the Colca Valley, with 91% of those occurring in high altitude regions. Inbar et al. (2000) quantitatively investigated sediment yield and analyzed the erosion of abandoned terraced fields. Their results indicate that soil erosion from abandoned traditional terraces id due to the failure of local irrigation systems. In the Mediterranean, more than 50% of abandoned terraced fields are exposed to gully erosion and landslides, leading to the collapse of rock canyons (Bellin et al., 2009). As post-collapse reconstruction costs are very high, resulting negative environmental consequences, beyond decreasing biodiversity, further exacerbating the condition of terraced fields, eventually leading to irreversible soil degradation and the permanent loss of vegetation and productivity (Duarte et al., 2008).

Multiple drivers are related to the abandonment of terraced fields, including the following: (1) decrease in labor and rural population, (2) reduced economic returns due to reduced agricultural product prices and high maintenance costs, and (3) limited accessibility of certain terraces (Dunjó et al., 2003; Galletti et al., 2013).

4. Shortcomings of related research

4.1. Lack of comparative studies

As there are different types of terraces, the effectiveness of terracing systems depends on the combination of factors (e.g., geographical location, climate, appearance, construction material, age, and vegetation cover) and not on individual variables. The function of terraces depends on geographical location and climatic conditions (Slámová et al., 2017). For example, in the southeast and northwest-central regions of China, forest terraces are highly beneficial in reducing runoff, while in the southwest and northeast, crop terraces are more effective (Chen et al., 2017). The soil erosion also changes with the type of terrace (Table 3).

The construction of graded terraces on slopes can reduce the risks associated with level terraces, although level terraces have a higher water retention efficiency. Compared with slope-separated terraces, level terraces have a greater capacity to reduce sediment loss and lower input-output ratios (Oliveira et al., 2012). Although it can be concluded that the ecological benefits of terraces differ significantly, depending on local typology and regions, few studies acknowledge this point. There are differences in the focus on different terraces types (Table 4). Regarding terrace structures (terraces can be categorized as level, slope-separated, zig, or sloping terraces (Liu, Li, et al., 2013), most researchers focus on level and sloping terraces (2795 and 1464 publications, respectively), while in terms of construction material (terraced fields can be classified as stone-dike, soil-ridge, and grass-ridge terraces), the majority of relevant literature is centered on stone-dike terraces (115 publications in total). Among the types of land use, including orchard, forest, and rice terraces, research mostly focuses on forest terraces (698 publications in total).

4.2. Terrace ecosystem service evaluation method is insufficient

Recent years have seen an increase in research on the economic value of ecosystem services of terraced fields (Tilliger et al., 2015). However, multiple factors, including the lack of a unified evaluation index system and socioeconomic complexities, make these types of quantitative evaluations very challenging. The evaluation of ecosystem services related to terracing, leads to the pricing of ecological resources and consequently, provides a theoretical basis for the planning, construction, and utilization of terraces (Miao

Table 4
Statistics on the number of different types of terraces.

	Type	CNKI	Web of science	Total
From the structure	Level terrace	327	2468	2795
	Slope-separated terrace	11	80	91
	zig terrace	6	11	17
	sloping terrace	38	1426	1464
From the building materials	Stone dike terrace	19	96	115
	soil ridge terrace	17	81	98
	Grass ridge terraces	3	6	9
From the land use	orchard terrace	6	6	12
	forest terrace	26	672	698
	rice terrace	21	179	200

Note: CNKI refers to “China national knowledge infrastructure”. Three key words (i.e., land terracing, terracing, and terrace) were used to search the existing literature from two sources: Web of Science and CNKI.

Table 5
Common methods for value assessment of terraced ecosystem services.

Types of ecosystem services	Method	Equation	Meaning	Advantages	Disadvantages
Flood regulation and storage	Shadow engineering method.	$V = s \times p$	V represents the value of flood regulation and storage, yuan; p is the total rainfall intercepted, m^3; and s is the construction cost of a reservoir per unit volume, yuan/m^3.	The ecological value, which is difficult to estimate directly, can be expressed by alternative engineering.	Substitution engineering is non-unique. Time and space of substitution engineering are quite different.
Soil retention	Opportunity cost technique	$V = h \times t \times d \times \sum(SOM,TN,TP,TK) \times s$	V represents the value of soil fertility retention; h is the area, m^3; t is the thickness of the soil, m; d stands for soil bulk density, $g \cdot cm^{-3}$;$\sum(SOM,TN,TP,TK) \times s$ represents the sum of the contents of organic matter, total nitrogen, total phosphorus, and total potassium in the soil multiplied by the corresponding fertilizer price; and s is the corresponding fertilizer price, yuan$\cdot kg^{-1}$.	Reflecting the ecological value of the resource system in an objective and comprehensive way that has high credibility.	Resources must be scarce.
Water resources conservation	Water balance method	$V = (j - r) \times a \times s$	V represents the value of water resource conservation, yuan; j stands for average annual precipitation, mm; r is the annual evaporation, mm;a is the area of terraces; and s is the cost for water resource conservation, yuan$\cdot m^{-3}$.		
Products production	Market value method	$V = m \times p$	V is the value of the product, yuan; m is the value of primary products, t; and p is the market price of the product, yuan$\cdot t^{-1}$.	The evaluation results are objective, more reliable, and less controversial.	Market is incomplete. Government intervention in the market may lead to price distortions.
Biodiversity	Equivalence method	$V = f \times d \times a$	V is the value of biodiversity, yuan; f is the value equivalent of ecosystem services; d represents the ecosystem system value of one standard equivalent factor, yuan$\cdot hm^{-2}$; and a is the area of terraces,hm^2.		
Cultural services	Market value method and Price substitution method	$V = SC + S_t$	V is the value of cultural services, yuan; SC is the input of terrace construction, yuan; and S_t is the income of terrace tourism, yuan.	Clearly reflects individual consumer preferences and true willingness to pay; data is easy to obtain. The valuation is relatively accurate. The credibility and recognition degree is high.	Ignores the indirect benefit so the result is one-sided. It is difficult to accurately calculate the added value of products.

Note: Liu et al. (2014), Miao et al. (2017), Nie et al. (2017), Chen et al. (2018), and Pappalardo et al. (2019) were referenced.

et al., 2017). Presently, monetary measurement methods are primarily used for the evaluation of terracing-related ecosystem services (Table 5).

Despite the high cost and challenges associated with these assessments, the monetary method is often used. Notably, in the last five years, several non-monetary evaluation methods have been developed, including expert scoring and index evaluations. Although a useful addition to monetary evaluations, these methods are rarely used in terrace-related research in China, due to only being developed recently and therefore, still being in the exploration phase. Additionally, current methods on the quantitative evaluation of soil conservation measures are incomplete, as they are primarily based on terraces constructed for soil and water saving purposes, and not focused on effects related to the transport of surface water and sediment. Furthermore, as terrace ecosystem services are dynamic, it is crucial to explore changing trends and thresholds affected by multiple factors including terrace management and sustainable development. However, current estimation methods are inadequate for the evaluation of dynamic ecosystem services.

4.3. Research gap: negative effects of terraces

Terraces can be considered within the context of anthropogenic topography due to human-induced soil characteristics and landform changes, which are often beneficial to humans (Kassie et al., 2011). However, there are also many negative effects. An objective and comprehensive analysis of the complexity of terraces is important for the implementation of terrace measures and land resource management, as current research is less focused on the negative effects of terraces and more on the role of terraces in improving ecosystem services and quantifying the related economic value.

5. Recommendation of countermeasures and future research directions

Over thousands of years and across the globe, terracing of hillslope has been considered as a practicable measure for natural-social-economic development. Nevertheless, it is should be stressed that unscientific terrace construction and maintenance may contribute to negative impacts, examples of terrace-induced gully erosion. But these negative impacts have been largely ignored. In addition, economic evaluation methods for terrace ecosystem services generally have a singular focus with a lack of integration across different terrace types. Terrace abandonment and collapse, due to inadequate maintenance and various natural or anthropogenic forces, has resulted in soil erosion and quality decline, threatening the human-land relationship (Kim et al., 2013). In the context of socioeconomic development and global climate change, understanding the complexity related to terracing, as well as the scientific management and sustainable development of terraces for the improvement of human wellbeing, are important research focus areas. Therefore, this paper put forward the following suggestions in order to provide reference for solving the above problems.

5.1. Recommendations for preventing the negative impacts of terraces

Some preventive and remedial measures are discussed so as to negate the possible bad impacts of terracing:

(i) The modern terraced system needs to change the whole hillslope morphology to adapt fields to mechanization (e.g., building terraces by machine, mechanized farming). However, terraced sustainability should not be ignored. More attention to protection than mechanized work should be considered so as to make modern terraces sustainable. Available design criteria must be developed and strictly followed. These criteria should take soil types depth, slope inclination, hydrological and rainfall characteristics into account (Ramos & Porta, 1997). These technical guidelines should involve the drainage channels and the determination of terrace design parameters (e.g., terraced width, terraced height, riser slope, riser length, riser height and vertical and horizontal intervals) yet. In general, reducing hillslope gradient and length of terrace and increasing the width of terraced bench are beneficial to an increase in infiltration rates, a reduction of runoff production and surface flow velocity at the local scale.

(ii) Dense and widespread vegetation (grass, scrub and forest) coverage improves soil conditions and prevent surface from raindrop impact, overland flow wash erosion and rill and gully incision (Poesen et al., 2003). Long-term development of weeds and forest cover attenuates the influence of terraced risers collapse on large-scale runoff connections, through promoting rainfall interception and evapotranspiration. Except vegetation development, surface armouring by rock fragment cover can also conduce to prevent erosion in newly built terraced (Moreno-de-las-Heras et al., 2019). The stabilizing function of rock fragment sieving crusts may become more crucial when terraces developed in dry environments, where vegetation growth imposed large constraints by climate conditions.

(iii) It should be noted that no single measure can thoroughly solve the problem of gully and rill erosion of terraces, and combined prevention and control measure measures, such as earth dams, suitable waterways, vegetation buffers, settling basins, are essential. By building earth dams and settling basins perpendicular to the terrace direction to reduce the effective catchment area of a terrace, thus becoming a series of rectangular depressions which save overland flow and intercept sediment during rain, especially in extreme rainstorms. Suitable waterways may convey the water to earth dams or down-slope without gully or rill erosion. Meanwhile, ridges are necessary. The interval and number of ridges are determined by the gradient and practical length of each terracing. The terraced ridge height lies on the height of adjacent shoulder bunds or contour ridges (Zhao et al., 2013). In addition, narrowing the gaps between the shoulder bunds and contour ridges and filling initial rill incision are effective measures (Wen et al., 2020).

5.2. Future research directions

5.2.1. Comparative studies of different terrace types

Compared with practical achievements of terraces, theoretical research is more lagging. Within the context of available technology and databases, it is possible and necessary to use spatial analysis tools and high-resolution remote sensing image data to determine the actual situation of terraced fields and their spatial boundaries (Huang et al., 2019). We suggest that future research focus on the establishment of a terrace-monitoring network combined with theoretical research (Strehmel et al., 2016). To provide a theoretical and scientific basis for the selection and optimal allocation of terracing techniques, we suggest that research consider on the following important points and related challenges: (1) systematic investigating of the medium and long-term role and influence of terraces across multiple scales; (2) investigation of the functional mechanism of terracing for small watershed ecosystems; and (3) functional characteristics and regional suitability of terraces. Terracing can then be adjusted according to local conditions and to support the relationship between humans and nature.

5.2.2. Research on the overall effects of terracing

Terraced fields are affected by many factors, including geographical environmental characteristics, land use, have different types. Nevertheless, there are few studies that combine terrace types with function, and few studies that focus on the effect of terracing on water circulation and vegetation cover. Therefore, the current research do not reveal the mechanism of action of terraces. Furthermore, there is a lack of research on terrace-related pollution and effective treatment plans. We suggest that future research focus on investigating the overall effect of terraces, taking into account their function and related mechanisms, as well as identifying feasible solutions for related problems.

5.2.3. Research on management of terraces

Terraced fields are a typical example of the connection between human engineering of ecosystems and the nature-human connection. Humans play a vital role in decision-making, management, and building of terracing. Terrace abandonment and improper utilization of terraces can result in environmental problems and threats related to socio-economic and food security of the region. Therefore, regular maintenance and appropriate management of terraces are essential for ensuring the sustainability of ecosystem services. Within this context, we suggest that future research investigate the socioeconomic development, demographic change, and national policies related to the following: (1) terrace maintenance and restoration, (2) establishment of quantitative objectives and tasks for sustainable terrace management, (3) protection and compensation for terrace construction (Bevan & Conolly, 2011), (4)

establishment of environmental legislation for terracing, (5) allotment of special funds and economic subsidies for terracing to encourage better management from farmers (Qiu et al., 2014), and (6) knowledge transfer from academia and policy makers to local farmers regarding terrace construction and sustainable land management (Iiyama et al., 2005). Research into these aspects may help to achieve the long-term coordinated and sustainable development of ecology, economy, and society (Zoumides et al., 2017).

Declaration of competing interest

The authors declare that they have no conflict of interest.

Acknowledgments

Financial support for this research was provided by the National Natural Science Foundation of China (No. U19A2047, 41877084), the Key Project of Department of Education of Hunan Province (No. 18A044), and the Water Resources Science and Technology Project of Hunan Province (Xiang shui ke ji [2017]230-40).

References

Adgo, E., Teshome, A., & Mati, B. (2013). Impacts of long-term soil and water conservation on agricultural productivity: The case of Anjenie watershed, Ethiopia. *Agricultural Water Management, 117*, 55–61. https://doi.org/10.1016/j.agwat.2012.10.026

Agnoletti, M., Errico, A., Santoro, A., Dani, A., & Preti, F. (2019). Terraced landscapes and hydrogeological risk. Effects of land abandonment in Cinque Terre (Italy) during severe rainfall events. *Sustainability, 11*. https://doi.org/10.3390/su11010235

Al Ali, Y., Touma, J., Zante, P., Nasri, S., & Albergel, J. (2008). Water and sediment balances of a contour bench terracing system in a semi-arid cultivated zone (El Gouazine, central Tunisia). *Hydrological Sciences Journal, 53*, 883–892. https://doi.org/10.1623/hysj.53.4.883

Antle, J. M., Stoorvogel, J. J., & Valdivia, R. O. (2006). Multiple equilibria, soil conservation investments, and the resilience of agricultural systems. *Environment and Development Economics, 11*, 477–492. https://doi.org/10.1017/S1355770X06003056

Arevalo, J. R., Tejedor, M., Jimenez, C., Reyes-Betancort, J. A., & Diaz, F. J. (2016). Plant species composition and richness in abandoned agricultural terraces vs. natural soils on Lanzarote (Canary Islands). *Journal of Arid Environments, 124*, 165–171. https://doi.org/10.1016/j.jaridenv.2015.08.012

Arnaez, J., Lana-Renault, N., Lasanta, T., Ruiz-Flano, P., & Castroviejo, J. (2015). Effects of farming terraces on hydrological and geomorphological processes. A review. *Catena, 128*, 122–134. https://doi.org/10.1016/j.catena.2015.01.021

Atta, H. A. E., & Aref, I. (2010). Effect of terracing on rainwater harvesting and growth of Juniperus procera Hochst. ex Endlicher. *International Journal of Environmental Science and Technology, 7*, 59–66. https://doi.org/10.1007/BF03326117

Bai, J., Yang, S., Zhang, Y., Liu, X., & Guan, Y. (2019). Assessing the impact of terraces and vegetation on runoff and sediment routing using the time-area method in the Chinese Loess Plateau. *Water, 11*. https://doi.org/10.3390/w11040803

Baryla, A., & Pierzgalski, E. (2008). Ridged terraces - functions, construction and use. *Journal of Environmental Engineering and Landscape Management, 16*. https://doi.org/10.3846/1648-6897.2008.16.104-109

Bazzofi, P., & Gardin, L. (2011). Effectiveness of the GAEC standard of cross compliance retains terraces on soil erosion control. *Italian Journal of Agronomy, 6*, 43–51.

Bellin, N., van Wesemael, B., Meerkerk, A., Vanacker, V., & Barbera, G. G. (2009). Abandonment of soil and water conservation structures in Mediterranean ecosystems A case study from south east Spain. *Catena, 76*, 114–121. https://doi.org/10.1016/j.catena.2008.10.002

Bevan, A., & Conolly, J. (2011). Terraced fields and Mediterranean landscape structure: An analytical case study from Antikythera, Greece. *Ecological Modelling, 222*, 1303–1314. https://doi.org/10.1016/j.ecolmodel.2010.12.016

Brunori, E., Salvati, L., Antogiovanni, A., & Biasi, R. (2018). Worrying about 'vertical landscapes': Terraced olive groves and ecosystem services in marginal land in Central Italy. *Sustainability, 10*. https://doi.org/10.3390/su10041164

Bryan, R., & Yair, A. (1982). Perspectives on studies of badland geomorphology. In Badland geomorphology and piping. Geobooks Norwich, 1-12. https://doi.org/10.2307/635017.

Calsamiglia, A., Fortesa, J., Garcia Comendador, J., Lucas Borja, M. E., Calvo Cases, A., & Estrany, J. (2018). Spatial patterns of sediment connectivity in terraced lands: Anthropogenic controls of catchment sensitivity. *Land Degradation & Development, 29*, 1198–1210. https://doi.org/10.1002/ldr.2840

Calsamiglia, A., Lucas-Borja, M. E., Fortesa, J., Garcia-Comendador, J., & Estrany, J. (2017). Changes in soil quality and hydrological connectivity caused by the abandonment of terraces in a mediterranean burned catchment. *Forests, 8*. https://doi.org/10.3390/f8090333

Cao, Y., Wu, Y., Zhang, Y., & Tian, J. (2013). Landscape pattern and sustainability of a 1300-year-old agricultural landscape in subtropical mountain areas, Southwestern China. *The International Journal of Sustainable Development and World Ecology, 20*, 349–357. https://doi.org/10.1080/13504509.2013.773266

Carlos, C., Goncalves, F., Crespo, L., Zina, V., Oliveira, I., Crespi, A., et al. (2019). How does habitat diversity affect ground-dwelling arthropods assemblages in Douro Demarcated Region terraced vineyards? *Journal of Insect Conservation, 23*, 555–564. https://doi.org/10.1007/s10841-019-00144-y

Cevasco, A., Pepe, G., & Brandolini, P. (2014). The influences of geological and land use settings on shallow landslides triggered by an intense rainfall event in a coastal terraced environment. *Bulletin of Engineering Geology and the Environment, 73*, 859–875. https://doi.org/10.1007/s10064-013-0544-x

Chen, S. K., Chen, Y. R., & Peng, Y. H. (2013). Experimental study on soil erosion characteristics in flooded terraced paddy fields. *Paddy and Water Environment, 11*, 433–444. https://doi.org/10.1007/s10333-012-0334-2

Chen, S. K., Liu, C. W., & Chen, Y. R. (2012). Assessing soil erosion in a terraced paddy field using experimental measurements and universal soil loss equation. *Catena, 95*, 131–141. https://doi.org/10.1016/j.catena.2012.02.013

Chen, B. X., Qiu, Z. M., Usio, N., & Nakamura, K. (2018). Conservation and contingent valuation of farming landscape amenities by visitors: A case study of terraced paddy fields in Central Japan. *Paddy and Water Environment, 16*, 561–570. https://doi.org/10.1007/s10333-018-0648-9

Chen, D., Wei, W., & Chen, L. D. (2017). Effects of terracing practices on water erosion control in China: A meta analysis. *Earth-Science Reviews, 173*, 109–121. https://doi.org/10.1016/j.earscirev.2017.08.007

Chen, D., Wei, W., & Chen, L. D. (2020). How can terracing impact on soil moisture variation in China? A meta-analysis. *Agricultural Water Management, 227*. https://doi.org/10.1016/j.agwat.2019.105849

Chen, D., Wei, W., Chen, L. D., & Yu, Y. (2016). Progress of the ecosystem services and management of terraces, 03 *Mountain Rsearch, 34*, 374–384 (in Chinese with English Abstract).

Chen, D., Wei, W., Daryanto, S., & Tarolli, P. (2020). Does terracing enhance soil organic carbon sequestration? A national-scale data analysis in China. *The Science of the Total Environment, 721*, 137751. https://doi.org/10.1016/j.scitotenv.2020.137751

Chow, T. L., Rees, H. W., & Daigle, J. L. (1999). Effectiveness of terraces/grassed waterway systems for soil and water conservation: A field evaluation. *Journal of Soil and Water Conservation, 54*, 577–583.

Crosta, G. B., Dal Negro, P., & Frattini, P. (2003). Soil slips and debris flows on terraced slopes. *Natural Hazards and Earth System Sciences, 3*, 31–42. https://doi.org/10.5194/nhess-3-31-2003

Damene, S., Tamene, L., & Vlek, P. L. G. (2013). Performance of exclosure in restoring soil fertility: A case of Gubalafto district in north Wello zone, northern highlands of Ethiopia. *Catena, 101*, 136–142. https://doi.org/10.1016/j.catena.2012.10.010

Díaz, A. R., Sanleandro, P. M., Soriano, A. S., Serrato, F. B., & Faulkner, H. (2007). The causes of piping in a set of abandoned agricultural terraces in southeast Spain. *Catena, 69*(3), 282–293.

Dick, R. P., Sandor, J. A., & Eash, N. S. (1994). Soil enzyme activities after 1500 years of terrace agriculture in the Colca Valley, Peru. *Agriculture, Ecosystems & Environment, 50*, 123–131. https://doi.org/10.1016/0167-8809(94)90131-7

Duarte, F., Jones, N., & Fleskens, L. (2008). Traditional olive orchards on sloping land: Sustainability or abandonment? *Journal of Environmental Management, 89*, 86–98. https://doi.org/10.1016/j.jenvman.2007.05.024

Dunjó, G., Pardini, G., & Gispert, M. (2003). Land use change effects on abandoned terraced soils in a Mediterranean catchment, NE Spain. *Catena, 52*, 23–37. https://doi.org/10.1016/S0341-8162(02)00148-0

Duran Zuazo, V. H., Rodriguez Pleguezuelo, C. R., Galvez Ruiz, B., Gutierrez Gordillo, S., & Francisco Garcia-Tejero, I. (2019). Water use and fruit yield of mango (Mangifera indica L.) grown in a subtropical Mediterranean climate. *International Journal of Fruit Science, 19*, 136–150. https://doi.org/10.1080/15538362.2018.1493960

Fashaho, A., Ndegwa, G. M., Lelei, J. J., Musandu, A. O., & Mwonga, S. M. (2020). Effect of land terracing on soil physical properties across slope positions and profile depths in medium and high altitude regions of Rwanda. *South African Journal of Plant and Soil, 37*(2), 91–100. https://doi.org/10.1080/02571862.2019.1665722

Feng, X., Cheng, W., Fu, B., & Lu, Y. (2016). The role of climatic and anthropogenic stresses on long-term runoff reduction from the Loess Plateau, China. *The Science of the Total Environment, 571*, 688–698. https://doi.org/10.1016/j.scitotenv.2016.07.038

Feng, T. J., Wei, W., Chen, L. D., Chen, D., Yu, Y., & Yang, L. (2017). [Comparison of soil hydraulic characteristics under the conditions of long-term land preparation and natural slope in Longtan catchment of the loess hilly region]. *Huanjing KeXue, 38*, 3860–3870. https://doi.org/10.13227/j.hjkx.201702126

Fu, B., Liu, Y., Lu, Y., He, C., Zeng, Y., & Wu, B. (2011). Assessing the soil erosion control service of ecosystems change in the Loess Plateau of China. *Ecological Complexity, 8*, 284–293. https://doi.org/10.1016/j.ecocom.2011.07.003

Fu, B., Wang, S., Su, C., & Forsius, M. (2013). Linking ecosystem processes and ecosystem services. *Current Opinion in Environmental Sustainability, 5*, 4–10. https://doi.org/10.1016/j.cosust.2012.12.002

Gallart, F., Llorens, P., & Latron, J. (1994). Studying the role of old agricultural terraces on runoff generation in a small Mediterranean mountainous basin. *Journal of Hydrology, 159*, 291–303. https://doi.org/10.1016/0022-1694(94)90262-3

Galletti, C. S., Ridder, E., Falconer, S. E., & Fall, P. L. (2013). Maxent modeling of ancient and modern agricultural terraces in the Troodos foothills, Cyprus. *Applied Geography, 39*, 46–56. https://doi.org/10.1016/j.apgeog.2012.11.020

Gao, P., Jiang, G., Wei, Y., Mu, X., Wang, F., Zhao, G., & Sun, W. (2015). Streamflow regimes of the Yanhe River under climate and land use change, Loess Plateau, China. *Hydrological Processes, 29*, 2402–2413. https://doi.org/10.1002/hyp.10309

Gao, J., Lu, Y., Chen, Z., Wang, L., & Zhou, J. (2019). Land-use change from cropland to orchard leads to high nitrate accumulation in the soils of a small catchment. *Land Degradation & Development, 30*(17), 2150–2161. https://doi.org/10.1002/ldr.3412

Garcia-Franco, N., Wiesmeier, M., Goberna, M., Martínez-Mena, M., & Albaladejo, J. (2014). Carbon dynamics after afforestation of semiarid shrublands: Implications of site preparation techniques. *Forest Ecology and Management, 319*, 107–115. https://doi.org/10.1016/j.foreco.2014.01.043

Garcia-Ruiz, J. M., Nadal-Romero, E., Lana-Renault, N., & Begueria, S. (2013). Erosion in Mediterranean landscapes: Changes and future challenges. *Geomorphology, 198*, 20–36. https://doi.org/10.1016/j.geomorph.2013.05.023

Gates, J. B., Scanlon, B. R., Mu, X., & Zhang, L. (2011). Impacts of soil conservation on groundwater recharge in the semi-arid Loess Plateau, China. *Hydrogeology Journal, 19*, 865–875. https://doi.org/10.1007/s10040-011-0716-3

Gebremichael, D., Nyssen, J., Poesen, J., Deckers, J., Haile, M., Govers, G., & Moeyersons, J. (2005). Effectiveness of stone bunds in controlling soil erosion on cropland in the Tigray Highlands, northern Ethiopia. *Soil Use & Management, 21*, 287–297. https://doi.org/10.1079/SUM2005321

Gibson, C. A., Koch, B. J., Compson, Z. G., Hungate, B. A., & Marks, J. C. (2018). Ecosystem responses to restored flow in a travertine river. *Freshwater Science, 37*, 169–177. https://doi.org/10.1086/696614

Guo, J., Yue, T., Li, X., & Yuan, Y. (2016). Heavy metal levels in kiwifruit orchard soils and trees and its potential health risk assessment in Shaanxi, China. *Environmental Science and Pollution Research, 23*(14), 14560–14566. https://doi.org/10.1007/s11356-016-6620-6

Hammad, A. A., Haugen, L. E., & Borresen, T. (2004). Effects of stonewalled terracing techniques on soil-water conservation and wheat production under Mediterranean conditions. *Environmental Management, 34*(5), 701–710. https://doi.org/10.1007/s00267-003-0278-9

Havlova, L., Hula, V., Niedobova, J., & Michalko, R. (2017). Effect of adjacent steppe-like habitats on spider diversity in vine plants. *Biocontrol, 62*, 757–768. https://doi.org/10.1007/s10526-017-9840-x

Hazel, D. W. (2008). Best management practices for reducing sediment loss from tobacco fields. *Journal of Soil and Water Conservation, 63*, 91A. https://doi.org/10.2489/jswc.63.3.91A

He, J. W. (2010). The exploitation of agricultural civilization heritages of minority community in Guangxi———a case study of Longsheng dragon back terrace, 06 *Journal of Landscape Research*, 80–83. https://doi.org/10.16785/j.issn1943-989x.2010.06.021.

Higson, J. L., & Singer, M. B. (2015). The impact of the streamflow hydrograph on sediment supply from terrace erosion. *Geomorphology, 248*, 475–488. https://doi.org/10.1016/j.geomorph.2015.07.037

Hrdalo, I., Trojanovic, A., & Tomic Reljic, D. (2019). The terraced landscape as a part of the Dubrovnik regional identity: Cross time study of the region Dubrovacko Primorje (Republic of Croatia). *Annales: Anali za istrske in mediteranske studije. Series historia et sociologia, 29*, 125–140. https://doi.org/10.19233/ASHS.2019.09

Huang, L., Wang, B., Niu, X., Gao, P., & Song, Q. (2019). Changes in ecosystem services and an analysis of driving factors for China's Natural Forest Conservation Program. *Ecology and Evolution, 9*, 3700–3716. https://doi.org/10.1002/ece3.4925

Hu, J. M., Hu, X., & Zuo, C. Q. (2005). Analysis on soil and water conservation benefit of terracing on red-soil slope land, 04 *Research of Soil and Water Conservation, 12*, 271–273 (in Chinese with English Abstract).

Iiyama, N., Kamada, M., & Nakagoshi, N. (2005). Ecological and social evaluation of landscape in a rural area with terraced paddies in southwestern Japan (vol 70, pg 301, 2005). *Landscape and Urban Planning, 73*, 59–71. https://doi.org/10.1016/j.landurbplan.2004.12.001

Inbar, M., & Llerena, C. (2000). Erosion processes in high mountain agricultural terraces in Peru. *Mountain Research and Development, 20*, 72–79. https://doi.org/10.1659/0276-4741(2000)020[0072:EPIHMA]2.0.CO;2

Jiao, J. Y., & Wang, W. Z. (1999). Quality and soil–water conservation effectiveness of level terrace on the Loess Plateau. *Transactions on CSAE, 15*(2), 59–63 (in Chinese with English Abstract).

Johnson, A. T., & Holly, T. (1992). Terraces for erosion and runoff: A program simulation (TERPS). *Computers and Electronics in Agriculture, 7*, 121–132. https://doi.org/10.1016/S0168-1699(05)80027-4

Kagabo, D. M., Stroosnijder, L., Visser, S. M., & Moore, D. (2013). Soil erosion, soil fertility and crop yield on slow-forming terraces in the highlands of Buberuka, Rwanda. *Soil and Tillage Research, 128*, 23–29. https://doi.org/10.1016/j.still.2012.11.002

Kassie, M., Köhlin, G., Bluffstone, R., & Holden, S. (2011). Are soil conservation technologies "win-win?" A case study of Anjeni in the north-western Ethiopian highlands. *Natural Resources Forum, 35*, 89–99. https://doi.org/10.1111/j.1477-8947.2011.01379.x

Kim, J. G., Park, J., & Hong, M. G. (2013). Relationship between early development of plant community and environmental condition in abandoned paddy terraces at mountainous valleys in Korea. *Journal of Ecology and Environment, 36*, 131–140. https://doi.org/10.5141/ecoenv.2013.017

Kladnik, D., Kruse, A., & Komac, B. (2017). Terraced landscapes: An increasingly prominent cultural landscape type. *Acta Geographica Slovenica-Geografski Zbornik, 57*, 73–81. https://doi.org/10.3986/AGS.4770

Kosmowski, F. (2018). Soil water management practices (terraces) helped to mitigate the 2015 drought in Ethiopia. *Agricultural Water Management, 204*, 11–16. https://doi.org/10.1016/j.agwat.2018.02.025

Koulouri, M., & Giourga, C. (2007). Land abandonment and slope gradient as key factors of soil erosion in Mediterranean terraced lands. *Catena, 69*, 274–281. https://doi.org/10.1016/j.catena.2006.07.001

Lasanta, T., Arnáez, J., Oserín, M., & Ortigosa, M. (2001). Marginal lands and erosion in terraced fields in the mediterranean mountains: A case study in the Camero Viejo (northwestern Iberian system, Spain). *Mountain Research and Development, 21*, 69–77. https://doi.org/10.1659/0276-4741(2001)021[0069:mlaeit]2.0.co2

Lee, S., & Kim, Y. P. (2011). A comparative study on the conservation of rice terraces as cultural landscapes in Korean and Japanese rural areas. *The Journal of Korean Institute of Forest Recreation, 15*, 1–14.

Lesschen, J. P., Cammeraat, L. H., & Nieman, T. (2008). Erosion and terrace failure due to agricultural land abandonment in a semi-arid environment. *Earth Surface Processes and Landforms, 33*, 1574–1584. https://doi.org/10.1002/esp.1676

Lesschen, J. P., Schoorl, J. M., & Cammeraat, L. H. (2009). Modelling runoff and erosion for a semi-arid catchment using a multi-scale approach based on hydrological connectivity. *Geomorphology, 109*, 174–183.

Liang, Y., Lal, R., Guo, S., Liu, R., & Hu, Y. (2018). Impacts of simulated erosion and soil amendments on greenhouse gas fluxes and maize yield in Miamian soil of central Ohio. *Scientific Reports, 8*. https://doi.org/10.1038/s41598-017-18922-6

Li, Y., & Lindstrom, M. J. (2001). Evaluating soil quality–soil redistribution relationship on terraces and steep hillslope. *Soil Science Society of America Journal, 65*, 1500–1508. https://doi.org/10.2136/sssaj2001.6551500x

Liu, S. L., Dong, Y. H., Li, D., Liu, Q., Wang, J., & Zhang, X. L. (2013). Effects of different terrace protection measures in a sloping land consolidation project targeting soil erosion at the slope scale. *Ecological Engineering, 53*, 46–53. https://doi.org/10.1016/j.ecoleng.2012.12.001

Liu, X., He, B., Li, Z., Zhang, J., Wang, L., & Wang, Z. (2011). Influence of land terracing on agricultural and ecological environment in the Loess Plateau regions of China. *Environmental Earth Sciences, 62*, 797–807. https://doi.org/10.1007/s12665-010-0567-6

Liu, C. A., Li, F. R., Zhou, L. M., Zhang, R. H., Yu, J., Lin, S. L., et al. (2013). Effect of organic manure and fertilizer on soil water and crop yields in newly-built terraces with loess soils in a semi-arid environment. *Agricultural Water Management, 117*, 123–132. https://doi.org/10.1016/j.agwat.2012.11.002

Liu, M. C., Xiong, Y., Yuan, Z., Min, Q. W., Sun, Y. H., & Fuller, A. M. (2014). Standards of ecological compensation for traditional eco-agriculture: Taking rice-fish system in Hani terrace as an example. *Journal of Mountain Science, 11*, 1049–1059. https://doi.org/10.1007/s11629-013-2738-x

Liu, C. A., & Zhou, L. M. (2017). Soil organic carbon sequestration and fertility response to newly-built terraces with organic manure and mineral fertilizer in a semi-arid environment. *Soil and Tillage Research, 172*, 39–47. https://doi.org/10.1016/j.still.2017.05.003

Li, Y. M., Wang, K. Q., Liu, Z. Q., Wang, J. Y., & Zhou, X. (2006). Effect of measure of engineering preparation to soil water in Yunnan dry-hot river valley. *Journal of Soil and Water Conservation, 1*(2), 15–19 (in Chinese with English abstract).

Londero, A. L., Minella, J. P. G., Deuschle, D., Schneider, F. J. A., Boeni, M., & Merten, G. H. (2018). Impact of broad-based terraces on water and sediment losses in no-till (paired zero-order) catchments in southern Brazil. *Journal of Soils and Sediments, 18*(3), 1159–1175. https://doi.org/10.1007/s11368-017-1894-y

Londoño, A. C., Williams, P. R., & Hart, M. L. (2017). A change in landscape: Lessons learned from abandonment of ancient Wari agricultural terraces in Southern Peru. *Journal of Environmental Management, 202*, 532–542. https://doi.org/10.1016/j.jenvman.2017.01.012

Lu, H. S., Zhu, Y. H., Skaggs, T. H., & Yu, Z. B. (2009). Comparison of measured and simulated water storage in dryland terraces of the Loess Plateau, China. *Agricultural Water Management, 96*, 299–306.

Mai, V. T., Van Keulen, H., Hessel, R., Ritsema, C., Roetter, R., & Phien, T. (2013). Influence of paddy rice terraces on soil erosion of a small watershed in a hilly area of Northern Vietnam. *Paddy and Water Environment, 11*(1–4), 285–298. https://doi.org/10.1007/s10333-012-0318-2

Martinez-Hernandez, C., Rodrigo-Comino, J., & Romero-Diaz, A. (2017). Impact of lithology and soil properties on abandoned dryland terraces during the early stages of soil erosion by water in south-east Spain. *Hydrological Processes, 31*, 3095–3109. https://doi.org/10.1002/hyp.11251

Meerkerk, A. L., van Wesemael, B., & Bellin, N. (2009). Application of connectivity theory to model the impact of terrace failure on runoff in semi-arid catchments. *Hydrological Processes, 23*, 2792–2803. https://doi.org/10.1002/hyp.7376

Merino, J. H., Rozas, L. P., Minello, T. J., & Sheridan, P. F. (2010). Effects of marsh terracing on nekton abundance at two locations in Galveston Bay, Texas. *Wetlands, 30*, 693–704. https://doi.org/10.1007/s13157-010-0079-x

Mesfin, S., Taye, G., Desta, Y., Sibhatu, B., Muruts, H., & Mohammedbrhan, M. (2018). Short-term effects of bench terraces on selected soil physical and chemical properties: Landscape improvement for hillside farming in semi-arid areas of northern Ethiopia. *Environmental Earth Sciences, 77*, 399. https://doi.org/10.1007/s12665-018-7528-x

Miao, J. Q., Wang, Z. Q., Yang, W. T., Sun, S., & Huang, G. Q. (2017). [Ecosystem services of Chongyi Hakka terraces]. *Journal of Applied Ecology, 28*, 1642–1652. https://doi.org/10.13287/j.1001-9332.201705.015

Miloš, B., & Bensa, A. (2019). Cd, Cu, Pb and Zn in terraced soil on flysch deposits of

Kastela Bay coastal area, Croatia. *Journal of Central European Agriculture, 20*, 974–985. https://doi.org/10.5513/JCEA01/20.3.2288
Mojeremane, W., Rees, R. M., & Mencuccini, M. (2010). Effects of site preparation for afforestation on methane fluxes at Harwood Forest, NE England. *Biogeochemistry, 97*, 89–107. https://doi.org/10.1007/s10533-009-9322-z
Momirski, L. A., & Kladnik, D. (2009). Terraced landscapes in Slovenia. *Acta Geographica Slovenica-Geografski Zbornik, 49*, 7–29. https://doi.org/10.3986/AGS49101
Moreno-de-las-Heras, M., Lindenberger, F., Latron, J., Lana-Renault, N., Llorens, P., Arnaez, J., et al. (2019). Hydro-geomorphological consequences of the abandonment of agricultural terraces in the Mediterranean region: Key controlling factors and landscape stability patterns. *Geomorphology, 333*, 73–91. https://doi.org/10.1016/j.geomorph.2019.02.014
Morgan, J. M., & Condon, A. G. (1986). Water use, grain yield, and osmoregulation in wheat. *Functional Plant Biology, 13*, 523–532. https://doi.org/10.1071/PP9860523
Nie, W., Ma, X., & Fei, L. (2017). Evaluation of infiltration models and variability of soil infiltration properties at multiple scales. *Irrigation and Drainage, 66*, 589–599. https://doi.org/10.1002/ird.2126
Ni, S. J., & Zhang, J. H. (2007). Variation of chemical properties as affected by soil erosion on hillslopes and terraces. *European Journal of Soil Science, 58*, 1285–1292. https://doi.org/10.1111/j.1365-2389.2007.00921.x
Nyssen, J., Poesen, J., Moeyersons, J., Deckers, J., Haile, M., & Lang, A. (2004). Human impact on the environment in the Ethiopian and Eritrean highlands—a state of the art. *Earth-Science Reviews, 64*(3–4), 273–320. https://doi.org/10.1016/s0012-8252(03)00078-3
Olesen, J. E., & Bindi, M. (2002). Consequences of climate change for European agricultural productivity, land use and policy. *European Journal of Agronomy, 16*, 239–262. https://doi.org/10.1016/S1161-0301(02)00004-7
Oliveira, J. R. S.d., Pruski, F. F., Silva, J. M. A.d., & Silva, D. P.d. (2012). Comparative analysis of the performance of mixed terraces and level and graded terraces. *Acta Scientiarum. Agronomy, 34*, 351–357. https://doi.org/10.4025/actasciagron.v34i4.14755
Pappalardo, G., Toscano, S., & Pecorino, B. (2019). Assessing willingness to pay for the terraced landscape of vineyards in Mt. Etna (Italy). *Quality-Access to Success, 20*, 440–445.
Pardini, G., & Gispert, M. (2012). Soil quality assessment through a multi-approach analysis in soils of abandoned terraced land in NE Spain. *Cuadernos De Investigacion Geografica, 38*, 7–30.
Pardini, G., Gispert, M., Emran, M., & Doni, S. (2017). Rainfall/runoff/erosion relationships and soil properties survey in abandoned shallow soils of NE Spain. *Journal of Soils and Sediments, 17*, 499–514. https://doi.org/10.1007/s11368-016-1532-0
Park, H., Lee, S. J., Cheong, S., Jeong, H. R., & Kim, J. G. (2017). Effects of small dam in a stream on benthic macro-invertebrate community. *Journal of Wetlands Research, 19*, 252–258.
Park, J. Y., Yu, Y. S., Hwang, S. J., Kim, C., & Kim, S. J. (2014). SWAT modeling of best management practices for Chungju dam watershed in South Korea under future climate change scenarios. *Paddy and Water Environment, 12*(1), S65–S75. https://doi.org/10.1007/s10333-014-0424-4
Peng, T., & Wang, S. J. (2012). Effects of land use, land cover and rainfall regimes on the surface runoff and soil loss on karst slopes in southwest China. *Catena, 90*, 53–62. https://doi.org/10.1016/j.catena.2011.11.001
Pepe, G., Mandarino, A., Raso, E., Scarpellini, P., Brandolini, P., & Cevasco, A. (2019). Investigation on farmland abandonment of terraced slopes using multitemporal data sources comparison and its implication on hydro-geomorphological processes. *Water, 11*. https://doi.org/10.3390/w11081552
Pietsch, D., & Mabit, L. (2012). Terrace soils in the Yemen Highlands: Using physical, chemical and radiometric data to assess their suitability for agriculture and their vulnerability to degradation. *Geoderma, 185*, 48–60. https://doi.org/10.1016/j.geoderma.2012.03.027
Poesen, J., Nachtergaele, J., Verstraeten, G., & Valentin, C. (2003). Gully erosion and environmental change: Importance and research needs. *Catena, 50*(2–4), 91–133. https://doi.org/10.1016/S0341-8162(02)00143-1
Posthumus, H., & De Graaff, J. (2005). Cost-benefit analysis of bench terraces, a case study in Peru. *Land Degradation & Development, 16*, 1–11. https://doi.org/10.1002/ldr.637
Posthumus, H., Deeks, L. K., Rickson, R. J., & Quinton, J. N. (2015). Costs and benefits of erosion control measures in the UK. *Soil Use & Management, 31*, 16–33. https://doi.org/10.1111/sum.12057
Preti, F., Guastini, E., Penna, D., Dani, A., Cassiani, G., Boaga, J., et al. (2018). Conceptualization of water flow pathways in agricultural terraced landscapes. *Land Degradation & Development, 29*, 651–662. https://doi.org/10.1002/ldr.2764
Price, S., & Nixon, L. (2005). Ancient Greek agricultural terraces: Evidence from texts and archaeological survey. *American Journal of Archaeology, 109*, 665–694. https://www.jstor.org/stable/40025693.
Qiu, Z., Chen, B., & Takemoto, K. (2014). Conservation of terraced paddy fields engaged with multiple stakeholders: The case of the Noto GIAHS site in Japan. *Paddy and Water Environment, 12*, 275–283. https://doi.org/10.1007/s10333-013-0387-x
Quine, T. A., Walling, D. E., Chakela, Q. K., Mandiringana, O. T., & Zhang, X. (1999). Rates and patterns of tillage and water erosion on terraces and contour strips: Evidence from caesium-137 measurements. *Catena, 36*, 115–142. https://doi.org/10.1016/S0341-8162(99)00006-5
Ramos, M. C., Cots-Folch, R., & Martínez-Casasnovas, J. A. (2007). Sustainability of modern land terracing for vineyard plantation in a Mediterranean mountain environment – the case of the Priorat region (NE Spain). *Geomorphology, 86*(1–2), 1–11. https://doi.org/10.1016/j.geomorph.2006.08.004
Ramos, M. C., & Porta, J. (1997). Analysis of design criteria for vineyard terraces in the mediterranean area of North East Spain. *Soil Technology, 10*, 155–166, 1997.
Rodewald, R., & Liechti, K. (2016). From Campagna to Arcadia: Changes in the reception of terraced landscapes in art and their practical implications. *Annales: Anali za istrske in mediteranske studije. Series historia et sociologia, 26*, 363–374. https://doi.org/10.19233/ASHS.2016.28
Romero Díaz, A., Marín Sanleandro, P., Sánchez Soriano, A., Belmonte Serrato, F., & Faulkner, H. (2007). The causes of piping in a set of abandoned agricultural terraces in southeast Spain. *Catena, 69*, 282–293. https://doi.org/10.1016/j.catena.2006.07.008
Ruecker, G., Schad, P., Alcubilla, M. M., & Ferrer, C. (1998). Natural regeneration of degraded soils and site changes on abandoned agricultural terraces in Mediterranean Spain. *Land Degradation & Development, 9*(2), 179–188.
Sang-Arun, J., Mihara, M., Horaguchi, Y., & Yamaji, E. (2006). Soil erosion and participatory remediation strategy for bench terraces in northern Thailand. *Catena, 65*, 258–264. https://doi.org/10.1016/j.catena.2005.11.010
Schilling, K. E., & Jacobson, P. J. (2016). Water and nutrient discharge to a high-value terrace-floodplain fen: Resilience and risk. *Ecohydrology, 9*, 1196–1207. https://doi.org/10.1002/eco.1718
Schönbrodt-Stitt, S., Behrens, T., Schmidt, K., Shi, X., & Scholten, T. (2013). Degradation of cultivated bench terraces in the Three Gorges Area: Field mapping and data mining. *Ecological Indicators, 34*, 478–493. https://doi.org/10.1016/j.ecolind.2013.06.010
Shao, H., Baffaut, C., Gao, J. E., Nelson, N. O., Janssen, K. A., Pierzynski, G. M., et al. (2013). Development and application of algorithms for simulating terraces within swat. *Transactions of the Asabe, 56*, 1715–1730. https://doi.org/10.13031/trans.56.10047
Shao, Y., Chen, H., Zhu, Z., & Li, B. (2019). Integrating environmental parameters and economic benefits to analyze the ecological agriculture (EA) application in the mountain rice paddy system of Chongqing, China. *Environmental Sciences Europe, 31*. https://doi.org/10.1186/s12302-019-0204-2
Sharda, V. N., Juyal, G. P., & Singh, P. N. (2002). Hydrologic and sedimentologic behavior of a conservation bench terrace system in a sub-humid climate. *Transactions of the ASAE, 45*(5), 1433–1441.
Shi, Z. H., Ai, L., Fang, N. F., & Zhu, H. D. (2012). Modeling the impacts of integrated small watershed management on soil erosion and sediment delivery: A case study in the three Gorges area, China. *Journal of Hydrology, 438*, 156–167. https://doi.org/10.1016/j.jhydrol.2012.03.016
Shi, Z. H., Cai, C. F., Ding, S. W., Wang, T. W., & Chow, T. L. (2004). Soil conservation planning at the small watershed level using RUSLE with GIS: A case study in the three Gorge area of China. *Catena, 55*, 33–48. https://doi.org/10.1016/S0341-8162(03)00088-2
Shi, Z. H., Chen, L. D., Cai, C. F., Li, Z. X., & Liu, G. H. (2009). Effects of long-term fertilization and mulch on soil fertility in contour hedgerow systems: A case study on steeplands from the three Gorges area, China. *Nutrient Cycling in Agroecosystems, 84*, 39–48. https://doi.org/10.1007/s10705-008-9223-x
Shimoda, S., & Koyanagi, T. F. (2017). Land use alters the plant-derived carbon and nitrogen pools in terraced rice paddies in a mountain village. *Sustainability, 9*. https://doi.org/10.3390/su9111973
Siriri, D., Tenywa, M. M., Raussen, T., & Zake, J. K. (2005). Crop and soil variability on terraces in the highlands of SW Uganda. *Land Degradation & Development, 16*(6), 569–579. https://doi.org/10.1002/ldr.688
Slámová, M., Krcmarova, J., Hroncek, P., & Kastierova, M. (2017). Environmental factors influencing the distribution of agricultural terraces: Case study of Horny Tisovnik, Slovakia. *Moravian Geographical Reports, 25*, 34–45. https://doi.org/10.1515/mgr-2017-0004
Soriano, M. A., & Herath, S. (2018). Quantifying the role of traditional rice terraces in regulating water resources: Implications for management and conservation efforts. *Agroecology and Sustainable Food Systems, 42*, 885–910. https://doi.org/10.1080/21683565.2018.1437497
Stanchi, S., Freppaz, M., Agnelli, A., Reinsch, T., & Zanini, E. (2012). Properties, best management practices and conservation of terraced soils in southern Europe (from mediterranean areas to the Alps): A review. *Quaternary International, 265*, 90–100. https://doi.org/10.1016/j.quaint.2011.09.015
Stavi, I., Rozenberg, T., Al-Ashhab, A., Argaman, E., & Groner, E. (2018). Failure and collapse of ancient agricultural stone terraces: On-site effects on soil and vegetation. *Water, 10*. https://doi.org/10.3390/w10101400
Strehmel, A., Jewett, A., Schuldt, R., Schmalz, B., & Fohrer, N. (2016). Field data-based implementation of land management and terraces on the catchment scale for an eco-hydrological modelling approach in the Three Gorges Region, China. *Agricultural Water Management, 175*, 43–60. https://doi.org/10.1016/j.agwat.2015.10.007
Tang, Q., Oki, T., Kanae, S., & Hu, H. (2008). A spatial analysis of hydro-climatic and vegetation condition trends in the Yellow River basin. *Hydrological Processes, 22*, 451–458. https://doi.org/10.1002/hyp.6624
Tarolli, P., Preti, F., & Romano, N. (2014). Terraced landscapes: From an old best practice to a potential hazard for soil degradation due to land abandonment. *Anthropocene, 6*, 10–25. https://doi.org/10.1016/j.ancene.2014.03.002
Tilliger, B., Rodriguez-Labajos, B., Bustamante, J. V., & Settele, J. (2015). Disentangling values in the interrelations between cultural ecosystem services and landscape ConservationA case study of the Ifugao rice terraces in the Philippines. *Land, 4*, 888–913. https://doi.org/10.3390/land4030888

Tiwari, K. R., Sitaula, B. K., Bajracharya, R. M., & Børresen, T. (2009). Runoff and soil loss responses to rainfall, land use, terracing and management practices in the Middle Mountains of Nepal. *Acta Agriculturae Scandinavica, 59*(3), 197–207. https://doi.org/10.1080/09064710802006021

Tokuoka, Y., & Hashigoe, K. (2015). Effects of stone-walled terracing and historical forest disturbances on revegetation processes after the abandonment of mountain slope uses on the Yura Peninsula, southwestern Japan. *Journal of Forest Research, 20*, 24–34. https://doi.org/10.1007/s10310-014-0471-0

Trinugraheni, T., Suyana, J., & Sumarno, S. (2017). Mulching with terrace strengthen on surface runoff, erosion, and sediment enrichment ratio. *Agrotechnology Research Journal, 1*. https://doi.org/10.20961/agrotechresj.v1i1.18868U. No 1 (2017).

Uchida, T., Furuno, M., Minami, T., Yamashita, S., Uchiyama, T., Arase, T., et al. (2015). Ecological significance of masonry revetments in plant biodiversity. *International Journal of Geomate, 9*, 1353–1359.

Uchida, E., Sato, K., Cunin, O., & Toyouchi, K. (2013). A reconsideration of the construction period of the Cruciform terraces and the elevated causeways in the Angkor monuments, based on the magnetic susceptibility of the sandstone blocks. *Archaeometry, 55*, 1034–1047. https://doi.org/10.1111/j.1475-4754.2012.00717.x

Van Dijk, A.I.J.M. (2002). reportWater and sediment dynamics in bench terraced agricultural steeplands in west Java, Indonesia. PhD thesis. Vrije Universiteit Amsterdam.

Van Dijk, A. I. J. M., & Bruijnzeel, L. A. (2004). Runoff and soil loss from bench terraces. 2. An event based erosion process model. *European Journal of Soil Science, 55*, 317–334. https://doi.org/10.1111/j.1365-0754.2004.00605.x

Van Dijk, A. I. J. M., Bruijnzeel, L. A., Vertessy, R. A., & Ruijter, J. (2005). Runoff and sediment generation on bench-terraced hillsides: Measurements and up-scaling of a field-based model. *Hydrological Processes, 19*(8), 1667–1685.

Varotto, M., & Lodatti, L. (2014). New family farmers for abandoned lands the adoption of terraces in the Italian Alps (Brenta valley). *Mountain Research and Development, 34*, 315–325. https://doi.org/10.1659/MRD-JOURNAL-D-14-00012.1

Verheijen, F. G. A., Jones, R. J. A., Rickson, R. J., & Smith, C. J. (2009). Tolerable versus actual soil erosion rates in Europe. *Earth-Science Review, 94*, 23–38.

Vogel, S., & Conedera, M. (2020). Effects of land use-induced vegetation and topography changes on soil chemistry in the Southern Alps (Ticino, Switzerland). *Plant Soil and Environment, 66*(2), 73–80. https://doi.org/10.17221/633/2019-PSE

Walle, R. J., & Sims, B. G. (1999). Fertility gradients in naturally formed terraces on Honduran hillside farms. *Agronomy Journal, 91*, 350–353. https://doi.org/10.2134/agronj1999.00021962009100020028x

Wang, P., Wang, K. Q., Li, T. X., & Li, Y. J. (2011). [Regulation effects of reverse-slope level terrace on the runoff and sediment yield in sloping farmland]. *Journal of Applied Ecology, 22*, 1261–1267. https://doi.org/10.13287/j.1001-9332.2011.0173

Wang, F., Yu, C., Xiong, L., & Chang, Y. (2019). How can agricultural water use efficiency be promoted in China? A spatial-temporal analysis. *Resources, Conservation and Recycling, 145*, 411–418. https://doi.org/10.1016/j.resconrec.2019.03.017

Wei, W., Chen, D., Wang, L., Daryanto, S., Chen, L., Yu, Y., et al. (2016). Global synthesis of the classifications, distributions, benefits and issues of terracing. *Earth-Science Reviews, 159*, 388–403. https://doi.org/10.1016/j.earscirev.2016.06.010

Wen, Y., Kasielke, T., Li, H., Zhang, B., & Zepp, H. (2020). May agricultural terraces induce gully erosion? A case study from the Black soil region of northeast China. *The Science of the Total Environment, 750*, 141715. https://doi.org/10.1016/j.scitotenv.2020.141715

Wen, B., Ren, Q., & Zhang, N. (2009). Soil nutrient vertical variance of Hani terraced field in Yuanyang county of Yunnan Province. *Journal of Yunnan Agricultural University, 24*, 78–93.

Wickama, J., Okoba, B., & Sterk, G. (2014). Effectiveness of sustainable land management measures in West Usambara highlands, Tanzania. *Catena, 118*, 91–102. https://doi.org/10.1016/j.catena.2014.01.013

Wu, F. Q., Zhang, Y. B., & Wang, J. (2004). Study on the benefits of level terrace on soil and water conservation, 01 *Science of Soil and Water Conservation*, 34–37 (in Chinese with English Abstract).

Xiao, L., Wang, Z. W., Yin, Q. Y., & Huang, C. M. (2019). Effect of terracing slope cropland on soil and water conservation in dry-hot valley of Jinsha river basin, southwest China. *Southwest China Journal of Agricultural Sciences, 32*(12), 2856–2861 (in Chinese with English Abstract).

Xu, Q. X., Wang, T. W., Cai, C. F., Li, Z. X., & Shi, Z. H. (2012). Effects of soil conservation on soil properties of citrus orchards in the Three-Gorges Area, China. *Land Degradation & Development, 23*(1), 34–42. https://doi.org/10.1002/ldr.1045

Xu, Q. X., Wu, P., Dai, J. F., Wang, T. W., Li, Z. X., Cai, C. F., et al. (2018). The effects of rainfall regimes and terracing on runoff and erosion in the Three Gorges area, China. *Environmental Science and Pollution Research, 25*, 9474–9484. https://doi.org/10.1007/s11356-018-1198-9

Xu, Y., Yang, B., Tang, Q., Liu, G., & Liu, P. (2011). Analysis of comprehensive benefits of transforming slope farmland to terraces on the Loess Plateau: A case study of the Yangou watershed in northern Shaanxi Province, China. *Journal of Mountain Science, 8*, 448–457. https://doi.org/10.1007/s11629-011-1058-2

Yang, Q., Meng, F. R., Zhao, Z., Chow, T. L., Benoy, G., Rees, H. W., et al. (2009). Assessing the impacts of flow diversion terraces on stream water and sediment yields at a watershed level using SWAT model. *Agriculture, Ecosystems & Environment, 132*, 23–31. https://doi.org/10.1016/j.agee.2009.02.012

Yu, Y., Wei, W., Chen, L., Feng, T., Daryanto, S., & Wang, L. (2017). Land preparation and vegetation type jointly determine soil conditions after long-term land stabilization measures in a typical hilly catchment, Loess Plateau of China. *Journal of Soils and Sediments, 17*, 144–156. https://doi.org/10.1007/s11368-016-1494-2

Zgaier, A. (2008). Landslides on agricultural hillslope terraces under Mediterranean climatic conditions. *Israel Journal of Earth Sciences, 57*, 249–261. https://doi.org/10.1560/ijes.57.3-4.249

Zhang, Y., He, L., Li, X., Zhang, C., Qian, C., Li, J., et al. (2019). Why are the Longji terraces in southwest China maintained well? A conservation mechanism for agricultural landscapes based on agricultural multi-functions developed by multi-stakeholders. *Land Use Policy, 85*, 42–51. https://doi.org/10.1016/j.ecolecon.2007.02.024

Zhang, Q. W., & Li, Y. (2014). Effectiveness assessment of soil conservation measures in reducing soil erosion in Baiquan County of Northeastern China by using 137Cs techniques. *Environmental Science. Processes & impacts, 16*, 1480–1488.

Zhang, Y., Long, Y., An, J., & Wang, X. (2014). Spatial patterns of 137 Cs inventories and soil erosion form earth-banked terraces in the Yimeng Mountains, China. *Journal of Environmental Radioactivity, 136*, 1–9.

Zhang, Y., Min, Q., Zhang, C., He, L., Zhang, S., Yang, L., et al. (2017). Traditional culture as an important power for maintaining agricultural landscapes in cultural heritage sites: A case study of the Hani terraces. *Journal of Cultural Heritage, 25*, 170–179. https://doi.org/10.1016/j.landusepol.2019.03.046

Zhang, J. H., Su, Z. A., & Liu, G. C. (2008). Effects of terracing and agroforestry on soil and water loss in hilly areas of the Sichuan Basin, China. *Journal of Mountain Science, 5*(3), 241–248. https://doi.org/10.1007/s11629-008-0189-6

Zhang, L., Wang, J. M., Bai, Z. K., & Lv, C. (2015). Effects of vegetation on runoff and soil erosion on reclaimed land in an opencast coal-mine dump in a loess area. *Catena, 128*, 44–53. https://doi.org/10.1016/j.catena.2015.01.016

Zhang, J. H., Wang, Y., & Li, F. C. (2015). Soil organic carbon and nitrogen losses due to soil erosion and cropping in a sloping terrace landscape. *Soil Research, 53*(1), 87–96. https://doi.org/10.1071/SR14151

Zhang, H., Wei, W., Chen, L., & Wang, L. (2017). Effects of terracing on soil water and canopy transpiration of Pinus tabulaeformis in the Loess Plateau of China. *Ecological Engineering, 102*, 557–564. https://doi.org/10.1016/j.ecoleng.2017.02.044

Zhang, Y., Wu, F., Zhang, X., & Cao, N. (2017). Pollution characteristics and ecological risk assessment of heavy metals in three land-use types on the southern Loess Plateau, China. *Environmental Monitoring and Assessment, 189*(9), 470. https://doi.org/10.1007/s10661-017-6140-y

Zhao, G., Mu, X., Wen, Z., Wang, F., & Gao, P. (2013). Soil erosion, conservation, and ecoenvironment changes in the Loess Plateau of China. *Land Degradation & Development, 24*(5), 499–510. https://doi.org/10.1002/ldr.2246

Zhou, K. Q., Sui, Y. Y., Liu, X. B., Zhang, X. Y., Jin, J., Wang, G. H., & Herbert, S. J. (2015). Crop rotation with nine-year continuous cattle manure addition restores farmland productivity of artificially eroded Mollisols in Northeast China. *Field Crops Research, 171*, 138–145. https://doi.org/10.1016/j.fcr.2014.10.017

Zoumides, C., Bruggeman, A., Giannakis, E., Camera, C., Djuma, H., Eliades, M., & Charalambous, K. (2017). Community-based rehabilitation of mountain terraces in Cyprus. *Land Degradation & Development, 28*, 95–105. https://doi.org/10.1002/ldr.2586

Zuazo, V. H. D., Pleguezuelo, C. R. R., Peinado, F. J. M., de Graaff, J., Martinez, J. R. F., & Flanagan, D. C. (2011). Environmental impact of introducing plant covers in the taluses of terraces: Implications for mitigating agricultural soil erosion and runoff. *Catena, 84*, 79–88. https://doi.org/10.1016/j.catena.2010.10.004

Zuo, C. Q., & Li, X. Q. (2004). Effects of terrace on soil and water conservation in red-soil hilly area. *Bulletin of Soil and Water Conservation, 6*, 79–81. https://doi.org/10.13961/j.cnki.stbctb.2004.06.020

International Soil and Water Conservation Research 9 (2021) 360–369

Contents lists available at ScienceDirect

International Soil and Water Conservation Research

journal homepage: www.elsevier.com/locate/iswcr

Short Communication

Soil conservation and sustainable development goals(SDGs) achievement in Europe and central Asia: Which role for the European soil partnership?

Hakkı Emrah Erdogan [a, *], Elena Havlicek [b], Carmelo Dazzi [c], Luca Montanarella [d], Marc Van Liedekerke [d], Borut Vrščaj [e, f], Pavel Krasilnikov [g], Gulchekhra Khasankhanova [h], Ronald Vargas [i]

[a] Republic of Turkey Ministry of Agriculture and Forestry, Ankara, Turkey
[b] Federal Office for the Environment FOEN, Soil and Biotechnology Division, 3003, Berne, Switzerland
[c] University of Palermo, Italy
[d] European Commission, Joint Research Centre, I-21027, Ispra, VA, Italy
[e] Department for Agro-ecology and Natural Resources, Centre for Soil and Environment, Agricultural Institute of Slovenia, Ljubljana, Slovenia
[f] Environmental Protection College, Velenje, Slovenia
[g] Lomonosov Moscow State University, Eurasian Centre for Food Security, Moscow, Russian Federation
[h] UZGIP Institute, Ministry of Water Resources, Tashkent, Uzbekistan
[i] Food and Agriculture Organization of the United Nations, Rome, Italy

ARTICLE INFO

Article history:
Received 10 September 2020
Received in revised form
22 February 2021
Accepted 27 February 2021
Available online 5 March 2021

Keywords:
Sustainable soil management
Soil partnership
Soil policy
Voluntary versus 52 mandatory approaches
Multilevel coordination
Communication and cooperation

ABSTRACT

Voluntary soil protection measures are not sufficient to achieve sustainable soil management at a global scale. Additionally, binding soil protection legislation at national and international levels has also proved to be insufficient for the effective protection of this almost non-renewable natural resource. The European Soil Partnership (ESP) and its sub-regional partnerships (Eurasian Sub-Regional Soil Partnership, Alpine Soil Partnership) were established in the context of FAO's Global Soil Partnership (GSP) with the mission to facilitate and contribute to the exchange of knowledge and technologies related to soils, to develop dialogue and to raise awareness for the need to establish a binding global agreement for sustainable soil management. The ESP has taken a role of an umbrella network covering countries in Europe and Central Asia. It aims to improve the dialogue in the whole region and has encouraged establishing goals that would promote sustainable soil management, taking into account various national and local approaches and priorities, as well as cultural specificities. The ESP first regional implementation plan for the 2017–2020 period was adopted and implemented along the five GSP pillars of action. Building on the experience of the last four years, this study demonstrates that establishing sub-regional and national partnerships is an additional step in a concrete sustainable soil management implementation process. It also suggests that a complementary approach between legal instruments and voluntary initiatives linked to the development of efficient communication and strong commitment is the key to success.

1. Introduction

The history of humankind has always been linked to the use of natural resources, they are currently linked and continue to be in the future. The successes or rise and failures of civilisations depend on people's awareness of how to sustainably manage natural resources such as air, water, and soil (Montgomery, 2012), and ultimately, how to avoid their loss or degradation. Like water and air, soils need to be protected against degradation from indiscriminate human activities. Chemical pollution is one the most notable threats affecting the three natural resources through direct or indirect inputs. However, contrary to the use of air and water, the use of soil (as a source of food, fibre, and fodder) since the inception of agriculture, inevitably entails a transformation of its basic

* Corresponding author.
E-mail address: hakki.erdogan@tarimorman.gov.tr (H.E. Erdogan).

https://doi.org/10.1016/j.iswcr.2021.02.003

properties and functioning and can lead to its intrinsic degradation. Hence, soil conservation involves both, protection against threats and sustainable management of multifunctional soils.

The complex nature of soils, that is, their high number of components and the interactions and feedbacks between these components (Havlicek & Mitchell, 2014) requires also a complex and a multidisciplinary sustainable soil management approach. Land use in general depends on soil properties and their potential functions (e.g. food or fibre production, water purification or climate regulation, and habitat); however, land use modifies soil properties and, therefore, affect provision of soil ecosystem services (Fig. 1).

The multiple and often unsustainable use of soils can lead to specific soil degradation, such as erosion, compaction, contamination, decline in soil organic matter, loss of soil biodiversity and others, which have been identified at national, regional, and global levels since the beginning of the Anthropocene. The matter has gained attention in the global environmental and development agenda, and many articles concerning soils were published in recent times stressing the importance of soil as a vital natural resource that performs many functions and provides ecosystem services (Drobnik et al., 2018). The capacity of soil for food production and the potential of climate change mitigation attract particular attention in the context of current environmental problems (Vermeulen et al., 2019).

In today's world, the sustainable use of soil depends not only on the management preferences and capabilities of local users—such as farmers, foresters, and land-use planners—but also on the development and implementation of widely adopted environment protection and climate mitigation policies at global or regional levels (Davies, 2017; Juerges & Hansjürgens, 2018; Montanarella, 2015). However, an approach and a legal framework based on the protection against soil threats alone are not sufficient to maintain multiple soil functions. Soil degradation with its associated social, economic and environmental impacts, costs, and problems require long-term regional and global funding, resource mobilisation, and expertise far beyond the solutions that are available to local users.

In response to the need of a global approach, the FAO established the Global Soil Partnership (GSP) in 2012 to develop synergies among national and international organisations for global action to stimulate a sustainable use of soil resources. The mission of the GSP is to "develop awareness and contribute to the development of capacities, build on best available science, and facilitate/contribute to the exchange of knowledge and technologies among stakeholders for the sustainable management and use of soil resources". The GSP encompasses nine regional soil partnerships (RSPs), covering the entire globe. The fundamental principle of the GSP and its RSPs is a country-driven, bottom-up approach. In this regard, regional partnerships play an important role to develop and steer dialogue between RSP's member countries. In Europe and Central Asia, this is performed by the European Soil Partnership (ESP), which was established in 2013. Given the vast geographic extent of the ESP, covering all Europe and Eurasia, the Eurasian Soil Partnership (EASP) was established in 2013 to account for sub-regional specificities and issues. The ESP, covering 40 member countries in Europe and Eurasia (Fig. 2), has identified the soil protection and sustainable soil management priorities with considering the major Europe-relevant soil threats, whereas the EASP has elaborated specific priorities for Eurasia.

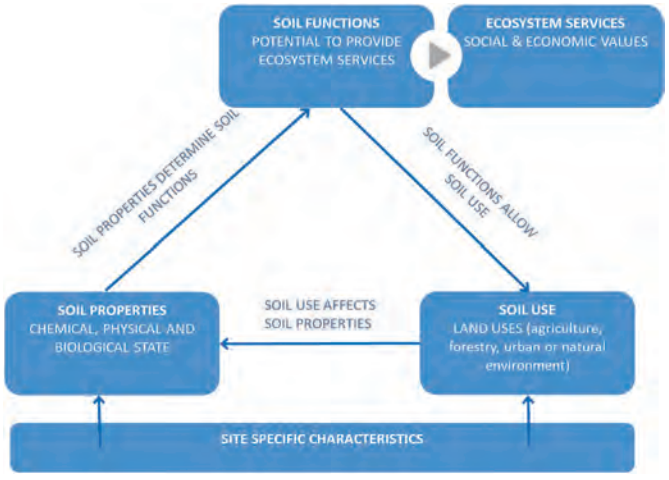

Fig. 1. Interrelations between soil properties, soil functions and soil use (adapted from FOEN, 2020).

The current study outlines the ESP and the EASP actions during the 2017–2020 period. Its objective is to present activities performed during the first implementation plan and to outline the challenges that had to be met. Moreover, further global reflections on the aspects of the concrete implementation of soil protection and management will be addressed.

2. Prioritised main UN SDG challenges and solutions at the European/Eurasian level

Maintenance and restoration of healthy soils along with its proper functioning is an underlying principle of several targets of the Sustainable Development Goals (SDGs). Since its inception, the GSP has been successfully raising awareness about soil at the global level, specifically on the UN SDGs and the 2030 Agenda. Soil, a cross-cutting theme, is not the subject of a specific multilateral environmental agreement (MEA), while it remains a relevant aspect in relation to climate change (UNFCCC), biodiversity (CBD) and desertification (UNCCD). However, many SDGs refer to targets that directly consider soil resources. For instance, poverty (SDG 1), food security (SDG 2), food safety (SDG 3), clean water (SDG 6), urban development (SDG 11), consumption and production pattern (SDG 12), climate regulation (SDG 13), land-based nutrient pollution of the seas (SDG 14), terrestrial ecosystem service sustainability (SDG 15), and partnership building for the Goals (SDG 17) all are dependent directly or indirectly, on the provision of ecosystem services where soils play a key role (https://sustainablesoils.org/soil-and-the-sdgs; Keesstra et al., 2016; Bouma et al., 2019) (Fig. 3).

Achieving soil-related SDGs in Europe and Central Asia requires an improved sharing of data and knowledge, incentives for research and monitoring, the analysis and design of adequate sustainable soil management options, and political and financial support. Regional implementation plans are the main tool for defining joint targets and priority actions; therefore, priorities and needs should be accurately defined and agreed on by the RSP's member countries. The implementation plans are organised along the GSP action framework, which is based on five pillars (Global Soil Partnership | Food and Agriculture Organization of the United Nations (fao.org)) (Fig. 4).

The main soil threats in Europe and Central Asia have been identified as soil sealing, salinization, and contamination (FAO, 2017 and FAO and ITPS, 2015). Additional threats include soil organic carbon changes, nutrient imbalance, soil compaction, soil erosion by wind and water, soil biodiversity loss, desertification, and landslides. Additionally, the EASP has recognised soil salinity as a main regional threat.

3. ESP and EASP policies and the 2017–2020 implementation plan

The 2017–2020 implementation plans of the ESP and the EASP have been developed according to regional soil threats and

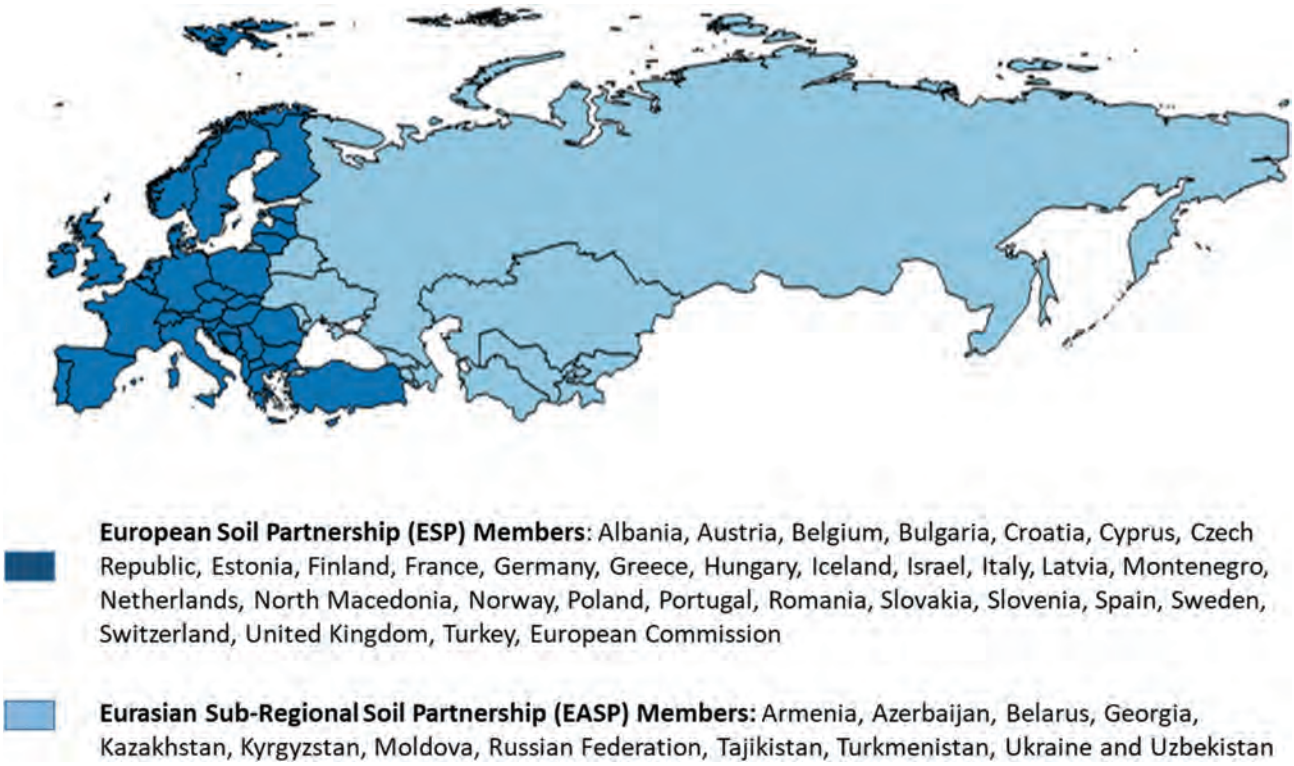

Fig. 2. Geographic extent of regional soil partnerships in Europe and Central Asia.

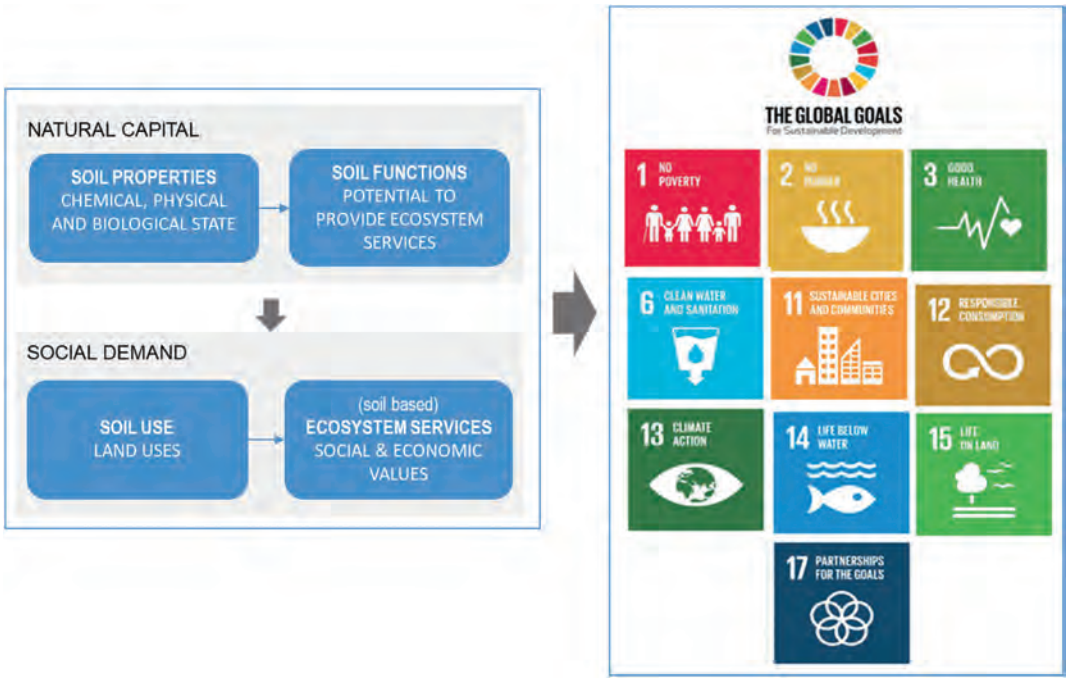

Fig. 3. Soils and cross-cutting themes.

considering their contribution to the achievement of the SDGs. They also prioritise an understanding of cross-border soil-related and land-based demands referring to soils by implementing SDGs 1, 2, 3, 6, 11, 12, 13, 14, 15, and 17 (FAO, 2017). In the following sub-chapters, the planned activities with their contribution to the SDGs will be described for each ESP pillar, and the key actors and the main challenges and opportunities will be outlined.

Fig. 4. The Global Soil Partnership action framework.

3.1. Promote sustainable management of soil resources for soil protection, conservation, and sustainable productivity (Pillar 1)

The European region is characterised by a large number and variety of institutions and organisations, and numerous regional-wide projects[1] whose objective is to study and implement sustainable soil management. Consequently, the main activities for Pillar 1 (Table 1) were set out to identify the key projects, institutions, and stakeholders and to bring together existing networks. The development of concrete solutions to soil-related problems, such as soil salinity in Central Asia, is essential to achieve land degradation neutrality (SDG 15.3).

The challenges associated with SSM implementation must be assessed including economic, technical, social-political, investment and partnership challenges. The ESP and EASP bring together partners and existing initiatives to improve global and regional solutions and practices towards improving and increase SSM for soil protection, conservation, and sustainable productivity (FAO, 2017).

The EASP has carried out activities in the context of awareness raising and dialogue for an integrative system approach and SSM technologies. Regarding this, several flagship reports have been published to support decision-making and policy development (EFCS 2018; FAO, 2016). In addition, guidance for the management of salty lands was published, which contributes to resolving the main threat in the region (FAO & ECFS, 2018). Most notably, between 2019 and 2020, 10 small projects on salinity mitigation and adaptation and 4 projects on soil organic carbon management were granted by the GSP Secretariat to the research groups in Armenia, Belarus, Moldova, Ukraine and Uzbekistan. A major part of the financial support for the EASP activities was provided in the frame of grant funded by the Russian Federation to the GSP Secretariat.

During the implementation period, having a guidance document such as the Voluntary Guidelines on Sustainable Soil Management (FAO, 2017), adopted by GSP member countries, was an important achievement but at the same time, the lack of policies to translate it into the action was challenging. Even if the EU Soil Thematic Strategy and EU Common Agricultural Policy are addressing soils in the 27 EU member countries, there is the need to develop a coherent sustainable soil management approach for the entire European region. A major role can be played in this sense by the European Environment Agency (EEA), that includes in its membership most of the countries in the region (EC, 2020; 2020a).

3.2. Encourage investment, technical cooperation, policy, education awareness, and extension in soils (Pillar 2)

Many of the actions under the other pillars addressed the general lack of societal awareness about the importance of soil in people's lives and for the well-being of the planet. In many cases, education deficiency in education of the environmental, societal and economic importance of soil is one of the underlying causes of unsustainable soil management practices, of the general lack of investment (both in education and in technical measures to protect soil), and of the widespread political reluctance to adopt short- and long-term measures to preserve and enhance soil conditions. Therefore, Pillar 2 activities of the ESP (Table 2) aimed to express the importance of soil to achieve SDGs 2, 11, 13 and 15. The promotion of outreach materials on best soil management practices, improving the dialogue between the scientific community, stakeholders, policy makers and the soil end users, and conducting integrated research programs were the main regional actions to enhance international support for implementing effective and targeted capacity-building for sustainable development (see Table 3).

A specific action has also been taken to increase soil awareness and research at the EU level. Such action concerns a request to revise and to update the panels of the European Research Council (ERC) whose mission is "to encourage the highest quality research in Europe through competitive funding and to support investigator-driven frontier research across all fields, on the basis of scientific excellence". However, the topic "soil science", does not appear with the importance that it deserves, and that has been acknowledged at a global level. Starting from this consideration, the ESP together with the European Society for Soil Conservation (ESSC) and the European Confederation of Soil Science Societies (ECSSS) prepared and signed a "petition" (also signed by the President of all the soil science societies of Europe) that has been sent to the ERC President.

[1] Examples of such projects are:- EJP Soil – a large H2020 programme that embeds internal projects related to main topics (e.g. carbon sequestration, erosion, soil ecosystem services, etc.); .); https://projects.au.dk/ejpsoil/- iSQAPER (Interactive Soil Quality assessment in Europe and China for Agricultural productivity and Environmental Resilience; http://www.isqaper-project.eu/);- SOILCARE (Soil Care for profitable and sustainable crop production in Europe, https://www.soilcare-project.eu/); - LANDMARK (Land Management Assessment Research Knowledge Base; http://landmark2020.eu/); - CACILM-II (Central Asian Countries Initiative for Land Management; http://www.cacilm.org/)- SPRINT (Sustainable Plant Protection Transition: A Global Health Approach; https://sprint-h2020.eu/.)- MINAGRIS (MIcro- and NAano-Plastics in AGRIgricultural Soils: sources, environmental fate and impacts on ecosystem services and overall sustainability).

Table 1
The ESP Pillar 1 2017–2020 implementation plan to promote sustainable management of soil resource in the Europe and Central Asia region.

Main activities	Partners/Key Stakeholders	Links with SDGs
Promoting an overview on the European soil threats and existing sustainable soil management (SSM) practices and stakeholder networks	In partnership with existing SSM-related projects and networks, and/or engaging farmer associations; ESP national focal points provide contacts to national projects	SDG 1.4 - equal access to ownership and control over land and other forms of property SDG 3.9 - substantially reduce the number of deaths and illnesses from hazardous chemicals and air, water, and soil pollution and contamination
Improve the multi-disciplinary dialogue	In partnership with existing networks from projects such assuch as iSQAPER, Soil Care, Landmark, and CACILM-II	SDG 14.1 - prevent and significantly reduce marine pollution of all kinds, from land-based activities
Support the mitigation and adaptation to soil pollution in Europe	EC-Joint Research Centre (JRC) on behalf of ESP secretariat, national focal points, national research organisations	SDG 15.3 - combat desertification, restoration of degraded land and soil
Support the mitigation and adaptation to soil salinity in Eurasia	Eurasian Center for Food Security (ECFS) on behalf of EASP secretariat, national focal points, national research organisations	SDG 17.16 - enhance the global partnership for sustainable development
Facilitate the development of a capacity-building strategy amongst stakeholders	EC- JRC on behalf of ESP secretariat, ECFS on behalf of EASP secretariat and FAO GSP, ESP and EASP national focal points provide information from national projects and extension services and farmer associations	
Report on the barriers preventing SSM implementation		

Table 2
ESP 2017–2020 implementation plan for Pillar 2.

Main activities	Partners/Key Stakeholders	Links with SDGs
Promote key messages to inform politicians and decision makers on the importance of soil	EC- JRC on behalf of ESP secretariat, ECFS on behalf of EASP secretariat and FAO GSP, ESP national focal points	SDG 2.4 - sustainable food production systems and resilient agricultural practices
Promote educational resources (multilingual), public outreach material and events, the definition of best practices, engagement with other scientific disciplines	Regional Soil Science Communities, NGOs	SDG 11.3 - inclusive and sustainable urbanisation
Establish an inclusive dialogue to address soil fertility management at the European level	European Commission and all other partners	SDG 13.1 - strengthen resilience and adaptive capacity to climate-related hazards and natural disasters in all countries
Conduct research calls (targeting of EU and national funding programme)		SDG 15.1 - conservation, restoration and sustainable use of terrestrial ecosystems and their services
Improving engagement between the soil science community and agricultural extension services to enhance the soil component in sustainable land use advisory activities	EC- JRC on behalf of ESP secretariat, ECFS on behalf of EASP secretariat and FAO GSP, ESP national focal points	SDG 15.2 - sustainable forest management, halt deforestation, restore degraded forests
For Central Asia, the establishment of a consultation service on soil management, for knowledge sharing and transfer	ECFS on behalf of EASP secretariat, with other possible partners such as the International Centre for Agricultural Research in the Dry Areas (ICARDA), and the International Centre for Biosaline Agriculture (ICBA)	SDG 17.9 - enhance international support for implementing effective and targeted capacity-building

Table 3
ESP Pillar 3 implementation plan 2017–2020 to improve regional soil research area.

Main activities	Partners/Key Stakeholders	Links with SDGs
Initiate a web-based platform for a structured inventory of soil research, and metadata on available soil information	EC- JRC on behalf of ESP secretariat, and FAO GSP, ESP national focal points, ESP Working Group members (or other voluntary contributors) of ESP and EASP	SDG 17.6 - enhance international cooperation and access to science, technology and innovation, and enhance knowledge sharing
Evaluate the impact/cost–benefit of soil research, stressing the cross-cutting role of soils in grand environmental and societal challenges		SDG 17.7 - promote the development, transfer, dissemination of environmentally sound technologies
Review the needs of inter- and transdisciplinary research for coherent action		SDG 17.14 - enhance policy coherence for sustainable development

The petition requested that the ERC establish a unique and specific ERC panel devoted to the field of “Soil Science” under the Life Sciences domain. A “Soil Science” panel will allow raising soil awareness and for a direct route to early-career soil scientists to apply for ERC grants.

During the first implementation period, the Eurasian Soil Portal was launched, and the EASP secretariat established cooperation on soil, with organisations such as the Dokuchaev Central Soil Museum, St. Petersburg (Russia). Additionally, a Pillar 2 workshop, “Giving soils more voice” was co-organised by the EC-JRC and the European Network of Soil Awareness (ENSA), supported by the European Land and Soil Alliance (ELSA). Although many well-developed local initiatives have been acknowledged, efforts to reach a wide audience and to make a societal impact remain a major challenge. In the EU, the communication aspects of the forthcoming Soil Health Mission of the new Horizon Europe research programme (2021–2027) has a high potential to provide opportunities to facilitate such outreach.

3.3. Promote targeted soil research and development focusing on identified gaps and priorities and synergies with related productive, environmental, and social development actions (Pillar 3)

Pillar 3 activities focus on needed improvement of soil knowledge, effective sharing of research results, evaluating their impact with cost-benefit analysis, and reviewing the needs of linkages

with cross-cutting issues, to ensure the access to science (SDGs 17.6), the development and transfer of environmentally sound technologies (SDG 17. 7), and to enhance policy coherence for sustainable development (SDG 17.14).

In Europe, many research and innovation projects have been funded under the EU Seventh Framework Programme for Research and Innovation (2007–2013) and the EU's funding instrument for the environment and climate action (LIFE programme) to address soil issues and to improve the knowledge base for action. LIFE has funded 147 soil-related projects covering different aspects of soil protection (soil sealing, soil biodiversity, soil carbon sequestration, soil monitoring, water and soil, sustainable agriculture and forestry, and land contamination). This effort continues under Horizon 2020 and LIFE+. The European Innovation Partnership (EIP) on agriculture also plays also a role.

At the EU level, the INSPIRATION project released the bottom-up demand-driven research need, including 14 integrated and 19 thematic areas. Additionally, the ESP became a member of the advisory board of the European Joint Program on Soil (EJP SOIL), which was established to identify soil research needs and propose research activities on priority topics for Europe. Recently, the Sino-EU Soil Observatory for Intelligent Land Use Management (SIEU-SOIL) consortium has been established to promote a research platform consisting of advanced crop and soil sensing tools, modelling and data fusion, digital soil mapping, and farm management information systems that will be developed to maximise land productivity and socio-economic benefits while minimising the environmental impacts.

In the EASP, the FAO and ECFS initiated a small grant facility for soil research projects to support targeted research and partnerships between scientists and local/national beneficiaries that would form a stable basis for long-term collaborative engagement to scale up the implementation of SSM practices to adapt or mitigate soil salinity and climate change.

Combining basic and applied research is pivotal in generating knowledge on adaptation of existing/traditional and integration of new, more environmental friendly soil management practices to adequately support SDGs. In soil research, the future development of the ESP would depend on the format of interaction with the new regional initiatives on soil research and knowledge exchange, which can support to the ambition of the EU Green Deal in relation to soil (Montanarella & Panagos, 2021) in the region.

3.4. Enhance the quantity, quality, and availability of soil data and information: data collection (generation), analysis, validation, modelling, reporting, monitoring and integration with other disciplines (Pillar 4)

In Europe, the building of information systems has a long history in terms of data exchange and networking. There are many soil data available, however gaps still exist and currently available data do not satisfy increasing user requirements (e.g. soil monitoring for agricultural, soil contamination, or soil biodiversity monitoring purposes). Current assessments of the status of the European soil resources are mainly based on rough estimates using largely nowadays considered legacy soil data that were compiled almost twenty years ago and cross-border harmonised to produce the Soil Geographical Database (SGDB) of Europe 1:1,000,000 (SGDB) in 2004, later published in the Soil Atlas of Europe in 2005. Yet, the relatively rough 1:1M scale of the SGDB and the needs on information of key soil properties calls for a spatial (resolution) and content improvement of uniform soil information at the European level.

The current situation in the Eurasian region is characterised by disaggregated, coarse and missing soil data. Even when soil data exist, they are often not shared or have limited availability. In this regard, there is need to develope a joint action and the ECFS as Secretariat of EASP can facilitate the dialogue among to countries for establishiıng a regional soil information system.

At the same time, data demands are high in the context of climate change (e.g. greenhouse gas inventories), SDGs, soil monitoring and soil research on soil pollution, and lack of data hinders advances in policy development and implementation, as well as research and innovation.

In the implementation plan, the investments in soil data collection were prioritised, and the activities were planned (Table 4) to support the establishment of regional soil information systems. Within this scope, ESP and EASP member countries agreed to prioritise the soil data collection investments to assess and monitor soil health in terms of soil quality (soil organic carbon, soil productivity, biodiversity, etc.), degradation (pollution, erosion, salinization, etc.), and ex-post/ex-ante impact assessment of human activities such as deforestation, restoration, and conservation. The SIS would allow the development of coherent policies and monitoring of policy implementations related to SDGs 3, 14, and 15.

In this direction, the ESP and EASP activities focus on contributing to the mapping exercise of the Global Soil Organic Carbon Map (GSOCmap), Global Soil Salinity Map (GSSmap), and planned Global Soil Erosion Map (GSEmap) as part of the development of the regional and global soil information system (GLOSIS). Globally, the International Soil Reference and Information Centre (ISRIC) in the Netherlands has taken role as a soil information facility centre and the EC-JRC facilitates the dialogue among EU member countries to establish a regional soil information system.

In Eurasia, national soil data centres have been established in Russia, Moldova, Belarus and Azerbaijan. The ECFS as an EASP secretariat provided support for establishing the Eurasian Soil Information System (EASIS) and for capacity-building at the regional level.

During this exercise, the ESP and EASP both experienced that developing a regional soil information system is challenging due to the need for a country-specific approach to map regional results in artefacts across geo-political borders, diversity of soil analytical methods and classification systems, and a lack of publicly available country-specific data that ultimately influence the assessment of country-specific situations. Therefore, ESP and EASP facilitated data sharing, model validation, and calibration experiments between countries.

3.5. Harmonisation of methods, measurements and indicators for the sustainable management and protection of soil resources (Pillar 5)

The main objective of the ESP's Pillar 5 was to develop an overarching mechanism for globally consistent and comparable harmonised soil monitoring for soil-related policies. The ESP implementation plan contained activities (Table 5) that contribute the Global Soil Laboratory Network (GLOSOLAN), the Universal Soil Classification and to the creation of global soil information exchange standards, to be called SoilML, that would allow access and use of data across a broad range of international initiatives (such as GEOSS and INSPIRE).

To support a European soil monitoring system, the EIONET-NRC Soil has initiated a task force to share details about national soil monitoring and associated information, and suggestions how this can be used to improve the current heterogeneous landscape in Europe for soil indicators, methods, and interpretation.

Moreover, the Regional Soil Laboratory Network for Eurasia and Europe (EUROSOLAN) was established in October 2019. Currently, 117 soil laboratories from Europe and Central Asia are registered.

Table 4
ESP Pillar 4 implementation plan to enhance quantity, quality, and availability of soil data and information between 2017 and 2020.

Main activities	Partners/Key Stakeholders	Links with SDGs
Joint technical meeting of European members of The International Network of Soil Information Institutions (INSII) and other soil information institutions to discuss ESP tasks related to soil information	ESP members of INSII, national soil research centres, European Soil Data Centre (ESDAC), EEA's European Topic Centre (ETC) on Urban/Land/Soil systems, European Soil Bureau Network (ESBN),	SDG 15.1 - conservation, restoration and sustainable use of terrestrial ecosystems and their services
Establish the Eurasian Soil information system and integrate with unified methodology and software (SOTER-type); specify data needs and identify gaps at different scales are assessed	EC- JRC on behalf of ESP secretariat, ECFS on behalf of EASP secretariat and FAO GSP, ESP national focal points	SDG 15.2 - sustainable forest management, halt deforestation, restore degraded forests and substantially increase afforestation and reforestation
Mobilise resources to implement new soil data collection and mapping and ensure comparable/harmonise soil data		
The global Pillar-4 Working Group data specifications: review and expansion to European conditions (e.g., representatively);	ESP members of International Network of Soil Information Institutions and ESP + EASP Pillar 4 Working Group Members	SDG 3.9 - substantially reduce the number of deaths and illnesses from hazardous chemicals and air, water and soil pollution and contamination
Conduct a design study (integrating national and Europe-wide approaches—JRC, EUROSTAT) to establish a soil monitoring system		

The EUROSOLAN aims to strengthen the performance of laboratories using standardised methods/protocols and harmonising soil analysis results so that soil information would be comparable and interpretable across laboratories, countries, and regions. In this regard, the first EUROSOLAN meetings concluded that improvements in the following areas are required in the future: 1) the unification process of national and international measurement methodologies; 2) investments in new equipment; 3) investment in human and financial resources; 4) getting funding; 5) high engagement of staff in research projects and teaching; 6) sufficient coverage of lab services by national projects; and 7) inclusion of methods (e.g. organic contaminants).

4. First ESP implementation plan 2017–2020: achievements, limitations and lessons

The period for the first implementation plan ended in 2020. During the last four years, the ESP partners together with the ESP Steering Committee and the 5 established Pillar Working Groups, held regular meetings and working sessions to improve dialogue on soil-related policies across the region. To what extent do they effectively contribute to the achievement of the ESP's objectives and to the promotion of SSM at global, regional, and national levels?

4.1. Facilitation of cooperation between the global, regional, and local level

The ESP National Focal Points and the ESP secretariat participated in all surveys launched by the GSP secretariat (Global Assessment of Soil Pollution report, Protocol for the Assessment of SSM, Assessment of the Global Status of Soil Biodiversity, SoiLEX platform). The ESP secretariat functioned as a channel for the transmission of information and the continuous efforts of the GSP secretariat to support the RSPs allowed for enhanced cooperation. Therefore, one of the core tasks of the regional partnership - to bring the region-specific aspect to the implementation of global actions - has been achieved.

During this first period, several bottom-up initiatives have led to the establishment of national or sub-regional partnerships. Several countries have set up national soil partnerships (e.g. Italy, Latvia, Portugal, Slovenia) that enable the transfer of the pillar tasks and activities from the global/regional to the national level. In the framework of the Interreg Alpine Space project Links4Soils, a sub-regional initiative led to the establishment of the Alpine sub-regional Soil Partnership (AlpSP) that considers the soil-related priorities and specificities of the Alpine Region. This is a region featuring specific ecological, economic and social conditions and is facing specific threats, such as soil sealing, erosion, landslides or permafrost thawing. The AlpSP efforts to address the soil resource

Table 5
The implementation plan to provide the opportunity on the harmonisation of the use of existing national/regional standards on the intergovernmental level.

Main activities	Partners/Key Stakeholders	Links with SDGs
Revision of the European soil mapping guidelines Support the development of a global soil profile description standard Support to the development of a universal soil classification system Interaction with global activities for developing best practice recommendations and procedures for soil sampling, storage, and soil laboratory analytics Analyse the implementation status for interoperable soil data according to INSPIRE, and the degree of soil data and data processing harmonisation	ESP representation of International Network of Soil Information Institutions (INSII), ESP representation of European Soil Laboratory Network (EUROSOLAN), National Research Centres, European Topic Centre on Urban, Land and Soil Systems, (ETC-ULS), European Soil Data Centre (ESDAC), ESP + EASP Pillar 5 Working Group, European Soil Bureau Network (ESBN),	SDG 15.1 - conservation, restoration and sustainable use of terrestrial ecosystems and their services SDG 15.2 - sustainable forest management, halt deforestation, restore degraded forests, and substantially increase afforestation and reforestation SDG 14.1 - prevent and significantly reduce marine pollution of all kinds, from land-use based activities. SDG 3.9 - substantially reduce the number of deaths and illnesses from hazardous chemicals and air, water and soil pollution, and contamination
Establish an ESP-wide network of soil laboratories building on existing initiatives	EC- JRC, on behalf of ESP secretariat, (ECFS) on behalf of the EASP secretariat and FAO GSP, ESP and EASP national focal points	
Develop a soil indicator concept about the state and response of soils expressing the effect of (soil) policies, management, and climate change	Pillar 5 Working Group	
Development and approval of new standards for saline and sodic soils for Central Asia	ECFS on behalf of the EASP secretariat and FAO GSP, ESP national focal points, Working Group Members	

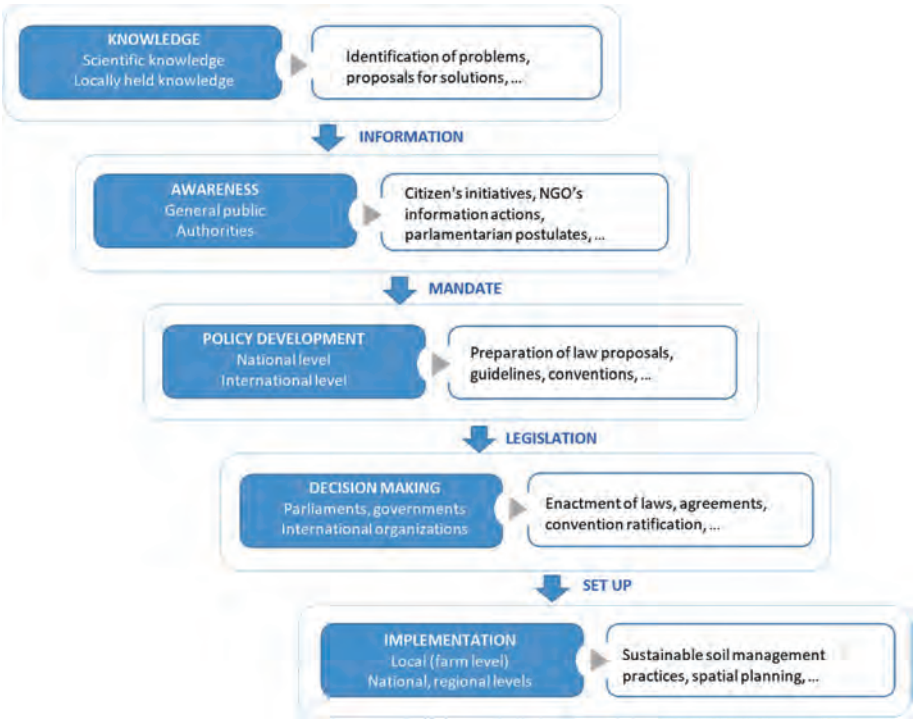

Fig. 5. Adoption of SSM practices: from problem and/or solution identification to the implementation, a multilevel process.

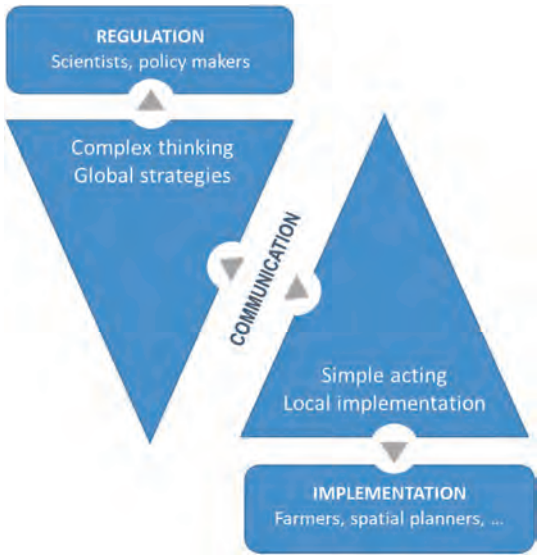

Fig. 6. Soils are complex systems and their comprehension requires complex thinking, however implementation of soil protection policy must be based on understandable and simple tools.

in line with the ESP implementation plan are a transnational contribution to fostering the implementation of the Alpine Convention's Soil Conservation Protocol (a binding international treaty ratified by virtually all parliaments of the Alpine countries) through the review of existing regional and national soil data, transferring knowledge and best management practices to local level policy-makers, decision makers, and other stakeholders in national languages.

Given that Europe encompasses a large array of ecological conditions, as well as many countries or regions with various local approaches and cultural specificities, national partnerships and sub-regional partnerships, such as the EASP, the Alpine Soil Partnership and the newly emerging Pyrenean Soil Partnership are essential and valuable initiatives linking local initiatives and activities to a larger/global – the GSP scale.

4.2. Exchange of data, knowledge, and technologies

Developing awareness and contributing to the development of capacities is a major part of the ESP mandate. During the last four years, the ESP succeeded in raising awareness on soil to support the prioritisation of sustainable soil management in various policies, as the European Commission presented in an ambitious package of measures within the Biodiversity Strategy 2030, the Farm to Fork and the European Climate Law. For instance, the Farm to Fork strategy addresses soil pollution with a 50% reduction in the use of chemical pesticides by 2030 and aims at a 20% reduction in fertiliser use plus a decrease in nutrient losses by at least 50%.

The necessity to set up an effective monitoring, reporting, and verification (MRV) system for soil in Europe and Central Asia is not a matter of doubt. A harmonised monitoring for evaluating the progress made in reversing the current negative trend is needed to support and adapt soil policies. Europe has an extensive history of harmonisation activities, mainly due to activities by the JRC and the EEA in cooperation with Europe-wide experts, groups, and networks (e.g. the European Soil Bureau Network, EIONET National reference Centre for Soil). However, given the challenges ahead and the stagnation of data harmonisation since the late 1990s, data harmonisation is a difficult and challenging area that still needs to be addressed. The newly launched EU Soil Observatory (EUSO) provides a great opportunity to streamline soil monitoring and indicator development harmonised into a single coherent system for monitoring, reporting, and verifying of policy-relevant soil data and indicators. In the new implementation period, the ESP should be in close collaboration with EUSO to develop a European soil information system.

In EASP, soil information systems are poorly harmonised, and there is a need for the integration of universal harmonised approaches rather than the development of regional systems. Currently, automated data exchange is a main challenge, and it is needed as a core element of the GLOSIS, while in Europe, detailed specifications for such data exchange exist (INSPIRE Directive). It is of high interest that global developments are consistent with the existing European experience. The EEA and EC-JRC are interested to conduct a study comparing the GLOSIS data exchange language with EU INSPIRE Directive data specifications for soil. The objective is to clarify the interoperability between data sets exchanged by INSPIRE and GLOSIS. Accordingly, in the new ESP implementation period, the activities related to soil data exchange should be conducted in connection with Pillar 3 (Research), and more importantly, successful implementation requires tight coordination or even combination with Pillar 4 (Soil information). Ultimately, the question of standardisation of methods and harmonisation of data, as defined in the Pillars 4 and 5, extends well beyond the regional dimension and should be spearheaded and coordinated at the global level. Conversely, awareness raising should be initiated at the local level as awareness depends on a person's intimate connection with his/her environment and personal experience with the "soil" (Michailova & Hutchings, 2006). That is why messages addressed to urban residents or farmers require a different approach, focus and emphasis and, more importantly, should be co-designed with practitioners and communication experts (Bouma, 2019). In this sense, the ESP in general, the ENSA in particular and the GSP pla a role as a formal or informal platform to facilitate the exchange of awareness raising experiences and compelling messages (e.g. World Soil Day website World Soil Day | Food and Agriculture Organization of the United Nations (fao.org)).

4.3. Communication, regulations, and implementation

The experience acquired during the first period of ESP's activities between 2017 and 2020 has highlighted that the adoption of concrete SSM practices is based on a process involving different steps and numerous stakeholders (Fig. 5).

The transfer of appropriate and comprehensible information between different levels and stakeholders constitutes a major challenge and a critical phase. Each stakeholder, whether farmer, citizen, scientist, policymaker, or parliamentarian, has its own language and its own understanding of the problem, priorities and needs. Therefore, promoting and supporting sustainable soil management at the heart of the GSP and ESP activities requires a solid soil literacy and "translation" skills. The VGSSM can be successfully implemented in Europe and Central Asia if end-users participate in the identification, dissemination, and implementation of best practices, and if evidence of economic and social benefits from SSM are adequately presented to the decision makers (politicians). Two levels are particularly relevant for the effective and concrete implementation of soil management measures: the end-users from different sectors (farmers, spatial/urban planners, environmentalists, etc.) and the regulators (policymakers, local and regional level decision makers) (Fig. 6). The former need social and economic conditions that allow for informed decisions and simple concrete actions; the latter require sufficient knowledge and information to adopt a transdisciplinary approach and a holistic view (Havlicek, 2012; Rodrigo-Comino et al., 2020). Moreover, scientists with ability to translate often complex science-based data and facts to commonly understandable information, messages and indicators are another essential link in the transfer of information.

By bringing together policymakers, scientists, and farmers' representatives, the ESP is creating a complementary way of protecting and managing soil resources.

5. Conclusion: mandatory versus voluntary approach

The fulfilment of the ESP fundamental function as an overarching mechanism for the many European organisations involved in the sustainable management of soils is currently based on a strong commitment and voluntary participation from ESP member countries, an active role of the GSP Secretariat, the substantial support of the European Commission and individual EU countries, participating national focal-points of EU countries and the voluntary based involvement of the members of the ESP steering committee and working groups. The design and successful implementation of the above-mentioned activities (Chapter 3) highly depend on a better institutionalisation and the availability of funding, continuous support from EU and international donors, and the commitment of regional and national institutions, including the updating of policies and laws. The successes of the sub-regional partnerships (EASP, AlpSP) achieved so far have also been made possible thanks to financial support from the European Commission, national governments, or research funding, respectively.

The willingness of partners and commitments of governments is the key to successful regional implementation of the VGSSM. Such effort can be realised if different ministries work together to integrate soil issues within their related activities at the national or local level, particularly in the environment, water, climate-change, and agriculture-related departments. Soil protection activities and best management practices need to find a way to specific geographic areas such as the Alps and Mediterranean, regional actors, and, when applicable, even to municipal actors where many soil-affecting decisions are made. On the one hand, binding legal instruments at national (Ronchi et al., 2019) and regional and sub-regional levels will be needed to fully protect available soil resources for future generations. Some instruments are already available, such as the Alpine Convention and its Soil Conservation Protocol (Schmid, 2018), but additional instruments are needed and should be the final aim of the ESP and EASP.

In contrast, capacity-building, awareness raising, and public-private partnerships can help build regional and local cooperation, develop, and implement good national and regional governance in soil management and protection. Complementarity between voluntary and mandatory approaches is a prerequisite to design smart regulation tools that include different instrument categories such as legal or economic instruments, self-regulation, or information strategies (Gunningham & Sinclair, 2017). The voluntary character of the RSPs cannot create any legally binding rights or obligations for its partners. However, the ESP and its sub-regional partnerships, with its voluntary and Europe-wide actions, complements the effectiveness and efficiency of soil conservation in Europe.

Declaration of competing interest

The authors confirm that there is no conflict of interest with the networks, organisations, and data centres referred to in the paper.

Acknowledgements

This study was possible thanks to the support of the Food and Agriculture Organization of the UN, the Global Soil Partnership Secretariat, and the voluntary contribution of the authors.

References

Bouma, J. (2019). How to communicate soil expertise more effectively in the information age when aiming at the UN Sustainable Development Goals. *Soil Use & Management, 35*(1), 32–38. https://doi.org/10.1111/sum.12415

Bouma, J., Montanarella, L., & Evanylo, G. (2019). The challenge for the soil science community to contribute to the implementation of the UN Sustainable Development Goals. *Soil Use & Management, 35*(4), 538–546. https://doi.org/10.1111/sum.12518

Davies, J. (2017). The business case for soil. *Nature, 543*, 309–311. https://doi.org/10.1038/543309a

Drobnik, T., Greiner, L., Keller, A., & Grêt-Regamey, A. (2018). Soil quality indicators–From soil functions to ecosystem services. *Ecological Indicators, 94*, 151–169. https://doi.org/10.1016/j.ecolind.2018.06.052

ECFS. (2018). *Report on taking stock of human capital in soil science for central Asia and the south caucasus*. Moscow, Russia: Eurasian Center for Food Security. https://ecfs.msu.ru/images/publications/CA_SC_report_WEB.pdf.

FAO, & ITPS. (2015). *Status of the World's soil resources (SWSR) – main report*. Rome, Italy: Food and Agriculture Organization of the United Nations and Intergovernmental Technical Panel on Soils. http://www.fao.org/3/a-i5199e.pdf.

FAO. (2016). *Regional implementation plan of the Eurasian soil partnership: Towards sustainable management of soil resources*. Rome, Italy: Food and Agriculture Organization of the United Nations. http://www.fao.org/3/a-bl101e.pdf.

FAO. (2017). *European soil partnership implementation plan 2017–2020*. Rome, Italy: Food and Agriculture Organization of the United Nations. http://www.fao.org/3/a-bs972e.pdf.

FAO, & ECFS. (2018). *Handbook for saline soil management*. Rome, Italy: Food and Agriculture Organization of the United Nations. http://www.fao.org/3/i7318en/I7318EN.pdf.

FOEN. (2020). *Swiss national soil strategy*. Swiss National Soil Strategy (admin.ch).

Gunningham, N., & Sinclair, D. (2017). Smart regulation, 133-148. In P. Drahos (Ed.), *Regulatory theory: Foundations and applications*. ANU Press. https://press-files.anu.edu.au/downloads/press/n2304/pdf/book.pdf.

Havlicek, E. (2012). Soil biodiversity and bioindication: From complex thinking to simple acting. *European Journal of Soil Biology, 49*, 80–84. https://doi.org/10.1016/j.ejsobi.2012.01.009

Havlicek, E., & Mitchell, E. A. (2014). Soils supporting biodiversity. In *Interactions in soil: Promoting plant growth* (pp. 27–58). Dordrecht: Springer. https://doi.org/10.1007/978-94-017-8890-8.

Juerges, N., & Hansjürgens, B. (2018). Soil governance in the transition towards a sustainable bioeconomy. *Journal of Cleaner Production, 170*, 1628–1639. https://doi.org/10.1016/j.jclepro.2016.10.143

Michailova, S., & Hutchings, K. (2006). National cultural influences on knowledge sharing: A comparison of China and Russia. *Journal of Management Studies, 43*(3), 383–405. https://doi.org/10.1111/j.1467-6486.2006.00595.x

Montanarella, L. (2015). Agricultural policy: Govern our soils. *Nature, 528*, 32–33. https://doi.org/10.1038/528032a

Montanarella, L., & Panagos, P. (2021). The relevance of sustainable soil management within the European Green Deal. *Land Use Policy, 100*. https://doi.org/10.1016/j.landusepol.2020.104950, 2021.

Montgomery, D. R. (2012). *Dirt: The erosion of civilizations*. Univ of California Press. https://doi.org/10.1525/9780520952119

Rodrigo-Comino, J., López-Vicente, M., Kumar, V., Rodríguez-Seijo, A., Valkó, O., Rojas, C., Pourghasemi, H. R., Salvati, L., Bakr, N., Vaudour, E., Brevik, E. C., Radziemska, M., Pulido, M., Di Prima, S., Dondini, M., de Vries, W., Santos, E. S., de Lourdes Mendoça-Santos, M., Yu, Y., & Panagos, P. (2020). Soil science challenges in a new era: A transdisciplinary overview of relevant topics. *Air, Soil and Water Research, 13*, 1–17. https://doi.org/10.1177/1178622120977491

Ronchi, S., Salata, S., Arcidiacono, A., Piroli, E., & Montanarella, L. (2019). Policy instruments for soil protection among the EU member states: A comparative analysis. *Land Use Policy, 82*, 763–780. https://doi.org/10.1016/j.landusepol.2019.01.017

Schmid, S. (2018). *The soil conservation Protocol of the Alpine convention: Why was the adoption possible*? In H. Ginzky, E. Dooley, I. Heuser, E. Kasimbazi, T. Markus, & T. Qin (Eds.), *International yearbook of soil law and policy 2017. International yearbook of soil law and policy 2017*. https://doi.org/10.1007/978-3-319-68885-5_20

Vermeulen, S., Bossio, D., Lehmann, J., Luu, P., Paustian, K., Webb, C., Augé, F., Bacudo, I., Baedeker, T., Havemann, T., & Jones, C. (2019). A global agenda for collective action on soil carbon. *Nature Sustainability, 2*, 2–4. https://doi.org/10.1038/s41893-018-0212-z

International Soil and Water Conservation Research 9 (2021) 370–380

Contents lists available at ScienceDirect

International Soil and Water Conservation Research

journal homepage: www.elsevier.com/locate/iswcr

Original Research Article

How to model the effect of mechanical erosion control practices at a catchment scale?

Elizeu Jonas Didoné [a, *], Jean Paolo Gomes Minella [a], Daniel Gustavo Allasia Piccilli [b]

[a] Federal University of Santa Maria, Department of Soil Science, 1000 Avenue Roraima, Camobi, CEP 97105-900, Santa Maria, RS, Brazil
[b] Federal University of Santa Maria, Department of Environmental and Sanitary Engineering, 1000 Avenue Roraima, Camobi, CEP 97105-900, Santa Maria, RS, Brazil

ARTICLE INFO

Article history:
Received 26 August 2020
Received in revised form
27 January 2021
Accepted 28 January 2021
Available online 9 February 2021

Keywords:
Conservation practices
Modeling
P-Factor
Planting efficiency

ABSTRACT

Conservation agriculture practices are a crucial factor in mitigating and controlling erosion by water. To address water erosion estimates, most environmental models use the USLE, RUSLE, and MUSLE models. Management practices that affect soil erosion by modifying the flow pattern, such as contour farming, strip farming, or terracing, are represented within these models as a support practice (P) factor. However, due to the difficulty in accurately mapping the P-factor, many studies choose to ignore it, using only the default value P-factor 1which represents the absence of sowing at the level or cultivation in strips. This study proposes a methodology that evaluates the current P-factor based on the angle between the crop row orientation and the elevation contour lines. The method was tested in four areas under soybean crop fields in southern Brazil, totaling 25 km^2. The reason for choosing four areas is to select different characteristics of rural properties and topographic conditions. The ideal values of the P-factor are expected to be between 0.5 and 0.6; however, in our case, a P-factor greater than 0.8 was obtained in 60% of the area, indicating the low occurrence of contour farming reduces erosion rates. The results show that policy-makers could potentially use this methodology (angle between the crop rows and contour lines) to run soil-erosion risk scenarios for a broader application of contour farming. This allows the P-factor to be quantified via a thematic map instead of assigning uniform P-factor values. With a detailed study of the P-factor on the slopes, there is a better understanding of where to target support practices to reduce erosion.

1. Introduction

Erosion from agricultural land has been recognized as an essential threat to the world's soil resources and natural (FAO & ITPS, 2015; Reicosky, 2015; USDA, 2015). Estimate soil erosion rates of arable or intensively grazed lands are 100–1000 times higher than natural background erosion rates (FAO, 2019a). Among the most critical factors negatively impacting erosion rates are monoculture and the inefficient use of conservation practices (Derpsch et al., 2014; Reicosky, 2015).

The Universal Soil Loss Equation (USLE) (Wischmeier & Smith, 1978) and its different versions and applications have been one of the most common ways of estimating soil loss through erosion (FAO, 2019b). The original USLE was revised, resulting in the more robust Revised Universal Soil Loss Equation (RUSLE) (Renard et al., 1997; USDA-ARS, 2008). The RUSLE computes the average annual erosion on-field slopes based on six several factors: Rainfall-runoff erosion (R), soil erodibility (K), slope length and steepness (LS), cover-management, and support practice (P). An example of the improvement of RUSLE is the new GIS-based algorithm for the estimation of LS estimative (Desmet & Govers, 1996; Moore & Burch, 1986; Patil, 2018; Zhang et al., 2013), providing greater precision in the management and evaluation of soil losses at the catchment scale (Patil, 2018; Zhang et al., 2013). While factors, such as the LS factor, evolved and adapted to new technologies, other factors, such as the factor related to support practices (P-factor), remain a source of uncertainty in the evaluation of soil losses despite its significant impact on erosion studies (Bernavidez et al., 2018; Morgan & Nearing, 2011; Panagos et al., 2015; Terranova

* Corresponding author. Avenida Roraima n° 1000, Prédio 42, sala 3311[a], Santa Maria, RS, CEP 97105-900, Brazil.
E-mail address: didoneagroufsm@gmail.com (E.J. Didoné).

https://doi.org/10.1016/j.iswcr.2021.01.007

et al., 2009; Xiong et al., 2019). In this light, the difficulty of accurately mapping support practice factors leads to many studies assuming P-factor as 1.0 (Benavidez et al., 2018; Panagos, Karydas, & Gitas, 2011, 2015). A P-factor equal to 1.0 may not represent the actual agricultural activities in southern Brazil because of the extensive adoption of contour farming (Freitas & Landers, 2014).

Several tables and empirical formulas proposing P-factor values for the different supporting conservation practices are found in the literature (e.g., Benavidez et al., 2018; Medeiros et al., 2016; Morgan, 2005; Renard et al., 1997; Terranova et al., 2009; Wischmeier & Smith, 1978; Yang et al., 2009). Studies have also considered P-factor as part of the cover-management factor (C-factor) or as a new combined CP-factor for lack of a representative P-factor (Benavidez et al., 2018; Bhandari et al., 2015; Liu et al., 2016; Morgan, 2005). Thus, factor P has a smaller representation concerning factor C (Renard et al., 1997). However, the few studies where P-factor values were assessed derived from studies carried out in relatively small areas (<2 km^2), suggesting that USLE-based models require improvement via the quantification of the P-factor, particularly for a regional and global scale (Panagos et al., 2015; Xiong et al., 2019). Some limited local information on P-factor values derived from very high-resolution (1 m) remote sensing datasets provided new insights for mapping landscape features representing a basis for assessing P-factor and information at a local scale. High-resolution images (3 m) from DEM (digital terrain model) are necessary to derive the P-factor. Determining the P-factor distributed in the landscape with the aid of modeling tools may provide valuable information for policymakers to simulate erosion risk scenarios and propose a more accurate conservation measures application. Thus, contour farming reduces P-factor values in different fractions, which may be used in conservation planning.

Often, due to poor farming techniques, sowing is not done parallel to the terrain level curves but in an angle varying from 0 (level sowing) to 90° (slope sowing), implying a variable P-factor between 0.5 to 1.0 based on this angle. The greater the inclination of the angle, the closer the P-factor will be to 1. The hypothesis is that mathematical modeling tools may promote better P-factor values in the same area. Based on these considerations, our study aims to propose a methodology to estimate the P-factor's spatial variability based on the vectorization of culture lines with the aid of remote sensing and contour curves.

2. Material and methods

2.1. Location of the study

This study was developed in Brazil's southernmost state (Rio Grande do Sul) in the Conceição river catchment. This catchment represents the soil conservation system pattern used in southern Brazil, and it is characterized by deep and weathering soils (Ferralsols and Nitisols). Amounts of clay in these soils may range from 45 to 60%, and are composed basically of kaolinite and oxides. Although these soils have an excellent physical structure, they are highly susceptible to degradation processes when compacted (Reichert et al., 2016). The catchment is predominantly cultivated with soybean using no-tillage farming as the leading soil management practice, without any correlated practices such as runoff control and crop rotation. Consequently, only low densities of biomass (i.e., the residues of previous crops) protect the soils against the erosive power of rainfall and runoff. The absence of additional conservation measures (mechanical/vegetative) has accelerated soil erosion along the slopes. Despite all the simplification of soil conservation practices, assigning a value of 1.0 to the P-factor for no-tillage farming does not correspond to the actual condition since the up-down farming creates distinct P-factor situations according to the characteristics of the relief.

Four test areas within the Conceição river catchment totaling approximately 25 km^2 were selected to capture different characteristics of rural properties and topographic conditions in the region (fig. 1). The area named "A" is formed by small rural properties; regions "B" and "C" include large farms characterized by a monoculture of soybean; region "D" comprises medium properties with different agricultural activity.

According to Köppen, the climate is of the Cfa type, humid subtropical without a dry season. The average annual precipitation varies between 1750 and 2000 mm, with an average temperature of 17 °C. The soils are weathered and deep, except for the area (A) composed of Ferralsols and Nitisols (FAO, 2015; all other areas (B, C, and D) are composed of Ferralsols. The local altitude varies from 258 to 472 m with a landscape characterized by medium to long slopes lengths (200 to 500 m) and soft slopes (6–9%) in the summit/back slopes and steeper slopes (10–14%) near the fluvial network.

In summer, soybean (*Glycine max*) is the most expressive culture and, in a smaller area, maize (*Zea mays*). In winter, wheat (*Triticum spp.*), oats (*Avena strigosa*), and, to a lesser extent, ryegrass (*Lolium multiflorium*) are predominant. There are systematic measures to control hydraulic forces exerted by the runoff on the soil surface (terraces, strip, or contour farming) in the catchment as crop alignment is performed by farmers at the most extended plot length regardless of the terrain level curves.

2.2. Estimation of P-factor

A sowing angle of 90° between crop rows and contour curves represents a contouring efficiency (Cef) of 0, and a sowing angle of 0° represents Cef of 1 (contour farming). This study sought to efficiently capture the variation of contouring angle between 0-90° for each pixel of the selected areas, determining the real values of the factor P with greater representativity.

Crop rows were manually vectorized from different satellite images spanning October to December 2017, obtained from Google Earth (Landsat). During this period, soybean sowing occurs, and, therefore, the crop rows are more evident. Contour lines were derived from 12.5m freely available DEM based on ALOS PALSAR imagery (Lagos et al., 2014) with a 10-m contour interval. Tests with coarser DEMs did not produce reliable results. After vectorization, the angle of intercession between crop rows and contour lines was determined in the example of fig. 2 using *Arc Gis 10.1,* as described in the supplementary material.

The support practice P-factor was estimated by multiplying the contouring support practice factor according to the slope (Pd) from Table 1 by the contouring efficiency (Cef), as shown in eq. (1).

$$Pfinal = 1 - Cef\,(1 - Pd) \quad (1)$$

Where P is the support practice factor, Pd is the contouring support practice factor, according to Shin (1999) (Table 1). The Cef is the contouring efficiency (Cef) that varies from 0 to 1 according to the intercession angle (0–90°).

The final P-factor was determined for each point according to the terrain unevenness and planting efficiency and later spatialized to the selected areas. The *semivariograms* were adjusted according to the values and later spatialized to the designated areas using the *Kriging* following Camargo (1998).

Distributed values obtained with the proposed methodology were then compared to those obtained using the traditional method proposed by Wischmeier and Smith (1978). P-factor was obtained, reclassifying slope and slope length according to Table 2

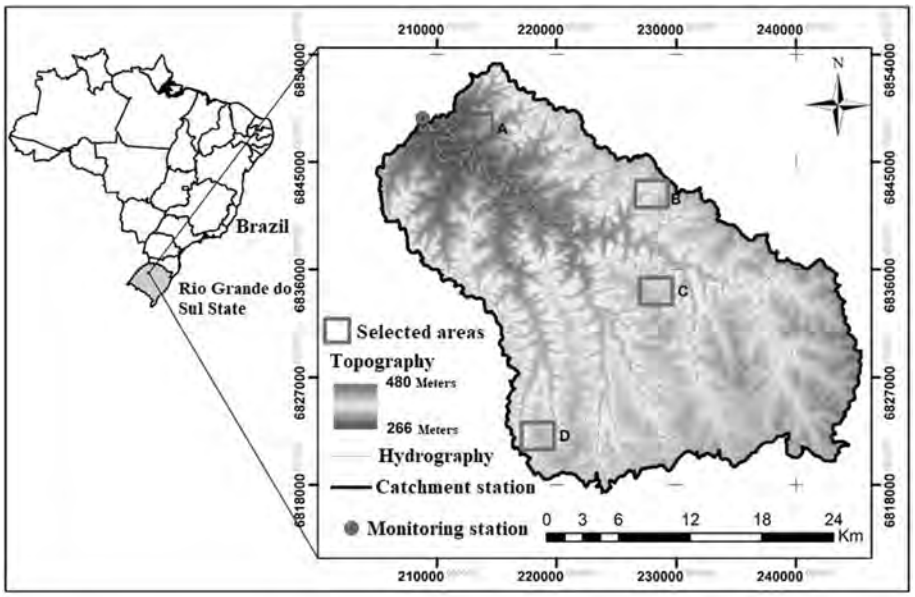

Fig. 1. - Location of the selected areas for the calculation of the P factor.

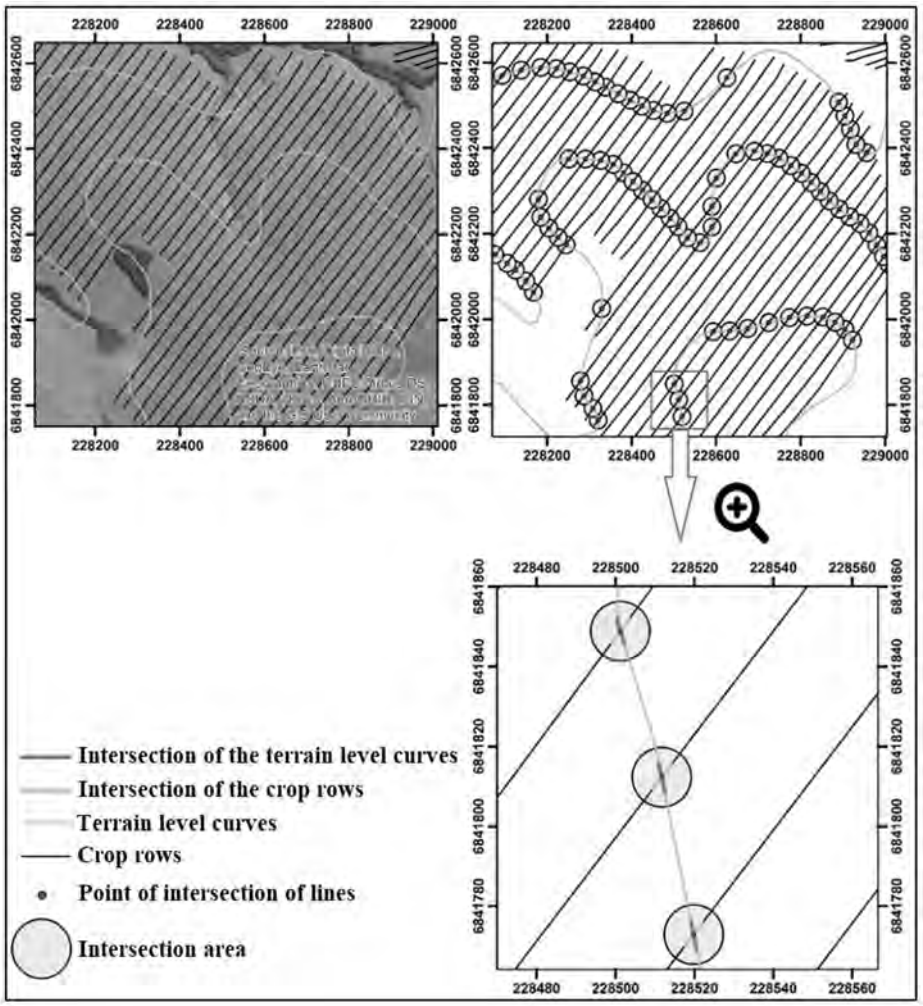

Fig. 2. - Representation of the intersections of crop rows and contour lines.

Table 1
Representation of planting values in contour farming (Pd) for different slopes.

(%) Slope of the terrain	[a]Contour farming Pd
0.0–7	0.55
7–11.3	0.6
11.3–17.6	0.8
17.6–26.8	0.9
>26.8	1

[a] Source: Adapted from Shin (1999).

Table 2
Supplementary practices of soil conservation (P factor) of the Universal Soil Loss Equation.

Cultivation in acclivity and slope		P = 1
Slope (%)	P-factor	
	Contour farming	Strip farming
1–2	0.6	0.3
3–5	0.5	0.25
6–8	0.5	0.25
9–12	0.6	0.3
13–16	0.7	0.35
17–20	0.8	0.4
21–25	1	0.45

Source: Wischmeier and Smith (1978).

using *Arc Gis 10.1* tools. As contour farming alone is not effective in controlling erosive processes (e. g., Karlen et al., 2009; Deuschle et al., 2019), an additional scenario considers contour and strip farming support measures in the region was also developed and compared.

Finally, soil erosion rates obtained using P = 1 were compared to those obtained using the proposed methodology.

2.3. Determination of R, K, LS, and C factors of RUSLE

For this study the version of RUSLE2 was used in which the parameters (R, K, LS, and C) were estimated following the general methodology proposed by Renard et al. (1997) and USDA-ARS (2008). Rainfall erosivity (R) was calculated based on a local equation developed by Cassol et al. (2007); specific soil erodibility (K) factor was estimated based on soil texture, organic matter, structure, oxides, and permeability following Roloff and Denardin (1994). The slope length and steepness (LS) factor were calculated based on Moore and Burch (1986). The more detailed effectiveness of R, K, LS, and C factors of RUSLE used in this study has been determined in previous studies conducted by Didoné et al. (2015, 2017).

3. Results and discussion

3.1. Determination of the P-factor based on contouring farming efficiency

The results confirm that sowing is not done perpendicular to terrain slope in the studied areas, observed as a variation in the angle between the crop rows and the contouring curves (fig. 3). The P-factor's different values are presented considering the crop rows' spatial variation and the P-factor frequency within the evaluated areas.

The values found for the P-factor in the selected areas varied from 0.5 to 1.0. Values above 0.8 were found in 60% of the evaluated areas, indicating that current conservation practices are much less effective than expected since the P-factor's typical values are foreseeable between 0.5 and 0.6. Values in this range were found only in 9% of the evaluated areas (Table 3), falling well below those recommended for a sustainable system (FAO, 2019a).

In the large properties (fig. 3, areas B and C), the P-factor values are concentrated above 0.8, indicating a lower efficiency due to the higher frequency of sowing oriented up or down-slope. A closer look showed that the crop rows were arranged following the largest dimension of the arable land where the mechanization has better operational efficiency, resulting in the overall increase in erosion processes in the region reported by previous studies by Didoné et al. (2015) and Deuschle et al. (2019).

Sowing oriented up-or-down-slope in the landscape may be associated with the field's size and the mechanical equipment available, such as tractors with a higher power, making it possible to sow the field in any direction (Levien et al., 2011). Whereas, small to medium farms are usually sown at the level (Fig. 3, areas A and D), which have better distribution between P-factor classes. Uneven sowing in the landscape has a greater risk of erosion processes. In these conditions, farming quality decreases, and excessive rolling of the wheels (tractor) displaces the ground cover, which disintegrates the surface and leaves a channel oriented towards the slope (Levien et al., 2011). The critical slope length characterizes residue failure and is defined by the slope distance from which there is a reduction of the residue's efficacy in controlling erosion (Leite et al., 2009). Residue failure may cause the shear stress to acquire enough energy to remove the residues that protect the soil, promoting erosion in the furrows, which can further concentrate the runoff favoring erosive processes (Barbosa et al., 2012). Thus, complementary conservation practices need to be used to control the erosive processes (Barbosa et al., 2012; Tiecher, 2015).

Another factor observed in the region is the lack of rotation of crops, lowering the input of organic matter, thus resulting in low integration of soil particles into aggregates, which leaves the soil vulnerable to rainfall events of great magnitude in terms of amount and intensity (Cogo et al., 2007; Tiecher, 2015)

The proposed technique to determine the P-factor was not used throughout the Conceição River catchment due to the computational capacity limitation to obtain large-scale crop row values. Automatic row delineation may be improved with techniques such as object-oriented image analysis explored by Karydas et al. (2009), IMAGE (http://www.earth.google.com), and Sobel filters for identifying physical obstacles (Panagos et al., 2014) or georeferenced crops considering the advances in tractors onboard GPS. Additional quality with improved topographic description should also be explored, considering the advances in available DEM information and the mentioned tractor GPS technology.

The scale may limit this methodology. Large areas of land (>100 km^2) require high-resolution data (3 m) and computational equipment with high processing capacity. The sowing lines must also be automatically vectorized, including specific instruments (computers, GIS programs) and human resources.

Automatic determination of the P-factor requires care concerning its spatialization in the landscape. When extrapolated to large areas, a reduced number of points may not be representative because P-factor values of areas under cultivation may be attributed to non-agricultural regions, such as rivers, forests, roads, and rural residences. The methodology may also be improved by analyzing all sowing lines (in scale catchment), which would give better representativeness to the P-factor in landscape-scale, reinforcing the results' reliability.

The different image resolutions can also affect the proposed method's accuracy by not capturing the sowing lines. There is a reduction in the number of values with fewer lines, with a low amount of final P-factor information to represent the area. Thus, the

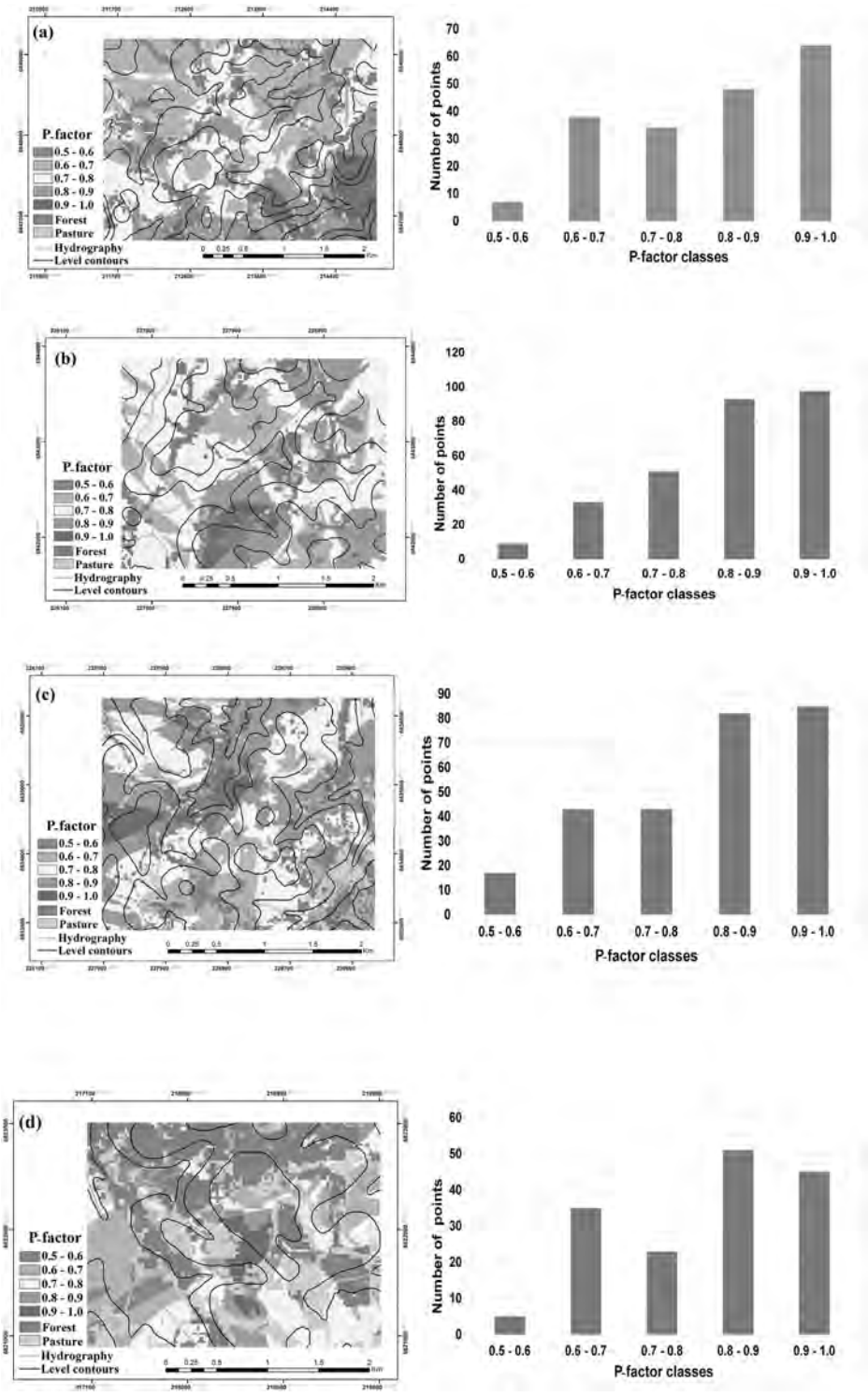

Fig. 3. - Spatial representation of the P factor for current conservation practices.

use of low-resolution images (30 m) should be avoided, as it could be a source of uncertainty. Another alternative is to use a GPS system integrated into a sowing machine which is less costly than acquiring high resolution images. In this way, the GPS may facilitate the P-factor derivation in small scales (<10 km^2).

However, even with these limitations, the results showed that even contour farming, one of the minimum expected support practices, is often ignored by farmers as observed in Table 3 and fig. 3, findings in agreement with the obtained by Karlen et al. (2009).

3.2. Estimating P-factor based on traditional tables for the different conservation practices

Our study was based on P-values proposed by Wischmeier & Smith, 1978) (Table 2), for contour farming. The results show (fig. 4 and Table 4) that strict support practices are present only in 56.3% of the evaluated area. Still, contour farming alone is not effective in controlling erosive processes in agreement with results from Karlen et al. (2009).

Table 3
Variation of the current P-factor for the different slopes according to the sowing efficiency in contour for each selected area.

(%) slope of the terrain	* Contour farming (Pd)	P final	% of area
0.0–7	0.55	0.5–0.6	9.03
7–11.3	0.6	0.6–0.7	20.20
11.3–17.6	0.8	0.7–0.8	29.48
17.6–26.8	0.9	0.8–0.9	23.21
>26.8	1	1	17.79

Source: Renard et al., 1997.

In the large properties (figs. 4bc, areas B and C), P-factor values for contour farming are near 1.0. Contour farming could significantly reduce erosive processes, even though other control measures, such as terraces, are also needed. When using contour farming, the P-factor values in all areas (figs. 4) show many values between 0.6-0.7, demonstrating its effects on control erosion.

Other support practices should be used in addition to contour farming (e.g., terracing), considering that it is effective for different slope lengths (Renard et al., 1997). The potential use of strip farming (Table 4 and fig. 5) associated with contour farming demonstrates an improvement of 13.2% of P-factor in the area than just using contour farming. Fig. 5 shows the spatial distribution of strip farming.

Strip farming contributes to erosion control due to the different densities, coverage rates, root systems, and the parceling of the slopes with alternating strips of greater and lesser susceptibility to erosion as a function of crop density (Lombardi, 1993). The alternating arrangement of different species cultivated on strips means that the erosion losses suffered in certain crops are in part controlled by the crops down the slope. This control is based on each crop's different morphological and physiological characteristics, with sowing and harvesting operations at different periods (Francis et al., 1985).

Strip farming can be of continuous exploration when the crops cultivated in the strips remain in the same place from one year to another (Lombardi, 1993). This method also prevents soil erosion and can improve soil fertility through crop rotation management (Exner et al., 1999). The crops used in the strip and the row width can be adjusted to obtain minimum soil loss. Under the most favorable conditions, soil erosion can be reduced by up to 75% through this technique (Moran et al., 1986).

When using strip farming as a conservationist measure, the medium size properties (fig. 5d) showed several occurrences for a P-factor of 0.3 in area D which indicates a very satisfactory condition for erosion control. In contrast, in the large (figs. 5bc) and small (fig. 5a) properties, the P-factor values for strip farming were more distributed between 0.3-0.35. This fact can be explained by the smaller declivity (Fig. 5d), in which strip farming comprised the second largest number of values for P-factor in the order of 0.3. It is important to emphasize that only the proposed strip farming would not be sufficient in controlling erosion for areas with a greater slope inclination, terracing the most effective measure (Londero et al., 2018).

In strip farming, it is essential to use different crops, for example, turnip greens or winter oats; and corn or soybeans in spring and summer as they provide different levels of soil protection since crop cycles represent distinct phytomass productions (Franchini et al., 2007; Silva et al., 2010).

Strip farming promotes micro-roughness between the different cultivation strips, which reduces the erosive processes along the slopes and up to 50% runoff rates when compared to a contour farming only scenario (Karlen et al., 2009). The adoption of strip cropping in up to 69.5% of the area could reduce erosion (Table 4); however, additional support practices such as terracing should be used, in the remaining 30.5% of the area, for erosion control as suggested by Londero et al. (2018).

3.3. Variation of erosion estimation with P-factor change

Several authors (e.g., Benavidez et al., 2018; Panagos et al., 2011; Panagos et al., 2015; Renard et al., 1997; Xiong et al., 2019) report on the difficulties in mapping complementary conservation practice factors where many studies assume P = 1. Table 5 and figs. 6-AB show the differences in the estimated erosion rates considering the P-factor mapped with our proposed methodology and using P = 1. This variability reflects the levels of erosion, as seen in Table 5.

The traditional P-factor = 1 used in modeling does not reflect the inclusion of complementary soil conservation practices observed in the field. Another issue that must be considered to understand the variability of P-factor values is each field's format. The variation in length, inclination, and shape of the area influence the farmer to choose the most suitable sowing direction (Denardin et al., 2008; Levien et al., 2011). All of these factors, when associated, influence erosion levels, as seen in Figs. 6 and 7.

The curvature (plan and profile) of the terrain influences the runoff speed and volume along the hillslope and erosion rate (Sensoy & Kara, 2014). The sloping topography, mainly in locations near the drainage network with a slope (>18%), favors erosive processes. This can be seen in Figs. 6 and 7, in areas A and B, which comprise small and large properties. Regardless of the P-factor used, both the estimated and the P-factor equal to 1, the erosion modeled at these locations is significant (12–25 t/ha/yr). In area D (Figs. 6 and 7), as occurs in pastures and forests in an environment with smaller slopes, the modeled erosion was lower. Therefore, the P-factor for different areas should be associated with the other RUSLE factors to better represent the areas with more significant degradation potential, thus using more effective conservation measures for its control.

The values obtained (Table 5 and fig. 6) show that erosion rates are overestimated by 20% when using a P-factor equal to 1 when compared to the spatially estimated P-factor (fig. 7), which is in agreement with modeling to the P-factor values of RUSLE2 (Yang et al., 2009). The values obtained with the technique presented in fig. 7 indicate spatial variability in the P-factor values. This change may influence the results of modeling for process representation.

The results of the erosion modeling using the P-factor estimated by the proposed methodology (Table 5; Figs. 6 and 7) reduced erosion by 18% in area D (medium properties) and 25% in area C (large properties). For the other areas, A small and B large properties, the reduction in erosion modeled using the P estimated was in the order of 20% concerning P-factor equal to one (Table 5). This indicates that regardless of the size of the properties, erosion processes are present where the slope and conservation practices used have a direct impact on erosion values.

When comparing the estimates of erosion (P = 1 and P estimated - Table 5) with the actual values of erosion observed for the region with the same soil type and conservation systems (0.13–1 t/ha/year - Cogo et al., 2003; Merten et al., 2015), the values of the modeled P factor are closer to the estimated erosion values. Didoné et al. (2015), using monitoring associated with modeling, quantified the average erosion in 4.4 t/ha/yr for the catchment scale (Conceição River). When using conservationist systems with crop rotation, the erosion levels were reduced to 1–2 t/ha/yr. Also, complementary conservation measures such as contour farming indicate a further reduction in erosion levels.

Concerning erosive models, the USLE uses indices based on the derivation of an empirical model. In comparison, the RUSLE is a hybrid model that combines indices and process-based equations.

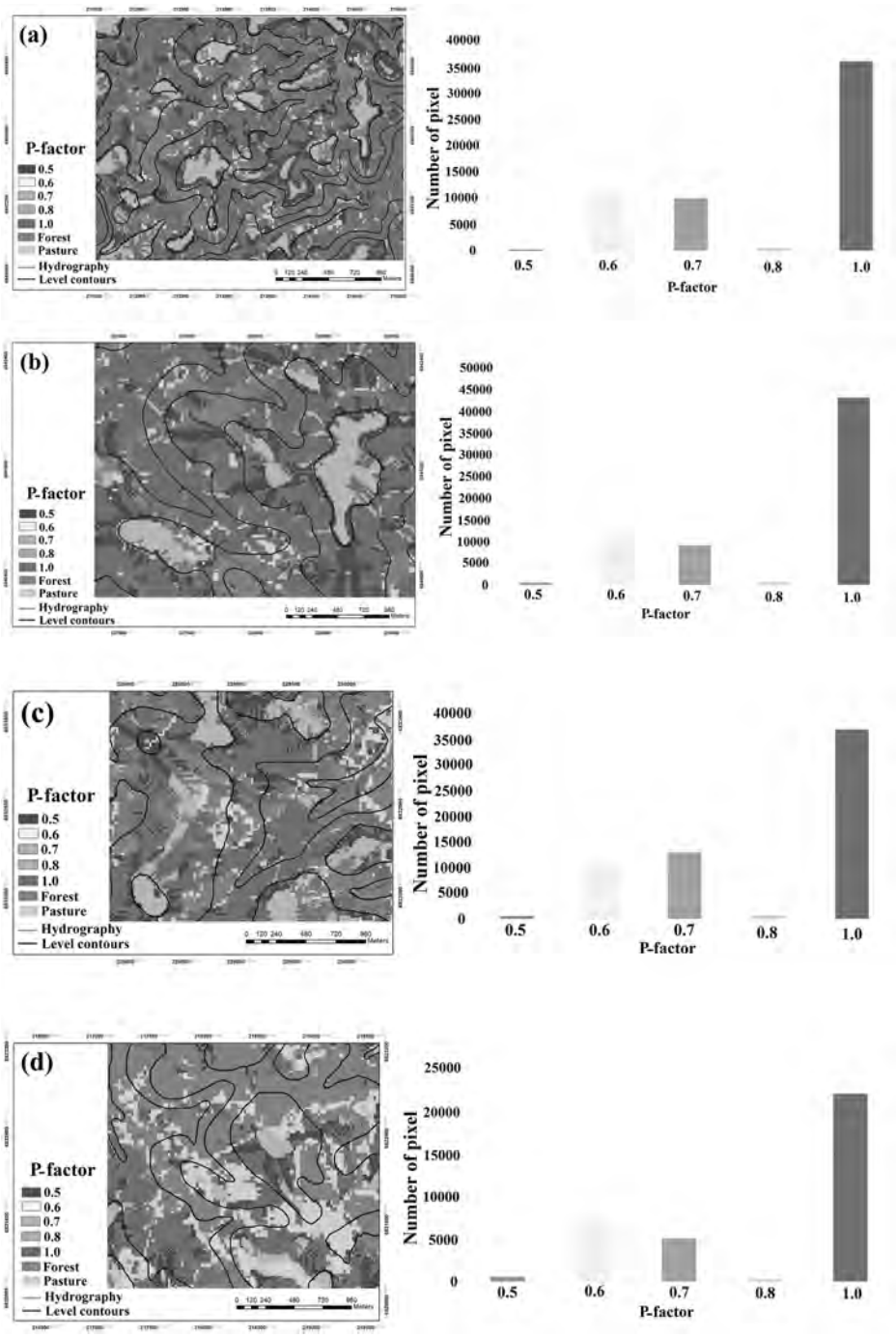

Fig. 4. Representation of the spatial distribution of the P factor predefined for contour farming.

Table 4
Representation of the P-factor for the selected areas of the Conceição River catchment with different complementary conservation practices.

Contour farming			Strip farming		
P factor	ha	% Area[a]	P factor	Ha	% Area[a]
0.5	510	28.3	0.25	582	32.3
0.6	21	1.2	0.3	460	25.6
0.7	458	25.4	0.35	153	8.5
0.8	25	1.4	0.4	25	1.4
1	786	43.7	0.45	31	1.7
–	–	–	1	549	30.5
	1800	100		1800	100

[a] Agricultural area.

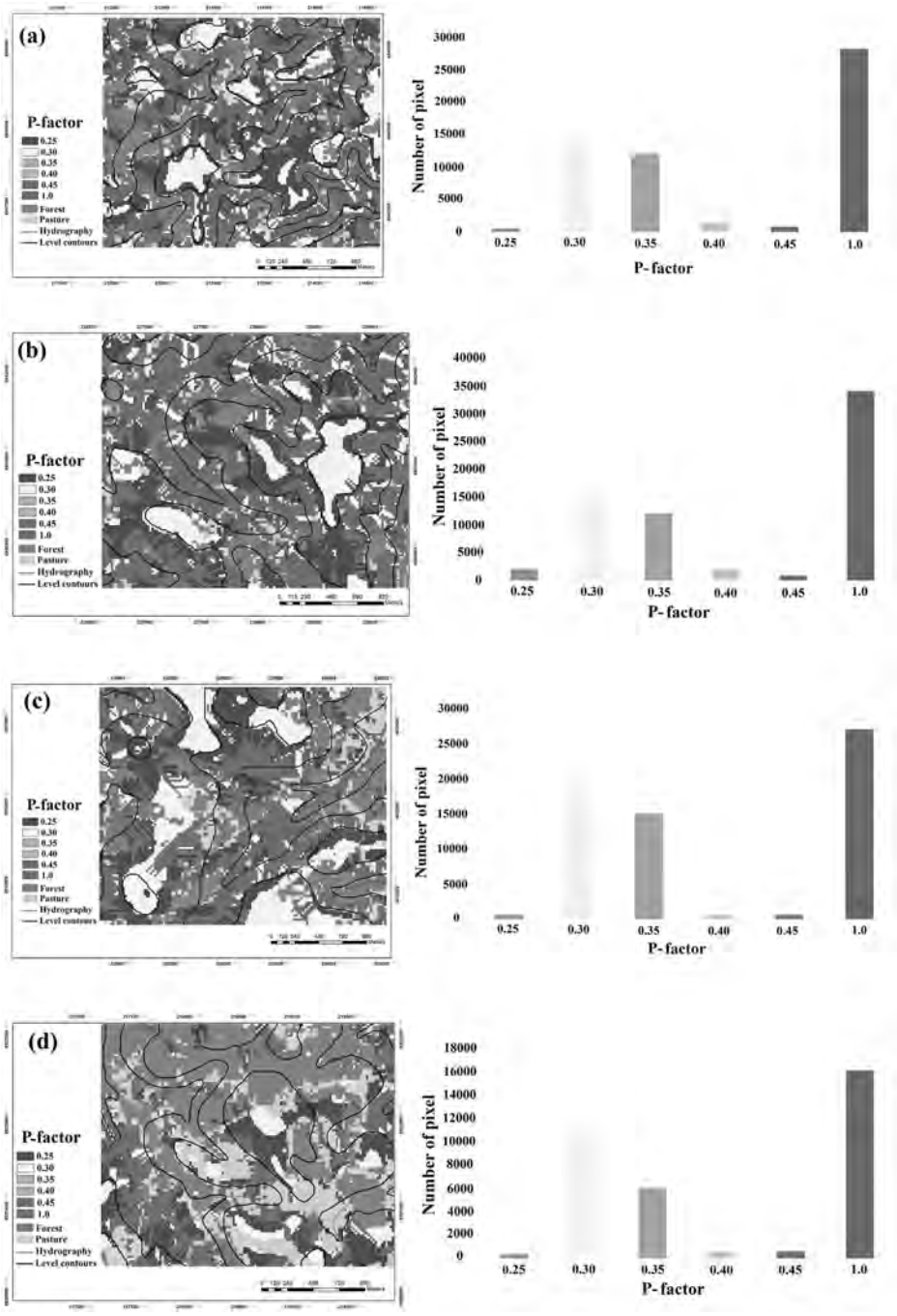

Fig. 5. Representation of the spatial distribution of the P factor predefined for strip farming.

Table 5
- Representation of erosion rates using values of P = 1 and P-factor estimated using the angles of the crop rows and contour lines.

	Area 1	Area 2	Area 3	Area 4	Average (t/ha/yr)
	Erosion (t/ha/yr)				
P - Estimated	2.70	2.85	1.82	1.32	2.17
P = 1	3.25	3.41	2.27	1.54	2.61
% Variation	20.33	19.64	24.72	18.18	20.48

Thus, RUSLE can analyze very complex slope shapes and spatial soil arrangements, coverage management, and slope support practices. RUSLE predicts the average soil loss and should not be applied to predict the specific erosion of independent rainfall events. Despite its limitations in terms of quantity, RUSLE is a useful tool for estimating vulnerability to soil erosion, allowing the identification of water erosion rates resulting from current land use and as a tool to subsidize ecological services aimed at sustainability (USDA-ARS, 2008). The insertion of distributed values of the P-factor for erosive models may present essential answers in the representation of erosion processes. The gains in results can minimize uncertainties associated with the representation of processes by mathematical models by representing the site's real conditions and providing the modeling subsidies to better represent the current condition of use. Authors such as Kuok et al. (2013) indicate that the

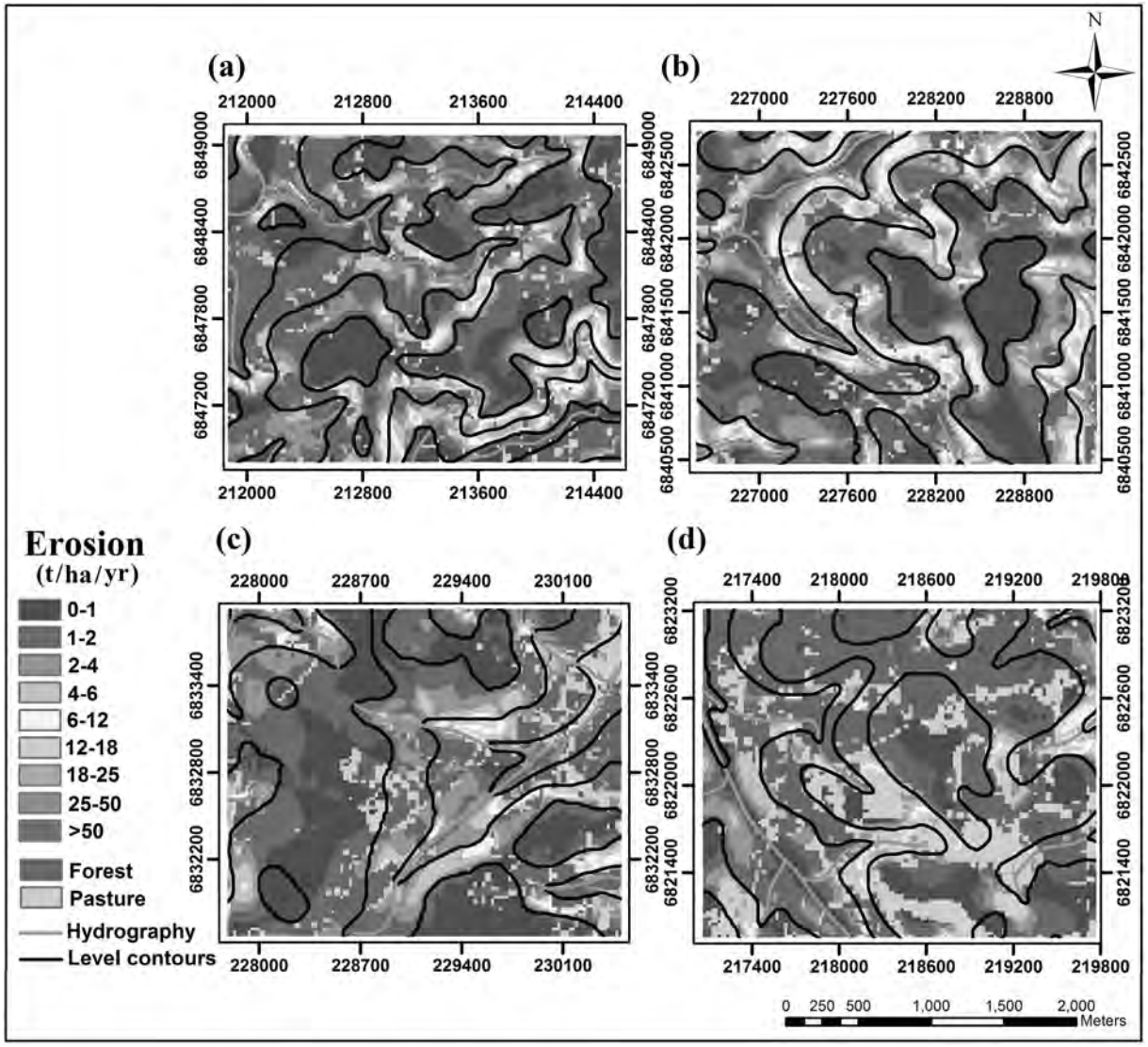

Fig. 6. Representation of erosion variation using P-factor = 1.

other RUSLE factors when associated with the P-factor may reduce sediment rates by up to 202%.

The current determination of the P factor requires the aid of tools capable of automating the process in determining the values for each location. Modeling practices must advance in the understanding of the determination of the effect of mechanical practices on erosive processes. New studies are needed to apply the obtained values in order to verify their response efficiency in using mathematical models that incorporate the values of conservation practices spatially, evaluating which effects the spatialized P-factor values influence the erosion estimates and the sensitivity of each model.

4. Conclusion

This study proposed a technique to estimate the P-factor's spatial variability based on a contour efficiency obtained by the vectorization of crop rows from remote sensing data and topographic information. Even if manual vectorization were used, more refined automatic crop row identification is needed for widespread adoption; this technique proved valuable for modeling and managing farming activities.

As there is difficulty capturing the effects of support practices in a distributed manner (P-factor), modeling studies associate C and P factors to minimize the absence of P-factor data. As factor C has better spatial quantification of land cover and less variability, it has greater weight in modeling than the P-factor. These factors are the only ones that can be directly altered, and P-factor has a more significant restriction in determining the spatial form. Tests on the use of complementary conservation measures in modeling should be used to assess the responses of different conservationist practices that influence the dynamics of surface runoff and its connections with rivers.

Results showed that disregarding the P-factor by assuming it equal to 1.0 may overestimate the erosion rates by 20% in the assessed area since P-factor values vary in the landscape according to the planting efficiency related to topography. Additionally, it showed the necessity to understand and consider farmers' decisions and technology to develop erosion assessments accurately.

The results of erosion modeling indicate that sites with greater slopes are more prone to erosive processes. Furthermore, current conservation practices are not sufficient to control erosion. On the other hand, more effective conservationist measures are needed to control the processes in all evaluated areas.

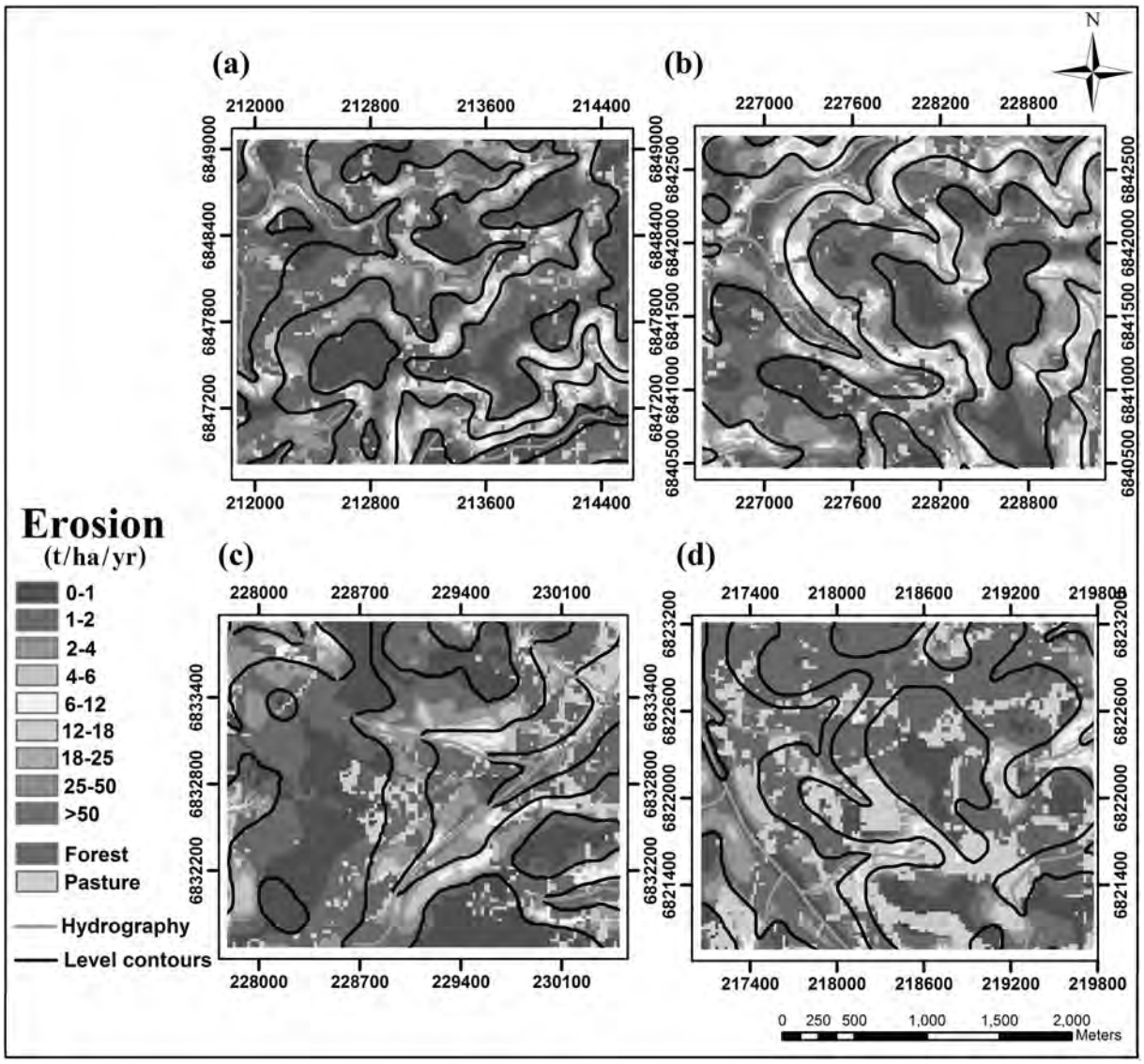

Fig. 7. Representation of erosion variation using P-factor estimated using the angles of the crop rows and contour lines.

Complementary soil conservation measures such as contour farming 56.3% and strip farming 69.5% showed that it reduces the need for more effective conservation measures such as terracing in most agricultural areas when used following technical recommendations. However, it is recommended to use terracing in 43.7% of the areas even with contour farming and 30.5% of the areas with strip farming.

All these measures spatially interfere with the P-factor values in the landscape and may assume different values among the classes of the slope. Further studies are necessary to apply the values obtained by the proposed methodology to verify their response efficiency in the use of mathematical models such as WaterShed and SWAT, these models should be tested to evaluate which spatialized values of the P-factor influence the erosion estimates.

Acknowledgments

This study was financed in part by the Coordenação de Aperfeiçoamento de Pessoal de Nível Superior - Brasil (CAPES) - Finance Code 001, Federal University of Santa Maria (UFSM) and Conselho Nacional de Desenvolvimento Científico e Tecnológico — CNPq.

Appendix A. Supplementary data

Supplementary data to this article can be found online at https://doi.org/10.1016/j.iswcr.2021.01.007.

References

Barbosa, F. T., Bertol, I., Werner, R. S., Ramos, J. C., & Ramos, R. R. (2012). Comprimento crítico de declive relacionado à erosão hídrica, em três tipos e doses de resíduos em duas direções de semeadura direta. *R. Bras. Ci. Solo, 36*, 1279–1290.

Benavidez, R., Jackson, B., Maxwell, D., & Norton, K. (2018). A review of the (revised) universal soil loss equation (R) USLE: With a view to increasing its global applicability and improving soil loss estimates. *Hydrology and Earth System Sciences, 22*, 6059–6086. https://doi.org/10.5194/hess-22-6059-2018, 2018.

Bhandari, K. P., Aryal, J., & Darnsawasdi, R. (2015). A geospatial approach to assessing soil erosion in a watershed by integrating socio-economic determinants and the RUSLE model. *Natural Hazards, 75*(1), 321–342.

Camargo, E. C. G. (1998). Geoestatística: Fundamento e Aplicações. In G. CAMARA, & J. S. MEDEIROS (Eds.), *Geoprocessamento em projetos ambientais. 2a*. São José dos Campos: INPE. Cap 5, 36pp.

Cassol, E. A., Martins, D., Eltz, F. L. F., Lima, V. S., & Bueno, A. C. (2007). Erosividade e padrões hidrológicos das chuvas de Ijuí (RS) no período de 1963 a 1993. *Rev Bras. de Agromet., Piracicaba, 15*(3), 220–231.

Cogo, N. P., Levien, R., & Schwarz, R. A. (2003). Perdas de solo e água por erosão hídrica influenciadas por método de preparo, classes de declive e níveis de

fertilidade do solo. *R. Bras. Ci. Solo, 27*, 743–753.
Cogo, N. P., Portela, J. C., Amaral, A. J., Trein, C. R., Gilles, L., Bagatini, T., & Chagas, J. P. (2007). Erosão e escoamento superficial em semeadura direta efetuada com máquina provida de hastes sulcadoras, influenciadas pela direção da operação de semeadura e pela cobertura da superfície do solo. In *CONGRESSO BRASILEIRO DE CIÊNCIA DO SOLO, 31, Gramado, 2007. Anais... Gramado*.
Denardin, J. E., Kochhann, R. A., Faganello, A., Sattler, A., & Manhago, D. D. (2008). "Vertical mulching" como prática conservacionista para manejo de enxurrada em sistema plantio direto. *Revista Brasileira de Ciência do Solo, 32*, 2847–2852.
Derpsch, R., Franzluebbers, A. J., Duiker, S. W., Reicosky, D. C., Koeller, K., Friedrich, T., et al. (2014). Why do we need to standardize no-tillage research? *Soil Till. Res., 137*, 16–22. https://doi.org/10.1016/j.still.2013.10.002
Desmet, P. J., & Govers, G. (1996). A GIS procedure for automatically calculating the USLE LS factor on topographically complex landscape units. *Journal of Soil and Water Conservation, 51*, 427–433.
Deuschle, D., Minella, J. P. G., Hörbe, T. A. N., Londero, A. L., & Schneider, F. J. A. (2019). Erosion and hydrological response in no-tillage subjected to crop rotation intensification in southern Brazil. *Geoderma, 340*, 157–163. https://doi.org/10.1016/j.geoderma.2019.01.010
Didoné, E. J., Minella, J. P. G., & Evrard, O. (2017). Measuring and modeling soil erosion and sediment yields in a large cultivated catchment under no-till of Southern Brazil. *Soil and Tillage Research, 174*, 24–33. https://doi.org/10.1016/j.still.2017.05.011
Didoné, E. J., Minella, J. P. G., & Merten, G. H. (2015). Quantifying soil erosion and sediment yield in a catchment in Southern Brazil and implications for land conservation. *Journal of Soils and Sediments, 15*, 2334–2346. https://doi.org/10.1007/s11368-015-1160-0
Exner, D. N., Davison, D. G., Ghaffarzadeh, M., & Cruse, R. M. (1999). Yields and returns from strip intercropping on six Iowa farms. *American Journal of Alternative Agriculture, 14*, 69–77.
FAO & ITPS. (2015). *Status of the world's soil resources (main report)*. Fao. p. Rome608 pp. (also available at http://www.fao.org/3/a-i5199e.pdf.
FAO. (2019a). *Soil erosion: The greatest challenge for sustainable soil management* (p. 104). Rome: Food and Agriculture Organization of the United Nations.
FAO. (2019b). *Outcome document of the global symposium on soil erosion. Rome*.
FAO (Food and Agriculture Organization of the United Nations). 7SS Working Group WRB. (2015). *World Reference Base for Soil Resources 2014, update 2015. International soil classification system for naming soils and creating legends for soil maps. World Soil Resources Reports No. 106*. Rome: FAO.
Franchini, J. C., Crispino, C. C., Souza, R. A., Torres, E., & Hungria, M. (2007). Microbiological parameters as indicators of soil quality under various soil management and crop rotation systems in southern Brazil. *Soil and Tillage Research, 92*(1–2), 18–29.
Francis, C. A., Barker, T. C., Goodman, S., & Wittier, K. (1985). Strip cropping potentials for corn and grain legumes. *Agronomy Abstracts*, 96.
Freitas, P. L., & Landers, J. N. (2014). The transformation of agriculture in Brazil through development and adoption of zero tillage conservation agriculture. *International Soil and Water Conservation Research, 2*(1), 35–46.
Karlen, D. L., Dinnes, D. L., Tomer, M. D., Meek, D. W., Cambardella, C. A., & Moorman, T. B. (2009). Is no-tillage enough? A field-scale watershed assessment of conservation effects. *Electronic Journal of Integrative Biosciences, 7*(2), 1–24.
Karydas, C. G., Sekuloska, T., & Silleos, G. N. (2009). Quantification and site-specification of the support practice factor when mapping soil erosion risk associated with olive plantations in the Mediterranean island of Crete. *Environmental Monitoring and Assessment, 149*(1–4), 19–28.
Kuok, K. K. K., Mah, D. Y. S., & Chiu, P. C. (2013). Evaluation of C and P factors in universal soil loss equation on trapping sediment: Case study of santubong river. *Journal of Water Resource and Protection, 5*(12), 1149–1154.
Leite, M. H. S., Couto, E. G., Amorim, R. S. S., Costa, E. L., & Maraschin, L. (2009). Perdas de solo e nutrientes num Latossolo Vermelho-Amarelo ácrico típico, com diferentes sistemas de preparo e sob chuva natural. *Revista Brasileira de Ciência do Solo, 33*, 689–699.
Levien, R., Furlani, C. E. A., Gamero, C. A., Conte, O., & Cavichioli, F. A. (2011). Semeadura direta de milho com dois tipos de sulcadores de adubo, em nível e no sentido do declive do terreno. *Ciência Rural, 41*(6), 1003–1010.
Liu, H., Blagodatsky, S., Giese, M., et al. (2016). Impact of herbicide application on soil erosion and induced carbon loss in a rubber plantation of Southwest China. *Catena, 145*, 180–192.
Lagos, L., Navarrete, O., Maruyama, F., Crowley, D.E., Cid, F., Mora, M.L., Jorquera, M.A. 2014. Bacterial community structures in rhizosphere microsites of ryegrass (Lolium perenne var. Nui) as revealed by pyrosequencing. Biol. Fert. Soils. 50, 1253–1266.
Lombardi, F. N. (1993). Cultura em faixas. In B. Raij (Ed.), *Manual técnico de manejo e conservação de solo e água. Volume III. Tecnologias para aumentar a cobertura vegetal e a infiltração de água no solo* (pp. 51–54). Campinas: CATI (Manual CATI; Nº 40).
Londero, A. L., Minella, G. P. G., Deuschle, D., Schneider, F. J. A., Boeni, M., & Merten, G. H. (2018). Impact of broad-based terraces on water and sediment losses in no-till (paired zero-order) catchments in southern Brazil. *Journal of Soils and Sediments, 18*, 1159–1175. https://doi.org/10.1007/s11368-017-1894-y
Medeiros, G. D. O. R., Giarolla, A., Sampaio, G., et al. (2016). Estimates of annual soil loss rates in the state of São Paulo, Brazil. *Revista Brasileira de Ciência do Solo, 40*, 1–18.
Merten, G. H., Araújo, A. G., Biscaia, R. C. M., Barbosa, G. M. C., & Conte, O. (2015). No-till surface runoff and soil losses in Southern Brazil. *Soil and Tillage Research, 152*, 85–93.
Moore, I. D., & Burch, G. J. (1986). Modelling erosion and deposition: Topographic effects. *Trans Am Soc Agric Eng, 29*, 1624–1630.
Moran, J. M., Morgan, M. D., & Wiersma, J. H. (1986). *Introduction to environmental science* (2nd ed.). New York: W. H. Freeman.
Morgan, R. P. C. (2005). *Soil erosion and conservation* (3rd ed., p. 304). Blackwell Science Ltd., ISBN 1-4051-1781-8.
Morgan, R. P. C., & Nearing, M. (2011). *Handbook of erosion modelling*. John Wiley & Sons.
Panagos, P., Borrelli, P., Meusburger, K., Zanden, E. H., Van Der, D., Poesen, J., & Alewell, C. (2015). Modelling the effect of support practices (P-factor) on the reduction of soil erosion by water at European scale. *Environmental Science & Policy, 51*, 23–34. https://doi.org/10.1016/j.envsci.2015.03.012
Panagos, P., Karydas, C. G., Ballabio, C., & Gitas, I. Z. (2014). Seasonal monitoring of soil erosion at regional scale: An application of the G2 model in crete focusing on agricultural land uses. *International Journal of Applied Earth Observation and Geoinformation, 27B*, 147–155.
Panagos, P., Karydas, C. G., & Gitas, I. Z. (2011). Monthly soil erosion monitoring based on remotely sensed biophysical parameters: A case study in strymonas river basin towards a functional pan-European service. *Int. J. Digit. Earth*, 461–487. https://doi.org/10.1080/17538947.2011.587897.
Patil, R. J. (2018). *Spatial techniques for soil erosion estimation: Remote sensing and GIS approach*. Cham: Springer International Publishing AG part of Springer Nature. https://doi.org/10.1007/978-3-319-74286-1
Reichert, J. M., da Rosa, V. T., Vogelmann, E. S., da Rosa, D. P., Horn, R., Reinert, D. J., et al. (2016). Conceptual framework for capacity and intensity physical soil properties affected by short and long-term (14 years) continuous no-tillage and controlled traffic. *Soil and Tillage Research, 158*, 123–136. https://doi.org/10.1016/j.still.2015.11.010
Reicosky, D. C. (2015). Conservation tillage is not conservation agriculture. *Journal of Soil and Water Conservation, 70*(5), 103A–108A. https://doi.org/10.2489/jswc.70.5.103A
Renard, K. G., Foster, G. R., Weesies, G. A., McCool, D. K., & Yoder, D. C. (1997). *Predicting soil erosion by water: A guide to conservation planning with the revised universal soil loss equation (RUSLE), Agriculture Handbook*.
Roloff, G., & Denardin, J. E. (1994). Estimativa simplificada da erodibilidade do solo. In *Reunião Brasileira de Manejo e Conservação do Solo e da Água, Florianópolis. 10., Anais. Florianópolis: Sociedade Brasileira de Ciência do Solo* (pp. 150–151).
Sensoy, H., & Kara, O. (2014). Slope shape effect on runoff and soil erosion under natural rainfall conditions. *IForest, 7*, 110–114.
Shin, G. J. (1999). *The analysis of soil erosion analysis in watershed using GIS*. Department of Civil Engineering, Gang-won National University. Ph.D. Dissertation.
Silva, A. P., Babujia, L. C., Franchini, J. C., Souza, R. A., & Hungria, M. (2010). Microbial biomass under various soil- and crop management systems in short and long-term experiments in Brazil. *Field Crops Research, 119*(1), 20–26.
Terranova, O., Antronico, L., Coscarelli, R., & Iaquinta, P. (2009). Soil erosion risk scenarios in the mediterranean environment using RUSLE and GIS: An application model for calabria (southern Italy). *Geomorphology, 112*, 228–245.
Tiecher, T. (2015). *Manejo e conservação do solo e da água em pequenas propriedades rurais no Sul do Brasil: Contextualizando as atividades agropecuárias e os problemas erosivos*. RS: Or: Tales Tiecher. URI - Frederico Westphalen, 152 pp.
USDA-ARS. (2008). *Draft user's reference guide, revised universal soil loss equation*. Version 2. Available at http://www.ars.usda.gov/sp2UserFiles/Place/64080510/RUSLE/RUSLE2_User_Ref_guide.pdf. (Accessed 3 September 2008).
USDA-United States Department of Agriculture, Wade, T., Claassen, R., & Wallander, S. (2015). *Conservation-practice adoption rates vary widely by crop and region, EIB-147*. U.S. Department of Agriculture, Economic Research Service. December 2015. Disponível em http://www.ers.usda.gov/media/1979972/eib147.pdf. Acesso em: abr. 2019.
Wischmeier, W. H., & Smith, D. D. (1978). *Predicting rainfall erosion losses - a guide to conservation planning. USDA handbook 537*. Washington, DC: USDA-Science and Education Administration.
Xiong, M., Sun, R., & Chen, L. (2019). Global analysis of support practices in USLE-based soil erosion modeling muqi Xiong research center for eco-environmental sciences, Chinese academy of sciences, China ranhao sun research center for eco-environmental sciences, Chinese academy of sciences, China liding chen. *Progress in Physical Geography, 43*(3), 391–409. https://doi.org/10.1177/0309133319832016
Yang, D., Shao, W., Yeh, P. J. F., Yang, H., Kanae, S., & Oki, T. (2009). Impact of vegetation coverage on regional water balance in the nonhumid regions of China. *Water Resources Research, 45*, 450–455. https://doi.org/10.1029/2008wr006948
Zhang, H., Yang, Q., Li, R., Liu, Q., Moore, D., He, P., Ritsema, C. J., & Geissen, V. (2013). Extension of a GIS procedure for calculating the RUSLE equation LS factor. *Computers & Geosciences, 52*, 177–188 (0).

International Soil and Water Conservation Research 9 (2021) 381–393

Contents lists available at ScienceDirect

International Soil and Water Conservation Research

journal homepage: www.elsevier.com/locate/iswcr

Original Research Article

Small dams/reservoirs site location analysis in a semi-arid region of Mozambique

António dos Anjos Luís [a], Pedro Cabral [b, *]

[a] Department of GIS and Regional Planning, Universidade Católica de Moçambique, Beira, Sofala, Mozambique
[b] NOVA Information Management School (NOVA IMS), Universidade Nova de Lisboa, 1070-312, Lisboa, Portugal

ARTICLE INFO

Article history:
Received 17 July 2020
Received in revised form
1 February 2021
Accepted 16 February 2021
Available online 27 February 2021

Keywords:
Water scarcity
Multi-criteria evaluation
Geographic information systems
Remote sensing
Mozambique

ABSTRACT

The water crisis is one of the biggest human problems in developing countries, especially in semi-arid regions where it can form an obstacle to irrigation and cultivation, cattle raising and people's survival. The construction of small dams/reservoirs are a possible solution to remediate this problem. These infrastructures must be located in suitable areas to be successful. This study aimed to find the most suitable locations for small dams/reservoirs in the Tete province region, Mozambique, which has a pronounced water deficit. A Geographical Information System (GIS) based approach was used to implement a multi-criteria evaluation (MCE) analysis through an Analytic Hierarchical Process (AHP), which included local experts' consultation. Three main categories of suitability were identified: "Not suitable" (15% of total area), "Modestly suitable" (78%), and "Suitable" (7%). We found that 35 of the 38 (92%) abandoned small dams/reservoirs were in areas classified as "Modestly suitable" confirming the robustness of our model. We also found that most of the dams/reservoirs currently operating (78%) and planned (73%) are in modestly suitable areas.

This finding suggests that the decision to construct dams/reservoirs may not have considered the most critical suitability factors identified in this study. More data and/or additional criteria are required for the full understanding of finding out why so many dams/reservoirs failed before building new ones to address the population's water needs in the region.

1. Introduction

Water is the basis of life and livelihoods since it supports the health of ecosystems and is the fundamental element for sustainable development (Guppy & Anderson, 2017). Its availability and storage are useful for drinking, field crop irrigation, and economic development (Raza, Shafique, Sikandar, Ahmad, & Shah, 2018). Hence, the United Nations recognized ensuring water security as a sustainable development goal (SDG) (Goal 6) (Gain, Giupponi, & Wada, 2016). However, many people worldwide do not have secure access to suitable water to meet their most basic needs (Detoni & Dondoni, 2008; UNICEF-WHO, 2019). The lack of water resources is likely to be one of the biggest human problems in the next decades (Rezaei, Rezaie, Nazari-Shirkouhi, Reza, & Tajabadi, 2013; Vörösmarty, Pahl-Wostl, Bunn, & Lawford, 2013).

Climate change will significantly impact the hydrological regime, water availability, and quality by increasing the frequency and severity of droughts and floods, rainfall variability, and higher temperatures (Luhunga, Chang'a, & Djolov, 2017). Thus, there is a great concern that climate change could worsen the water resource crisis in areas with water scarcity (Abu-Allaban, El-Naqa, Jaber, & Hammouri, 2015; Malinowski & Skoczko, 2018). Projections for Africa by 2020, as a consequence of climate change, point to an increase in water stress with a reduction in agricultural incomes of 50% in some regions, severely compromising the access to food (Ammar, Riksen, Ouessar, & Ritsema, 2016).

Water scarcity is a critical issue in many developing countries (Ibrahim, Rasul, Hamid, Ali, & Dewana, 2019). Particularly in arid and semi-arid areas where evaporation exceeds precipitation, water scarcity affects livelihoods and food security since in the majority of the available water comes from the rain during the rainy season or the groundwater close to the land surface (Abdalla et al., 2017).

The need to have a continuous and stable water supply for

* Corresponding author.
E-mail address: pcabral@novaims.unl.pt (P. Cabral).

https://doi.org/10.1016/j.iswcr.2021.02.002

human activities implies building dams and/or reservoirs to store water during the rainy season and use it in the drought season (Sayl, Muhammad, Yaseen, & El-shafie, 2016). Dams are transverse barriers to the direction of the flow of a water course to accumulate or raise the level of the water body (Ghazal & Salman, 2015). A reservoir is an artificial water body usually created in a river valley due to water-retaining constructions for accumulation and storage of water (Nagy, Asante-Duah, & Zsuffa, 2002). The construction of dams/reservoirs may provide water supplies for human needs and livestock, small-scale irrigation, and may play an important factor in improving the livelihoods of rural populations (Senzanje, Boelee, & Rusere, 2008; World Bank, 2007). Small dams/reservoirs have the advantage of being operationally efficient, flexible, close to potential users, and require relatively fewer issues for management (Keller, Sakthivadivel, & Seckler, 2000). Experiences with small and medium-size dams demonstrate that these contribute significantly to rural poverty reduction by increasing agricultural productivity and household food security, diversifying local economies and improving local incomes (World Bank, 2007).

In general, the process of selecting the location for the installation of dams/reservoirs is carried out through empirical knowledge and/or according to political interests (Al-Ruzouq, Shanableh, Yilmaz, et al., 2019). An imprecise assessment of the dam/reservoir site and below recommended standards can have harmful effects in the long run and result in incalculable negative impacts on the environment and livelihoods of the local population (Behera, 2013). The combination of Geographic Information Systems (GIS) and Remote Sensing (RS) enables time savings and containment of financial expenses by providing reliable and up-to-date information for water resource management (Mugo & Odera, 2019). These techniques play a fundamental role in identifying potential sites for water storage infrastructure combined with hydrological analysis and modeling (Ahmad & Verma, 2018); RS technology because it allows covering large and inaccessible areas in a short time and different resolutions, providing different environmental and hydrologic parameters for the analysis, and GIS tools because it integrates all these thematic layers together (Elbeih, 2015).

GIS and RS through approaches together with multi-criteria evaluation (MCE) techniques, such as Analytic Hierarchy Process (AHP), Boolean logic, fuzzy logic, Technique for Order of Preference by Similarity to Ideal Solution (TOPSIS), among others, allow the articulation and aggregation of geospatial information to perform dam site suitability mapping and analysis (Al-Ruzouq, Shanableh, Yilmaz, et al., 2019; Jozaghi et al., 2018; Lee, Hyun, Lee, & Lee, 2020).

The selection of modeling techniques used to analyze dam/reservoir suitability varies according to the available data, expertise and local context. When using MCE analysis, several factors that affect dam/reservoir site suitability can be considered, such as the character of foundations, topography, hydrological aspects, spillway capacity, availability of construction materials, submerged land value, accessibility and living facilities (Duggal & Soni, 1996). Al-Ruzouq, Shanableh, Yilmaz, et al. (2019) provide a comprehensive list of factors and respective techniques used in dam suitability studies in many regions of the world, such as Iraq, Pakistan, Sweden, India, and Malaysia. Many other studied locations can be found in the literature, such as the United Arab Emirates (Al-Ruzouq, Shanableh, Yilmaz, et al., 2019), Iran (Jamali, Randhir, & Nosrati, 2018; Yasser, Jahangir, & Mohmmad, 2013), South Korea (Choo, Ahn, Yang, & Yun, 2017), among other locations. However, studies are rare for Mozambique's semi-arid region, which struggles significantly against water scarcity. This study fills this gap by providing the first dam/reservoir suitability mapping study for a semi-arid region in Mozambique. This aspect is crucial since one of the strategic and priority objectives of the Mozambican government is to reduce the vulnerability of rural communities to climate risks and natural disasters through the rehabilitation and construction of 80 small dams/reservoirs to support irrigation for small producers and increase production in drought agricultural areas and improve food security (AR, 2020). This paper aims to identify the most suitable dam/reservoir sites for the semi-arid zone of the Tete Province, Mozambique. Specifically, we aim to:

- Identify the biophysical and socioeconomic factors based on a literature review;
- Use an AHP with local expert opinion to create a dam/reservoir suitability map; and
- Validate the results obtained through the abandoned dam/reservoirs and provide an outlook on the current operational and planned dam/reservoir infrastructure.

Results are expected to contribute with relevant information to support the Southern African Development Community water protocol signed in Johannesburg in 2002. Within this protocol, Mozambique established a regional agreement among the countries in which an action plan for drought mitigation has been delineated, including measures to expand the access to drinking water to populations, particularly in arid and semi-arid areas, and the creation of infrastructures to increase the storage capacity and reduction of water loss (MICOA, 2005).

2. Study area

The study area is in the south of the Tete province, Mozambique, in the districts of Cahora Bassa, Changara, Chiuta, City of Tete, Luenha, Magoe, Maraza, Moatize and Mutarara covering an area of 48454.4 km^2, considered one of the semi-arid regions of Mozambique (Fig. 1). According to the census, there were 1,070,712 people living in these districts in 2017 (INE, 2019). The region is inhabited mainly by a rural population whose survival depends fundamentally on agriculture. Agriculture is the largest sector of the country's economy. About 80% of households are involved in the agricultural sector, contributing up to 29% of the Gross Domestic Product (GDP) (FAO, 2016).

The population's agricultural practice and food security are affected by problems related to climate change problems, such as drought, floods, and cyclones (Engelman, 2009). The vulnerability of this region is partly due to irregular precipitation since the rainy season often does not start as predicted resulting in unpredictable seeding seasons (Fig. 2). Rainfall events concentrate in very short periods causing soil erosion by the surface runoff (MICOA, 2005). The southern region of the Tete Province, north of Sofala and Manica and Inhambane and Gaza provinces are the most critical regions with a high-risk drought level (INGC, 2017) (Fig. 3).

The lack of water in Tete's semi-arid region is related to the severity of climate and to the lack of infrastructures to store water. There is insufficient groundwater extraction through the excavation of artesian wells allied to a low quantity of dams/reservoirs with the capacity to meet population's demand. Recently, the National Institute of Disasters showed a great interest in implementing the Johannesburg agreement and intends to find better ways to increase water availability for inhabitants, crop and livestock production by creating dams/reservoirs in the best available areas. Due to the water scarcity in the region, the development of artificial water storage is necessary and mandatory for ensuring reliable water supply during periods of reduced natural water availability (droughts) as well as for retaining excessive water during periods of floods (World Bank, 2007).

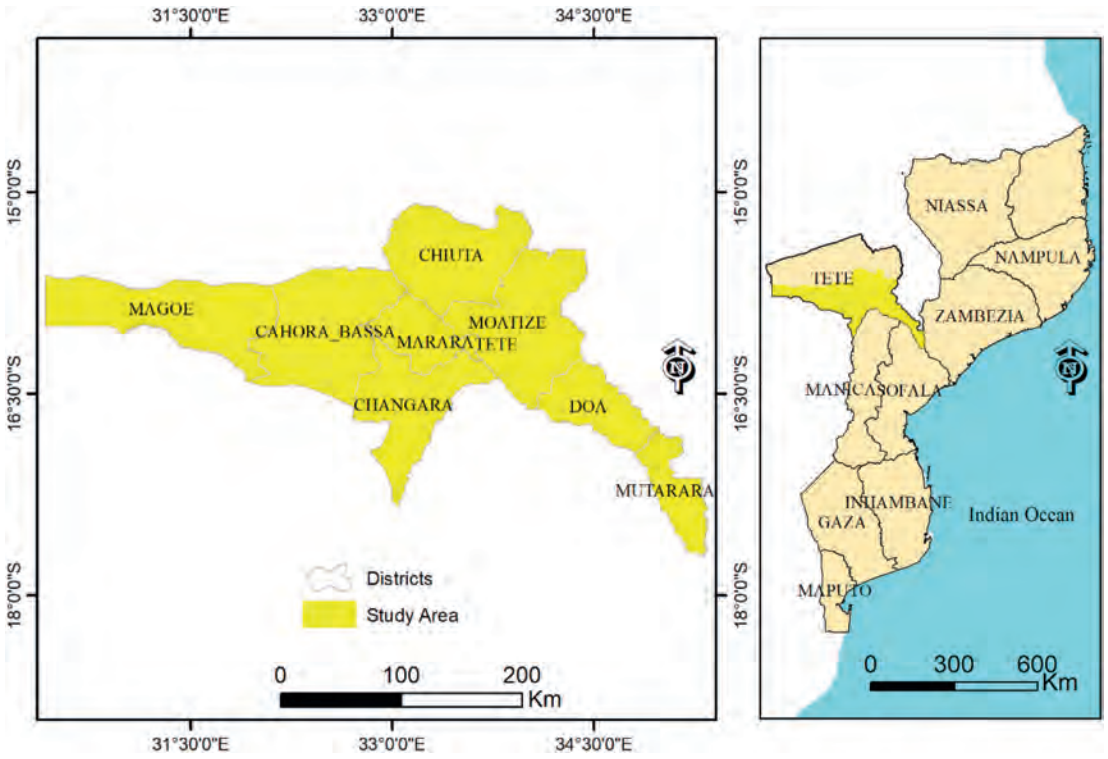

Fig. 1. Geographic location of the study area.

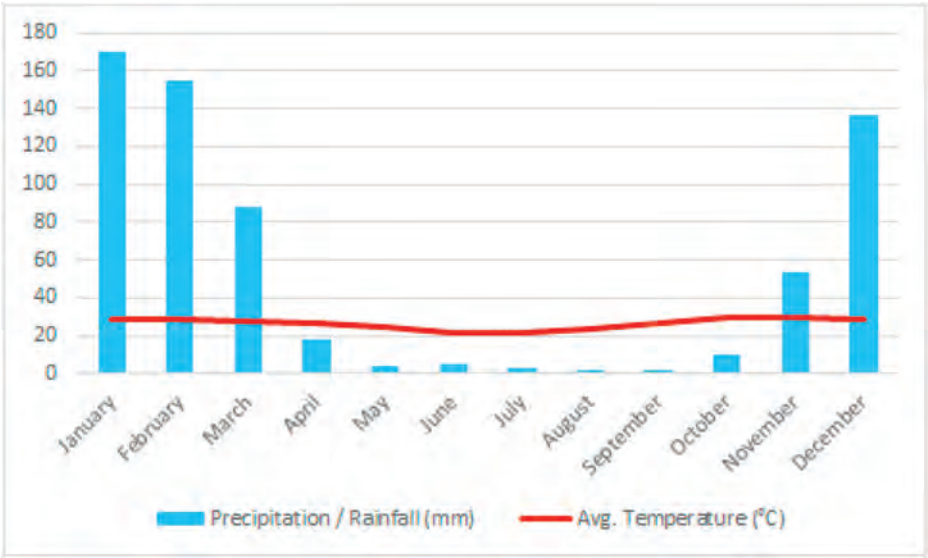

Fig. 2. Tete average rainfall and precipitation (Source: https://en.climate-data.org).

3. Data and methods

3.1. Methodological approach

Multi-Criteria Evaluation (MCE) methods provide a framework for facilitating decision making through information exchange and negotiation among stakeholders (Kiker, Bridges, Varghese, Seager, & Linkov, 2005; Malczewski, 2006). An approach involving several geospatial operations was adopted to determine the suitability of siting small dams/reservoirs based on multiple criteria and an Analytic Hierarchy Process (AHP) (T. L. Saaty, 1986) (Fig. 4).

3.2. Identification of criteria

A literature review was carried out to determine the most relevant criteria to locate dams/reservoirs. This exercise included identifying factors, constraints, and exclusionary areas considering Tete's region specific biophysical and socioeconomic conditions and data availability (Table 1).

3.3. Data sources and preprocessing

Several spatial datasets in vector and raster formats and with

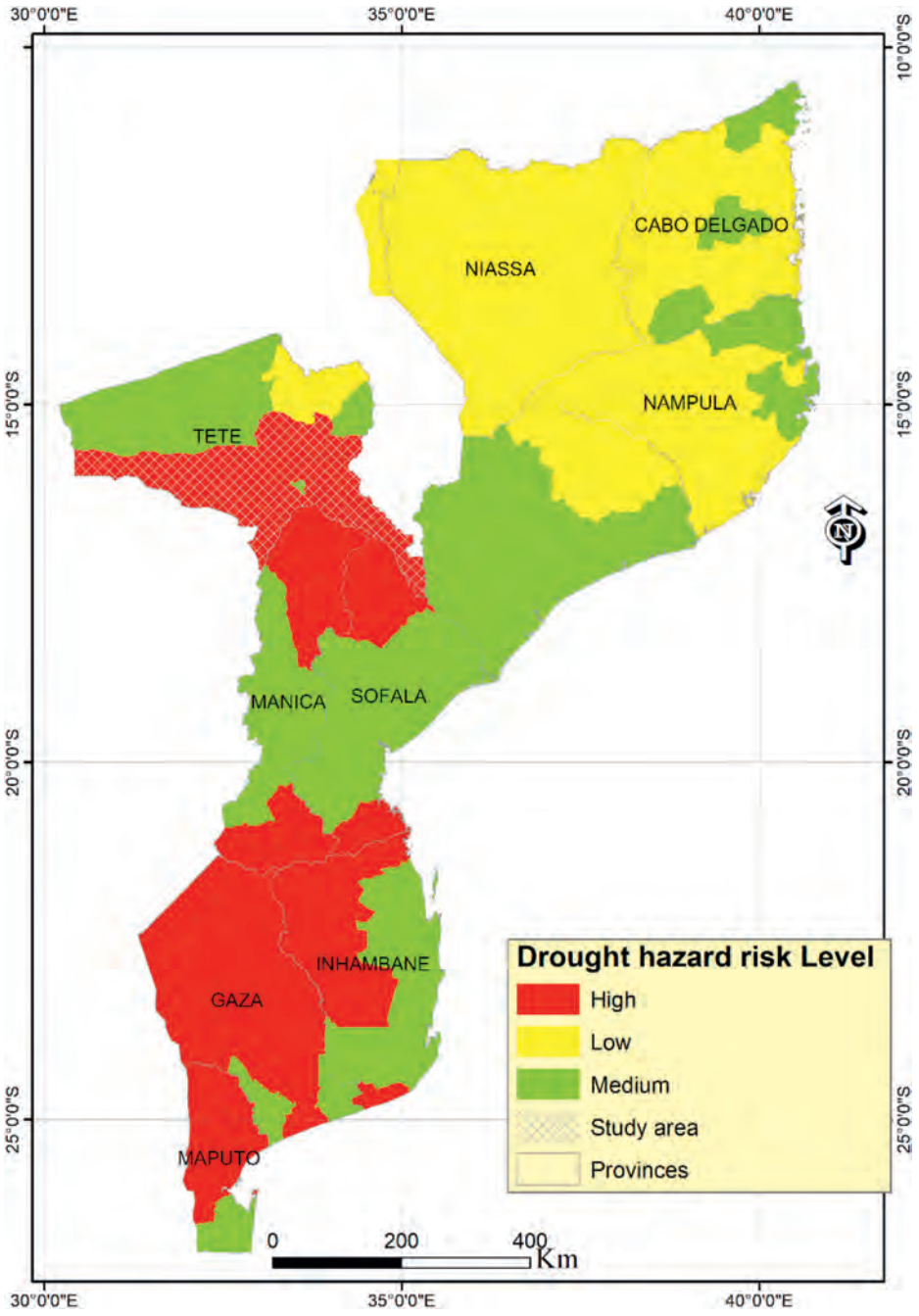

Fig. 3. Mozambique drought hazard risk level (Adapted from INGC, 2017).

different scales and resolutions were used in the study to create the factors to be included in the MCE modelling (Table 2).

The study area dataset was obtained from CENACARTA (CENACARTA, 1997). The lineament structure was derived using the lineament extraction algorithm in PCI Geomatica software (PCI, 2018). Because of the ease in distinguishing between types of rocks and minerals, band 6 of the Landsat 8 satellite was used to map these geological structures (Aretouyap, Billa, Jones, & Richter, 2020; Epuh et al., 2020). Short-wave infrared (SWIR 1) and band 6 of the Landsat 8 image for 2016 were downloaded from the EarthExplorer platform (United States Geological Survey, n.d.) using the following path and row: 167/72 (12-Aug), 168/72 (19-Aug), 168/71 (28 Aug), 169/71(26-Aug) and 170/71 (17 Aug). The distance to roads and villages were obtained using the Euclidian distance tool of ArcGIS (ESRI, 2017). A Digital Elevation Model (DEM) (NASA JPL & NASA/METI, 2012) with a resolution of 30 m was obtained for the Tete Region with elevation ranging from 0 to 1545 m (above sea level). The slope was derived from the DEM using the surface tool of the Spatial analyst extension of ESRI ArcGIS software (ESRI, 2017). Soil data for the study area were obtained from the National Soil map, scale 1:1000000 (DTA-INIA, 1995). The rainfall data based on the mean annual rainfall were obtained from WorldClim (Fick & Hijmans, 2017). WorldClim is a set of global climate layers (gridded data) with a spatial resolution of 1 km^2. The data for this criterion were derived from the DEM using the hydrology extension of ArcGIS software (ESRI, 2017), after proceeding with the sink fill,

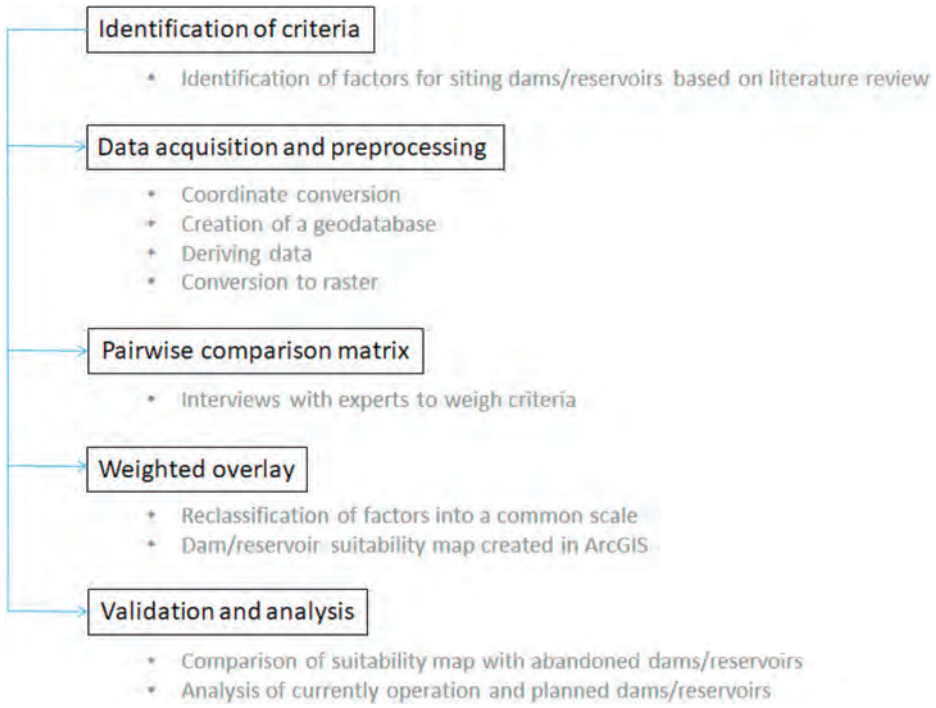

Fig. 4. Flowchart of research methodology.

Table 1
Used criteria and rationale.

Criteria	Rationale	References
Elevation	Elevation influences the location of dams/reservoirs since it affects the water accumulation and movement. Lower elevations are preferable to higher elevations.	Al-Ruzouq, Shanableh, Merabtene, et al. (2019)
Slope	Higher slopes have a higher risk of landslides and put more pressure on the foundation of the infrastructures. The higher the slope in the construction site the lower the potential for storing water and sediment, meaning that lower slopes have more storage volumes.	Ahmad and Verma (2018)
Distance to roads	The presence of roads and settlements close to the proposed sites will reduce the costs of water transportation.	Othman et al. (2020)
Rainfall	Is the primary source of runoff water recharge. Rainfall intensity and its distribution are some of the pre-requisites for designing a water harvesting system.	Prinz and Singh (2000)
Lineaments	Lineaments are linear features on the Earth's surface which reflect the geological structure such as faults or fractures. Areas near lineaments are potential weakness zones for installing infrastructures.	(Elbeih, 2015; Othman et al., 2020)
Distance to villages	The closer dams/reservoirs are to populations the lower will be the costs of water transportation.	Mugo and Odera (2019)
Land use land cover	Areas proposed for constructing of dams/reservoirs should be in or close to agricultural land to reduce the distances of farmers searching for water and the cost of transferring water from the reservoir to agricultural land. In addition, the primary objective of the dam/reservoir proposed for the study area is to assist crops field irrigation.	Mugo and Odera (2019)
Soil type	The type of soils is influenced by its texture, structure and depth which determine soil infiltration rates and the amount of runoff.	Jha, Chowdary, Kulkarni, and Mal (2014)
Stream density	Provides the necessary runoff water for dam/reservoir function, since different drainage network levels indicate different amounts of runoff water when the streams are upper stream tributaries and main downstream streams. Areas with high drainage density are ranked higher in suitability compared to areas of low drainage.	(Jha et al., 2014; Mbilinyi, Tumbo, Mahoo, & Mkilamwinyi, 2014)

flow direction identification, calculation of the flow accumulation and definition of the stream network. Stream density was calculated using the Spatial Analyst Density tool in ArcGIS (ESRI, 2017).

After acquiring and pre-processing all data, these were converted into raster and stored in a spatial geodatabase using a World Geodetic System (WGS) 84, Universe Transverse Mercator (UTM) coordinate system with 30 m spatial resolution.

3.4. Pair-wise comparison matrix

AHP was originally developed by (T. L. Saaty, 1986) and has been applied to many fields (Choudhary & Shankar, 2012; Colak, Memisoglu, & Gercek, 2020; Dedeoğlu & Dengiz, 2019; Martins, Silva, & Cabral, 2012). The implementation of AHP involves the creation of a comparative decision-making preference matrix and determining the factor weights (T. L. Saaty, 1986). The pairwise comparison is applied on all criteria using the fundamental scale proposed by Saaty (1986) (Table 3). In the comparison process, a scale of numbers is used indicating how many times more important one element is over another element with respect to the criterion or property to which they are compared (T. L. Saaty, 2008). This method enables a decision-making group to focus on areas of agreement and disagreement when setting criterion weights (Drobne & Lisec, 2009).

A structured interview was undertaken with four local experts with a background in geology, water resource management,

Table 2
Data used and their sources.

Data	Description	Scale/Spatial resolution	Source
Study Area	Polygon with boundary of semi-arid region of Tete Province	1:250000	CENACARTA (CENACARTA, 1997)
Band 6 of Landsat 8 OLI (2016)	Shortwave infrared band used for lineament extraction (Landsat scene 170/72)	30 m	USGS (USGS, 2016)
Roads	Polylines data with existing roads		CENACARTA (CENACARTA, 1997)
Villages	Point data with the main settlements	1:250000	CENACARTA (CENACARTA, 1997)
Digital Elevation Model (DEM)	Raster dataset with elevation	30 m	ASTER GDEM (NASA JPL & NASA/METI, 2012)
Land use/Land Cover	Polygons with land use and land cover categories (2018)	_	MITADER (MITADER, 2018)
Soil	Polygons with soil types	_	DPA-INIAM (DTA-INIA, 1995)
Rainfall	Raster dataset showing the mean of rainfall	1 km^2 Global Climate data	Fick and Hijmans (2017)
Dams/reservoirs	Point data with the dams/reservoirs	_	ARA-ZAMBEZE (ARAZAMBEZE, 2020)

Table 3
Relative importance. Adapted from Saaty (1986)..

Intensity of relative importance	Definition	Explanation
1	Equal importance	Two criteria contribute equally to the objective
3	Moderate importance	Experience and judgment slightly favor one criterion over another
5	Strong importance	Experience and judgment strongly favor one criterion over another
7	Very strong or demonstrated importance	A criterion is favored very strongly over another; its dominance is demonstrated in practice
9	Extreme importance	The evidence favoring one criterion over another is of the highest possible order of affirmation
2, 4, 6, and 8	Intermediate	Can be used if necessary

hydrology, and civil engineering, respectively. The interview, carried out in January 2020, aimed at exploring their opinions regarding the relative importance of the selected criteria for dam/reservoir siting and the creation of the pairwise comparison matrix. The weighted vector of this matrix was normalized, and the normalized weight vectors were obtained according to the relative level of importance of the criteria used (T. L. Saaty, 1986). A consistency ratio (CR), which measures how consistent the judgments have been relative to large samples of purely random judgments, is computed from the resulting normalized vector values (T. L. Saaty, 1986) (Eq. (1)). If the CR is over 0.1, then the judgments should be considered untrustworthy.

$$CR = CI / RI \quad (1)$$

where CR is the consistency ratio, CI is the consistency index (Eq. (2)), and RI represents a random consistency index derived from a sample of randomly generated reciprocal matrixes (R. W. Saaty, 1987; T. L. Saaty, 1986).

$$CI = (\lambda_{max} - n) / (n - 1) \quad (2)$$

where $\lambda_{max}$is the principal Eigen value, i.e. the value obtained from the summation of products between each element of the Eigen vector and the sum of the columns of the reciprocal matrix, and n is the number of factors.

3.5. Suitability index

After determining the weights, all the criteria were reclassified into a common evaluation scale before performing the weighted overlay analysis in ESRI's ArcGIS Spatial Analyst (ESRI, 2017). Five classes of suitability were used in this process: “Highly unsuitable”; “Not suitable”; “Modestly suitable”; “Suitable” and “Highly suitable”. Highly faulted areas are not suitable for dam/reservoir construction, so dam sites should be located at least 100 m away from lineaments (Othman et al., 2020). The lineaments were reclassified in two classes of suitability; less than 100 m (“Highly unsuitable”) and more than 100 m (“Highly suitable”). Soil classes were reclassified according to their level of suitability (DTA-INIA, 1995). All the remaining input rasters were reclassified using Natural Breaks (Jenks) classification method available in ArcGIS. This method identifies real classes within the data, creating accurate representations of trends in the data (Karlsson, Kalantari, Mörtberg, Olofsson, & Lyon, 2017; Oswald Beiler & Treat, 2015).

In this study, we used a Weighted Linear Combination (WLC), which is based on a weighted average that can easily be understood and implemented within a GIS environment using map algebra operations and cartographic modeling (Chen, Zhang, & Zhu, 2011; Malczewski, 2000). By obtaining the summation of the product of the relative importance weight (percentage of influence) of each criterion with its standard suitability score, a suitability index was determined (Eq. (3)):

$$SI = \sum w\,i\,s\,i \quad (3)$$

where SI is the suitability index, *wi* corresponds to the relative importance of criterion *i* and *si* is the standardized suitability score of criterion i.

3.6. Analysis of current and future situation

In the study area, a total of 38 dams/reservoirs were abandoned, 37 are in use, and 15 are in the process of being built (ARAZAMBEZE, 2020). The infrastructures' georreferenced points were overlaid with the suitability map to check the coincidence level between these data sources providing an outlook of the water infrastructure in the region.

4. Results

4.1. Suitability criteria and reclassification

The nine criteria were reclassified using the suitability level presented in Table 4. This process resulted in nine maps presented in Fig. 5.

Table 4
Site selection criteria used and level of suitability.

Criteria	Suitability Level				
	Highly unsuitable	Not suitable	Modestly suitable	Suitable	Highly suitable
Elevation (m)	715–1545	493–715	361–493	214–361	0–214
Slope (°)	23,5–68,6	14,4–23.4	8,2–14.3	4,1–8.1	0–4
Soil	Arenosol, Calcaric Cambis, Ferric Lixisol, Rhodic Ferralso	Calcic Vertisol, Eutric Leptsol,	Stagnic or Hapl, Ferratic Arenosol, Chromic Luvisol	Mollic Fluvisol, Gleysol	Eutric fluvisol, Fluvisol
Stream density	0-0,18	0,18–0,30	0,30–0,39	0,39–0,49	0,49–0,75
Lineaments (m)	0–100	–	–	–	100–70225
Distance to Villages (km)	0–1	>64,4	34,01–64,4	24,1–34,0	1-24,1
Land Use Land Cover	Evergreen forest, Bare Areas, Artificial water bodies	Grassland, Shrub lands, deciduous forest, Thickets	Closed to open forest with shift cultivation, Regularly Flooded shrub lands	Open forest, Aquatic/Regularly flooded	Cultivated area, Natural water bodies, shifting cultivation to open forest
Rainfall (mm)	599,1–672,0	672,0–751,3	751,3–850,4	850,4–964,7	964- 1107,9
Distance to Roads (km)	42,3–65,4	28,2–42,3	16,6–28,2	1-16,6	0–1

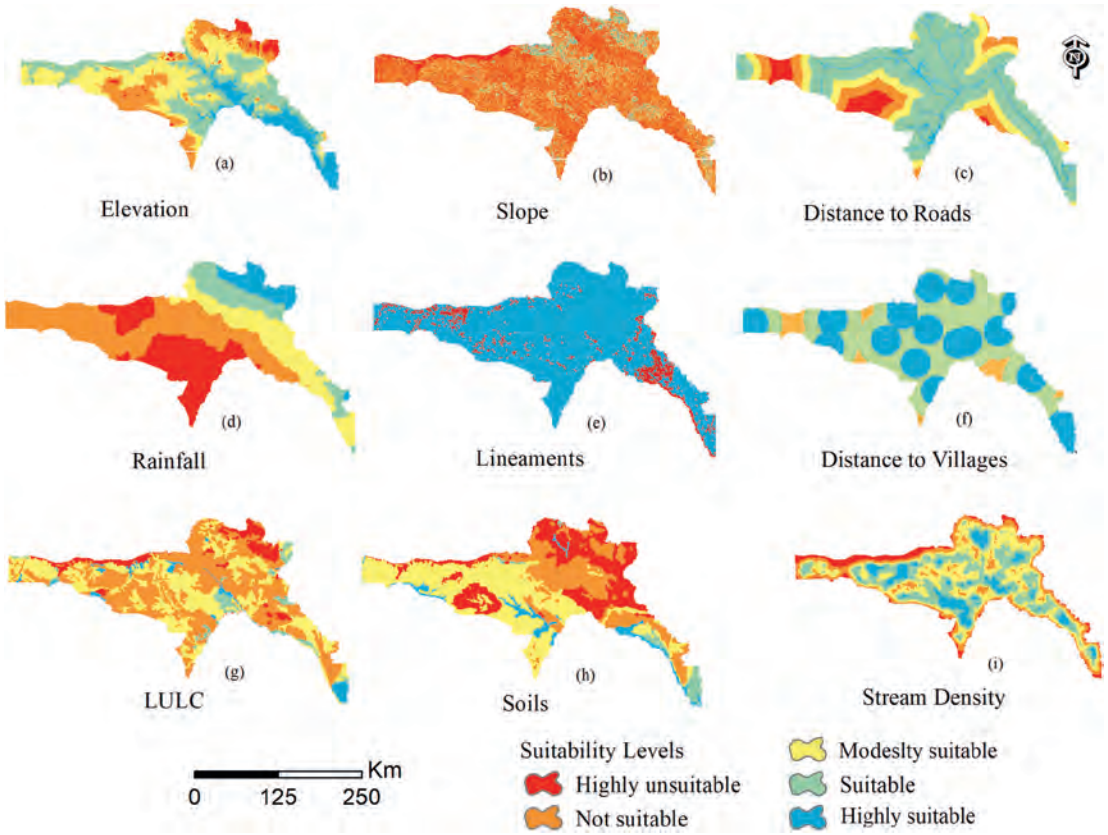

Fig. 5. Standardised criteria for small dam/reservoir site selection.

A low elevation was considered suitable for dam/reservoir siting since it enables the accumulation of precipitated water. Groundwater is also higher at a lower elevation (Fig. 5a). The slope ranged up to 68,9°. The best locations were the ones with gentle slopes, i.e. areas up to 8,1% slope (Fig. 5b). The range of distance to roads for the study area was from 0 to 65.4 km. Areas within 0–1 km were assigned as "Highly suitable" and larger distances were considered from "Suitable" to "Highly unsuitable" (Fig. 5c). A high priority for siting dam/reservoir was given to locations with precipitation ranging from 964 mm to 1107,9 mm (Fig. 5d). Regarding the lineaments, and because these geological structures can obstruct the normal stream-flow and cause the water reserves to collapse, the areas with or close to lineaments should be excluded from consideration to site a dam/reservoir (Noori, Pradhan, & Ajaj, 2019). For the study area, the more distant a lineament is, the better the location for the dam/reservoir is (Fig. 5e). The proximity of the dams relative to residential areas can facilitate the task of finding a skilled workforce for the construction and maintenance work of the dam/reservoir itself, as well as making the transfer of water less expensive for rural populations (Emamgholi, Shahedi, Solimani, &

Khaledian, 2007; Safavian & Amani, 2015). In this study, the areas closer to the village were classified as the most suitable (Fig. 5f). The increase in vegetation density results in an increase in the loss of interception, retention and infiltration rates, resulting in decreased flow volume. In turn, cultivated fields are suitable for certain types of rainwater harvesting technologies, while the riparian vegetation is not adequate (Mbilinyi et al., 2014). In this study, the most suitable LULC considered were the cultivated areas, natural water bodies, and areas shifting cultivation to open forest (Fig. 5g). The most suitable soils for dam/reservoir site locations should have a higher capacity for water retention (Adham, Riksen, Ouessar, Abed, & Ritsema, 2017). For the study area *Mollic fluvisol* and *Gleysol eutric fluvisol* were considered the most suitable because of their low permeability and higher water-holding ability (Othman et al., 2020) (Fig. 5h). For the stream density factor, a high priority was given to the locations where there was a high drainage density (0,79–0,75/ km^2) when compared to areas of low drainage (Fig. 5i).

4.2. Pairwise comparison of criteria

Based on the local experts and decision makers' opinion, a matrix comparison with weight for all criteria was produced and then normalized (Table 5). Stream density was the most important factor (31%). Both distances to villages and roads were considered the least important factors (2%). We found a $\lambda_{max} = 10.14$, $n = 9$, CI = 0.1425 and a CR of 0.098. Since the CR obtained was less than 0.1, the judgments of the experts were considered consistent (T. L. Saaty, 2008).

4.3. Suitability map

A suitability map for the dam/reservoir in the semi-arid zone of the Tete province was produced together with a histogram showing area and percentage for the different categories of suitability (Fig. 6). Although five classes of suitability were predefined, the results of the weighted overlay of the criteria revealed only three levels of suitability: "Not suitable", "Modestly suitable" and "Suitable". The suitability classes "Highly unsuitable" and "Highly suitable" were not found.

The "Modestly suitable" class occupies most of the study area (78%). The "Not suitable" class is predominant in the western zone of the study area, covering about 15% of the region, with emphasis on the districts of Cahora Bassa, Magoe and Changara, most likely due to reduced levels of rainfall and predominance of a drainage network with very low water flow. It is also possible to observe that Tete City districts, Marara and Mutarara contain only "Modestly suitable" and "Suitable" classes. The "Suitable" class only occupies 7% of the region. The individual analysis of the districts shows that Mutara, Doa, Moatize, Magoe and Cahora-Bassa are the districts with the highest coverage of suitable areas, in contrast to the districts of Marara, Changara and Tete city that have a lower coverage in this class. The comparative analysis by district reveals that although all districts have most of their area classified as "Modestly suitable", the districts of Moatize, Magoe and Chiuta are the ones with the largest proportional area in this class (Fig. 7).

Table 5
Normalized pairwise comparison (1: Slope; 2: Elevation; 3: Stream Density; 4: Land Use Land Cover; 5: Soil; 6: Distance to Roads; 7: Rainfall; 8: Distance to Villages; 9: Lineaments).

Criteria	1	2	3	4	5	6	7	8	9	Weight
1	0.05	0.05	0.04	0.07	0.13	0.14	0.05	0.13	0	8%
2	0.05	0.05	0.05	0.07	0.13	0.1	0.05	0.13	0	7%
3	0.39	0.36	0.33	0.5	0.3	0.16	0.29	0.17	0.3	31%
4	0.05	0.05	0.05	0.07	0.17	0.12	0.1	0.09	0.2	10%
5	0.02	0.02	0.05	0.02	0.04	0.14	0.07	0.09	0.1	6%
6	0.01	0.01	0.04	0.01	0.01	0.02	0.03	0.02	0	2%
7	0.29	0.31	0.33	0.21	0.17	0.16	0.29	0.17	0.3	24%
8	0.01	0.01	0.04	0.01	0.01	0.02	0.03	0.02	0	2%
9	0.15	0.15	0.08	0.04	0.04	0.16	0.1	0.17	0.1	11%

4.4. Analysis of current and future situation

Recent data provided by AraZambeze (ARAZAMBEZE, 2020) indicates that the study area has 38 abandoned dams/reservoirs built with concrete and mortar stone, spatially distributed by the districts of Changara (15), Marara (11), Chiuta (4), Cahora-Bassa (3), Magoe (2), Moatize (2) and Doa (1). The spatial overlay of the abandoned dams and the streams order layers over the suitability level map shows that 35 out of the 38 abandoned dams were in the areas considered as modestly suitable, two dams were in not suitable areas, and only one abandoned dam was in a suitable area. All overlapping points coincide with areas with a stream order of less than 5, i.e., a very low runoff (Fig. 8).

Currently, the region has 37 dams in operation located in the districts of Changara (19), Marara (7), Magoe (5), Cahora Bassa (4), Chiuta (1), and Moatize (1). As shown in Fig. 8, Changara and Marara districts, in the central area of the study area, have the largest number of dams (70.2%), whereas in the eastern districts Doa and Mutarara there is no operational dam. It is also noted that of 37 dams/reservoirs in operation, 78% overlap with the modestly suitable zones, 16.2% are in suitable areas and 5.4% are in not suitable areas. Most of these dams/reservoirs are found in rivers with little flow (stream order less than 5). To increase the number of dams/reservoirs to improve water availability to local communities in the dry season, different governmental entities and NGOs have financed the construction of new dams in the study area. Presently, 15 irrigation dams are under construction, located in the districts of Changara (4), Cahora Bassa (3), Moatize (3), Chiuta (2), Doa (1), Magoe (1), Marara (1). The overlay of these dams with the suitability map show that three dams are in areas considered "Suitable", 11 are in "Modestly suitable" areas and only one dam is in a "Not suitable" zone. Only two dams will be built in a stream order greater than 4 (Fig. 9).

5. Discussion

5.1. Main findings and contribution

This paper contributes with a case study for locating the best places for building small dams/reservoirs in a semi-arid region of Mozambique using a GIS-based MCE approach with an AHP. We found that the stream density (31%), rainfall (24%), and lineaments (11%) were the most critical factors in determining the location of these infrastructures according to local expert knowledge. These factors have also been identified in previous studies as the most important ones (Al-Ruzouq, Shanableh, Yilmaz, et al., 2019; Elbeih, 2015). The study also compared the resulting suitability map with current and abandoned dams/reservoirs. This analysis showed that most of the study area falls inside modestly suitable areas (78%), 15% are in not suitable areas, and only 7% of the area is suitable for dam/reservoir construction confirming that in this area the rainfall regime is very low and with severe drought. According to the interviewed experts from AraZambeze, the lack of water in most of the year, silting, rupture, and erosion are the main causes of these dams' abandonment. The overlay of the layers of the dams/reservoirs that were abandoned (92%), operational (78%), and planned (or under construction) (73%) with the suitability map shows that most of these are in modestly suitable areas. This finding suggests that the decision to construct dams/reservoirs may not have

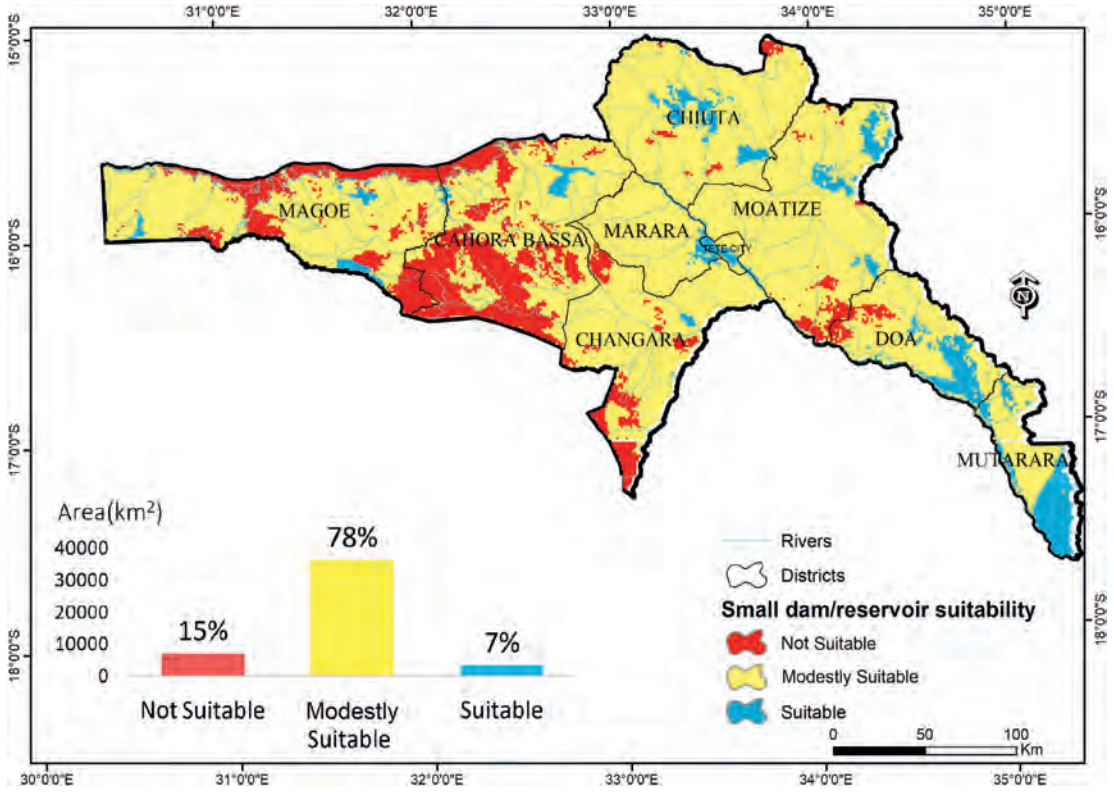

Fig. 6. Small dam/reservoirs suitability categories for the study area.

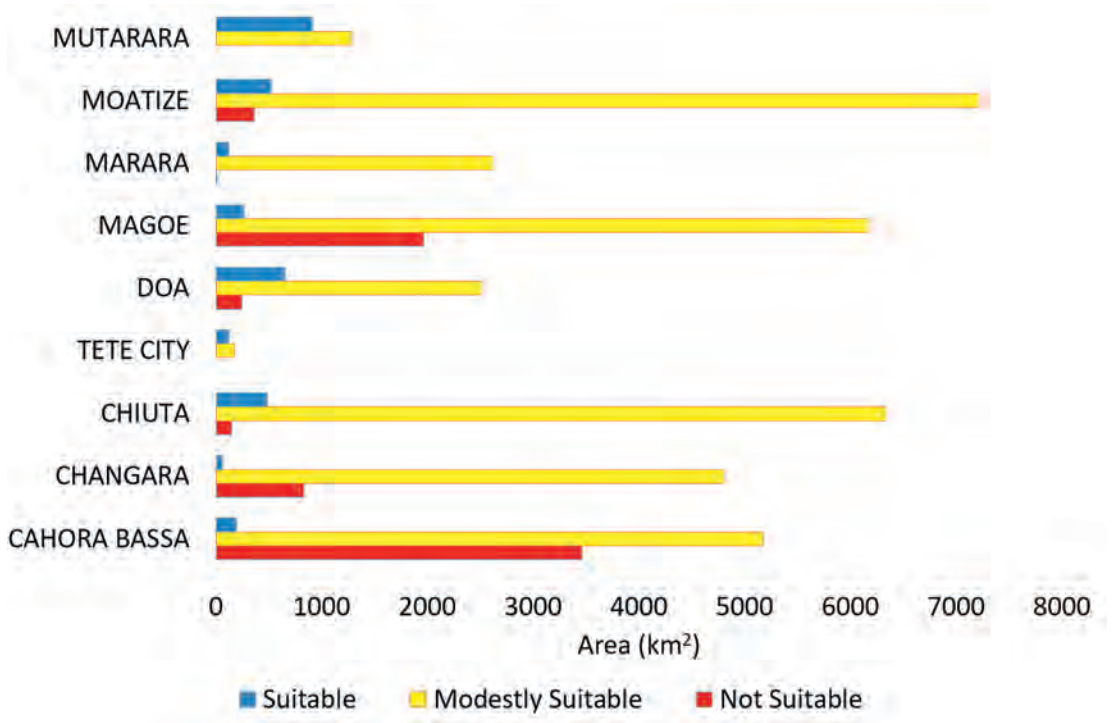

Fig. 7. Level of suitability per district.

considered the most critical suitability factors identified in this study. Since most of the dams/reservoirs still in operation are also in modestly suitable areas, the suitability criteria used may not fully explain whether these infrastructures are still in operation. It may be possible that the low suitability of a site may have contributed to the abandonment. The full understanding of finding out why so many dams/reservoirs failed seems important before building new ones and requires further analysis with more data and/or additional

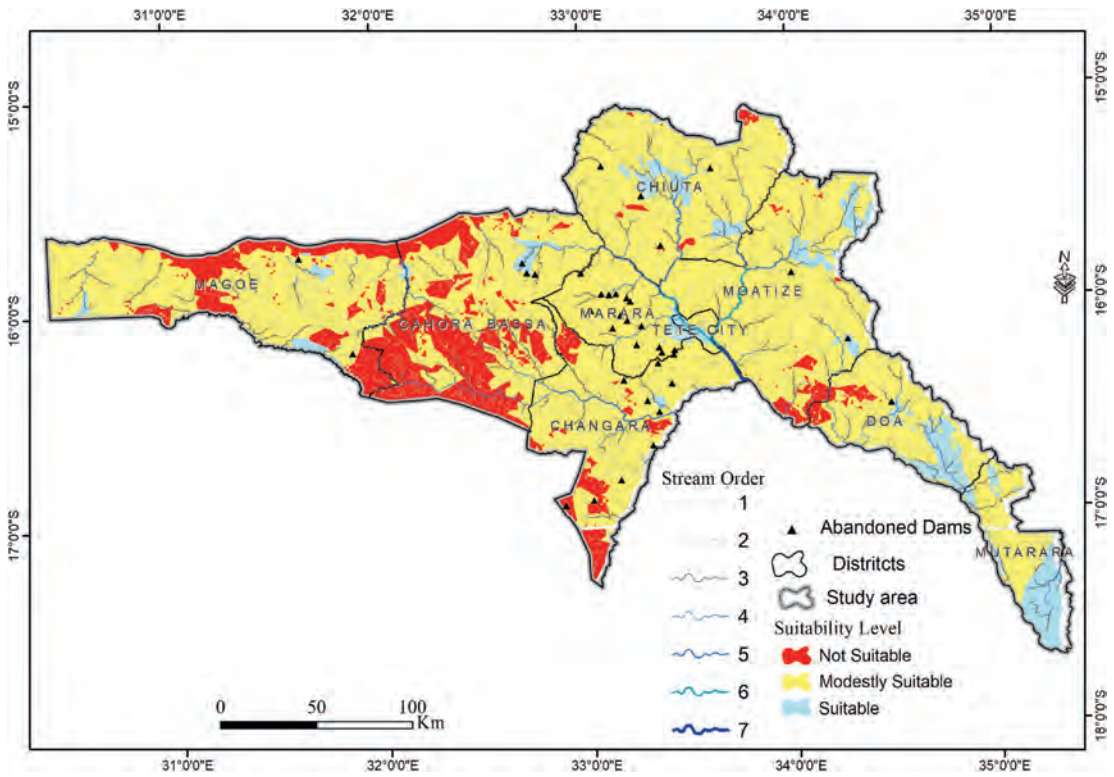

Fig. 8. Abandoned dams/reservoirs overlaid with suitability map and streams.

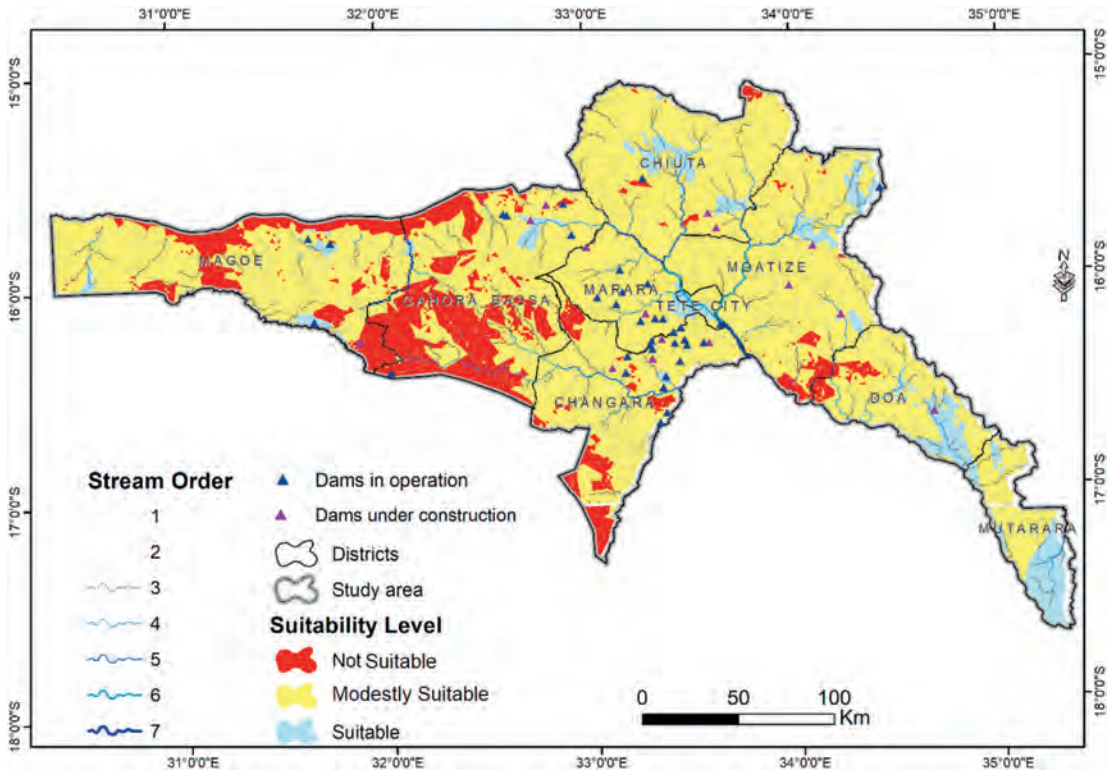

Fig. 9. Geographic location of dams in operation and under construction.

criteria.

5.2. Limitations and future developments

The results need to be interpreted with caution since there are limitations that should be considered in future developments of this study. For instance, the MCE modeling approach followed used WLC, which is an additive model that should, ideally, only use independent criteria (Karlsson et al., 2017). Otherwise, some of the factors used may be correlated, resulting in double-counting (Karlsson et al., 2017). However, as Malczewski (2000) pointed out, the requirements of decomposability and non-redundancy are difficult to justify in spatial decision problems. Future versions of this study should incorporate a strategy to avoid redundancy, such as the factor interaction method (A., M., Kheir, & C., 2001).

Another limitation was the lack of a sensitivity analysis. Despite not being so commonly used in suitability analysis (Delgado & Sendra, 2004), a sensitivity analysis was not implemented. We could have varied the weights of the criteria to test if these significantly changed the results obtained. However, in this study, we wanted to incorporate the knowledge of credible local experts who have unique technical and local knowledge about the study area; three of them work for the Regional Water Administration and one has worked as a hydraulic engineer in an infrastructure building international company operating in Mozambique. Since AHP judgments were considered consistent, and the suitability model's results were validated by the abandoned dams/reservoirs, this option was not further explored.

The number of experts who participated in this study is low as in other previous studies with AHP (Alemdar, Kaya, & Çodur, 2020; Dash & Sar, 2020; Peterson, Silsbee, & Schmoldt, 1994). Although, it would have been desirable to have more experts to possibly bring more relevant knowledge for the decision process, we had to work with the ones we could find for this study area in Mozambique. Nevertheless, a variability and confidence analysis regarding experts' level of knowledge about each criterion should be envisaged in future versions of this study to bring more credibility to the results (Campagne, Roche, Gosselin, Tschanz, & Tatoni, 2017; Elliott et al., 2020). The dams/reservoirs' location would also benefit from a participatory process with stakeholders (Luijten, Knapp, Sanz, & Jones, 2003; Roozbahani, Abbasi, Schreider, & Hosseinifard, 2020). Thus, for the process to be considered community property, it is recommended to conduct fieldwork for community consultation to assess the population's point of view regarding the construction of the dams/reservoirs in the proposed locations. Local communities and other stakeholders' involvement in water projects is crucial as it brings transparency, acceptability, support, and ensures the sustainability of the process (Dungumaro & Madulu, 2003). This element will prevent, for instance, land-use conflicts and will involve populations in the resolution of possible problems, such as erosion, siltation, and others. Future works aiming to improve results' quality and reliability should consider participatory events with all relevant stakeholders.

Aspects, such as local knowledge and the ability to maintain the dam/reservoir or access to better alternative water sources could also cause dam/reservoir failure. A more structured in-depth research using the same suitability criteria to determine the exact reasons for abandoning dams/reservoirs could have been done. This action would enable verifying if the criteria used for the suitability analysis were well chosen. Unfortunately, we did not have data to check precisely why each dam/reservoir failed. We only had information about their location and operational status. To pinpoint why each specific dam failed would involve field work which we could not do due to lack of resources. However, future versions of this work should include this aspect since it would validate the results more consistently.

Another possible improvement for this study is data. For instance, we could use locally measured rainfall data instead of interpolated global data (Fick & Hijmans, 2017), which is known to have substantial discrepancies (Faye, Herrera, Bellomo, Silvain, & Dangles, 2014). Although we tried to use the best possible data, future versions of the suitability model will benefit from more accurate datasets when these are made available.

6. Conclusion

Identifying suitable areas for building small dams/reservoirs is essential for the study area, a semi-arid region with important water deficits. The approach followed in this study based on GIS-based MCE together with an AHP enabled us to obtain information about the relevant variables (i.e., slope, elevation, rainfall, stream density, lineaments, soil, land-use land cover and two socioeconomic factors, distance to roads and distance to villages) to create a small dam/reservoir suitability map for the region of Tete, Mozambique. Results show that most of the currently operating and planned small dams/reservoirs are located in modestly suitable areas. This means that the main location factors for building a dam are not being considered, reinforcing the need to use a spatial MCE approach. This information raises concerns about the future effectiveness of these infrastructures and should be carefully analyzed by planners to better address the population's water needs in the region. The methodology is flexible enough to easily consider additional criteria, experts/stakeholders, and up-to-date data in the process of deciding where to locate these infrastructures in semi-arid regions or any other locations facing water scarcity problems.

Acknowledgements

This work was partially supported by national funds through FCT (Fundação para a Ciência e a Tecnologia) under the project UIDB/04152/2020 - Centro de Investigação em Gestão de Informação (MagIC). The authors would like to express their gratitude to the interviewed experts: António Melembe and Angelo Pereira (ARA Centro), Francisco Macaringue (ARA Zambeze) and Johane Moiane for their valuable contribution to this research and evaluating the site selection criteria.

References

Abdalla, O., Kacimov, A., Chen, M., Al-Maktoumi, A., Al-Hosni, T., & Clark, I. (2017). *Water resources in arid areas: The way forward*. Springer Water. https://doi.org/10.1007/978-3-319-51856-5

Abu-Allaban, M., El-Naqa, A., Jaber, M., & Hammouri, N. (2015). Water scarcity impact of climate change in semi-arid regions: A case study in Mujib basin, Jordan. *Arabian Journal of Geosciences, 8*(2), 951–959. https://doi.org/10.1007/s12517-014-1266-5

Adham, A., Riksen, M., Ouessar, M., Abed, R., & Ritsema, C. (2017). Development of methodology for existing rainwater harvesting assessment in (semi-)Arid regions. In *Water and land security in drylands* (pp. 171–184). Cham: Springer International Publishing. https://doi.org/10.1007/978-3-319-54021-4_16.

Ahmad, I., & Verma, M. K. (2018). Application of analytic hierarchy process in water resources planning: A GIS based approach in the identification of suitable site for water storage. *Water Resources Management, 32*(15), 5093–5114. https://doi.org/10.1007/s11269-018-2135-x

Al-Ruzouq, R., Shanableh, A., Merabtene, T., Siddique, M., Khalil, M. A., Idris, A., et al. (2019). Potential groundwater zone mapping based on geo-hydrological considerations and multi-criteria spatial analysis: North UAE. *Catena, 173*, 511–524. https://doi.org/10.1016/j.catena.2018.10.037

Al-Ruzouq, R., Shanableh, A., Yilmaz, A. G., Idris, A. E., Mukherjee, S., Khalil, M. A., et al. (2019). Dam site suitability mapping and analysis using an integrated GIS and machine learning approach. *Water, 11*(9), 1880. https://doi.org/10.3390/w11091880

Alemdar, K. D., Kaya, Ö., & Çodur, M. Y. (2020). A GIS and microsimulation-based MCDA approach for evaluation of pedestrian crossings. *Accident Analysis & Prevention, 148*, 105771. https://doi.org/10.1016/j.aap.2020.105771

Ammar, A., Riksen, M., Ouessar, M., & Ritsema, C. (2016). Identification of suitable sites for rainwater harvesting structures in arid and semi-arid regions: A review. *International Soil and Water Conservation Research, 4*(2), 108–120. https://doi.org/10.1016/j.iswcr.2016.03.001

AR. (2020). *Proposta de Programa Quinquenal do Governo: 2020-2024. Maputo: Assembleia da Republica, IX Legislatura*.

ARAZAMBEZE. (2020). Represas do vale do Zambeze. *Tete: Administração Regional de Águas do Zambeze*.

Aretouyap, Z., Billa, L., Jones, M., & Richter, G. (2020). Geospatial and statistical interpretation of lineaments: Salinity intrusion in the kribi-campo coastland of Cameroon. *Advances in Space Research, 66*(4), 844–853. https://doi.org/10.1016/j.asr.2020.05.002

Behera, D. K. (2013). Dams , development and inclusion of indigenous groups A case from odisha. In S. Uwe, et al. (Eds.), *Navigating social Exclusion and Inclusion in contemporary India and beyond , str ... (Anthem pre)*. London, UK: British Library.

Campagne, C. S., Roche, P., Gosselin, F., Tschanz, L., & Tatoni, T. (2017). Expert-based ecosystem services capacity matrices: Dealing with scoring variability. *Ecological Indicators, 79*, 63–72. https://doi.org/10.1016/j.ecolind.2017.03.043

CENACARTA. (1997). *Mozambique GIS data*. Maputo, Mozambique: Centro Nacional de Cartografia e Teledetecção.

Chen, J., Zhang, X., & Zhu, Q. (2011). Multi-objective decision making for land use planning with ordered weighted averaging method. *Systems Engineering Procedia, 2*, 434–440. https://doi.org/10.1016/j.sepro.2011.10.063

Choo, T. H., Ahn, S. H., Yang, D. U., & Yun, G. S. (2017). A Study on the Estimating Dam Suitable Site based on Geographic Information using AHP. *In ICDET-17, FABMS-17, RIECAE-17, RTET-17, ABMS-17 Feb. 2017*, 50–56. https://doi.org/10.17758/EIRAI.DIR0217032. EIRAI.

Choudhary, D., & Shankar, R. (2012). An STEEP-fuzzy AHP-TOPSIS framework for evaluation and selection of thermal power plant location: A case study from India. *Energy, 42*(1), 510–521. https://doi.org/10.1016/j.energy.2012.03.010

Colak, H. E., Memisoglu, T., & Gercek, Y. (2020). Optimal site selection for solar photovoltaic (PV) power plants using GIS and AHP: A case study of Malatya province, Turkey. *Renewable Energy, 149*, 565–576. https://doi.org/10.1016/j.renene.2019.12.078

Dash, P., & Sar, J. (2020). Identification and validation of potential flood hazard area using GIS-based multi-criteria analysis and satellite data-derived water index. *Journal of Flood Risk Management, 13*(3). https://doi.org/10.1111/jfr3.12620

Dedeoğlu, M., & Dengiz, O. (2019). Generating of land suitability index for wheat with hybrid system aproach using AHP and GIS. *Computers and Electronics in Agriculture, 167*, 105062. https://doi.org/10.1016/j.compag.2019.105062

Delgado, M. G., & Sendra, J. B. (2004). Sensitivity analysis in multicriteria spatial decision-making: A review. *Human and Ecological Risk Assessment: An International Journal, 10*(6), 1173–1187. https://doi.org/10.1080/10807030490887221

Detoni, T. L., & Dondoni, P. C. (2008). A escassez da água: Um olhar global sobre a sustentabilidade e a consciência acadêmica. *Revista Ciências Administrativas, 14*(2), 191–204.

Drobne, S., & Lisec, A. (2009). Multi-attribute decision analysis in GIS : Weighted linear combination and ordered weighted averaging. *Informatica, 33*, 459–474. https://doi.org/10.1017/CBO9781107415324.004

DTA-INIA. (1995). *Carta Nacional de Solos. Maputo, Mozambique: Serie Terra e Água, Comunicação No. 73*. Departamento de Terra e Água), Instituto Nacional de Investigação Agronómica (INIA).

Duggal, K. N., & Soni, J. P. (1996). Elements of Water Resources Engineering. *Ludhiana: New Age International*.

Dungumaro, E. W., & Madulu, N. F. (2003). Public participation in integrated water resources management: The case of Tanzania. *Physics and Chemistry of the Earth, 28*(20–27), 1009–1014. https://doi.org/10.1016/j.pce.2003.08.042

Elbeih, S. F. (2015). An overview of integrated remote sensing and GIS for groundwater mapping in Egypt. *Ain Shams Engineering Journal, 6*(1), 1–15. https://doi.org/10.1016/j.asej.2014.08.008

Elliott, R. M., Motzny, A. E., Majd, S., Chavez, F. J. V., Laimer, D., Orlove, B. S., et al. (2020). Identifying linkages between urban green infrastructure and ecosystem services using an expert opinion methodology. *Ambio, 49*(2), 569–583. https://doi.org/10.1007/s13280-019-01223-9

Emamgholi, M., Shahedi, K., Solimani, K., & Khaledian, V. (2007). Suitable site selection for gabion check dams construction using analytical hierarchy process and decision making methods. *Journal of Soil Environment, 2*(4), 170–179.

Engelman, R. (2009). *State of world population 2009. Facing a changing world: women, population and climate. New York*. Retrieved from https://www.unfpa.org/publications/state-world-population-2009.

Epuh, E. E., Okolie, C. J., Daramola, O. E., Ogunlade, F. S., Oyatayo, F. J., Akinnusi, S. A., et al. (2020). An integrated lineament extraction from satellite imagery and gravity anomaly maps for groundwater exploration in the Gongola Basin. *Remote Sensing Applications: Society and Environment, 20*, 100346. https://doi.org/10.1016/j.rsase.2020.100346

ESRI. (2017). *November 20). ArcGIS*. Redlands, USA: Environmental Systems Research Institute. Retrieved from www.esri.com.

FAO. (2016). Mozambique. Socio-economic context and role of agriculture. Country fact sheet on food and agriculture policy trends. *Food and agriculture organization of the united Nations*. Retrieved from http://www.fao.org/3/a-i5931e.pdf.

Faye, E., Herrera, M., Bellomo, L., Silvain, J.-F., & Dangles, O. (2014). Strong discrepancies between local temperature mapping and interpolated climatic grids in tropical mountainous agricultural landscapes. *PloS One, 9*(8), Article e105541. https://doi.org/10.1371/journal.pone.0105541

Fick, S. E., & Hijmans, R. J. (2017). WorldClim 2: New 1-km spatial resolution climate surfaces for global land areas. *International Journal of Climatology, 37*(12), 4302–4315. https://doi.org/10.1002/joc.5086

Gain, A. K., Giupponi, C., & Wada, Y. (2016). Measuring global water security towards sustainable development goals. *Environmental Research Letters, 11*(12). https://doi.org/10.1088/1748-9326/11/12/124015

Ghazal, N. K., & Salman, S. R. (2015). Determining the optimum site of small dams using remote sensing techniques and GIS. *International Journal of Scientific Engineering and Research, 3*(9), 4–8.

Guppy, L., & Anderson, K. (2017). *Water crisis report - the facts*. Hamilton, Canada: United Nations University Institute for Water, Environment and Health.

Ibrahim, G. R. F., Rasul, A., Hamid, A. A., Ali, Z. F., & Dewana, A. A. (2019). Uitable site selection for rainwater harvesting and storage case study using dohuk governorate. Water. *S*. https://doi.org/10.3390/w11040864

INE. (2019). *Censo 2017, IV recenseamento geral da população e habitação*. Maputo, Mozambique: INE: Instituto Nacional de Estatística. Retrieved from http://www.ine.gov.mz.

INGC. (2017). *HQ VAM analysis of CHIRPS rainfall estimates*. Maputo: National Institute of Disaster Management.

Jamali, A. A., Randhir, T. O., & Nosrati, J. (2018). Site suitability analysis for subsurface dams using Boolean and fuzzy logic in arid watersheds. *Journal of Water Resources Planning and Management, 144*(8), Article 04018047. https://doi.org/10.1061/(ASCE)WR.1943-5452.0000947

Jha, M. K., Chowdary, V. M., Kulkarni, Y., & Mal, B. C. (2014). Rainwater harvesting planning using geospatial techniques and multicriteria decision analysis. *Resources, Conservation and Recycling, 83*, 96–111. https://doi.org/10.1016/j.resconrec.2013.12.003

Jozaghi, A., Alizadeh, B., Hatami, M., Flood, I., Khorrami, M., Khodaei, N., et al. (2018). A comparative study of the AHP and TOPSIS techniques for dam site selection using GIS: A case study of sistan and Baluchestan province, Iran. *Geosciences, 8*(12), 494. https://doi.org/10.3390/geosciences8120494

Karlsson, C. S. J., Kalantari, Z., Mörtberg, U., Olofsson, B., & Lyon, S. W. (2017). Natural hazard susceptibility assessment for road planning using spatial multi-criteria analysis. *Environmental Management, 60*(5), 823–851. https://doi.org/10.1007/s00267-017-0912-6

Keller, A., Sakthivadivel, R., & Seckler, D. (2000). *Water scarcity and the role of storage in development. Research Report (IWMI)*. Sri Lanka: Colombo.

A, S., M, K., Kheir, R. B., & C, A. (2001). Assessment of road instability along a typical mountainous road using GIS and aerial photos, Lebanon - eastern Mediterranean. *Bulletin of Engineering Geology and the Environment, 60*(2), 93–101. https://doi.org/10.1007/s100640000092

Kiker, G. A., Bridges, T. S., Varghese, A., Seager, T. P., & Linkov, I. (2005). Application of multicriteria decision analysis in environmental decision making. *Integrated Environmental Assessment and Management, 1*(2), 95. https://doi.org/10.1897/IEAM_2004a-015.1

Lee, S., Hyun, Y., Lee, S., & Lee, M.-J. (2020). Groundwater potential mapping using remote sensing and GIS-based machine learning techniques. *Remote Sensing, 12*(7), 1200. https://doi.org/10.3390/rs12071200

Luhunga, P., Chang'a, L., & Djolov, G. (2017). Assessment of the impacts of climate change on maize production in the wami ruvu Basin of Tanzania. *Journal of Water and Climate Change, 8*(1), 142–164. https://doi.org/10.2166/wcc.2016.055

Luijten, J. C., Knapp, E. B., Sanz, S. I., & Jones, J. W. (2003). A role for GIS-based simulation for empowering local stakeholders in water resources negotiations in developing countries: Case studies for two rural hillside watersheds in Honduras and Colombia. *Water Policy, 5*(3), 213–236. https://doi.org/10.2166/wp.2003.0013

Malczewski, J. (2000). On the use of weighted linear combination method in GIS: Common and best practice approaches. *Transactions in GIS, 4*(1), 5–22. https://doi.org/10.1111/1467-9671.00035

Malczewski, J. (2006). GIS-based multicriteria decision analysis: A survey of the literature. *International Journal of Geographical Information Science, 20*(7), 703–726. https://doi.org/10.1080/13658810600661508

Malinowski, Ł., & Skoczko, I. (2018). Impacts of climate change on hydrological regime and water resources management of the Narew river in Poland. *Journal of Ecological Engineering, 19*(4), 167–175. https://doi.org/10.12911/22998993/91672

Martins, V. N., Silva, D. S., & Cabral, P. (2012). Social vulnerability assessment to seismic risk using multicriteria analysis: The case study of vila Franca do campo (são Miguel island, azores, Portugal). *Natural Hazards, 62*(2), 385–404. https://doi.org/10.1007/s11069-012-0084-x

Mbilinyi, B. P., Tumbo, S. D., Mahoo, H. F., & Mkilamwinyi, F. (2014). Identification of suitable indices for identification of potential sites for rainwater harvesting. *Tanzania Journal of Agricultural Sciences, 12*(2), 35–46.

MICOA. (2005). *Avaliação da vulnerabilidade as mudanças climáticas e estratégias de adaptação. Ministério para a Coordenação da Acção Ambiental*. Maputo.

MITADER. (2018). *Uso e Nível de Referência de Emissões Florestais de Moçambique para Redução de Emissões por Desflorestamento de Florestas Nativas*. Maputo.

Mugo, G. M., & Odera, P. A. (2019). Site selection for rainwater harvesting structures in Kiambu County-Kenya. *The Egyptian Journal of Remote Sensing and Space Science, 22*(2), 155–164. https://doi.org/10.1016/j.ejrs.2018.05.003

Nagy, I. V., Asante-Duah, K., & Zsuffa, I. (2002). Planning for dams and reservoirs: Hydrologic design elements and operational characteristics of storage reservoirs. In *Hydrological dimensioning and operation of reservoirs* (pp. 29–60). Water Science and Technology Library. https://doi.org/10.1007/978-94-015-9894-1_3.

NASA JPL, & NASA/METI. (2012). *ASTER global DEM data (GDEM V2), 49 nasa jpl §*. California: NASA Jet Propulsion Laboratory. https://doi.org/10.5067/ASTER/ASTGTM.002

Noori, A. M., Pradhan, B., & Ajaj, Q. M. (2019). Dam site suitability assessment at the Greater Zab River in northern Iraq using remote sensing data and GIS. *Journal of*

Hydrology, 574, 964–979. https://doi.org/10.1016/j.jhydrol.2019.05.001
Oswald Beiler, M. R., & Treat, C. (2015). Integrating GIS and AHP to prioritize transportation infrastructure using sustainability metrics. *Journal of Infrastructure Systems, 21*(3), Article 04014053. https://doi.org/10.1061/(ASCE)IS.1943-555X.0000245
Othman, A. A., Al-Maamar, A. F., Al-Manmi, D. A. M. A., Liesenberg, V., Hasan, S. E., Obaid, A. K., et al. (2020). GIS-based modeling for selection of dam sites in the kurdistan region, Iraq. *ISPRS International Journal of Geo-Information, 9*(4), 244. https://doi.org/10.3390/ijgi9040244
PCI. (2018). PCI Geomatica training guide. Canada: Geomatica. Retrieved from https://www.pcigeomatics.com/.
Peterson, D. L., Silsbee, D. G., & Schmoldt, D. L. (1994). A case study of resources management planning with multiple objectives and projects. *Environmental Management, 18*(5), 729–742. https://doi.org/10.1007/BF02394636
Prinz, D., & Singh, A. (2000). *Technological potential for improvements of water harvesting. Gutachten für die World Commission on Dams*. Cape Town, South Africa.
Raza, S. H., Shafique, M., Sikandar, A., Ahmad, N., & Shah, K. (2018). Site selection of water storage based on multi-criteria decision analysis. *Int. J. Hum. Capital Urban Manage, 3*(4), 265–278. https://doi.org/10.22034/IJHCUM.2018.04.01
Rezaei, P., Rezaie, K., Nazari-Shirkouhi, S., Reza, M., & Tajabadi, J. (2013). Application of fuzzy multi-criteria decision making analysis for evaluating and selecting the best location for construction of underground dam. *Acta Polytechnica Hungarica, 10*(7).
Roozbahani, R., Abbasi, B., Schreider, S., & Hosseinifard, Z. (2020). A basin-wide approach for water allocation and dams location-allocation. *Annals of Operations Research, 287*(1), 323–349. https://doi.org/10.1007/s10479-019-03345-5
Saaty, T. L. (1986). Axiomatic foundation of the analytic hierarchy process. *Management Science, 32*(7). https://doi.org/10.1287/mnsc.32.7.841
Saaty, R. W. (1987). The analytic hierarchy process—what it is and how it is used. *Mathematical Modelling, 9*(3–5), 161–176. https://doi.org/10.1016/0270-0255(87)90473-8
Saaty, T. L. (2008). Decision making with the analytic hierarchy process. *International Journal of Services Sciences, 1*(1), 83. https://doi.org/10.1504/IJSSCI.2008.017590
Safavian, A., & Amani, M. (2015). Analysis of land suitability for small earth dams using multi criteria evaluation (MCE) in the geographic information system (GIS). *International Letters of Natural Sciences, 42*, 38–46. www.scipress.com/ilns.42.38.
Sayl, K. N., Muhammad, N. S., Yaseen, Z. M., & El-shafie, A. (2016). Estimation the physical variables of rainwater harvesting system using integrated GIS-based remote sensing approach. *Water Resources Management, 30*(9), 3299–3313. https://doi.org/10.1007/s11269-016-1350-6
Senzanje, A., Boelee, E., & Rusere, S. (2008). Multiple use of water and water productivity of communal small dams in the Limpopo Basin, Zimbabwe. *Irrigation and Drainage Systems, 22*(3–4), 225–237. https://doi.org/10.1007/s10795-008-9053-7
UNICEF-WHO. (2019). 1 in 3 people globally do not have access to safe drinking water. Retrieved, from https://www.who.int/news-room/detail/18-06-2019-1-in-3-people-globally-do-not-have-access-to-safe-drinking-water-unicef-who. (Accessed 11 January 2019).
United States Geological Survey. EarthExplorer (n.d.), Retrieved November 15, 2018, from https://earthexplorer.usgs.gov/.
USGS. (2016). US geological survey earth resources observation and science center. Retrieved May 11, 2019, from http://earthexplorer.usgs.gov/.
Vörösmarty, C. J., Pahl-Wostl, C., Bunn, S. E., & Lawford, R. (2013). Global water, the anthropocene and the transformation of a science. *Current Opinion in Environmental Sustainability, 5*(6), 539–550. https://doi.org/10.1016/j.cosust.2013.10.005
World Bank. (2007). *Mozambique country water resources assistance strategy: Making water work for sustainable growth and poverty reduction*. Washington, DC.
Yasser, M., Jahangir, K., & Mohmmad, A. (2013). Earth dam site selection using the analytic hierarchy process (AHP): A case study in the west of Iran. *Arabian Journal of Geosciences, 6*(9), 3417–3426. https://doi.org/10.1007/s12517-012-0602-x

International Soil and Water Conservation Research 9 (2021) 394–404

Contents lists available at ScienceDirect

International Soil and Water Conservation Research

journal homepage: www.elsevier.com/locate/iswcr

Original Research Article

Seasonal changes of soil erosion and its spatial distribution on a long gentle hillslope in the Chinese Mollisol region

Lei Wang [a, f], Fenli Zheng [a, b, *], Gang Liu [a, b], Xunchang J. Zhang [c], Glenn V. Wilson [d], Hongqiang Shi [a], Xujun Liu [e]

[a] State Key Laboratory of Soil Erosion and Dryland Farming on the Loess Plateau, Institute of Soil and Water Conservation, Northwest A&F University, Yangling, 712100, Shaanxi, PR China
[b] Institute of Soil and Water Conservation, CAS & MWR, Yangling, 712100, Shaanxi, PR China
[c] USDA-ARS Grazinglands Research Laboratory, El Reno, 73036, OK, USA
[d] USDA-ARS National Sedimentation Laboratory, Oxford, 38655, MS, USA
[e] Heilongjiang Province Hydraulic Research Institute, Harbin, 150080, Heilongjiang, PR China
[f] Sichuan Provincial Engineering Laboratory for Monitoring and Control of Soil Erosion on Dry Valleys, China West Normal University, Nanchong, 637000, Sichuan, PR China

ARTICLE INFO

Article history:
Received 26 September 2020
Received in revised form
23 January 2021
Accepted 5 February 2021
Available online 10 February 2021

Keywords:
Deposition
Erosive force
Soil detachment
Sediment transport
Rare earth elements

ABSTRACT

Understanding seasonal soil erosion and deposition rates and their spatial distribution along sloping farmlands are necessary for erosion prediction technology and implementing effective soil conservation practices. To date seasonal change of soil erosion and soil redistribution on long gentle hillslopes are not fully quantified due to the variable erosive forces in different seasons. A multi-tracer method using rare earth elements (REE) was employed to discriminate seasonal changes of soil erosion and its spatial distribution on a sloping farmland driven by snowmelt runoff, wind force and rainfall-runoff. A long-slope runoff plot with 5 m wide and 320 m long located in the typical Mollisol region of China was divided into eight segments, each of which was 40 m long and tagged with one of eight REE oxides. The spot method of a partial-area tagging scheme was employed and a grid-based layout was used for REE application. Results showed that annual soil erosion rate was 3251.0 t km^{-2} for the whole runoff plot, in which snowmelt runoff erosion contributed 537.3 t km^{-2}, wind erosion 363.1 t km^{-2} and rainfall-runoff erosion 2350.6 t km^{-2}. Surface runoff is the main external erosive force of hillslope soil erosion, accounting for 88.8% of the total annual soil loss. Furthermore, for the eight slope segments of the 320-m long hillslope, the sediment transport ratios of each slope segment caused by snowmelt runoff and rainfall-runoff erosion were more than 23.5% and 34.7%, respectively. The results will enrich the understanding of seasonal soil erosion on long hillslopes.

1. Introduction

Soil erosion on agricultural lands is a worldwide environmental problem, which causes serious land degradation and results in crop yield reduction. In natural conditions of middle and high latitude regions, croplands suffer from multiple erosive forces, such as freeze-thaw action, snowmelt, wind, and rainfall (Rodzik et al., 2009; Jia et al., 2015; Liu et al., 2017). These multiple erosive forces occur with seasonally variations within a year and, superposed in space, and their interaction poses a serious threat to land productivity. It is important to quantify how the multiple erosive forces interact across time and space to affect soil erosion. Current studies on soil erosion mainly focused on event, annual and longer time scales (Polyakov & Nearing, 2004; Kimoto et al., 2006; Polyakov et al., 2009), but there are few literatures on the seasonal variation of soil erosion within a year. Seasonal change of soil erosion is controlled by different erosive forces, which includes the erosion patterns of a single dominant erosive force (water, wind, freeze-thaw effect, etc.) and the interaction of multiple forces. Different seasons usually have one dominant erosion force, such as

* Corresponding author. 26, Xi'nong Road, Institute of Soil and Water Conservation, Yangling, 712100, Shaanxi, PR China.
E-mail address: flzh@ms.iswc.ac.cn (F. Zheng).

https://doi.org/10.1016/j.iswcr.2021.02.001

snowmelt runoff erosion and wind erosion in spring, rainfall and inflow water erosion in summer, and freeze-thaw action in winter and spring. To date, studies on seasonal change of soil erosion mainly focused on snowmelt runoff erosion in spring and rainfall erosion in summer (Kirby & Mehuys, 1987; Lundekvam & Skoien, 1998), but the seasonal erosion change in different erosive forces within a year are rarely reported. Detachment and deposition distribution along a hillslope exposed to seasonal changes of erosive forces is a serious knowledge gap that has great impact on the effective implementation of conservation measures. Therefore, research of these spatial and temporal patterns is worthy of attention (Feng et al., 2018; Wall et al., 1988).

Erosive forces in different seasons may cause various spatial patterns of sediment distribution. Spatial distribution of soil erosion-deposition provides a better understanding for erosion process and quantitative description of the source-sink pathways of soil on hillslope, which is important for soil erosion control measures on hillslope and physically based erosion prediction models (Polyakov & Nearing, 2004; Yang et al., 2006; Zhang, 2017a). Previous studies on spatial distribution of soil erosion have been conducted by field survey (Verachtert et al., 2010), by applying Universal Soil Loss Equation (USLE) or Revised Universal Soil Loss Equation (RUSLE) model integrated with geographical information system (GIS) (Irvem et al., 2007; Chen et al., 2011), by Water Erosion Prediction Project (WEPP) Model (Zhang, 2017a), and by using tracer methods including fallout radionuclides, rare earth elements (REE), magnetism, dye and other tracers (Guzmán et al., 2013; Yang et al., 2006; Yue et al., 2019).

Rare earth element (REE) tracers provide an alternative to the approaches described above for soil redistribution. It is an ideal tracer that has been successfully used in many studies (Deasy & Quinton, 2010; Liu et al., 2004; Polyakov et al., 2009; Zhang et al., 2001, 2016) because it satisfies a set of properties such as strong binding ability with soil particles, sensitivity to analysis, low background in soils and multiple elements available for selection. Zhang et al. (2001) proved the feasibility of direct mixing rare earth elements oxides with soil materials to trace soil erosion at a plot scale, which provided the possibility for tracing soil erosion on larger field runoff plots. Liu et al. (2004) used the band application method of REE technique to study the soil erosion of a 100 m long hillslope over a four year period. They proved that the soil loss amount based on measurement was similar to the soil loss amount based on REE technique. Kimoto et al. (2006) used six REE elements to represent different morphological elements in a 0.68 ha watershed and found that REE technique is suitable for sediment source tracing.

The utilization of REE technique can provide information for identifying sediment sources and spatial erosion-deposition patterns (Kimoto et al., 2006; Polyakov et al., 2009). However, the spatial redistribution of sediment eroded from different locations on the hillslope is still one of the most difficult problems to be overcome by the tracer technique. Therefore, in this study, multiple REE tracers were employed to identify the source and fate of the sediment, which makes it possible to evaluate the relative source contributions of sediment at different slope locations in each season driven by various erosive forces. The objectives of this study were to 1) identify the seasonal soil losses caused by different erosive forces on long gentle farmland hillslope; 2) quantify the spatial distribution of soil erosion/deposition and contributions of different slope segments to sediment transport under different erosive agents. The results will provide understanding for sediment transportation and redistribution on hillslopes as a reference for the spatially dependent application of soil erosion control measures.

2. Materials and methods

2.1. Study area and field runoff plot

The study area is located in Keshan County, Heilongjiang Province (125°49′56″ E, 48°3′46″ N), which belongs to the typical Mollisol region in Northeast China (MWR, CAS, & CAE, 2010). Gentle and long slope lengths are basic topographical characteristics of the Mollisol region. A 5 m wide, 320 m long runoff plot with an average slope gradient of 2° was established on a national farm in Keshan County. A set of runoff and sediment automatic collection device (XYZ-2 type, Harbin Bailiang Technology Development Co. LTD.) was installed at the outlet of the runoff plot. The surface treatment of the runoff plot was bare fallow and plough depth was 25 cm, which was similar to the surface treatment of local farmland. The spot method of a partial-area tagging scheme with a grid-based layout was used for rare earth element application (Fig. 1). The long-slope runoff plot was divided into eight segments with each segment being 5 m wide by 40 m long. Each tagged soil spot or zone involved a circle with a diameter of 50 cm. The tagged soil depths were 2 cm and 5 cm for the upper three segments (0–120 m) and lower five segments (120–320m), respectively. Each circle was spaced 1 m or 1.25 m in the direction parallel to the contour line, and 5 m in the direction perpendicular to the contour line. There were 28 tagged soil zones in total for each 40 m segment. A total of 224 points were applied on the whole 320 m long slope runoff plot.

2.2. Meteorological characteristics during the observation period

The study began before snowfall in 2017, and the sampling was conducted in different seasons of 2018. An ONSET HOBO U30-NRC professional small automatic weather station (Onset Computer Corporation, Bourne, MA) was installed beside the runoff plot, and the rainfall and wind speed and direction were recorded at 5 min interval. The snowfall amount was 31.8 mm in 2017–2018 and rainfall amount was 485 mm in 2018. The first rainfall event occurred on Jun. 7 and the last one occurred on Sep. 29 (Fig. 2). The prevailing winds were from Northwest and North-northwest, which accounted for 29.8% of all directions. Calms refer to wind speed of 0 m s^{-1}, which accounted for 32.32% (Fig. 3).

2.3. Soil and rare earth oxide characteristics

Eight different rare earth oxides (Eu_2O_3, Gd_2O_3, Tb_4O_7, Sm_2O_3, CeO_2, La_2O_3, Yb_2O_3 and Nd_2O_3) in powder form were employed in this study. Selection was based on cost considerations, amount required and analytical detection methodology (Liu et al., 2004). The detailed characteristics of the application of REE oxides were shown in Table 1. The rare earth oxides must be mixed with the blank soil, i.e. sieved soil that has not been mixed with any REE oxides (Michaelides et al., 2010), prior to application. Topsoil (0–20 cm) was collected from agricultural land beside the plot. The soil is classified as a Mollisol (USDA NRCS, 1999) with approximately 9.3% sand, 61.3% silt and 29.4% clay. The organic matter content was 23.8 g kg^{-1} determined by the potassium dichromate oxidation-external heating method. The pH in water was 6.1, measured with a 1:2.5 solid-to-water ratio on a weight basis. The soil collected was air-dried to a water content of about 11% by weight and screened by a 2 mm sieve.

2.4. REE mixing and tagging

In order to fully and uniformly mix the REE oxides with the blank soil, this study combined the two methods of gradual dilution and sieving. The REE oxides were firstly diluted with the blank soil,

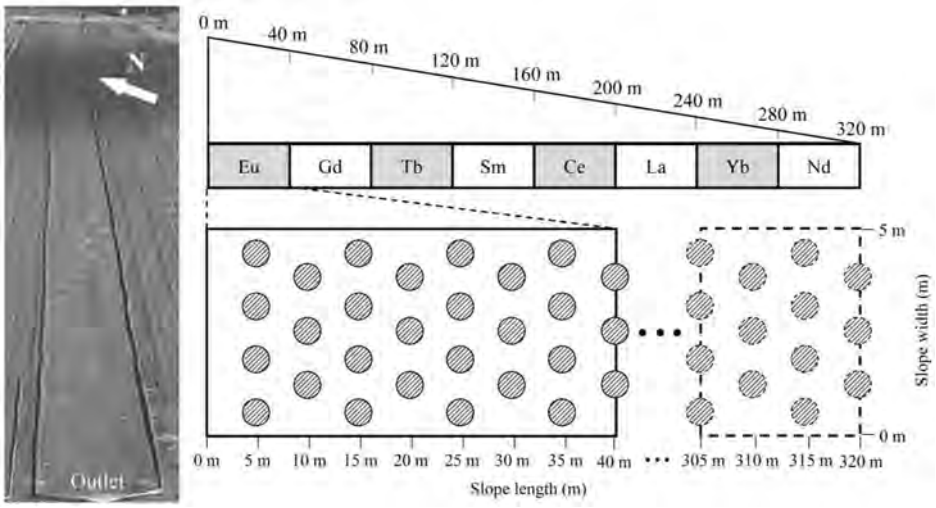

Fig. 1. Photo and schematic diagram of the long slope runoff plot and rare earth element spot application. Each 40 m hillslope segment was applied with a different RRE. Each element was applied in 28 circular areas (dashed circles) aligned in 7 downslope transects.

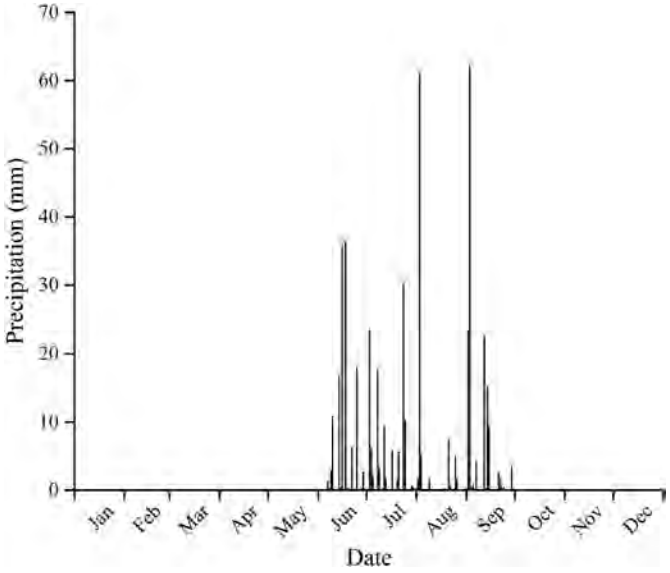

Fig. 2. Individual rainfall events in the study area from Jan. 1 to Dec. 31, 2018.

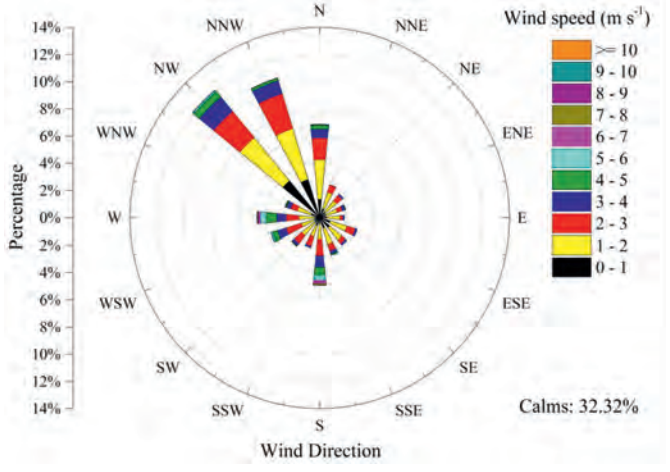

Fig. 3. Wind direction and speed in the study area from Jan. 1 to Jun. 31, 2018.

and then the REE-soil mixtures were mixed with the blank soil through sieving. In the process of mixing, it is necessary to ensure that there is no cross contamination between various rare earth elements. The steps used were as follows: 1) the soil amount of each target location on the plot was calculated by multiplying the volume by the soil bulk density (Liu et al., 2004). 2) The pre-determined quantity of rare earth oxide powder was calculated and weighed by a ten-thousandth scale and mixed thoroughly with 200 g of the prepared blank soil (Michaelides et al., 2010). After that, the REE-soil mixture was screened through a 2 mm sieve. Then 500 g of blank soil was added and mixed thoroughly and sieved again. After that, 1.5 kg of blank soil was added, then the above steps were repeated until a pre-determined quantity of blank soil needed to fill the tagged zones had been added (4.12 kg and 10.30 kg for tagged zones of 2 and 5 cm deep, respectively).

2.5. REE-soil mixture placement

A metal mold (marked on the inner wall) with a height of 10 cm and a diameter of 50 cm was used for the REE-soil mixture placement (Fig. 4). Two tape measures were used to determine the position of the application point of REE-soil mixture. The metal mold was inserted into the soil to the pre-determined depth. The soil in the metal mold was removed with the bottom leveled (Fig. 4a). After that, the prepared REE-soil mixture was placed into the empty metal mold. A hand trowel was used to smooth the surface and pat it gently for compaction to the original surface level (Fig. 4b). A prepared fine steel stick (50 cm in length) marked at 30 cm position from the bottom was inserted in the center of the tagged soil zone to the depth of 30 cm. Then, the tagged soil zones were wetted with a water spray in order to facilitate REE-soil binding and the soil surface outside the circle was restored to the original shape (Fig. 4c).

2.6. Post-placement sampling

In order to prevent disturbing the soil surface during sampling, a metal bridge with 6 m long, 0.2 m wide and 0.3 m high was used (Fig. 5a). REE-soil mixture samples were collected in the tagged soil zones where REE-soil mixture was applied (Michaelides et al., 2010). Five cores were collected in each tagged soil zone, and these five sub-samples were combined into one representative

Table 1
Parameters of the application of rare earth element (REE) oxides and the topographic information of the hillslope.

Hillslope segment (m)	Average slope gradient of each segment (°)	REE oxide	Application depth (cm)	Soil background concentration (mg kg^{-1})	REE application Concentration (mg kg^{-1})
0–40	1.2	Eu_2O_3	2	1.08	43.2
40–80	1.4	Gd_2O_3	2	4.44	177.6
80–120	1.4	Tb_4O_7	2	0.68	33.8
120–160	2.0	Sm_2O_3	5	5.51	165.3
160–200	2.1	CeO_2	5	61.70	1234.0
200–240	2.7	La_2O_3	5	31.30	626.0
240–280	2.8	Yb_2O_3	5	2.33	93.2
280–320	2.2	Nd_2O_3	5	31.10	622.0

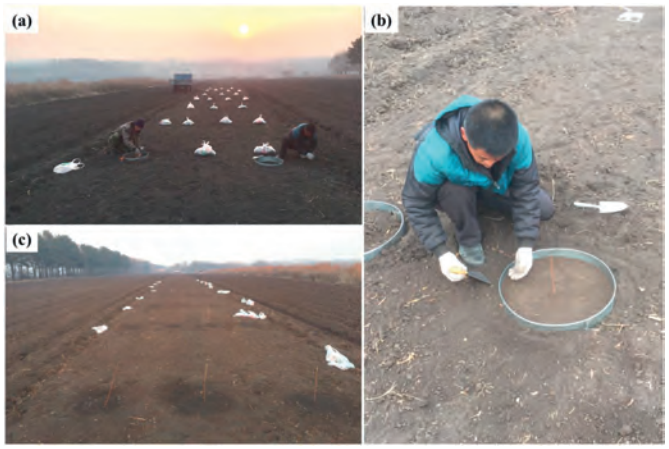

Fig. 4. A metal template was used for the (a, b) placement of REE tagged soil mixture and (c) the tagged zones were wetted afterwards.

sample of the zone (Fig. 5b). Based on the marked point on the fine steel stick, the tagged zone can be identified as a net erosion area or a net deposition area prior to sampling. As shown in Fig. 6, the sampling depth was determined according to the REE application depth and the conditions of soil erosion and deposition in the tagged zone. It was ensured that all the applied REE was sampled. In the erosion zone, the sampling depth is equal to the application depth. In deposition zone, the sampling depth is greater than the application depth. Soil samples were collected following the end of the snow melt period (Mar. 20, 2018), the period of wind season (Jun. 3, 2018) and the period of rainy season (Oct. 14, 2018). In order to make sure that the positions of the five sampling points of different sampling times were not overlapped, a metal circle was used to determine the sampling location, followed by a fine stick inserted into the point where the sample was taken. After that, the sampling holes were back-filled with blank soil and the slope surface was restored to the original shape. The positions of the five sampling points were shifted clockwise to the un-sampled area in the circle at next sampling. Soil samples collected from each tagged soil zone were bagged and labeled.

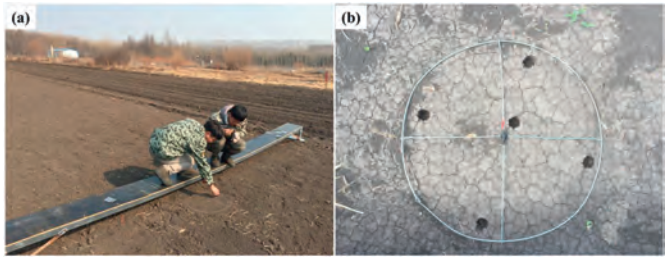

Fig. 5. A metal bridge was used for sampling and five cores were collected in each tagged soil zone for each erosion period.

2.7. Laboratory analysis and data processing

The REE extraction and Inductively Coupled Plasma Mass Spectrometry (ICP-MS) analysis were carried out according to Xiao et al. (2017). The calculations of soil erosion and deposition were based on the methods conducted by previous studies (Michaelides et al., 2010; Zhang et al., 2003), which are expressed as follows for the applied REE at each application spot:

$$M_c \cdot C_i = M_i \cdot O_i + M_b \cdot C_b \quad (1)$$

$$M_i = M_c - M_b \quad (2)$$

where M_c is the total mass of the core, g; C_i is the final concentration of the *in situ* REE in the core, mg g^{-1}; M_i is the mass of remaining tagged soil, g; O_i is the initial spiked-REE concentration, mg g^{-1}; M_b is the mass of the soil not tagged with the *in situ* REE, g; C_b is the background concentration of the *in situ* REE in the soil, mg g^{-1}. Equations (1) and (2) are applied sequentially to all other REEs present in the core-sample that were not tagged *in situ* to calculate the mass of soil deposited at the zone from other locations on the hillslope (Michaelides et al., 2010).

Soil erosion and deposition in three seasons were calculated by taking the end value of the previous sampling as the starting value of the current sampling. That is, the calculated concentration of the first sampling (after snowmelt runoff erosion period) is based on the application concentration, the calculated concentration of the second sampling (after wind erosion period) is based on the result of the first sampling, and the calculated concentration of the third sampling (after rainfall-runoff erosion period) is based on the result of the second sampling. Spatial distribution maps of soil erosion and deposition were drawn using a Kriging method in this study.

3. Results

3.1. Spatial distribution of seasonal soil detachment-deposition under different erosive forces

From snowfall to snow melt in the spring of the following year (November to March), soil erosion mainly occurred within a few days since snowmelt runoff generation. Snowmelt runoff erosion/deposition rates on the long gentle hillslope ranged between −4.4 (negative refers to erosion) and 3.4 (positive refers to deposition) kg m^{-2} (Fig. 7). The annual snowmelt runoff erosion rate was −537.3 t km^{-2}. As shown in Fig. 7, the snowmelt runoff erosion presents strong and weak alternations from the top to the foot of the slope. The severe erosion mainly occurs in the 120–280 m segments, among which the most severe soil erosion occurred in

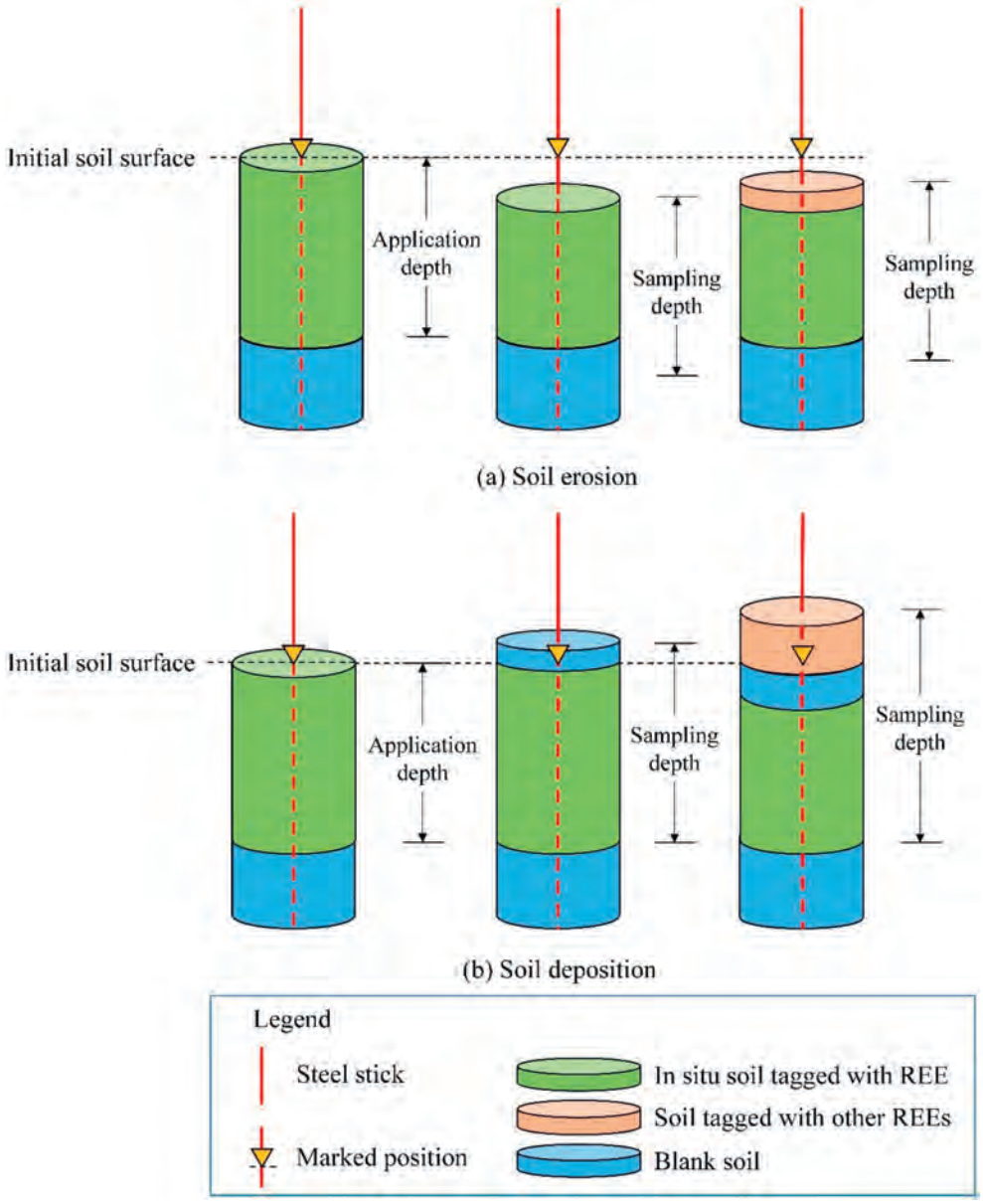

Fig. 6. Sketches of the sampling depth under conditions of (a) soil erosion: if erosion occurred in the tagged zone, the sampling depth is equal to the application depth; (b) soil deposition: if deposition occurred in the tagged zone, the sampling depth is greater than the application depth.

the slope segments of 120–160 m. Soil deposition mainly occurred in the 30 m at the foot of the slope.

After snow melt period, the agricultural lands in the study area were mainly affected by wind erosion until the rainy season (March to June) due to bare and fallow surface condition, which continues until after plant emergence following the seeding period in mid-to-late April. The wind erosion/deposition rate on the hillslope ranged between −3.6 and 3.0 kg m^{-2} (Fig. 8). The wind erosion rate was −363.1 t km^{-2}. Due to the influence of surface roughness and micro-topographic fluctuation of the runoff plot on near-surface wind field, soil erosion and deposition distribution along the hillslope had no obvious spatial pattern, while soil erosion and deposition from the slope top to foot had an alternating patchy distribution. Some deposition was observed at the top of the plot, which might have been related to the prevailing wind directions.

The runoff plot was mainly affected by rainfall-runoff erosion (June to October) after the wind erosion period and before freezing and snowfall periods. As shown in Fig. 9, soil erosion rate of the hillslope caused by rainfall-runoff was between −0.4 and −9.3 kg m^{-2}, and the deposition rate was between 0.5 and 5.1 kg m^{-2}. The annual rainfall-runoff erosion rate was −2350.6 t km^{-2}. Soil erosion gradually increased along the slope length and reached its maximum in the 120–240 m slope segments, with an average erosion rate of −4.4 kg m^{-2}. Soil deposition mainly occurred in the 290–320 m segment of the hillslope, i.e. slope toe, with an average deposition rate of 2.7 kg m^{-2}.

The meteorological observation results near the long-slope runoff indicate that the annual rainfall of the runoff plot site is 485.0 mm. A total of 13 erosive rainfall events were observed to generate runoff during 2018, and the erosive rainfall was 374.8 mm, resulting in soil loss of 2776.8 t km^{-2} (Fig. 10), which was basically consistent with the REE tracer observation results. Soil erosion caused by rainfall and upslope inflow in the rainy season was the

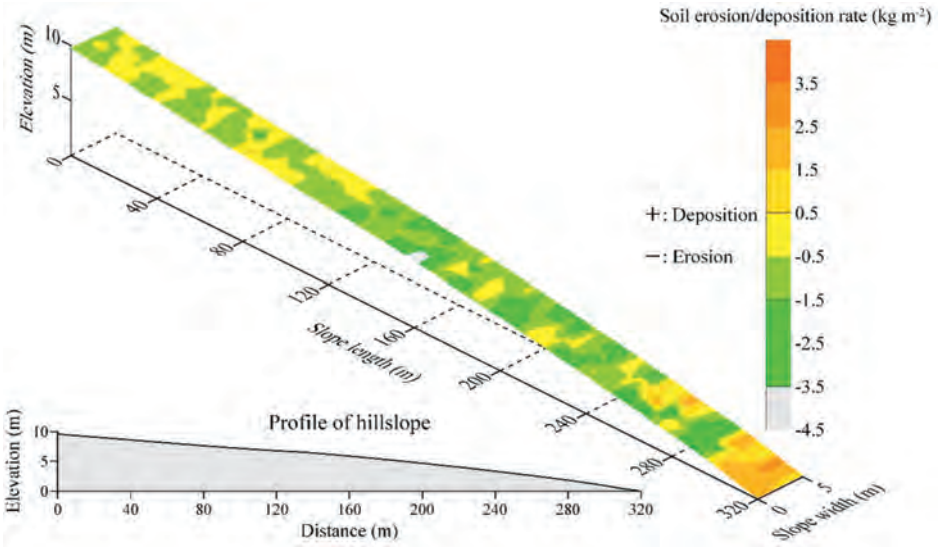

Fig. 7. Soil erosion-deposition distribution along slope length of the runoff plot after snowmelt period (Mar. 20, 2018).

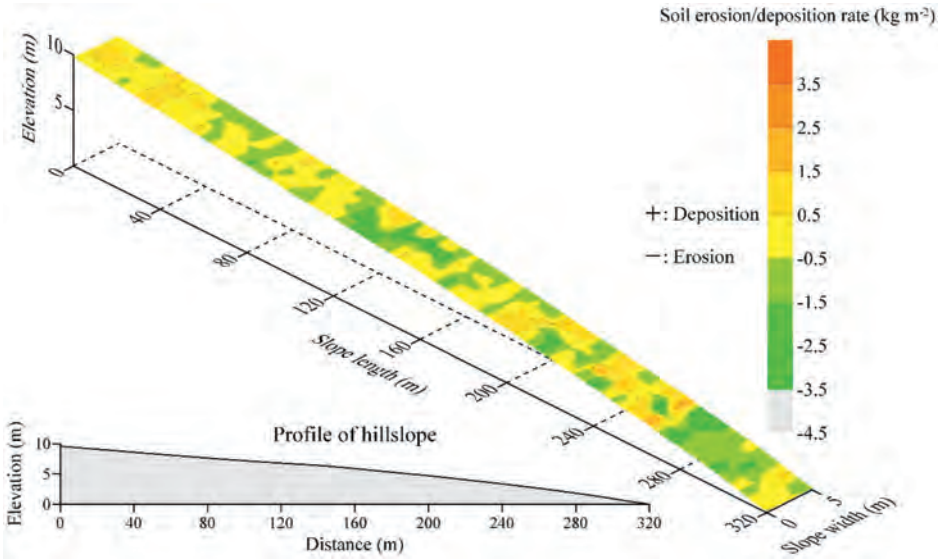

Fig. 8. Soil erosion-deposition distribution along slope length of the runoff plot after the wind erosion season (Jun. 3, 2018).

most severe in the whole year. As shown in Fig. 12, soil erosion caused by two rainstorms on August 3 (61.0 mm) and September 3 (62.2 mm) was the most serious, which were 887.4 t km^{-2} and 975.6 t km^{-2}, respectively, the sum of them accounted for 67.1% of the total annual soil loss on the hillslope.

3.2. Spatial patterns of sediment transport under snowmelt runoff and rainfall-runoff erosion

The water erosion by snowmelt runoff and rainfall-runoff were analyzed for their sediment transport characteristics by tagging different rare earth elements in different slope segments. As shown in Fig. 11, snowmelt runoff caused relatively weak sediment transport on the hillslope. The percent sediment eroded from the Eu, Gd, Tb, Sm, Ce, La, Yb and Nd slope segments (40, 80, 120, 160 200, 240, 280, 320 m of slope length) that deposited downslope from these eight segments were 76.5%, 52.8%, 44.4%, 24.5%, 13.2%, 13.9%, 4.5% and 0, respectively. These sediment delivery percentages were calculated by dividing the total percentage deposited downslope by eroded percentage of the original application. Sediments eroded from the three upslope segments (40, 80, 120 m of slope length) were mainly deposited on the downslope, while the sediment eroded in the last five slope segments (160 200, 240, 280, 320 m of slope length) were mostly transported out of the runoff plot.

After the rainy season, sediment transport was much greater. REE-tagged soil was detached from each segment and deposited in the lower parts of the hillslope. Due to the effects of rainfall and upslope inflow, the sediment detached from the REE-tagged segment was almost all distributed over the hillslope segment downstream from that tagged segment (Fig. 12). The proportion of sediment eroded from the Eu, Gd, Tb, Sm, Ce, La, Yb and Nd slope segments deposited downslope from these segments were 61.6%, 65.3%, 58.9%, 22.4%, 23.5%, 30.1%, 10.0% and 0, respectively. Sediments eroded from the three upslope segments (40, 80, and 120 m of slope length) that deposited on the downslope were relatively

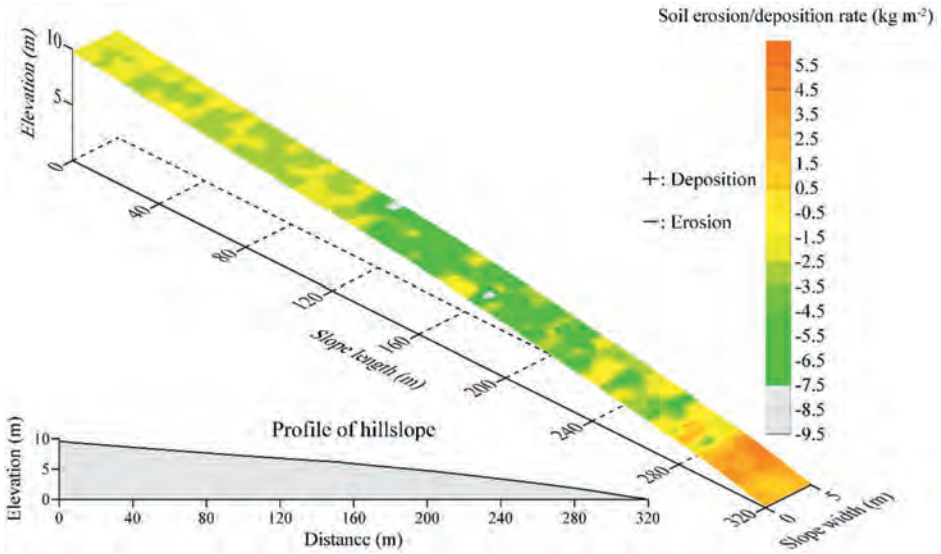

Fig. 9. Soil erosion-deposition distribution along slope length of the runoff plot after the rainy season (Oct. 14, 2018).

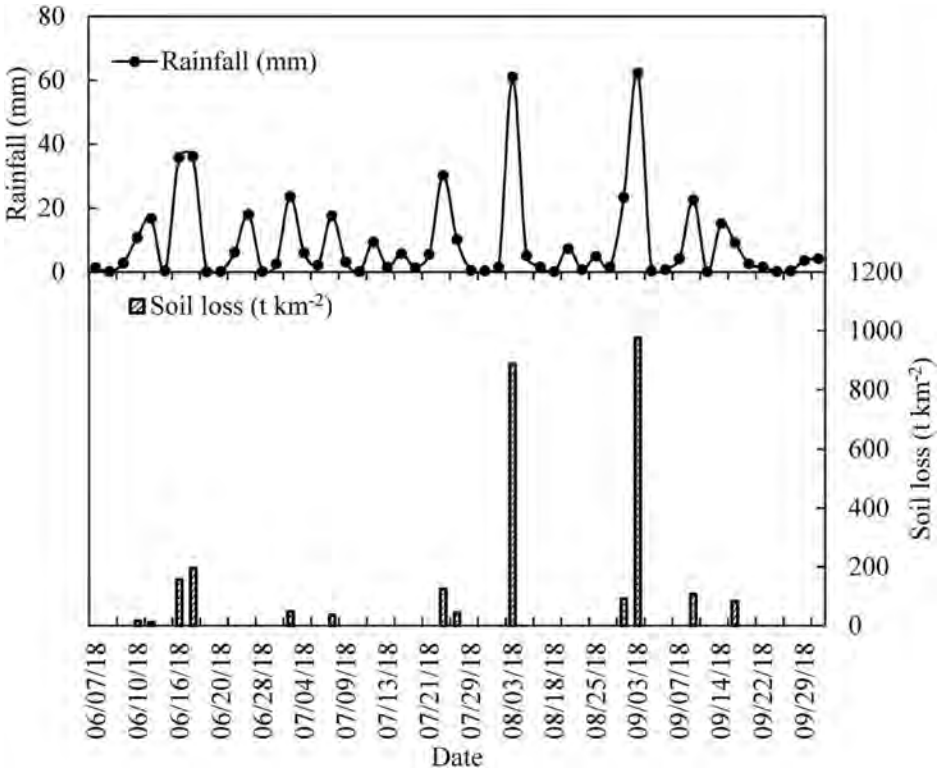

Fig. 10. Characteristics of individual rainfall events and soil losses on the runoff plot.

high, while the depositions on the following segments were low.

4. Discussion

4.1. Impacts of different erosive forces on seasonal soil erosion

Seasonal soil erosion is affected by changes in the erosive forces as the processes involved change from freeze-thaw action, to wind, rainfall and/or upslope inflow, etc. Soil erosion in each season is often dominated by one of these forces or the integration of several erosive forces. As calculated by REE tracing, the contributions of soil erosion amounts caused by three such erosive forces (snowmelt runoff, wind and rainfall) in different seasons to annual soil loss were 16.5%, 11.2% and 72.3%, respectively. At the beginning of the year in the study area, almost no wind erosion occurred because the soil surface was covered with snow although wind was intensive and frequent. Moreover, exposed soil surfaces were frozen and particles were tightly cemented together. Thus, wind had no or only minor effects on surface soil detachment during this period.

In spring, snow begins to melt as temperatures rise. The

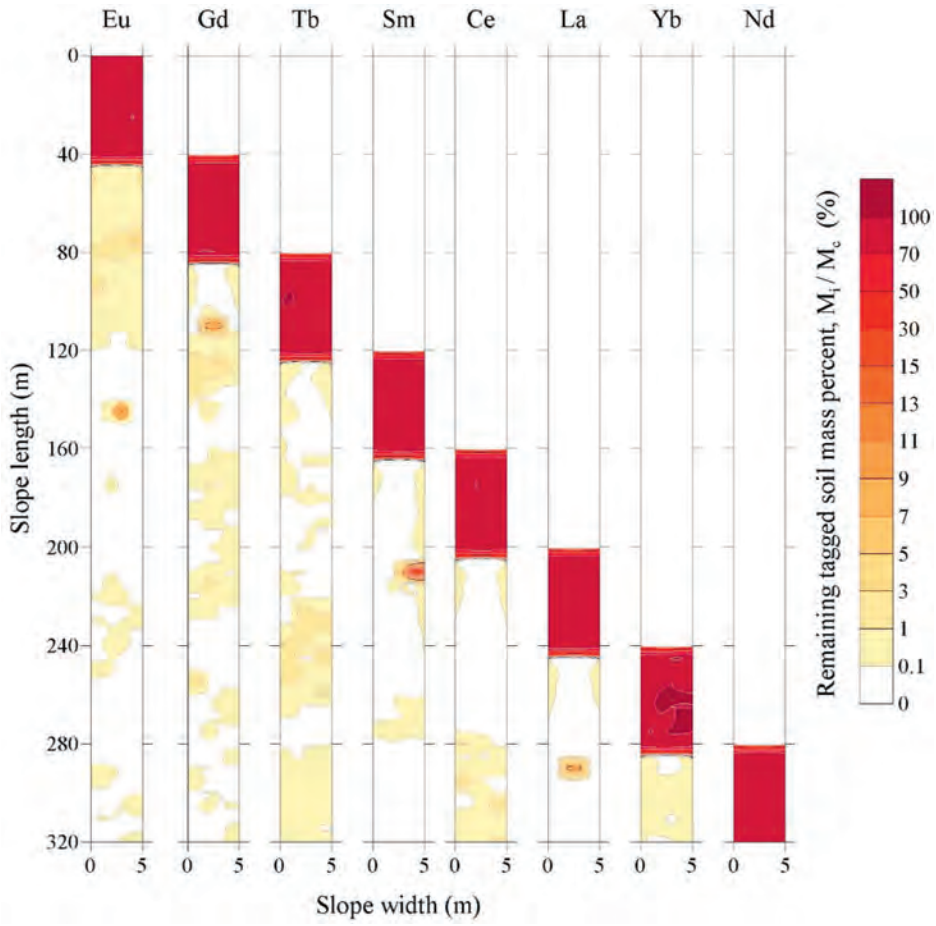

Fig. 11. Spatial patterns of sediment transport in different REE-tagged segments after snow melting. Remaining tagged soil mass percent refers to the percent of the initial tagged soil mass either remained in the original application zone or deposited downslope.

snowmelt runoff formed as concentrated flow, which caused rill and ephemeral gully erosion on the gentle slope farmland with longitudinal ridge-tillage (Fig. 13). Although snow melting finished within about one week, due to the long slope length and large upslope drainage area, it could produce a great inflow from upslope areas. Consequently, snowmelt runoff erosion was obvious and significant, especially at the lower parts of the hillslope. Snowmelt runoff erosion was mainly affected by two of the factors, i.e., the thawed surface soil and the frozen subsoil (Zuzel et al., 1982), which showed a two-way melting from top (soil surface) to bottom (underground) and from bottom to top. A study by Ollesch et al. (2005) in a catchment in the Harz Mountains of Germany showed that soil erosion in winter caused by snowmelt runoff in combination with soil frost was higher than summer rainfall events. These were different from our results where rainfall was the dominant contributor to soil loss and snowmelt runoff erosion caused only 16.5% of total annual soil loss. This is largely a result of the short time period in which snowmelt runoff contributed.

After the snow melt period, thawed soil surfaces tend to be loose and generally weak (Formanek et al., 1984). Wang et al. (2019) reported that the number of freeze-thaw cycles of the surface soil in the study area in spring was less than 12, while after 6 freeze-thaw cycles, soil aggregate stability decreased by about 20% (Oztas & Fayetorbay, 2003). This may be due to the high soil moisture content caused by snowmelt and the gradual fragmentation of soil aggregates under successive freeze-thaw cycles (Oztas & Fayetorbay, 2003). There was seldom precipitation from the snow melt period to the rainy season. This period usually lasts about 2–3 months. Loose topsoil provides a rich source of material for wind erosion following the snow melt period. Zhang et al. (2018) reported that wind erosion was linearly or exponentially related to the slope gradient, and convex reliefs generated high erosion patches. This was consistent with our results, which showed higher wind erosion rates at the convex terrain locations of about 120 m and 280 m.

During the rainy season, hillslope soil erosion was dominated by water erosion (Fig. 14). Erosion included both processes of raindrop caused particle detachment and runoff caused detachment and sediment transport. For the long gentle slope of farmland in this study, transport of soil particles directly by raindrop splash is very limited due to the gentle slope gradient. However, raindrops provide a large source of detached soil particles for runoff transport in shallow flows (Lu et al., 2016). The major erosive force is overland flow generated by the large upslope drainage area (Xu et al., 2017; Wang et al., 2020). This was proved in spatial patterns of sediment transport in Fig. 12, as sediment transport ratios of each segment tended to increase downslope, indicating the flow-driven transport was more efficient than the raindrop-driven transport (Zhang et al., 2017b).

4.2. Soil redistribution on long gentle slope in different seasons

Deposition rates were obtained by calculating the concentration of REE deposited downslope of each tagged segment and the spatial

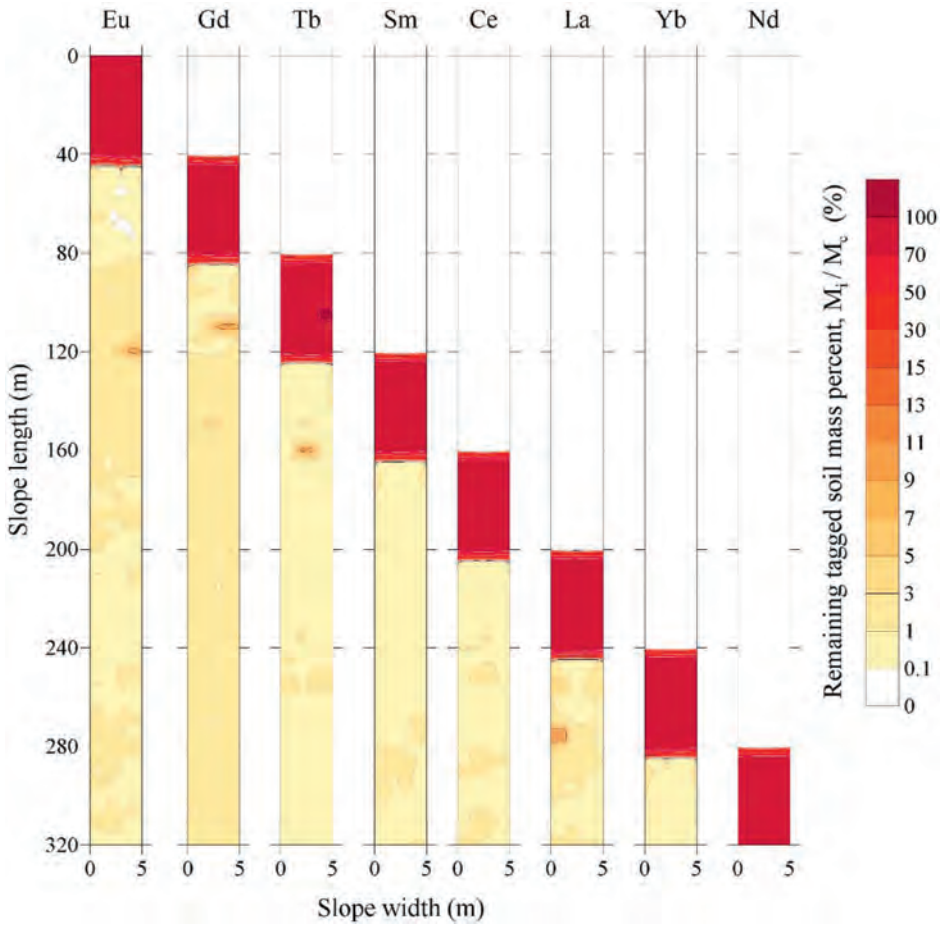

Fig. 12. Spatial patterns of sediment transport in different REE-tagged segment after the rainy season. Remaining tagged soil mass percent refers to the percent of the initial tagged soil mass either remained in the original application zone or deposited downslope.

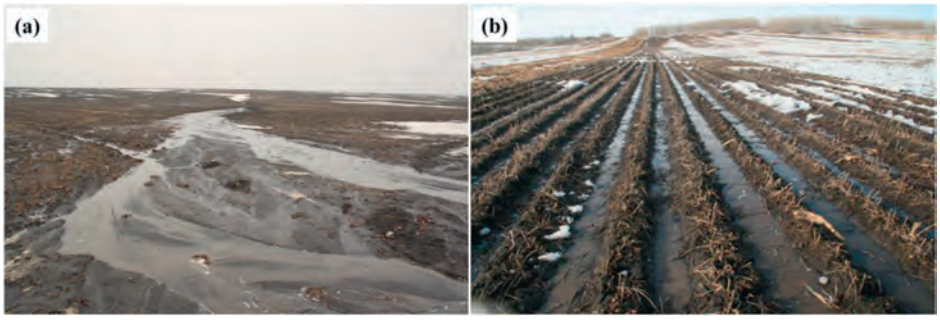

Fig. 13. Snowmelt erosion in spring in the study area.

patterns of sediment deposit in each segment. It appeared from Figs. 11 and 12 that a large proportion of sediment detached from Eu (0–40 m) and Gd (40–80 m) segments was deposited in the following 80 m segments. Sediment detached from the Tb (80–120 m) segment showed negligible deposition in the following 80 m segments, which coincided with the severe soil erosion in the 120–240 m segments according to Figs. 7 and 9. Another reason for severe soil erosion in the 120–240 m segments is that the slope gradient had changed in this position. The hillslope shows a slight convex profile. Dividing the hillslope by 40 m segments, the upstream slope gradient was about 1 degree, and the downstream slope gradient was about 2–3 degrees. The steeper the slope gradient, the greater the runoff sediment carrying capacity (Fox & Bryan, 2000; Zhang et al., 2009). Since slope gradient increases from 1.2-1.4 degree at 0–120 m slope length to 2.0–2.8 degree at 120–240 m slope length, the runoff detachment and transport capacity of the upper slope (0–120 m segments) was weak and the sediment moving distance was relatively short. For the following 120 m segment (120–240 slope length), the increase of slope gradient increased the runoff detachment and transport capacity, which resulted in a decrease in sediment deposition in these segments. The slope gradient near the outlet decreased again, which caused great deposition in this area, but a large amount of sediment was still transported out of the plot by runoff.

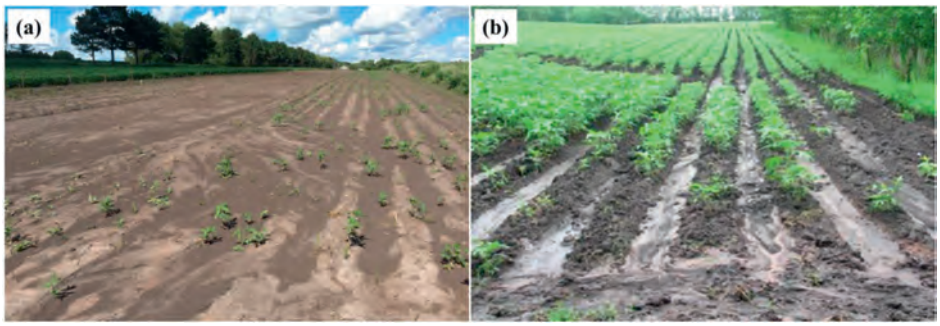

Fig. 14. Soil erosion after rainy season in the study area.

For the long gentle hillslope studied here, sediment transport visibly represented a sheet erosion pattern. This may be due to the gentle slope gradient of the runoff plot. As for wind erosion, soil erosion-deposition presented an alternating distribution pattern with a large depositional area observed on the upper slope that which might be attributed to the prevailing wind direction (Fig. 8). However, we need to collect further data to explain its complexity and haphazard or random distribution. In the snow melt and rainfall periods, the soil erosion-deposition patterns that caused mainly by water erosion showed similar patterns with no obvious changes on upper slope, strong erosion in the middle and lower parts of the hillslope, and deposition at the toe slope. Sediment delivery on the slope after snowmelt runoff and rainfall-runoff was dominated by the runoff transport process without transport capacity being exceeded except at the lower slope position (Zhang et al., 2017b). Surface runoff discharge would increase as slope length increased and result in higher erosion rates in the lower parts of the hillslope. As shown in Figs. 7 and 9, soil erosion rate was relatively weak in the upper slopes of 0–120 m segments and severe soil loss in the 120–280 m segments, which may attribute to the gradual flow accumulation (Polyakov & Nearing, 2004). Moreover, the slight variation in slope gradient also cannot be ignored. Compared with 0–120 m slope segments, the slope gradient at 120–240 m slope length increased from 1.2 to 2.8 degree. The increase in slope gradient accelerated the overland flow velocity and increased the transport capacity of runoff in these segments (Fox & Bryan, 2000). Relevant studies in the Mollisol region of China showed that soil loss increased by more than 17% as slope gradient increased from 5° to 10° (Lu et al., 2016; Shen et al., 2018).

4.3. The advantages and limitations of this study

The tracer technique has already been proven to have high accuracy and it has been applied in both laboratory and field conditions (Lei et al., 2006; Stevens & Quinton, 2008). Moreover, this method provides an approach to quantify the spatial patterns of soil redistribution. However, the soil disturbance caused by REE-soil mixture tagging may lead to uncertainty in soil loss calculation. The original structure of soil aggregates was changed by soil sieving, which caused soil erosion of the remodeled soil may be different from that of the undisturbed (original) soil. Moreover, a metal mold was used for the REE-soil mixture placement, which may cause unconformity between the remolded soil inside the mold and undisturbed soil outside. Thus, in order to fully and uniformly mix the rare earth elements (REE) oxides with the soil, before mixing the REE oxides with soil, the soil was screened through a 2 mm sieve to ensure that both of REE oxides and soil particles are fully mixed.

This is the first time that the spot method of a partial-area tagging scheme using rare earth elements has been applied to the study of soil erosion in a long-slope runoff plot in the field. On the one hand, the spot method used in this study was labor intensive and relatively expensive; on the other hand, this method provided high spatial resolution for the identification of sediment sources. Compared with previous studies, the method such as spreading the mixture of rare earth elements on the soil surface can obtain more comprehensive slope erosion information (Polyakov & Nearing, 2004; Kimoto et al., 2006; Polyakov et al., 2009), but it could only reflect the characteristics of the thin surface layer of soil. The *in situ* tagging approaches such as band method and spot method are relatively more accurate in determining the soil erosion depth at certain locations (Michaelides et al., 2010). The spot method used in this study was a grid-based method between band application and whole slope application, which has the advantage of using a statistical basis to provide greater spatial resolution of the sediment sources (Haddadchi et al., 2019). Nevertheless, both the band method and the spot method are approaches that use parts to represent the whole, which may ignore the effect of partial changes in untagged areas on the overall change of the whole hillslope to some extent.

5. Conclusion

The spot method of a partial-area tagging scheme using rare earth elements was employed to quantitatively investigate seasonal changes in soil erosion and its spatial distribution driven by different erosive forces in the Mollisol region of China. Based on distinguishing eight slope segments and sampling across different erosion periods, the study provides valuable information on seasonal changes in soil erosion and deposition rates driven by snowmelt runoff, wind and rainfall-runoff erosive forces. Results showed that soil erosion rates and their spatial distribution varied with season and hillslope position due to different erosive forces. (1) The spatial distribution of soil erosion caused by water erosion was characterized as slight erosion in the upper parts of the hillslope and severe erosion in middle and lower parts of hillslope. (2) The spatial distribution of soil erosion caused by wind force was not obvious with random distribution characteristics across the hillslope. (3) Water erosion caused by snowmelt runoff and rainfall-runoff was the dominant erosive force and both erosion amounts occupied 88.8% of the total annual soil loss. (4) The flow-driven sediment transport was more efficient than the raindrop-driven transport due to the large upslope drainage area and gentle slope gradient. (5) Hillslope soil erosion is affected by local topographic changes, where convex locations are more susceptible to water and wind erosion. Results of this study are helpful to enhance the understanding of seasonal soil erosion, and provide a reference for the spatially dependent application of soil and water conservation

measures on long gentle farmland hillslopes.

Declaration of competing interest

The authors declare that they have no known competing financial interests or personal relationships that could have appeared to influence the work reported in this paper.

Acknowledgements

This study was financially supported by the National Key R&D Program of China (No. 2016YFE0202900), Strategic Priority Research Program of the Chinese Academy of Sciences (No. XDA23060502) and the National Natural Science Foundation of China (No. 41571263).

References

Chen, T., Niu, R. Q., Wang, Y., Li, P. X., Zhang, L. P., & Du, B. (2011). Assessment of spatial distribution of soil loss over the upper basin of Miyun reservoir in China based on RS and GIS techniques. *Environmental Monitoring and Assessment, 179*(1–4), 605–617.

Deasy, C., & Quinton, J. (2010). Use of rare earth oxides as tracers to identify sediment source areas for agricultural hillslopes. *Solid Earth, 1*(2), 111–118.

Feng, Q., Xiao, F., Du, Y., & Wang, L. H. (2018). Evaluation of seasonal soil erosion distribution in typical area of Danjiangkou. *Environmental Science and Technology, 41*(6), 168–174 (in Chinese).

Formanek, G. E., McCool, D. K., & Papendick, R. I. (1984). Freeze-thaw and consolidation effects on strength of a wet silt loam. *Transactions of the ASAE, 27*(6), 1749–1752.

Fox, D. M., & Bryan, R. B. (2000). The relationship of soil loss by interrill erosion to slope gradient. *Catena, 38*(3), 211–222.

Guzmán, G., Quinton, J. N., Nearing, M. A., Mabit, L., & Gómez, J. A. (2013). Sediment tracers in water erosion studies: Current approaches and challenges. *Journal of Soils and Sediments, 13*(4), 816–833.

Haddadchi, A., Hicks, M., Olley, J. M., Singh, S., & Srinivasan, M. S. (2019). Grid-based sediment tracing approach to determine sediment sources. *Land Degradation & Development, 30*(17), 2088–2106.

Irvem, A., Topaloğlu, F., & Uygur, V. (2007). Estimating spatial distribution of soil loss over Seyhan River Basin in Turkey. *Journal of Hydrology, 336*(1–2), 30–37.

Jia, H., Wang, G., Guo, L., Zhuang, J., & Tang, L. (2015). Wind erosion control utilizing standing corn residue in Northeast China. *Soil and Tillage Research, 153*, 112–119.

Kimoto, A., Nearing, M. A., Shipitalo, M. J., & Polyakov, V. O. (2006). Multi-year tracking of sediment sources in a small agricultural watershed using rare earth elements. *Earth Surface Processes and Landforms, 31*(14), 1763–1774.

Kirby, P. C., & Mehuys, G. R. (1987). The seasonal variation of soil erosion by water in southwestern Quebec. *Canadian Journal of Soil Science, 67*(1), 55–63.

Lei, T. W., Zhang, Q. W., Zhao, J., & Nearing, M. A. (2006). Tracing sediment dynamics and sources in eroding rills with rare earth elements. *European Journal of Soil Science, 57*(3), 287–294.

Liu, P. L., Tian, J. L., Zhou, P. H., Yang, M. Y., & Shi, H. (2004). Stable rare earth element tracers to evaluate soil erosion. *Soil and Tillage Research, 76*(2), 147–155.

Liu, T., Xu, X., & Yang, J. (2017). Experimental study on the effect of freezing-thawing cycles on wind erosion of black soil in Northeast China. *Cold Regions Science and Technology, 136*, 1–8.

Lundekvam, H., & Skoien, S. (1998). Soil erosion in Norway. An overview of measurements from soil loss plots. *Soil Use and Management, 14*(2), 84–89.

Lu, J., Zheng, F., Li, G., Bian, F., & An, J. (2016). The effects of raindrop impact and runoff detachment on hillslope soil erosion and soil aggregate loss in the Mollisol region of Northeast China. *Soil and Tillage Research, 161*, 79–85.

Michaelides, K., Ibraim, I., Nord, G., & Esteves, M. (2010). Tracing sediment redistribution across a break in slope using rare earth elements. *Earth Surface Processes and Landforms, 35*(5), 575–587.

MWR, CAS, & CAE. (2010). *Soil erosion control and ecological security in China: Mollisol region*. Beijing: Science Press (in Chinese).

Ollesch, G., Sukhanovski, Y., Kistner, I., Rode, M., & Meissner, R. (2005). Characterization and modelling of the spatial heterogeneity of snowmelt erosion. *Earth Surface Processes and Landforms, 30*(2), 197–211.

Oztas, T., & Fayetorbay, F. (2003). Effect of freezing and thawing processes on soil aggregate stability. *Catena, 52*(1), 1–8.

Polyakov, V. O., Kimoto, A., Nearing, M. A., & Nichols, M. H. (2009). Tracing sediment movement on a semiarid watershed using rare earth elements. *Soil Science Society of America Journal, 73*(5), 1559–1565.

Polyakov, V. O., & Nearing, M. A. (2004). Rare earth element oxides for tracing sediment movement. *Catena, 55*(3), 255–276.

Rodzik, J., Furtak, T., & Zglobicki, W. (2009). The impact of snowmelt and heavy rainfall runoff on erosion rates in a gully system, Lublin Upland, Poland. *Earth Surface Processes and Landforms, 34*(14), 1938–1950.

Shen, H. O., Wen, L. L., He, Y. F., Hu, W., Li, H. L., Che, X. C., & Li, X. (2018). Rainfall and inflow effects on soil erosion for hillslopes dominated by sheet erosion or rill erosion in the Chinese Mollisol region. *Journal of Mountain Science, 15*(10), 2182–2191.

Stevens, C. J., & Quinton, J. N. (2008). Investigating source areas of eroded sediments transported in concentrated overland flow using rare earth element tracers. *Catena, 74*(1), 31–36.

USDA NRCS. (1999). *Soil taxonomy: A basic system of soil classification for making and interpreting soil surveys. Agric. Handbook* (2nd ed., Vol. 436). Washington, DC: US Government Printing Office.

Verachtert, E., Van Den Eeckhaut, M., Poesen, J., & Deckers, J. (2010). Factors controlling the spatial distribution of soil piping erosion on loess-derived soils: A case study from central Belgium. *Geomorphology, 118*(3), 339–348.

Wall, G. J., Dickinson, W. T., Rudra, R. P., & Coote, D. R. (1988). Seasonal soil erodibility variation in southwestern Ontario. *Canadian Journal of Soil Science, 68*(2), 417–424.

Wang, L., Zheng, F., Zhang, X. J., Wilson, G. V., Qin, C., He, C., & Zhang, J. (2020). Discrimination of soil losses between ridge and furrow in longitudinal ridge-tillage under simulated upslope inflow and rainfall. *Soil and Tillage Research, 198*, 104541.

Wang, Y., Zheng, F., Zhou, X., Qin, C., Fu, H., Zuo, X., … Zhang, J. (2019). Soil profile temperature variation in farmlands during freeze-thaw period in Mollisol region. *Bulletin of Soil and Water Conservation, 39*(3), 57–64 (in Chinese).

Xiao, H., Liu, G., Liu, P., Zheng, F., Zhang, J., & Hu, F. (2017). Developing equations to explore relationships between aggregate stability and erodibility in Ultisols of subtropical China. *Catena, 157*, 279–285.

Xu, X., Zheng, F., Wilson, G. V., & Wu, M. (2017). Upslope inflow, hillslope gradient and rainfall intensity impacts on ephemeral gully erosion. *Land Degradation & Development, 28*(8), 2623–2635.

Yang, M. Y., Tian, J. L., & Liu, P. L. (2006). Investigating the spatial distribution of soil erosion and deposition in a small catchment on the Loess Plateau of China, using ^{137}Cs. *Soil and Tillage Research, 87*(2), 186–193.

Yue, Y., Keli, Z., Liang, L., Qianhong, M., & Jianyong, L. (2019). Estimating long-term erosion and sedimentation rate on farmland using magnetic susceptibility in northeast China. *Soil and Tillage Research, 187*, 41–49.

Zhang, X. C. (2017a). Evaluating water erosion prediction project model using Cesium-137-derived spatial soil redistribution data. *Soil Science Society of America Journal, 81*(1), 179–188.

Zhang, X. C., Friedrich, J. M., Nearing, M. A., & Norton, L. D. (2001). Potential use of rare earth oxides as tracers for soil erosion and aggregation studies. *Soil Science Society of America Journal, 65*(5), 1508–1515.

Zhang, Q., Lei, T., & Huang, X. (2016). Quantifying the sediment transport capacity in eroding rills using a REE tracing method. *Land Degradation & Development, 28*(2), 591–601.

Zhang, G. H., Liu, Y. M., Han, Y. F., & Zhang, X. C. (2009). Sediment transport and soil detachment on steep slopes: I. Transport capacity estimation. *Soil Science Society of America Journal, 73*(4), 1291–1297.

Zhang, X. C., Nearing, M. A., & Garbrecht, J. D. (2017b). Gaining insights into interrill erosion processes using rare earth element tracers. *Geoderma, 299*, 63–72.

Zhang, X. C., Nearing, M. A., Polyakov, V. O., & Friedrich, J. M. (2003). Using rare-earth oxide tracers for studying soil erosion dynamics. *Soil Science Society of America Journal, 67*(1), 279–288.

Zhang, J., Yang, M., Deng, X., Liu, Z., Zhang, F., & Zhou, W. (2018). Beryllium-7 measurements of wind erosion on sloping fields in the wind-water erosion crisscross region on the Chinese Loess Plateau. *The Science of the Total Environment, 615*, 240–252.

Zuzel, J. F., Allmaras, R. R., & Greenwalt, R. (1982). Runoff and soil erosion on frozen soils in northeastern Oregon. *Journal of Soil and Water Conservation, 37*(6), 351–354.

International Soil and Water Conservation Research 9 (2021) 405–418

Contents lists available at ScienceDirect

International Soil and Water Conservation Research

journal homepage: www.elsevier.com/locate/iswcr

Original Research Article

Characteristics of unsaturated soil slope covered with capillary barrier system and deep-rooted grass under different rainfall patterns

Yangyang Li [a], Alfrendo Satyanaga [b], Harianto Rahardjo [c, *]

[a] School of Civil and Environmental Engineering, Nanyang Technological University, Block N1, 50 Nanyang Avenue, Singapore
[b] School of Engineering and Digital Sciences, Nazarbayev University, Kabanbay Batyr Ave. 53, Nur-Sultan, 010000, Kazakhstan
[c] School of Civil and Environmental Engineering, Nanyang Technological University, Block N1, #1B-36, 50 Nanyang Avenue, 639798, Singapore

ARTICLE INFO

Article history:
Received 23 July 2020
Received in revised form
9 December 2020
Accepted 17 March 2021
Available online 1 April 2021

Keywords:
Unsaturated
Slope stability
Unsaturated soil
CBS
Vetiver grass

ABSTRACT

Rainfall-induced slope failures commonly occur in residual soil slopes. Slope failures are triggered by the reduction in soil strength. This is attributed to the decrease in soil suction due to rainwater infiltration. Slope covers like capillary barrier system and vegetative cover are effective methods that can be used to prevent rainfall-induced slope failures. The capillary barrier system is able to limit the rainwater infiltration, and vegetation can contribute to the increase in soil strength. Vetiver grass is widely planted in tropical and subtropical areas of the world for soil and water conservation. This study investigates the characteristics of unsaturated soil slope covered with capillary barrier system and Vetiver grass in comparison with the original slope through numerical analyses and field measurements. The analyses were carried out under the advanced, normal, and delayed rainfall patterns. The results of the analyses indicated that the capillary barrier system played a more significant role than the Vetiver grass in maintaining slope stability, although both the capillary barrier system and Vetiver grass contributed to the slope stability. In addition, both numerical analyses and field measurements showed that under the delayed and normal rainfall patterns, when antecedent rainwater infiltration could increase the soil moisture, the capillary barrier system performed much better compared to Vetiver grass in maintaining soil matric suctions and slope stability.

1. Introduction

Climate change has been a worldwide concern, and it impacts many parts of the planet. Climate change is not limited to temperature but also precipitation. Rainfall-induced slope failures are commonly observed within unsaturated soils located in different geological settings such as pyroclastic deposits (Comegna et al., 2016; Forte et al., 2019; Pirone, 2015), extensively weathered residual soils (Rahardjo et al., 2013; Pradhan & Kim, 2015), and colluvial weathered deposits (Sorbino and Nicotera, 2013). A higher number of rainfall-induced slope failures could occur (Rahardjo et al., 2013; Zhang et al., 2019) as heavy rainfalls become more frequent (Meteorological Services Singapore, 2018). Slope fails as rainwater infiltrates into the residual soil slope and soil strength decreases due to a decrease in the matric suction within the unsaturated zone of residual soil slope (Oh & Lu, 2015; Xion et al., 2019). Rainfall-induced slope failures can cause significant damage to infrastructure or even loss of life. It is important to protect slopes with appropriate measures. Two possible preventive measures against rainfall-induced slope failures are related to slope stabilization using capillary barrier system and vegetations.

The capillary barrier system has been studied and widely used as an effective soil cover in reducing rainfall infiltration (Ross, 1990; Stormont, 1996). It comprises a fine-grained layer of non-cohesive soil overlying a coarse-grained layer of non-cohesive soil. As the capillary barrier system is generally unsaturated, the difference in permeability of the fine-grained layer and the coarse-grained layer limits the water movement downward into the slope (Yan et al., 2019). When rainfall occurs, infiltrated water will be held in the fine-grained layer by the capillary force and water will be drained laterally from the fine-grained layer if the fine-coarse interface is sloped. The water can also be removed by evapotranspiration from

* Corresponding author.
E-mail addresses: yangyang.li@ntu.edu.sg (Y. Li), alfrendo.satyanaga@nu.edu.kz (A. Satyanaga), chrahardjo@ntu.edu.sg (H. Rahardjo).
URL: http://www.ntu.edu.sg/cee/staff/infrastructure/academic/chrahardjo.asp

https://doi.org/10.1016/j.iswcr.2021.03.004

the fine-grained layer, though restricted by climate (Morris & Stormont, 1999). Breakthrough occurs when water percolates into the coarse-grained layer and fine-grained layer approaches saturation. The precipitation exceeds the total of evapotranspiration and lateral diversion, and the capillary barrier is not effective in this case (Stormont, 1996).

A lower-cost slope preventive measure is utilizing vegetation for covering the slope. Vegetation can affect slope stability by affecting soil hydrological and mechanical properties (Schwarz et al., 2010; Wang et al., 2019). Structural roots of trees and shrubs provide additional mechanical reinforcement to stabilize slopes significantly while fine roots of vegetations can help increase the shear strength of soil. Furthermore, rainwater could be intercepted by vegetation and soil water could be removed through the evapotranspiration process. These hydrological reinforcements result in a decrease in soil moisture and an increase in soil strength (Greenwood et al., 2004). However, many studies have shown that evapotranspiration was minimal and can be ignored during rainfall events (Leung et al., 2015; Ni et al., 2018). Compared to the effect of evapotranspiration, the root-induced changes in soil-water characteristic curve (SWCC) affected slope stability more than other factors (Ni et al., 2018). However, the effect of root-induced change in SWCC was not as significant as the effect of root-induced change in soil saturated permeability on slope stability (Leung et al., 2015). The hydrological reinforcement was predominantly contributed by the change in the saturated permeability. It was found that shallow soil was effectively reinforced by the mechanical effect of roots while deep soil was more reinforced by the hydrological effects of roots (Ni et al., 2018). In addition, soil permeability could increase due to the root channels formed by the macropores that were created by dying and decaying roots, which could endanger slope stability (Ni et al., 2018). On the other hand, Ghestem et al. (2011) suggested that both alive and dead roots can form preferential flow paths, and the effects can be adverse or beneficial to slope stability depending on the root arrangement and architecture in the slope.

Both capillary barrier system (CBS) and vegetations help to stabilize the slope. However, the comparison of the effectiveness of both methods on stabilizing an unsaturated soil slope was seldom studied. Furthermore, slopes may also behave differently under different rainfall patterns such as advanced rainfall, normal rainfall, and delayed rainfall (Rahimi et al., 2011). Ng et al. (2001) found that rainfall patterns influenced the pore-water pressure changes significantly, although the resultant change in slope stability was not investigated. Rahimi et al. (2011) studied the effect of three typical rainfall patterns on slopes with two different soil types (with high and low permeability) and found that the slope stability of low permeability soil slope was affected more than the slope stability of high permeability soil slope by the rainfall patterns. Brand et al. (1984) also suggested that landslides in Hong Kong were mostly induced by rainfall with short duration and high intensity. In addition, the effect of antecedent rainfall was very limited due to the high permeability of local soils in Hong Kong.

Issues related to runoff and soil erosion due to rainfall have been extensively studied by Cuomo et al. (2015; 2016a; 2016b) in different scales. In our case, soil erosion due to runoff was not considered because Singapore is an urbanized city with very good drainage systems. Soils in Singapore are relatively stiff and not much erosive. Most slopes are engineered slopes and the soil was well compacted. In addition, our cumulative precipitation applied in this study was less than 400 mm and runoff can hardly occur, based on a study by Cuomo and Della Sala (2013) for slopes under rainfall intensity higher than the initial hydraulic soil permeability but lower than the saturated permeability.

In this study, the characteristics of three different slopes, i.e., one original residual soil slope, one residual soil slope covered with CBS, and another residual soil slope covered with deep-rooted Vetiver grass were investigated. The main objective of this study is to compare the characteristics of these three different slopes under the advanced, normal, and delayed rainfall patterns. The effectiveness of the two different slope stabilization methods under different rainfall patterns were compared through parametric studies and field measurements. The parametric studies were conducted numerically on the performance of different slopes under different rainfall patterns. On the other hand, field monitoring measurements of soil suctions at different depths were used to evaluate the characteristics of different slopes under different rainfall patterns.

2. Method of analyses

2.1. Rainfall patterns in parametric studies

Parametric studies were carried out numerically to investigate the performance of three slopes under three rainfall patterns. Seepage analyses were conducted first using SEEP/W (Geo-slope international Ltd, 2012a; Geo-slope international Ltd, 2012b) to obtain the pore-water pressure changes due to rainwater infiltration, to be exported to SLOPE/W (Geo-slope international Ltd, 2012a; Geo-slope international Ltd, 2012b) for calculation of factor of safety (FOS). The three slopes investigated in this study comprised original residual soil slope, residual soil slope covered with CBS, and residual soil slope covered with Vetiver grass. The three rainfall patterns applied in the transient seepage analyses were advanced rainfall, normal rainfall, and delayed rainfall following the study by Rahimi et al. (2011). According to a study by Rahardjo et al. (2008), the highest pore-water pressure profile was observed when a total of 5-day antecedent rainfall was received by the slope, and the contribution of the subsequent rainfall to the pore-water pressure was insignificant. It was also found that a 5-day antecedent rainfall of 92–109 mm was the threshold to produce the highest pore-water pressure profiles in the residual soil derived from Bukit Timah Granite. Therefore, a 5-day rainfall of 100 mm was used in the simulation because it resulted in the highest pore-water pressure profile and the most unfavourable condition for slope stability. To distinguish the different antecedent rainfall patterns, the 5-day rainfall was divided into 15 time-intervals with 8 h duration for each time interval. The three rainfall patterns are shown in Fig. 1.

2.2. Site overview and soil properties

A slope investigated in this study is located at Ang Mo Kio St. 21 in Singapore. The slope consists of the residual soil from Bukit Timah granite. The slope was repaired upon major failures triggered by rainfall in 2008. The height and the slope angle of the repaired slope were 5 m and 33° respectively. One section of the slope was covered with CBS and another section of the slope was covered with Vetiver grass, as shown in Fig. 2. Each section of the slope had a total area of approximately 140 m^2. In the construction of CBS, granite chip was used as the coarse-grained material and fine sand was used as the fine-grained material. Each layer of the CBS system had a thickness of 20 cm. A related study about the performance of the same CBS slope through field instrumentations was discussed by Rahardjo et al. (2012). The vegetated slope was assumed to have a root depth of 40 cm for an estimation of short-term slope stability after planting Vetiver grass.

The undisturbed soil samples were taken using a Mazier sampler in the field. For the vegetated slope, the grass above the ground surface was removed first, and topsoil with roots was

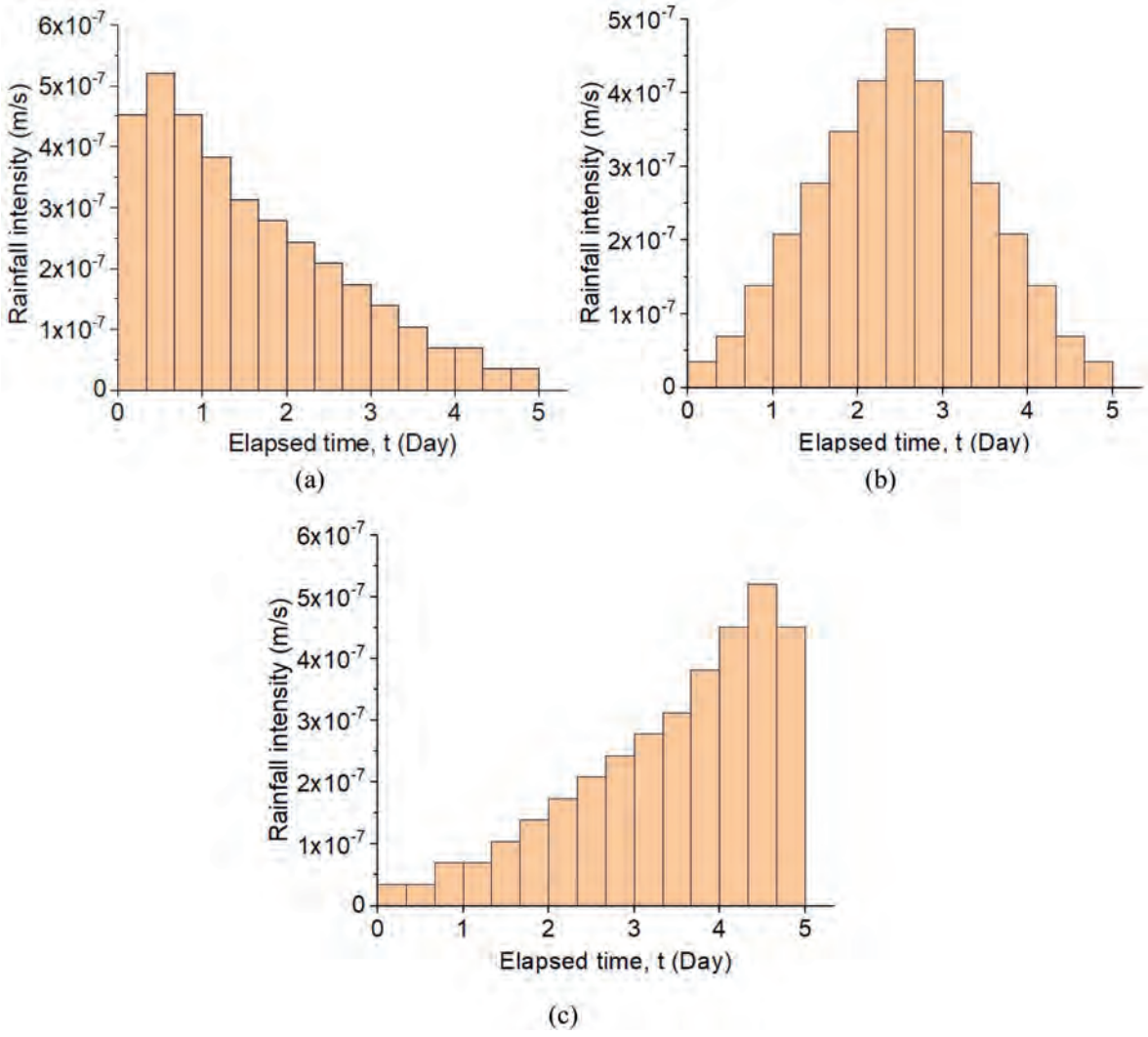

Fig. 1. The (a) advanced rainfall pattern, (b) normal rainfall pattern and (c) delayed rainfall pattern.

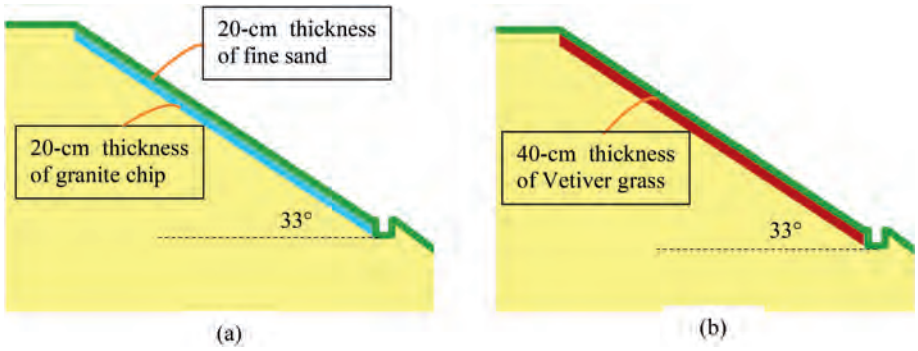

Fig. 2. (a) Slope covered with CBS and (b) slope cover with Vetiver grass.

sampled directly below the ground surface using block sampling. Index property tests, saturated permeability tests, and shear strength tests were carried out on those undisturbed samples in the laboratory. The saturated permeability tests were conducted using two back pressures triaxial system (Satyanaga et al., 2019). A summary of the basic properties of the soil used in this study is presented in Table 1.

The soil-water characteristic curve (SWCC) describes the relationship between the volumetric water content and matric suction of a soil. The air-entry value is the matric suction value when air starts to enter the pores during drying process and the water-entry value is the matric suction value when water starts to enter the pores during wetting process. The water-entry value is also called as the breakthrough head or breakthrough suction because

Table 1
List of soil index properties.

Index Properties	Residual soil	Fine sand	Granite chip	Topsoil with Vetiver grass
Unified soil classification system	SM-MH	SP	GP	SP
Specific gravity	2.64–2.68	2.65	2.69	2.64
Liquid limit (%)	53–66			
Plastic limit (%)	36–38			
Water content (%)	46–54			17.2
D_{60} (mm)	0.25	0.6	18	1.1
D_{30} (mm)	0.02	0.4	15	0.5
D_{10} (mm)	0.00	0.3	11.27	0.23
Coefficient of uniformity	92.86	2	1.6	4.89
Coefficient of curvature	0.63	0.89	1.11	1.01
Gravel (>4.75 mm; %)	0	5.4	98.5	11.9
Sand (%)	54	94.3	1.48	85.7
Fines (<0.075 mm; %)	46	0.3	0.002	2.4
Dry density (Mg/m^3)	1.51	1.56	1.65	1.86
Void ratio	0.74–0.77	0.70	0.64	0.4
Saturated coefficient of permeability (m/s)	6×10^{-6}	2.7×10^{-4}	5.1×10^{-1}	2.6×10^{-5}

breakthrough occurs when the matric suction at the interface between the fine-grained layer and coarse-grained layer is lower than the water-entry suction of the coarse-grained layer. Breakthrough occurs faster and easier when the water-entry value of the coarse-grained layer is higher. The SWCCs were best fitted using Fredlund and Xing (1994) Equation, which was found to fit data ranging from 0 to 1,000,000 kPa:

$$\theta = C(\psi)\frac{\theta_s}{\left\{\ln\left[e + \left(\frac{\psi}{a}\right)^n\right]\right\}^m} \quad (1)$$

where θ is the calculated volumetric water content for a specified matric suction; θ_s is the saturated volumetric water content; $C(\psi)$ is the correction factor and was suggested to be equal to 1 by Leong and Rahardjo (1997); ψ is the matric suction; and a, n, and m are empirically-derived variables related to the air-entry value of soil, the maximum slope of the SWCC and the curvature of the slope of SWCC, respectively.

Unsaturated permeability is determined from the measured saturated permeability and the integration of the SWCC (Fredlund et al., 1994; Zhai & Rahardjo, 2015):

$$k_w(\psi) = \frac{\int_{\ln(\psi)}^{b} \frac{\theta(e^y) - \theta(\psi)}{e^y}\theta'(e^y)dy}{\int_{\ln(\psi_{aev})}^{b} \frac{\theta(e^y) - \theta_s}{e^y}\theta'(e^y)dy}k_s \quad (2)$$

where b is equal to ln (100000); $k_w(\psi)$ is the calculated unsaturated permeability for a specified matric suction ψ (m/s); k_s is the coefficient of saturated permeability and y is a dummy variable of integration representing the logarithm of matric suction.

Tempe cell and pressure plates were the two instruments used to obtain SWCC data points. Fig. 3 shows the wetting SWCCs and permeability functions calculated from the measured saturated permeability and SWCC for the residual soil, fine sand, granite chips, and topsoil with Vetiver grass. The best-fitting parameters are summarized in Table 2. A simple scaling method proposed by Pham et al. (2005) was used for estimating the wetting curve for the granite chip in the coarse-grained layer.

Shear strength of unsaturated soils can be obtained using Equation (3), as proposed by Fredlund et al. (1978):

$$\tau = c' + (\sigma - u_a)\tan\varphi' + (u_a - u_w)\tan\varphi^b \quad (3)$$

where c' is the effective cohesion, φ' is the frictional angle, u_a is the pore-air pressure; $(\sigma - u_a)$ is the net normal stress; $(u_a - u_w)$ is matric suction and φ^b is the angle indicating the rate of change in shear strength with respect to the change in matric suction.

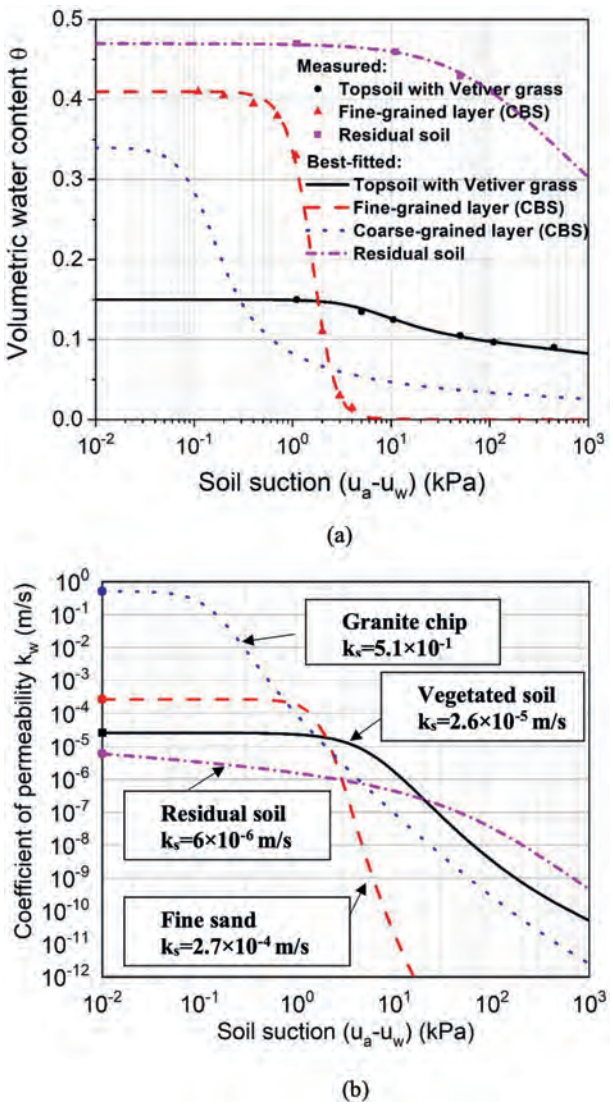

Fig. 3. (a) SWCCs and (b) permeability functions of the soils.

Table 2
Best-fitting parameters for the SWCCs.

Parameters	Residual soil	Fine sand	Granite chip	Topsoil with Vetiver grass
Saturated volumetric water content θ_s	0.47	0.41	0.34	0.15
a (kPa)	84.39	1.81	0.11	4.31
n	0.92	3.19	2.72	2
m	0.42	3.74	0.79	0.23

Multistage consolidated drained triaxial tests were carried out to obtain the shear strength parameters. Triaxial tests were conducted on the saturated soil specimens to obtain φ' and c'. Triaxial tests were conducted on the unsaturated soil specimens under a constant net normal stress but different matric suctions to estimate φ^b. More related details can be referred to the studies by Rahardjo et al. (2014) and Satyanaga et al. (2019). The shear strength parameters of the soils used in this study are shown in Table 3.

As illustrated in Fig. 4 and Fig. 5, steel J-pins of 1.5 m length were used to secure the CBS onto the slope. Each J-pin has a pull-out resistance of 10 kPa and a shear force of 15 kN.

2.3. Seepage and slope stability analyses in parametric studies

Seepage analyses were carried out to obtain the pore-water pressure changes due to different rainfall patterns. The initial ground water table was set to estimate the initial pore-water pressure head and the corresponding volumetric water content in the numerical analyses. The initial groundwater table was assumed the same for all three slopes. Fig. 6 illustrates the boundary conditions applied in SEEP/W. Unit flux was applied to simulate rainfall on the ground surface. No ponding selection was enabled by limiting the resultant maximum pore-water pressure to zero. Runoff was allowed and excess accumulation of rainwater on slope surface could be avoided. The total head of left boundary and right boundary were kept constant at 116.5 m and 115 m according to the position of groundwater table on site, respectively. At the bottom boundary, no flow was allowed. In addition, as illustrated in Fig. 6, a horizontal drain was installed to draw down the water level and reduce the excess pore water pressure in the slope.

At the end of each time interval (8 h), the factor of safety (FOS) was computed using Slope/W based on the pore-water pressures obtained from the previous seepage analysis for each slope. Bishop's simplified method of slices (Bishop, 1955) was used.

2.4. Field instrumentations and slope stability analyses

Three sections of the slope at Ang Mo Kio were instrumented with jet fill tensiometers for measurements of the negative pore-water pressure within the original slope, slope covered with CBS, and slope covered with Vetiver grass. The tensiometers were installed in mid-slope at depths of 0.5 m, 1 m, 1.5 m and 2 m with a spacing of 0.5 m. Maintenance was performed regularly to remove accumulated air resulted from cavitation of water by flushing the tensiometers and refilling deaired water into the jet-fill reservoir. Three piezometers were installed at the crest, middle and toe of the slope to monitor the position of groundwater table during dry and rainy periods. From September 2008 to October 2008, manual monitoring and maintenance of tensiometers were conducted three times a week at the same time of each day. The rainfall data were obtained from the nearest weather station, Ang Mo Kio weather station which was located 0.9 km distance away from the investigated site (i.e., Ang Mo Kio St. 21). Soil properties from the site as presented in Section 2.2 were incorporated in the numerical analyses of field instrumentation data.

Slope stability analyses were performed by incorporating the measured matric suction values from field monitoring in Slope/W using the total cohesion method (Fredlund & Rahardjo, 1993). The soil model was divided into five sublayers based on the following depths: 0–0.75 m, 0.75–1.25 m, 1.25–1.75 m, 1.75–2.25 m and the soil layer below 2.25 m. Based on the extended Mohr-Coulomb yield criterion for unsaturated soil (Fredlund et al., 1978) (i.e., $\tau = c' + (\sigma - u_a)\tan\varphi' + (u_a - u_w)\tan\varphi^b$), total cohesion c was defined as the summation of effective cohesion c' and additional cohesion from matric suction in unsaturated soil $(u_a - u_w)\tan\varphi^b$ (i.e. $c = c' + (u_a - u_w)\tan\varphi^b$). Total cohesions within the four soil layers close to the ground surface were calculated from the matric suctions observed from the field monitoring in each corresponding layer. A higher or lower matric suction reflected by the effect of rainwater infiltration resulted in a higher or lower additional cohesion from matric suction. The total cohesion was assumed constant and not to vary with depth within each layer.

Total cohesion method was used for the calculation of shear strength of the soil layers shallower than 2.25 m. For the soil deeper than 2.25 m without matric suction measurements, the soil shear strength was estimated based on the position of the ground water table as measured in the field. The extended Mohr-Coulomb yield criterion for unsaturated soil was applied with the shear strength parameters as listed in Table 3. The variations in matric suctions with depth were obtained based on the position of the groundwater table from the field measurements. It was assumed that all the three slopes shared the same groundwater table as measured in the field. In other words, the effect of Vetiver grass and CBS on groundwater level was not considered.

3. Results and discussions

3.1. Slope stability from parametric studies

Fig. 7 presents the results of stability analyses under three typical rainfall patterns (i.e., advanced rainfall pattern, normal rainfall pattern. and delayed rainfall pattern) from parametric

Table 3
Shear strength parameters of the soils.

Parameters	Residual soil	Fine sand	Granite chip	Topsoil with Vetiver grass
Unit weight γ (kN/m^3)	20	24	24	21.4
$\mathbf{c'}$ (kPa)	2	0	0	10
φ' (°)	30	34	36	34
$\varphi^{\mathbf{b}}$(°)	18	15	17	19

Fig. 4. J-pins before (a) and after (b) installation.

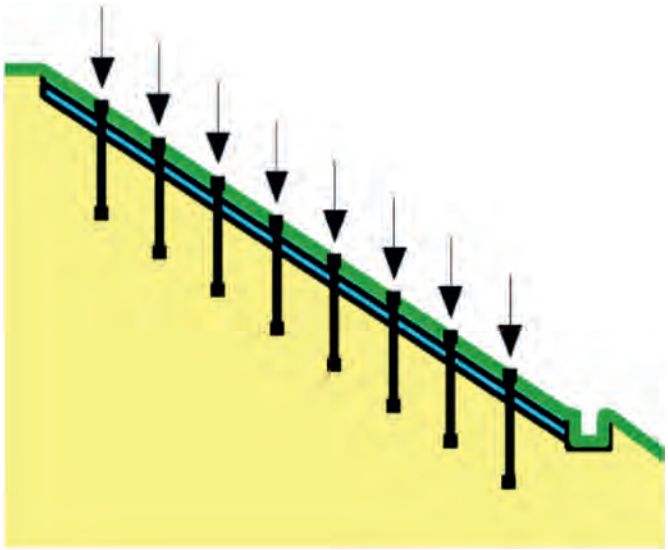

Fig. 5. Illustration of J-pins on slope covered with CBS.

studies, respectively. CBS, VG and OS represent the results of the CBS slope, the vegetated slope, and the original slope, respectively. The difference in the FOS of the CBS slope and the original slope, as well as the difference in the FOS of the vegetated slope and the original slope were plotted for comparison.

In general, the FOS of the CBS slope and the vegetated slope were higher than that of the original slope, which implied that both CBS and vegetations help to stabilize the slope. However, the FOS of the CBS slope was much higher than those of vegetated slope. Based on the analyses under the advanced rainfall pattern, the FOS of the CBS slope was about 15–20% higher than those of original slope, while the FOS of the vegetated slope was only about 2.5% higher than those of the original slope. Based on the analyses under the normal rainfall pattern, the FOS of the CBS slope was about 14–25% higher than those of the original slope, while the FOS of the vegetated slope was only about 2–4% higher than those of the original slope. Based on the analyses under the delayed rainfall pattern, the FOS of the CBS slope was about 17–25% higher than the FOS of the original slope, while the FOS of the vegetated slope was only about 2.5% higher than those of the original slope. The results of the slope stability analyses under different rainfall patterns

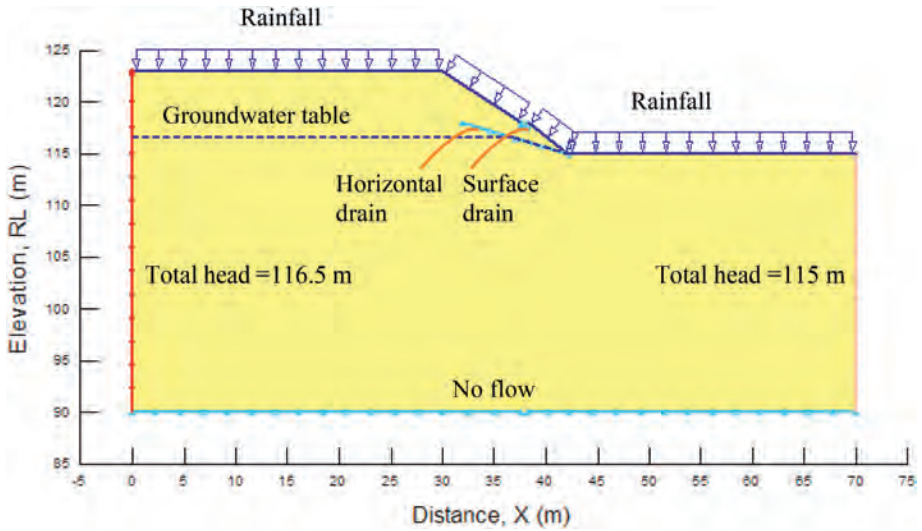

Fig. 6. Boundary conditions applied in seepage analyses.

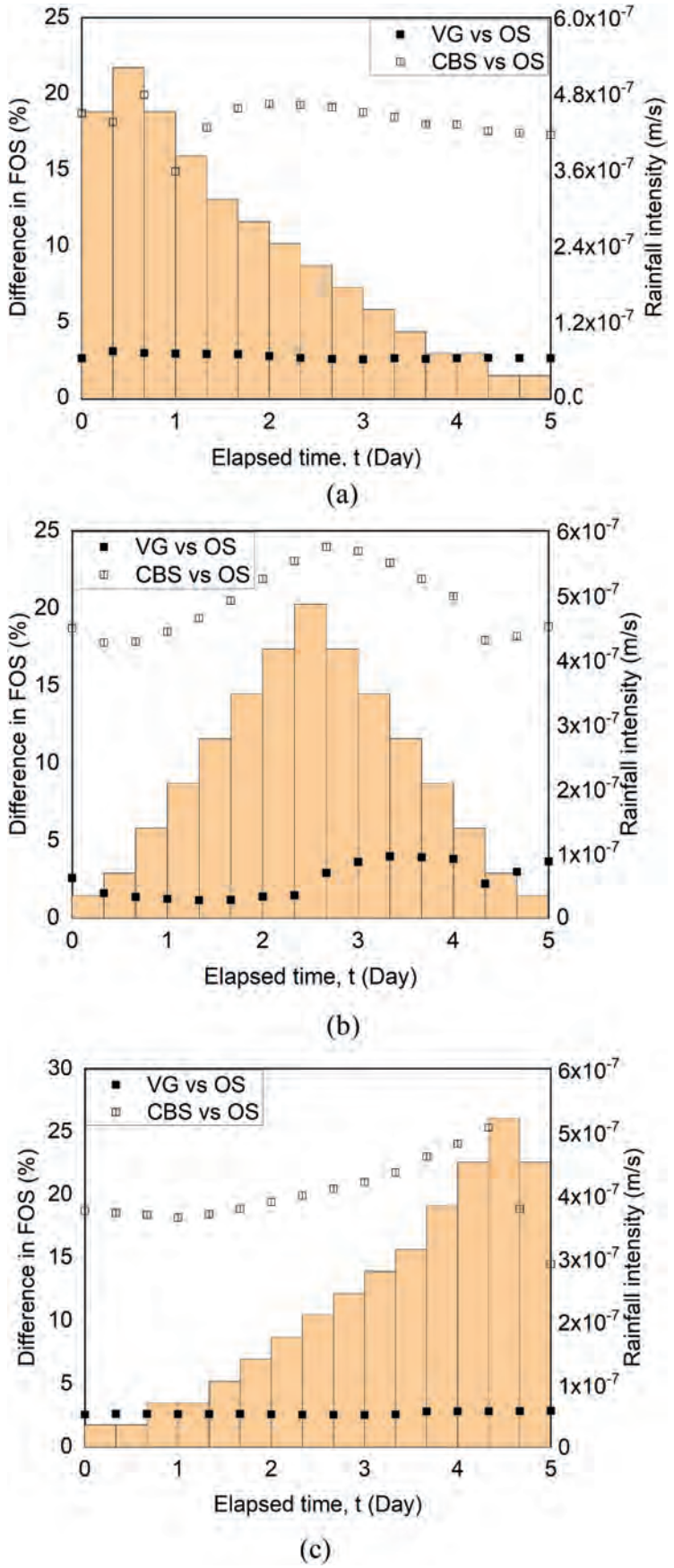

Fig. 7. The results of difference in the FOS of the vegetated slope, CBS slope and original slope under the (a) advanced rainfall pattern, (b) normal rainfall pattern and (c) delayed rainfall pattern.

indicated that the stability of the CBS slope might experience a significant drop during the application of rainfall with high intensity, as a result of the breakthrough. Breakthrough was observed from the results of seepage analyses on days with a high rainfall intensity. As the infiltrated rainwater within the fine-grained layer was diverted down to the lower part of the slope, breakthrough first occurred at the toe of the covered slope and in the end, it occurred at the top of the covered slope. Breakthrough was a progressive process under the prolonged light rainfall condition. However, under the short-duration heavy rainfall, breakthrough occurred at the same time along the slope because the infiltration rate was larger than the diversion capacity and the infiltrated water was not able to flow downwards before breakthrough occurred (Li et al., 2013). Significant infiltration into the underlying residual soil after breakthrough at a certain location lowered the FOS of the CBS slope. The distance from the top of the covered slope to the breakthrough position is called diversion length. Under the advanced rainfall pattern, breakthrough started immediately from the beginning of precipitation and reached a minimum diversion length of 3 m at the end of the first day. The FOS also reached the minimum value at the same time. Under the normal rainfall pattern, breakthrough started from the morning of the 2nd day and the FOS started to decrease. The minimum diversion length was about 6 m at the end of the third day. The minimum FOS also occurred at the same time. Under the delayed rainfall pattern, breakthrough started from the 4th day of precipitation and reached a minimum diversion length of 3 m at the end of the 5th day. The FOS also reached minimum at the same time. It was found that the minimum FOS occurred at the same time when the diversion length reached the minimum in all three analyses under different rainfall patterns. Moreover, a shorter diversion length resulted in a lower FOS. It was also observed that the stability of the CBS slope was more sensitive to the change in rainfall patterns, as a result of breakthrough, compared to the stability of the original slope and the vegetated slope.

In the parametric studies, the contribution of the Vetiver grass on the evapotranspiration was ignored and this may cause an underestimate of the computed FOS values of the vegetated slope.

3.2. Field measurements

Variations in groundwater level with the daily precipitation in September and October 2008 at Ang Mo Kio slope are presented in Fig. 8. As observed, the groundwater level at the toe of the slope was maintained at the ground surface due to the presence of the horizontal drain.

Figs. 9–11 show the field measurements of matric suctions at various depths for the original slope, vegetated slope and CBS slope in September and October 2008. The daily precipitation data from the nearest weather station located 0.9 km away was also plotted.

It was observed that the matric suction values from field monitoring of the CBS slope were generally higher than those measured in the vegetated slope and original slope, which contributed to the additional shear strength of soil at the CBS slope. In addition, the J-pins installed in the CBS slope also contributed partly to the stability of the slope. Hence, the stability of a CBS slope can be maintained during rainfall. The highest daily precipitation of 100 mm was recorded on September 3 that resulted in a significant drop in matric suctions of all three slopes. The range of the matric suction from field monitoring of the CBS slope varied from 2.5 to 20 kPa while those of the vegetated slope and original slope varied from 0 to 11 kPa and from 0 to 6 kPa, respectively. Furthermore, there was a relatively high daily precipitation of 44 mm on September 26. However, the matric suction of the CBS slope was maintained between 20 and 40 kPa varying with depth while the matric suction of the vegetated slope and original slope dropped to a range between 2 and 18 kPa and between 7 and 9 kPa, respectively. It implied that the stability of the CBS slope might not be affected by rainwater since CBS impeded the rainwater infiltration while the vegetated slope and original slope were much more affected by the rainwater infiltration. In October 2008, although the daily precipitation was not higher than 22 mm, there was a long period of continuous precipitation from October 13 to October 22. Due to this long period of rainfall, the matric suction of all three slopes dropped significantly. However, CBS was still effective as a slope cover since it can maintain a relatively higher matric suction.

In both September and October, the matric suction values from field measurements of the vegetated slope at 0.5 m and 1 m depth were the lowest among all slopes. However, the matric suction values at 1.5 m of the vegetated slope were much higher than that of the original slope, which can be observed clearly from the plots of matric suctions for all slopes with respect to different depths as shown in Figs. 12–15. The shallow layer (i.e., 0-1 m) of the vegetated slope may have a higher storage of water due to the existence of vegetations. Matric suction decreased more significantly within the shallow soil layer instead of the deeper soil layer, implying lesser rainwater infiltration into the deeper soil layer below 1 m. The high suction of the vegetated slope at 1.5 m depth was also contributed by a concentration of roots above the depth. However, the soil suction at 2 m depth was not as high as the soil suction at 1.5 m because 2 m depth was close to the groundwater table (i.e., 2-5 m between middle and crest of slope). The observed low suctions at shallow soil (i.e., 0-1 m) and high suctions at deep soil (i.e., 1.5 m) of the vegetated slope implied the same conclusion from the study by Ni et al. (2018) that the shallow soil (i.e., 0-1 m) was more reinforced by the mechanical effect of roots while deep soil (i.e., 1-2 m) was more reinforced by the hydrological effects of roots.

It was also observed that the rainwater infiltration into the layer below the CBS slope was reduced. As a result, the matric suction within the layer near the ground surface of the CBS slope was also maintained at a higher suction value as compared to that of the vegetated slope and original slope. This could be attributed to the lateral diversion of rainwater within the fine-grained layer of the CBS slope. Then, the rainwater was dissipated into the main drain further downslope. Therefore, the difference in the matric suction between field measurements from the CBS slope and the original slope was observed to be small at 0.5 m depth since the infiltrated rainwater flowed within the fine-grained layer. On the other hand, the difference in the matric suction between field measurements from the CBS slope and the original slope was observed to be large at the deeper soil layer since only limited rainwater was able to infiltrate into the soil layer below CBS.

3.3. Slope stability from field measurements

Slope stability analyses that incorporates the field measurements of matric suctions and groundwater table were then performed in Slope/W using total cohesion method. The periods of field measurements to be incorporated in the slope stability analyses were selected based on a period with similar rainfall patterns as used in the parametric studies. Fig. 16 presents the computed FOS based on the analyses under the advanced, normal and delayed rainfall patterns. Meanwhile, the difference in the FOS from analyses of the CBS slope and the original slope, as well as the difference in the FOS from the analyses of the vegetated slope and the original slope was calculated and plotted.

In general, both CBS and vegetations helped to stabilize the slope as the FOS of the CBS slope and the vegetated slope were higher than that of the original slope. However, CBS performed better in maintaining the slope stability since the FOS of the CBS

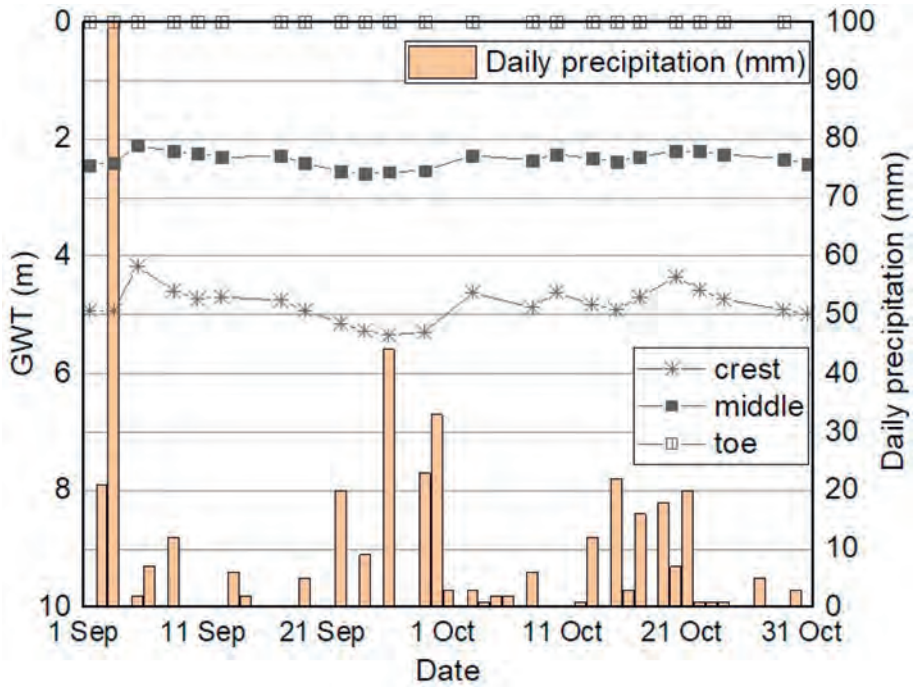

Fig. 8. Piezometer measurements at the crest, middle and toe of slope.

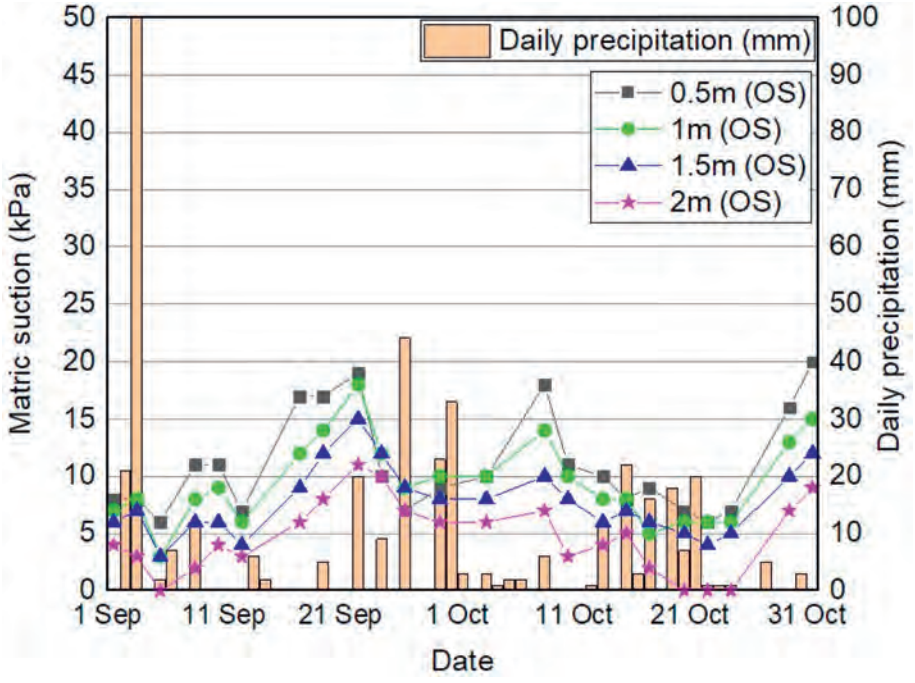

Fig. 9. Tensiometer measurements at various depths for the original slope.

slope was higher than that of the vegetated slope. The minimum FOS for the CBS slope was 1.4, 1.5 and 1.6 based on the stability analyses under the advanced, normal and delayed rainfall patterns, respectively. The minimum FOS for the vegetated slope were 1.4 based on the stability analyses under the advanced and normal rainfall patterns and 1.5 based on the stability analyses under the delayed rainfall pattern. The minimum FOS for the original slope were 1.3 based on the stability analyses under the advanced and normal rainfall patterns and 1.5 based on the stability analyses under the delayed rainfall pattern. The analyses on certain rainy days (i.e., Sep 26 and Oct 22) indicated that the FOS of the CBS slope did not decrease with the help of the capillary layer to minimize the rainwater infiltration, while those of the vegetated slope and the original slope decreased.

Based on the stability analyses under the advanced rainfall pattern, the FOS of the CBS slope was about 4–11% higher than the FOS of the original slope, while the FOS of the vegetated slope was about 1.5–8% higher than the FOS of the original slope. Based on the stability analyses under the normal rainfall pattern, the FOS of the CBS slope was about 6–12% higher than those of the original

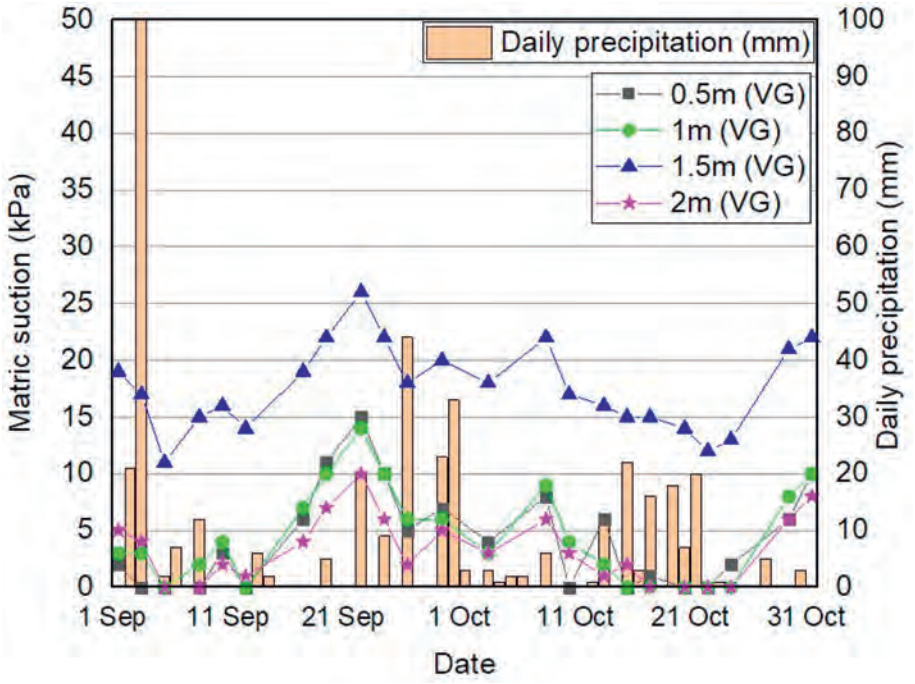

Fig. 10. Tensiometer measurements at various depths for the vegetated slope.

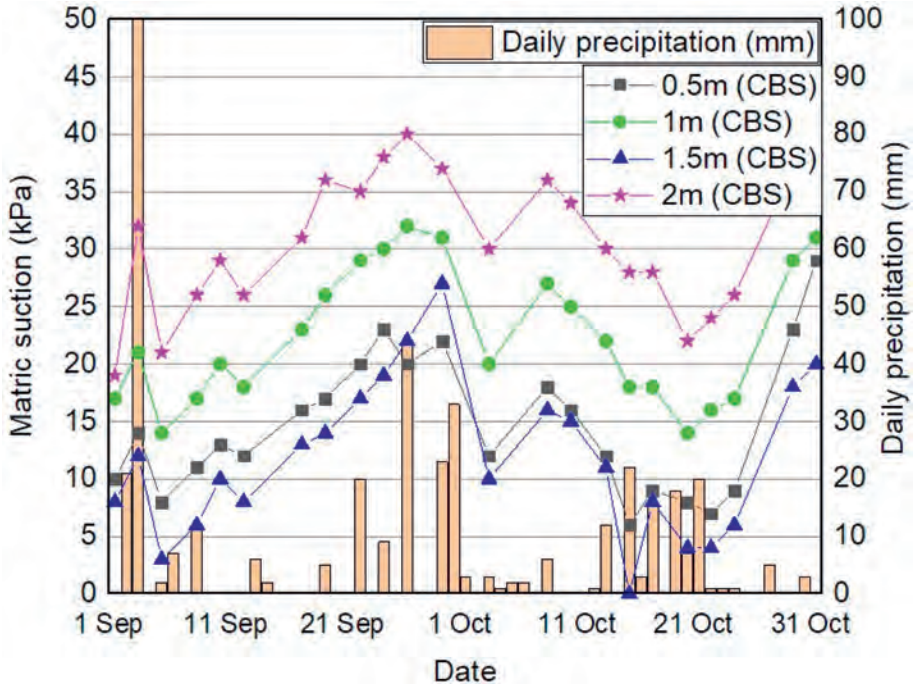

Fig. 11. Tensiometer measurements at various depths for the CBS slope.

slope, while the FOS of the vegetated slope was about 3–7% higher than those of the original slope. Based on the stability analyses under the delayed rainfall pattern, the FOS of the CBS slope was about 2.5–7% higher than those of the original slope, while the FOS of the vegetated slope was about 1.5–2% higher than those of the original slope.

In Table 4, the effectiveness of CBS and Vetiver grass in slope stability under different rainfall patterns were compared by summarizing the difference in the FOS from both parametric studies and field measurements. CBS performed better when compared to Vetiver grass in maintaining slope stability under the delayed and normal rainfall patterns than under the advanced rainfall pattern, implying that the antecedent rainwater infiltration under the delayed and normal rainfall patterns could affect the vegetated and original slopes more than the CBS slope.

It was also observed that the differences in the effectiveness of CBS and Vetiver grass observed from the analyses incorporating field measurements were not as large as observed from the

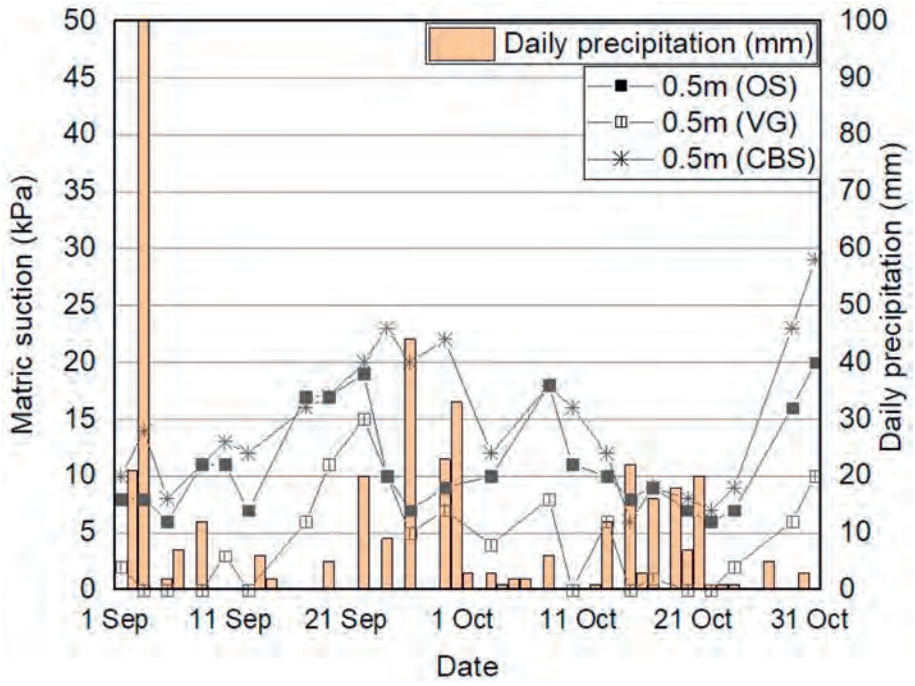

Fig. 12. Tensiometer measurements at 0.5 m for the original slope, vegetated slope and CBS slope.

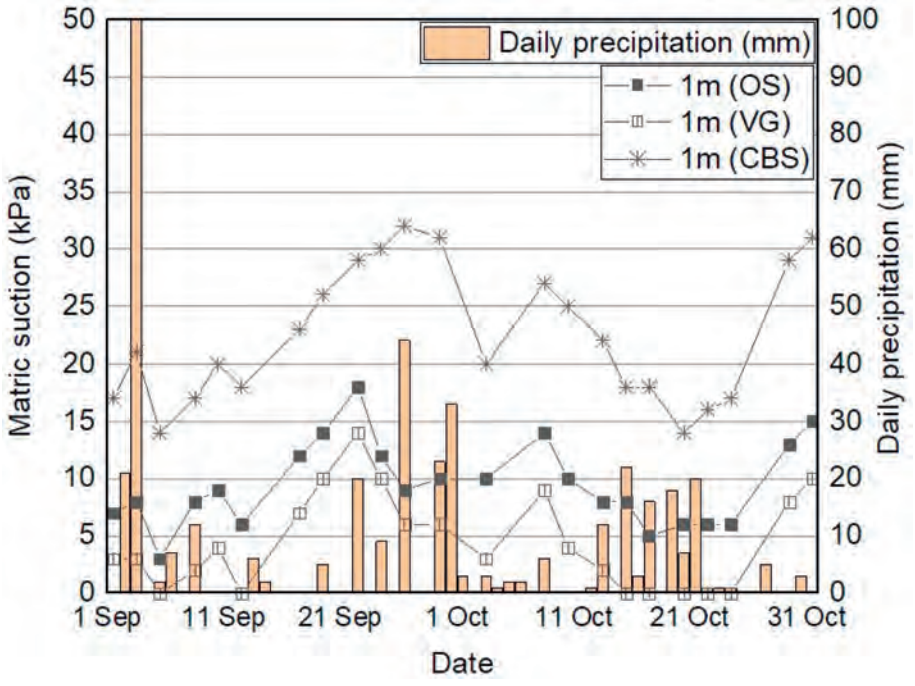

Fig. 13. Tensiometer measurements at 1 m depth for the original slope, vegetated slope and CBS slope.

analyses in the parametric studies. Based on the field measurements data, CBS was able to help increase the FOS of the slope by a maximum of 12% while Vetiver grass was able to help increase the FOS of the slope by a maximum of 8%. However, in the parametric studies, CBS was shown to help increase the FOS of the slope by a maximum of 25% while Vetiver grass helped to increase the FOS of the slope by a maximum of 4%. This could be attributed to the growth of roots of Vetiver grass with time that contributes matric suctions due to transpiration and therefore, the additional strength of the soil. This phenomenon could be captured from the instrumentation data, but it could not be reflected in the parametric studies.

4. Conclusions

The effect of CBS and Vetiver grass on slope stability was investigated through numerical analyses in terms of parametric studies and based on field measurements. The computed FOS from

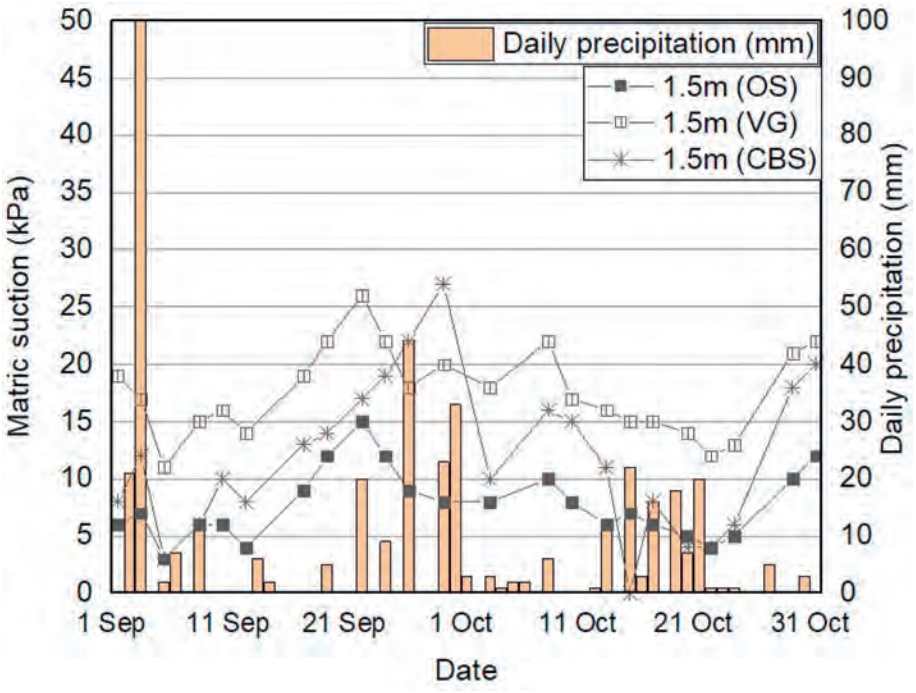

Fig. 14. Tensiometer measurements at 1.5 m depth for the original slope, vegetated slope and CBS slope.

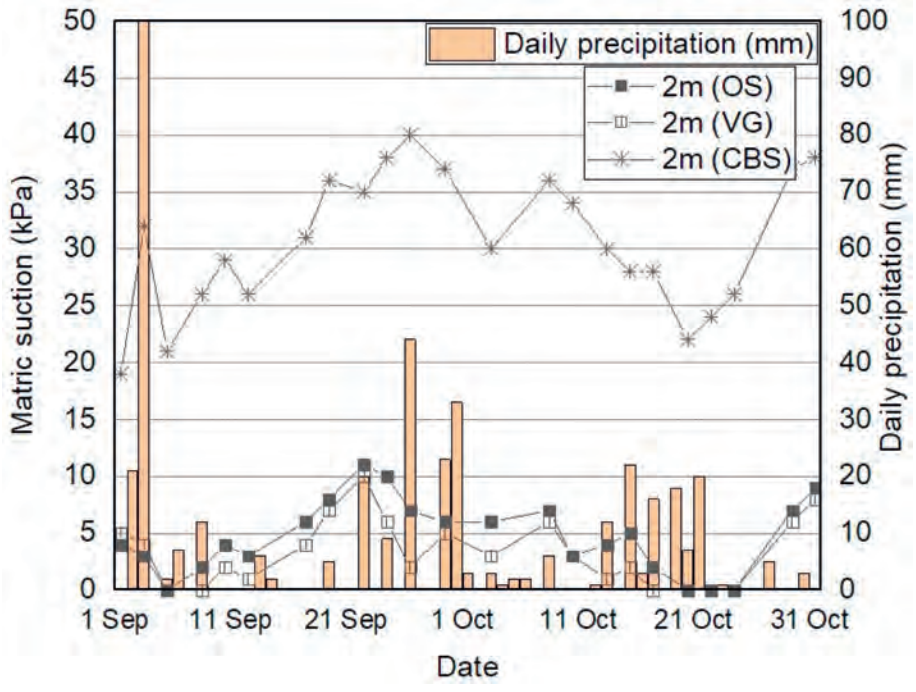

Fig. 15. Tensiometer measurements at 2 m depth for the original slope, vegetated slope and CBS slope.

numerical analyses results from the parametric studies and from the analyses by incorporating field measurements show that both CBS and Vetiver grass were able to stabilize slopes. However, it was observed that the CBS performed better than the vegetation in maintaining the stability of the slope in this study. It was also found that from the slope stability analyses in both parametric studies and field measurements, the CBS played a more effective role in limiting antecedent rainwater infiltration compared to the Vetiver grass, especially under the advanced and delayed rainfall patterns.

In future studies, it is recommended that the effect of vegetation growth on slope stability to be evaluated. The effect of vegetation growth on SWCC and permeability function of soil, as well as the evapotranspiration flux boundary can be incorporated in the seepage analyses. Moreover, the effect of vegetation growth on soil strength can be incorporated in the slope stability analyses.

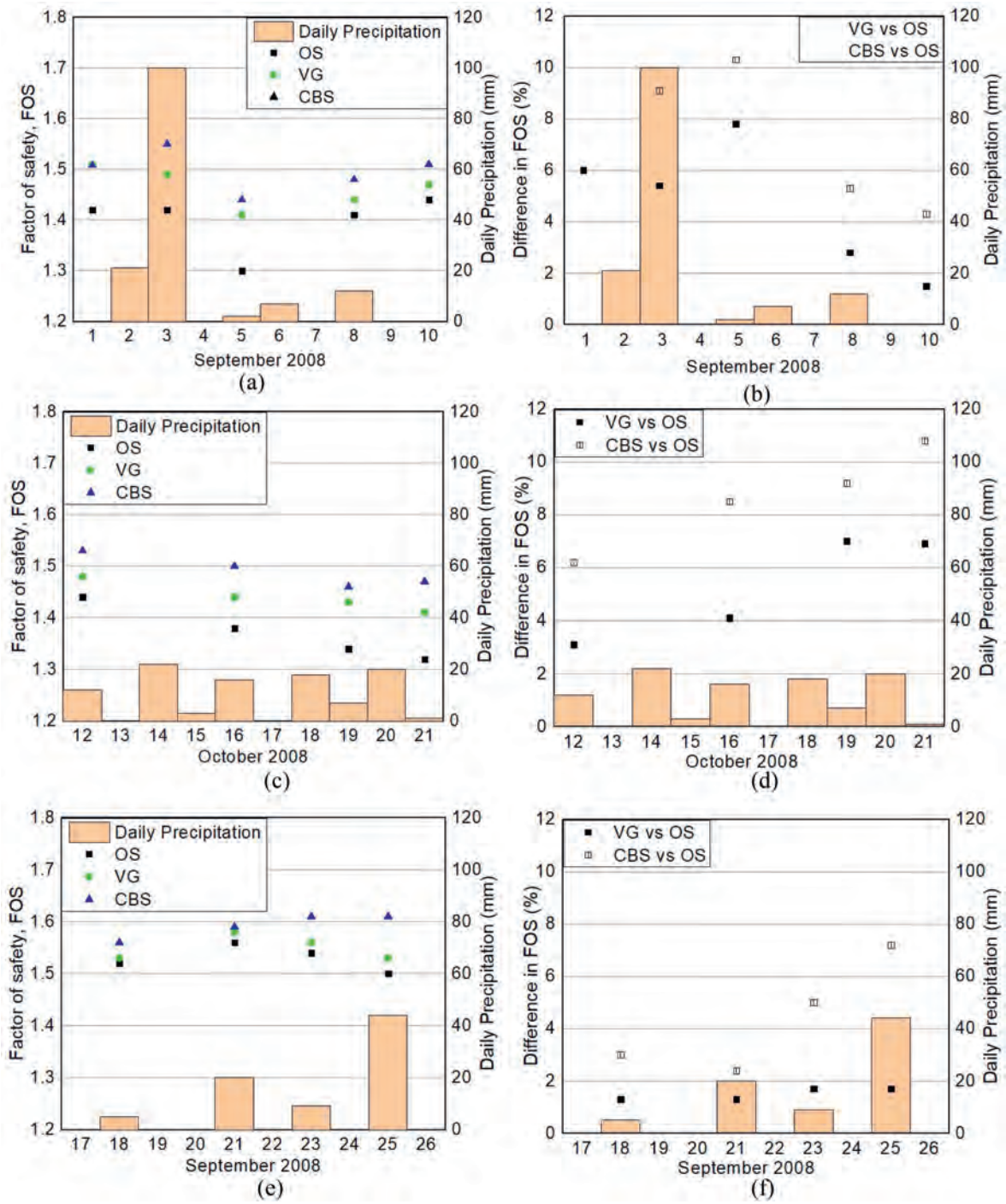

Fig. 16. The results of the FOS and difference in the FOS of the vegetated slope, CBS slope and original slope under the (a) (b) advanced rainfall pattern, (c) (d) normal rainfall pattern and (e) (f) delayed rainfall pattern.

Table 4
Comparison of effectiveness of CBS and Vetiver grass.

Max percentage of increase in the FOS compared to the original slope	Delayed rainfall pattern	Normal rainfall pattern	Advanced rainfall pattern
CBS (parametric studies)	25%	25%	20%
Vetiver Grass (parametric studies)	2.5%	4%	2.5%
Difference = CBS − Vetiver Grass (parametric studies)	22.5%	21%	17.5%
CBS (field)	7%	12%	11%
Vetiver Grass (field)	2%	7%	8%
Difference = CBS − Vetiver Grass (field)	5%	5%	3%

Declaration of competing interest

The authors declare that they have no known competing financial interests or personal relationships that could have appeared to influence the work reported in this paper.

Acknowledgement

This study was supported by the Housing and Development Board and Nanyang Technological University, Singapore.

References

Bishop, A. W. (1955). The use of the slip circle in the stability analysis of slopes. *Géotechnique, 5*(1), 7–17.

Brand, E. W., Premchitt, J., & Phillipson, H. B. (1984, September). Relationship between rainfall and landslides in Hong Kong. In *Proceedings of the 4th international symposium on landslides* (Vol. 1, pp. 377–384). Toronto: Canadian Geotechnical Society.

Comegna, L., Damiano, E., Greco, R., Guida, A., Olivares, L., & Picarelli, L. (2016). Field hydrological monitoring of a sloping shallow pyroclastic deposit. *Canadian Geotechnical Journal, 53*(7), 1125–1137.

Cuomo, S., Chareyre, B., d'Arista, P., Della Sala, M., & Cascini, L. (2016a). Micromechanical modelling of rainsplash erosion in unsaturated soils by Discrete Element Method. *Catena, 147*, 146–152.

Cuomo, S., & Della Sala, M. (2013). Rainfall-induced infiltration, runoff and failure in steep unsaturated shallow soil deposits. *Engineering Geology, 162*, 118–127.

Cuomo, S., Della Sala, M., & Novità, A. (2015). Physically based modelling of soil erosion induced by rainfall in small mountain basins. *Geomorphology, 243*, 106–115.

Cuomo, S., Della Sala, M., & Pierri, M. (2016b). Experimental evidences and numerical modelling of runoff and soil erosion in flume tests. *Catena, 147*, 61–70.

Forte, G., Pirone, M., Santo, A., Nicotera, M. V., & Urciuoli, G. (2019). Triggering and predisposing factors for flow-like landslides in pyroclastic soils: The case study of the lattari mts.(southern Italy). *Engineering Geology, 257*, Article 105137.

Fredlund, D. G., Morgenstern, N. R., & Widger, R. A. (1978). The shear strength of unsaturated soils. *Canadian Geotechnical Journal, 15*(3), 313–321.

Fredlund, D. G., & Rahardjo, H. (1993). *Soil mechanics for unsaturated soils*. John Wiley & Sons.

Fredlund, D. G., & Xing, A. (1994). Equations for the soil-water characteristic curve. *Canadian Geotechnical Journal, 31*(4), 521–532.

Fredlund, D. G., Xing, A., & Huang, S. (1994). Predicting the permeability function for unsaturated soils using the soil-water characteristic curve. *Canadian Geotechnical Journal, 31*(4), 533–546.

Geo-slope international Ltd. (2012a). *SEEP/W*. Calgary, Alberta, Canada: GEO-SLOPE International Ltd.

Geo-slope international Ltd. (2012b). *SLOPE/W*. Calgary, Alberta, Canada: GEO-SLOPE International Ltd.

Ghestem, M., Sidle, R. C., & Stokes, A. (2011). The influence of plant root systems on subsurface flow: Implications for slope stability. *BioScience, 61*(11), 869–879.

Greenwood, J. R., Norris, J. E., & Wint, J. (2004). Assessing the contribution of vegetation to slope stability. *Proceedings of the Institution of Civil Engineers-Geotechnical Engineering, 157*(4), 199–207.

Leong, E. C., & Rahardjo, H. (1997). Permeability functions for unsaturated soils. *Journal of Geotechnical and Geoenvironmental Engineering, 123*(12), 1118–1126.

Leung, A. K., Garg, A., & Ng, C. W. W. (2015). Effects of plant roots on soil-water retention and induced suction in vegetated soil. *Engineering Geology, 193*, 183–197.

Li, J. H., Du, L., Chen, R., & Zhang, L. M. (2013). Numerical investigation of the performance of covers with capillary barrier effects in South China. *Computers and Geotechnics, 48*, 304–315.

Meteorological Services Singapore. (2018). Past climate trends. http://www.weather.gov.sg/climate-past-climate-trends/.

Morris, C. E., & Stormont, J. C. (1999). Parametric study of unsaturated drainage layers in a capillary barrier. *Journal of Geotechnical and Geoenvironmental Engineering, 125*(12), 1057–1065.

Ng, C. W., Wang, B., & Tung, Y. K. (2001). Three-dimensional numerical investigations of groundwater responses in an unsaturated slope subjected to various rainfall patterns. *Canadian Geotechnical Journal, 38*(5), 1049–1062.

Ni, J. J., Leung, A. K., Ng, C. W. W., & Shao, W. (2018). Modelling hydro-mechanical reinforcements of plants to slope stability. *Computers and Geotechnics, 95*, 99–109.

Oh, S., & Lu, N. (2015). Slope stability analysis under unsaturated conditions: Case studies of rainfall-induced failure of cut slopes. *Engineering Geology, 184*, 96–103.

Pham, H. Q., Fredlund, D. G., & Barbour, S. L. (2005). A study of hysteresis models for soil-water characteristic curves. *Canadian Geotechnical Journal, 42*(6), 1548–1568.

Pirone, M., Papa, R., Nicotera, M. V., & Urciuoli, G. (2015). In situ monitoring of the groundwater field in an unsaturated pyroclastic slope for slope stability evaluation. *Landslides, 12*(2), 259–276.

Pradhan, A. M. S., & Kim, Y. T. (2015). Application and comparison of shallow landslide susceptibility models in weathered granite soil under extreme rainfall events. *Environmental Earth Sciences, 73*(9), 5761–5771.

Rahardjo, H., Leong, E. C., & Rezaur, R. B. (2008). Effect of antecedent rainfall on pore-water pressure distribution characteristics in residual soil slopes under tropical rainfall. *Hydrological Processes: International Journal, 22*(4), 506–523.

Rahardjo, H., Santoso, V. A., Leong, E. C., Ng, Y. S., & Hua, C. J. (2012). Performance of an instrumented slope covered by a capillary barrier system. *Journal of Geotechnical and Geoenvironmental Engineering, 138*(4), 481–490.

Rahardjo, H., Satyanaga, A., & Leong, E. C. (2013). Effects of flux boundary conditions on pore-water pressure distribution in slope. *Engineering Geology, 165*, 133–142.

Rahardjo, H., Satyanaga, A., Leong, E. C., Santoso, V. A., & Ng, Y. S. (2014). Performance of an instrumented slope covered with shrubs and deep-rooted grass. *Soils and Foundations, 54*(3), 417–425.

Rahimi, A., Rahardjo, H., & Leong, E. C. (2011). Effect of antecedent rainfall patterns on rainfall-induced slope failure. *Journal of Geotechnical and Geoenvironmental Engineering, 137*(5), 483–491.

Ross, B. (1990). The diversion capacity of capillary barriers. *Water Resources Research, 26*(10), 2625–2629.

Satyanaga, A., Rahardjo, H., & Hua, C. J. (2019). Numerical simulation of capillary barrier system under rainfall infiltration in Singapore. *ISSMGE International Journal of Geoengineering Case Histories, 5*(1), 43–54.

Schwarz, M., Preti, F., Giadrossich, F., Lehmann, P., & Or, D. (2010). Quantifying the role of vegetation in slope stability: A case study in tuscany (Italy). *Ecological Engineering, 36*(3), 285–291.

Sorbino, G., & Nicotera, M. V. (2013). Unsaturated soil mechanics in rainfall-induced flow landslides. *Engineering Geology, 165*, 105–132.

Stormont, J. C. (1996). The effectiveness of two capillary barriers on a 10% slope. *Geotechnical & Geological Engineering, 14*(4), 243–267.

Wang, K., Xu, Z. M., Tian, L., Ren, Z., Yang, K., Tang, Y. J., & Luo, J. Y. (2019). Estimating the dynamics of the groundwater in vegetated slopes based on the monitoring of streams. *Engineering Geology, 259*, Article 105160.

Xiong, X., Shi, Z., Xiong, Y., Peng, M., Ma, X., & Zhang, F. (2019). Unsaturated slope stability around the Three Gorges Reservoir under various combinations of rainfall and water level fluctuation. *Engineering Gceology, 261*, Article 105231.

Yan, C. G., Wan, Q., Xu, Y., Xie, Y., & Yin, P. (2018). Experimental study of barrier effect on moisture movement and mechanical behaviors of loess soil. *Engineering Geology, 240*, 1–9.

Zhai, Q., & Rahardjo, H. (2015). Estimation of permeability function from the soil–water characteristic curve. *Engineering Geology, 199*, 148–156.

Zhang, S., Zhang, X., Pei, X., Wang, S., Huang, R., Xu, Q., & Wang, Z. (2019). Model test study on the hydrological mechanisms and early warning thresholds for loess fill slope failure induced by rainfall. *Engineering Geology, 258*, Article 105135.

International Soil and Water Conservation Research 9 (2021) 419–432

Contents lists available at ScienceDirect

International Soil and Water Conservation Research

journal homepage: www.elsevier.com/locate/iswcr

Original Research Article

The soil configuration on granite residuals affects Benggang erosion by altering the soil water regime on the slope

Xiaoqian Duan, Yusong Deng, Yu Tao, Yangbo He, Lirong Lin, Jiazhou Chen*

Key Laboratory of Arable Land Conservation (Middle and Lower Reaches of Yangtze River) of the Ministry of Agriculture, College of Resources and Environment, Huazhong Agricultural University, Wuhan, 430070, People's Republic of China

ARTICLE INFO

Article history:
Received 23 October 2020
Received in revised form
6 February 2021
Accepted 17 March 2021
Available online 27 March 2021

Keywords:
Gully erosion
Saturated hydraulic conductivity
Water retention capacity
Shear strength
VADOSE/W model

ABSTRACT

A permanent collapsing gully, locally called Benggang, formed on slopes with deep granite red soil and is a type of unique gully erosion widely prevalent in southern China. Three different soil configurations (SC), ie, red-transition-sandy (SC I, the transition is the soil layer between the red soil and the sandy soil layer), transition-sandy (SC II) or sandy (SC III) are usually present in the soil profile of the Benggang slope. However, little attention has been paid to impacts of SCs on the triggering of Benggang erosion. In this study, we aimed to explore the relationships between soil water content (SWC) and triggering of Benggang erosion under different SC conditions. The soil properties of different soil layers were measured and the SWC at depths of 20, 40, 60, and 80 cm were monitored at 5-min intervals along a typical Benggang (SC I) during 2016–2018. The SWC of Benggang slopes with different SCs were simulated by VADOSE/W model. Results showed that the red soil layer had a higher water retention capacity and shear strength than the sandy soil layer. Even if the SWC is higher (e.g., 0.42 cm^3/cm^3) at red soil layer or transition layer, the corresponding shear strength is greater than that of sandy soil layer with a lower SWC (e.g., 0.32 cm^3/cm^3). Relationships between shear strength and SWC of different soil layers indicate that Benggang erosion is triggered by an increase in the SWC in the deep sandy layer. Results also showed that differences exist in the SWC distribution among the different SCs. The SWC is higher in topsoil than in deeper soil in SC I and SC II, while in SC III, the opposite trend is observed. These results revealed that the presence of the red soil or transition layer can reduce the infiltration of rainwater into the deep sandy layer, thus can reduce the possibility of collapse. Our results show that the SC affects the stability of the headwall, and results provide great significances to guide the mitigation of Benggang erosion.

1. Introduction

Gully erosion, in which runoff water accumulates and removes soils from gully areas, is one of the main soil erosion types and is a major source of sediment at the small-watershed and regional scales (Bingner et al., 2016; Chen et al., 2013; Momm et al., 2015; Wells et al., 2013). The triggering of gully erosion commonly requires a large drainage area and is attributed to flow from surface runoff and seepage, which is concentrated into channels and rills. Over time, these features enlarge into deep trenches in the land surface, resulting in headwall retreat (collapse) (Amare et al., 2019; Arabameri et al., 2019; Qin et al., 2018; Thomas et al., 2009; Vanwalleghem et al., 2005; Chaplot et al., 2013).

A special type of gully erosion, associated with a permanent collapsing gully on a low hillslope developed from granite red soil, is present in South China, and locally called Benggang (Zhong et al., 2013). As an erosion landform, Benggang is partially similar to "Badland" in southeast Spain, and other areas in the world, and both types of soil erosion are closely related to high intensity rainfall (Cerdà, 1999). However, the material conditions and development mechanism of their formation are not completely consistent (Xu, 1996). In addition, the Benggang is also similar to the soil erosion occurring in other areas in the world, such as the "Lavaka" in Madagascar in southern Africa (Cox et al., 2010;

* Corresponding author. College of Resources and Environment, Huazhong Agricultural University, Wuhan 430070, China.
E-mail addresses: duanxq@webmail.hzau.deu.cn (X. Duan), dennyus@163.com (Y. Deng), 389801805@qq.com (Y. Tao), kathy@mail.hzau.edu.cn (Y. He), lrlin@mail.hzau.edu.cn (L. Lin), jzchen@mail.hzau.edu.cn (J. Chen).

https://doi.org/10.1016/j.iswcr.2021.03.003

Voarintsoa et al., 2012), the "Vocoroca" in southeastern Brazil (Bacellar er al., 2005), "Calanchi" in Italy (Caraballo-Arias et al., 2014; Neugirg et al., 2016) and "Crumbling" in Japan (Lin, 2008, pp. 1–293). All of them are deeply collapsed gullies under the action of precipitation in deep soil conditions.

Previous results show that the most important causes of Lavaka, Benggang, and other erosional gullies worldwide are water erosion (fluvial shearing process) and gravity erosion (gravitational shearing process) (Vanwalleghem et al., 2005; Wells et al., 2013). Gully erosion is mainly triggered by the erosion induced by surface runoff, which causes the gully head to retreat in the process of river shearing, and this process usually requires a large drainage area (Qin et al., 2018; Thomas et al., 2009; Chaplot et al., 2011). However, the drainage area of a Benggang can be small or even nonexistent, and the headwall can retreat (collapse) regardless of the upper slope drainage area, eventually reaching the ridge of the slope (Deng et al., 2018; Jiang et al., 2014). Thus, the gravitational shearing process has an important influence on the triggering of Benggang erosion. At present, most of the research on Benggang erosion has focused on the water erosion process, with emphasis on the surface water sediment movement and runoff characteristics. It is believed that surface processes, such as rainfall and surface runoff, wash away the drainage area, promoting the development of Benggang erosion (Jiang et al., 2014; Wang et al., 2016). Due to the complex causes of gravity erosion and the many factors affecting gravity erosion, research on gravity erosion has been paid little attention, and the influence of the alteration of the soil water content on gravity erosion remain poorly constrained (Thiemann et al., 2005; Wen et al., 2015; Xue et al., 2009).

The alteration of soil water content has an important impact on shear strength (Horn, 2003), which is an important component influencing a soil's resistance to erosion and the headwall stability. An increase in the soil water content leads to a decrease in the shear strength and is thus a driving force for the formation of mass movements and headwall retreat, affects the process of gravity erosion, which can lead to the development of Benggang erosion (Fox & Willson, 2010; Rachman et al., 2003; Stefano et al., 2013; Wuddivira et al., 2013). These phenomena indicate that apart from the effects of surface runoff, the alteration of soil water content is the most important trigger of Benggang erosion.

Previous results show that the alteration of soil water content are influenced by soil properties, such as particle size distribution, bulk density, hydraulic conductivity, and differences in soil configuration (Assouline, 2013; Beven & Germann, 2013; Buczko & Gerke, 2005; Rahardjo et al., 2012; Wang et al., 2014; Yang et al., 2006). Different soil configurations lead to the variation of soil properties, which result in different alterations in soil water content (Li et al., 2014; Cui et al., 2018). In addition to the influence of soil properties on soil water content, shear strength, is also affected by soil properties and exhibits significant heterogeneity under different soil configurations (Lin et al., 2018; Wuddivira et al., 2013; Zhang et al., 2018). And different trends in the relationship between soil water content and shear strength properties have been reported for different soil configurations (Al-Shayea, 2001; Fan & Su, 2008; Hoyos et al., 2014; Rahardjo et al., 2012). These findings indicate that the impact of soil configurations on alterations in soil water content and shear strength and their relationships plays an important role in the formation of Benggang erosion. Similarly, related studies indicate that Lavaka formation is closely related to soil properties and water status (Voarintsoa et al., 2012). Obviously, it is essential to pay attention to the impact of soil configurations on gully erosion.

Soil has a heterogeneous soil profile in the vertical direction, and it is easy to produce different soil configurations in the process of soil erosion. For example, granite red soil has soil profiles that are commonly heterogeneous, with different soil properties and hydraulic properties in individual layers (Tao et al., 2017; Gui and Zhu, 2018; Wei et al., 2018). There are three types of layers exposed to the surface after long-term water erosion: a red soil layer, a transition layer (the red soil layer has been eroded), and a sandy soil layer (the red soil layer as well as the transition layer have been eroded). Therefore, Benggang, which develops from granite red soil, generally has three different soil configurations: red-transition-sandy, transition-sandy and sandy. Some studies have focused on the relationship between soil configurations and Benggang erosion. These works have shown that the shear strength decreases with increasing profile depth (Wei et al., 2019), the suction stress of the lower soils is significantly lower than that of the upper soils under the same matric suction (Deng et al., 2018), the abundance of sandy particles in the lower soils is higher than that in the upper soils (Deng et al., 2015; Liao et al., 2019), and the saturated hydraulic conductivity is high in the red soil layer and sandy soil layer and low in the transition layer (Duan et al., 2018). Thus, the soil properties vary among the different soil layers in Benggang slopes, and variations in these properties influence Benggang development. However, most of these studies focused on a certain soil property, without considering the impact of the spatial distribution of these properties on Benggang erosion, the comprehensive impacts of different soil configurations on the triggering of Benggang erosion are unclear.

We hypothesize that different soil configurations promote gully erosion to a great extent by affecting the soil water content distribution. The main objectives of this study were to (1) monitor the effect of alterations of soil water content on typical Benggang (with a red-transition-sandy soil configuration), events Benggang erosion and (2) simulate the effect of alterations of soil water content on different soil configurations of a Benggang slope by using the VADOSE/W model to exactly reveal this effect. These results can provide useful information on the conditions that trigger gully erosion in different soil configurations and reveal the mechanism of gully erosion.

2. Materials and methods

2.1. Description of the experimental site and soil sampling

The experimental site is located in Tongcheng County, Hubei Province (113°46′18″E, 29°20′05″ N). This county features a subtropical monsoon climate, with an average annual temperature of 15.5–16.7 °C. The annual precipitation is 1450–1600 mm, and most of the rainfall occurs from March to September. The zonal soil is derived from granite residues and is classified as an Utisol (Soil Taxonomy of the US) or red soil, as it is locally called. The land use pattern is the mixture of sparse secondary grass and shrub composed mainly of *Dicranopteris linearis*. The Tongcheng granite formed during the Yanshanian and the thickness of the granite weathering crust in this area is more than 10 m (Xu, 1996). Gradational variations in the pedogenic differentiation of granite-derived soils with depth can be observed on the basis of soil texture and color from the surface downwards, and the soil can be divided into four layers: the surface soil layer, the red soil layer, the transition layer, and the sandy soil layer (Deng et al., 2017).

Under the rainy climate and mountainous topography in Tongcheng County, 1102 Benggang slopes have actively developed in this region. Due to different degrees of water erosion of the topsoil, the vertical combination of soil layers differs. On some Benggang slopes, the red soil layer has been eroded, and the transition layer is exposed due to erosion by surface runoff. On some Benggang slopes, the red soil as well as the transition layers have been eroded, and the sandy soil layer is exposed. Therefore, according to the

combination of soil layers in the vertical profile, there are three different SCs of Benggang soil according to the degree of erosion: red-transition-sandy (SC I, intact granitic soil profile), transition-sandy (SC II, the red soil layer has been eroded) and sandy (SC III, the red soil layer as well as the transition layer have been eroded). The SC I with a intact granitic soil profile and is naturally formed in the process of soil occurrence. Unlike those in SC I, the soil profiles of SC II and SC III are not complete, and they are formed in places with large erosion or after artificial damage, resulting in a sparse distribution.

For typical soil sampling in the field, we selected the Benggang slope with a intact granitic soil profile (SC I: red-transition-sandy) as the sampling site. The hillslope is 35 m in length from the headwall to the dividing ridge, and the average slope of the watershed is 35°. According to transitions in color and texture, the four soil layers on the granite slope of the test site are further divided into 10 sublayers from top to bottom: surface layer I (0–15 cm), surface layer II (15–25 cm), red soil layer I (25–65 cm), red soil layer II (65–125 cm), red-transition layer (125–165 cm), transition layer (165–195 cm), transition-sandy layer (195–225 cm), sandy soil layer I (225–255 cm), sandy soil layer II (255–400 cm), and strongly weathered layer (>400 cm) (Fig. 1).

Considering the accessibility of soil sampling in the field, we selected samples at the lower slope position near the headwall (the distance to the ridge of the slope was 28 m). To clarify the physical properties of different soil layers in the vertical profile of the Benggang slope, soil samples were collected from the surface to the deep soil layer in the vertical profile according to the above mentioned soil layer division method using an environment sampling instrument (GeoProbe 54DT, GEOPROB Co., Ltd, America). Cutting ring soil samples were collected from the ten different layers by the GeoProbe 54DT, and the basic physical properties and hydraulic properties of the soil were measured. Additionally, cutting ring soil samples (height 20.0 mm and inner diameter 61.8 mm) were collected from red soil layer I, the transition layer, and sandy soil layer I to measure the shear strength. Approximately 1~2 kg of the scattered soil samples was collected from red soil layer I, the transition layer, and sandy soil layer I for the analysis of the soil Atterberg limits (liquid limit and plastic limit).

2.2. Determination of soil properties

The bulk density (BD) was determined using a cutting ring and the dry weighing method (dried at 105 °C), the total porosity (TP) was calculated by BD and PD (soil particle density) as TP = 1 - (BD/PD) (Cerdà & Doerr, 2010). The particle size distribution was determined using the sieve and pipette method, and soil particles were divided into three sizes: sand (2–0.05 mm), silt (0.05–0.002 mm), and clay (<0.002 mm) (Gee et al., 1986). According to the textural classification of the United States Department of Agriculture, the results were expressed in terms of clay loam, loam, sandy loam, loamy sand and sand. Saturated hydraulic conductivity (K_s) was measured by the cutting ring constant head method in the laboratory, and the hydraulic head was 9.88 cm. The aeration porosity (>0.015 mm) and capillary porosity (0.015–0.0002 mm) and soil water retention curve (SWRC) were determined using high speed centrifuge (GR21G, HITACHI). For the detailed process of determination, we refer to the operation method of Khanzode et al. (2002). Soil Atterberg limits (liquid limit and plastic limit) were determined using the air-dried soil for each layer according to the cone penetrometer and the thread roll method (Stanchi et al., 2012). For a detailed discussion of the measurement process refer to Deng et al. (2017).

Five soil water contents (SWCs) of the soil samples were applied for the shear strength test: 0.15, 0.20, 0.25, 0.35, and 0.45 cm^3/cm^3 for the red soil layer I; 0.10, 0.15, 0.25, 0.35, and 0.40 cm^3/cm^3 for the transition layer; 0.05, 0.15, 0.25, 0.35, and 0.40 cm^3/cm^3 for the sandy soil layer I. Three replicate soil samples were conducted for each SWC. To maintain a constant hydraulic stress path, all the core samples were placed in stacked saturators and fully saturated before testing. The saturated samples were dehydrated uniformly in a container with constant temperature (25 °C) and humidity (40%) under continuous weight monitoring until approximately reaching the designed water content. Then, the target soil samples were placed into an airtight container for 24 h to attain moisture equilibrium and used for the shear strength testing by the quadruple direct shear apparatus (LH-DDS-4, Nanjing TKA Technology Co., Ltd, Shanghai, China). The shear rate is 4 r/min, and the coefficient of measuring ring is C = 1.541 kPa/0.01 mm and the shear tests were conducted under four effective con-fining stresses (σ= 50, 100, 150 and 200 kPa) (Rahardjo et al., 2012). According to the Mohr-Coulomb failure criterion (Fredlund & Rahardjo, 1993), the cohesion strength and internal friction angle were calculated as follows:

$$\tau = c + \sigma \tan \varphi \quad (1)$$

Where τ is the limit shear strength (kPa); c is the cohesion strength (kPa); σ is the effective normal stress on soil (kPa); and φ is the internal friction angle (°).

2.3. Monitoring of the SWC on the test Benggang slope

To obtain the alteration of SWC on the test Benggang slope (SC I: red-transition-sandy), two parallel zones above the headwall along the slope were carefully chosen as soil water monitoring sites. To follow the general method of monitoring slope water distribution and the possible differences in soil water content of the three sites (upper, middle, and lower slope sites) were considered. Therefore, to obtain an accurate record of the water distribution in the Benggang slope, three soil water monitoring sites were set up at three slope sites (upper, middle, and lower slope sites) and their distances to the ridge of the slope were 18 m, 24 m and 28 m, respectively. To install the soil moisture sensor, a pit (40 × 20 × 80 cm) was carefully excavated to ensure the least disturbance to the soil at each site, with the 40 cm-length side oriented along the hillslope. Four soil sensors (WS SMEC 300 SM/EC/Temp Sensor, Spectrum Technologies, Inc.) were installed horizontally to obtain the soil profiles at depths of 20, 40, 60, and 80 cm and were connected to a datalogger (Watchdog 2400, Spectrum Technologies, Inc.) at each site. The sensors were 7 cm in length and were calibrated before installation. Further experimental observations showed that with increasing distance from the headwall, the clay content increased, the aeration porosity decreased (Tao et al., 2017). Therefore, K_s gradually decreasing with increasing distance from the headwall (Duan et al., 2018). The K_s reflects the soil infiltration and seepage properties affect the migration of water in soil and controls soil water dynamics (Bonsu, 1992; Rezaei et al., 2016). Combining this information with the results of previous research on the influence of texture and K_s on the water distribution, setting monitoring sites at different locations on the slope was suitable. A rain gauge was also placed beside the slope. The instrument installation was performed in June 2015. After seven months of test runs, the SWC values at all sites were recorded at 5-min intervals from January 2016 to December 2018.

Two Benggang erosion initiation events occurred in 2016–2018, and both were recorded in the experiment. During the initiation of Benggang erosion, the soil failed at the headwall, and the gully retreated (collapsed). The first event occurred on June 2, 2016, and

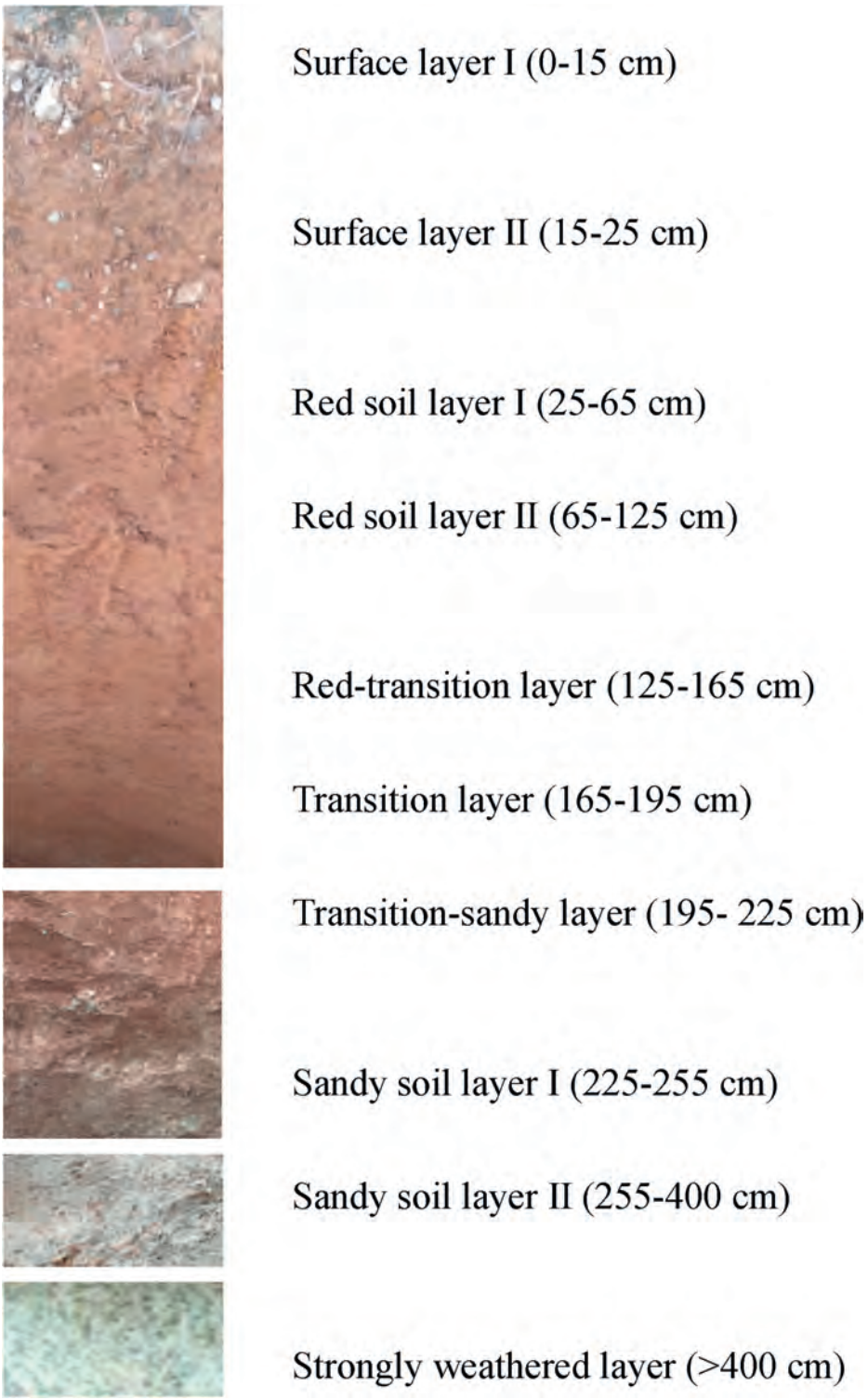

Fig. 1. Soil configuration of intact granite red soil (SC I, red-transition-sandy). The soil profile can be divided into four soil layers and further divided into 10 sublayers from top to bottom:surface layer (I and II), red soil layer (I and II), transition layer (red-transition layer, transition layer, transition-sandy layer), and sandy soil layer (I, II and strongly weathered layer). The topsoil layer is easily eroded by water erosion, so there are two other soil configurations (SCs) of Benggang soil: transition-sandy (SC II, the red soil layer has been eroded) and sandy (SC III, the red soil layer as well as the transition layer have been eroded).

the gully retreated by 0.5 m; the second event occurred on June 23, 2017, and the gully retreated by 0.6 m. Both events were triggered by heavy rainfall, with an accumulated amount of more than 105 mm in 24 h, and high antecedent soil water content (ASWC), with values of 0.39, 0.36, and 0.32 cm^3/cm^3 in the upper slope, middle slope, and lower slope, respectively. No Benggang erosion was triggered under other conditions (when the conditions of a high ASWC and heavy rainfall were not met).

2.4. Simulation of the SWC of three SC Benggang slopes

To obtain the alteration of the SWC under more soil configurations, the SWCs of three SCs Benggang slopes (SC I: red-transition-sandy, SC II: transition-sandy, SC III: sandy) were evaluated by finite element analysis using the two-dimensional seepage VADOSE/W model.

VADOSE/W can mathematically simulate the real physical process of water flowing through a particulate medium; the program is formulated on the basis that the seepage, heat, vapor, and gas flow through both saturated and unsaturated soil follows an appropriate form of a Darcy-type flow law, and a solution is obtained by the finite element method. In VADOSE/W, all meshing is fully automatic, the size of the elements for the entire mesh can be altered at a global level (Geo-Slope International Ltd, 2014). VADOSE/W plays an important role in seepage analysis and can be formulated for simultaneous application under hydraulic, thermal and gas transfer boundary conditions (Garg & Ng, 2015; Zhang et al., 2016; Zhao et al., 2017).

The three soil configurations were established in the VADOSE/W model. For the three SC Benggang slopes established in the model, the slope was 35 m in length from the headwall to the dividing ridge, and the average slope of the watershed was 35°; these conditions were all consistent with the Benggang test slope (SC I). The soil properties used in the model were established according to the measurement results from the test Benggang slope. The input data for places where no actual measurements existed were established by linear interpolation. Only the soil layers in the direction of the vertical profile are different between different SCs in the VADOSE/W. For SC I, the texture and thickness of different soil layers were completely consistent with the test Benggang slope: the first layer is composed of a surface layer with an average thickness of 25 cm (the thicknesses of surface layers I and II were 15 and 10 cm, respectively); the second layer consisted of a red soil layer with an average thickness of 100 cm (the thicknesses of red soil layers I and II were 40 and 60 cm, respectively); the third layer is composed of a transition layer with an average thickness of 100 cm (the thicknesses of the red-transition layer, transition layer, and transition-sandy layer were 40, 30, and 30 cm, respectively); and the layer underneath the third was composed of a sandy soil layer (the thicknesses of sandy soil layers I and II were 30 and 145 cm, respectively, and underneath them was a strongly weathered layer) (Fig. 2). For SC II, we divided the soil into two layers: the first layer was composed of a transition layer with an average thickness of 100 cm (the thicknesses of the red-transition layer, transition layer, and transition-sandy layer were 40, 30, and 30 cm, respectively), and the layer underneath the second was composed of a sandy soil layer (the thicknesses of sandy soil layers I and II were 30 and 145 cm, respectively, and underneath them was a strongly weathered layer). For SC III, the topsoil to deep soil consisted of sandy soil layer I.

The adaptive time stepping method and a mesh of 0.5 m elements were used during the simulations for SC I, SC II, and SC III. The domain was discretized as a finite element mesh comprising 3650 elements.

The upper and right boundaries of the model are the climatic boundaries, and the VADOSE/W climate boundary condition calculates evaporation from unsaturated soil using the Penman-Wilson equation (Wilson et al., 1994). The boundary between the granite bedrock and accumulation was set as the lower boundary, and the lower boundary was defined as the free drainage boundary, while the left boundary was set as the zero flow boundary in the model. We specified the initial conditions directly by using the draw initial water table command in VADOSE/W.

The calibration of the model was based on a comparison between the SWCs of the simulated results for SC I and the time domain reflectometry (TDR) monitoring results on the test Benggang slope at four soil depths (20, 40, 60, and 80 cm) and three slope positions (upper, middle, and lower slope) under different climatic conditions. We selected the three climatic conditions of drought (rainfall of 0 mm in 24 h), light rain (rainfall of 0.1–9.9 mm in 24 h) and heavy rain (rainfall of 100.0–249.9 mm in 24 h) to compare the results of the model with the monitoring results. The simulation effect was verified using R^2 (coefficient of determination), RE (relative error), and RMSE (root mean squared error) as evaluation indexes. The simulation showed high accuracy, with an RE range of 1.40–6.13%, an R^2 range of 0.88–0.99 and an RMSE range of 1.03×10^{-2}-2.42×10^{-2}.

After correcting of the model, we simulated the alteration of SWC of different SC Benggang slopes under different conditions. Gully erosion becomes more active during heavy rainfall (Dehotin et al., 2015; Ries et al., 2017; Wang et al., 2018), and according to the actual meteorological data, we selected two high-rainfall conditions (rainfall is 54 and 143 mm) conditions. ASWC can affect the partitioning of rainwater into infiltration, consequently influencing runoff and soil erosion (Zonta et al., 2012). We selected two different ASWC conditions (ASWC is 0.24, and 0.36 cm^3/cm^3) conditions for simulation. We selected a total of 4 conditions that can trigger the Benggang erosion for the simulations.

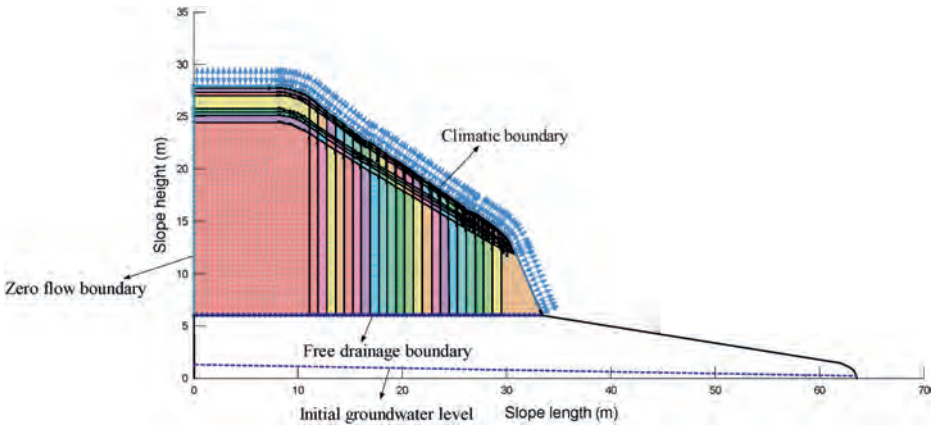

Fig. 2. The two-dimensional structure of a typical intact configuration (SC I) Benggang slope and the element division and boundary conditions in VADOSE/W simulation. The domain was discretized as a finite element mesh comprising 3650 elements. The soil properties used in the model were established according to the measurement results from the test Benggang. SC II, SC III and SC I are the same except for the soil layers material division (No red soil layer in the SC II, no red soil and transition layer in the SC III).

2.5. Analysis of data

Each soil sensor registered soil water measurements daily. The real-time data were used to demonstrate the soil water dynamics during heavy rainfall events, and the rainfall was determined as the total rainfall per hour. The simulated SWC results at depths of 0.3 m, 2 m, and 4 m were selected in SC I, SC II, and SC III for analysis, and the SWC after the end of a rainfall event was selected. The relationships between SWC and cohesion strength (c), and between SWC and internal friction angle (φ) were fitted with nonlinear regression equations.

3. Results

3.1. Soil hydraulic and mechanical properties of different SC Benggang slopes

With an increase in depth, the clay content (particle size<0.002 mm) gradually decreases, the soil texture gradually increased with soil depth as the texture transitioned from clay to sand (Table 1). The aeration porosity (>0.015 mm) in the transition layer are obviously lower than those in the red and sandy soil layers. Combine with Fig. 3 and Fig. 4, the red soil layer with high clay content and aeration porosity had high K_s and water retention capacity; the transition layer with high clay content and lower aeration porosity had the lowest K_s values and larger soil water retention capacity; the sandy soil layer with high sand content and aeration porosity had higher K_s and poor soil water retention capacity. That is the K_s first decreases then increases with increasing soil depth, and the red soil layer and transition layer have a larger soil water retention capacity than the sandy soil layer. And the differences in soil properties are mainly divided into three categories: the red soil layer (including red soil layer I and red soil layer II), transition layer (including the red-transition layer, transition layer, and transition-sandy layer) and sandy soil layer (including sandy soil layer I, sandy soil layer II, and the strongly weathered layer). Therefore, we only measured the shear strength, liquid limit and plastic limit of red soil layer I, the transition layer and sandy soil layer I.

As shown in Fig. 5 and Fig. 6, the cohesion strength (c) and internal friction angle (φ) of red soil layer I, the transition layer, and sandy soil layer I decrease with increasing SWC values. The relationships between cohesion strength and SWC in the red soil layer, transition layer and sandy soil layer are $c = -85.14\ln(swc) - 58.04$ ($R^2 = 0.95$), $c = -41.63\ln(swc) - 12.76$($R^2 = 0.85$), and$c = -15.72\ln(swc) - 2.91$ ($R^2 = 0.94$), respectively. The relationships between friction angle and SWC in the red soil layer, transition layer and sandy soil layer are $\phi = 56.07e^{(-SWC/0.16)} + 20.9$($R^2 = 0.99$), $\phi = 22.22e^{(-SWC/0.20)} + 20.79$ ($R^2 = 0.97$) and$\phi = 56.07e^{(-SWC/2.25)} - 79.35$ ($R^2 = 0.99$) in the red soil layer, transition layer and sandy soil layer, respectively. When the SWC of the red soil layer is 0.40 cm^3/cm^3, the internal friction angle is 26.25°, and the cohesion is 18.49 kPa; when the SWC of the transition layer is 0.40 cm^3/cm^3, the internal friction angle is 21.84°, and the cohesion is 23.12 kPa; and when the SWC of the sandy soil layer is 0.40 cm^3/cm^3, the internal friction angle is 21.84°, and the cohesion is 12.84 kPa. These results show that the cohesion strength and internal friction angle of sandy soil layer I (which has a low clay content) are less than those of red soil layer I and the transition layer (which have a higher clay content). Interestingly, as shown in Fig. 7, when the SWC of red soil layer I and the transition layer is higher (e.g., 0.42 cm^3/cm^3), the corresponding shear strength is greater than that of sandy soil layer I at a lower SWC (e.g., 0.32 cm^3/cm^3). Furthermore, the increase in shear strength is directly proportional to the increase in effective normal stress in a specific range of SWCs. The increase in shear strength caused by normal pressure at low SWC is more obvious than that at high SWC.

As shown in Table 2, the liquid limit and plastic limit of red soil layer I are 0.83 cm^3/cm^3 and 0.45 cm^3/cm^3, respectively; the liquid limit and plastic limit of the transition layer are 0.64 cm^3/cm^3 and 0.36 cm^3/cm^3, respectively; and the liquid limit and plastic limit of sandy soil layer I are 0.48 cm^3/cm^3 and 0.30 cm^3/cm^3, respectively. Obviously, the type and amount of clay govern the liquid and plastic limits of the soil; the higher the clay content is, the greater the liquid and plastic limits. The liquid limit and plastic limit of red soil layer I and the transition layer (which have a high clay content) are higher than those of sandy soil layer I (which has a lower clay content).

Table 1
Basic physical properties of soil in the test Benggang slope.

Soil layer		Sample collected depth (cm)	Bulk density (g/cm^3)	Saturated water content (cm^3/cm^3)	Aeration porosity (%)	Capillary porosity (%)	Particle size distribution (%)			Texture
					>0.015 mm	0.015 −0.0002 mm	2 −0.05 mm	0.05 −0.002 mm	<0.002 mm	(USDA)
Surface layer	Surface layer I	15	1.25	0.53	10.33	13.09	44.06	19.98	35.96	Clay loam
	Surface layer II	25	1.41	0.47	5.11	15.63	36.06	43.96	19.98	Loam
Red soil layer	Red soil layer I	65	1.43	0.46	4.23	16.23	40.06	31.97	27.97	Clay loam
	Red soil layer II	125	1.40	0.47	1.94	14.29	44.00	28.00	28.00	Clay loam
Transition layer	Red -transition layer	165	1.37	0.48	1.73	19.62	48.00	28.00	24.00	Loam
	Transition layer	195	1.41	0.47	1.58	18.84	52.05	31.97	15.98	Sandy loam
	Transition-sandy layer	225	1.41	0.47	1.93	23.61	60.00	24.00	16.00	Sandy loam
Sandy soil layer	Sandy soil layer I	255	1.40	0.47	2.57	26.61	76.02	19.98	4.00	Loamy sand
	Sandy soil layer II	400	1.42	0.46	2.64	28.96	73.05	24.00	2.95	Loamy sand
	Strongly weathered layer	2000	1.45	0.45	4.34	28.04	90.00	8.00	2.00	Sand

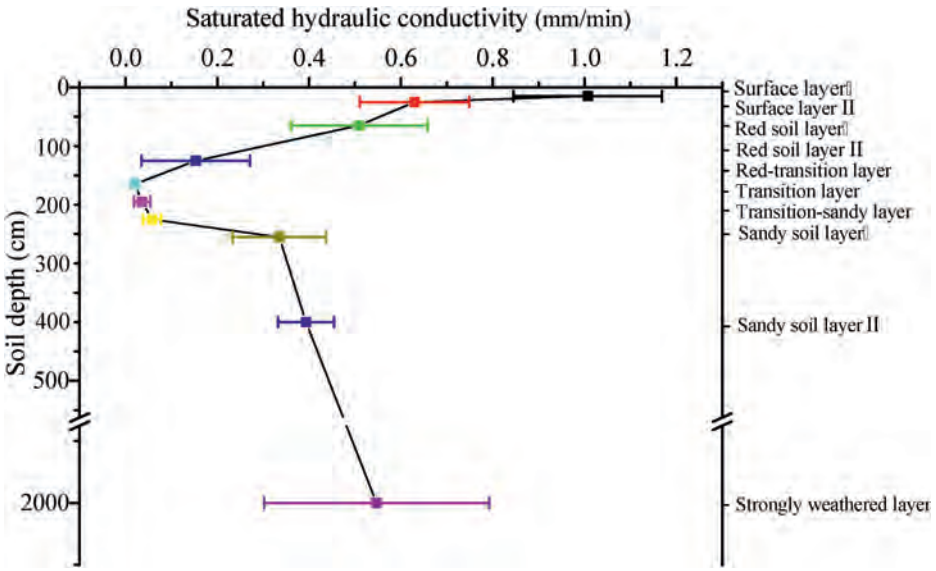

Fig. 3. Saturated hydraulic conductivity (K_s) at different soil layers in the test Benggang slope. Soil samples were collected from ten different soil layers and the depth of each soil samples was shown in Table 1.

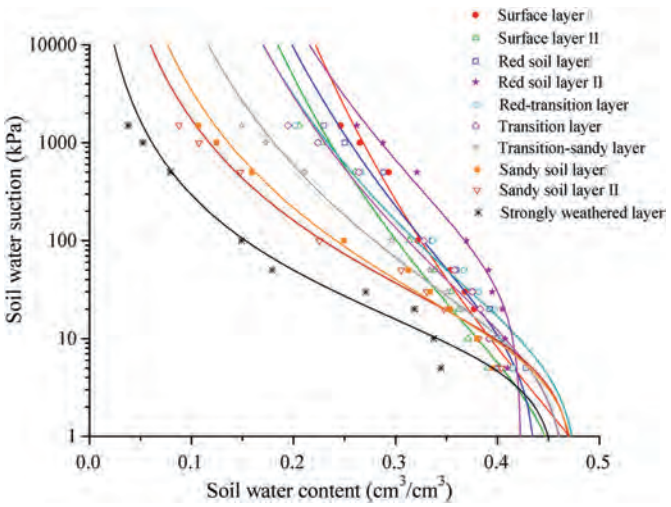

Fig. 4. Soil water retention curve (SWRC) for the different soil layers. Soil samples were collected from ten different soil layers and the depth of each soil samples was shown in Table 1.

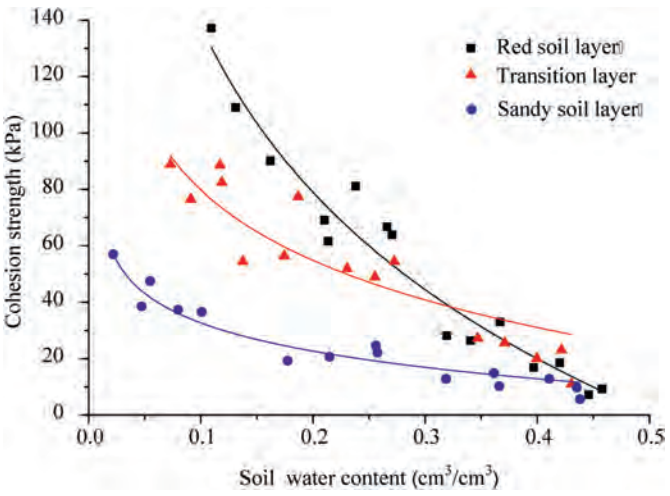

Fig. 5. Cohesion strength of different soil layers (red soil layer I, transition layer, and sandy soil layer I) with different soil water contents.

3.2. Monitoring results of the SWC during Benggang erosion triggering on the test Benggang slope (SC I)

At the initiation of Benggang erosion, the SWC obviously increases at the four soil depths (20, 40, 60, 80 cm) and at the three slope sites (upper, middle, and lower slope) (Fig. 8). The SWC at the four soil depths increased rapidly at the same time, and the average SWCs at the four soil depths were 0.40, 0.38, and 0.34 cm^3/cm^3 at the upper, middle, and lower slope sites, respectively. The SWC at the lower slope site was less than those at the middle and upper slope sites at the four soil depths during the initiation of Benggang erosion.

3.3. Simulation results of SWC on different SC Benggang slopes

As shown in Figs. 9–11, even under the same rainfall and ASWC amounts, the alteration of the SWC in the vertical profile and among the slope positions in the horizontal direction differs among the three Benggang slopes with different SCs. In the vertical profile, a similar trend in SWC behavior is observed for SC I and SC II-the SWC is higher in topsoil than in deeper soil-while SC III has the opposite trend. Among the three Benggang slopes with different SCs, the SWC of the deep sandy layer of SC I is lower than that of SC II and SC III under the same conditions. The SWC of the deep sandy layer of SC I varies greatly under different conditions. In detail, when the ASWC is 0.24 cm^3/cm^3 and the rainfall is 54 and 143 mm, the SWC at the sandy soil layer is lower than 0.32 cm^3/cm^3, and when the ASWC is 0.36 cm^3/cm^3 and the rainfall is 54 and 143 mm, the SWC at the sandy soil layer obviously increases, especially near the headwall, with SWC values close to 0.40 cm^3/cm^3. Among the slope positions, for SC I, the SWC at the red soil layer in the lower slope is lower than that at the middle and upper slopes. For SC II and SC III, the SWC is basically evenly distributed along the slope. In addition, the SWC of the deep sandy layer of all three SCs slopes position is higher at the lower slope position than at the middle and upper slope positions.

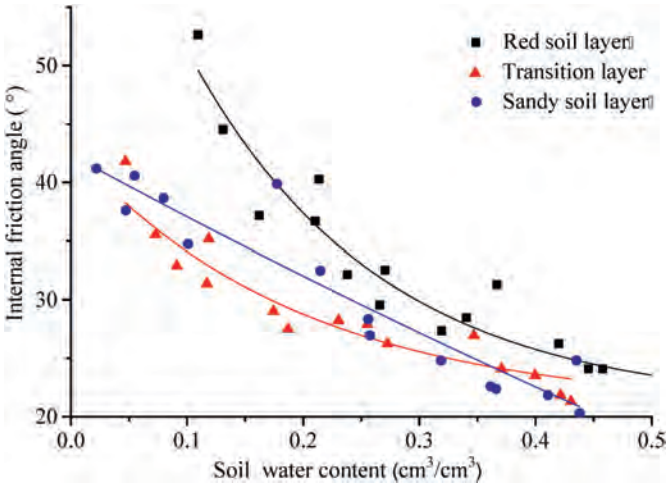

Fig. 6. Internal friction angle of different soil layers (red soil layer I, transition layer, and sandy soil layer I) with different soil water contents.

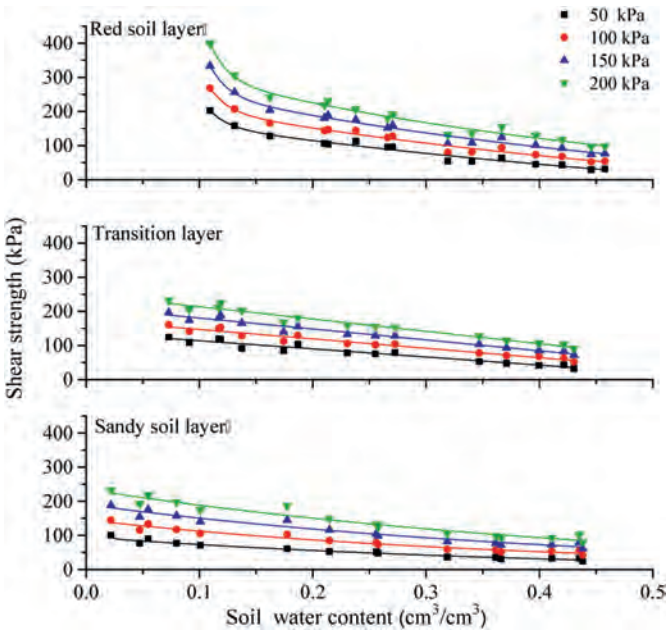

Fig. 7. Shear strength with soil water content for different soil layers (red soil layer I, transition layer, and sandy soil layer I) at different effective normal stress (50, 100, 150 and 200 kPa).

To further analyze the alteration of SWC of Benggang slopes with different SCs, the pore water pressure distributions under different conditions are compared. With an increase in rainfall from 54 to 143 mm and an increase the ASWC from 0.24 to 0.36 cm^3/cm^3, for SC I, the average pore water pressures at depths of 0.3 m (red soil layer), 2 m (transition layer), and 4 m (sandy soil layer) increase from −25 to −10 kPa, −40 to 5 kPa, and −45 to −20 kPa, respectively; for SC II, the average pore water pressures at depths of 0.3 m (transition layer), 2 m (sandy soil layer), and 4 m (sandy soil layer), increase from −8 to −7 kPa, −18 to −10 kPa, and −15 to 4 kPa, respectively; and for SC III, the average pore water pressures at depths of 0.3 m (sandy soil layer), 2 m (sandy soil layer), and 4 m (sandy soil layer) increase from −25 to −10 kPa, −15 to-5 kPa, and −5 to 5 kPa, respectively. For SC I, a positive pore pressure first appears at a depth of 2 m (transition layer), whereas in SC II and SC III, positive pore pressure first appears in the deep sandy layer.

4. Discussions

4.1. Differences in the SC of Benggang slopes affect the SWC

The SWCs of the Benggang slopes with different SCs (SC I, SC II, and SC III) were simulated (Figs. 9–11), and the results show that even when the rainfall and ASWC conditions are consistent, the water distribution varied with the soil depth in the vertical profiles and along the slope position in the horizontal direction of Benggang slopes with different SCs (SC I, SC II, and SC III).

Two SC characteristics were observed to affect the SWC in the vertical profile. (1) For SC I and SC II, the SWC is higher in the topsoil than in the deeper soil, while for SC III, the opposite trend is observed. (2) For SC I, a positive pore pressure first occurs in the transition layer, and for SC II and SC III, a positive pore pressure first occurs in the deep sandy layer (Figs. 9–11). These differences are mainly due to the following reasons: (1) The K_s values of different soil layers are different. The points noted are that the K_s values are higher in the red soil layer (0.51 mm/min) and sandy soil layer (0.34 mm/min) but lower in the transition layer (0.04 mm/min) (Fig. 3). Water storage and movement are affected by K_s (Bonsu, 2013), for SC I, the water concentrated in the transition layer and the deep sandy layer will not easily become saturated and the water content will remain stable for a long time. (2) The soil retention capacity varies with the soil layer. The field capacities of the red soil and transition layers are greater than 0.38 cm^3/cm^3, and the field capacity of the sandy soil layer is only 0.27 cm^3/cm^3 (Fig. 4). This difference occurred due to the red soil and transition layers contain higher contents of fine particles and small pores, while the sandy soil dominated by coarser particles, result in larger gaps between particles and a lower water retention capacity (Ashrafi et al., 2002; Gupta et al., 2009; Miller et al., 2002; Siyal et al., 2009; Tarantino & Tombolato, 2005). At this condition, the topsoil of SC I (red soil layer and transition layer) and SC II (transition layer) can retain large amounts of infiltration water. If the red soil layer and transition layer has been eroded (SC III), rainwater can quickly infiltrates into the deeper layer, and the increase of soil water content in deep sand layer inevitably occurs. (3) The thicknesses of the soil layer above the sandy layer are different for SC I and SC II. For SC II, the red soil layer has been eroded, and the thickness of the soil layer above the sandy layer is less than that of SC I, which leads to a higher SWC in the deep sandy layer of SC II compared to that of SC I.

In addition to the vertical profile, the SCs exhibit two characteristic effects on the SWC along the slope positions. (1) For SC I, the SWC at a depth of 0.3 m at the lower slope is lower than that at the middle and upper slopes. For SC II and SC III, the SWCs are basically

Table 2
Liquid limit and plastic limit of different soil layers.

Soil layer	Liquid limit cm^3/cm^3	Plastic limit cm^3/cm^3	Plastic line cm^3/cm^3
Red soil layer I	0.83	0.45	0.38
Transition layer	0.64	0.36	0.28
Sandy soil layer I	0.48	0.30	0.18

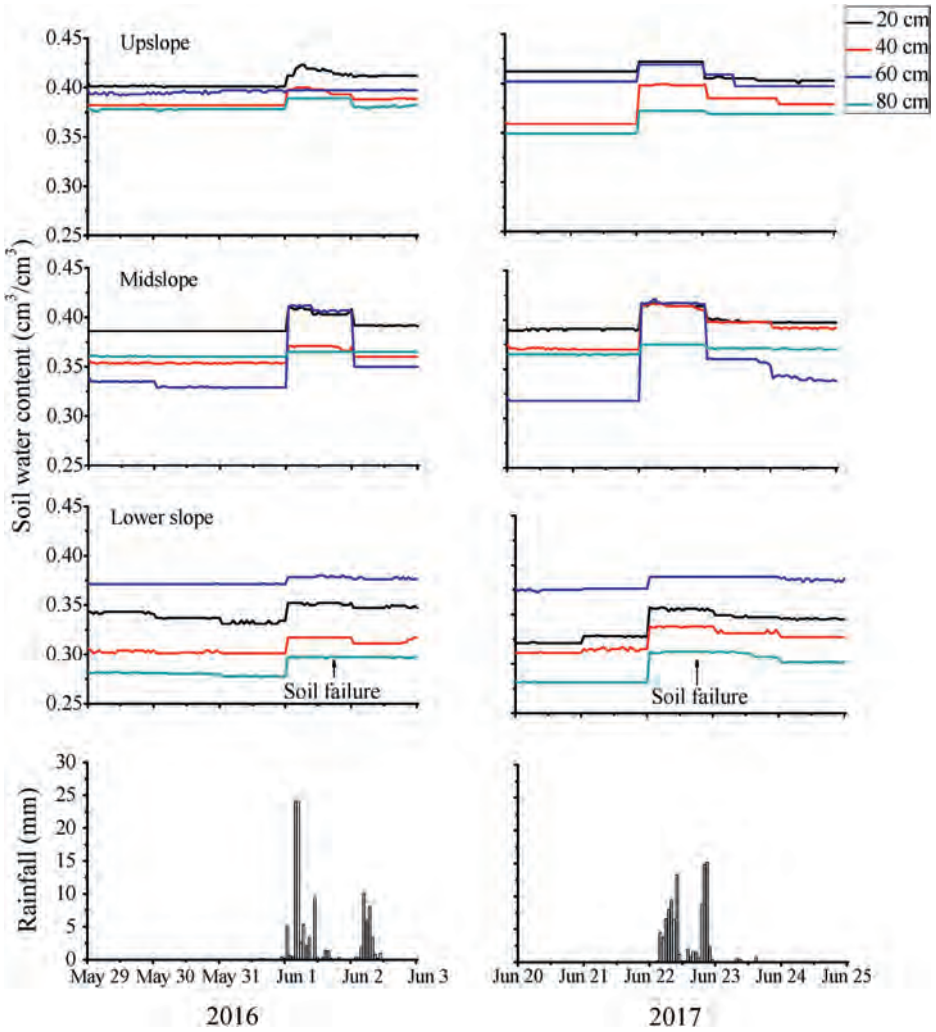

Fig. 8. The soil water content at different soil depths during the triggering of a Benggang erosion event. Two events of Benggang erosion triggering were captured on June 2, 2016 and June 23, 2017.

evenly distributed along the slope. (2) The SWC of the deep sandy layer of the three SCs is higher at the lower slope than at the middle and upper slopes. These differences are mainly due to the following reasons: (1) The soil properties, such as K_S, determines the maximum capacity of water transport in saturated soil and reflects the infiltration characteristics that affect the change of SWC (Moradi et al., 2016). For SC I, the depth of 0.3 m corresponds to the red soil layer and has a high water conductivity and water retention capacity. The lower slope near the headwall is affected by tensile fractures, which induce higher content of macropores than that of middle or upper slope (Duan et al., 2018). Hence, K_S is higher at the lower slope than middle and upper slopes, which assist in the rainwater infiltrate into deeper layer during rainfall at the lower slope, resulting in a lower SWC in the topsoil at the lower slope than at the middle and upper slopes. Unlike that in SC I, the topsoil in SC II is a transition layer with a low water conductivity and a high water retention capacity, the water cannot flow through this layer easily, which makes the rainwater tends to be uniformly distributed across the whole slope. The topsoil in SC III is a sandy soil layer with a high water conductivity and a low water retention capacity, the water can flow through this layer easily, therefore, the water tends to be occurs distributed across the whole slope. (2) The slope position has a great influence on the water distribution. In the deep sandy layer, the SWC is higher at the lower slope position than at the middle and upper slope positions. This lower-heavy and upper-light water distribution pattern observed for deep layers for the three SC slopes is mainly controlled by the slope position. Compared to the soil in the upper slope, the soil in the lower slope is actually higher; thus, the soil water is more likely to percolate into the gully bottom.

In summary, there is a difference in the distribution of SWC on slopes with different SCs, indicating that it is necessary to understand which SC slope is more likely to trigger Benggang erosion.

4.2. Which SC slope is more likely to trigger Benggang erosion?

Which SC slope is more likely to trigger of Benggang erosion is a complex question in that different SC slopes have different SWC patterns, pore water pressures and shear strengths, which are all factors that have importance in affecting erosion.

In this study, the SWC on the test Benggang slope (SC I) was continuously monitored. Rainfall events trigger Benggang erosion (SC I) when the ASWC is high, and rainfall is heavy (Fig. 8). Under these conditions, the SWC was high before rain and increased obviously in the deeper layer. A similar variation in the SWC was found in the VADOSE/W simulated results for SC I—the SWC and

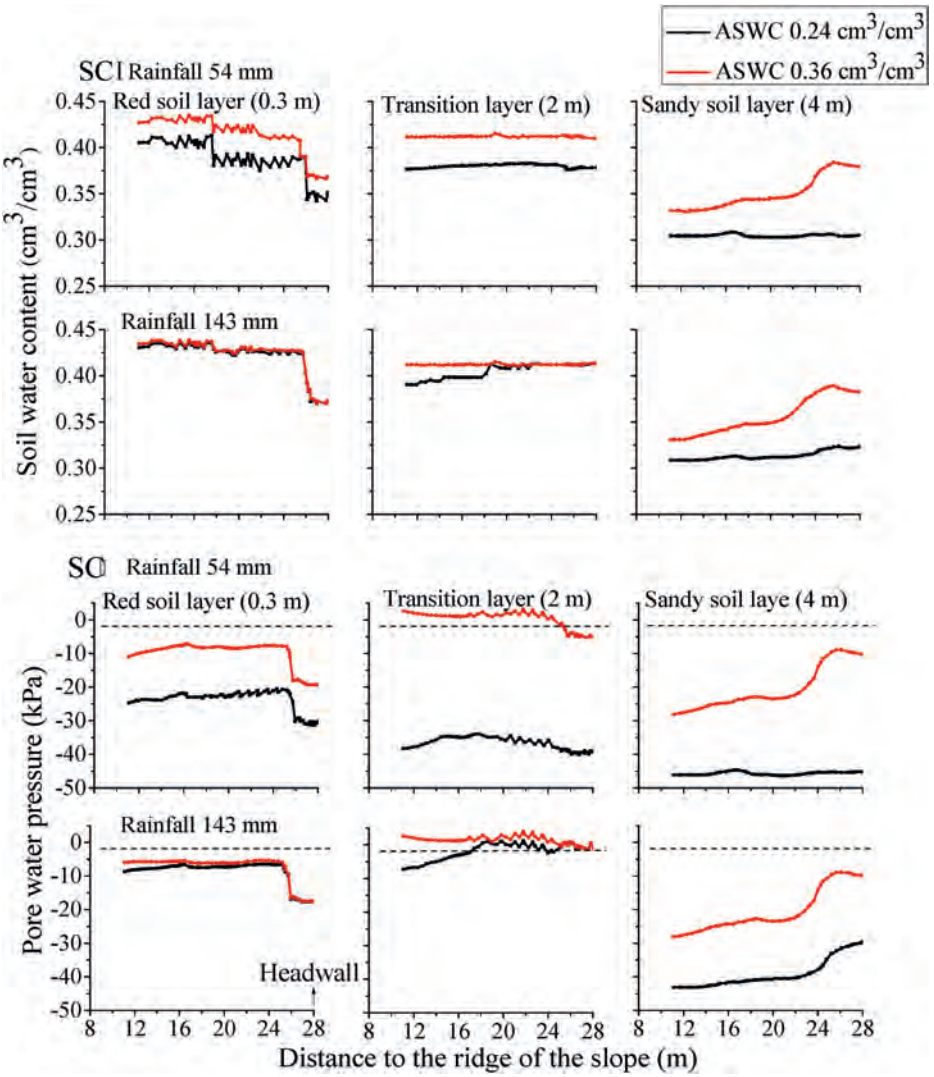

Fig. 9. The soil water content and pore water pressure at the different soil depths, at the depth of 0.3 m (red soil layer), 2 m (transition layer), and 4 m (sandy soil layer) along the slope of SC I. Simulated during the two higher rainfall events (rainfall is 54 and 143 mm in 24 h) and two antecedent soil water content (ASWC is 0.24 and 0.36 cm^3/cm^3).

pore water pressure increased obviously in the deep sandy layer near the headwall, under a high ASWC and heavy rainfall (ASWC of 0.36 cm^3/cm^3 and rainfall of 54 and 143 mm) (Fig. 9). Increases in the SWC lead to reductions in shear strength (Fig. 7), these reductions in the shear strength are the reason behind the instability and collapse of the headwall (Xu et al., 2018; Stark et al., 2005). The specific indications in terms of the SWC and shear strength are helpful to understand the mechanism of the Benggang erosion. Interestingly, we found that the shear strength of the red soil layer and transition layer under a high SWC level (e.g., 0.42 cm^3/cm^3) is still greater than that of the sandy soil layer under a low SWC level (e.g., 0.31 cm^3/cm^3) (Fig. 7). The shear strength is affected by the particle size distribution and bulk density (Zhang et al., 2018; knapen et al., 2007). The fine particles in soil act as cementation materials between the soil particles, which can effectively increase the shear strength of the soil (Eid et al., 2015; Schnellmann et al., 2013). Therefore, the shear strength of sandy soil layer is less than that of the red soil layer and transition layer due to the low content of fine particles in the sandy soil layer. In addition, the liquid limit and plastic limit of the red soil layer and the transition layer are higher than those of the sandy soil layer (Table 2). Under a high ASWC and heavy rainfall, the SWC increased obviously and the pore water pressure was close to positive pressure in the deep sandy layer at the lower slope position, and a positive pore pressure instantaneously causes soil liquefaction in the sandy layer. At this condition, the local shear strength of the sandy layer at the lower slope disappears, and destabilizing the soil mass. This phenomenon suggests that although the red soil layer and the transition layer have high SWCs, they are not necessarily responsible for slope instability, and Benggang erosion may be more easily triggered by an increase in the SWC of the deep sandy layer.

Only under the conditions of a high ASWC and heavy rainfall, does the SWC of the deep sandy layer of SC I increase obviously, potentially triggering Benggang erosion. For SC II and SC III, the topsoil has been eroded, and the deep sandy layer more easily reaches a higher SWC (Figs. 10 and 11). Especially for SC III, when the ASWC is 0.24 cm^3/cm^3 and the rainfall is 143 mm, the SWC is already at a high level in the deep sandy layer, and a positive pore pressure appears near the headwall (Fig. 11). The present study is the first one to analyze the variations of the SWC for different SCs, under the same ASWC and rainfall. Our findings suggest that if the topsoil (red soil layer and transition layer) is eroded, the possibility of triggering Benggang erosion increases.

The specific indication of the SWC in different SCs is helpful to understand the impacts of SCs on the triggering of gully erosion. The SCs can affect the development of gully erosion was also

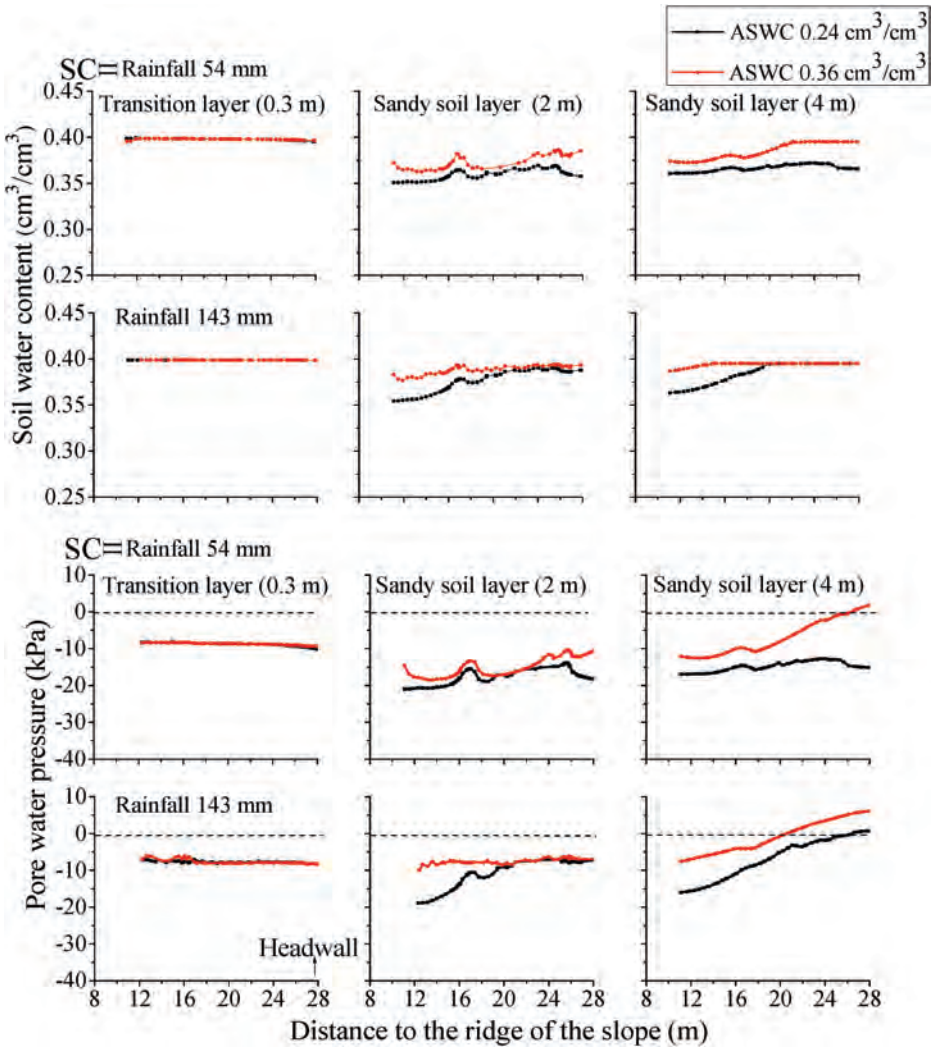

Fig. 10. The soil water content and pore water pressure at the different soil depths, at the depth of 0.3 m (transition layer), 2 m (sandy soil layer), and 4 m (sandy soil layer) along the slope of SC II. Simulated during the two higher rainfall events (rainfall is 54 and 143 mm in 24 h) and two antecedent soil water content (ASWC is 0.24 and 0.36 cm^3/cm^3).

reported in the formation of South Africa. Mararakanye et al. (2017) and Laker (2004) indicated that in South Africa, various mudstones are susceptible to gully erosion, mainly due to the presence of highly erodible duplex soils. They highlighted that the duplex soils favor continuous gully development, mainly due to having a lower organic matter content and lower amounts of exchangeable calcium and magnesium than those of the nonduplex soils in the same study area (Seitlheko, 2003). Several studies have noted that for duplex soil, the marked increase in the clay content from the topsoil to the deep soil horizon exhibits an abrupt transition between the topsoil and the deep soil and that this abrupt transitions is related to the soil texture, structure and consistency. The surface horizon is usually dispersive and prone to crusting, which makes duplex soils prone to gullying through tunneling above the impermeable layer, where water moves along a subsurface flow, causing tunnel erosion under rainfall (Rienks et al., 2000; Roux & Sumner, 2012).

These conclusions appear to be contrary to our research results, possibly because these conclusions were based on landforms that occur in environmental conditions that differ from those of Benggang. Although these previously studied gully erosional landforms and Benggang are rainfall-induced heavily collapsed gullies in deep soil conditions, the gully erosion investigated in previous studies occurred in an area with annual precipitation varying from 600 to 1200 mm. Benggang slopes are located in areas with an annual precipitation of 1300–2000 mm. The granites that developed Benggang were distributed in a hot and rainy climate, and these granites underwent intense physical and chemical weathering, which resulted in the formation of deep sandy soil layers. In addition, the topsoil has undergone strong chemical weathering, which promotes the formation of clay particles, resulting in the formation of a clay topsoil and deeper sandy layer in Benggang slopes. Deep sandy layers have collapsible grain structures, and these soils are usually dispersive and easily lose aggregation (Havaee et al., 2015). Extraordinary rainfall events trigger Benggang erosion when rainwater infiltrates into the deep sandy layer. The amounts of exchangeable calcium and magnesium in Benggang soil are low, with no differences among the soil layers (Deng et al., 2018). For SC III, from topsoil to deep soil both are sandy soil layers, this allows the deep sandy layer can more easily reach a higher SWC, which favors Benggang erosion development.

5. Conclusion

The soil mass of Benggang slopes has a heterogeneous soil profile in the vertical direction, with different soil properties and hydraulic properties in individual layers. The water retention

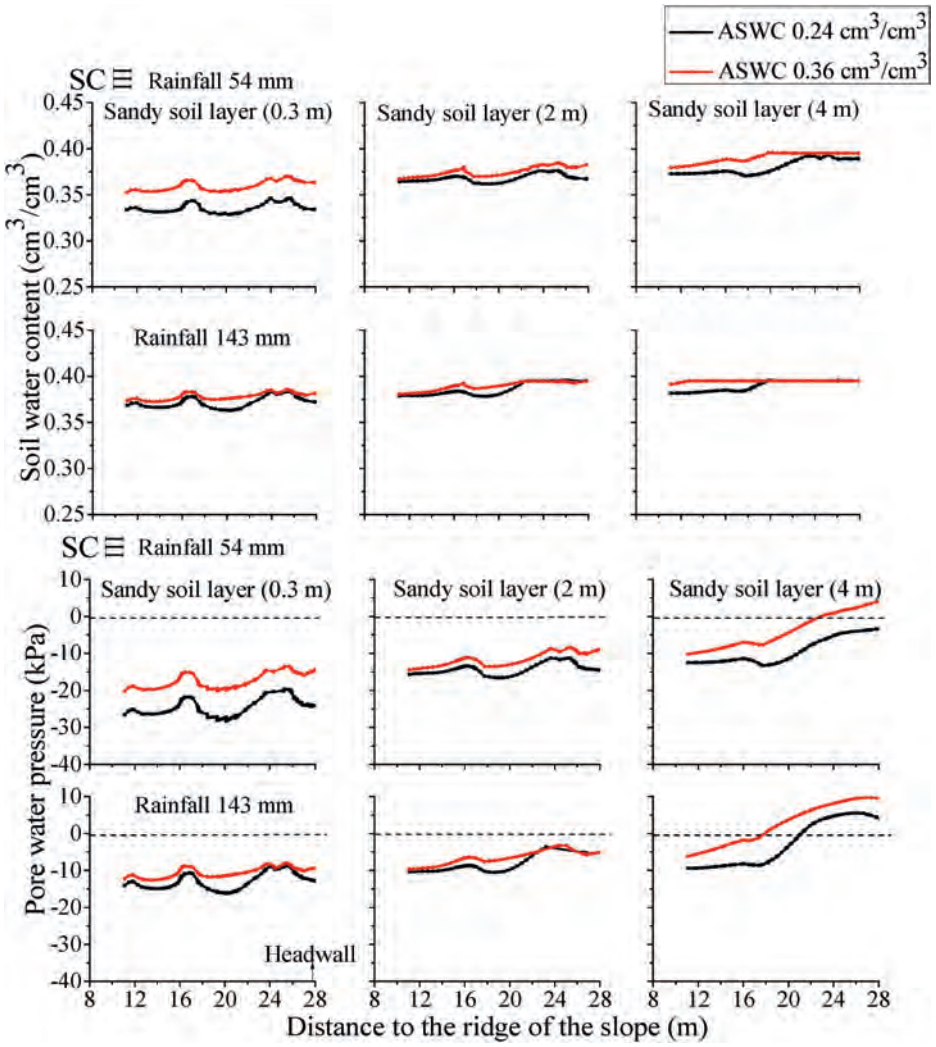

Fig. 11. The soil water content and pore water pressure at the different soil depths, at the depth of 0.3 m (sandy soil layer), 2 m (sandy soil layer), and 4 m (sandy soil layer) along the slope of SC III. Simulated during the two higher rainfall events (rainfall is 54 and 143 mm in 24 h) and two antecedent soil water content (ASWC is 0.24 and 0.36 cm^3/cm^3).

capacity and shear strength decreased with increasing granitic profile depth, topsoil (red soil layer and transition layer) has higher water retention capacity and shear strength than the sandy soil layer, which is the unique material basis for the occurrence of Benggang erosion. Our study reveals that the Benggang erosion is triggered by an increase in the soil water content (SWC) in the deep sandy layer. The high SWC in deep sandy soil and the buildup of positive pore water pressure and reduce shear strength result in the triggering of Benggang erosion. SC II and SC III increase precipitation infiltration and the water content of the deeper sandy soil layer compared to SC I, even when the rainfall and antecedent soil water content conditions are consistent. The current measures such as the construction of drainage ditches and horizontal terraces may make the red soil layer shallower or expose the sandy layer, which artificially leads to the formation of Benggang slope of SC I into SC II and SC III, it is easily to cause Benggang erosion. Therefore, the key to preventing the Benggang erosion is to protect the topsoil (red soil and transition layer).

Declaration of competing interest

No conflict of interest exits in the submission of this manuscript, and manuscript is approved by all authors for publication. I would like to declare on behalf of my co-authors that the work described is our original research that has not been published previously, nor under consideration for publication elsewhere, in whole or in part. All the authors listed have approved the submission of the manuscript enclosed.

Acknowledgements

Financial support for this research was provided by the National Natural Science Foundation of China (No. 41571258, 42007055 and 41630858).

Appendix A. Supplementary data

Supplementary data to this article can be found online at https://doi.org/10.1016/j.iswcr.2021.03.003.

References

Al-Shayea, N. A. (2001). The combined effect of clay and moisture content on the behavior of remolded unsaturated soils. *Engineering Geology, 62*, 319–342. https://doi.org/10.1016/S0013-7952(01) 00032-1

Amare, S., Keesstra, S., van der Ploeg, M., Langendoen, E., Steenhuis, T., & Tilahun, S. (2019). Causes and controlling factors of valley bottom gullies. *Land, 8*(9), 141.

https://doi.org/10.3390/land8090141
Arabameri, A., Cerda, A., & Tiefenbacher, J. P. (2019). Spatial pattern analysis and prediction of gully erosion using novel hybrid model of entropy-weight of evidence. *Water, 11*(6), 1129. https://doi.org/10.3390/w11061129
Ashrafi, S., Gupta, A. D., Babel, M. S., Izumi, N., & Loof, R. (2002). Simulation of infiltration from porous clay pipe in subsurface irrigation. *Hydrological Sciences Journal, 47*(2), 253–268. https://doi.org/10.1080/02626660209492928
Assouline, S. (2013). Infiltration into soils: Conceptual approaches and solutions. *Water Resources Research, 49*(4), 1755–1772. https://doi.org/10.1002/wrcr.20155
Bacellar, L. D. A. P., Netto, A. L. C., & Lacerda, W. A. (2005). Controlling factors of gullying in the Maracujáaracuj, 2005. *Controlling factors of gullyinProc Land, 30*, 1369–1385. https://doi.org/10.1002/esp.1193
Beven, K., & Germann, P. (2013). Macropores and water flow in soils revisited. *Water Resources Research, 49*(6), 3071–3092. https://doi.org/10.1002/wrcr.20156
Bingner, R. L., Wells, R. R., Momm, H. G., Rigby, J. R., & Theurer, F. D. (2016). Ephemeral gully channel width and erosion simulation technology. *Natural Hazards, 80*, 1949–1966. https://doi.org/10.1007/s11069-015-2053-7
Bonsu, M. (1992). A study of a texture-based equation for estimating the saturated hydraulic conductivity of an alfisol in the Sudan savannah ecological zone, Ghana. *Hydrological Sciences Journal, 37*(6), 599–606. https://doi.org/10.1080/02626669209492626
Buczko, U., & Gerke, H. H. (2005). Estimating spatial distributions of hydraulic parameters for a two-scale structured heterogeneous lignitic mine soil. *Journal of Hydrology, 312*(1–4), 109–124. https://doi.org/10.1016/j.jhydrol.2005.02.040
Caraballo-Arias, N. A., Conoscenti, C., Di Stefano, C., & Ferro, V. (2014). Testing gis-morphometric analysis of some Sicilian badlands. *Catena, 113*, 370–376. https://doi.org/10.1016/j.catena.2013.08.021
Cerdà, A. (1999). Seasonal and spatial variations in infiltration rates in badland surfaces under Mediterranean climatic conditions. *Water Resources Research, 35*(1), 319–328. https://doi.org/10.1029/98WR01659
Cerdà, A., & Doerr, S. H. (2010). The effect of ant mounds on overland flow and soil erodibility following a wildfire in eastern Spain. *Ecohydrology, 3*(4), 392–401. https://doi.org/10.1002/eco.147
Chaplot, V. (2013). Impact of terrain attributes, parent material and soil types on gully erosion. *Geomorphology, 186*, 1–11. https://doi.org/10.1016/j.geomorph.2012.10.031
Chen, A., Zhang, D., Peng, H., Fan, J., Xiong, D., & Liu, G. (2013). Experimental study on the development of collapse of overhanging layers of gully in Yuanmou Valley, China. *Catena, 109*, 177–185. https://doi.org/10.1016/j.catena.2013.04.002
Cox, R., Zentner, D. B., Rakotondrazafy, A. F. M., & Rasoazanamparany, C. F. (2010). Shakedown in Madagascar: Occurrence of lavakas (erosional gullies) associated with seismic activity. *Geology, 33*, 179–182. https://doi.org/10.1130/G30670.1
Cui, G., & Zhu, J. (2018). Prediction of unsaturated flow and water backfill during infiltration in layered soils. *Journal of Hydrology, 557*, 509–521. https://doi.org/10.1016/j.jhydrol.2017.12.050
Dehotin, J., Breil, P., Braud, I., de Lavenne, A., Lagouy, M., & Sarrazin, B. (2015). Detecting surface run off location in a small catchment using distributed and simple observation method. *Journal of Hydrology, 525*, 113–129. https://doi.org/10.1016/j.jhydrol.2015.02.051
Deng, Y. S., Cai, C. F., Xia, D., Ding, S. W., Chen, J. Z., & Wang, T. W. (2017). Soil atterberg limits of different weathering profiles of the collapsing gullies in the hilly granitic region of southern China. *Solid Earth, 8*(2), 499–513. https://doi.org/10.5194/se-8-499-2017
Deng, Y. S., Ding, S. W., Liu, C. M., Xia, D., Zhang, X. M., & Lv, G. A. (2015). Soil moisture characteristics of collapsing gully wall in granite area of Southeastern Hubei. *Journal of Soil & Water Conservation, 29*, 132–137.
Deng, Y. S., Duan, X. Q., Ding, S. W., Cai, C. F., & Chen, J. Z. (2018). Suction stress characteristics in granite red soils and their relationship with the collapsing gully in south China. *Catena, 171*, 505–522. https://doi.org/10.1016/j.catena.2018.07.043
Duan, X. Q., Deng, Y. S., Tao, Y., He, Y. B., Lin, L. R., & Chen, J. Z. (2018). Variation in soil saturated hydraulic conductivity along the hillslope of collapsing granite gullies. *Hydrological Sciences Journal, 63*(5), 803–817. https://doi.org/10.1080/02626667.2018.1453610
Eid, H. T., Amarasinghe, R. S., Rabie, K. H., & Wijewickreme, D. (2015). Residual shear strength of fine-grained soils and soil-solid interfaces at low effective normal stresses. *Canadian Geotechnical Journal, 52*(2), 198–210. https://doi.org/10.1139/cgj-2014-0019
Fan, C. C., & Su, C. F. (2008). Role of roots in the shear strength of root-reinforced soils with high moisture content. *Ecological Engineering, 33*(2), 157–166. https://doi.org/10.1016/j.ecoleng.2008.02.013
Fox, G. A., & Willson, G. V. (2010). The role of subsurface flow in hillslope and stream bank erosion: A review. *Soil Science Society of America Journal, 74*, 717–733. https://doi.org/10.2136/sssaj2009.0319
Fredlund, D. G., & Rahardjo, H. (1993). *Soil mechanics for unsaturated soils*. John Wiley and Sons.
Garg, A., & Ng, C. W. W. (2015). Investigation of soil density effect on suction induced due to root water uptake by Schefflera heptaphylla. *Journal of Plant Nutrition and Soil Science, 178*(4), 586–591. https://doi.org/10.1002/jpln.201400265
Gee, G. W., Bauder, J. W., & Klute, A. (1986). *Particle-size analysis, methods of soil analysis, part 1. Physical and mineralogical methods*. Madison, WI: Soil since Society of America. Inc.
Geo-Slope International Ltd. (2014). *Seepage modeling with VADOSE/W-an engineering methodology*. May 2014 (Edition). GEO-SLOPE International Ltd.
Gupta, A. D., Babel, M. S., & Ashrafi, S. (2009). Effect of soil texture on the emission characteristics of porous clay pipe for subsurface irrigation. *Irrigation sci, 27*(3), 201–208. https://doi.org/10.1007/s00271-008-0129-9
Havaee, S., Mosaddeghi, M. R., & Ayoubi, S. (2015). In situ surface shear strength as affected by soil characteristics and land use in calcareous soils of central Iran. *Geoderma, 237*, 137–148. https://doi.org/10.1016/j.geoderma.2014.08.016
Horn, R. (2003). Stress-strain effects in structured unsaturated soils on coupled mechanical and hydraulic processes. *Geoderma, 116*, 77–88. https://doi.org/10.1016/s0016-7061(03)00095-8
Hoyos, L. R., Velosa, C. L., & Puppala, A. J. (2014). Residual shear strength of unsaturated soil via suction-controlled ring shear testing. *Engineering Geology, 172*, 1–11. https://doi.org/10.1016/j.enggeo. 2014.01.001
Jiang, F. S., Huang, Y. H., Wang, M. K., Lin, J. S., Zhao, G., & Ge, H. L. (2014). Effects of rainfall intensity and slope gradient on steep colluvial deposit erosion in southeast China. *Soil Science Society of America Journal, 78*(5), 1741–1752. https://doi.org/10.2136/sssaj2014.04.0132
Khanzode, R. M., Vanapalli, S. K., & Fredlund, D. G. (2002). Measurement of soil-water characteristic curves for fine-grained soils using a small-scale centrifuge. *Canadian Geotechnical Journal, 39*(5), 1209–1217. https://doi.org/10.1139/t02-060
Knapen, A., Poesen, J., Govers, G., Gyssels, G., & Nachtergaele, J. (2007). Resistance of soils to concentrated flow erosion: A review. *Earth-Science Reviews, 80*, 75–109. https://doi.org/10.1016/.j.earscirev.2006.08.001
Laker, M. C. (2004). Advances in soil erosion, soil conservation, land suitability evaluation and land use planning research in South Africa, 1978-2003. *South African Journal of Plant and Soil, 21*(5), 345–368. https://doi.org/10.1080/02571862.2004.10635069
Liao, Y., Yuan, Z., Zheng, M., Li, D., Nie, X., Wu, X., Huang, B., Xie, Z. Y., & Tang, C. T. (2019). The spatial distribution of benggang and the factors that influence it. *Land Degradation & Development, 30*(18), 2323–2335. https://doi.org/10.1002/ldr.3418
Lin, Z. L. (2008). *Introduction to preservation sand: Prediction and prevention of soil disaster*. Kyoto: Chuangrong Book Printing Co.
Lin, J. S., Zhu, G. L., Wei, J., Jiang, F. S., Wang, M. K., & Huang, Y. H. (2018). Mulching effects on erosion from steep slopes and sediment particle size distributions of gully colluvial deposits. *Catena, 160*, 57–67. https://doi.org/10.1016/j.catena.2017.09.003
Mararakanye, N., & Sumner, P. D. (2017). Gully erosion: A comparison of contributing factors in two catchments in South Africa. *Geomorphology, 288*, 99–110. https://doi.org/10.1016/j.geomorph.2017.03.029
Miller, C. J., Yesiller, N., Yaldo, K., & Merayyan, S. (2002). Impact of soil type and compaction conditions on soil water characteristic. *J. Geotech. Geoenviron., 128*(9), 733–742. https://doi.org/10.1061/(ASCE)1090-0241(2002)128:9(733)
Momm, H. G., Wells, R. R., & Bingner, R. L. (2015). GIS technology for spatiotemporal measurements of gully channel width evolution. *Natural Hazards, 79*, S97–S112. https://doi.org/10.1007/s11069-015-1615-z
Moradi, F., Moosavi, A. A., & Moghaddam, B. K. (2016). Spatial variability of water retention parameters and saturated hydraulic conductivity in a calcareous inceptisol (khuzestan province of Iran) under sugarcane cropping. *Archives of Agronomy and Soil Science, 62*(12), 1686–1699. https://doi.org/10.1080/03650340.2016.1164308
Neugirg, F., Stark, M., Kaiser, A., Vlacilova, M., Della Seta, M., Vergari, F., Schmidt, J., Becht, M., & Haas, F. (2016). Erosion processes in calanchi in the Upper Orcia Valley, Southern Tuscany, Ita-ly based on multitemporal high- resolution terrestrial Li-DAR and UAV surveys. *Geomorphology, 269*(15), 8–22. https://doi.org/10.1016/j.geomorph.2016.06.027
Qin, C., Zheng, F., Wells, R. R., Xu, X., Wang, B., & Zhong, K. (2018). A laboratory study of channel sidewall expansion in upland concentrated flows. *Soil Till. Res., 178*, 22–31. https://doi.org/10.1016/j.still.2017.12.008
Rachman, A., Anderson, S. H., Gantzer, C. J., & Thompson, A. L. (2003). Influence of long term cropping systems on soil physical properties related to soil erodibility. *Soil Science Society of America Journal, 67*, 637–644. https://doi.org/10.2136/sssaj2003.6370
Rahardjo, H., Satyanaga, A., Leong, E. C., Ng, Y. S., & Pang, H. T. C. (2012). Variability of residual soil properties. *Engineering Geology, 141–142*(4), 124–140. https://doi.org/10.1016/j.enggeo.2012.05.009
Rezaei, M., Seuntjens, P., Shahidi, R., Joris, I., Boënne, W., Al-Barri, B., & Cornelis, W. M. (2016). The relevance of in-situ and laboratory characterization of sandy soil hydraulic properties for soil water simulations. *Journal of Hydrology, 534*(1), 251–265. https://doi.org/10.1016/j.jhydrol.2015.12.062
Rienks, S. M., Botha, G. A., & Hughes, J. C. (2000). Some physical and chemical properties of sediments exposed in a gully (donga) in northern KwaZulu-Natal, South Africa and their relationship to the erodibility of the colluvial layers. *Catena, 39*(1), 11–31. https://doi.org/10.1016/S0341-8162(99)00082-X
Ries, F., Sechmidt, S., Sauter, M., & Lange, J. (2017). Controls of runoff generation along a steep climatic gradient in the Eastern Mediterranean. *J. Hydrol. Reg. Stud., 9*, 18–33. https://doi.org/10.1016/j.ejrh.2016.11.001
Roux, J. J. L., & Sumner, P. D. (2012). Factors controlling gully development: Comparing continuous and discontinuous gullies. *Land Degradation & Development, 23*(5), 440–449. https://doi.org/10.1002/.ldr.1083
Schnellmann, R., Rahardjo, H., & Schneider, H. R. (2013). Unsaturated shear strength of a silty sand. *Engineering Geology, 162*, 88–96. https://doi.org/10.1016/j.enggeo.2013.05.011
Seitlheko, E. M. (2003). Gully initiation and expansion in Lesotho: A case of the

buasono area. *South African Geographical Journal, 85*(2), 175–181. https://doi.org/10.1080/03736245.2003.9713799
Siyal, A. A., Van Genuchten, M. T., & Skaggs, T. H. (2009). Performance of pitcher irrigation system. *Soil Science, 174*(6), 312–320. https://doi.org/10.1097/ss.0b013e3181a97532
Stanchi, S., Freppaz, M., & Zanini, E. (2012). The influence of Alpine soil properties on shallow movement hazards, investigated through factor analysis. *Nat. Hazard Earth Sys, 12*, 1845–1854. https://doi.org/10.5194/nhess-12-1845-2012, 2012.
Stark, T. D., Choi, H., & McCone, S. (2005). Drained shear strength parameters for analysis of landslides. *J. Geotech. Geoenviron., 131*(5), 575–588. https://doi.org/10.1061/(ASCE) 1090-0241(2005)131:5(575)
Stefano, C. D., Ferro, V., Pampalone, V., & Sanzone, F. (2013). Field investigation of rill and ephemeral gully erosion in the Sparacia experimental area, South Italy. *Catena, 101*, 226–234. https://doi.org/10.1016/j.catena.2012.10.012
Tao, Y., He, Y. B., Duan, X. Q., Zou, Z. Q., Lin, L. R., & Chen, J. Z. (2017). Preferential flows and soil moistures on a Benggang slope: Determined by the water and temperature co-monitoring. *Journal of Hydrology, 553*, 678–690. https://doi.org/10.1016/j.jhydrol.2017.08.029
Tarantino, A., & Tombolato, S. (2005). Coupling of hydraulic and mechanical behaviour in unsaturated compacted clay. *Géotechnique, 55*(4), 307–317. https://doi.org/10.1680/.geot.2005.55.4.307
Thiemann, S., Schütt, B., & Förch, G. (2005). Assessment of erosion and soil erosion processes-a case study from the Northern Ethiopian Highland. *FWU Water Resour. Publ, 3*, 173–185.
Thomas, J. T., Iverson, N. R., & Burkart, M. R. (2009). Bank-collapse process in a valley-bottom gully, western Iowa. *Earth Surface Processes and Landforms, 34*, 109–122. https://doi.org/10.1002/esp.1699
Vanwalleghem, T., Poesen, J., Nachtergaele, J., & Verstraeten, G. (2005). Characteristics, controlling factors and importance of deep gullies under cropland on loess-derived soils. *Geomorphology, 69*, 76–91. https://doi.org/10.1016/j.geomorph.2004.12.003
Voarintsoa, N. R. G., Cox, R., Razanatseheno, M. O. M., & Rakotondrazafy, A. F. M. (2012). Relation between bedrock geology, topography and Lavaka distribution in Madagascar. *South African Journal of Geology, 115*, 225–250. https://doi.org/10.2113/gssajg.115.225
Wang, Q. X., Ding, S. W., Deng, Y. S., & Ma, Y. (2016). Characteristics of runoff and sediment of different soil layers in granite collapse region under artificial rainfall simulation condition. *Journal of Soil & Water Conservation, 30*(6), 7–12. https://doi.org/10.13870/j.cnki.stbcxb.2016.06.002, 2016.
Wang, C., Mao, X., & Hatano, R. (2014). Modeling ponded infiltration in fine textured soils with coarse interlayer. *Soil Science Society of America Journal, 78*(3), 745–753. https://doi.org/10.2136/sssaj 2013.12.0535
Wang, Y. F., You, W., Fan, J., Jin, M., Wei, X. B., & Wang, Q. J. (2018). Effects of subsequent rainfall events with different intensities on runoff and erosion in a coarse soil. *Catena, 170*, 100–107.
Wei, Y. J., Wu, X. L., Li, X. Y., Xia, J. W., Cai, C. F., & Hassanikhah, A. (2018). A novel and facile method for characterizing shrinkage geometry along the granitic soil profile. *Soil Science Society of America Journal, 82*, 20–30. https://doi.org/10.2136/sssaj2017.05.0160
Wei, Y. J., Wu, X. L., Xia, J. W., Miller, G. A., Cai, C. F., Guo, Z. L., & Hassanikhah, A. (2019). The effect of water content on the shear strength characteristics of granitic soils in South China. *Soil Till. Res., 187*, 50–59. https://doi.org/10.1016/j.still.2018.11.013
Wells, R. R., Momm, H. G., Rigby, J. R., Bennett, S. J., Bingner, R. L., & Dabney, S. M. (2013). An empirical investigation of gully widening rates in upland concentrated flows. *Catena, 101*, 114–121. https://doi.org/10.1016/j.catena.2012.10.004
Wen, L. L., Zheng, F. L., Shen, H. O., Bian, F., & Jiang, Y. L. (2015). Rainfall intensity and inflow rate effects on hillslope soil erosion in the Mollisol region of Northeast China. *Natural Hazards, 79*(1), 381–395. https://doi.org/10.1007/s11069-015-1847-y
Wilson, G. W., Fredlund, D. G., & Barbour, S. L. (1994). Coupled soil-atmosphere modelling for soil evaporation. *Canadian Geotechnical Journal, 31*(2), 151–161. https://doi.org/10.1139/t94-021
Wuddivira, M. N., Stone, R. J., & Ekwue, E. I. (2013). Influence of cohesive and disruptive forces on strength and erodibility of tropical soils. *Soil Till. Res., 133*, 40–48. https://doi.org/10.1016/.j.still.2013.05.012
Xu, J. X. (1996). Benggang erosion: The influencing factors. *Catena, 27*, 249–263. https://doi.org/10.1016/0341-8162(96)00014-8
Xu, C., Wang, X., Lu, X., Dai, F., & Jiao, S. (2018). Experimental study of residual strength and the index of shear strength characteristics of clay soil. *Engineering Geology, 233*, 183–190. https://doi.org/10.1016/.j.enggeo.2017.12.004
Yang, H., Rahardjo, H., & Leong, E. C. (2006). Behavior of unsaturated layered soil columns during infiltration. *Journal of Hydrologic Engineering, 11*(4), 329–337. https://doi.org/10.1061/(ASCE) 1084-0699(2006)11:4(329)
Zhang, W., Sun, C., & Qiu, Q. (2016). Characterizing of a capillary barrier evapotranspirative cover under high precipitation conditions. *Environ. Earth Sci., 75*(6), 1–11. https://doi.org/10.1007/s12665-015-5214-9
Zhang, C. L., Wang, X. S., Zou, X. Y., Zou, X., Tian, J., Liu, B., Li, J., & Wu, Y. (2018). Estimation of surface shear strength of undisturbed soils in the eastern part of northern China's wind erosion area. *Soil Till. Res., 178*, 1–10. https://doi.org/10.1016/j.still.2017.12.014
Zhao, W., Yu, P., Ma, X., Sheng, J., & Zhou, C. (2017). Numerical simulation of soil evaporation with sand mulching and inclusion. *Water, 9*(4), 294–301. https://doi.org/10.3390/w9040294
Zhong, B. L., Peng, S. Y., Zhang, Q., Ma, H., & Cao, S. (2013). Using an ecological economics approach to support the restoration of collapsing gullies in southern China. *Land Use Policy, 32*, 119–124. https://doi.org/10.1016/j.landusepol.2012.10.005
Zonta, J. H., Martinez, M. A., Pruski, F. F., Silva, D. D., & Santos, M. R. (2012). Effect of successive rainfall with different patterns on soil water infiltration rate. *Braz. J. Soil Sci., 36*, 377–388. https://doi.org/10.1038/417459a

International Soil and Water Conservation Research 9 (2021) 433–444

Contents lists available at ScienceDirect

International Soil and Water Conservation Research

journal homepage: www.elsevier.com/locate/iswcr

Original Research Article

Soil erosion assessment by RUSLE with improved P factor and its validation: Case study on mountainous and hilly areas of Hubei Province, China

Pei Tian [a, *], Zhanliang Zhu [a, b], Qimeng Yue [a, b], Yi He [a], Zhaoyi Zhang [c], Fanghua Hao [a], Wenzhao Guo [d], Lin Chen [c], Muxing Liu [a]

[a] Key Laboratory for Geographical Process Analysis & Simulation of Hubei Province, Central China Normal University, Wuhan, 430079, PR China
[b] School of Geosciences, The University of Edinburgh, EH89XP, UK
[c] Department of Geography, University of Montreal, H2V 0B3, Montreal, QC, Canada
[d] State Key Laboratory of Soil Erosion and Dryland Farming on the Loess Plateau, Institute of Water and Soil Conservation, Northwest A&F University, Yangling, 712100, Shaanxi, PR China

ARTICLE INFO

Article history:
Received 21 February 2021
Received in revised form
9 April 2021
Accepted 13 April 2021
Available online 26 April 2021

Keywords:
RUSLE
Conservation practice factor (P)
Soil and water conservation measure
Soil erosion
Land use
Monitoring data

ABSTRACT

The Revised Universal Soil Loss Equation (RUSLE) is widely used to estimate regional soil erosion. However, quantitative impacts of soil and water conservation (SWC) measures on conservation practice factor (P) of the RUSLE remain largely unclear, especially for the mountainous and hilly areas. In this study, we improved the RUSLE by considering quantitative impacts of different SWC measures on the P factor value. The improved RUSLE was validated against the long-term (2000–2015) soil erosion monitoring data obtained from 96 runoff plots (15–35°) in mountainous and hilly areas of Hubei Province, China; the result presented a high accuracy with the determination coefficient of 0.89. Based on the erosion monitoring data of 2018 and 2019, the Root Mean Square Error of the result by the improved RUSLE was 28.0% smaller than that by the original RUSLE with decrement of 19.6%–24.0% in the average P factor values, indicating that the soil erosion modelling accuracy was significantly enhanced by the improved RUSLE. Relatively low P factor values appeared for farmlands with tillage measures ($P < 0.53$), grasslands with engineering measures ($P < 0.23$), woodlands with biological measures ($P < 0.28$), and other land use types with biological measures ($P < 0.51$). The soil erosion modulus showed a downward trend with the corresponding values of 1681.21, 1673.14, 1594.70, 1482.40 and 1437.50 t km^{-2} a^{-1} in 2000, 2005, 2010, 2015 and 2019, respectively. The applicability of the improved RUSLE was verified by the measurements in typical mountainous and hilly areas of Hubei Province, China, and arrangements of SWC measures of this area were proposed.

1. Introduction

Soil erosion, a worldwide environmental problem, seriously threatens natural resources (Pimentel, 2006), agriculture (Robinson et al., 2017), and the ecological environment (Owens & Collins, 2006). The increasing human activities exacerbate the risk of soil erosion, including excessive agricultural production, grazing, and forest destruction (Chuenchum et al., 2020). In order to ameliorate this situation, many studies have been conducted to help governments to formulate soil erosion management policies (Guerra et al., 2016; Wang & Su, 2020; Xu et al., 2020). Clarifying the occurrence process of regional soil erosion is the basis of formulating scientific and reasonable measures to control soil erosion (Alewell et al., 2019; Duan, Rong, et al., 2020; Tamene et al., 2017). Moreover, the implementation of soil and water conservation (SWC) measures has become increasingly urgent to quantify the inhibitory effects of soil erosion, especially in mountainous and hilly areas that are highly susceptible to soil erosion (Chen et al., 2019). Therefore, it is imperative to conduct high-precision regional soil erosion research in mountainous and hilly areas.

Soil erosion model is the basic tool to accurately assess and

* Corresponding author.
E-mail address: tianpei@mail.bnu.edu.cn (P. Tian).

https://doi.org/10.1016/j.iswcr.2021.04.007

predict the status of the soil erosion intensity at the regional scale (Biddoccu et al., 2020). Some physics-based models (Foster et al., 1981; Morgan et al., 1998) and empirical models (Wischmeier & Smith, 1978; Liu & Zhang, 2002) have proved the effectiveness for predicting soil erosion. The physical process model, such as the Water Erosion Prediction Project (WEPP) (Nearing et al., 1989), is limited for modelling soil erosion at large regional scales mainly due to the large amount of precise data required (Foster et al., 1995). While the empirical statistical model, such as the Revised Universal Soil Loss Equation (RUSLE) (Renard et al., 1997), is commonly utilized to estimate the regional soil erosion due to its uncomplicated model form and relatively high accuracy and applicability (Farhan & Nawaiseh, 2015). Meanwhile, with the rise of geographic information system (GIS) and remote sensing (RS) techniques, the advantages in the large-scale research of soil erosion could be better compatible with the RUSLE (Behera et al., 2020; Islam et al., 2020; Zhang et al., 2019). Although the RUSLE was developed based on soil erosion experiments in the United States, some studies have been conducted on the adaptability of the RUSLE parameters for different geomorphic features (e.g., mountains and intricate plateau regions) (Duan, Rong, et al., 2020; Fu et al., 2005; Wang & Su, 2020), different soil types (Chen et al., 2020; Tu et al., 2018), different land use types (Kebede et al., 2020; Liu & Zhang, 2002; Nyssen et al., 2009), and different soil conservation measures (Belachew et al., 2020; Diyabalanage et al., 2017) in other countries or climatic regions (Islam et al., 2020; Polykretis et al., 2020; Taye et al., 2018) around the world.

The RUSLE parameters include rainfall erosivity factor (R), soil erodibility factor (K), slope length and slope gradient factor (LS), cover management factor (C) and conservation practice factor (P). Among these factors, the P factor is one of the most difficult factors to determine (Wang & Su, 2020), especially since the realization of SWC measures has an increasingly significant effect on the calculation process of the P factor value. Hence, the validated P factor against locally measured data will increase the reliability of RUSLE in soil loss prediction (Kebede et al., 2020). The determination of the P value in the RUSLE was mainly affected by the land use types combined with the slope (Behera et al., 2020; Nyssen et al., 2009). The SWC measures have been proven to be able to effectively control soil erosion all over the world, which even could reduce nearly 70.0% of the amount of soil erosion on steep slopes (<25°) (Tu et al., 2018). The SWC measures should be cautiously implemented, since they could alter hydrological and ecological cycles (Fang, 2021; Liu & Zhang, 2002), while the impact of SWC measures reflected in the RUSLE was mainly concentrated in the P value. The lower value it is, the better the effect of controlling soil erosion (Diyabalanage et al., 2017). Chen et al. (2011) used the BP Algorithm to calculate the C and P values and assumed the P value as 1.0 due to limited conservation practices, which was difficult to accurately conform to the actual situation. Duan, Rong, et al. (2020) proposed an accurate calculation method of the SWC measures by high-resolution images in China, while SWC measures were considered in the E and T factors of the Chinese Soil Loss Equation (CSLE). The P value was regarded as the ratio of soil loss before and after the implementation of SWC measures (Chen et al., 2019). Taye et al. (2018) and Kebede et al. (2020) calculated the P value by considering SWC measures in the plateau terrain, and quantitative analysis was conducted with seasonal soil loss investigations in their research. Therefore, the quantitative consideration of SWC measures on the P factor has been confirmed in some studies.

Although the consideration of SWC measures on the P factor has been confirmed in previous studies, there is insufficient research addressing the quantitative impact of various SWC measures on the P factor at the regional scale of soil erosion, and the P factor was mainly based on literature experience and land use types to assign values (Zhu, 2015). In addition, current studies mainly focused on the impact of single or separate SWC measures on the P factor (Taye et al., 2018). Field investigations were overly concentrated in plateau regions, which limited their applicability and efficiency of the P factor improvement in the RUSLE (Kebede et al., 2020). We considered that the impacts of SWC measures on the P factor could be roughly divided into three parts: biological measures, engineering measures and tillage measures, which were mainly reflected in affecting the seasonal soil loss rate. Meanwhile, the slope distribution of mountainous and hilly areas should be analysed simultaneously due to the divergent effects of various SWC measures applied to different land use types. Therefore, in the process of obtaining the P value in the RUSLE, through GIS and RS techniques, the difference in seasonal soil loss caused by various SWC measures in different land use types should be considered.

Generally, plateaus and mountainous terrain with fragile ecology are vulnerable to soil erosion. The applications of the RUSLE for estimating regional soil erosion in the Loess Plateau (Fu et al., 2005), Yunnan Plateau (Duan, Rong, et al., 2020), Qinba Mountains (Wang & Su, 2020) and other plateau and mountainous areas (Chen et al., 2007) of China have been reported in the literature. However, few studies of the RUSLE focus on the validation and application in the mountainous and hilly area of Hubei Province, China. Hubei Province, as the core water source area of the Three Gorges Reservoir and the Middle Route of the South-to-North Water Diversion Project (Song et al., 2020), is located in the central of China which belongs to the pivotal area of the Yangtze River Economic Belt. Moreover, the topography varies greatly with the mountainous and hilly areas accounting for nearly 70.0% of the total area of Hubei Province, and the soil erosion area accounts for as high as 17.2% of the whole land area (Hubei Provincial Department of Water Resources, 2017). The current soil erosion research in Hubei Province focuses on key areas in the Three Gorges Reservoir and Danjiangkou Reservoir (Yu et al., 2010), and the application of the RUSLE is relatively rare.

Therefore, in this study, we selected the typical mountainous and hilly areas of Hubei Province in China as the study area. The objectives are to (1) improve the calculation method of the P factor of the RUSLE by considering the quantitative impact of various SWC measures and land use types, (2) validate the adaptability and the modelling accuracy of the improved RUSLE with the soil erosion monitoring data of runoff plots during 2000–2019 in the study area, and (3) illustrate the temporal and spatial distribution of soil erosion intensity from 2000 to 2019 and provide a reference for the reasonable allocations of the SWC measures in the study area. This study aims to introduce the improved RUSLE by modifying the P factor and verify its applicability for estimating regional soil erosion in typical mountainous and hilly areas of Central China, as well as provide a scientific guide for soil erosion control practices of the study area.

2. Materials and methods

2.1. Study area

Hubei Province (29°05′–33°20′N; 108°21′–116°07′E) is located in the middle reaches of the Yangtze River and central part of China (Zhu et al., 2009). The study area contains four typical mountainous and hilly areas in Hubei Province (Fig. 1). The soil types in the study area mainly include yellow soil, red soil and yellow-brown soil, while brown soil is mostly distributed in the middle and upper parts of mountains with high altitudes. The climatic features of the study area are typical subtropical monsoon climate, with sufficient sunshine, four distinct seasons, rain and heat in the same period. The average annual sunshine hours are between 1100 and 2150 h,

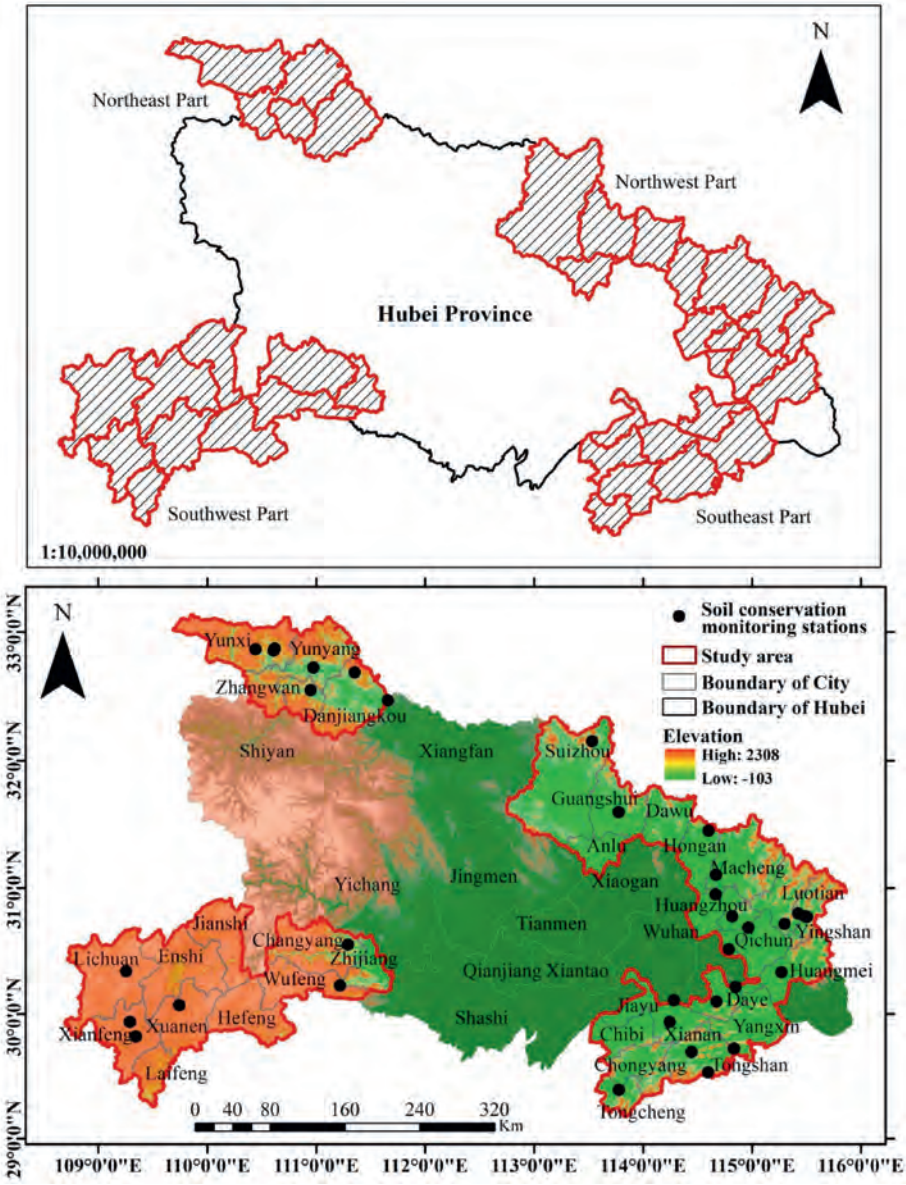

Fig. 1. Hubei Province in China and the location of the study area.

the annual average temperature is between 15 and 17 centigrade, and the average rainfall is between 800 and 1600 mm (Wang & Li, 2016). It mainly belongs to the northern subtropical monsoon climate zone, with the climatic characteristics of the transition from subtropical to warm temperate zone.

Table 1
Area percentage and vegetation coverage of different slope grades in the study area.

Slope grades	Area (%)	Vegetation Coverage (%)
<2°	3.1	21.5
2–5°	4.3	17.1
5–15°	12.9	14.6
15–25°	35.7	34.3
25–35°	26.7	46.2
>35°	17.3	35.6

Note: Vegetation coverage refers to the percentage of woodland and grassland areas in the whole study area. For instance, 21.5% means that the area of woodland and grassland occupied 21.5% of the whole region where the slope grade is less than 2°.

The total land area is 77988 km^2, while the area with slope grades below 35° accounts for approximately 80.0% (Table 1). Moreover, the study area is located in the transition zone from the second ladder to the third ladder of Chinese terrain. According to the topographic characteristics of this study area, the proportion of extremely steep slopes (susceptible to gravity erosion) is less than 18.0%.

2.2. Methods

2.2.1. Revised Universal Soil Loss Equation

Revised Universal Soil Loss Equation (RUSLE) is an empirical soil erosion model, which is used to estimate the long-term annual average soil loss rate of the sheet and rill erosion, and generally applied in a certain area with specific slope attributes, land use, and land management combinations (Renard et al., 1997; Sonneveld & Nearing, 2003; Wischmeier & Smith, 1978). Considering the impact of the SWC measures on the P factor, we conducted

quantitative applicability of the RUSLE, established by Renard et al. (1997), to estimate the soil loss rate from 2000 to 2019 in mountainous and hilly areas of Hubei Province, China. The formula of the RUSLE is as follows:

$$A = R*K*LS*C*P \quad (1)$$

where A (t hm^{-2} a^{-1}) is the predicted soil loss on the average unit area; R (MJ mm hm^{-2} h^{-1} a^{-1}) is the rainfall erosivity factor; K ($t \cdot h \cdot MJ^{-1} \cdot mm^{-1}$) is the soil erodibility factor; LS is the terrain factor (dimensionless); C is the cover management factor (dimensionless); and P is the conservation practice factor (dimensionless).

2.2.2. Improved conservation practice (P) factor

Land use types and slope gradients were considered when determining the P value of the RUSLE (e.g., Behera et al., 2020; Tu et al., 2018). Moreover, there were some studies addressing the impact of SWC measures on the P factor (Panagos et al., 2015; Taye et al., 2018), which was calculated by the slope gradients (contouring) and the seasonal soil loss rate with SWC measures. These studies mainly focused on partial SWC measures by field investigations, but lacking the consideration of multiple SWC measures. Therefore, the impact of multiple SWC measures on the P factor should be properly considered at the regional scale (Chen et al., 2020), along with the terrain of the mountainous and hilly areas.

In this study, we improved the calculation method of the P factor by considering the quantitative effects of multiple SWC measures (biological measures, engineering measures and tillage measures) at the regional scale. The identification of different SWC measures mainly relied on the collected Landsat images (resolution of 30.0 m) for land use surveys and Google Earth images (resolution of 2.5 m) for identification and verification of SWC measures, combined with statistical data. Biological measures were mainly embodied in vegetation construction, including different contour hedgerows, economic forests and shelter forests. After dividing different land use types, the image data (resolution of 2.5 m) was divided into polygons, and the changes of different vegetation patches in adjacent years and the verification of statistical data were used to determine whether biological measures have occurred. The identification of engineering measures (building terraces and stone embankments) was based on the slope gradient and terraces, combining with image features of shape, colour, position, crop and so on (Duan, Rong, et al., 2020). Tillage measures were collected by the images and statistical data of crop planting and rotation. Based on the characteristics in the study area, the improved P factor was calculated by two subfactors ($P_{struc.}$ and $P_{cont.}$) (Angima et al., 2003; Taye et al., 2018):

$$P = P_{struc.} \cdot P_{cont.} \quad (2)$$

$$P_{struc.} = SL_{S,SWC} / SL_{S,cont.} \quad (3)$$

where $P_{struc.}$ is the P value for SWC measures, $SL_{s,swc}$ is seasonal soil loss rate with SWC measures on the monitoring site, $SL_{s,cont.}$ is seasonal soil loss rate without SWC measures on the same control plot. $P_{cont.}$ is mainly determined by contour fluctuations, and its value is determined according to the method proposed by Renard et al. (1997). When $P_{struc.}$ is 1.0, it means that there are no SWC measures.

2.2.3. Other factors in the RUSLE

The rainfall erosivity (R) factor is the main driving force of soil erosion. The rainfall erosivity index of different years in the study area was acquired by calculating the accumulation of rainfall erosivity for half a month (Huang et al., 2019; Zhang et al., 2002). The formulas are as follows:

$$R = \sum_{k=1}^{24} M \quad (4)$$

$$M = \alpha \sum_{j=1}^{k} (P_j)^{\beta} \quad (5)$$

$$\beta = 0.8363 + \frac{18.177}{P_{d12}} + \frac{24.455}{P_{y12}} \quad (6)$$

$$\alpha = 21.586 \beta^{-7.1891} \quad (7)$$

where R (MJ mm hm^{-2} h^{-1} a^{-1}) represents average annual rainfall erosivity, M is the rainfall erosivity of k-th half-months (15 days), k is the number of half-months (15 days); P_j is the erosive rainfall on the j-th day, and erosive rainfall is defined as rainfall exceeding 12 mm P_{d12} is the daily average erosive rainfall, and P_{y12} is the annual average erosive rainfall.

The soil erodibility (K) factor in the RUSLE could be affected by the characteristics of different soil types, and soil erodibility is significantly related to soil texture (Wischmeier & Smith, 1978):

$$K = \left[2.1 \times 10^{-4} M^{1.14} (12 - OM) + 3.25(S_c - 2) + 2.5(P_c - 3)\right] \Big/ 100 \quad (8)$$

$$M = N_1 (100 - N_2) \quad (9)$$

where K (t h MJ^{-1} mm^{-1}) represents soil erodibility, N_1 (0.002–0.1 mm) represents the percentage of silt (0.002–0.05 mm) plus very fine sand (0.05–0.1 mm), N_2 (<0.002 mm) is the clay fraction, OM is the soil organic matter content (%), S_c is the soil structure code, and P_c is the soil permeability code.

The slope length (L) and the slope gradient (S) factors represent the influence of terrain indices on soil erosion in the RUSLE (Qiu et al., 2018; Tian et al., 2020). The calculation method of LS on steep slopes was revised (Liu & Zhang, 2002; Qiu et al., 2018), avoiding the limitation (slope gradient ≤18.0%) in the calculation of LS in the RUSLE:

$$L = (\lambda / 22.13)^m \quad (10)$$

$$m = \begin{cases} 0.2 & \theta < 1\% \\ 0.3 & 1\% \leqslant \theta < 3\% \\ 0.4 & 3\% \leqslant \theta < 9\% \\ 05 & \theta \geqslant 9\% \end{cases} \quad (11)$$

where L is the slope length factor, λ is the slope length of each cell, m is the slope length exponent which is calculated by slope θ.

The formula of the S factor is as follows:

$$S = \begin{cases} 10.8 \sin\theta + 0.03 & \theta < 9\% \\ 16.8 \sin\theta - 0.05 & 9\% \leqslant \theta < 18\% \\ 21.9 \sin\theta - 0.96 & \theta \geqslant 18\% \end{cases} \quad (12)$$

where S is the slope gradient factor which is calculated by slope θ.

The cover management (C) factor in the RUSLE is closely related to the Normalized Difference Vegetation Index (NDVI) (Yan et al., 2020; Zhou et al., 2006), and its calculation formula is as follows:

Table 2
The information of runoff plots in four parts of typical mountainous and hilly areas used for validation of the improved RUSLE.

Study areas	Location	Number of plots	Sample sizes	Slope (°)	Length and width (m × m)	Soil type	Land use	SWC measures
SW	Changyang	4	20	5–30	20 × 5	RS	F, G	TP
	Wufeng	3	15	5–25	20 × 5	YS	F, G, O	BH, TP
	Lichuan	6	26	15	10 × 5	YBS	G, O	TP, TR
	Enshi	8	24	5–30	20 × 5	YS	G, W	BH, BE
	Xianfeng	4	18	10–25	20 × 5	RS	W, O	TP
	Xuan'en	6	16	25	20 × 5	PS	F, O	BH, ET
NW	Yunxi	2	17	5–25	20 × 5	YS	G, W, O	ET, EE
	Danjiangkou	4	21	20	20 × 5	YBS	F, O	TP
	Maojian	2	18	15	20 × 5	RS	F	TP
	Yunyang	4	26	5–25	20 × 5	PS	F, G	ET, TP
NE	Macheng	6	26	15–25	20 × 5	YBS	F, G	TP, TR
	Yingshan	4	20	10–25	20 × 5	YBS	F, O	BH, BS
	Tuanfeng	4	15	25	20 × 5	RS	F, W, G	BH, BE, ET
	Qichun	3	17	10–25	20 × 5	YS	F, O	TP
	Luotian	4	26	5–15	10 × 5	YS	W, O	TP, TR
	Hong'an	2	18	15	20 × 5	YBS	F, O	ET, TR
	Huanggang	2	31	10–25	20 × 5	YBS	F, G, O	BH, BE, TP
	Xinzhou	4	26	5–30	20 × 5	PS	F, O	BH, BE, ET
	Zengdu	3	23	10–25	20 × 5	RS	F, G, O	TP
SE	Daye	4	29	25	20 × 5	YBS	F, W, O	BH, BE, TP
	Yangxin	3	19	15–30	20 × 5	RS	F, O	ET, TP
	Tongcheng	8	27	5–30	20 × 5	RS	F, G, O	BH, BE
	Tongshan	2	38	5–15	20 × 5	YBS	W, O	TP
	Xianning	4	26	15–25	20 × 5	YS	F, W, O	BH, BE, TP
Total	24	96	559	–	–	4	4	7

Note: SW, NW, NE and SE refer to southwest part, northwest part, northeast part and southeast part of mountainous and hilly areas of Hubei province, respectively. RS, YS, YBS and PS mean Red Soil, Yellow Soil, Yellow-brown Soil and Purple Soil respectively. F, W, G and O represent the farmland, woodland, grassland and other land use types respectively. BH, BE and BS refer to the biological measures with contour hedgerows, economic forests and shelter forests, respectively; ET and EE mean the engineering measures with terraces and stone embankments, respectively; TP and TR mean tillage measures with crop planting and rotation, respectively.

$$\begin{array}{ll} C = 1 & f < 0.1 \\ C = 0.6508 - 0.3436\lg f & 0.1 \leqslant \theta \leqslant 0.783 \\ C = 0 & f > 0.783 \end{array} \quad (13)$$

$$f = \frac{NDVI - NDVI_s}{NDVI_v - NDVI_s} \quad (14)$$

where C is the cover management factor, f is the vegetation coverage, $NDVI_s$ and $NDVI_v$ are the $NDVI$ values for pure bare soil pixels, and pure vegetation pixels respectively.

2.2.4. Validation of the improved RUSLE by the monitoring data

We used the measured data of 96 runoff plots in four mountainous and hilly areas and classified them according to the land use types, slope and SWC measures (Table 2), due to the lack of the large-scale measured data obtained from the soil conservation monitoring stations in this study area. The land use types of the runoff plots include farmland (mainly peanuts and corn), woodland (economic forest tea trees), grassland and planting hedgerow, the main soil types are yellow soil and yellow-brown soil, with a slope range of 5–30°. These runoff plots are relatively evenly distributed in four parts of the typical mountainous and hilly area of Hubei Province, with 31 in the southwest part, 12 in the northwest part, 32 in the northeast part and 21 in the southeast part (Table 2).

Table 3
The standard for classification and grading of soil erosion intensity.

Soil erosion intensity	SEM (t km^{-2} a^{-1})
Slight	<500
Mild	500–2500
Moderate	2500–5000
Strong	5000–8000
Very strong	8000–15,000
Severe	>15,000

Due to the span of the study period and the limitation of data acquisition, we used the measured soil erosion data of different runoff plots in 2000, 2005, 2010 and 2015 as the true value (Table 2), and the improved RUSLE prediction results to determine the coefficient of determination (R^2) (Hessel et al., 2014) and Root Mean Square Error (RMSE) (Chen et al., 2007) verification.

$$R^2 = \left(\frac{\sum_{i=1}^{n} \left(O_i - \overline{O}\right)\left(P_i - \overline{P}\right)}{\sqrt{\sum_{i=1}^{n} \left(O_i - \overline{O}\right)^2} \sqrt{\sum_{i=1}^{n} \left(P_i - \overline{P}\right)^2}} \right) \quad (15)$$

$$RMSE = \sqrt{\frac{1}{n} \sum_{i=1}^{n} (P_i - O_i)^2} \quad (16)$$

where n is the total number of runoff cells, i is the runoff cell number, O and P are the observed and predicted values, respectively; $\overline{P}$ and $\overline{O}$ are the average of the observed and predicted values, respectively.

2.2.5. Classification of soil erosion intensity

According to the "Soil Erosion Classification and Grading Standard" (Table 3) issued by the Ministry of Water Resources of the People's Republic of China (2008), the soil erosion intensity was classified into six levels. Due to the difference between the unit of the grading standard and Eq. (1), we regrouped the unit with the grading standard. Areas with a soil erosion modulus (SEM) greater than 500 (slight erosion intensity) were identified as erosion areas in this study.

2.3. Data sources

The data involved in this research include statistical yearbooks,

bulletin data, and remote sensing data. The statistics and bulletin data are sourced from the research district government website (http://slt.hubei.gov.cn), and it includes the soil erosion monitoring data of different 96 runoff plots with 559 erosion records in the four mountainous and hilly areas of Hubei province, which is used to verify the accuracy of the improved RUSLE. The monitoring data includes the *SEM*, land use types, SWC measures and basic properties of runoff plots (area, slope, etc.) recorded from 2000 to 2019.

The remote sensing data includes land cover, land use data and NDVI data in the study year from Google Earth Engine (https://developers.google.com/earth-engine), the data sources include Landsat ETM+ and Landsat 7 ETM data, rainfall data comes from China Meteorological Network (http://data.cma.cn), soil type data and soil erodibility data are obtained from the National Earth System Science Data Center, National Science & Technology Infrastructure of China (http://www.geodata.cn), the digital elevation model (DEM) data is SRTM data with resolution of 30 m data (https://www.usgs.gov). The administrative district boundary refers to the 1:18 million Chinese administrative district boundary data (http://www.resdc.cn). In order to reduce the error, all data was sampled at 30.0 m in ArcGIS 10.2.

3. Results

3.1. Validating the applicability of the improved RUSLE

To verify the accuracy of the improved RUSLE, the measured soil erosion modulus (*SEM*) derived from 96 runoff plots and the improved RUSLE were fitted (Fig. 2). The fitting results showed the high fitting accuracy with the R^2 of 0.89, and the RMSE of 44.71 t km^{-2} a^{-1}. The measured and predicted average *SEM* were 308.90 t km^{-2} a^{-1} and 373.20 t km^{-2} a^{-1}, respectively, with the standard deviation of 391.19 t km^{-2} a^{-1} and 415.40 t km^{-2} a^{-1}. The relative errors between measured and predicted *SEM* for farmland, grassland, woodland and other land types were less than 20.0%. In addition, more than 63.0% of the predicted result by the improved RUSLE had absolute errors within 50.00 t km^{-2} a^{-1}, and absolute errors of more than 42.0% were less than 20.00 t km^{-2} a^{-1} (Fig. 2). Therefore, a small RMSE value reflected an efficient prediction result. The verification results of the improved RUSLE in the study area showed high accuracy, but generally overestimated the *SEM* (Fig. 2).

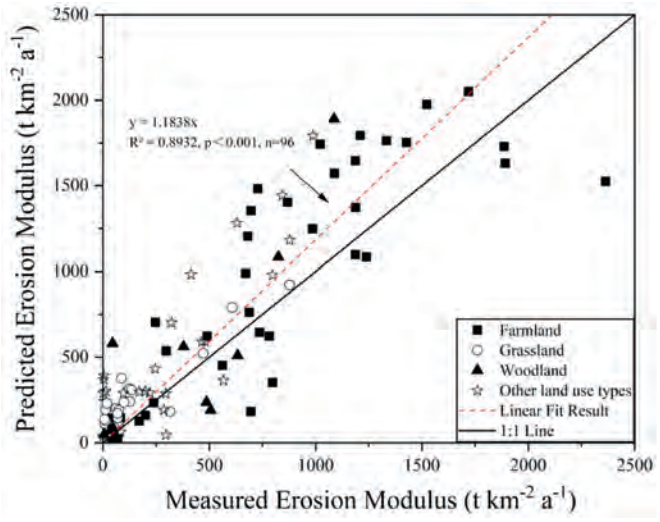

Fig. 2. Validation of predicted soil erosion modulus (*SEM*) by the improved RUSLE based on the monitoring data of 96 runoff plots with different land use types in 2000, 2005, 2010 and 2015.

3.2. Improved P factor of the RUSLE

The P values ranged from 0 to 1 in the whole study area with an average of 0.48, 0.38, 0.47, and 0.35 in 2000, 2005, 2010, and 2015, respectively, showing a downward trend. Areas with high P values were distributed in the northwest and southwest parts (Fig. 3). The southwest Hubei was the region with the largest range of changes, with an average P value increased by more than 25.0%.

The calculated subfactor ($P_{struc.}$) values for different SWC measures, subfactor ($P_{cont.}$) values for contouring, and overall P values with SWC measures for different land use types in the study area were presented in Table 4. The $P_{struc.}$ values for farmland with tillage measures ($P_{struc.} < 0.74$) and grasslands with engineering measures ($P_{struc} < 0.59$) were relatively low (Table 4). Areas with biological measures were prone to have low $P_{struc.}$ values on woodlands ($P_{struc} < 0.55$) and other land use types ($P_{struc} < 0.79$). The $P_{cont.}$ values for farmlands, grasslands, woodlands and other land use types were 0.72, 0.39, 0.51 and 0.64 respectively, which were calculated by slope gradient (contour) for various land use types. Relatively low P values tended to exist on farmlands ($0.30 < P < 0.53$) with tillage measures, grassland ($0.13 < P < 0.23$) with engineering measures, woodlands ($0.14 < P < 0.28$) with biological measures, and other land use types ($0.42 < P < 0.51$) with biological measures.

Overall, the P values ranged from 0.30 to 0.72 on farmland, with an average value of 0.55, which was the highest among the four land use types. Seasonal soil loss could be suppressed by SWC measures, while relatively high subfactors ($P_{cont.}$) values of farmlands might lead to relatively high P values. The P values ranged from 0.13 to 0.37 on woodlands, with an average value of 0.27. The P values ranged from 0.13 to 0.25 on grassland, with an average value of 0.18, which was the lowest. P values ranged from 0.42 to 0.60 on other land use types, with an average value of 0.49.

3.3. The RKLSC factors of the RUSLE

R values, ranging from 1657 to 6340 MJ mm^{-1} ha^{-1} h^{-1} a^{-1}, had an average value of 3920 MJ mm^{-1} ha^{-1} h^{-1} a^{-1} in 2000, 3487 MJ mm^{-1} ha^{-1} h^{-1} a^{-1} in 2005, 3961 MJ mm^{-1} ha^{-1} h^{-1} a^{-1} in 2010, 3671 MJ mm^{-1} ha^{-1} h^{-1} a^{-1} in 2015, indicating that the erosion potential caused by rainfall had a downward trend. Areas with high R values were mainly concentrated in the southeast and northeast parts of the study area.

K values, ranging from 0 to 0.0135 t h MJ^{-1} mm^{-1}, had the highest value in purple soil, while the lowest value in red soil. High K values tended to distribute in the northwest and southwest parts. The areas with more than 100 m of slope length occupied nearly 41.0% of the total areas, and L values ranged from 0 to 13.1. The slope gradient was 25.1° on average, and S values ranged from 0 to 20.6. Areas with low LS values were mainly distributed in the basin parts.

The distribution of C values had a strong correlation with land use types and vegetation coverage. Low C values were mainly distributed on the woodland, while high C values were mainly distributed on the farmland of southeast and northeast parts. The C values ranged from 0 to 1, with average values of 0.1482, 0.1521, 0.1530, and 0.1578 in 2000, 2005, 2010, and 2015 respectively.

3.4. Temporal and spatial distribution of soil erosion intensity

The average soil erosion modulus (*SEM*) in 2000, 2005, 2010, 2015 and 2019 were 1681.21, 1673.14, 1594.70, 1482.40 and 1437.50 t km^{-2} a^{-1}, respectively (Fig. 4). The erosion areas were 46,462, 42,330, 38,034, 33,240 and 25,679 km^2 in 2000, 2005, 2010,

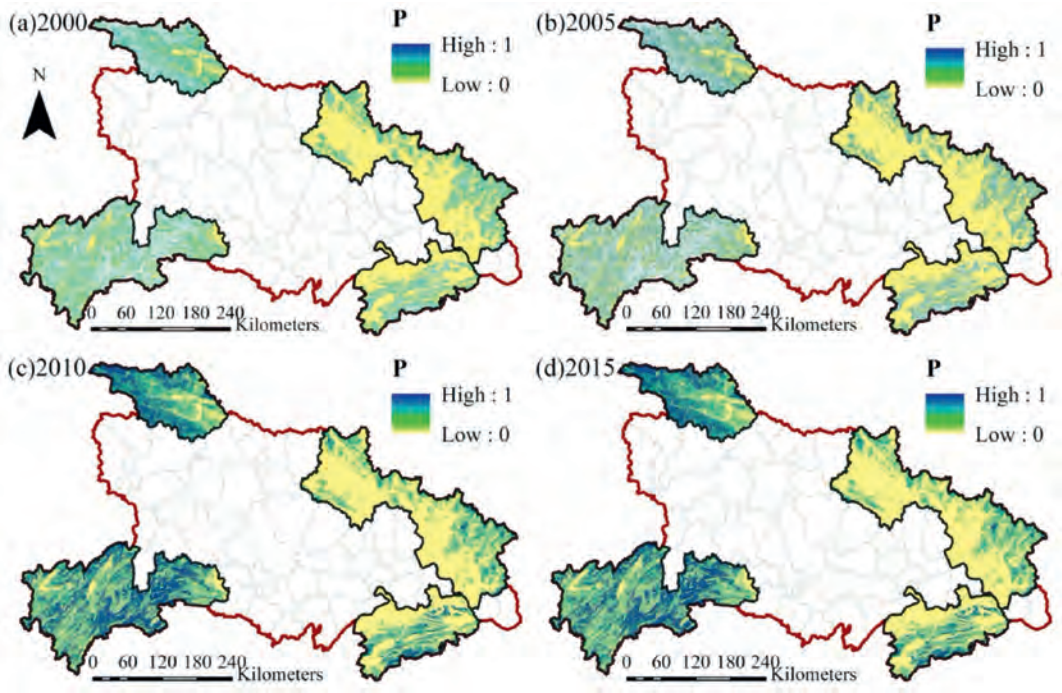

Fig. 3. Spatial variances of conservation practice factor (P) of the typical mountainous and hilly areas in Hubei Province in the improved RUSLE in 2000, 2005, 2010, and 2015.

Table 4
Calculated subfactor ($P_{struc.}$) values for different SWC measures, subfactor ($P_{cont.}$) values for contouring, and overall P values for different land use types of 2000, 2005, 2010 and 2015.

Type	Year	$P_{struc.}$	$P_{cont.}$	P	Year	$P_{struc.}$	$P_{cont.}$	P	Year	$P_{struc.}$	$P_{cont.}$	P	Year	$P_{struc.}$	$P_{cont.}$	P
F–B	2000	1.00	0.72	0.72	2005	1.00	0.72	0.72	2010	1.00	0.72	0.72	2015	1.00	0.72	0.72
F-E	2000	0.46	0.72	0.33	2005	0.72	0.72	0.52	2010	0.78	0.72	0.56	2015	0.81	0.72	0.58
F-T	2000	0.41	0.72	0.30	2005	0.52	0.72	0.37	2010	0.72	0.72	0.52	2015	0.74	0.72	0.53
W–B	2000	0.27	0.51	0.14	2005	0.47	0.51	0.24	2010	0.55	0.51	0.28	2015	0.52	0.51	0.27
W-E	2000	0.26	0.51	0.13	2005	0.51	0.51	0.26	2010	0.61	0.51	0.31	2015	0.56	0.51	0.29
W-T	2000	0.59	0.51	0.30	2005	0.73	0.51	0.37	2010	0.67	0.51	0.34	2015	0.69	0.51	0.35
G-B	2000	0.41	0.39	0.16	2005	0.57	0.39	0.22	2010	0.41	0.39	0.16	2015	0.44	0.39	0.17
G-E	2000	0.34	0.39	0.13	2005	0.59	0.39	0.23	2010	0.44	0.39	0.17	2015	0.37	0.39	0.14
G-T	2000	0.45	0.39	0.18	2005	0.64	0.39	0.25	2010	0.47	0.39	0.18	2015	0.36	0.39	0.14
O–B	2000	0.71	0.64	0.45	2005	0.79	0.64	0.51	2010	0.68	0.64	0.44	2015	0.66	0.64	0.42
O-E	2000	0.66	0.64	0.42	2005	0.81	0.64	0.52	2010	0.73	0.64	0.47	2015	0.76	0.64	0.49
O-T	2000	0.84	0.64	0.54	2005	0.94	0.64	0.60	2010	0.79	0.64	0.51	2015	0.78	0.64	0.50

Note: F refers to Farmlands, W refers to Woodlands, G refers to Grasslands, O refers to Other land use types. B represents Biological measures of SWC; E represents Engineering measures and T represents Tillage measures of SWC. For instance, F–B means Farmlands with Biological measures of SWC.

2015 and 2019, respectively, with a decline of 44.7% for 19 years.

The soil erosion intensity of the typical mountainous and hilly areas in Hubei Province showed temporal and spatial heterogeneity. Based on the soil erosion intensity classification standard, the soil erosion intensity in northeast part of the study area was mainly slight, mild and severe erosion, accounting for more than 50.0% in 19 years. The soil erosion intensity in the southeast part was mainly slight, moderate and strong erosion, while strong and very strong erosion accounted for the most in the northwest area, despite Danjiangkou maintained a slight intensity in 19 years. The soil erosion intensity in southwest Hubei was mainly strong, very strong and severe erosion. In general, the degree of soil erosion of the study area has changed from strong, very strong and severe erosion to slight erosion dominating.

During the period from 2000 to 2019, the area of mild erosion, moderate erosion, strong erosion and very strong erosion all showed a certain degree of decline, and the proportion of their erosion areas were reduced to 20.2%, 16.5%, 2.6% respectively (Fig. 5). By contrast, the area of slight erosion increased to 39.9% in 2019. In addition, the decrease in the average *SEM* and erosion areas also indicated that the soil erosion in the study area had been controlled to a certain extent.

4. Discussion

4.1. Modelling soil erosion by the improved RUSLE

The improved RUSLE has been validated by the measured soil erosion data of 96 runoff plots over the 2000–2015 period ($R^2 = 0.89$). To analyse the predicted accuracy of the improved RUSLE in the study area, we compared the modelling soil erosion results by the original RUSLE and by the improved RUSLE, as well as the monitoring soil erosion data during 2018–2019. The calculation methods for other factors (RKLSC) of the original RUSLE used for comparison were consistent with the improved RUSLE proposed in this paper. In addition, the original RUSLE also considered the

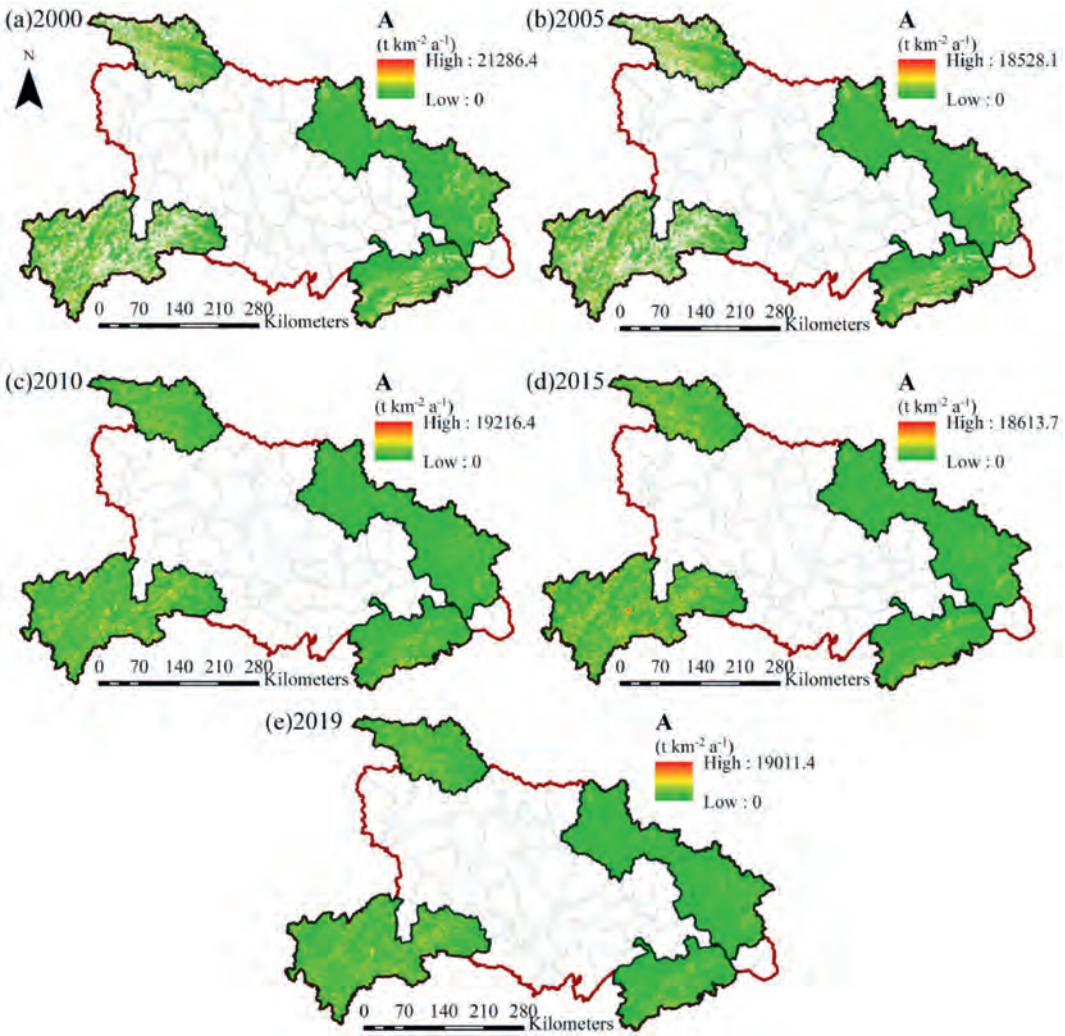

Fig. 4. Spatial variances of soil erosion modulus (*SEM*) of the typical mountainous and hilly areas in Hubei Province by the improved RUSLE of 2000, 2005, 2010, 2015 and 2019.

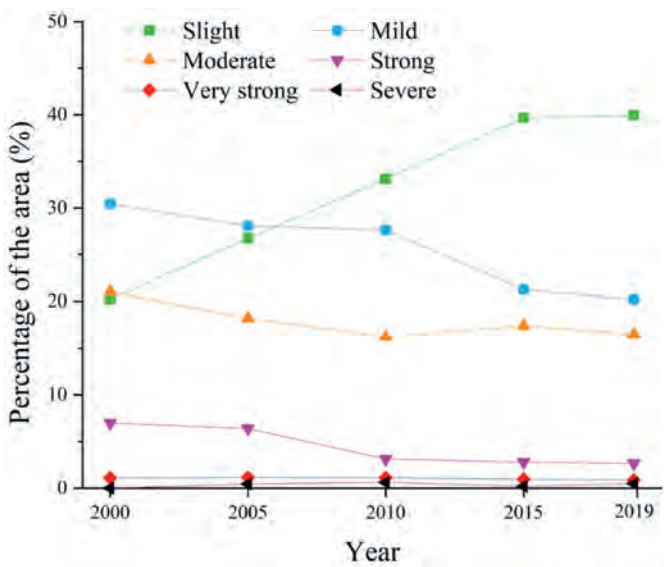

Fig. 5. Temporal variations of different soil erosion intensity of the typical mountainous and hilly areas in Hubei Province in 2000, 2005, 2010, 2015 and 2019.

influence of the slope gradient, land use types and partial SWC measures (terraces and cropping) in the calculation of the P factor (Panagos et al., 2015). Correspondingly, in order to clarify the accuracy of modelling soil erosion, we quantitatively compared the effectiveness for considering SWC measures in the P factor value by the original RUSLE and the improved RUSLE.

With the land use data obtained in 2018 and 2019, areas with highly similar SWC measures, soil types, soil erodibility, slope length, and multi-year average rainfall were selected for simulation. The *SEM* in 2018 and 2019 was predicted by the improved RUSLE and the original RUSLE respectively, and was verified by the monitoring data of runoff plots in the study area. The RMSE of our improved RUSLE (42.15 t km^{-2} a^{-1}) was 28.0% smaller than that of the original RUSLE (58.54 t km^{-2} a^{-1}), indicating a high accuracy of soil erosion simulation. In addition, comparing SEM for farmland, grassland, woodland and other land use types, the overall relative error in the improved RUSLE was smaller than that in the original RUSLE. Although some scholars considered the impact of SWC measures on the P value (Kebede et al., 2020; Taye et al., 2018), they mainly addressed the engineering measures (e.g., stone embankment). Inadequate consideration of various SWC measures might bring unexpected errors to the P value, especially in areas where multiple SWC measures exist. The SWC measures are significant for controlling surface soil loss, and the improved RUSLE has more

detailed calculation of the P factor for regions with SWC measures, thus avoiding errors caused by insufficient consideration of these measures. In addition, the traditional P factor calculation method is too general to summarize the value of woodland, grassland and farmland at different slopes, which will overestimate the degree of soil loss in some areas with SWC measures. Therefore, the RUSLE with improved P factor proposed in this paper is highly effective and accurate for modelling soil erosion of the mountainous and hilly areas of Hubei Province.

4.2. The P factor improvement

The results in Table 4 showed the effectiveness of considering different SWC measures during 2000–2015. The $P_{struc.}$ values of the improved RUSLE were mainly determined by the seasonal soil loss rate, while the $P_{struc.}$ values could be significantly reduced by SWC measures for various land use types. The average $P_{struc.}$ Values for farmland, grassland, woodland and other land use types in 2019 were 0.60, 0.44, 0.45 and 0.71 respectively, while $P_{cont.}$ were 0.72, 0.39, 0.51 and 0.64 respectively. In addition, the average P value obtained from the modelling results of the improved RUSLE in 2019 was 0.39, which was 35.8% lower than that by the original RUSLE. From 2000 to 2019, the SWC measures carried out by Hubei Province focused on biological measures (e.g., vegetation construction, operating economic fruit forests and afforestation), engineering measures (e.g., building terraces and stone embankment) and tillage measures (e.g., crop rotation) (Chen et al., 2019) (Fig. 6). The growth in land use data and statistics showed a steady upward trend. Incorporating with the implementation of SWC measures, the P value reflected varying degrees of impact on farmland, grassland, woodland and other land use types (Taye et al., 2018). In the study area, grassland and woodland were assigned a value of 1.00 when SWC measures were not involved (Wang & Su, 2020), and the average P value after considering SWC measures was 0.18 and 0.27 respectively. The average P value of farmlands was 0.67 in the original RUSLE, while 0.55 in the improved RUSLE. Overall, the average P values of the improved RUSLE in 2000, 2005, 2010, 2015 and 2019 were 0.32, 0.40, 0.39, 0.38 and 0.39, respectively, which were 11.8%–31.2% lower than those of the original RUSLE. Therefore, with the consideration of SWC measures, the average value of P factor was smaller in comparison to the original RUSLE, indicating that *SEM* could be estimated more reasonably and avoid overestimation results due to 11.8%–31.2% relative reduction of the average P values of the improved RUSLE (Table 5).

To determine the P value, the most important part is to identify the quantitative impacts of SWC measures. Biological measures were obtained by extracting vegetation changes and new artificial vegetation. The accuracy limitation of remote sensing data and the verification of statistical data might lead to certain deviations. The pixel features in remote sensing data might be not enough to be considered as SWC measures, but SWC measures actually exist. The verification of engineering measures and tillage measures for terrains and crop rotation also relies on the support of statistical data, and objectively there will be a certain range of verification deviations. Thus, it is necessary to use high-resolution image data to maximally reduce the impact of uncertainty in the recognition process on the results.

4.3. Targeted soil erosion prevention measures

Targeted SWC measures for different regions could be suggested by quantitatively assessing the effect of different SWC measures on the P value (Kebede et al., 2020). In the mountainous and hilly areas of Hubei Province, we successfully tested the effects of different SWC measures on different land use types, which was mainly reflected in the P values. With the 0.05 significance level, relatively low average P values tended to appear on farmland with tillage measures ($P = 0.34$), grassland with engineering measures ($P = 0.13$), woodland with biological measures ($P = 0.18$), and other land use types with biological measures ($P = 0.36$) during 2000–2019 (Fig. 7).

The low P values of farmland with the implementation of tillage measures is due to more plant covers during the process of crop rotation, which indicates that the implementation of tillage

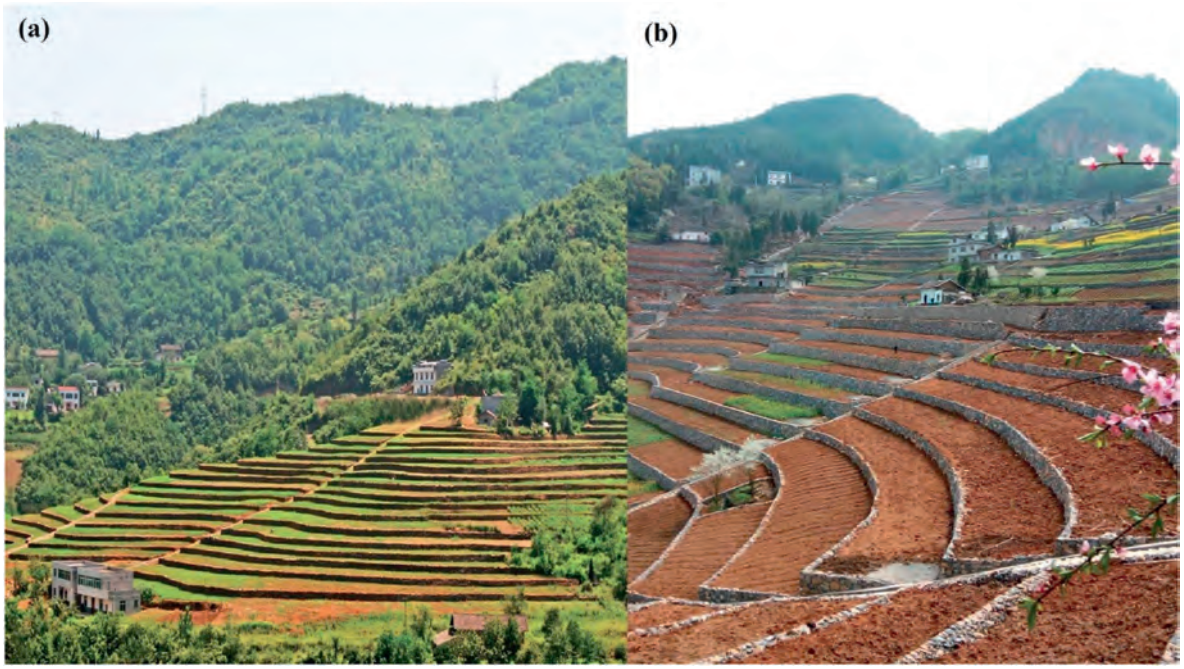

Fig. 6. The SWC measures for woodland and farmland include stone embankment (Engineering measures) and crop rotation (Tillage measures) in the mountainous and hilly areas of the northwest (a) and southwest (b) Hubei Province, China. Data from: Soil and Water Conservation Bulletin of Hubei Province in 2019.

Table 5
Comparison of predicted and measured *SEM* of farmland, grassland, woodland and other land use types in 2018 and 2019.

Land use types	2018 (*SEM*, t km^{-2} a^{-1})			Relative error (%)		2019 (*SEM*, t km^{-2} a^{-1})			Relative error (%)		RMSE (*SEM*, t km^{-2} a^{-1})	
	RUSLE	Improved RUSLE	Monitoring data	RUSLE	Improved RUSLE	RUSLE	Improved RUSLE	Monitoring data	RUSLE	Improved RUSLE	RUSLE	Improved RUSLE
Farmland	724.70	672.40	692.40	4.7	2.9	772.30	720.50	731.40	5.6	1.5	58.54	42.15
Grassland	102.50	90.20	72.40	41.6	24.6	192.40	109.70	131.50	46.3	16.6		
Woodland	331.60	291.40	251.40	31.9	15.9	298.20	279.60	258.60	15.3	8.1		
Other types	84.30	81.60	70.60	19.4	15.6	181.40	137.90	153.80	17.9	10.3		
Total	1243.10	1135.60	1086.80	14.4	4.5	1444.30	1247.70	1275.30	13.3	2.2		

Note: Other means other land use types; numbers refer to the soil erosion modulus (*SEM*) of 2018 and 2019; RUSLE means the original RUSLE; RMSE is the abbreviation of Root Mean Square Error; The calculation method of the P factor was calculated by $P_{cont.}$ (the contouring subfactor) and P_{swc} (terraces and cropping subfactors) (Panagos et al., 2015), while the $P_{cont.}$ values were consistent with that in the improved RUSLE due to the congruous slope gradients and land use types and the P_{swc} values were based on the two SWC measures (terraces and cropping) in the study area.

measures is an effective way to control soil loss. For the grassland, engineering measures, as an effective control method, should be promoted to reduce the soil erosion of fragile grassland caused by erosive rainfall. By contrast, for the woodland and other land use types, the results showed that biological measures (vegetation construction) were useful to reduce the P value, thus the soil loss rate could be reduced accordingly. Therefore, the inhibitory effect of biological measures on soil erosion in these two land use types should be strengthened. Arrangements of SWC measures for the study area are proposed: in the southeast and northeast part where farmlands dominate, the promotion of tillage measures should be considered due to the significant effects of soil conservation and economic benefits of farming; in the southwest part where woodlands are widely distributed, the implementation of biological measures is crucial; in the northwest part where grasslands mainly occupy, the promotion of engineering measures is urgent for soil loss control.

5. Conclusions

In this study, the RUSLE was improved by considering the quantitative impacts of various SWC measures on determining the P factor value. The applicability of the improved RUSLE was validated against the long-term (2000–2015) soil erosion monitoring data obtained from 96 runoff plots in typical mountainous and hilly areas of central China. The application of the improved RUSLE in the study area showed high efficiency ($R^2 = 0.89$). Based on the soil erosion monitoring data of 2018 and 2019, the soil erosion modelling accuracy of the improved RUSLE obviously increased (28.0%) in comparison to that of the original RUSLE, due to decrement (11.8%–31.2%) in the average P values of the improved RUSLE. There were relatively low average P values for farmlands with tillage measures, grasslands with engineering measures, woodlands with biological measures, and other land use types with biological measures, which illustrated that the SWC measures obviously reduced the P values for different land use types. The average soil erosion modulus in 2000, 2005, 2010, 2015 and 2019 of the study area were 1681.21, 1673.14, 1594.70, 1482.40 and 1437.50 t km^{-2} a^{-1}, respectively, showing a downward trend. In addition, arrangements of SWC measures for the study area were proposed: tillage measures should be strengthened in the southeast and northeast parts where farmlands dominate, biological measures should be promoted in the southwest part where woodlands are widely distributed, and engineering measures are crucial in the northwest part where grasslands mainly occupy.

The RUSLE with improved P factor considering various SWC measures showed high accuracy in this study, and it was verified with the soil erosion monitoring data of local runoff plots with slope gradients of 15–35°. In future research, the slope divisions of all terrains and related monitoring soil erosion data in the specific area should be covered, and higher-precision remote sensing data for identifying the SWC measures needs to be utilized. In this case, the obtained P value of the RUSLE in different combinations of land use types could better reflect the reduction effect of soil loss rate by the conservation practice.

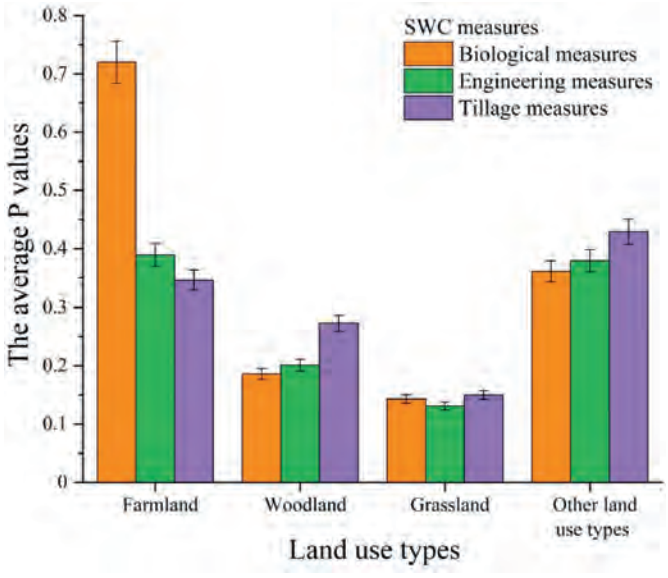

Fig. 7. The average P values of the RUSLE in the areas with different land use types and SWC measures during 2000–2019. At the 0.05 significance level, the P factor value in our study has significant differences in different SWC measures, while there is no significant difference in the P factor value in different land use types.

Declaration of competing interest

We declare that we have no known competing financial interests or personal relationships that could have appeared to influence the work reported in this paper.

Acknowledgments

This research was jointly funded by the Natural Science Foundation of China Project (41907061), the National Key Research and Development Program (2016YFC0503506), the Research Program from the State Key Laboratory of Soil Erosion and Dryland Farming on the Loess Plateau (A314021402-2005), and the Research Center on Mountain Torrent & Geologic Disaster Prevention of the Ministry of Water Resources, Changjiang River Scientific Research Institute (CKWV2019761/KY).

References

Alewell, C., Borrelli, P., Meusburger, K., & Panagos, P. (2019). Using the USLE: Chances, challenges and limitations of soil erosion modelling. *International Soil and Water Conservation Research, 7*(3), 203–225. https://doi.org/10.1016/j.iswcr.2019.05.004

Angima, S. D., Stott, D. E., O'neill, M. K., Ong, C. K., & Weesies, G. A. (2003). Soil erosion prediction using RUSLE for central Kenyan highland conditions. *Agriculture, Ecosystems & Environment, 97*(1–3), 295–308. https://doi.org/10.1016/S0167-8809(03)00011-2

Behera, M., Sena, D. R., Mandal, U., Kashyap, P. S., & Dash, S. S. (2020). Integrated GIS-based RUSLE approach for quantification of potential soil erosion under future climate change scenarios. *Environmental Monitoring and Assessment, 192*(11), 1–18. https://doi-org.ezproxy.is.ed.ac.uk/10.1007/s10661-020-08688-2.

Belachew, A., Mekuria, W., & Nachimuthu, K. (2020). Factors influencing adoption of soil and water conservation practices in the northwest Ethiopian highlands. *International Soil and Water Conservation Research, 8*(1), 80–89. https://doi.org/10.1016/j.iswcr.2020.01.005

Biddoccu, M., Guzmán, G., Capello, G., Thielke, T., Strauss, P., Winter, S., Zaller, J. G., Nicolai, A., Cluzeau, D., Popescu, D., Bunea, C., Hoble, A., Cavallo, E., & Gómez, J. A. (2020). Evaluation of soil erosion risk and identification of soil cover and management factor (C) for RUSLE in European vineyards with different soil management. *International Soil and Water Conservation Research, 8*(4), 337–353. https://doi.org/10.1016/j.iswcr.2020.07.003

Chen, T., Niu, R., Li, P., Zhang, L., & Du, B. (2011). Regional soil erosion risk mapping using RUSLE, GIS, and remote sensing: A case study in Miyun watershed, North China. *Environmental Earth Sciences, 63*(3), 533–541. https://doi.org/10.1007/s12665-010-0715-z

Chen, Y., Pan, W., & Cai, Y. (2007). Assessment of soil erosion sensitivity in watershed based on RUSLE——a case study of Jixi watershed [J]. *Journal of Mountain Science, 4*, 017. (In Chinese with English abstract).

Chen, J., Xiao, H., Li, Z., Liu, C., Ning, K., & Tang, C. (2020). How effective are soil and water conservation measures (SWCMs) in reducing soil and water losses in the red soil hilly region of China? A meta-analysis of field plot data. *The Science of the Total Environment, 735*, 139517. https://doi.org/10.1016/j.scitotenv.2020.139517

Chen, S., Zha, X., Bai, Y., & Wang, L. (2019). Evaluation of soil erosion vulnerability on the basis of exposure, sensitivity, and adaptive capacity: A case study in the Zhuxi watershed, Changting, Fujian Province, southern China. *Catena, 177*, 57–69. https://doi.org/10.1016/j.catena.2019.01.036

Chuenchum, P., Xu, M., & Tang, W. (2020). Estimation of soil erosion and sediment yield in the Lancang–Mekong river using the Modified revised universal soil loss equation and GIS techniques. *Water, 12*(1), 135. https://doi.org/10.3390/w12010135

Diyabalanage, S., Samarakoon, K. K., Adikari, S. B., & Hewawasam, T. (2017). Impact of soil and water conservation measures on soil erosion rate and sediment yields in a tropical watershed in the Central Highlands of Sri Lanka. *Applied Geography, 79*, 103–114. https://doi.org/10.1016/j.apgeog.2016.12.004

Duan, X., Bai, Z., Rong, L., Li, Y., Ding, J., Tao, Y., Li, J., Li, J., & Wang, W. (2020). Investigation method for regional soil erosion based on the Chinese Soil Loss Equation and high-resolution spatial data: Case study on the mountainous Yunnan Province, China. *Catena, 184*, 104237. https://doi.org/10.1016/j.catena.2019.104237

Duan, X., Rong, L., Bai, Z., Gu, Z., Ding, J., Tao, Y., Li, J., Li, J., Wang, W., & Yin, X. (2020). Effects of soil conservation measures on soil erosion in the Yunnan Plateau, southwest China. *Journal of Soil and Water Conservation, 75*(2), 131–142. https://doi.org/10.2489/jswc.75.2.131

Fang, H. (2021). Impacts of soil conservation measures on runoff and soil loss in a hilly region, Northern China. *Agricultural Water Management, 247*, 106740. https://doi.org/10.1016/j.agwat.2021.106740

Farhan, Y., & Nawaiseh, S. (2015). Spatial assessment of soil erosion risk using RUSLE and GIS techniques. *Environmental Earth Sciences, 74*(6), 4649–4669. https://doi-org.ezproxy.is.ed.ac.uk/10.1007/s12665-015-4430-7.

Foster, G. R., Flanagan, D. C., Nearing, M. A., Lane, L. J., Risse, M. M., & Finkner, S. C. (1995). Hillslope erosion component. In D. C. Flanagan, & M. D. Nearing (Eds.), *USDA–Water erosion prediction Project, technical documentation, NSER report 10. National soil erosion research laboratory, west lafayette*.

Foster, G. R., Lane, L. J., Nowlin, J. D., Laflen, J. M., & Young, R. A. (1981). Estimating erosion and sediment yield on field-sized areas. *Transactions of the ASAE, 24*(5), 1253–1262.

Fu, B. J., Zhao, W. W., Chen, L. D., Zhang, Q. J., Lü, Y. H., Gulinck, H., & Poesen, J. (2005). Assessment of soil erosion at large watershed scale using RUSLE and GIS: A case study in the Loess Plateau of China: Assessment OF soil erosion using RUSLE and GIS. *Land Degradation & Development, 16*(1), 73–85. https://doi.org/10.1002/ldr.646

Guerra, C. A., Maes, J., Geijzendorffer, I., & Metzger, M. J. (2016). An assessment of soil erosion prevention by vegetation in Mediterranean Europe: Current trends of ecosystem service provision. *Ecological Indicators, 60*, 213–222. https://doi.org/10.1016/j.ecolind.2015.06.043

Hessel, R., Daroussin, J., Verzandvoort, S., & Walvoort, D. (2014). Evaluation of two different soil databases to assess soil erosion sensitivity with MESALES for three areas in Europe and Morocco. *Catena, 118*, 234–247. https://doi.org/10.1016/j.catena.2014.01.012

Huang, J., Zhang, F., Hu, Z., & Chen, S. (2019). Climatology of rainfall erosivity during 1961–2012 in Jiangsu Province, southeast China. *Natural Hazards, 98*(3), 1155–1168. https://doi.org/10.1007/s11069-018-3391-z

Hubei Provincial Department of Water Resources. (2017). Hubei Province soil and water conservation Plan (2016-2030. Retrieved from: http://www.hubei.gov.cn/zwgk/hbyw/hbywqb/201708/t20170816_1487264.shtml.

Islam, M. R., Jaafar, W. Z. W., Hin, L. S., Osman, N., & Karim, M. R. (2020). Development of an erosion model for Langat river basin, Malaysia, adapting GIS and RS in RUSLE. *Applied Water Science, 10*(7), 1–11. https://doi-org.ezproxy.is.ed.ac.uk/10.1007/s13201-020-01185-4.

Kebede, B., Tsunekawa, A., Haregeweyn, N., Adgo, E., Ebabu, K., Meshesha, D. T., Tsubo, M., Masunaga, T., & Fenta, A. A. (2020). Determining C-and Ps of RUSLE for different land uses and management practices across agro-ecologies: Case studies from the Upper Blue Nile basin, Ethiopia. *Physical Geography*, 1–23. https://doi.org/10.1080/02723646.2020.1762831

Liu, B., & Zhang, K. X. Y. (2002). An empirical soil loss equation. *Proc. 12th ISCO Conf, 2*, 21–25.

Ministry of Water Resources of the People's Republic of China. (2008). Standards for classification and gradation of soil erosion. Retrieved from http://zwgk.mwr.gov.cn/jsp/yishenqing/appladd/biaozhunfile/flash/preview.jsp?bzMax=SL190-2007.

Morgan, R. P. C., Quinton, J. N., Smith, R. E., Govers, G., Poesen, J. W. A., Auerswald, K., Chisci, G., Torri, D., & Styczen, M. E. (1998). The European soil erosion model (EUROSEM): A dynamic approach for predicting sediment transport from fields and small catchments. *Earth Surface Processes and Landforms: The Journal of the British Geomorphological Group, 23*(6), 527–544.

Nearing, M. A., Foster, G. R., Lane, L. J., & Finkner, S. C. (1989). A process-based soil erosion model for USDA-Water Erosion Prediction Project technology. *Transactions of the ASAE, 32*(5), 1587–1593.

Nyssen, J., Poesen, J., Haile, M., Moeyersons, J., Deckers, J., & Hurni, H. (2009). Effects of land use and land cover on sheet and rill erosion rates in the Tigray highlands, Ethiopia. *Zeitschrift f?? R Geomorphologie, 53*(2), 171–197. https://doi.org/10.1127/0372-8854/2009/0053-0171

Owens, P. N., & Collins, A. J. (2006). *Soil erosion and sediment redistribution in river catchments: Measurement, modelling and management. CABI*.

Panagos, P., Borrelli, P., Meusburger, K., van der Zanden, E. H., Poesen, J., & Alewell, C. (2015). Modelling the effect of support practices (P-factor) on the reduction of soil erosion by water at European scale. *Environmental Science & Policy, 51*, 23–34. https://doi.org/10.1016/j.envsci.2015.03.012

Pimentel, D. (2006). Soil erosion: A Food and environmental threat. *Environment, Development and Sustainability, 8*(1), 119–137. https://doi.org/10.1007/s10668-005-1262-8

Polykretis, C., Alexakis, D. D., Grillakis, M. G., & Manoudakis, S. (2020). Assessment of intra-annual and inter-annual variabilities of soil erosion in Crete Island (Greece) by incorporating the Dynamic "Nature" of R and C-Factors in RUSLE modeling. *Remote Sensing, 12*(15), 2439. https://doi.org/10.3390/rs12152439

Qiu, H., Cui, P., Regmi, A. D., Hu, S., Wang, X., & Zhang, Y. (2018). The effects of slope length and slope gradient on the size distributions of loess slides: Field observations and simulations. *Geomorphology, 300*, 69–76. https://doi.org/10.1016/j.geomorph.2017.10.020

Renard, K. G., Foster, G. R., Weesies, G. A., Mccool, D. K., & Yoder, D. C. (1997). Predicting soil erosion by water: A guide to conservation planning with the revised universal soil loss equation (RUSLE). In *Agriculture handbook 703* (p. 404). Washington: United States Department of Agriculture.

Robinson, D. A., Panagos, P., Borrelli, P., Jones, A., Montanarella, L., Tye, A., & Obst, C. G. (2017). Soil natural capital in europe; a framework for state and change assessment. *Scientific Reports, 7*(1), 6706. https://doi.org/10.1038/s41598-017-06819-3

Song, F., Yang, X., & Wu, F. (2020). Catastrophe progression method based on MK test and correlation analysis for assessing water resources carrying capacity in Hubei province. *Journal of Water and Climate Change, 11*(2), 556–567. https://doi.org/10.2166/wcc.2018.114

Sonneveld, B. G. J. S., & Nearing, M. A. (2003). A nonparametric/parametric analysis of the universal soil loss equation. *Catena, 52*(1), 9–21. https://doi.org/10.1016/S0341-8162(02)00150-9

Tamene, L., Adimassu, Z., Aynekulu, E., & Yaekob, T. (2017). Estimating landscape susceptibility to soil erosion using a GIS-based approach in Northern Ethiopia. *International Soil and Water Conservation Research, 5*(3), 221–230. https://doi.org/10.1016/j.iswcr.2017.05.002

Taye, G., Vanmaercke, M., Poesen, J., WeSEMael, B. V., Tesfaye, S., Teka, D., Nyssen, J., Deckers, J., & Haregeweyn, N. (2018). Determining RUSLE P- and C-factors for stone bunds and trenches in rangeland and cropland, North Ethiopia. *Land Degradation & Development, 29*(3), 812–824. https://doi.org/10.1002/ldr.2814

Tian, P., Pan, C., Xu, X., Wu, T., Yang, T., & Zhang, L. (2020). A field investigation on rill development and flow hydrodynamics under different upslope inflow and slope gradient conditions. *Hydrology Research, 51*(5), 1201–1220. https://doi.org/10.2166/nh.2020.168

Tu, A., Xie, S., Yu, Z., Li, Y., & Nie, X. (2018). Long-term effect of soil and water conservation measures on runoff, sediment and their relationship in an orchard on sloping red soil of southern China. *PloS One, 13*(9), Article e0203669. https://doi.org/10.1371/journal.pone.0203669. e0203669.

Wang, R., & Li, C. (2016). Spatiotemporal analysis of precipitation trends during 1961–2010 in Hubei province, central China. *Theoretical and Applied Climatology, 124*(1–2), 385–399. https://doi.org/10.1007/s00704-015-1426-x

Wang, Z., & Su, Y. (2020). Assessment of soil erosion in the Qinba mountains of the southern shaanxi Province in China using the RUSLE model. *Sustainability, 12*(5),

1733. https://doi.org/10.3390/su12051733
Wischmeier, W. H., & Smith, D. D. (1978). *Predicting rainfall erosion losses: A guide to conservation planning. Department of agriculture, science and education administration*.
Xu, S., Liu, Y., Gong, J., Wang, C., & Wang, Z. (2020). Comparing differences among three ecosystem service proxies for soil erosion prevention and their combination characteristics at local scales. *Ecological Indicators, 110*, 105929. https://doi.org/10.1016/j.ecolind.2019.105929
Yan, H., Wang, L., Wang, T. W., Wang, Z., & Shi, Z. H. (2020). A synthesized approach for estimating the C-factor of RUSLE for a mixed-landscape watershed: A case study in the Gongshui watershed, southern China. *Agriculture, Ecosystems & Environment, 301*, 107009. https://doi.org/10.1016/j.agee.2020.107009
Yu, G., Feng, J., Che, Y., Lin, X., Hu, L., & Yang, S. (2010). The identification and assessment of ecological risks for land consolidation based on the anticipation of ecosystem stabilization: A case study in Hubei Province, China. *Land Use Policy, 27*(2), 293–303. https://doi.org/10.1016/j.landusepol.2009.03.004
Zhang, K., Chao, L., Wang, Q., Huang, Y., Liu, R., Hong, Y., Tu, Y., Qu, W., & Ye, J. (2019). Using multi-satellite microwave remote sensing observations for retrieval of daily surface soil moisture across China. *Water Science and Engineering, 12*(2), 85–97. https://doi.org/10.1016/j.wse.2019.06.001
Zhang, W.-B., Xie, Y., & Liu, B.-Y. (2002). Rainfall erosivity estimation using daily rainfall amounts. *Scientia Geographica Sinica, 22*(6), 705–711 (In Chinese with English abstract).
Zhou, Z. C., Shangguan, Z. P., & Zhao, D. (2006). Modeling vegetation coverage and soil erosion in the Loess Plateau Area of China. *Ecological Modelling, 198*(1–2), 263–268. https://doi.org/10.1016/j.ecolmodel.2006.04.019
Zhu, M. (2015). Soil erosion assessment using USLE in the GIS environment: A case study in the Danjiangkou Reservoir region, China. *Environmental Earth Sciences, 73*(12), 7899–7908. https://doi.org/10.1007/s12665-014-3947-5
Zhu, D., Wang, T. W., Cai, C. F., Li, L., & Shi, Z. H. (2009). Large-scale assessment of soil erosion using a neuro-fuzzy model combined with GIS: A case study of Hubei Province, China. *Land Degradation & Development, 20*(6), 654–666. https://doi.org/10.1002/ldr.956

International Soil and Water Conservation Research 9 (2021) 445–460

Contents lists available at ScienceDirect

International Soil and Water Conservation Research

journal homepage: www.elsevier.com/locate/iswcr

Original Research Article

Generation of a long-term daily gridded precipitation dataset for the Upper Indus Basin (UIB) through temporal Reconstruction, Correction & Informed Regionalization-"ReCIR"

Asim Jahangir Khan [a, *], Manfred Koch [a]

[a] Department of Geohydraulics and Engineering Hydrology, University of Kassel, 34125, Kassel, Germany

ARTICLE INFO

Article history:
Received 3 September 2020
Received in revised form
15 January 2021
Accepted 19 January 2021
Available online 27 January 2021

Keywords:
Precipitation
Temporal reconstruction
Orographic correction factor (OCF)
Soil and water assessment tool (SWAT)
Glacier/water mass balance
Upper indus basin (UIB)

ABSTRACT

This study attempted to generate a long-term (1961–2010) daily gridded precipitation dataset for the Upper Indus Basin (UIB) with orographic adjustments so as to generate realistic precipitation estimates, enabling hydrological and water resource investigations that can close the water balance, that is difficult, if not impossible to achieve with the currently available precipitation data products for the basin. The procedure includes temporal reconstruction of precipitation series at points where data were not recorded prior to the mid-nineties, followed by a regionalization of the precipitation series to a smaller scale across the basin (0.125 ° × 0.125 °), while introducing adjustments for the orographic effect and changes in glacier storage. The reconstruction process involves interpolation of the precipitation at virtual locations of the current (1995-) dense observational network, followed by corrections for frequency and intensity and adjustments for temporal trends at these virtual locations. The data generated in this way were further validated for temporal and spatial representativeness through evaluation of SWAT-modelled streamflow responses against observed flows across the UIB. The results show that the calibrated SWAT-simulated daily discharge at the basin outlet as well as at different sub-basin outlets, when forcing the model with the reconstructed precipitation of years 1973–1996, is almost identical to that when forcing it with the reference precipitation data (1997–2008). Finally, the spatial distribution pattern of the reconstructed (1961–1996) and reference (1997–2008) precipitation were also found consistent across the UIB, reflecting well the large-scale atmospheric-circulation pattern in the region.

1. Introduction

High resolution climatic datasets are the primary input to spatially distributed rainfall-runoff models and water balance calculations. The quality of input climatic data is for sure the most important factor capable of influencing the simulation results (Andréassian et al., 2001; Duncan et al., 1993; Kobold & Sušelj, 2005; Leander et al., 2008; Rueland et al., 2010; Singh & Kumar, 1997) so that any errors in the input are amplified in the output (the runoff simulations) (Liu Y.B. and De Smedt F. 2004).

The spatial as well as the temporal precipitation patterns could be extremely variable, especially over mountainous catchments, (Archer & Fowler, 2004). Therefore it is extremely challenging to capture the true spatial distribution, owing in most cases to the overly limited spatial density of gauging networks (RODDA, 1971), but also due to the inability of the mostly lower altitude gauging stations, to capture the orographic effect (Khan & Koch, 2018a). The hydrological investigations in such catchments may therefore find "water imbalances", whereby streamflow totals exceed precipitation estimates. The problem could be further exaggerated by data quality issues, inhomogeneity or discontinuities in the temporal precipitation records.

The Upper Indus Basin (UIB) is not an exception to this recurrent problem in proper streamflow modelling as the observed precipitation data available for this basin also suffer from these problems. The unavailability of in-situ observational data, that have appropriate spatial, altitudinal and temporal coverage, is one of the major hindrances for hydro-meteorological investigations and climate change impact studies in the UIB (Khan & Koch, 2018a).

* Corresponding author.
E-mail addresses: asimjkw@gmail.com (A.J. Khan), kochm@uni-kassel.de, manfred_kochde@yahoo.de (M. Koch).

https://doi.org/10.1016/j.iswcr.2021.01.005

Similarly, as the climate station network in UIB are historically comprised of very few low altitude valley based stations, a long-term observational precipitation dataset in the high-altitude areas of the region is absent, (Ren et al., 2017; Sun et al., 2017; Zhan et al., 2017), although, since the mid-nineties, there are growing efforts to improve the observational network via installations of several higher altitude automatic weather stations. Nevertheless, the coverage is still very thin and the data less representative, especially for different elevation zones. Furthermore, the available data also needs a lot of pre-processing as it is uncorrected raw precipitation readings and need checking for quality issues and correction for gaps and losses. Similarly, while most of the weather stations have become operational after the mid-nineties, long-term data, that is needed for assessing local and regional hydro-climatology or climate change associated hydrological impacts, is only available at limited gauge points.

Over the last couple of decades substantial progress has been made in constructing a wide variety of global and/or regional scale gridded precipitation products and analysed fields. The most common and widely used products include gridded data sets such as:

- "ERA-Interim", the third generation global atmospheric reanalysis product by the European Centre for Medium-Range Weather Forecasts (Dee et al., 2011);

- "WFDEI", the Water and Global Change Project (WATCH) Forcing Data methodology applied to ERA-Interim data (Weedon et al., 2014);

- "TEMPA-TRMM", the Tropical Rainfall Measuring Mission -Multi-satellite Precipitation Analysis data (Huffman et al., 2007);

- "APHRODITE", the Asian Precipitation-highly Resolved Observational Data Integration Towards Evaluation of Water Resources (Yatagai et al., 2012), and so on.

These data products are in most cases merged or derived versions that are sourced from individual or multiple precipitation data product out of observed, satellite estimates and/or climate model reanalysis etc. Although these precipitation products and others have been of great help in providing a wider range of alternatives but are not without limitations, especially in their applicability to hydro-meteorological studies at regional scale. This is because most of these products are subject to either limited spatial resolution (Khan & Koch, 2018a; Lutz et al., 2016; Palazzi et al., 2013; Tahir, Chevallier, Arnaud, & Ahmad, 2011) or limited temporal resolution (Khan & Koch, 2018a; Lutz et al., 2016), or both. These limitations are further amplified, especially in regions with complex topography, such as the upper Indus basin (UIB) where the representation of a realistic precipitation regime is made difficult by factors like the complexity of the underlying atmospheric physics, limited efficiency of sensors to accurately account for precipitation of all forms (Andermann et al., 2011), or the insufficient coverage by the observational network, especially at higher altitudes or for longer durations (Khan & Koch, 2018a; Lutz et al., 2016; Tahir, Chevallier, Arnaud, & Ahmad, 2011). Resultantly, none of the data products is suitable enough for hydro-meteorological investigations at regional to catchment scales. These concerns have been reverberated by many researchers by indicating the evident overestimations by the ERA-interim estimates (Dahri et al. 2016, 2018) and considerable under estimations by all the other major gridded precipitation products that are derived wholly or partially based on the satellite remote sensing or the observational data (Dahri et al. 2016, 2018; Khan & Koch, 2018a; Lutz et al., 2016; Reggiani & Rientjes, 2015).

Overall, owing to the complex orography, extreme topographic and climate heterogeneity and the strong horizontal and vertical gradients in precipitation of the Hindu Kush Himalayan region (HKH) (Qiu, 2008; Sharma et al., 2016; Yanai & Li, 1994; Yao et al., 2012), neither the sensors based datasets nor the sparse observed station data or gridded data products based on them, fully represent the precipitation regime of the region (Palazzi et al., 2013; Wijngaard et al., 2017; Yatagai et al., 2012). These claims are in line with the fact that the average precipitation amounts over the UIB are unrealistically lower than the magnitudes required to sustain the observed discharge at the basin outlet (Immerzeel et al., 2015; Khan & Koch, 2018a) and this holds true for not only the estimates derived from the observed data set or the gridded data products based on the available sparse and low-altitude climatic station network, but also for the sensors-based gridded precipitation products (Khan et al., 2018; Khan & Koch, 2018a).

Though these issues have compelled many researchers to find ways to assess and employ methods for precipitation correction, capable of arriving at a more realistic water balance (Valéry et al., 2010), or to utilize a variety of reference climate data from different sources (which have higher spatial or longer temporal coverage), either directly or with prior modifications and adjustments for hydro-climatic investigations in the UIB region, (e.g. modified APHRODIT - (Lutz et al., 2016), modified WFDEI data - (Wijngaard et al., 2017) etc), the UIB still lacks a reliable precipitation dataset that has a longer temporal coverage and is, at the same time, able to account for the spatial and altitudinal precipitation patterns, adjusted for orographic effects and, so, exhibiting more realistic magnitudes which are more consistent with the observed UIB total streamflow discharge. None of the precipitation data sets available for UIB possess both these attributes, may it be the sensors based (e.g. TRMM) (Khan et al.) or the data products based on the "low altitude observational networks" (e.g. gauge station records, APHRODITE, WFDEI, etc.) (Khan & Koch, 2018a), leading to limitations in hydro-meteorological investigations, namely their inability to close the water balance of mountainous catchments, such as the UIB (Khan et al.; Khan & Koch, 2018a).

In light of these imminent issues, the current study aims at generating a long-gridded precipitation dataset that is not only based on the maximum available gauge station precipitation records of varied temporal coverages at different locations, but is, at the same time, subjected to adjustments for orographic effects. To that avail, we propose a simple method to construct long-term gridded precipitation dataset for the UIB, by creating precipitation time series through: (1) generation of time series of rain events at virtual stations, i.e. by interpolation of the available recorded data, for locations in the present rain gauge network which are newer and had no rain gauge installation previously (1961–1996); (2) correction for frequency, intensity and adjustments for temporal trends at the generated data at virtual location; and, finally, (3) orographic adjustment and regionalization through application of an "Interpolation/Informed Regionalization method" (Khan & Koch, 2018a), to construct gridded precipitation dataset (0.125° by 0.125°) for the UIB.

It is worth mentioning here that the "Interpolation/Informed Regionalization method" (IR), that has already been developed and tested by Khan and Koch (2018a), is adopted as an added step to induce regionalized orographic adjustment to the precipitation data, reconstructed during this study.

The data generated using these techniques is intended to provide a valuable alternative for climate change or hydrological impact studies in the UIB and might be the only gridded precipitation product that would be based on: (1) the maximum available in situ observations, supplemented by (2) all the available hydro-glaciological information of the UIB, as well as (3) correction through a "reverse hydrology" approach based on the observed flows in the basin, and, therefore, (4) enables hydrological investigations that can close the water balance over the UIB.

2. Materials and methods

2.1. Study area-the Upper Indus River Basin (UIB)

The portion of the Indus River upstream of Tarbela Dam, that comprises the upper Indus river basin (UIB), (Figs. 1 and 2), has an estimated length of about 1150 km and drains an area of about 165,400 km^2, as per our findings. The UIB span over three mighty mountain ranges, i.e. Hindu Kush, Karakorum and Himalayan (HKH) and contains the largest area of perennial glacial ice cover (15,062 km^2) outside the polar regions, with 2173.52 km^3 of total ice reserves (Bajracharya et al., 2015), and that extends even further during the winter season. The altitude within the UIB ranges from as low as 455 m to a high of 8611 m and, as a result, the climate varies greatly within the basin (Tahir, Chevallier, Arnaud, & Ahmad, 2011). The UIB draw its water mainly (over 50% - (Lutz et al., 2016)) from melting of the seasonal and/or permanent snow cover and glaciers in the HKH region (Ali & Boer, 2007; Archer, 2003; Immerzeel et al., 2009; Tahir, Chevallier, Arnaud, Neppel, & Ahmad, 2011).

Most of the UIB's annual precipitation originates in the west, resulting from the mid-latitude western disturbances and which mostly falls in solid form during winter and spring (Ali & Boer, 2007; Hasson, 2016; Hewitt, 2011; Wake, 1989), whereas occasional rains are brought by the monsoonal incursions to trans-Himalayan areas (Wake, 1989), but even during the summer months, the trans-Himalayan areas do not derive all precipitation from monsoon sources (Wake, 1989).

The strongly varying topographic altitudes usually have strong influence on the climatic variables in the UIB. This is evident by the fact that the northern valley floors are mostly drier, with annual precipitation of only around 100–200 mm, but as the elevation increases, considerably higher totals are witnessed, reaching up to 600 mm at an elevation of 4400 m (Hewitt, 2007), wherefore around two-third accumulates as winter snowfall at higher altitudes caused by westerly circulation and cyclonic storms (Hewitt, 2007; Shroder, 2005). The same trends are reported by different glaciological studies which suggest even higher annual accumulation rates of as much as 1500–2000 mm at 5500 m elevation (Wake, 1989). The average snow cover area in the Upper Indus River Basin changes from 10% to 70% over the year, wherefore the snow cover is at a maximum of 70–80% in the winter (December to February) snow accumulation period and at a minimum of 10–15% in the summer (June, July and August) snow melt period (Tahir, Chevallier, Arnaud, Neppel, & Ahmad, 2011).

2.2. Observed hydro-climate

2.2.1. Observed precipitation data

The precipitation data of a total of twenty meteorological stations operative in the study area (UIB) (Fig. 1) were used in this study, out of which six (6) stations are operated by the Pakistan Meteorological Organization (PMD), while fourteen (14) automated weather stations, called data collection platforms (DCPs) are under the jurisdiction of the Water & Power Development Authority, Pakistan (WAPDA). The stations operated by PMD have daily time step climate data available for longer periods. Though the recent records are fairly consistent, the stations operated by PMD being all low altitude stations, do not represent the precipitation at higher altitudes of UIB. The remaining 14 climate stations operated by WAPDA are fairly new and located at higher altitudes and have data for a shorter time period (1995 onwards at most locations) and also prone to some inconsistencies (Table 1).

With these imponderabilities, the current study utilized precipitation records of the six (6) PMD operated stations for the duration of 1961–2010 and of fourteen (14) weather stations

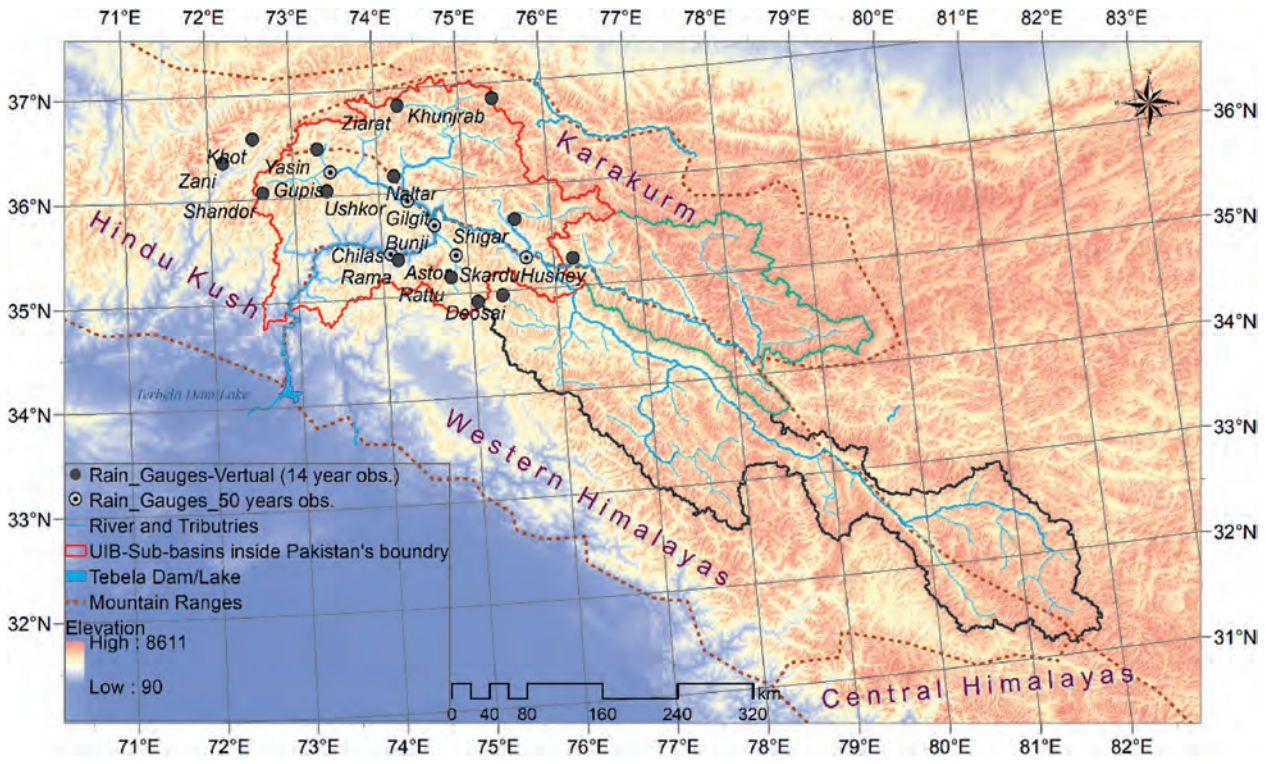

Fig. 1. Map of Upper Indus Basin (UIB) indicating main sub-basins; the network of meteorological stations with six stations with observed data for longer periods, and fourteen (14) automated weather stations with observed data for shorter period and reconstructed/virtual data for the remaining period; streams and tributaries; mountain ranges and administrative boundaries.

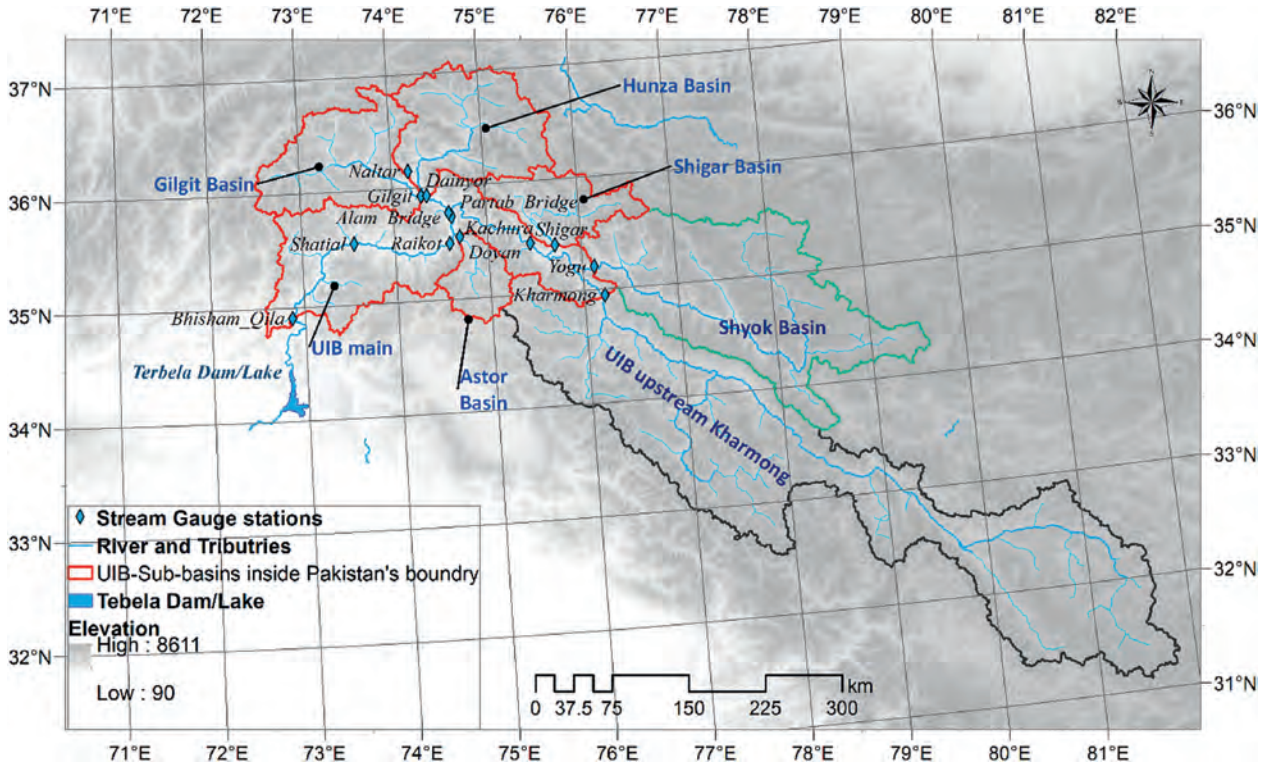

Fig. 2. Map of Upper Indus Basin (UIB) indicating main sub-basins; network of stream gauge stations; streams and tributaries; mountain ranges and administrative boundaries.

Table 1
Geographical attributes of the Precipitation gauge Network.

Station group	No.	Station name	Duration of data used in this study	Latitude (°)	Longitude (°)	Altitude (m)
High altitude (2367–4440 m.a.s.l.) stations operated by Water and Power Development Authority, Pakistan (WAPDA)	1	Burzil	1997–2010	34.906	75.902	4030
	2	Deosai	1997–2010	35.09	75.54	4149
	3	Hushe	1997–2010	35.42	76.37	3075
	4	Khot Pass	1997–2010	36.517	72.583	3505
	5	Khunjrab	1997–2010	36.84	75.42	4440
	6	Naltar	1997–2010	36.17	74.18	2898
	7	Ramma	1997–2010	35.36	74.81	3179
	8	Rattu	1997–2010	35.15	74.8	2718
	9	Shendoor	1997–2010	36.09	72.55	3712
	10	Shigar	1997–2010	35.63	75.53	2367
	11	Ushkore	1997–2010	36.05	73.39	3051
	12	Yasin	1997–2010	36.454	73.3	3350
	13	Zani	1997–2010	36.334	72.167	3895
	14	Ziarat	1997–2010	36.77	74.46	3020
Low altitude (1250–2210 m.a.s.l) stations operated by Pakistan Meteorological Department (PMD)	15	Chillas	1961–2010	35.42	74.1	1250
	16	Astore	1961–2010	35.37	74.9	2168
	17	Bunji	1961–2010	35.67	74.63	1372
	18	Gilgit	1961–2010	35.92	74.33	1460
	19	Gupis	1961–2010	36.17	73.4	2156
	20	Skardu	1961–2010	35.3	75.68	2210

(DCPs) operated by WAPDA for the duration of 1997–2010.

In addition to the above mentioned precipitation records, for parts of the UIB outside Pakistan's boundary that include "Shyok basin" and the "parts of the UIB upstream of Kharmong" (Fig. 2), we utilized a modified version (using the here-proposed Informed Regionalization method) of the APHRODITE daily gridded precipitation dataset for Asia which is based on a dense network of rain gauges. (Yatagai et al., 2012). This data has a spatial resolution of 25 km^2 and is available for the time period 1951–2007 (Version -APHRO_MA_V1101) and for the time period 1998–2015 (version -APHRO_MA_V1901). We utilized APHRO_MA_V1101 for the period of 1961–2007 and APHRO_MA_V1901 for the period of 2008–2010.

2.2.2. Observed discharge data

The daily river discharge and flow data in the study area was collected from the Water & Power Development Authority, Pakistan (WAPDA). The acquired discharge data at the UIB outlet (Bisham Qila), covered a period of 39 years (1969–2008), out of which data from 1973 to 2008 was used for validation of the reconstructed precipitation. To validate the reconstructed data for spatial representativeness at sub-basin scale, data for several other discharge gauge stations were also acquired for cross validation purposes during the study, but as these stations covered variable durations, only the discharge data for the duration of 1985–2008 was utilized (Table 2, Fig. 2).

3. Methodology

For the temporal reconstruction and the "informed" spatial regionalization of the precipitation in the UIB, three main procedures were carried out, prior to finally applying the "regionalization and orographic adjustment" proposed by (Khan & Koch, 2018a). The procedures for the "Temporal reconstruction" of the data included:

(1) Quality check & correction of systematic errors in the raw precipitation data;
(2) interpolation of the available recorded data, for (virtual) locations in the present rain gauge network which are newer and had no rain gauge installation previously (1961–1996), basically to get the occurrences of precipitation events rather than magnitudes; followed by
(3) correction and adjustments for frequencies, intensities as well as temporal trends of the generated data at virtual location.

Once the long duration data was generated at all the point locations of the target high altitude stations, it was adjusted for the orographic effect by employing "Informed Regionalization" (IR) technique, which have already been developed and tested by outhors (Khan & Koch, 2018a), but for an observed data from a denser precipitation observational network covering a limited duration. While applying this technique the point data (observed or generated) is at first adjusted through application of "Orographic Correction Factor's (OCF's) of point data to the mean catchment elevation. The adjusted data at mean catchment elevation is than interpolated through ordinary kriging to the desired grid/denser point location. The interpolated data is than finally readjusted through OCR, applied as precipitation lapse rate (PLR) adjustment at the grid-average/point elevations. In the current work we applied this "IR" technique to the newly generated long term data set, to get orographic adjustment similar to those applied to the precipitation data for the reference period by Khan and Koch (2018a).

The application of the IR technique during the current work is further described in section 3.3, while the full account of the development, application and validation process for the IR technique is covered in (Khan & Koch, 2018a).

It is worth noting that the coverage of the observational network prior to the mid-nineties (with precipitation data available at only six climate stations for part of UIB inside Pakistan's boundary) were regarded too thin to generate reliable precipitation estimates over extended distances, especially in a region with complex orography, or to reconstruct the details of the precipitation field using some spatialization or interpolation methods.

Although most available gridded data products have utilized these observed timeseries at the limited locations as their reference observed data, we opted for a different approach. It was decided to interpolate the available precipitation timeseries mainly as indication of the occurrences of precipitation events at regional scale rather than the frequencies and intensities or the temporal trends. The frequencies, intensities and the temporal trends were instead corrected by applying methods similar to the approaches applied for bias removal in climate model simulations.

Secondly, as the low density of the observational data points hindered application of a direct validation of the results acquired through interpolation or spatialization, therefore we opted for an unconventional set of indirect verification that included: (1) the evaluations and comparison of the long term generated data against the observed data (available post mid-ninties) at same locations through various statistical indices, and (2), validation of the resulting precipitation data (once the observed and generated data at virtual/point location were finally adjusted and spatialized) through application of a hydrological model and validation of hydrological response against the observed hydrological flow regime.

The details of reconstruction, spatialization or verification and validation steps are discussed in the subsequent sub-sections. Of course, prior to the application of all of these correction methods, the observed precipitation data was checked for inhomogeneity and outliers.

The overall procedures followed during the Temporal reconstruction & Informed Regionalization "ReCIR" methodology are summarized in the schematic diagram of Fig. 3.

3.1. Correction of systematic errors

The first step included the correction of systematic errors in the raw precipitation data. As the observed precipitation data available for the UIB are uncorrected raw observations, procedures were needed to remove any systematic errors in the precipitation measurements and the possible precipitation-under-catch during snowfall, particularly under windy conditions. For this purpose different methods recommended by the World Meteorological Organization (WMO) were reviewed, and the method based on the work of Ma et al. (Ma et al., 2015) was selected eventually, as it required less observed parameters and had also previously been applied in the study region.

The (Ma et al., 2015) method (see also (Yang & Ohata, 2001)) employs various equations to account for wind-induced errors, wetting losses, evaporation losses and trace amounts. These equations are as follows:

$$Pc = K(Pm + \Delta Pw + \Delta Pe + \Delta Pt) \quad (1)$$

$$K = 1/CR \quad (2)$$

where **Pc** is the 'true' precipitation, ***Pm*** is the measured value by gauges, ***ΔPw*** denote wetting losses, ***ΔPe*** are evaporation losses, ***ΔPt*** is the trace amount, and ***K*** is the adjustment coefficient due to the wind-induced error, for which ***CR*** is the catch ratio (%), defined as a function of wind speed. The values of ***ΔPw, ΔPe, ΔPt and CR*** suggested by Ma et al. (Ma et al., 2015) and Yang et al. (Yang &

Table 2
Geographical attributes of the hydrometric stations.

Serial No.	River/Tributary	Station name	Area (km^2)	Mean discharge (m^3/s)	Elevation (m.a.s.l)	Time period available (years)	Time period used (years)
1	Astore River	Doyan	3906.15	138	1580	1974–2010	1985–2008
2	Gilgit River	Gilgit	12,777.89	303	1430	1970–2010	1985–2008
3	Hunza River	Dainyor	13,761.15	294	1420	1966–2010	1985–2008
4	Shyok River	Yugo	32,934.58	410	2460	1974–2010	1985–2008
5	Indus River	Kharmong	3906.15	460	2500	1982–2010	1985–2008
6	Indus River	Kachura	113,744.60	1151	2180	1970–2010	1985–2008
7	Indus River	Besham Qila	165,610.93	2425	600	1969–2010	1973–2008

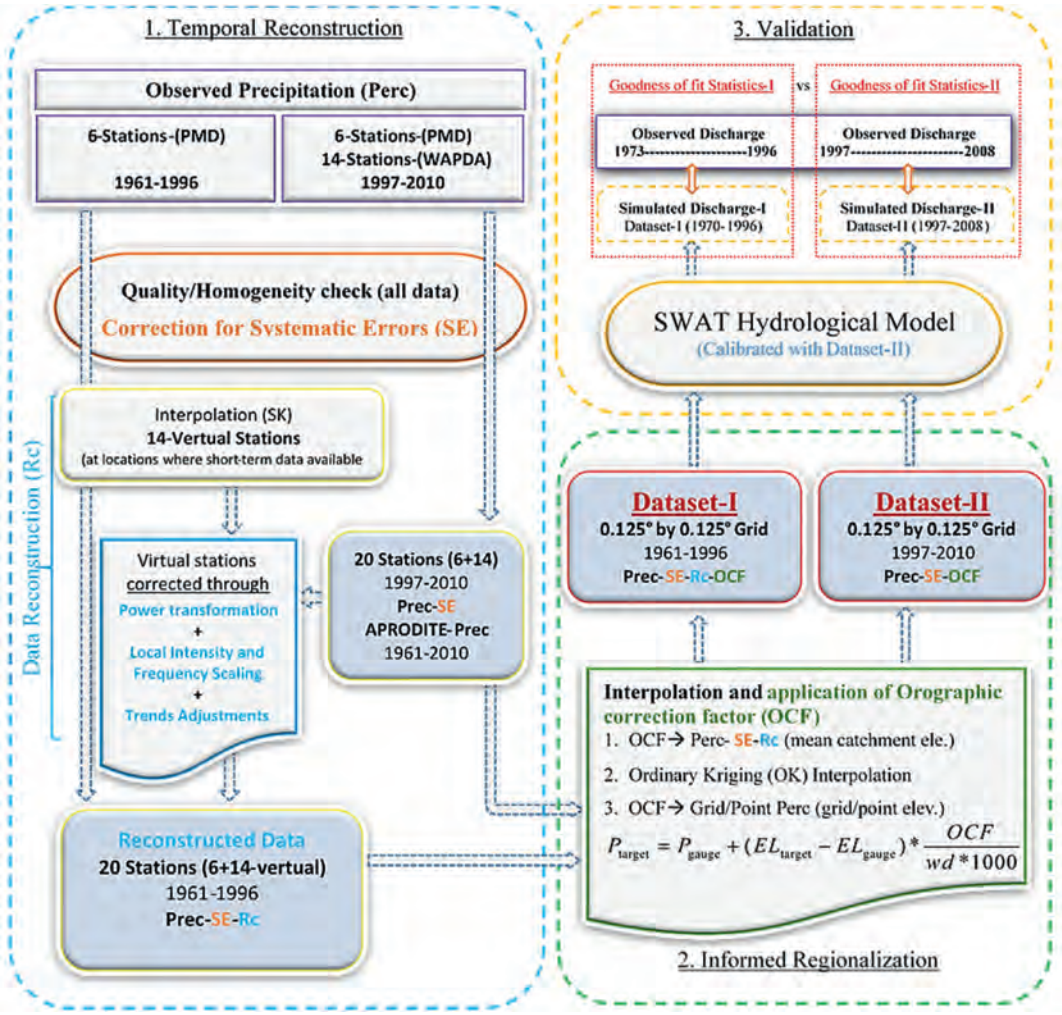

Fig. 3. Schematic outline of the "Temporal Reconstruction and Informed Regionalization" process for daily rainfall estimation.

Ohata, 2001) and used in this study are listed in Table 3.

For allocating values for ***ΔPw***, ***ΔPe***, ***ΔPt*** and ***CR*** during the calculations, the precipitation during the (1) winter months December, January and February (DJF) was considered as snow, (2) summer months- June, July and August (JJA) as **r**ain**,** and (3) spring and autumn March, April, and May, as well as September, October and November (MAM and SON) as mixed. Additionally, prior to applying correction for the systematic errors, raw observed precipitation data was also pre-checked for inhomogeneity and outliers. For this purpose we used a software "Multiple Analysis of Series for Homogenization (MASH v3.03) developed by (Tamás Szentimrey, 2013).

3.2. Temporal reconstruction-ReC

As mentioned, for 14 locations in the UIB, climate data have been available only for a shorter time, as there were no stations available before mid-nineties at those locations. The data at these locations, though short, and so may find less applicability in certain types of studies, definitely provides a deep understanding of the site/region specific orography as well as the amounts, spatial patterns and seasonality of the precipitation there. Similarly, as the 6 locations where longer precipitation data are available, are spread through major sub-basins in the region, the precipitation data at these locations provide a good indication of the seasonality and spatial distributions of storm events across the basin. So basically, if precipitation data of these 6 stations are interpolated to the 14 locations (where data for shorter period is available) to form virtual stations and corrected based on the shorter period of available precipitation data, a reconstructed precipitation time series can be derived for the past, with a reasonably accurate temporal sequence of rain event distribution (based on 6 stations data for 1961–1996) as well as site specific orography, amounts, spatial patterns and seasonality of precipitation (based on short duration data at same locations).

Testing this idea involved three steps where, firstly, the daily precipitation data from 1961 to 1996 at the 6 locations were interpolated via Inverse Distance Weighting (IDW) to the 14 locations for which only short duration data was available. The data were then corrected in the second step with a monthly scaling

Table 3
Values for ΔPw, ΔPe, ΔPt and CR used in the calculations.

Variable	Snow	Mixed	Rain
ΔPw	0.15	0.15	0.20
ΔPe	0.10	0.30	0.30
ΔPt	0.10	0.10	0.10
CR	100×1.13^{-1}	100×1.05^{-1}	

Source (Ma et al., 2015).

factor for amounts of events and magnitude (Local Intensity Scaling). Finally, in the third step, adjustments for trends in the mean and occurrences of events were made.

3.2.1. Inverse Distance Weighting (IDW)

The IDW method explicitly implements the assumption that observations closer to one another are more alike than those farther apart, which means that the method weighs the points closer to the prediction location stronger than those farther away. To that avail, the following equation is used:

$$Z^*(x_o) = \frac{1}{\sum_{i=1}^{n}\lambda_i}\sum_{i=1}^{n}\lambda_i Z(x_i) with \lambda_i(x) = \frac{1}{|x_o - x_i|^p} \quad (3)$$

where n represents the number of sample data values around the unsampled location to be used in the interpolation, $Z^*(x_o)$ is the interpolated value at location x_o while $Z(x_i)$ is the sampled or observed data value at location x_i, λ denotes the weight of the sampled data at location x_i, p is the power of the distance between unsampled location x_o and sampled location x_i, usually taken as $p = 1$ (linear) or $p=2$ (quadratic) (stronger decay of the influence of most distant points x_i).

3.2.2. Correction of generated data for intensity and frequency

The correction of the generated data for biases in intensities, frequencies followed a combination of two methods: Power transformation (PT) and Local Intensity and Frequency Scaling (LIS), suggested by (Schmidli et al., 2006) and (Khan & Koch, 2018b).

This combination of bias correction methods was selected based on our previous work (Khan & Koch, 2018b), with an overview of the different methods (except the two described here) that were evaluated, along with their comparative performances, is given in the "supplementary materials", appendix A & B.

According to (Khan & Koch, 2018b), each of the two methods has its own strength and weaknesses, for example, the PT method can yield results with a very good match of the corrected data, especially as far as peak precipitation magnitude is concerned, but may not be very efficient in adjusting the number of wet days if the generated modelled data have highly exaggerated wet days counts. The second method (LIS), on the other hand, is very efficient in adjusting the probability of wet days, but may not be able to give as good results regarding peak magnitude of the daily precipitation. Thus, when these two methods are combined, the strengths of each can be used, while the weaknesses can be avoided to a large extent.

- Power transformation of precipitation (PT)

Power transformation allows for adjusting differences in the variance. To do this, a non-linear correction in an exponential form (Leander et al., 2008), may be used to exactly apply adjustments to the variance statistics of a precipitation time series. In this correction each of the daily precipitation amount P is converted to a corrected P (P_{corr}) using:

$$P_{corr} = P^o \quad (4)$$

where the parameter b is determined iteratively, following Brent's method (Brent, 1971), whereby the coefficient of variation (CV) of the corrected daily historical precipitation (P_{corr}) is matched with the CV of the observed daily precipitation (P) for each month m. This is done with a distribution-free approach on a monthly basis using an interval of 30 days before and after the month considered. The so identified b is then applied to correct the simulated series. In this way, the CV is only a function of the parameter b.

- Local intensity and frequency scaling (LIS)

The local intensity and frequency scaling method (LIS) used here is a slightly modified version of the method suggested by (Schmidli et al., 2006) for bias correction of modelled data. This method corrects the generated precipitation series at the virtual stations by effectively matching them with the climatological wet-day frequency and intensity of the observations. The LIS method consists internally also of two steps. In the first step at each virtual station, a wet-day threshold for the m^{th} month "$\boldsymbol{WDT_P}$" is determined from the daily interpolated and variance-adjusted precipitation (PT) series (1961–1996), such that the threshold exceedance matches the wet-day frequency at the same location in the observed precipitation series (1997–2010).

In a second step, a scaling factor sf_m is calculated from the wet-day intensities for each month by:

$$sf_m = \frac{\mu\left(P_{m,d}^{obs}\right)}{\mu\left(P_{m,d}^{V} given\ P_{m,d}^{V} \geq WDT_{m,d}^{P}\right)} \quad (5)$$

This scaling factor for each month is applied to the daily time series of the virtual stations (above the threshold) to ensure that the mean of the corrected precipitation match that of the observed precipitation at these locations, i.e.

$$P_{(cor)}^{V} = \begin{cases} 0, & if \quad P_{m,d}^{V} < WDT_{m,d}^{P} \\ P_{m,d}^{V} \times sf_m & otherwise \end{cases} \quad (6)$$

In the equations above $P_{m,d}^{o\ b\ s}$ and $P_{m,d}^{V}$ denote the daily precipitation values of the observations and the virtual stations for a specific month, respectively, μ indicates the long term average, $WDT_{m,d}^{P}$ is the wet-days threshold for each month, and $P_{(cor)}^{V}$ is the corrected precipitation (at the virtual stations for the period 1961–1996).

The local intensity and frequency scaling method could be calibrated on a monthly, seasonal or annual scale. In the current study, the precipitation series at the virtual stations were corrected for wet-day frequencies and intensities on a monthly scale. During this exercise, a total of 24 fitting parameters were determined, including 12 $WDT_{m,d}^{P}$ and 12 sfm (one for each month of a year).

3.2.3. Adjustment for trends in mean and occurrences (AfT)

The sfmas well as the $WDT_{m,d}^{P}$ were further adjusted at each virtual station, based on the difference/departure in the trends of the mean precipitation and the wet-day frequency in comparison with those of the reference period (1997–2008), and three time period segments (1961–1972; 1973–1984; and 1985–1996), derived from the observed time series recorded at the 6 locations. The adjustment factors are derived as follows:

$$P_E = P_d + \left(EL_T - EL_{gauge}\right) x\ \frac{OCF}{wd\ x\ 1000} \quad (7)$$

where $AfT_{mean}$and AfT_{WD} are the adjustment factors for precipitation amount and wet-days frequency, respectively, P_T and P_R are the mean precipitation during the target period and the reference period, while WD_T and WD_R represent the number of wet days in the target and reference period, respectively.

For each virtual station, the adjustment factor used for the precipitation means or the wet day's frequency, is a "weighted average" (based on distance Δs) of the three nearest observed locations, i.e.:

$$\overline{AfT_{virtualst.}} = \frac{\sum_{i=1}^{n=3}\left(\left(\frac{1}{\Delta s}\right)_i.(AfT)_i\right)}{\sum_{i=1}^{n=3}\left(\frac{1}{\Delta s}\right)_i} \quad (8)$$

In case of the scaling factor (sf_m), these are directly multiplied by the adjustment factors at the virtual stations ($\overline{AfT_{virtual\ st.}}$),r the different periods, whereas for the wet-day threshold ($WDT^P_{m,d}$), the adjustment factors are applied in a similar way to the original wet-day frequencies prior to the determination of the final $WDT^P_{m,d}$.

3.3. Informed Regionalization- IR (orographic correction and stepwise interpolation)

Following the above-mentioned methodology, we obtained a long duration precipitation time series at all the 20 locations i.e. observed precipitation time series at 6 locations operated by PMD, for duration of 1961–2010 and observed precipitation time series at the 14 stations operated by WAPDA since 1995, for periods covering 1995/1997–2010 and reconstructed (virtual) at the same 14 locations for periods covering 1961–1994/1996. As the data at the 14 stations, though in most cases available from the year 1995, had sometimes inconsistencies and quality issues during the initial period, we utilized observed precipitation at these locations for periods prior to 1997 only when it showed consistency and better quality.

In the third step, the reconstructed long-duration precipitation dataset at the 20 location still needed adjustment for orographic effects. The methodology used is based on the work by (Khan & Koch, 2018a) who proposed and developed a new approach for the interpolation and regionalization of point observational precipitation series, with adjustments for the orographic effect and to a smaller spatial scale, specifically in the UIB. The current study adopted and applied this approach to the long-term precipitation time series generated at the 20 locations. This approach, called the "Informed Regionalization-IR" (orographic correction and stepwise interpolation method), is capable of adjusting the long-term reconstructed precipitation data for orographic effect and interpolate them to a 0.125° by 0.125° grid in a step-wise procedure. A brief description of the procedure is given here, while details can be checked in (Khan & Koch, 2018a). In the first step of this "stepwise interpolation/regionalization" all observed time series were adjusted at mean catchment elevation with the OCF as:

$$P_E = P_d + (EL_T - EL_{gauge})\ x\ \frac{OCF}{wd\ x\ 1000} \quad (9)$$

where P_E is the precipitation at target elevation (mm); P_d is precipitation at recorded at gauge station (mm); EL_T is elevation at target point/grid; EL_{gauge} is elevation at gauge station (m) and *OCF* is the Orographic Correction Factor (in terms of precipitation lapse rate) for the catchment (mm/km). The OCF's are adopted from our previous work (Khan & Koch, 2018a) and given in Table 4, for which further details can be checked in (Khan & Koch, 2018a).

In the second step the data adjusted at mean catchment elevation were interpolated using "Ordinary Kriging" (OK) (Goovaerts 1997, 2000), which assumes a stationary local mean in the vicinity of the interpolated point - to a 0.125° by 0.125° grid. While in the third step, the interpolated data were readjusted from the mean catchment elevation to the grid elevation according to the OCF, applying Eq. 10.

For areas of the UIB not covered by the observational data acquired, we utilized the APHRODITE daily gridded precipitation dataset for Asia (Yatagai et al., 2012). This data was adjusted/corrected as well, using the orographic adjustment factors ($OCF_{multiplicative}$) as given in Table- 3. We used APHRO_MA_V1101 and APHRO_MA_V1901 for the periods of 1961–2007 and 2008–2010, respectively.

3.4. Validation methods

Any of these techniques or strategies, which can be used for correction, reconstruction and regionalization of data, needs calibration and validation by means of historical data information (Lanza et al., 2001), either directly or indirectly by evaluating the results against observed or comparison of the outputs of spatially distributed hydrological models against the observed hydrological regime, respectively. In the current study, to check the performance of the temporal reconstruction method, both methods were applied in some form. Therefore, the validation process consists also of a two-step approach.

3.4.1. Validation of generated data at virtual stations

The precipitation time series (1961–1996) obtained as an intermediate product at the 14 virtual stations were evaluated to see, firstly, how good the generated data match the seasonal cycle, means, extremes, and frequencies of the observed data collected at these locations during 1997–2008, and, secondly, how well the generated data at these 14 virtual stations depict the departure from the "means" in the region observed over the reconstruction period of 1961–1996. For evaluation and validation purposes, the 36 years-duration reconstructed precipitation was divided into three equal segments of 12 years each. The lengths of these segments were kept the same as the reference data acquired, to avoid any miss match in the population size for the calculation of various statistical indices.

These indices included: root mean squared error (RSME), average annual precipitation (Av. Annual), 99th percentile (P99), probability of Wet-Days (W.D. Prob) and Intensity of Wet-Days (W.D. Int). In addition, the seasonal cycles of original and reconstructed data were visually compared.

3.4.2. Validation of output by means of the SWAT hydrological model

To validate the final product of the proposed **Re-C**onstruction & **I**nformed **R**egionalization (ReCIR) method, the calibrated "Soil and Water Assessment Tool" (SWAT) hydrological model was forced with the two precipitation data series, i.e. (1) reconstructed precipitation (1961–1996), and (2) regionalized reference precipitation (1997–2008), and the "goodness of fit" statistical parameters: coefficient of determination (R^2), Percent bias (*PBIAS*) and Nash–Sutcliffe efficiency (*NS*) were computed by assessing the simulated hydrological responses for the streamflow against the observed flow data. These goodness of fit statistics for simulated flows resulting from the two sets of input precipitation data were then compared to check the validity of the proposed methods. In the following paragraphs a short description, setup and calibration of the SWAT-model is provided.

3.4.2.1. SWAT model description. The Soil and Water Assessment Tool (SWAT) is a hydrological model developed for the US Department of Agriculture (USDA), Agricultural Research Service (ARS) by Dr. Jeff Arnold. SWAT model is a continuous time (long-term yield), process-based semi-distributed model, capable of simulating hydrological processes in river basins/watersheds, based on specific information pertaining to the watershed, such as weather, topography, soil properties, land cover, land use and management practices (Arnold et al., 1998; Srinivasan et al., 1998).

Table 4
Mean annual precipitation and orographic correction factors (OCF) for catchments of UIB (Khan & Koch, 2018a).

Catchment	Mean annual Precipitation			OCF_{plapse} [c] per 1000 m Elev. (Corrected Observed)	$OCF_{multiplicative}$ [a] Raw Observed/ APHRODITE	$OCF_{multiplicative}$ [b] (Corrected −Observed)
	Raw Observed/ APHRODITE [+]	Corrected [++] (Observed)	True [+++] (Estimated)			
	(mm)	(mm)	(mm)	(mm/km)	(multipl)	(multipl)
Astor	581	788	1254	300	2.16	1.59
Gilgit	265	473	874	620	3.30	1.85
Hunza	360	493	795	320	2.21	1.61
Shigar	341	509	938	190	2.75	1.84
Indus**	343	481	820	380	2.39	1.71
Shyok	140	–	456	–	3.25	–
Kharmong*	221	–	360	–	1.63	–
UIB (whole)	367	544	608	–	1.66	1.12

* UIB upstream of Kharmong including Shingo, Zanskar; ** UIB downstream of Kharmong without main tributary catchment,+APHRODITE data is used only for Shyok and Kharmong basins, [++] Observed gauge station records, corrected for systematic errors through Eq. (1), [+++] True areal precipitation estimated based on Eq. (5).
[a] Applicable to raw gauge precipitation records.
[b] Applicable to gauge precipitation records already corrected for systematic errors.
[c] Applicable to gauge precipitation records already corrected for systematic errors as additive factor per 1000 m.

In the SWAT model, a river basin or watershed is partitioned into larger sub-units called sub basins draining into the stream network and the river-system. These sub-basins are further divided into a series of smaller units: the hydrological response units (HRUs), which are spatial uniform units, each representing unique combinations of soil, land-use and slope. The calculations and simulations of various hydrological variables (and other quantities, like sediment yield, and biological and chemical nutrients/contaminants, but which are of no interest here) are first carried out for each HRU and then routed and aggregated for the various sub basins and, finally, for the whole watershed. A more detailed general description of the SWAT methodology can be found in (Arnold et al., 1998; Srinivasan et al., 1998), and in relation to its specific application to the UIB in (Khan & Koch, 2018a).

3.4.2.2. SWAT-model setup and calibration. In the current study, we used "ArcSWAT-2012", which is an ArcGIS-ArcView extension and graphical user input interface for the SWAT model. The input data used for SWAT during this study include: a void-filled, and hydrologically conditioned, 3 arc-seconds digital elevation model (DEM) from Hydro-SHEDS (Lehner et al., 2008); FAO-UNESCO global soil map (FAO-UNESCO, 2007); and "Global Land Cover Characterization (GLCC) at 1 km spatial resolution (USGS EROS Data Center, 2002). During the watershed delineation process, the total simulated watershed area of 165610.9 km^2 was configured with 173 sub-basins, divided into 2825 discrete HRUs.

The weather/climate forcing for the two SWAT-models comprised the same inputs for all variables except for precipitation, for which two input sets were used: (a) "reconstructed precipitation" (1961–1996); and (b) "corrected & regionalized" precipitation (1997–2010).

Before using it as an indirect validation option for the temporal reconstruction of the precipitation, the SWAT model was first calibrated and validated against the daily discharge data at the UIB outlet (Bisham Qila) through parameter optimization using the "Sequential Uncertainty Fitting" SUFI-2 algorithm (Abbaspour, 2015; Abbaspour et al., 2007) of the SWAT-CUP program (Abbaspour, 2015). For the evaluation of the calibration/validation results, the named goodness of fit statistics R^2, PBIAS, and NS were computed. Further information on SWAT Model setup, input physical data as well as calibration and validation parameters are presented in supplementary materials, Appendix C.

4. Results and discussion

4.1. Validation results-reconstructed precipitation at 14 stations

The precipitation time series (1961–1972, 1973–1984 and 1985–1996), obtained as an intermediate product after the reconstruction procedure at the 14 virtual stations, were evaluated for two aspects: (1) How good is the match of the seasonal cycle, means, extremes, and frequencies of the generated and the observed data, collected at these locations during 1997–2008; and (2) how well do the generated data at the 14 virtual stations depict the observed departure from the means in the region over the reconstruction period of 1961–1996?

Indeed, the results show a good match, as the generated precipitation time series at corresponding locations, not only exhibit a comparable seasonal cycle, means, extremes, and frequencies for the 12 year (1997–2008) observed precipitation data (Fig. 4 & Table 4), but were also able to depict the departure trends of mean annual precipitation observed over the region during the corresponding periods.

All the monthly precipitation indices (Table 5) during the three reconstruction periods 1961–1972, 1973–1984, and 1985–1996 are in a close range of the same indices observed during the reference period (1997–2008) and the reconstructed variations followed the same pattern as the observed data at the six stations for during these time periods.

The mean annual precipitation over the whole UIB was 726.28, 567.26 and 641.05 mm during the three "time periods" 1961–1972, 1973–1984 and 1985–1996, respectively, all of which are in a close range of the mean annual precipitation during the reference period (1997–2008). Indeed, the virtual stations show a departure of +15%, −10% and +1.4% from the mean reference period annual precipitation, in comparison to a departure of 12%, 10.30% and 4% at the 6 observed locations, for the period of 1961–1972, 1973–1984 and 1985–1996, respectively.

The 99^{th} percentiles of the monthly precipitation for the three periods, though, are with 17.22, 15.18 and 16.82 mm, respectively, a bit on the lower side, in comparison with that for the reference period (21.41 mm), but appear to be still in an acceptable range. The probability and intensity of the wet-days also show minor differences for all three periods, but are still in close proximity of their corresponding values in the observed period (Fig. 4).

The reconstructed data at the 14 virtual stations also follow the

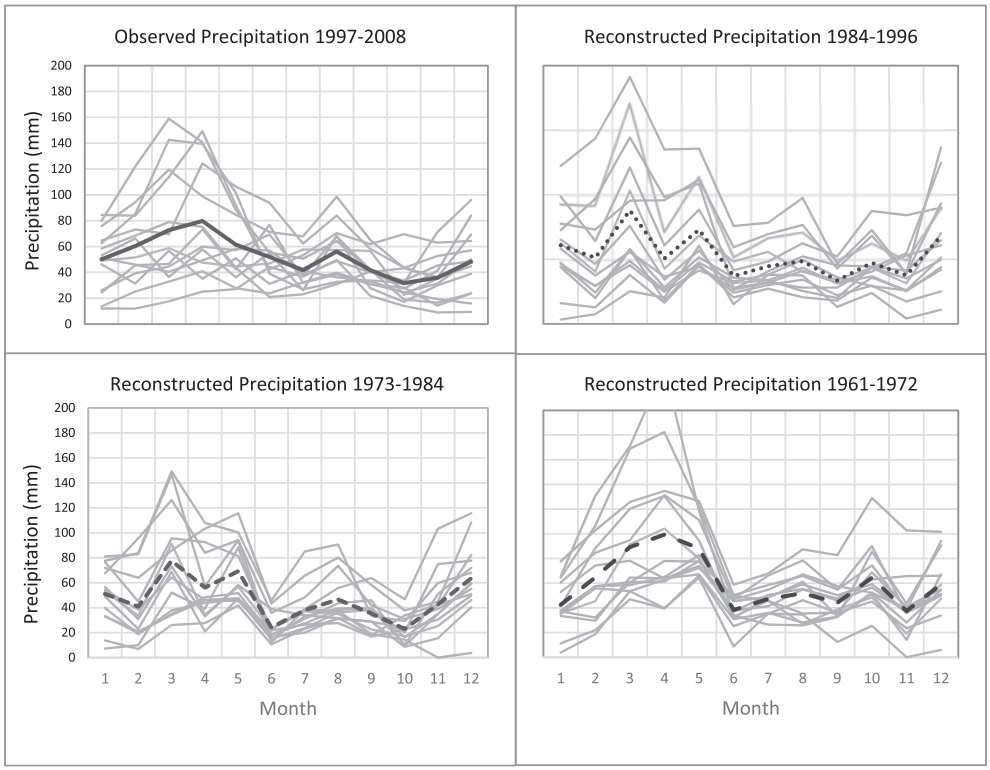

Fig. 4. Average observed (1999–2008) and reconstructed monthly precipitation for the three time periods as indicated at 14 virtual stations, with mean annual precipitation; 99th percentile; probability of wet days; and intensity of wet days listed. The thick line in each plot denotes the averages for all 14 stations.

Table 5
Validation indices for observed and reconstructed precipitation, including: average annual precipitation (Av. Annual), 99th percentile (P99), number of Wet-Days (W.D. No.), intensity of Wet-Days (W.D. Int) and root mean squared error (RSME) of generated precipitation.

	Stations	Burzil	Deosai	Hushey	Khot	Khunjrab	Naltar	Rama	Rattu	Shandour	Shigar	Ushkor	Yasin	Zani	Ziarat	Astor	Bunji	Chilas	Gilgit	Gupis	Skardu
Duration	Indices	14 Stations (Observed data 1997-2008, Reconstructed Data 1961-1996)														6 stations (Observed data 1961-2008)					
1961-1972	Av. An (mm)	1058.2	615.7	617.2	719.	302.6	936.6	782.3	1058.	626.8	521.5	630.4	669.	1197.	431.2	886.	227.	211.6	194.8	241.5	227.1
	P99 (mm)	31.2	23.2	14.6	14.5	15	16.2	15.8	30.4	10.9	15.7	9.6	10.4	22.8	10.8	37.9	11.3	12	8.4	11.6	12.1
	W.D. No.	167.8	112.2	138.1	124.	64.3	133.7	106.8	157.3	118.3	129.8	127.2	117.	127.8	106.8	104.	82.8	65.7	75.8	68.2	69.8
	W.D. Int (mm/day)	6.3	5.5	4.5	5.8	4.7	7	7.3	6.7	5.3	4	5	5.7	9.4	4	8.5	2.8	3.2	2.6	3.5	3.3
	RSME	10.8	7.1	5.1	5.2	3.8	7.5	7.8	12.9	7	6.7	5.3	5.5	8.3	3.5	15.5	3.6	3.8	3.8	6.8	4.6
1973-1984	Av. An (mm)	786.3	474.8	501.3	534.	321.8	877.9	929.8	711	445.9	404.6	412.9	429.	836.2	274.5	570.	196.	317.4	189.6	160.2	291.6
	P99 (mm)	18.3	15.4	11.7	19	15.8	17.4	16.7	17.3	12.3	11.2	11.2	12.4	25	8.7	24.6	12.1	14	9.1	8.2	15
	W.D. No.	185.9	120.8	153	80.9	54.7	116.8	119.3	173.3	80.8	141.3	83.9	65.6	88.5	60.6	125.	52.3	96.1	74.6	35.8	66.3
	W.D. Int (mm/day)	4.2	3.9	3.3	6.6	5.9	7.5	7.8	4.1	5.5	2.9	4.9	6.6	9.4	4.5	4.5	3.8	3.3	2.5	4.5	4.4
	RSME	5.9	4.6	4.5	5.5	4.1	7.5	9.1	7.8	7.2	5.8	5.4	5.7	8.5	3.6	6.7	3.5	7.2	3.5	7.4	4.8
1985-1996	Av. An (mm)	983.1	640.9	453	565.	260.8	903.9	1275.	860.4	548.1	385.1	432.8	452.	901	311.5	666.	201.	292.7	208.5	214.2	353.7
	P99 (mm)	25.2	23.8	10.9	15.9	12.7	17.2	15.1	23.3	17.2	10.6	12.2	13.7	25.1	12.6	29.2	11.7	10.8	10.1	15.2	18.5
	W.D. No.	176.3	125.3	163.1	99.2	50.5	117.8	168.4	166.9	86.3	140.7	83.1	62.4	91.2	59.4	121.	41.8	125.7	80	26	61.8
	W.D. Int (mm/day)	5.6	5.1	2.8	5.7	5.2	7.7	7.6	5.2	6.3	2.7	5.2	7.3	9.9	5.2	5.5	4.8	2.3	2.6	8.2	5.7
	RSME	6.9	5.8	4.5	5.2	3.7	7.5	7.8	8.3	7.2	5.8	5.4	5.5	8.5	3.6	7.3	3.8	3.6	3.6	6.8	5.2
1997-2008	Av. An (mm)	928.7	578	553.1	567.	278.5	885.3	954.3	862.4	513.7	467.5	476.5	503.	947.6	327.2	485.	194.	214.3	195.4	349.9	309.8
	P99 (mm)	20.6	15.1	16.5	17.8	7.2	27.3	33.7	34.5	25	26.8	15.2	18.2	32.1	9.7	20.6	9.6	13.3	8.3	21.1	16.2
	W.D. No.	179.3	194.4	148.7	133	119	142.3	139.1	138.5	116.5	98.8	125.6	116.	143.8	113.5	81.8	42.8	40.5	68.1	32.8	60.5
	W.D. Int (mm/day)	5.2	3	3.7	4.3	2.3	6.2	6.9	6.2	4.4	4.7	3.8	4.3	6.6	2.9	5.9	4.5	5.3	2.9	10.7	5.1

same trends of departure from the reference period's mean annual precipitation, as was shown by the observed data at the 6 locations used for interpolation.

4.2. Validation results – SWAT modelled response

The precipitation data series constructed at the 14 virtual stations for the time period 1961–1996 as an intermediate product

(along with the observed time series at six gauge stations) were further processed to generate a 0.125° by 0.125° grid of precipitation time series through the "Informed-regionalization" methodology (Khan & Koch, 2018a) covering whole UIB.

The SWAT hydrological model, which had already been calibrated for the reference period, was then forced with the reconstructed precipitation and the modelled flows were assessed for "goodness of fit" with the observed discharges at the UIB outlet (Fig. 5) as well as at outlets at all the major tributary catchments inside the UIB (Fig. 6). The simulated discharges at the outlets from all the major tributary catchments during the period of 1985–1996 were evaluated against those simulated for the reference period 1997–2008. The "goodness of fit" statistics for the major tributary catchments for the two periods are listed in Table 6.

The "goodness of fit" numbers listed in Fig. 5 and Table 6 indicate that the performance of the SWAT model in simulating the flows during the reference period is very good, with an overall NS value of 0.85 for the outflow at the basin outlet, and *NS*- values of 0.69 or above for the outlet discharges from different tributaries in the UIB. Regarding the other performance indices, the SWAT-simulated flows during the periods when forced with the reconstruction precipitation, result in R^2, *NS* or *PBIAS* values that are almost identical to those obtained for the reference period at the outlets of the different tributary catchments and an even higher *NS* (0.88) for the UIB outlet.

The simulated flows at the different evaluated sub-basin gauge points match the observed discharges also very well, both for peaks and low flows (Fig. 7), meanwhile the goodness of fit statistics for both precipitation forcings (reconstructed and reference precipitation) are almost identical (see Table 6).

These results establish the validity of the reconstructed precipitation dataset, as the SWAT-modelled discharges based on this data depict all the temporal and spatial patterns observed in the flow regimes of the UIB almost as good as the SWAT-modelled flows forced by the reference precipitation (Figs. 5 and 6). Indeed, the simulated flows show a good visual fit with the observed flows for all the evaluated catchments, with a very good representation of the daily and monthly high and low flows, as well as the seasonal cycle. The match of simulated daily flows with the observed flows during the reconstructed period is as good as the one for during the reference period, confirming the suitability of the generated precipitation data set also for application at finer temporal scales, such as daily or weekly time steps.

The "Flow Duration Curves" (FDC) of SWAT modelled flows against observed flows for different (12 years) time segments in the UIB for reconstructed and reference precipitation forcing also showed promising indications of the validity of the reconstructed data.as the FDC for observed and simulated flows show a good match for the different time segments, especially across peak flows and low flows. It may be noted that, although for the upper-lower to mid-range, the FDC of simulated flows show a slightly higher exceedance, it may only be indicative of the hydrological model limitations rather than discrepancies in the reconstructed precipitation input data because the differences between the observed and the modelled flows are almost identical regardless if the simulations are forced with reference or reconstructed precipitation data.

4.3. Spatial distribution patterns of precipitation

Maps showing the spatial distribution of the precipitation across the UIB are illustrated in **Fig- 8**. During the reference period (1997–2008), the distribution of mean annual precipitation shows a distinct spatial pattern across the UIB (Fig. 8a). Thus, the north-western parts of the UIB, which lie inside Pakistan's boundary, shows the highest mean annual precipitation, especially over the Gilgit and Astor river catchments, reaching a mean annual precipitation of over 1800 mm/year.

There is a gradual decrease of the mean annual precipitation to the north of these two catchments, with Hunza and Shigar catchments having lower precipitation. A similar precipitation gradient is witnessed in the West-East direction, where across the whole UIB, a steady decrease is visible in west-eastward direction, with the lowest mean precipitation witnessed in the easternmost parts of the basin. The distributions of the reconstructed mean annual precipitation across the UIB during the reconstructed periods 1961–1972 (Figs. 8d), 1973–1984 (Figs. 8c), and 1985–1996 (Fig. 8b), show similar patterns as that of the reference period, with only minor disagreements.

The spatial distribution of the reconstructed precipitation complies with the reported hydro-climatology of the region, whereby the mid-latitude western disturbances bring most of the annual precipitation during winter and spring. As they are originating and contributing maximum in the west, they have a diminishing influence towards the east (Ali & Boer, 2007; (Hasson, 2016); Hewitt, 2011; Wake, 1989). The monsoonal incursions to trans-Himalayan areas, which bring occasional rains (Ali & Boer, 2007; Ali et al., 2015; Wake, 1989), are also observed in the reconstructed precipitation, which exhibits higher values in the southern parts of the UIB which are not located in the rain shadows.

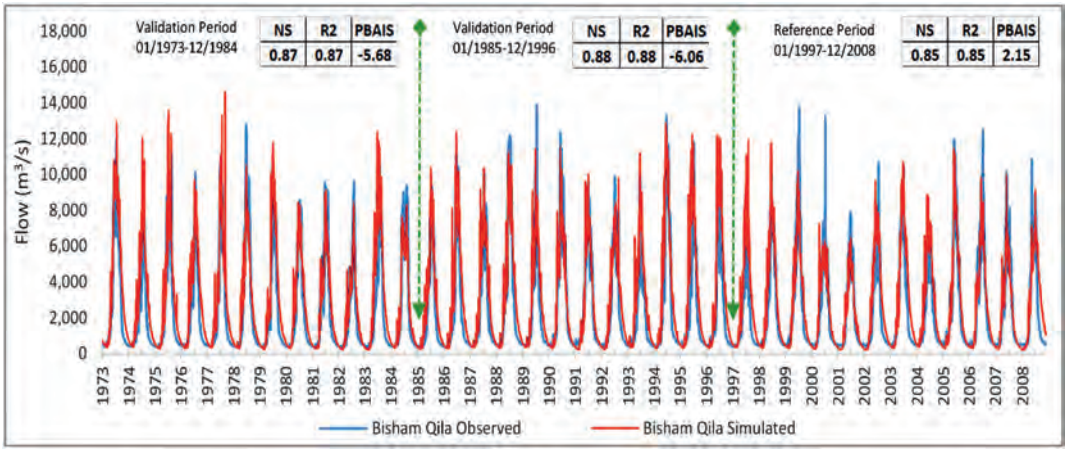

Fig. 5. Comparison of SWAT modelled flows with observed flow at UIB outlet for reconstructed and reference precipitation forcings.

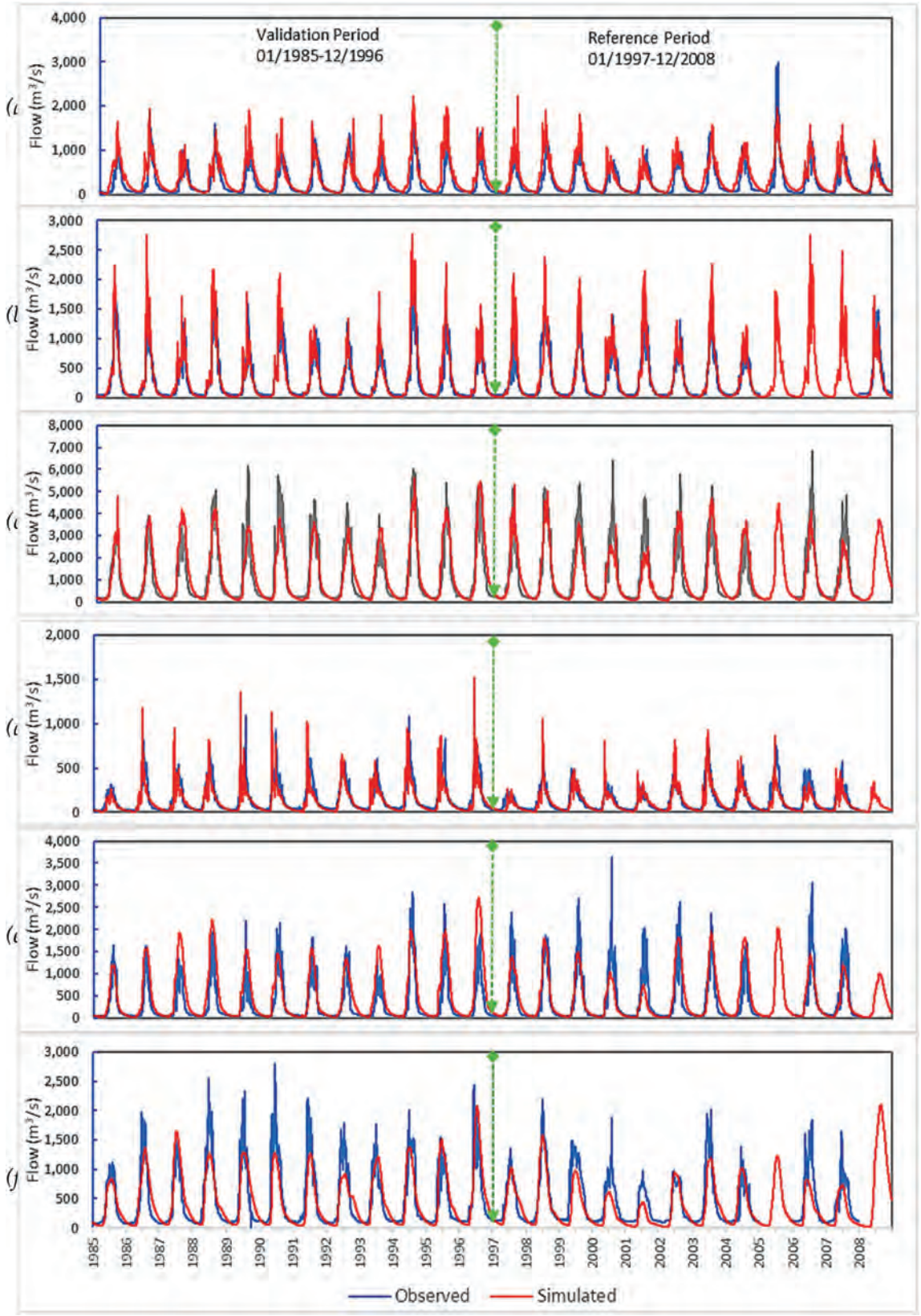

Fig. 6. Comparison of SWAT modelled flows with observed flows at the different sub-basin outlets in the UIB for reconstructed and reference precipitation forcing: (a) Gilgit (Gilgit River); (b) Dainor (Hunza River); (c) Kachura (Indus River); (d) Astor (Astor River); (e) Yugo (Shigar River); (f) Kharmong (Indus River-upstream).

Table 6
Goodness of fit statistics for SWAT-modelled discharge with the two different input precipitation datasets, i.e., reference precipitation (1997–2008) and reconstructed precipitation (1961–19996).

Goodness of fit indices	Reconstructed precipitation (1985-1996)			Reference precipitation (1997-2008)		
Gauge Station (River)	R^2	NS	PBIAS	R^2	NS	PBIAS
Gilgit (Gilgit)	0.76	0.59	-25.74	0.74	0.69	-18.15
Dainor (Hunza)	0.88	0.82	-7.50	0.85	0.85	-2.58
Doyan (Astor)	0.75	0.73	19.73	0.75	0.77	14.39
Kachura (Indus) for Shigar	0.85	0.84	-4.35	0.80	0.81	7.54
Yugo (Shyok)	0.68	0.52	-25.85	0.79	0.73	-12.90
Kharmong (Indus)	0.75	0.75	2.67	0.79	0.79	19.80
Bisham Qila (Indus-UIB outlet)	0.88	0.88	-6.06	0.85	0.85	2.15

4.4. Limitations of the study

The main aim of the current study with the proposed methods was to produce a precipitation data set that not only have longer temporal coverage, but that also addresses inherent issues of data quality as well as spatio-altitudinal representativeness of precipitation data. Although this study aim was essentially achieved, certain limitations were unavoidable and need to be discussed.

First of all, the study adopted a series of different methods for the reconstruction of precipitation time series, where each method or process has an inherent potential of inducing uncertainties. Furthermore, although the number of precipitation gauge stations (observed or virtual) which have been used here to generate the gridded precipitation product, are considerably higher than those used up to date for generating any other observation based gridded product for the UIB, resulting in a marked improvement in the spatial representativeness of the product, the generation of the data at the virtual stations, naturally, could not be achieved without added uncertainties.

Similarly, the IR technique of Khan and Koch (2018a) used here which consists in applying "orographic correction factors" (OCF's), are estimated values, one each for each gauged-catchment and based on reverse hydrology and glacier mass balance of that particular "catchment" of the UIB. The IR correction may, can therefore, only present a crude estimate of the reality and can only apply an adjustment that makes the product spatially and altitudinally representative at the spatial scale of the gauge-catchment used in deriving these factors, rather than of the grid/point scale of the product. Additionally, the use of a reverse-hydrology-based correction factor may have also assisted in achieving better calibration and validation statistics when using a distributed hydrological model (SWAT) as validation tool for the proposed data product.

Despite these obvious limitations, the adopted approach made it possible for us to present a valuable alternative precipitation product in the UIB, that might be the only gridded precipitation

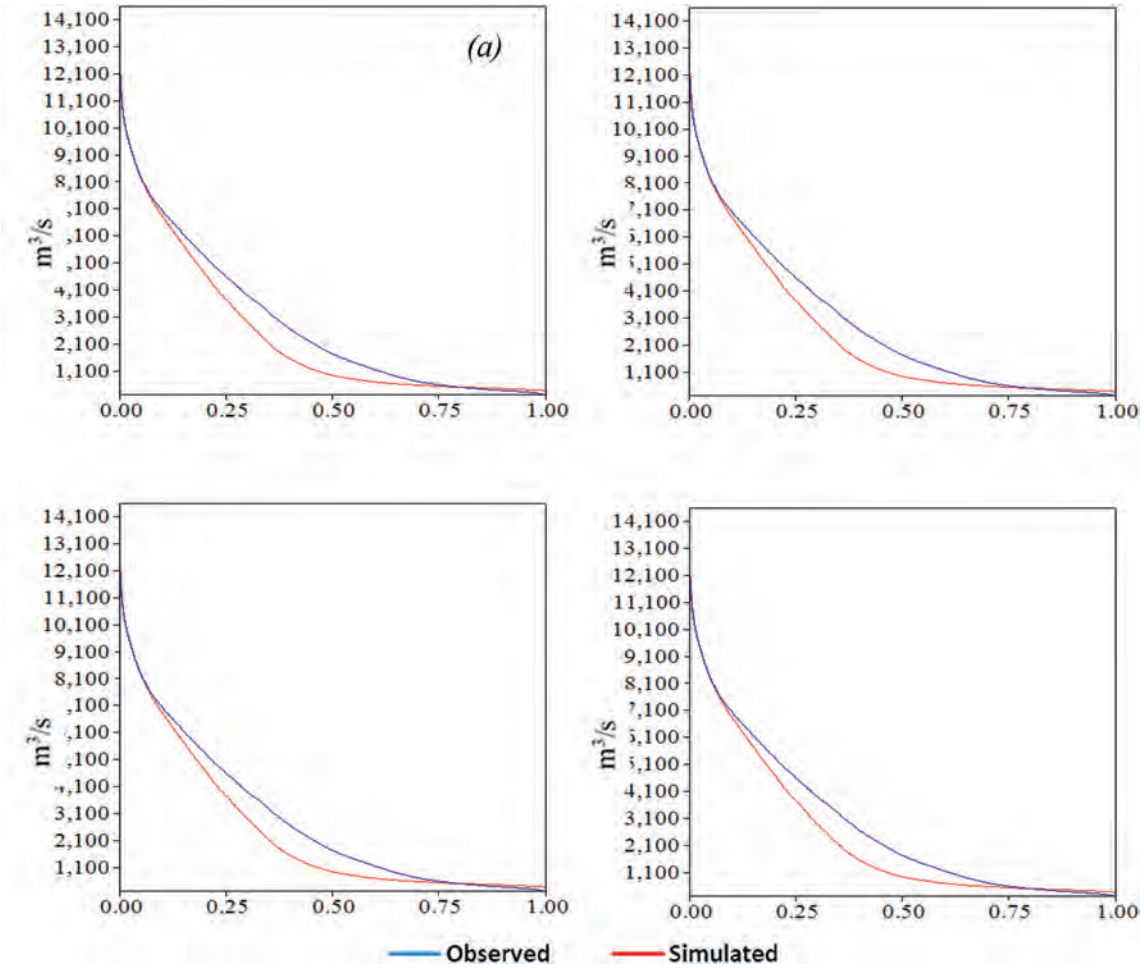

Fig. 7. Flow Duration Curves of SWAT modelled flows against observed flows for different (12 years) time segments in the UIB for reconstructed and reference precipitation forcing: *(a)* time segment 1973–1984; *(b)* time segment 1985–1996; *(c)* reference period 1997–2008; *(d)* Flow Duration Curves for the whole period of 1973–2008.

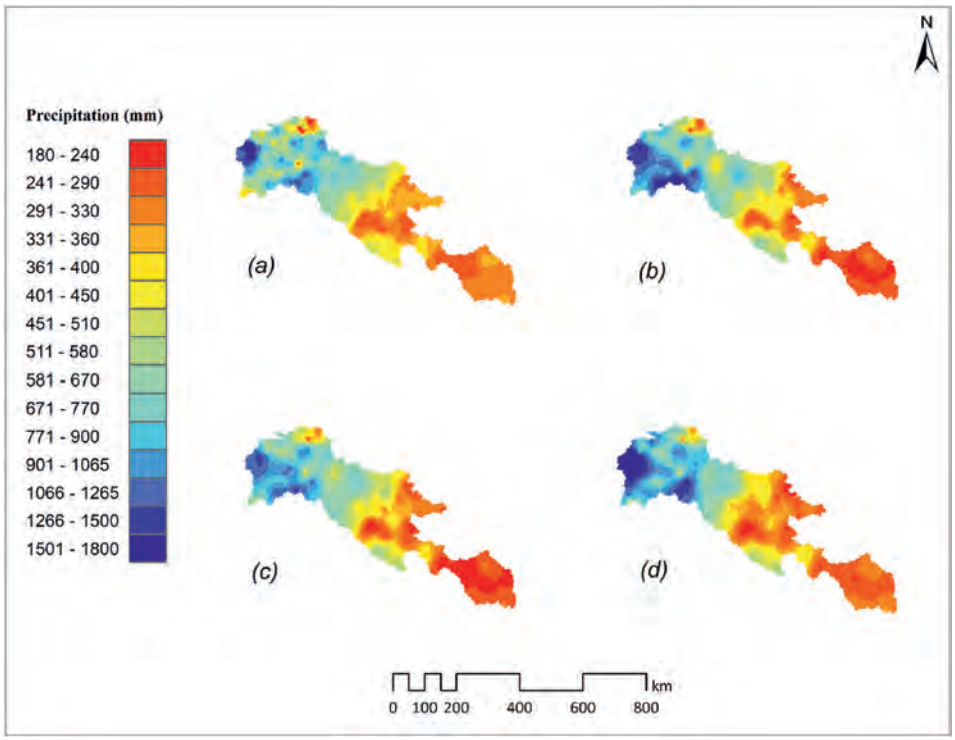

Fig. 8. Average annual precipitation over the UIB: (a) reference precipitation (1997–2008); (b) reconstructed precipitation for 1985–1996; (c) reconstructed precipitation for 1973–1984; and (d) reconstructed precipitation for 1961–1972.

product which have sufficiently long temporal coverage, while utilizing the maximum available in-situ observations, supplemented by hydro-glaciological information of the UIB and "reverse hydrology" of the observed flows, and so to reconstruct the missing data points and correct for the orographic under-estimation of the precipitation amounts. And using this multi-step- corrected precipitation product as input in the SWAT model proved it to be capable of closing the (hitherto) observed water balance gap over the UIB which, eventually, makes the product also a good candidate for use in other hydrological climate impact studies in the region.

5. Summary and conclusions

Poor spatial and temporal coverage of the available in-situ observational precipitation data is one of the major hurdles in accurately investigating the hydrometeorology of the Upper Indus basin (UIB). This study endeavored to address these issues by constructing a long-term precipitation series on regular grid of 0.125° by 0.125°. Initial precipitation time series were generated at locations (virtual stations), where there were no precipitation data available prior to the mid-nineties, corrected and adjusted for frequency, intensity and temporal trends based on: (1) observed precipitation during the reconstruction period (1961–1996) as well as (2) precipitation time series for recent years (1997–2008) available for these locations. This was followed by regionalization of the precipitation series to the name smaller grid scale across the basin, while incorporating adjustments for the orographic effect and changes in glacier storage.

The precipitation time series generated at the 14 virtual locations as an intermediate step, resulted in values for the statistical indices mean annual precipitation, 99th percentiles, intensities and frequencies of wet days in similar ranges as the observed data at these locations (1997–2008). The final product (gridded precipitation at 0.125 ° × 0.125 ° resolution) generated by means of this 2-step CIR methodology (Khan & Koch, 2018a) was further validated by evaluating SWAT-modelled streamflow response against observed flows across the UIB, for reference –as well as reconstructed precipitation forcing. The results show that for all the different stream gauge stations evaluated the daily SWAT-modelled discharges with the reconstructed precipitation is almost identical to those using the reference precipitation data. The low and high flows as well as the monthly and seasonal cycles during the reconstructed data period are all mimicked with similar accuracy as those during the reference period.

The spatial distribution pattern of the precipitation in the UIB observed during the reference period (1997–2008) are also well represented by the reconstructed time series of the historical period (1961–1996) and reflect the large scale atmospheric circulation pattern in the UIB, as also reported in the literature.

The 1961–1996 reconstructed precipitation time series we present here as the major outcome of the present study is possibly the only product which is based on the maximum available in situ observations, supplemented by all the available hydro-glaciological information of UIB as well as "reverse hydrology", based on observed and SWAT-simulated flows in the basin. As such the present CIR-data, which has already been checked for its suitability in other studies involving hydrological modelling at monthly or daily time scales (Khan & Koch, 2018a), may also prove to be a valuable alternative for climate change induced hydrological impact studies.

Conflicts of interest

The authors declare no conflict of interest.

Acknowledgments

We acknowledge provision of data by the following sources: Hydro-Shed-3sec GRID: Conditioned DEM, courtesy of the U.S. Geological Survey; FAO-UNESCO Soil Map of the World, version 3.6;

courtesy of the Food and Agriculture Organization of the United Nations. FAO GEONETWORK, 2007; GLCC—Global Land Cover Characteristics Data Base, Version 2.0; courtesy of the U.S. Geological Survey, USGS EROS Data Centre; and Water and Power Development Authority (WAPDA) and Pakistan Meteorological Department (PMD), for their exchange of the valuable hydrological and climate data to complete our research.

Appendix A. Supplementary data

Supplementary data to this article can be found online at https://doi.org/10.1016/j.iswcr.2021.01.005.

Author contributions

Conceptualization, A.J.K.; Formal analysis, A.J.K.; Investigation, A.J.K.; Methodology, A.J.K.; Resources, M.K.; Supervision, M.K.; Validation, A.J.K.; Writing—original draft, A.J.K.; Writing—review & editing, M.K.

Funding

This research received no external funding.

References

Abbaspour, K. C. (2015). *SWAT-CUP. SWAT calibration and uncertainty program—a user manual*. SWAT-CUP SWATCalibration and Uncertainty Programs.

Abbaspour, K. C., Yang, J., Maximov, I., Siber, R., Bogner, K., Mieleitner, J., Zobrist, J., & Srinivasan, R. (2007). Modelling hydrology and water quality in the pre-alpine/alpine Thur watershed using SWAT. *Journal of Hydrology, 333*, 413–430. https://doi.org/10.1016/j.jhydrol.2006.09.014

Ali, K. F., & de Boer, D. H. (2007). Spatial patterns and variation of suspended sediment yield in the upper Indus River basin, northern Pakistan. *Journal of Hydrology, 334*, 368–387. https://doi.org/10.1016/j.jhydrol.2006.10.013

Ali, S., Li, D., Congbin, F., & Khan, F. (2015). Twenty first century climatic and hydrological changes over Upper Indus Basin of Himalayan region of Pakistan. *Environmental Research Letters, 10*, 14007. https://doi.org/10.1088/1748-9326/10/1/014007

Andermann, C., Bonnet, S., & Gloaguen, R. (2011). Evaluation of precipitation data sets along the Himalayan front. *Geochemistry, Geophysics, Geosystems, 12*. https://doi.org/10.1029/2011GC003513. n/a-n/a.

Andréassian, V., Perrin, C., Michel, C., Usart-Sanchez, I., & Lavabre, J. (2001). Impact of imperfect rainfall knowledge on the efficiency and the parameters of watershed models. *Journal of Hydrology, 250*, 206–223. https://doi.org/10.1016/S0022-1694(01)00437-1

Archer, D. (2003). Contrasting hydrological regimes in the upper Indus Basin. *Journal of Hydrology, 274*, 198–210. https://doi.org/10.1016/S0022-1694(02)00414-6

Archer, D. R., & Fowler, H. J. (2004). Spatial and temporal variations in precipitation in the Upper Indus Basin, global teleconnections and hydrological implications. *Hydrology and Earth System Sciences, 8*, 47–61. https://doi.org/10.5194/hess-8-47-2004

Arnold, J. G., Srinivasan, R., Muttiah, R. S., & Williams, J. R. (1998). Large area hydrologic modeling and assessment part I: Model development. *Journal of the American Water Resources Association, 34*, 73–89. https://doi.org/10.1111/j.1752-1688.1998.tb05961.x

Bajracharya, S. R., Maharjan, S. B., Shrestha, F., Guo, W., Liu, S., Immerzeel, W., & Shrestha, B. (2015). The glaciers of the Hindu Kush himalayas: Current status and observed changes from the 1980s to 2010. *International Journal of Water Resources Development, 31*, 161–173. https://doi.org/10.1080/07900627.2015.1005731

Brent, R. P. (1971). An algorithm with guaranteed convergence for finding a zero of a function. *The Computer Journal, 14*, 422–425. https://doi.org/10.1093/comjnl/14.4.422

Dahri, Z. H., Ludwig, F., Moors, E., Ahmad, B., Khan, A., & Kabat, P. (2016). An appraisal of precipitation distribution in the high-altitude catchments of the Indus basin. *The Science of the Total Environment, 548–549*, 289–306. https://doi.org/10.1016/j.scitotenv.2016.01.001

Dahri, Z. H., Moors, E., Ludwig, F., Ahmad, S., Khan, A., Ali, I., & Kabat, P. (2018). Adjustment of measurement errors to reconcile precipitation distribution in the high-altitude Indus basin. *International Journal of Climatology, 38*, 3842–3860. https://doi.org/10.1002/joc.5539

Dee, D. P., Uppala, S. M., Simmons, A. J., Berrisford, P., Poli, P., Kobayashi, S., Andrae, U., Balmaseda, M. A., Balsamo, G., Bauer, P., Bechtold, P., Beljaars, A. C. M., van de Berg, L., Bidlot, J., Bormann, N., Delsol, C., Dragani, R., Fuentes, M., Geer, A. J., … Vitart, F. (2011). The ERA-interim reanalysis: Configuration and performance of the data assimilation system. *Quarterly Journal of the Royal Meteorological Society, 137*, 553–597. https://doi.org/10.1002/qj.828

Duncan, M. R., Austin, B., Fabry, F., & Austin, G. L. (1993). The effect of gauge sampling density on the accuracy of streamflow prediction for rural catchments. *Journal of Hydrology, 142*, 445–476. https://doi.org/10.1016/0022-1694(93)90023-3

FAO-UNESCO. (2007). FAO-UNESCO soil map of the World. In *Food and agriculture organization of the united Nations*. FAO GEONETWORK.

Goovaerts, P. (1997). Geostatistics for natural resources evaluation. In *Applied geostatistics series*. New York, Oxford: Oxford University Press.

Goovaerts, P. (2000). Geostatistical approaches for incorporating elevation into the spatial interpolation of rainfall. *Journal of Hydrology, 228*, 113–129. https://doi.org/10.1016/S0022-1694(00)00144-X

Hewitt, K. (2007). Tributary glacier surges: An exceptional concentration at panmah glacier, Karakoram himalaya. *Journal of Glaciology, 53*, 181–188. https://doi.org/10.3189/172756507782202829

Hewitt, K. (2011). Glacier change, concentration, and elevation effects in the Karakoram himalaya, upper Indus basin. *Mountain Research and Development, 31*, 188–200. https://doi.org/10.1659/MRD-JOURNAL-D-11-00020.1

Huffman, G. J., Bolvin, D. T., Nelkin, E. J., Wolff, D. B., Adler, R. F., Gu, G., Hong, Y., Bowman, K. P., & Stocker, E. F. (2007). The TRMM multisatellite precipitation analysis (TMPA): Quasi-global, multiyear, combined-Sensor precipitation estimates at fine scales. *Journal of Hydrometeorology, 8*, 38–55. https://doi.org/10.1175/JHM560.1

Immerzeel, W. W., Droogers, P., de Jong, S. M., & Bierkens, M. F. P. (2009). Large-scale monitoring of snow cover and runoff simulation in Himalayan river basins using remote sensing. *Remote Sensing of Environment, 113*, 40–49. https://doi.org/10.1016/j.rse.2008.08.010

Immerzeel, W. W., Wanders, N., Lutz, A. F., Shea, J. M., & Bierkens, M. F. P. (2015). Reconciling high-altitude precipitation in the upper Indus basin with glacier mass balances and runoff. *Hydrology and Earth System Sciences, 19*, 4673–4687. https://doi.org/10.5194/hess-19-4673-2015

Khan, A., & Koch, M. (2018a). Correction and informed regionalization of precipitation data in a high mountainous region (upper Indus basin) and its effect on SWAT-modelled discharge. *Water, 10*, 1557. https://doi.org/10.3390/w10111557

Khan, A., & Koch, M. (2018b). Selecting and downscaling a set of climate models for projecting climatic change for impact assessment in the upper Indus basin (UIB). *Climate, 6*, 89. https://doi.org/10.3390/cli6040089

Khan, A., Koch, M., & Chinchilla, K. (2018). Evaluation of gridded multi-satellite precipitation estimation (TRMM-3B42-V7) performance in the upper Indus basin (UIB). *Climate, 6*, 76. https://doi.org/10.3390/cli6030076

Kobold, M., & Sušelj, K. (2005). Precipitation forecasts and their uncertainty as input into hydrological models. *Hydrology and Earth System Sciences, 9*, 322–332. https://doi.org/10.5194/hess-9-322-2005

Lanza, L. G., Ramírez, J. A., & Todini, E. (2001). Stochastic rainfall interpolation and downscaling. *Hydrology and Earth System Sciences, 5*, 139–143. https://doi.org/10.5194/hess-5-139-2001

Leander, R., Buishand, T. A., van den Hurk, B. J. J. M., & de Wit, M. J. M. (2008). Estimated changes in flood quantiles of the river Meuse from resampling of regional climate model output. *Journal of Hydrology, 351*, 331–343. https://doi.org/10.1016/j.jhydrol.2007.12.020

Lehner, B., Verdin, K., & Jarvis, A. (2008). New global hydrography derived from Spaceborne elevation data. *Eos Trans. AGU, 89*, 93. https://doi.org/10.1029/2008EO100001

Liu, Y. B., & De Smedt, F. (2004). *WetSpa extension, A GIS-based hydrologic model for flood prediction and watershed management: Documentation and user manual*. Belgium, Brussel, Belgium: Department of Hydrology and Hydraulic Engineering, Vrije Universiteit Brussel.

Lutz, A. F., Immerzeel, W. W., Kraaijenbrink, P. D. A., Shrestha, A. B., & Bierkens, M. F. P. (2016). Climate change impacts on the upper Indus hydrology: Sources, Shifts and extremes. *PloS One, 11*, Article e0165630. https://doi.org/10.1371/journal.pone.0165630

Ma, Y., Zhang, Y., Yang, D., & Farhan, S. B. (2015). Precipitation bias variability versus various gauges under different climatic conditions over the Third Pole Environment (TPE) region. *International Journal of Climatology, 35*, 1201–1211. https://doi.org/10.1002/joc.4045

Palazzi, E., von Hardenberg, J., & Provenzale, A. (2013). Precipitation in the hindu-Kush Karakoram himalaya: Observations and future scenarios. *Journal of Geophysical Research - D: Atmospheres, 118*, 85–100. https://doi.org/10.1029/2012JD018697

Qiu, J. (2008). China: The third pole. *Nature, 454*, 393–396. https://doi.org/10.1038/454393a

Reggiani, P., & Rientjes, T. H. M. (2015). A reflection on the long-term water balance of the Upper Indus Basin. *Hydrology Research, 46*, 446–462. https://doi.org/10.2166/nh.2014.060

Ren, Y.-Y., Ren, G.-Y., Sun, X.-B., Shrestha, A. B., You, Q.-L., Zhan, Y.-J., Rajbhandari, R., Zhang, P.-F., & Wen, K.-M. (2017). Observed changes in surface air temperature and precipitation in the Hindu Kush Himalayan region over the last 100-plus years. *Advances in Climate Change Research, 8*, 148–156. https://doi.org/10.1016/j.accre.2017.08.001

RODDA, J. C. (1971). Report on precipitation. International association of Scientific hydrology. *Bulletin, 16*, 37–47. https://doi.org/10.1080/02626667109493783

Rueland, D., Larrat, V., & Guinot, V. (2010). *A comparison of two conceptual models for the simulation of hydro-climatic variability over 50 years in a large Sudano-*

Sahelian catchment. IAHS publication (Vol. 340). Wallingford: International Association of Hydrological Sciences, 0144-7815.

Schmidli, J., Frei, C., & Vidale, P. L. (2006). Downscaling from GCM precipitation: A benchmark for dynamical and statistical downscaling methods. *International Journal of Climatology, 26*, 679–689. https://doi.org/10.1002/joc.1287

Sharma, E., Molden, D., Wester, P., & Shrestha, R. M. (2016). The Hindu Kush himalayan monitoring and assessment programme: Action to sustain a global asset. *Mountain Research and Development, 36*, 236–239. https://doi.org/10.1659/MRD-JOURNAL-D-16-00061.1

Shroder, J. F., Jr. (2005). *Himalaya to the sea: Geology, geomorphology and the quaternary* (1st ed.). Abingdon, Oxon: Taylor and Francis.

Singh, P., & Kumar, N. (1997). Effect of orography on precipitation in the western Himalayan region. *Journal of Hydrology, 199*, 183–206. https://doi.org/10.1016/S0022-1694(96)03222-2

Srinivasan, R., Ramanarayanan, T. S., Arnold, J. G., & Bednarz, S. T. (1998). Large area hydrologic modeling and assessment part II: Model application. *Journal of the American Water Resources Association, 34*, 91–101. https://doi.org/10.1111/j.1752-1688.1998.tb05962.x

Hasson, Shabeh ul (2016). Future water availability from hindukush-Karakoram-himalaya upper Indus basin under conflicting climate change scenarios. *Climate, 4*, 40. https://doi.org/10.3390/cli4030040

Sun, X.-B., Ren, G.-Y., Shrestha, A. B., Ren, Y.-Y., You, Q.-L., Zhan, Y.-J., Xu, Y., & Rajbhandari, R. (2017). Changes in extreme temperature events over the Hindu Kush himalaya during 1961–2015. *Advances in Climate Change Research, 8*, 157–165. https://doi.org/10.1016/j.accre.2017.07.001

Szentimrey, T. (2013). *Multiple analysis of series for homogenization (M A S H v3.03): CARPATCLIM-report annex 3 – description of MASH and MISH algorithms*. http://www.carpatclim-eu.org/docs/mashmish/mashmish.pdf.

Tahir, A. A., Chevallier, P., Arnaud, Y., & Ahmad, B. (2011). Snow cover dynamics and hydrological regime of the Hunza River basin, Karakoram range, Northern Pakistan. *Hydrology and Earth System Sciences, 15*, 2275–2290. https://doi.org/10.5194/hess-15-2275-2011

Tahir, A. A., Chevallier, P., Arnaud, Y., Neppel, L., & Ahmad, B. (2011). Modeling snowmelt-runoff under climate scenarios in the Hunza River basin, Karakoram range, Northern Pakistan. *Journal of Hydrology, 409*, 104–117. https://doi.org/10.1016/j.jhydrol.2011.08.035

USGS EROS Data Center. (2002). GLCC - global land cover Characteristics data Base. In *Earth resources observation and science (EROS) cente* (2nd ed.). USGS.

Valéry, A., Andréassian, V., & Perrin, C. (2010). Regionalization of precipitation and air temperature over high-altitude catchments – learning from outliers. *Hydrological Sciences Journal, 55*, 928–940. https://doi.org/10.1080/02626667.2010.504676

Wake, C. P. (1989). Glaciochemical investigations as a tool for determining the spatial and seasonal variation of snow accumulation in the central Karakoram, Northern Pakistan. *A. Glaciology., 13*, 279–284. https://doi.org/10.3189/S0260305500008053

Weedon, G. P., Balsamo, G., Bellouin, N., Gomes, S., Best, M. J., & Viterbo, P. (2014). The WFDEI meteorological forcing data set: WATCH forcing data methodology applied to ERA-interim reanalysis data. *Water Resour. Res., 50*, 7505–7514. https://doi.org/10.1002/2014WR015638

Wijngaard, R. R., Lutz, A. F., Nepal, S., Khanal, S., Pradhananga, S., Shrestha, A. B., & Immerzeel, W. W. (2017). Future changes in hydro-climatic extremes in the upper Indus, ganges, and brahmaputra river basins. *PloS One, 12*, Article e0190224. https://doi.org/10.1371/journal.pone.0190224

Yanai, M., & Li, C. (1994). Mechanism of heating and the boundary layer over the Tibetan plateau. *Monthly Weather Review, 122*, 305–323. https://doi.org/10.1175/1520-0493(1994)122<0305:MOHATB>2.0.CO;2

Yang, D., & Ohata, T. (2001). A bias-corrected Siberian regional precipitation climatology. *Journal of Hydrometeorology, 2*, 122–139. https://doi.org/10.1175/1525-7541(2001)002<0122:ABCSRP>2.0.CO;2

Yao, T., Thompson, L. G., Mosbrugger, V., Zhang, F., Ma, Y., Luo, T., Xu, B., Yang, X., Joswiak, D. R., Wang, W., Joswiak, M. E., Devkota, L. P., Tayal, S., Jilani, R., & Fayziev, R. (2012). Third Pole environment (TPE). *Environmental Development, 3*, 52–64. https://doi.org/10.1016/j.envdev.2012.04.002

Yatagai, A., Kamiguchi, K., Arakawa, O., Hamada, A., Yasutomi, N., & Kitoh, A. (2012). Aphrodite: Constructing a long-term daily gridded precipitation dataset for Asia based on a dense network of rain gauges. *Bulletin of the American Meteorological Society, 93*, 1401–1415. https://doi.org/10.1175/BAMS-D-11-00122.1

Zhan, Y.-J., Ren, G.-Y., Shrestha, A. B., Rajbhandari, R., Ren, Y.-Y., Sanjay, J., Xu, Y., Sun, X.-B., You, Q.-L., & Wang, S. (2017). Changes in extreme precipitation events over the Hindu Kush Himalayan region during 1961–2012. *Advances in Climate Change Research, 8*, 166–175. https://doi.org/10.1016/j.accre.2017.08.002

International Soil and Water Conservation Research 9 (2021) 461–473

Contents lists available at ScienceDirect

International Soil and Water Conservation Research

journal homepage: www.elsevier.com/locate/iswcr

Original Research Article

In-depth analysis of soil management and farmers' perceptions of related risks in two olive grove areas in southern Spain

José A. Gómez [a, *], Ana Sánchez Montero [a], Gema Guzmán [a], María-Auxiliadora Soriano [b]

[a] Institute for Sustainable Agriculture, CSIC, Cordoba, Spain
[b] Agronomy Department, University of Cordoba, Cordoba, Spain

ARTICLE INFO

Article history:
Received 15 December 2020
Received in revised form
15 January 2021
Accepted 19 January 2021
Available online 25 January 2021

Keywords:
Tillage
Cover crops
Olive yield
Erosion risk
Irrigation
Questionnaire

ABSTRACT

This manuscript presents a questionnaire-based study aimed to provide a detailed analysis on the different soil management carried out by olive farmers in two representative olive-growing areas in southern Spain (Cordoba and Estepa), their perceptions on cover crop use and the possible influence of the different types of farms and farmers' typologies on these perceptions. Our results show a relatively large variability of soil management, with fourteen options, as a result of a combination of different alternatives for bare soil and cover crops with the use or not of pruning residues, but with a great similarity between both areas. The results indicate a high adoption of soil conservation measures in the two study areas, with 63% of farmers using cover crops and 80% a mulch of pruning residues, higher than that reported in previous studies in Southern Spain, and a trend of lower use of these techniques by less experienced and younger farmers. This high penetration of soil conservation measures resulted in a significant reduction of soil erosion risk, as indicated by the relatively low values for the cover and management factor (C) of RUSLE, also calculated and presented in this study, but also the possibility of focusing further efforts on farmers with less experience. Our results indicate the persistence of a minor, but relevant, percentage of farmers using bare soil management (37%) and no mulching (20%), with a moderate concern on the impact of soil erosion on soil degradation and provision of ecosystem services. This suggests the need to concentrate efforts also on this cluster of farmers to enhance the success of what seems to be a remarkable expansion of the use of soil conservation measures in recent decades in Southern Spain, but also in similar areas in the Mediterranean basin.

1. Introduction

Olive trees cover approximately 10.5 Mha worldwide (FAOSTAT, 2020). This area is larger than the cultivated area of other widely distributed woody crops such as vineyards or apple trees, 7.2 and 4.9 Mha respectively, although smaller than the area devoted to field crops for vegetable oils like soybean or sunflower, 124.9 and 27.5 Mha, respectively (FAOSTAT, 2020). Due to the climatic requirements of olive trees, around 95% of the total area is cultivated in the Mediterranean basin and seven countries concentrate 84% of the olive grove area (Spain, Tunisia, Italy, Morocco, Greece, Turkey and Syria, in order of decreasing extension). In these countries olive is a major cash crop, having municipalities where olive groves occupy more than 70% of all available land (e.g. some areas in southern Spain, REDIAM, 2020). Olive is also a cornerstone of cultural and landscape values after more than two millennia of its continuous cultivation (Loumou & Giourga, 2003).

Olive acreage has grown steadily over the last decades worldwide, with an average annual increase of 5.7% since the early 1960's (FAOSTAT, 2020) as a response to the increasing demand for olive oil. In parallel to this market success, olive cultivation has been associated with several sustainability problems (e.g. Beaufoy, 2001; El Hanandeh & Gharaibeh, 2016; Gómez, 2009; Gómez-Limón et al., 2012; Scheidel & Krausmann, 2011), particularly in countries where its expansion has been more intense, like Spain. Among these sustainability issues are a reduction of biodiversity, overexploitation of water resources, decreasing profitability for farmers, offsite contamination, and soil degradation by accelerated water erosion processes (Gómez, 2009).

Due to the combination of topographic and climatic factors

* Corresponding author.
E-mail address: joseagomez@ias.csic.es (J.A. Gómez).

https://doi.org/10.1016/j.iswcr.2021.01.003

(sloping land and Mediterranean climate prone to sporadically intense rainfall events) and agricultural practices (low tree density, small crown size and bare soil management aimed at ensuring tree survival during drought periods), soil erosion has historically been identified as a serious environmental problem in Mediterranean olive groves. Besides this, erosion rates have increased during the last decades of the 20th century due to olive farming intensification (Vanwalleghem et al., 2011).

To our knowledge, the first recommendations regarding the introduction of systematic measures for reducing soil erosion in olive growing areas appeared in technical literature in the 1960's (Bennet, 1960; Ruiz de Castroviejo, 1969). Since then, several soil management strategies have been promoted to substitute bare soil approaches (using tillage or herbicide) by alternative ones which maintain ground cover. These can be summarized as: i) temporary cover crops during the rainy season (from fall to early spring) to minimize the risk of competition for water and nutrients and to avoid reduced olive yields (Gómez, 2016); and ii) mulch of chopped olive-tree pruning residues along the alleys to provide ground cover and improve soil properties (Bombino et al., 2020). Their use has grown in recent decades, as noted by some local studies (e.g. Calatrava et al., 2007).

Regarding the adoption of pruning mulch in olive groves, one of the few studies available is that of Calatrava and Franco (2011) in the Granada province (southern Spain). This study was based in a survey of 215 olive farmers and found that pruning mulch was used by 43% of them 20 years after its first introduction in the province. There are some more studies, but not many, on the use of cover crops in olive groves. Thus, Calatrava et al. (2007) evaluated, by means of a survey of 223 farmers, the use of soil conservation practices in olive orchards in mountainous areas of southern Spain. They found that 51% of the farmers used a temporary cover crop, mostly controlled with herbicide, and that this number had risen from a mere 4% in 1989. The difficulty of tillage due to the high slopes might explain this relatively high use of cover crops in these mountainous areas, which contrasts with the results found for cover crop use in other areas. For instance, Sastre et al. (2017) in a survey of 119 olive farmers in the flatter and drier areas of central Spain found that only 6% of the farmers used cover crops. Recently, Rodriguez-Sousa et al. (2020) in a survey of 55 olive farmers in the Estepa region (a rolling landscape area in southern Spain) noted a common use of cover crops and pruning mulch in the area, although they did not quantify their use, since they classified the farmers by the production system (organic *vs.* integrated pest management). Analogous studies in other Mediterranean countries also show contrasting results. Kourouxou et al. (2005), in a study based on surveys and interviews on the Greek island of Taxos, found divergent views on the introduction of more sustainable soil management, depending among other factors, on the farmers' age and level of academic education. These authors also classified the farmers according to production systems (intensive, extensive, organic) with scarce information on the specific details of soil management implemented within each system. This generalization, using the production system (e.g. organic *vs.* conventional) as a proxy for soil management, seems to be a common approach in other environmentally-related studies in olives, e.g. Giomi et al. (2018) in their evaluation of agri-environment schemes to reduce the use of agrochemicals in Tuscany. This approach might be justified by the purposes of these studies, oriented towards the identification of farmers'attitudes, their perceptions regarding the future of olive production and their affinity to change practices. However, they provide very limited knowledge on details that are critical for a better appraisal of the impact of soil management on erosion risk, which can vary widely within broad categories such as conventional or organic (Gómez, 2016). This fact has been well documented in other woody crops, such as in vineyards where Bidoccu et al. (2020) detected a large variability in the erosion risk of apparently similar soil management grouped within the same category (i.e., cover crops or bare soil). That variability was highlighted when the details of soil management reported by each individual farmer were considered. This large, still poorly understood, farm-to-farm variability on cover crops and mulching use, and the need for more in-depth research, is in line with the results reported by Roesch-McNally et al. (2018) on the adoption of cover crops in field crops in the USA Midwest. These authors indicated how the adoption of cover crops by farmers seems to be the result of simultaneously addressing field-level challenges (which are mainly site-specific) and structural barriers (e.g. market forces). They suggest that farmers are using, implicitly, a system approach not only based on agronomic concerns, highlighting the limited available information to understand this process.

Our review of available studies on soil conservation measures in olive-growing countries indicates the need for research aimed to provide a more detailed description of soil management currently implemented by farmers, and exploring its potential link to farm types and farmers' typologies and perceptions. In this regard, new research might contribute to improving soil conservation and, in general, the provision of ecosystems services in olive-growing areas. Furthermore, it could identify the most successful practices and strategies to enhance their widespread adoption, as well as identifying blind spots where additional efforts should be concentrated. For these reasons, we carried out this study, with the objective of developing a detailed analysis on different soil management used by farmers in two representative olive-growing areas in southern Spain (Cordoba and Estepa), exploring the possible relationship between its frequency of use with the possible differences among farms and farmers' typologies and perceptions.

2. Materials and methods

2.1. Study area

The study area covered two different olive-growing areas in southern Spain. One was the Protected Appellation of Origin (DOP) of Estepa (hereafter Estepa), which covers approximately 40,000 ha of olive trees that cover approximately 54.5% of all the land corresponding to the municipalities included in the DOP, distributed across the provinces of Cordoba and Seville, Fig. 1. It is located in the mid-southern section of the Guadalquivir river valley and it has a hot-summer Mediterranean climate (Csa) according to the Köppen classification (Gómez-Zotano et al., 2015). This area of rolling landscapes on sedimentary materials has as dominant soil types, Calcic Regosol and Calcic Cambisol (according to the world reference soil groups; IUSS, 2015) with a moderate presence of Vertic soils according to the soil map of Andalusia (Consejería de Medio Ambiente, 2005).

The other study area was the "comarca" (county-like) area of Cordoba (hereafter Cordoba), which is in the center of the Guadalquivir river valley, Fig. 1. It is also an area of rolling landscape, with a hot-summer Mediterranean climate (Csa). At the time of this study, there were approximately 17,500 ha of olive groves, that is, 14.0% of the total area of Cordoba. The dominant soil types are Vertic soils, followed in extension by Calcic Regosol and Calcic Cambisol, with a moderate presence of Fluvisol and Luvisol (Consejería de Medio Ambiente, 2005; IUSS, 2015).

2.2. Survey methodology

The study was carried out based on questionnaires aimed at obtaining an in-depth response from olive farmers in relation to the

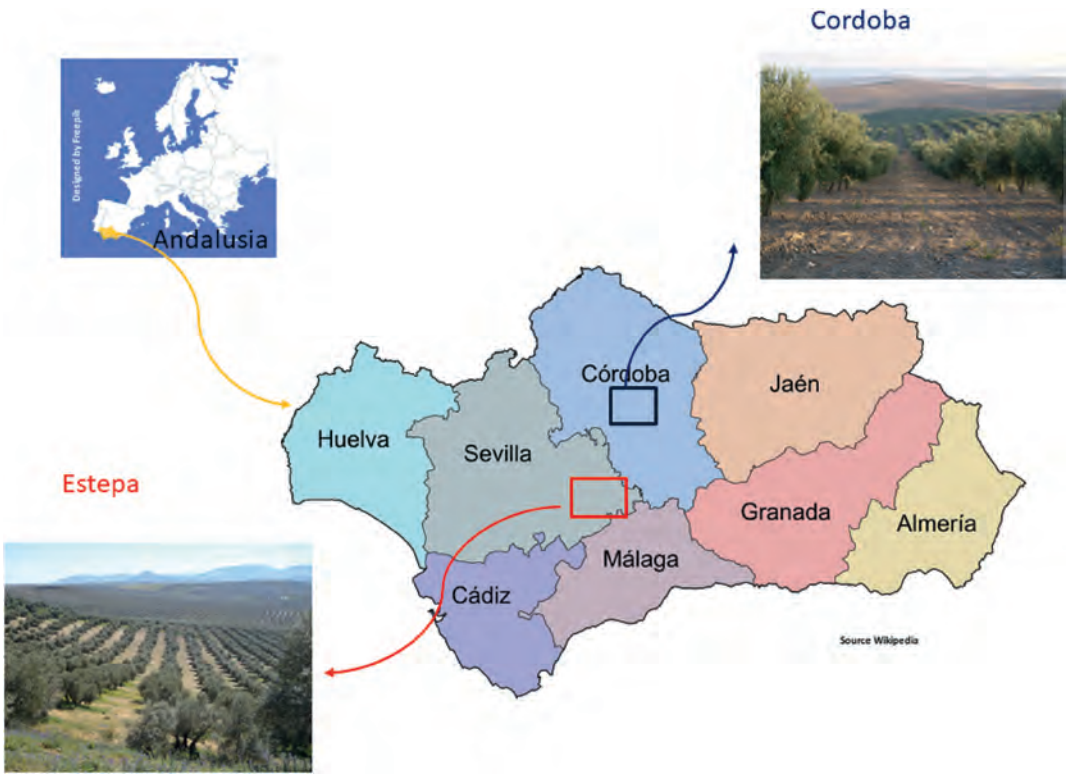

Fig. 1. Location map and view of the olive groves in the two study areas.

actual soil management carried out on their farms and their perception about the advantages and risks of alternative soil management based on cover crops or mulch of pruning residues, compared to traditional bare soil-based methods. This questionnaire was filled out in both study areas using two complementary ways during June–December 2019.

The first approach consisted of filling out the questionnaire personally, after a soil management and cover crop use seminar for farmers held on June 4th in Cordoba and June 22nd in Estepa. This was followed by a second on-line round, through the websites of the DOP Estepa and ASAJA (the majority farmers' association in the Cordoba area). This campaign was active from July 1st to December 8th, 2019, and participating farmers received a sample of cover crop seed mixture for their contribution. Overall,146 questionnaires were filled out, 84 from Estepa (19 personally and 65 on-line) and 62 from Cordoba (24 personally and 38 on-line). The questionnaire was divided into five sections (S), which covered different aspects. S1: characterization of farms, farmers and soil management (Table 1); S2: motivations for using cover crops *vs.* bare soil management (Table 2); S3: limitations perceived by farmers for using cover crops (Table 3); S4: beneficial effects observed by farmers using cover crops (Table 4); and S5: farmers' concerns regarding the negative effects of soil erosion on their farms (Table 5). Most of the answers were in the form of categorical variables, with the exception of farm area and olive yield.

2.3. Data analysis

Questionnaires were checked, discarding those that were mostly incomplete, resulting in a total of 136 to be analysed: 69 from Estepa (18 personally and 61 on-line) and 57 from Cordoba (20 personally and 37 on-line). Data from the questionnaires were analysed in three stages. First, we compared the results obtained between the two olive grove areas and in relation to farm access to irrigation. Secondly, the answers on management details were analysed to describe and quantify the different soil management options resulting from the use of herbicides and/or tillage *vs.* cover crops, and considering the use of chopped pruning residues as mulch. This analysis was complemented with the evaluation of the erosion risk for the different management through the soil cover and management factor of the Revised Universal Soil Loss Equation, RUSLE (Renard et al., 1997) running the ORUSCAL tool (Bidoccu et al., 2020). Given the relative proximity of both olive grove areas, the rainfall erosivity R corresponding to Cordoba was used in the evaluation. Thirdly, we evaluated the possible differences among farm types and farmers' typologies and perceptions regarding the use of cover crops (Tables 1–4) according to the three main types of soil management identified (Table 1) and the use or not of pruning residues as mulch. Statistical analyses were performed using STATA/SE 15 (StataCorp, College Station, TX) using a Fisher's exact test for categorical variables and a Kruskal-Wallis test for numerical (farm surface and olive yield) variables.

3. Results

3.1. Differences in olive-farms and farmer's typologies and perceptions by area and access to irrigation

Fig. 2A summarizes the differences (statistically significant at $p < 0.10$) in farms and in farmers' typologies and benefits and limitations regarding the use of cover crops between the two olive grove areas, with full results in Table 6. Farmers in Cordoba tend to manage larger farms than those in Estepa, 142 *vs.* 65 ha respectively, being in both areas dominantly owned (82%). Their academic level differed, with a higher proportion of farmers with college education in Cordoba (71%) as compared to Estepa (46%).

Table 1
Description of variables used in the questionnaire and values assigned to characterize farms, farmers and soil management.

Abbreviation	Description	Value
Area	Area where the olive farms are located	1 = Cordoba area 2 = D.O·P. Estepa
Irrig	Access to irrigation water	1 = Only rainfed 2 = Only irrigated 3 = Partly rainfed and the rest irrigated
RegProp	Own or leased land	1 = Owns all or majority of land 2 = Leases all or majority of land
Education	Academic level	1 = University 2 = Secondary school 3 = Primary school
Age	Age group	1 = Less than 30 years old 2 = 30–40 years old 3 = 40–50 years old 4 = 50–60 years old 5 = More than 60 years old
Experience	Years farming olive trees	1 = Less than 5 years 2 = 5–15 years 3 = 15–25 years 4 = More than 25 years
Surface	Cultivated area of olive trees	Numerical variable, in ha
YieldRain	Olive yield, in rainfed farms	Numerical variable, in kg ha^{-1}
YieldIrrig	Olive yield, in irrigated farms	Numerical variable, in kg ha^{-1}
SoilMan	Type of soil management	1 = Bare soil (tillage and/or herbicide) 2 = Cover crop 3 = Bare soil in rainfed farms and cover crop in irrigated ones
Herb	Use of herbicides to control cover crops	1 = Yes 2 = No
Mow	Use of mowing to control cover crops	1 = Yes 2 = No
NatCC	Cover crops of natural vegetation present	1 = Yes 2 = No
SeedCC	Seeded cover crop	1 = Yes 2 = No
SumPlow	Light tillage in summer to cover soil cracks	1 = Yes 2 = No
Prun	Use of chopped pruning residues as mulch	1 = Yes 2 = No

Table 2
Description of variables used in the questionnaire to analyze farmers' motives for using cover crops as an alternative to bare soil management.

Abbreviation	Description	Value
M_Erosion	To reduce accelerated water erosion	1 = No 2 = Yes
M_Fert	To improve soil fertility	1 = No 2 = Yes
M_Gully	To control gully erosion	1 = No 2 = Yes
M_Econom	To improve farm profitability	1 = No 2 = Yes
M_OrgC	To increase soil organic carbon	1 = No 2 = Yes
M_Energ	To reduce energy use	1 = No 2 = Yes
M_Biodiv	To improve biodiversity	1 = No 2 = Yes
M_Pests	Reduction of pests and/or diseases	1 = No 2 = Yes
M_CAP	Due to Common Agricultural Policy cross compliance	1 = No 2 = Yes

Farmers in both areas tended to have a similar age, with dominant age group (38%) ranging from 40 to 50 years, and a similar long trajectory in agriculture, with the dominant group (33%) with more than 25 years of farming. Among the most relevant features that did not show differences between areas, but which are worth mentioning, are the relatively high access to irrigation, 48%, although deficit irrigation, and the lack of differences in the average declared olive fruit yield, 5901 kg ha^{-1} $year^{-1}$ (Table 6).

Farmers in Estepa presented higher motivation for the use of cover crops related to the improvement of soil fertility, pest/disease control and fulfillment of the Common Agricultural Policy (CAP) requirements, compared to those in Cordoba. Farmers in Estepa also noted the high cost of seeds as a limitation for the use of cover crops and energy savings as a beneficial effect of using cover crops (93 and 86% of farmers, respectively) more frequently than those in Cordoba (73 and 66% of farmers, Fig. 2A).

However, in both areas, farmers' most frequent motivation to use cover crops was to reduce soil erosion (88% of answers on average), followed by the two already commented: fulfillment of the CAP requirements (76%) and improvement of soil fertility (75%). The most frequently noted limitations for the use of cover crops were technical in general terms, related to difficulties implanting cover crops and the high cost of cover crop seeds (83% on average), and the need for availability of seeds and an adequate mower for cover crops (74% of answers). Half of the farmers did not mention a greater difficulty for harvesting as a limitation. Farmers using cover crops in both areas have a similar perception about their benefits, with the most frequently-named benefits (81–86% of farmers) related to soil (increased soil organic carbon, improvement of soil structure and fertility and soil erosion reduction), and with an increased biodiversity and reduction of pest/disease damages (Table 6).

Farmers in both areas also had similar concerns about the negative effects of soil erosion, with loss of soil fertility and development of gullies being the most frequent concern, 73 and 79% of answers respectively, with a higher concern in Cordoba in

Table 3
Description of variables used in the questionnaire to analyze the limitations that farmers perceive to implement cover crops.

Abbreviation	Description	Values
L_Yield	Olive yield reduction	1 = Relevant 2 = Not relevant
L_Harvest	Difficulty in harvesting	1 = Relevant 2 = Not relevant
L_Cost	Increase in farming costs	1 = Relevant 2 = Not relevant
L_Pests	Increase in pests and/or diseases	1 = Relevant 2 = Not relevant
L_IncEnerg	Increase of energy costs	1 = Relevant 2 = Not relevant
L_Implant	Difficulties in implanting the cover crop	1 = Relevant 2 = Not relevant
L_Expensiv	High cost of cover crop seeds	1 = Relevant 2 = Not relevant
L_Availab	No availability of cover crop seeds	1 = Relevant 2 = Not relevant
L_Mower	Need to purchase a mower for cover crops management	1 = Relevant 2 = Not relevant

Table 4
Description of variables used in the questionnaire to analyze the beneficial effects observed by farmers using cover crops.

Abbreviation	Description	Values
B_Erosion	Reduction of soil erosion	1 = Relevant 2 = Not relevant
B_Fert	Improvement of soil fertility	1 = Relevant 2 = Not relevant
B_Econom	Improvement of farm profitability	1 = Relevant 2 = Not relevant
B_OrgC	Increase in soil organic carbon	1 = Relevant 2 = Not relevant
B_Energ	Reduction of energy use	1 = Relevant 2 = Not relevant
B_Biodiv	Increase in biodiversity	1 = Relevant 2 = Not relevant
B_Pests	Reduction of pests and/or diseases	1 = Relevant 2 = Not relevant
B_SoilStr	Improvement of soil structure	1 = Relevant 2 = Not relevant

Table 5
Description of variables used in the questionnaire to appraise farmers' concerns regarding the negative effects of soil erosion in their farms.

Abbreviation	Description	Values
N_Yield	Olive yield reduction	1 = Concerned 2 = Not concerned
N_Fert	Reduction of soil fertility	1 = Concerned 2 = Not concerned
N_Traffic	Difficulty for traffic on the farm	1 = Concerned 2 = Not concerned
N_CostFert	Increase in fertilizers cost	1 = Concerned 2 = Not concerned
N_Gully	Acceleration of gully erosion	1 = Concerned 2 = Not concerned
N_Trees	Loss of olive trees	1 = Concerned 2 = Not concerned
N_Lands	Reduction of landscape values	1 = Concerned 2 = Not concerned
N_Biodiv	Reduction of biodiversity	1 = Concerned 2 = Not concerned

relation to gully development (87% of farmers compared to 71% in Estepa). There were between 36 and 53% of farmers who indicated no concern about the negative effects of erosion on the reduction of olive yield, biodiversity, landscape values and trafficability on farms, finding differences between both olive grove areas in their concern about loss of olive trees (67% of the farmers in Cordoba and 51% in Estepa, Table 6).

Fig. 2B summarizes the differences (statistically significant at $p < 0.10$) among the three possibilities of access to irrigation (Table 1) for the same questions addressed between the two olive grove areas, with complete results in Table 6. In relation to cultivated surface and olive trees farming experience, there were no differences between farmers managing exclusively rainfed or irrigated orchards, while farmers managing simultaneously rainfed and irrigated orchards managed more land and had more years of farming experience (Table 6). Differences in yield were in the expected direction, with fully irrigated farms declaring 9545 kg ha^{-1} $year^{-1}$of olive-fruit, as compared to 4692 and 6427 kg ha^{-1} $year^{-1}$for rainfed and partially-irrigated, respectively.

Rainfed farmers perceived less frequently the benefits of cover crops in relation to energy savings and improved farm profitability, as well as seed availability as a limitation to using cover crops. On the other hand, farmers managing only irrigated orchards perceived less frequently the reduction of erosion as a benefit of using cover crops, as well as gully control as a motivation for their use. This might be due to the need to exclude irrigation from the steepest slopes, even if using drip irrigation as it is the case in the area. Beyond these differences, there was a similar perception among groups of farmers according to their access to irrigation in relation to motivations, limitations and benefits observed of using cover crops. No differences were detected in concerns about the negative effects of erosion.

3.2. Analysis of soil management strategies in the two olive-growing areas and impact on erosion risk

Fig. 3 summarizes the different soil management identified in the two study areas, showing a large number of different approaches: fourteen. The frequency distribution of the different soil management was similar in both areas, with only some minor differences. Overall, there is a dominance of cover crop-based management in both areas with 63% of farmers using some kind of cover crop as compared to 35% of farmers keeping bare soil (with or without pruning residues). There were no statistically significant differences in the use of cover crops between the olive growers in Cordoba and Estepa, according to Fisher's exact test($p < 0.10$). Almost all the cover crops are based on the spontaneous vegetation of the farms, with only a very small percentage of farmers seeding a cover crop in the Cordoba area. There was a moderate effect

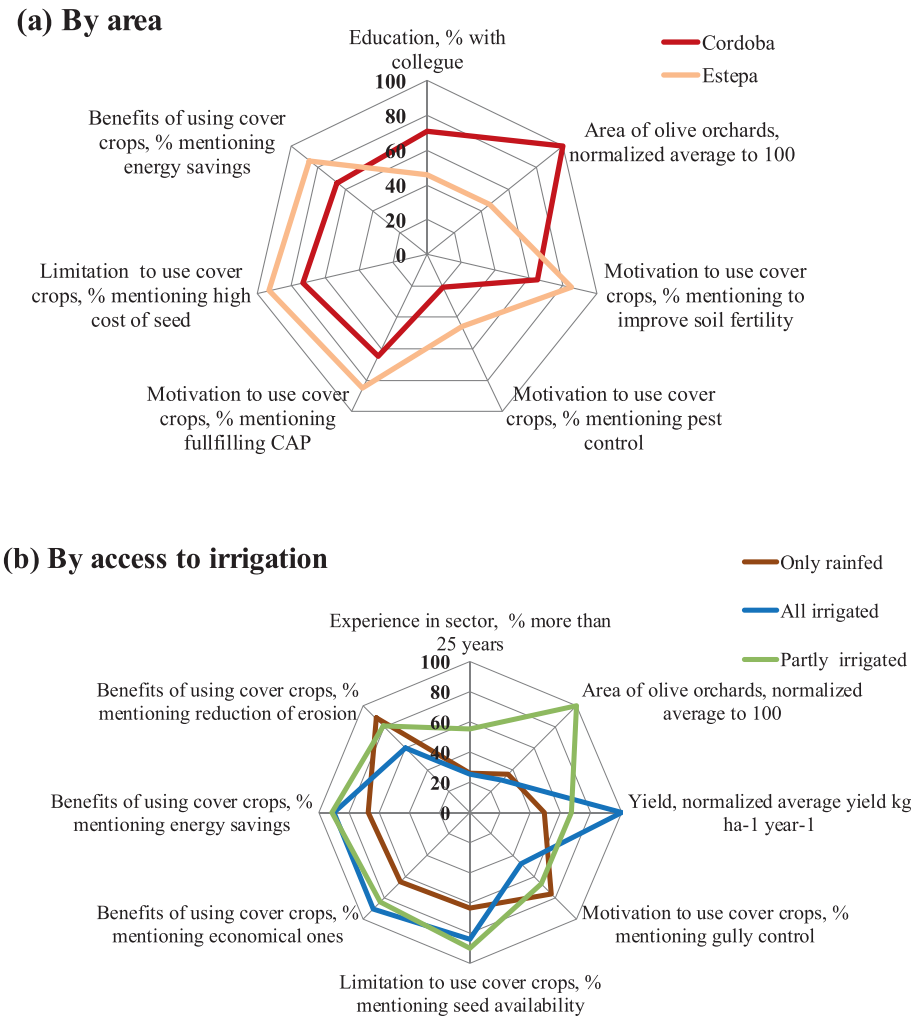

Fig. 2. Spider graph summarizing statistically significant differences ($p < 0.1$) in olive farms and in farmers' typologies and limitations and benefits regarding the use of cover crops according to the location of the olive orchards, (a) top, and access to irrigation, (b) bottom).

($p = 0.097$, according to Fischer's exact test) of the access to irrigation in the use of cover crops by farmers, so 67% of rainfed farmers used cover crops, as compared to 48% of farmers managing only irrigated olive orchards, and 71% of farmers managing both rainfed and irrigated orchards. A mulch of chopped pruning residues along the lanes was used by 83% of the farmers, without significant difference between both areas. Access to irrigation had a significant effect on the use of pruning mulch ($p = 0.005$, according to Fischer's exact test), so 79 and 69% of farmers managing only rainfed or only irrigated orchards, respectively, used this technique, while it was used by 94% of farmers managing both rainfed and irrigated orchards.

Fig. 4 presents, aggregated due to the lack of significant differences between the two areas, the differences in hillslope water-erosion risk according to different soil management, using as a proxy the value of the soil cover and management factor C of RUSLE, with Fig. 5 showing its cumulative probability distribution. A relatively small fraction of the farmers (<5%, Fig. 5) declared a soil management presenting a very high erosion risk, as noted by C values above 0.4. These managements were those based on bare soil management using herbicides or tillage, without the use of a mulch of pruning residues. The soil management mostly implemented in both areas, based on increasing the soil cover with cover crops, mulch of pruning residues or both, resulted in a much lower erosion risk, in the range of 0.12–0.22 for C values (Fig. 4), roughly halving the water erosion risk. Among the different managements with cover crops, those not using a pruning mulch resulted in lower C values (around 0.12) than those using it (C around 0.16), considering a lower development of the cover crop due to the impact of mulching.

3.3. *Differences in farmer's typologies and perceptions using different soil management*

Fig. 6A summarizes the significant differences between the three main groups of farmers based on their soil management approaches (Table 1), with the full results in Table 7. Farmers using bare-soil management tended to have less farming experience (40% with less than 5 years in the sector) and were slightly younger (30% of farmers in the dominant age group of 40–50 year) than those using a cover crop (always or partially). Thirty-nine percent of farmers always using cover crops had more than 25 years of experience growing olive trees, and 60% of those using them partially had between 15 and 25 years of experience, with 44% of farmers in the dominant age group of 40–50 years and 40% in that of those older than 60 years always or partially using cover crops, respectively. Farmers using bare-soil management managed significantly less olive area, 71 ha, than those using always or

Table 6
Summary of olive farmers' characteristics, motivations and perceived limitations and observed benefits by farmers using cover crops, and concerns about negative effects related to soil erosion, according to olive grove area (Area) and access to irrigation water (Irrig). Percentages in bold-brackets indicate the number of farmers who answered to that question. The significance of the differences among farmers by area or access to irrigation according to the Fisher's exact test (or Kruskal-Wallis for surface and yield) is shown for $p < 0.10$ (grey highlighted), NS=Not significant. (CO is Cordoba and ES is Estepa; R: rainfed; I: irrigated; R + I: farmer with irrigated and rainfed farms). Percentages within each block summarize the most frequent answer (average value) according to the description and values assigned in Tables 1–5

Farmers' characteristics	RegProp (94%)	Education (97%)	Experience (96%)	Age (94%)	Olive surface (96%)	Yield (81, 90%)	Irrig (94%)		
Area	NS; 1 (owners): 82%	p=0.001; 1 (college): 71% in CO, 46% in ES	NS; 4 (more than 25 years): 33%	NS; 3 (40–50 year): 38%	p=0.050; 142 ha in CO and 65 ha in ES	NS; 5901 kg ha^{-1}	NS; 1 (R): 52%		
Irrig	NS; 1 (owners): 82%	NS; 1 (college): 61%	p=0.017; 4 (more than 25 year): 26% R, 25% I, 55% R + I	NS; 3 (40–50 year): 38%	p=0.0871; 71 ha R., 60 ha I, 201 ha R + I	p=0.001; 4692 kg ha−1 R, 9545 kg ha−1 I, 6427 kg ha−1 R + I	–		
Motivation	**M_Erosion (99%)**	**M_Fert (99%)**	**M_Gully (99%)**	**M_Econom (99%)**	**M_OrgC (99%)**	**M_Energ (99%)**	**M_Biodiv (99%)**	**M_Pests (99%)**	**M_CAP (99%)**
Area	NS; Yes 88%	p=0.009; Yes: 65% in CO, 85% in ES	NS; Yes 67%	NS; No 66%	NS; No 53%	NS; No 71%	NS; Yes 59%	p=0.002; No: 79% in CO, 54% in ES	p=0.030; Yes: 65% in CO, 85% in ES
Irrig	NS; Yes 88%	NS; Yes 75%	p=0.030; Yes: 76% R, 48% I, 67% R + I	NS; No 66%	NS; No 53%	NS; No 71%	NS; Yes 59%	NS; No 67%	NS; Yes 76%
Limitations	**L_Yield (62%)**	**L_Harvest (60%)**	**L_Cost (61%)**	**L_Pests (57%)**	**L_IncEner (3.7%)**	**L_Implant (57%)**	**L_Expensiv (51%)**	**L_Availab (53%)**	**L_Mower (49%)**
Area	NS; Import. 67%	NS; No Import. 50%	NS; Import. 69%	NS; Import. 63%	–	NS; Import. 83%	p=0.018; Import.: 73% in CO, 93% in ES	NS; Import. 74%	NS; Import. 74%
Irrig	NS; Import. 67%	NS; No Import. 50%	NS; Import. 69%	NS; Import. 63%	–	NS; Import. 83%	NS; Import. 75%	p=0.044; Import.: 63% R, 84% I, 90% R + I	NS; Import. 74%
Beneficial	**B_Erosion (77%)**	**B_Fert (75%)**	**B_Econom (72%)**	**B_OrgC (63%)**	**B_Energ (68%)**	**B_Biodiv (70%)**	**B_Pests (64%)**	**B_SoilStr (74%)**	
Area	NS; Import. 81%	NS; Import. 81%	NS; Import. 75%	NS; Import. 86%	p=0.026; Import.: 66% in CO, 86% in ES	NS; Import. 82%	NS; Import. 81%	NS; Import. 84%	
Irrig	p=0.036; Import.: 88% R, 60% I, 81% R + I	NS; Import. 81	p=0.050; Import.: 65% R, 90% I, 84% R + I	NS; Import. 86%	p=0.040; Import.: 67% R, 90% I, 91% R + I	NS; Import. 82%	NS; Import. 81%	NS; Import. 84%	
Negative	**N_Yield (88%)**	**N_Fert (88%)**	**N_Traffic (90%)**	**N_CostFert (85%)**	**N_Gully (84%)**	**N_Trees (90%)**	**N_Lands (85%)**	**N_Biodiv (85%)**	
Area	NS; Concer. 64%	NS; Concer. 73%	NS; Concer. 60%	NS; No Concer. 53%	p=0.041; Concer.: 87% in CO, 71% in ES	p=0.097; Concer.: 67% in CO, 51% in ES	NS; Concer. 61%	NS, Concer. 61%	
Irrig	NS; Concer. 64%	NS; Concer. 73%	NS; Concer. 60%	NS; No Concer. 53%	NS; Concer. 79%	NS; Concer. 59%	NS; Concer. 61%	NS, Concer. 61%	

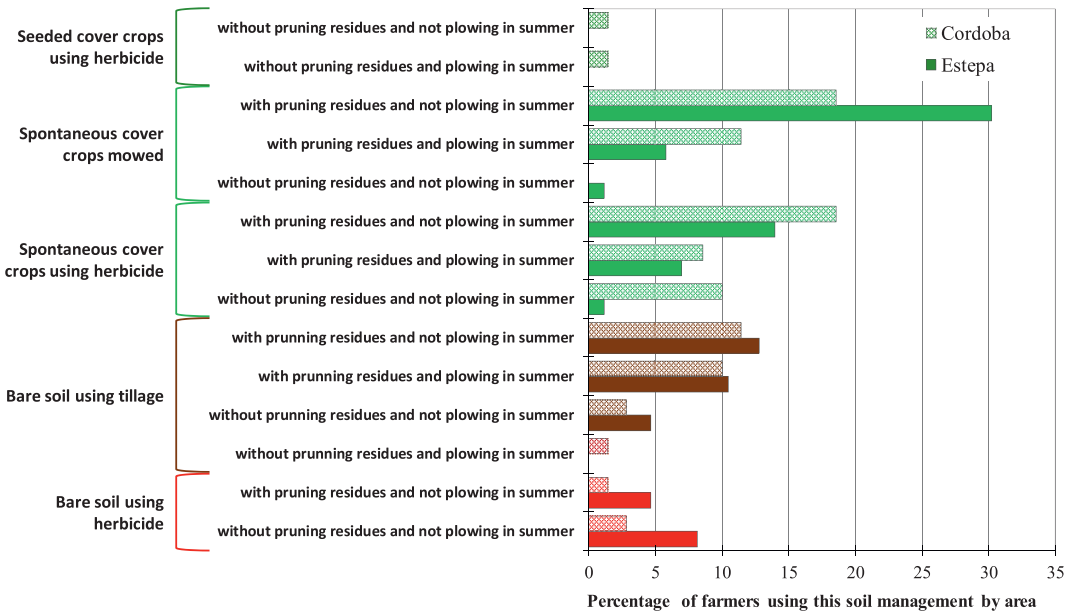

Fig. 3. Frequency of farmers (%) using the different soil management in the two study areas, Cordoba and Estepa.

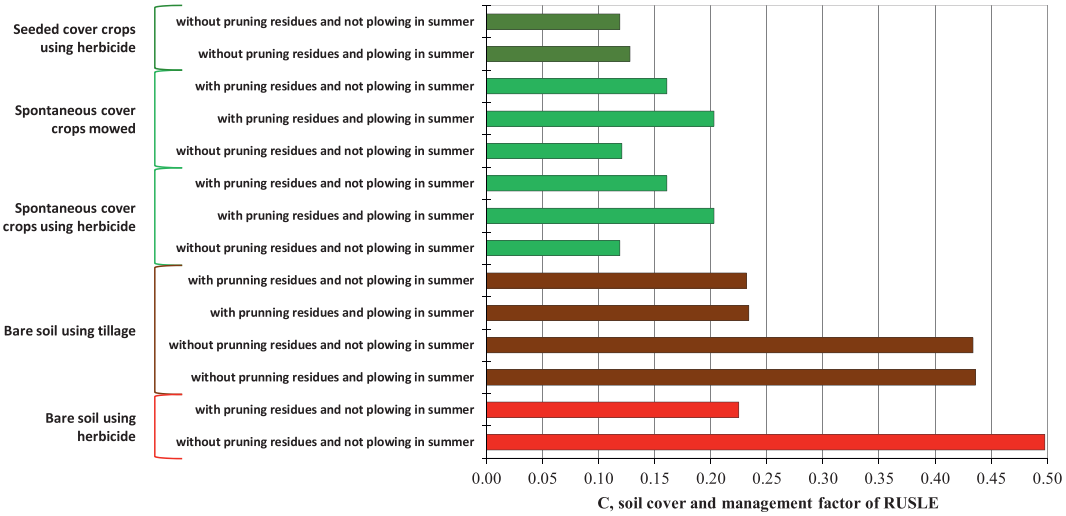

Fig. 4. Estimated value of the soil cover and management factor C of RUSLE for the different soil management declared by farmers in both study areas.

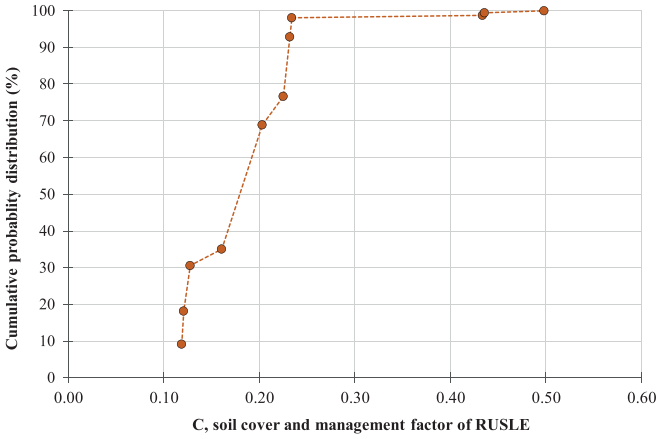

Fig. 5. Cumulative probability distribution of the soil cover and management factor C of RUSLE for the different soil management declared by farmers in both study areas, according to the percentage of farmers using each management.

partially a cover crop, 111 and 316 ha, respectively.

Regarding the motivations for using cover crops among the three soil management groups, the major differences appeared between the group that always used cover crops and the other two groups, bare-soil or partial-use of cover crops. Farmers who always use cover crops seemed to present a higher motivation for their use in relation to erosion and gully control and improvement of soil fertility, in the range of 74–96% of them, compared to 56–80% of farmers in the other two management groups. Bare-soil farmers regarded improving farm profitability much less of a potential motivation for using cover crops (only 9% answered yes) than farmers already using, exclusively or partially, cover crops, with 48 and 40% of positive answers respectively. Farmers always using cover crops also noted a higher motivation in relation to improving biodiversity and energy savings, 68 and 38% of positive answers respectively, as compared to the farmers using bare soil, 43 and 14% of positive answers, or partially using a cover crop, 40 and 30% of positive answers respectively. Farmers using a cover crop highlighted as a limitation seed availability more frequently (70–100% of farmers) than the farmers using bare soil (40% of them). Farmers always using a cover crop less frequently noted difficulty in harvesting or higher cost of farming, 38 and 60% respectively, than those using bare soil (total or partially) which noted this limitation in the ranges of 60–64 and 80–100% respectively, (Table 7). Among features that did not present differences between the three groups of farmers, according to soil management, and that are worth mentioning are the academic level, or the declared olive yield, Table 7.

Fig. 6B summarizes the significant differences between the two groups of farmers according to whether or not they use a mulch of pruning residues, with complete results in Table 7. Farmers using a pruning mulch were more experienced (39% of them with more than 25 years of farming experience), and older (39% in the dominant age group of 40–50 year) than those not using it, with 38% of them in the experience group of 15–25 years, and 33% in the age group of 30–40 years. The farmers using a mulch of pruning residues managed more olive area (105 *vs.* 102 ha) and had a higher declared olive yield in rainfed conditions (4851 *vs.* 3823 kg ha^{-1} $year^{-1}$). Farmers using a pruning mulch presented a higher motivation in relation to improvement of soil fertility, biodiversity and energy savings (80, 64 and 33%), than those not using a mulch, who noted a motivation of 54, 35 and 12% respectively. Farmers using a pruning residue mulch also perceived more frequently limitations in relation to the availability of seeds and an adequate mower for the use of cover crops (68 and 77% respectively) than those not using the mulch (44 and 53% respectively).

4. Discussion

4.1. Differences in olive-farms and farmer's typologies and perceptions by area and access to irrigation

The two olive grove areas evaluated in our study are in the upper range of yield within southern Spain (Andalusia) as reported in previous studies. For instance, Areal and Riesgo (2014) reported values in the range of 2.1–5.7 and 3.7–6.5 t ha^{-1} $year^{-1}$ for rainfed and irrigated orchards respectively. A large proportion of the interviewed farmers in our study (48%) managed orchards with access to irrigation, which in the area is exclusively deficit irrigation (1500–2500 m^3 ha^{-1} $year^{-1}$), without differences between areas. This access to irrigation was higher than that reported for other areas in southern Spain in previous studies which ranged between 5.5 and 24.4% (Areal & Riesgo, 2014; Calatrava & Franco, 2011), with the exception of La Loma county (Jaen province) which has 89%. This fact, combined with good climate and edaphic conditions can

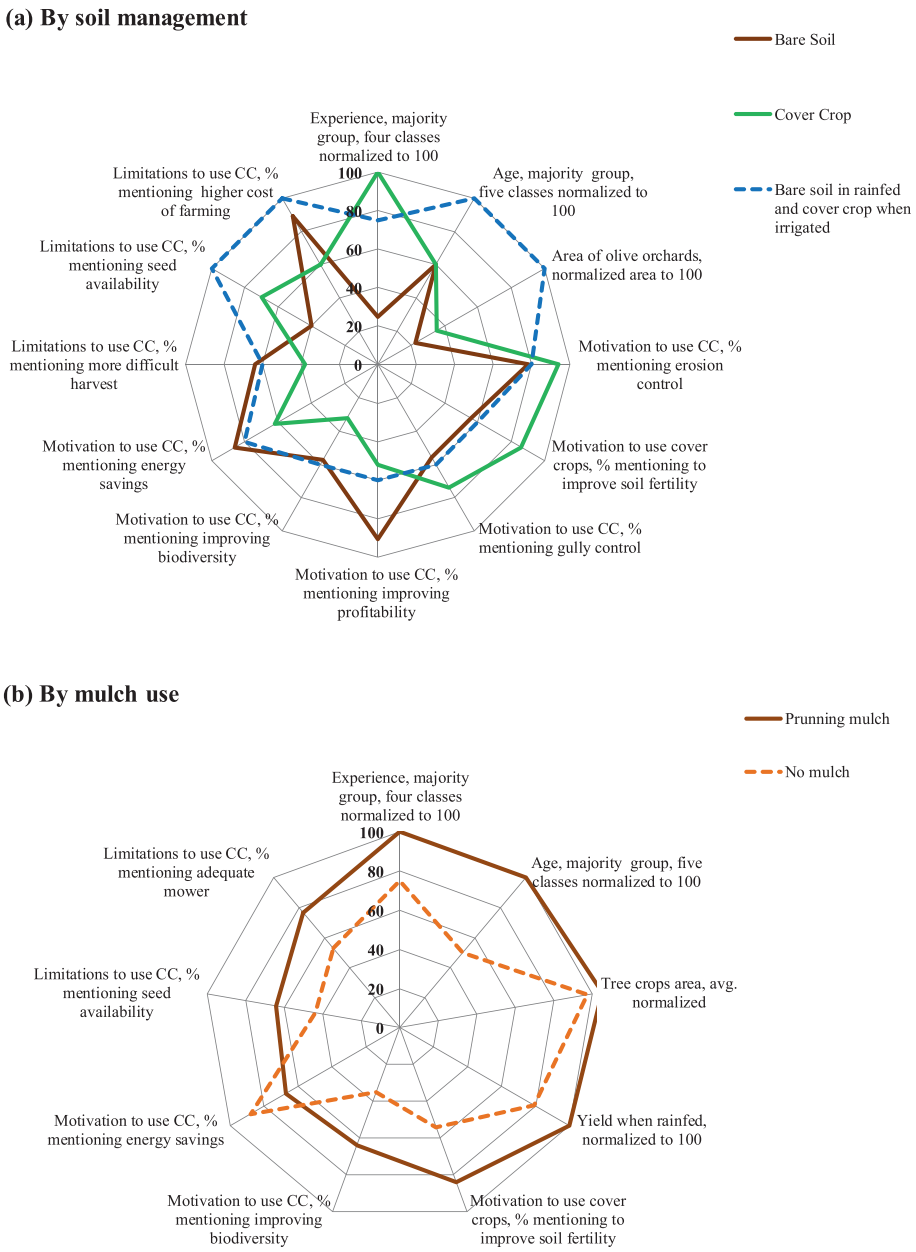

Fig. 6. Spider graph summarizing significant differences ($p < 0.1$) in olive farms and farmers' typologies and perceptions regarding the use of cover crops according to soil management (A, top) and use of mulch of pruning residues (B, bottom).

explain the relatively high olive yield levels found in our study. The farmers answering to our interviews seem to represent a group of professionalized farmers, as noted by the large area managed by the average farmer (142 and 65 ha in Cordoba and Estepa, respectively), and a high percentage of college-educated farmers, ranging from 46 to 71% in Estepa and Cordoba. These olive growers manage larger areas than the averages shown by Areal and Riesgo (2014) in Andalusia, in the range of 8.5–22.5 ha, although similar to the 119 ha reported by Sastre et al. (2017) in central Spain. The academic level of the farmers of our study also differed from those found by Areal and Riesgo (2014) who found a percentage of college-educated farmers in the range of 5.9–13%. However, it was similar to the 53% of college education recently reported by Rodriguez-Souza et al. (2020) for the organic farmers in the Estepa region, albeit in our case the majority of interviewed famers in the Estepa area were certified as integrated producers, while in Cordoba the majority were conventional, that is, not certified as organic or integrated farmers. In both areas, the dominant group of farmers were those in the age group of 40–50 years (38%) with more than 25 years of farming experience (33%). The age group is similar to the age range described by Rodriguez-Souza et al. (2020) for the Estepa region, and older than the dominant age group (less than 40 years old) described by Calatrava et al. (2007) for the Granada province. In short, it is apparent that the results presented in this study reflect a population of farmers who tend to be more productive and professionalized than others found in previous studies in Andalusia, but with a similar experience and age distribution.

Farmers interviewed in Cordoba and Estepa, despite some small differences, seemed to share a similar perception about motivations and limitations for using cover crops, and about the observed benefits of their use. They seemed to be in line with results from

Table 7
Summary of olive farmers' characteristics, motivations and perceived limitations and observed benefits by farmers using cover crops, and concerns about negative effects related to soil erosion, according to soil management (SoilMan) and use of mulch of pruning residues (Mulch). Percentages in bold-brackets indicate the number of farmers who answered to that question. The significance of the differences among farmers by soil management or use of pruning residues according to the Fisher's exact test (or Kruskal-Wallis for surface and yield) is shown for $p < 0.10$ (grey highlighted), NS=Not significant. (P: mulch with pruning; NP: no mulch with pruning; BS: bare soil; CC: cover crop; B: cover crop in irrigated farms and bare soil in rainfed ones). Yield results distinguish rainfed orchards (R) and total or partial access to irrigation (I). Percentages within each block summarize the most frequent answer (average value) according to Tables 1–5

Farmers' characteristics	RegProp (94%)	Education (97%)	Experience (96%)	Age (94%)	Olive surface (96%)	Yield (81%)			
SoilMan	NS; CC used by 63%	NS; CC used by 63%	p=0.001; 1 (less than 5 years) 40% BS, 4 (more than 25 years) 39% CC, 3 (15–25 years) 60% B	p=0.000; 3 (40–50 years) 30% BS, 3 (40–50 years) 44% CC, 5 (>60 years) 40% B	*p*=0.019; 71 ha BS, 111 ha CC, 316 ha B	NS; 4718 kg ha^{-1} in R NS; 9459 kg ha^{-1} in I			
Mulch	NS; P used by 80%	NS; P used by 80%	p=0.000; 4 (more than 25 year) 39% P, 2 (5–15 year) 38% NP	p=0.000; 3 (40–50 years) 39% P, 2 (30–40 years) 33% NP	p=0.028; 105 ha P, 102 ha NP	p=0.065; 4851 kg ha−1 P, 3823 kg ha−1 NP when both R NS; 9459 kg ha−1 for I			
Motivation	**M_Erosion (99%)**	**M_Fert (99%)**	**M_Gully (99%)**	**M_Econom (99%)**	**M_OrgC (99%)**	**M_Energ (99%)**	**M_Biodiv (99%)**	**M_Pests (99%)**	**M_CAP (99%)**
SoilMan	*p*=0.016; Yes: 78% BS, 94% CC, 80% B	*p*=0.000; Yes: 56% BS, 86% CC, 60% B	*p*=0.094; Yes: 56% BS, 74% CC, 60% B	*p*=0.000; No: 91% BS, 52% CC, 60% B	NS; No 54%	*p*=0.008; No: 86% BS, 62% CC, 80% B	*p*=0.030; No: 57% BS, 32% CC, 60% B	NS; No 66%	NS; Yes 76%
Mulch	NS; Yes 82%	*p*=0.011; Yes: 80% P, 54% NP	NS; Yes 67%	NS; Yes 66%	NS; No 54%	*p*=0.032; No: 67% P, 88% NP	*p*=0.008; Yes: 64% P, 35% NP	NS; No 66%	NS; Yes 76%
Limitations	**L_Yield (62%)**	**L_Harvest (60%)**	L_Cost (61%)	**L_Pests (57%)**	**L_IncEner (3.7%)**	**L_Implant (57%)**	**L_Expensiv (51%)**	**L_Availab (53%)**	**L_Mower (49%)**
SoilMan	NS; Import. 62%	*p*=0.046; Import.: 64% BS, 38% CC, 60% B	*p*=0.007; Import.: 89% BS, 60% CC, 100% B	NS; Import. 59%	–	NS; Import. 75%	NS; Import. 75%	*p*=0.008; Import.: 40% BS, 70% CC, 100% B	NS; Import. 54%
Mulch	NS; Import. 62%	NS; No Import. 53%	NS; Import. 70%	NS; Import. 59%	–	NS; Import. 75%	NS; Import. 75%	*p*=0.009; Import.: 68% P, 44% NP	*p*=0.072; Import.: 77% P, 53% NP.
Beneficial	**B_Erosion (77%)**	**B_Fert (75%)**	**B_Econom (72%)**	**B_OrgC (63%)**	**B_Energ (68%)**	**B_Biodiv (70%)**	**B_Pests (64%)**	**B_SoilStr (74%)**	
Only cover crops farmers	Import. 81%	Import. 80%	Impor, 75%	Import. 86%	Import. 77%	Import. 82%	Import. 80%	Import. 84%	
Negative	**N_Yield (88%)**	**N_Fert (88%)**	**N_Traffic (90%)**	**N_CostFert (85%)**	**N_Gully (84%)**	**N_Trees (90%)**	**N_Lands (85%)**	**N_Biodiv (85%)**	
SoilMan	NS; Concer. 64%	NS; Concer. 73%	NS; Concer. 60%	NS; No Concer. 60%	*p*=0.019; Concer.: 68% BS, 86% CC, 50% B	NS; Concer. 59%	NS; Concer. 61%	*p*=0.022; Concer.: 64% BS, 64% CC, 0% B	
Mulch	NS; Concer. 64%	NS; Concer. 73%	NS; Concer. 60%	NS; No Concer. 60%	*p*=0.059; Concer.: 83% P, 61% NP	NS; Concer. 59%	NS; Concer. 61%	NS; Concer. 61%	

previous studies in which soil degradation by water erosion is a major concern (Areal & Riesgo, 2014; Calatrava et al., 2007; Rodriguez-Souza et al., 2020). Differences with previous studies might be explained, partly, by the distinctions in the survey methodology, especially in the way to access the farmers, a key methodological aspect not fully explained in most of the studies consulted. Calatrava and Franco (2011) used a stratified sampling to capture the variability in farm size within each municipality, while other authors, like Areal and Riesgo (2014) or Rodriguez-Sousa et al. (2020) used a random sampling. Regardless of the approach, none of these studies provided in-depth discussion on the risk of missing farmers that are simply not motivated, for multiple reasons, to participate in this kind of study. Given the low return of responses for questionnaire-based studies quantified by Giomi et al. (2016) in a 7.6% for olive farmers in Tuscany (Italy), and the recognized bias that can be introduced in these kinds of studies (Spiegelhalter, 2020), it is a point worth raising for more in-depth research in the future. Due to the method of contacting farmers in our study, we are aware that our results are an output from motivated farmers who participated in a seminar on soil conservation (those who filled out the questionnaire personally) or answered an on-line request from the DOP Estepa or ASAJA Cordoba, both associations they belong to.

4.2. Analysis of soil management strategies in the two areas and impact on erosion risk

The types of soil management used in most of the available documents tend to follow the four classes defined by Gómez et al. (2003) in a study aimed to provide values of the C factor of the RUSLE: bare soil using herbicide, bare soil using tillage, temporary cover crop on the lanes finalized early in spring, and cover crop on

the whole plot finalized in mid-May. Adaptations of this classification have been used in further social studies on olives (e.g. Areal & Riesgo, 2014; Rodriguez-Sousa et al., 2020). Mollenhauer et al. (2002) also developed C factor values for different tillage strategies in Western Anatolia, including some practices that been based on avoiding tillage during fall and winter, were similar to a temporary cover crop. The results presented in Figs. 3 and 4 could enrich the description of soil management in olive orchards normally used in the scientific literature, providing a more comprehensive view of existence practices and helping to prevent an oversimplification in future analysis on their impact on erosion risk analysis. Bidoccu et al. (2020) have already noted the need to include this higher variability in soil management in the analysis on erosion risk for another woody crop, vineyards. Additionally, our analysis also appraises the effect on erosion risk of the use of a mulch of pruning residues, from which, to our knowledge, no comparative analysis of the modelling of erosion risk, or calibration of the C values, in olives has been published. Results in Fig. 4 illustrate the full range of practices identified, proposing C values for a mature olive grove with a 31% ground cover by the canopy, which are complemented with C values for other values of olive tree canopy cover in Table S1. The range of C values found in our study is similar to the range proposed independently by Mollenhauer et al. (2002) in olive trees in Western Anatolia. There is very limited experimental validation of the accuracy of published C values for erosion predictions in olive groves. To our knowledge, only Marín (2013) has tested preliminarily the performance of the C values for bare soil with tillage or herbicide and temporary cover crops following Gómez, Battany, Renschler, & Fereres, (2003) against a limited dataset of long-term runoff plot with natural rainfall (23 years from two locations). Marín's (2013) results showed a root mean square error (RMSE) of 4.6 t ha^{-1} $year^{-1}$ and a Nash-Sustcliffe model efficiency of 0.83 for the average annual soil loss predictions for each site and management. These results, which are in the range of those found by Risse et al. (1993) for RUSLE who used a much larger experimental dataset, suggest that the proposed C values, refined in the present study, might capture the overall range of the variability in erosion rates in olive groves among the different managements. However, the limited research on validation of these erosion rates in olives indicates that a more rigorous validation is required. This more rigorous validation should aim to provide a better understanding of the uncertainty of the prediction of absolute erosion rates, as well as the actual significance of moderate differences in C values in different soil management, which might be irrelevant if the uncertainty of model predictions happens to be larger than those differences.

Both study areas presented a high degree of use of conservation practices, with 63% of farmers using some kind of cover crop based management. This is higher than the 51% reported by Calatrava et al. (2007) in the Granada and Jaen provinces, and much higher than the 6% of use reported by Sastre et al. (2017) for farmers in drier central Spain. The percentage of use of a mulch of olive-pruning residues found in Cordoba and Estepa areas (83%) was also higher than the 45% reported by Calatrava and Franco (2011) in the Granada province. An analysis of the cumulative distribution of the C values (Fig. 5) indicates how the combination of a high proportion of farmers using mulching and cover crops results in an overall low erosion risk, with 80% of the farmers with relatively high levels of ground cover (Fig. 3), above 50% of farmers providing a high ground cover found by Areal and Riesgo (2014) in several areas of the provinces of Cordoba and Jaen. With the caveat, already mentioned, on the difficulty of validating the representativeness of farmers participating in a survey as that of the whole farmers' population in the two study areas (of intense and professionalized olive cultivation) there is a large group of farmers that are implementing soil conservation measures with a clear impact on the reduction of erosion risk. This can be partly explained by the continuous efforts on training and regulation, particularly related to the CAP, which have gone on for decades in the region (e.g. Areal & Riesgo, 2014). Currently, these CAP regulations require the maintenance of structural elements, such as terraces, already in place to control erosion. They also require the use of a temporary cover crop during the rainy season and in olive orchards with an average slope higher than 10%, forbidding soil turning tillage on plots with an average slope above 15%. It can also be partially explained by the high social capital of the participating farmers who are related to the DOP and ASAJA, which provide an interactive and self-governance approach to soil conservation that complement the top-down approach of the CAP (Giomi et al., 2018).

A better estimation of the actual impact of soil conservation measures and erosion risk in both olive-growing areas, or for that sake in any other area, should rely on detailed information on actual management on each farm. This might be done exploiting information already generated for the purposes of regulatory processes related to the CAP. There are already pilot initiatives to facilitate access of that information for additional uses: for instance, the Farm Sustainability Tool for Nutrients (FaST, European Commission, 2019), which is a digital platform promoted by the EC and several state members for implementation of CAP at farm level. It should be relatively straightforward, with a moderate effort, to elaborate a plot/farm-based erosion risk map incorporating actual management by farmers. For this approach, a realistic description of soil management implemented by olive farmers, which might be selected from a catalogue of practices like the ones described in this manuscript, will be required. This approach would leave unchecked the actual level of ground cover achieved by each farmer at their plot, a level that has been shown to vary significantly among farms in olives and other Mediterranean woody crops (Guzmán et al., 2019; Vicente-Vicente et al., 2017). Analysis of vegetation indexes using satellite images, which to date are available at short regular intervals and many at minimum or no cost, and which have proven to be successful in evaluating different degrees of ground cover by vegetation (Boumadhi, 2019; Weissteiner et al., 2011) might provide a complementary check. The identification of non-green living material, like the pruning residues used as a mulch, remains challenging due to the higher similarity with the soil spectral signal. Nevertheless, recent progress suggests that this might be done in the mid/near future using satellite images (Alexakis et al., 2016).

4.3. Differences in farmer's typologies and perceptions using different soil management

Despite the relatively large use of cover crops and a mulch of pruning residues among the farmers interviewed in our study areas there are some differences in the farmer's typologies and perceptions on the use of soil conservation measures that might provide insight to improving soil conservation in olive-growing areas. In Cordoba and Estepa, farmers with more experience (and older) are more prone to use a cover crop-based management and a pruning mulch, a trend in which literature is not conclusive. Calatrava and Franco (2011) detected a lack of correlation in the use of pruning mulchwith farmers' age, while Calatrava et al. (2007) found an increasing chance of adopting cover crops by farmers younger than 40 years old. Our interpretation of the results from our study areas is that less experienced farmers still find the implementation of these techniques challenging due to higher complexity, as compared to the conventional, bare-soil based management practices. This suggests that there is scope for improving training of younger farmers, as well as agricultural students, to increase the

use of soil conservation measures, ideally linking them with more experienced farmers already implementing them. This is in line with the results of Rodríguez-Entrena et al. (2014), which highlighted the positive effect of better training and social capital on the adoption of cover crop management.

It is interesting to note that we did not find a significant difference in the adoption of cover crop management in relation to the declared yield level, although the risk of a decrease in olive yield is a latent threat when using temporary cover crops in Mediterranean conditions (Gómez, 2016). It is probable that the large variability in declared yield among the farmers, reflecting a combination of environmental and agronomic factors, might mask individual situations where this might be a key concern. In fact, the dual response of some farmers with access to irrigation suggests that this risk of yield remains in their decision-making process on how to manage their soil on their farm. Further research focusing on these farmers, rather than on general population analysis like the one shown in this manuscript, might provide useful insight into this capital aspect to improve agronomic management and adoption of cover crops by farmers in olive-growing areas. Regarding the motivation for using cover crop, our results indicate a higher motivation by farmers actually using cover crops, something that was somehow expected from the nature of the survey. What it is more interesting for the olive sector, is that after decades of training and education on improving soil conservation, there is still a significant percentage of farmers not using cover crops or pruning mulch and without finding significant concern for the impact of soil erosion on yield (46%), reducing soil fertility (27%), fractionating the farm by gully erosion (21%) or improving biodiversity (39%). These levels of unconcerned farmers are similar to those found for similar questions by Rodríguez-Souza et al. (2020), an average of 47% when farmers in integrated olive production were asked about their respect the environment when taking decisions on farm management. This indicates again that there is a cluster of olive farmers to whom training and awareness efforts to enhance the adoption of soil management practices best adapted to the provision of ecosystems services, should be focused - probably with a different, or complementary, approach than the one followed to date. It is also apparent from the limitations perceived by farmers in this study, that efforts to enhance the availability at a lower cost of seed for cover crops, and facilitating the use of mowers, particularly for farmers combining them with pruning residues, should be given priority in R + D + i future efforts of soil conservation in olive groves.

5. Conclusions

This manuscript presents the results of a detailed analysis of different soil management carried out by farmers in two representative olive-growing areas in southern Spain (Cordoba and Estepa). It shows a relative large variability of soil management, with fourteen options, as a result of a combination of different alternatives for bare-soil and cover crops with the use or not of pruning residues, but with a great similarity between both areas. The results indicate a high incorporation of soil conservation measures in both olive-growing areas, 63% of farmers using cover crops and 80% a mulch of pruning residues, higher than those presented in previous studies in Andalusia (Southern Spain). This change results in a significant reduction of erosion risk, as indicated by the relatively low values for the cover and management factor (C) of RUSLE, also calculated and presented in this study. This description of soil management and characterization of C values might be useful for a better appraisal of soil erosion risk in these areas. Given the uncertainty of the type of farmer left behind (for not being willing to participate in questionnaire-based studies), further analysis based on farmers' CAP declarations or remote sensing approaches are recommended, taking advantage of the progress in easiness of use of both approaches. Our results indicate the persistence of a minority, but relevant, percentage of farmers using bare-soil management (37%) and no pruning mulch (20%), with a moderate concern for the impact of soil erosion, soil degradation and the provision of ecosystem services. This suggests the need to concentrate efforts on this cluster of farmers to enhance the success of what seems to be a remarkable expansion of the use of soil-conservation measures in recent decades in this area of southern Spain.

Declaration of competing interest

None.

Acknowledgments

This work was supported by P12-AGR-0931 (Andalusian Government), AGL2015-65036-C3-1-R and PID2019-105793RB-I00 (Spanish Government), SHui (European Commission Grant Agreement number: 773903) and EU-FEDER funds, as well as by the cooperative agreement between the DOP Estepa and the University of Cordoba. All this support is gratefully acknowledged. The authors would also like to thank to the staff of ASAJA Cordoba and the DOP Estepa for their dedicated support for the interview process.

Appendix A. Supplementary data

Supplementary data to this article can be found online at https://doi.org/10.1016/j.iswcr.2021.01.003.

References

Alexakis, D. D., Sarris, A., Kalaitzidis, C., Papadopoulos, N., & Soupios, P. (2016). Integrated use of satellite remote sensing, GIS, and ground spectroscopy techniques for monitoring olive oil mill waste disposal areas on the island of Crete, Greece. *International Journal of Remote Sensing, 37*, 669–693.

Areal, F. J., & Riesgo, L. (2014). Famers' view on the future of olive farming in Andalusia, Spain. *Land Use Policy, 36*, 543–553.

Beaufoy, G. (2001). *EU Policies for olive farming, Unsustainable on all counts*. Brussels: Bird Life International. WWF.

Bennet, H. H. (1960). Soil erosion in Spain. *Geographical Review, 50*, 59–72.

Bidoccu, M., Guzmán, M., Capello, G., Thielke, T., Strauss, P., Winter, S., Zaller, J. G., Nicolai, A., Cluzeau, D., Popescu, D., Bunea, C., Hoble, A., Cavallo, E., & Gómez, J. A. (2020). Evaluation of soil erosion risk and identification of soil cover and management factor (C) for RUSLE in European vineyards with different soil management. *International Soil and Water Conservation Research, 8*, 337–353.

Bombino, G., Denizi, P., Gómez, J. A., & Zema, D. A. (2020). Mulching as best management practice to reduce surface runoff and erosion in steep claey olive groves. *International Soil and Water Conservation Research*. https://doi.org/10.1016/j.iswcr.2020.10.002 (in press).

Boumadhi, A. (2019). *Análisis de los Elementos Diversificadores del Paisaje Agrario en las Explotaciones Olivareras de la campiña de Córdoba*. Master Thesis. Spain: University of Cordoba.

Calatrava, J., & Franco, J. A. (2011). Using pruning residues as mulch: Analysis of its adoption and process of diffusion in southern Spain in olive orchards. *Journal of Environmental Management, 92*, 620–629.

Calatrava, J., Franco, J. A., & González, M. C. (2007). Analysis of the adoption of soil conservation practices in olive groves: The case of mountainous areas in southern Spain. *Spanish Journal of Agricultural Research, 5*, 249–258.

Consejería de Medio Ambiente de la Junta de Andalucía. (2005). *Mapa de suelos de Andalucía 1:400000*. Available at: http://www.juntadeandalucia.es/medioambiente/site/rediam/menuitem.04dc44281e5d53cf8ca78ca731525ea0/?vgnextoid=0a45239671e0a210VgnVCM2000000624e50aRCRD&vgnextchannel=36faa7215670f210VgnVCM1000001325e50aRCRD&vgnextfmt=rediam&lr=lang_es#apartadoc945239671e0a210VgnVCM2000000624e50a. (Accessed 10 November 2020).

El Hanandeh, A., & Gharaibeh, M. A. (2016). Environmental Efficiency of olive oil production by small and micro-scale farmers in northern Jordan: Life cycle assessment. *Agricultural Systems, 148*, 169–177.

European Commission. (2019). *Future of the common agricultural policy*. https://ec.

europa.eu/info/news/new-tool-increase-sustainable-use-nutrientsacross-eu-2019-feb-19_en.
FAOSTAT. (2020). *Statistics of the food and agriculture organization of the united nations*. http://www.fao.org/faostat/en/#home. (Accessed 20 November 2020).
Giomi, T., Runhaar, P., & Runharr, H. (2018). Reducing agrochemical use for nature conservation by Italian olive farmers: En evaluation of public and private governance strategies. *International Journal of Agricultural Sustainability, 16*, 94–105.
Gómez, J. A. (Ed.). (2009). *Sostenibilidad de la producción de olivar en Andalucía*. Sevilla: Junta de Andalucía.
Gómez, J. A. (2016). Sustainability using cover crops in Mediterranean tree crops, olives and vines. Challenges and current knowledge. *Hungarian Geographical Bulletin, 66*, 13–28.
Gómez, J. A., Battany, M., Renschler, C. S., & Fereres, E. (2003). Evaluating the impact of soil management on soil loss in olive orchards. *Soil Use and Management, 19*, 127–134.
Gómez-Limón, J. A., Picazo-Tadeo, A. J., & Reig-Martínez, E. (2012). Eco-efficiency assessment of olive farms in Andalusia. *Land Use Policy, 29*, 395–406.
Gómez-Zotano, J., Alcántara-Manzanares, J., Olmedo-Cobo, J. A., & Martínez-Ibarra, E. (2015). La sistematización del clima mediterráneo: Identificación, clasificación y caracterización climática de Andalucía (España). *Revista de Geografía, Norte Grande, 61*, 161–180.
Guzmán, G., Cabezas, J. M., Sánchez-Cuesta, R., Lora, A., Bauer, T., Strauss, P., Winter, S., Zaller, J. G., & Gómez, J. A. (2019). A field evaluation of the impact of temporary cover crops on soil properties and vegetation communities in southern Spain vineyards. *Agriculture, Ecosystems & Environment, 272*, 135–145.
IUSS Working Group WRB. (2015). *World reference base for soil resources 2014, update 2015*. International soil classification system for naming soils and creating legends for soil maps. World Soil Resources Reports No. 106. Rome: FAO.
Kourouxou, M. I., Siardos, G. K., Iakovidou, O. I., & Kalburtji, K. L. (2005). Olive trees farmers: Agricultural management, attitudes and behaviors towards environment. *Proceedings of the 9th International Conference on Environmental Science and Technology, Vol A oral presentations, Pts A and B*, 829–835.
Loumou, A., & Giourga, C. (2003). Olive groves: "The life and identity of the mediterranean". *Agriculture and Human Values, 20*, 87–95.
Marín, V. J. (2013). *Interfaz gráfica para la valoración de las pérdidas de suelo en parcelas de olivar*. Spain: Graduation Thesis. University of Cordoba.
Mollenhauer, K., Taysun, A., & Frede, H. G. (2002). C-factors of the universal soil loss equation for olive plantations in water Anatolia (central Egean region). *Journal of Plant Nutrition and Soil Science, 165*, 313–319.
REDIAM. (2020). *Red de Información Ambiental de Andalucía*. Available at: http://www.juntadeandalucia.es/medioambiente/site/rediam/menuitem.04dc44281e5d53cf8ca78ca731525ea0/?vgnextoid=ca74d2aa40504210VgnVCM1000001325e50aRCRD&vgnextchannel=7b3ba7215670f210VgnVCM1000001325e50aRCRD. (Accessed 20 November 2020).
Renard, K. G., Foster, G. R., Weesies, G. A., McCool, D. K., & Yoder, D. C. (1997). *Predicting soil erosion by water: A guide to conservation planning with the revised universal soil loss equation (RUSLE)*. Washington DC: USDA. US Department of Agriculture Agricultural Handbook No. 703.
Risse, L. M., Nearing, M. A., Laflen, J. M., & Nicks, A. D. (1993). Error assessment in the universal soil loss equation. *Soil Science Society of America Journal, 57*, 825. https://doi.org/10.2136/sssaj1993.03615995005700030032x
Rodríguez-Entrena, M., Arriaza, M., & Gómez-Limón, J. A. (2014). Determining Economic and social factors in the adoption of cover crops under mower control in olive groves. *Agroecology and Sustainable Food Systems, 38*, 69–91.
Rodriguez-Sousa, A. A., Parra, C., Sayadi, S., Barandica, J. M., & Rescia, A. J. (2020). Evaluation of the objectives of farmers to apply different agricultural managements in olive groves: The case of Estepa region (southern Spain). *Land, 9*, 366. https://doi.org/10.3390/land9100366
Roesch-McNally, G. E., Basche, A. D., Arbuckle, J. G., Tyndall, J. C., Miguez, F. E., Bowman, T., & Clay, R. (2018). The trouble with cover crops: Farmers' experiences with overcoming barriers to adoption. *Renewable Agriculture and Food Systems, 33*, 322–333.
Ruiz de Castroviejo, J. (1969). Explotación de olivares en asociación con trébol subterráneo. *Agricultura, 443*, 135–139.
Sastre, B., Barbero-Sierra, C., Bienes, R., Marques, M. J., & García-Díaz, A. (2017). Soil loss in an olive grove in Central Spain under crops and tillage treatments, and farmer perceptions. *Journal of Soils and Sediments, 17*, 873–888.
Scheidel, A., & Krausmann, F. (2011). Diet, trade and land use: A socio-ecological analysis of the transformation of the olive system. *Land Use Policy, 28*, 47–56.
Spiegelhalter, D. (2020). *The art of statistics. Learning from data*. Penguin Random House.
Vanwalleghem, T., Amate, J. I., de Molina, M. G., Fernández, D. S., & Gómez, J. A. (2011). Quantifying the effect of historical soil management on soil erosion rates in Mediterranean olive orchards. *Agriculture, Ecosystems & Environment, 142*, 341–351.
Vicente-Vicente, J. L., Gómez-Muñoz, B., Hinojosa-Centeno, M. B., Smith, P., & García-Ruiz, R. (2017). Carbon saturation and assessment of soil organic carbon fractions in Mediterranean rainfed olive orchards under plant covermanagement. *Agriculture, Ecosystems & Environment, 245*, 135–146.
Weissteiner, C. J., Strobl, P., & Sommer, S. (2011). Assessment of status and trends of olive farming intensity in EU-Mediterraneancountries using remote sensing time series and land cover data. *Ecological Indicators, 11*, 601–610.

International Soil and Water Conservation Research 9 (2021) 474–484

Contents lists available at ScienceDirect

International Soil and Water Conservation Research

journal homepage: www.elsevier.com/locate/iswcr

Original Research Article

Rainfall partitioning in young clonal plantations Eucalyptus species in a subtropical environment, and implications for water and forest management

Décio Oscar Cardoso Ferreto [a], José Miguel Reichert [a, *], Rosane Barbosa Lopes Cavalcante [b], Raghavan Srinivasan [c]

[a] Soils Department, Universidade Federal de Santa Maria (UFSM). Avenida Roraima 1000, Santa Maria, RS, Brazil
[b] Instituto Tecnológico Vale. Rua Boaventura da Silva, 955, Umarizal, Belém, PA, Brazil
[c] Department of Ecology and Conservation Biology, Texas A&M University (TAMU) 534 John Kimbrough Blvd., Room 305, College Station, TX, USA

ARTICLE INFO

Article history:
Received 5 October 2020
Received in revised form
8 January 2021
Accepted 15 January 2021
Available online 23 January 2021

Keywords:
Water balance
Blue-green water
Forest hydrology
Rainfall interception
Rainfall throughfall

ABSTRACT

Different canopy characteristics of industrial eucalyptus may lead to differences in water evaporation and availability to plants. This study aims to understand rainfall partitioning in a young clonal plantation (age of 2–4.5 years) of three eucalyptus species by relating tree parameters: diameter at breast height, total height, and leaf area index. We measured rainfall, throughfall, stemflow and litter interception, along with the tree parameters. The eucalyptus trees had rainfall interception varying between 22 mm (for 178 mm of rainfall) and 42 mm (for 87 mm of te rainfall), throughfall between 106 mm (for 186 mm of rainfall) and 44 mm (for 74 mm of rainfall), and stemflow between 0.5 mm (for 92 mm of rainfall) and 1.4 mm (for 24 mm of rainfall). For the three species, rainfall interception varied between 12 and 48%, throughfall between 57 and 90%, and stemflow between 0.3 and 5.4%. The coefficient of determination between interception and rainfall was 0.76, indicating interception depends on other variables, possibly including antecedent rainfall, rainfall intensity, and seasonality. Interception decreased with a reduction in leaf area index caused by eucalyptus defoliation. The E. benthamii had 0.75 mm of throughfall per 1 mm of rainfall, whereas in E. dunnii and *E. saligna*, these ratios were 0.71 and 0.68, respectively. Stemflow in E. benthamii and E. dunii had a higher positive relationship with the diameter at breast height of the trees, whereas in *E. saligna* the highest relationship was with the rainfall. These results contribute to establishing management strategies, such as choosing suitable eucalyptus species to local climate, and to improve the synchronization of crop-demand versus soil-water-supply while maintaining streamflow to fulfill ecological and production needs.

1. Introduction

Brazil has 5.7 million ha of Eucalyptus spp. Plantations, leading in eucalyptus productivity of 35.7 m^3 ha-1 yr-1 (IBÁ 2017). Approximately 15% of these plantations are in subtropical climate (southern Brazil), subject to higher thermal amplitudes and low temperatures in winter. Among the eucalyptus species that are both frost-tolerant and able to handle thermal stress are E. dunnii and E. benthamii (Santos, Resende, et al., 2013). Commercial plantations with these species are poorly studied compared with plantations in tropical environments or with genetic materials with greater plasticity commonly planted in southern Brazil.

Despite their importance in the timber industry, eucalyptus plantations are often scrutinized concerning their hydrological (Ferreto et al., 2020; Nosetto et al., 2012; Reichert et al., 2017) and erosion impacts (Ebling et al., 2020; Rodrigues et al, 2014, 2018; Valente et al., 2020). Eucalyptus has high water-loss by transpiration (Rohatyn et al., 2018) and interception (Ferreto et al., 2020; Reichert et al., 2017) compared to smaller vegetation, and productivity of eucalyptus plantations is linked to water availability (Cavalli et al., 2020; Santos et al., 2015; Stape et al., 2010), and depends on rainfall volume and partitioning in the canopy.

* Corresponding author.
E-mail address: reichert@ufsm.br (J.M. Reichert).

https://doi.org/10.1016/j.iswcr.2021.01.002

Furthermore, afforestation distinctly affects the portioning of rainfall into green and blue water systems (Falkenmark & Rockström, 2004, 2006, 2010).

When rain falls on to a vegetated surface, a portion of the rainfall reaches the forest floor by passing through or dripping from canopy (throughfall, Tf) or flowing through branches and stems (stemflow, Sf). The other portion is intercepted by the canopy and is lost by evaporation (canopy interception) (Chang, 2012). Of the rainfall that falls on the forest floor, a share is intercepted by the litter (IL) and then evaporated to the atmosphere. The percentage of each of these components of the hydrologic cycle is dependent on weather conditions, e.g., wind and duration, intensity and frequency of rainfall, and vegetation characteristics that vary with the species and forest composition, e.g., canopy structure, leaf size, and slope, and plant density (Crockford & Richardson, 2000; Levia et al., 2011; Shi et al., 2012).

A significant share of the gross precipitation in forest areas is intercepted by forest canopy (Savenije, 2004). This interception is a vital component of watersheds' water balance (David et al., 2005). However, despite its importance for determining the total precipitation that reaches the soil, interception is frequently neglected or underestimated in hydrological modeling studies (Savenije, 2004).

Most studies in vegetation interception in Brazil were carried out in tropical forests, and little is known about these processes in other Brazilian environments (Giglio & Kobiyama, 2013). For eucalyptus plantation in the Brazilian Pampa or Southern Grasslands biome, in which grasslands are substituted by forest plantations and annual crops (Oliveira et al., 2017), the studies usually analyzed only one-year of data and one species (Baunhardt, 2014; Correa et al., 2019; Momolli et al., 2019; Santos et al., 2014; Sari et al., 2016; Souza et al., 2019), except for the studies of Dick et al. (2018), Reichert et al. (2017) and Valente et al. (2016) who used two years of data and Consensa et al. (2012) who compared two species. Moreover, we did not find any study in the region that analyzed the interception in the E. benthamii. A longer monitored period is important because of the strong influence of the climate variability on the interception, and comparing species allows analysis of forest management options for each plantation.

Considering different canopy structures and local climatic characteristics, further studies are needed to propose management strategies with improved synchronization between crop demand and soil supply of water, while maintaining local water availability for other uses (Ferraz et al., 2013). Our study aimed to evaluate rainfall partitioning in commercial plantations of clones of three young Eucalyptus species (*E. saligna*, E. benthamii, and E. dunnii), during 2.5 years, as affected by rainfall amount and growth (diameter at breast height, DBH, and total height, Ht) and canopy (leaf area index, LAI) variables in subtropical Brazil. The study novelty is connecting forestry (species and age) and ecosystem processes (forest water balance components) in a subtropical environment, contributing to afforestation planning in the Pampa biome, southern South America.

2. Material and methods

2.1. Study area and experimental conditions

The experiment was conducted in an experimental area with eucalyptus stands (2nd rotation) grown for pulp production in the southernmost state of Brazil (Fig. 1). The soil is classified as Neossolo Regolítico by the Brazilian Soil Classification System (Santos, Resende, et al., 2013) or Entisol by Soil Taxonomy (USDA, 1999). The regional climate is Cfa (Köppen classification), humid subtropical, with well-defined summer and winter seasons. The average annual rainfall is 1356 mm, well distributed throughout the year. The average annual temperature is 19 °C, with mean annual maximum and minimum temperatures of 26 °C and 15 °C, respectively (Alvares et al., 2013) and occasional below-zero temperatures in winter months and temperatures near 40 °C in summer. The average elevation is 270 m, and the mean slope is 6.2%.

The study was conducted with three eucalyptus species (Eucalyptus benthamii, E. dunnii, and *E. saligna*) in three blocks (replications), from March 2016 to September 2018. Planting was carried out in May 2014 in plots 660 m2 (10 rows and 10 plants per row) with 3.0 × 2.2 m spacing, totaling 100 plants of each species per plot. Throughfall (Tf), stemflow (St), litter interception (IL), growth variables (Ht and DBH), and LAI were monitored in each plot, as described in the following sections. A schematic of the setup for field instrumentation and their placement inside the plot is shown in Fig. 2.

2.2. Rainfall partitioning evaluation

2.2.1. Rainfall

Gross precipitation (P) was measured near the experimental area using two automatic pluviographs (tipping bucket, model CS700) at 10-min intervals, and four manual pluviometers used for quantification of rainfall at biweekly intervals. Since tipping bucket pluviographs are known to possibly underestimate precipitation (Lida et al., 2018), especially at very high intensities, we corrected the data based on a relationship with rainfall quantified in manual pluviometers.

Total P during the study period (from March 2016 to September 2018) was 5010.3 mm (monthly mean of 161.6 mm), 32.8% greater than the climatological normal from 1981 to 2010 for the region (INMET, 2009). The monthly values of P are shown in Fig. 3.

2.2.2. Throughfall

Throughfall (Tf) was determined by four linear pluviometers (0.1 m wide and 1.9 m long) installed per plot, as shown in Fig. 2. Two of them were installed next and parallel to the tree row, and two in-between and transversal to the tree row. This method of long flumes has uncertainties, given there was no rotation of the pluviometers. However, considering the uniformity of the plantation and trees, coupled with a more extensive sampling area than would be available with circular pluviometers, this strategy is useful for Tf quantification. Furthermore, this linear configuration allows monitoring of locations featuring variable Tf (Sato et al.,

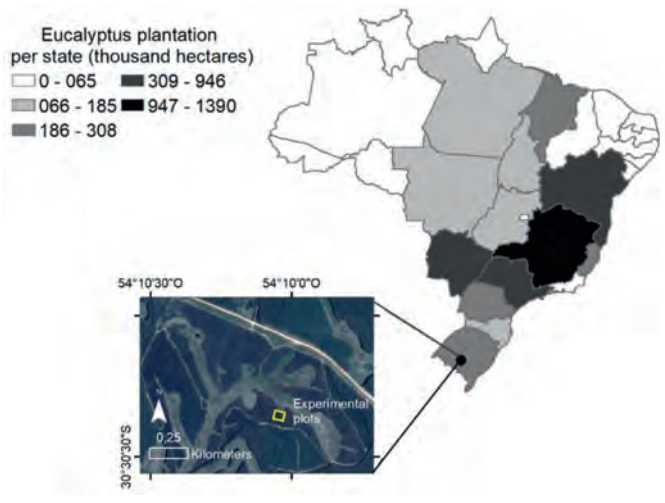

Fig. 1. Area of Eucalyptus plantation per state and location of the experimental sites.

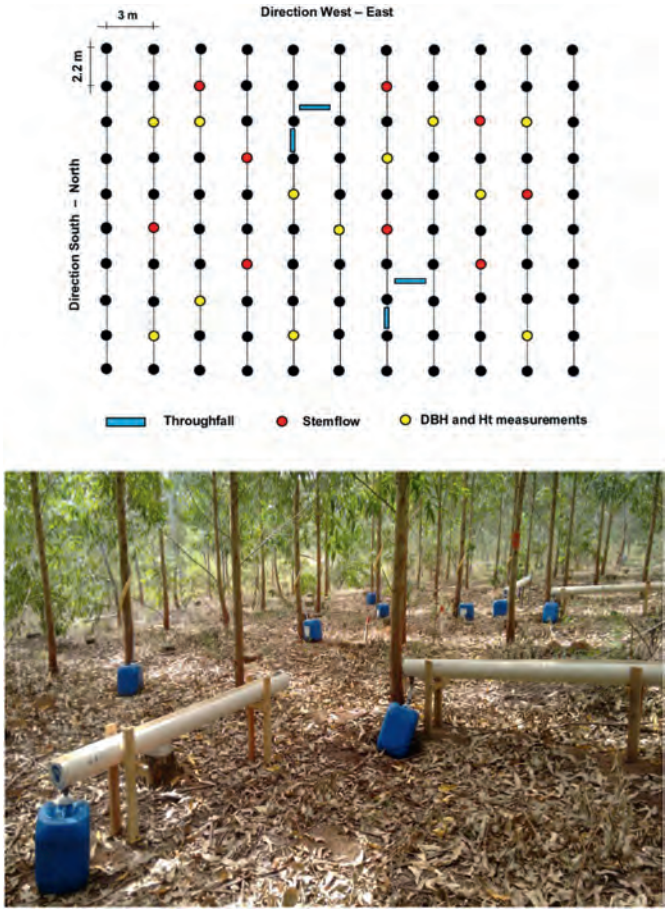

Fig. 2. Illustration and picture of the collectors distribution in a plot.

2011). The Tf was quantified at biweekly intervals or after rainfall events greater than the canopy water storage capacity (CWS).

2.2.3. Stemflow

Stemflow (Sf) was measured for nine trees in each plot. The collectors, constructed from plastic, were sealed to the stem in a spiral pattern, and the water diverted into collection vessels on the forest floor. The Sf was quantified concurrently with Tf, and it was measured on trees with a representative diameter at breast height.

2.2.4. Litter interception and total interception by vegetation

Litter interception (IL) was determined using a methodology adapted from Sacramento Neto (2001). Litter samples were artificially-wetted and covered to prevent evaporation during water drainage and later oven-dried (to 65 °C). The water retention capacity (WRL) was determined by the difference between the wet and dry biomass weights. This procedure was done every three months, including rainy and dry periods, of defoliation and renewal of the plants' bark. The residual litter moisture (RML) was monitored after rainfall events to measure moisture variation and it was determined as described above for WRL. The IL was determined in each rainfall event with greater P than CWS, by determining the difference between WRL and RML.

The CWS was estimated as the x-axis intercept (Tf = 0) of the upper envelope of the data dispersion of Tf and P for major events, as proposed by Lleyton et al. (1965). Three high-intensity rainfall events were monitored, and the mean CWS values obtained for the species *E. saligna*, E. dunnii, and E. benthamii were 2.9, 1.7, and 1.2 mm. The results are in accordance with the leaf slope, which is higher in E. benthamii and lower in *E. saligna*.

Total interception by vegetation (INT), which includes canopy and litter interception, was determined by equation (1). The INT consists of the portion of rainfall stored and later evaporated from leaves, branches, stems, and litter.

$$INT = P - Tf - Sf + IL \quad (1)$$

where INT is the total interception by vegetation, P is the gross rainfall, Tf is the throughfall, Sf is the stemflow, and IL is the litter interception, all in mm.

2.3. Leaf area index, diameter, and total height

Leaf area index (LAI) was assessed with a non-destructive canopy analyzer, LAI-2200. Estimates were made at dawn, sunset, or daytime periods with a high incidence of cloud cover, every three months, to explore phenological differences in different seasons of the year. For each area, ten consecutive LAI readings were taken below the canopy, in four replications, following to the measurement protocol for row crops described in the instrument instruction manual (LAI-2200, version 1.0). The readings were made at even intervals across the row along two diagonal transects between the rows, crossing the different row distances and representing the various canopy closure degrees.

Diameter at breast height (DBH, with hypsometer) and height of eucalyptus trees (Ht, tape measure) were determined for each tree in the plots on April 2016, August 2016, August 2017, November 2017, March 2018, and June 2018. These dates correspond to 23, 27, 38, 41, 45, and 48 months of the plantation.

2.4. Statistical analysis

Variance analysis (ANOVA) was performed for Tf, Sf, IL, INT, LAI, and growth variables (DBH and Ht), considering a completely randomized design, through the software Free Statistical Software SAS® University Edition. When analysis of variance was significant ($p < 0.05$), the Tukey test was performed for comparison averages between species at 5% significance. Rejecting the null hypothesis means that the differences in the observed values between species are unlikely to be due to random chance.

3. Results

3.1. Crop growth

Among the growth variables, only DBH was different ($p < 0.05$ by the Tukey test) among the eucalyptus species (Table 1). A reduction in plant growth (mainly in the DBH) occurred from November 2017 to March 2018, the period with the largest soil water deficit. This reduction was more pronounced in E. benthamii, where DBH increased only 0.003 m from November 2017 to June 2018. The E. benthamii was also the species most affected by the bronze bug. The E. dunnii and the *E. saligna* showed an increase of, respectively, 0.007 and 0.008 m in this period (Table 1). In March 2018, favored by dry weather conditions, an infestation of the insect Thaumastocoris peregrinus (bronze bug) occurred in the study area, causing forest defoliation (Fig. 4).

3.2. Throughfall (Tf)

Considering the variance between the nine samples measured for each species in each date, only the Tf during May to July 2016 and during September 2017 were statistically (Tukey test, $p < 0.05$)

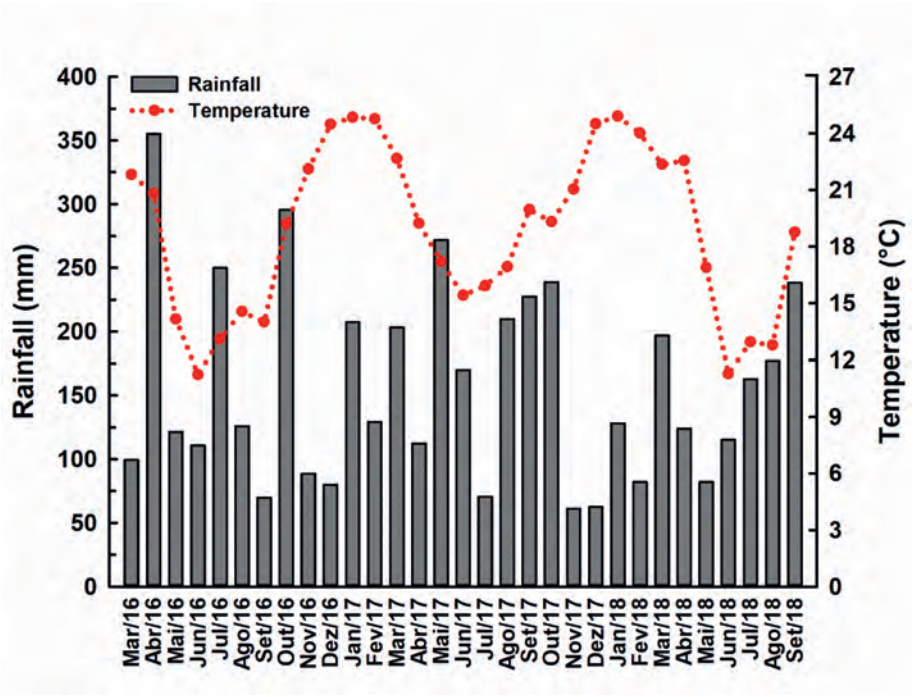

Fig. 3. Total monthly rainfall and mean temperature in the study area from March 2016 to September 2018.

different between species. The Tf (in % of P) values along the 2.5 years and the average values for 6-months intervals are shown, respectively, in Fig. 5 and Table 2. As a general trend, Tf decreased with crop growth until the age of 3.5 years. For all species, the lowest Tf occurred from May to October 2017, when the eucalyptus was between 3.0 and 3.5 years of age (Fig. 5). The highest rainfall also happened during this period (Table 2).

From November 2017 to February 2018, there was low rainfall in the study area, which caused a soil water deficit. In March 2018, favored by dry weather conditions, an infestation of bronze bug occurred, causing forest defoliation (Fig. 3). As a result, the Tf in E. benthamii increased from April 2018, remaining high until early September 2018. The Tf also increased in the other two eucalyptus species, but less pronounced and persisted only until May 2018 (Fig. 5). For the whole series, the Tf among species was E. benthamii > E. dunnii > *E. saligna*.

The E. benthamii, which had the lowest LAI, presented the greatest Tf most of the time, whereas the *E. saligna*, with the greatest LAI, showed the lowest Tf most of the time. Furthermore, high variation in LAI in *E. saligna* was associated with greatest amplitude in Tf (53.2–83.7% of P), whereas in E. dunnii the Tf ranged from 57.1 to 85.9% of P, and in E. benthamii it ranged from 60.7 to 89.7% (Fig. 5). However, there was no linear correlation between Tf and LAI for E. benthamii ($R = -0.08$) and for E. dunnii ($R = 0.36$) and low correlation for *E. saligna* ($R = -0.69$).

The Tf of the three species were strongly correlated with P ($R^2 > 0.93$). The angular coefficients, representing the mm of Tf per mm of P, were 0.75, 0.71, and 0.68 respectively for E. benthamii, E. dunnii, and *E. saligna* (Fig. 6).

Table 1
Total height, diameter at breast height, and leaf area index of Eucalyptus saligna, E. dunnii and E. benthamii plantations of different ages. Means followed by the same letter in the row (lowercase) and in the column (uppercase) do not differ from each other by the Tukey test ($p < 0.05$).

Month/year	Age	Species		
	(months)	Eucalyptus saligna	E. dunnii	E. benthamii
Total height (m)				
Apr/16	23	10.0 a	9.8 a	9.8 a
Aug/16	29	12.7 a	12.6 a	12.3 a
Aug/17	39	16.5 a	16.5 a	16.5 a
Nov/17	42	17.9 a	18.0 a	17.5 a
Mar/18	46	19.4 a	19.9 a	18.3 a
Jun/18	49	19.9 a	20.1 a	19.2 a
Diameter at breast height (m)				
Apr/16	23	0.095 a	0.097 a	0.088 b
Aug/16	29	0.120 a	0.115 a	0.109 b
Aug/17	39	0.148 a	0.137 b	0.136 b
Nov/17	42	0.157 a	0.143 b	0.141 b
Mar/18	46	0.160 a	0.146 b	0.142 b
Jun/18	49	0.165 a	0.150 b	0.144 b
Leaf area index (m2 m-2)				
Jun/17	37	3.08 aA	2.13 bB	2.03 bA
Sep/17	40	3.37 aA	2.48 bB	2.43 bA
Jan/18	43	3.44 aA	3.59 aA	2.20 bA
Apr/18	47	3.09 aA	2.59 bB	2.49 bA
Aug/18	51	2.68 aB	2.52 abB	2.09 bcA

3.3. Stemflow (Sf)

The Sf (in % of P) was greater ($p < 0.05$) in *E. saligna* than in E. dunnii and E. benthamii species in most of the study period (Fig. 7). This difference was statistically significant (Tukey test, $p < 0.05$) for about 40% of the measurements. The highest Sf in *E. saligna* occurred on 15 September and October 26, 2017 ($p < 0.05$) and September 30, 2018.

In E. dunnii and E. benthamii, the Sf remained low during the first year of the study, varying between 0.5% and 1.3% of P. The Sf for these two species were not influenced by high rainfall events (Fig. 7), as shown by the low coefficient of determination obtained in the relationship between Sf and P for these species (Fig. 8).

The E. benthamii and E. dunnii presented greater increase in Sf with the increase of DBH than the *E. saligna*, as can be seen in the linear regression equation and determination coefficient between these variables in Fig. 9. On the other hand, for the *E. saligna*, St was

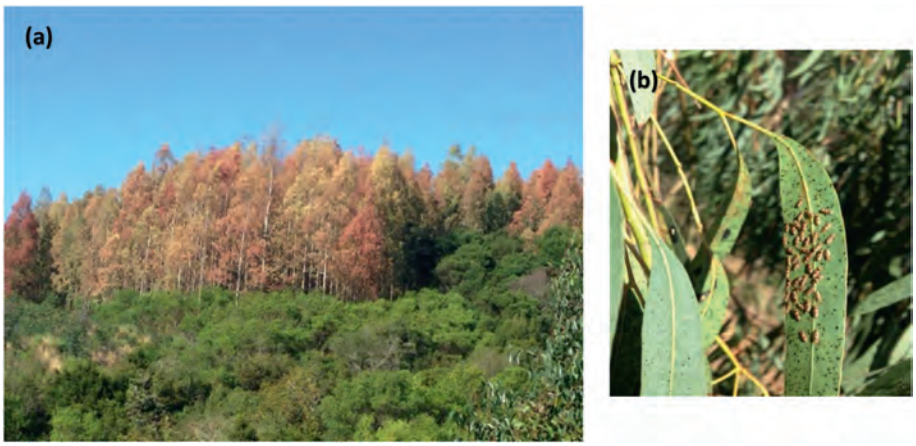

Fig. 4. Injury caused by Thaumastocoris peregrinus (bronze bug) on Eucaliptus benthamii (a), and adult T. peregrinus insects on eucalyptus leaves (b), in the study area.

more strongly correlated with the rainfall (Fig. 8). The differences in leaf inclination between the species can be responsible for the differences in the correlations of St. Mean Sf values by semester are shown in Table 2. For the whole series, the Sf among species was *E. saligna* > E. benthamii = E. dunnii.

3.4. Litter (IL)

From April 2016 to January 2017 (22–32 months of plants age), the percentage of P intercepted by litter (IL) was greater in *E. saligna* than in the other two species (Fig. 10). The difference was statisticaly significant (Tukey test, $p < 0.05$) for about 45% of the measuments. From February 2017 to January 2018 (23–44 months), the IL was greater in E. dunnii, and from February 2018 to September 2018, the IL was similar among the species (Fig. 10). The average IL values by plants age are presented in Table 2. The highest value of IL occurred on March 17, 2018 (14.2%), when the defoliation caused by bronze bug ocurred. The IL showed an increasing trend from November 2017 to May 2018, months with low rainfall (Fig. 10).

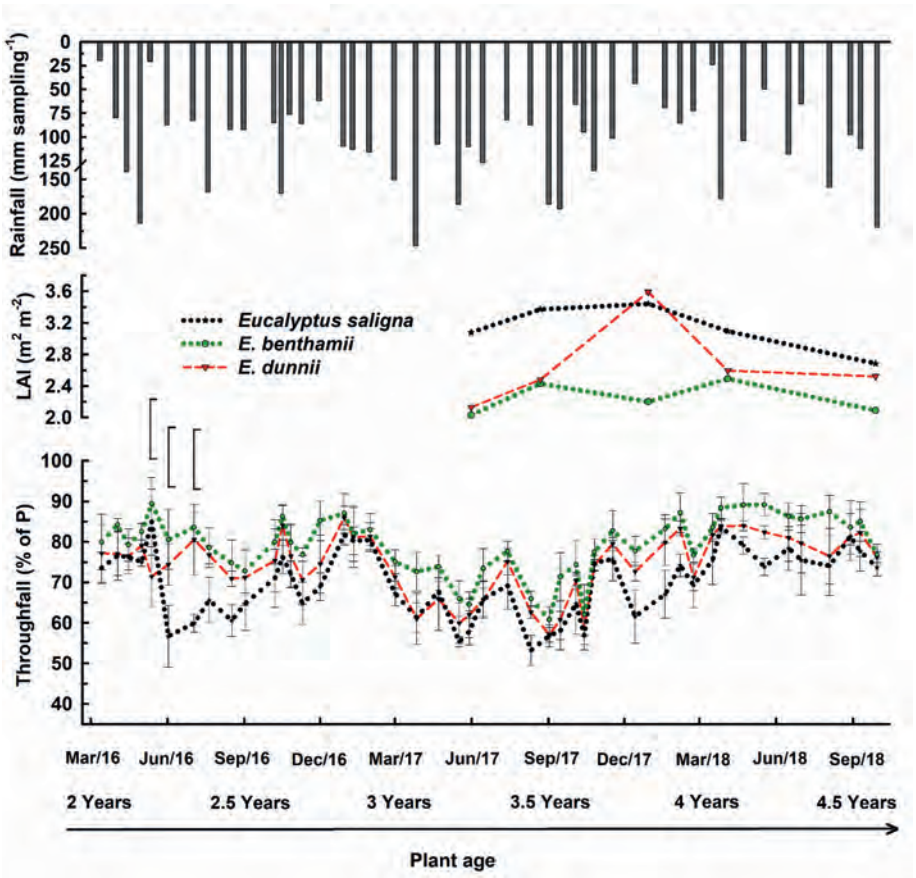

Fig. 5. Rainfall (P), leaf area index (LAI) and throughfall (Tf) in the study area from March 2016 to September 2018. On the throughfall plot, vertical bars on data represent standard deviation and, and on top of plot indicate the minimum significant difference ($p < 0.05$) and, when absent, insignificant ($p > 0.05$) by Tukey test.

Table 2
Throughfall, stemflow, and litter interception (in % of rainfall) for different eucalyptus species and ages.

Age (months)	P (mm mo-1)	Tf (% of P)			Sf			IL		
		Eb	Ed	Es	Eb	Ed	Es	Eb	Ed	Es
24–30	145.8	80.6	75.7	69.6	0.8	1.1	2.4	2.2	3.0	5.4
30–36	165.2	79.5	74.0	71.6	1.1	0.9	1.7	2.2	3.5	4.4
36–42	211.8	68.5	63.3	59.8	1.3	1.6	2.9	3.0	5.1	3.2
42–48	120.3	84.2	79.8	73.5	2.4	1.3	3.7	6.9	7.0	7.3
48–52	197.3	85.6	81.6	77.4	2.2	1.9	2.8	3.9	3.6	4.0
24–52	166.0	79.7	74.8	70.4	1.6	1.4	2.7	3.6	4.4	4.9

P is rainfall; Tf is throughfall; Sf is stemflow; IL is litter interception.
Eb is Eucalyptus bentamii; Ed is E. dunnii; Es is *E. saligna*.

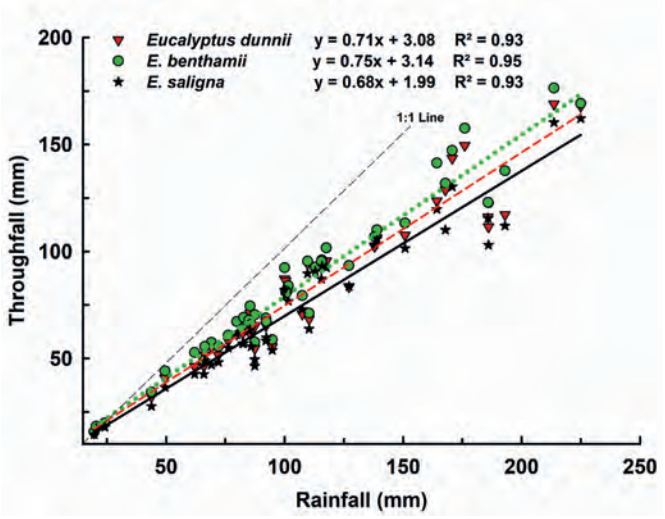

Fig. 6. Regression between throughfall and rainfall in mm in the area under Eucalyptus dunnii, E. benthamii, and *E. saligna*.

3.5. Total interception (INT)

The INT was influenced by plant development stage and by eucalyptus species (Fig. 11). The results were significantly (Tukey test, $p < 0.05$) different between species during most of the time. From March 2016 to March 2017 (21–33 months of plants age), the percentage of P intercepted was higher in *E. saligna* than in E. dunnii and E. benthamii. The average INT in this period was 31.5, 26.2, and 20.8% of P, respectively. Therefore, the soil under E. benthamii trees received, on average, about 10% more water than the soil under *E. saligna* during these months. The highest INT happened from March 2017 to March 2018, when mean values of 37.3, 36.3 and 29.4% of INT were observed in *E. saligna*, E. dunnii and E. benthamii, respectively. In this period, the plants were aged between 3 and 4 years (Fig. 11). For the whole series, the INT among species was *E. saligna* > E. dunnii > E. benthamii.

The highest relationship between INT and P was found for *E. saligna* with R2 of 0.76 (Fig. 12). This indicates that INT depends on other variables, possibly including antecedent rainfall, rainfall intensity, and seasonality. Low values of INT were observed between April and August 2018, probably influenced by LAI reduction caused by eucalyptus defoliation previously mentioned. This reduction was more pronounced in E. benthamii than in this period had average of 15.3% of P, while for *E. saligna* and E. dunnii species the INT means over this period were 23.6 and 20.6% of P, respectively (Fig. 11). However, there was no linear correlation between INT and LAI for E. benthamii ($R = 0.18$) and E. dunnii ($R = 0.02$), we only obtained linear correlation for *E. saligna* ($R = 0.84$).

4. Discussion

4.1. Comparation with previous studies in eucalyptus plantations in the Brazilian Pampa biome

Considering all species and measurements during the study period (eucalyptus 2–4.5 years old), our results show that 12–48% of rainfall (P) corresponds to interception (INT), 57–90% is throughfall (Tf), and 0.3–5.4% is stemflow (Sf). Thus, we observed higher INT and Sf and lower Tf than observed in the Brazilian Atlantic and Amazonian Forests, based on a literature review done by Giglio and Kobiyama (2013), where the first biome shows 8.4–20.6% INT, 47.6–97,4% Tf, and 0.2–3.3% Sf, and the latter has respectively 7.2–22.6%, 76.8–91% and 0.6–1.8% of total rainfall.

Previous studies of rainfall partition in eucalyptus in the Brazilian Pampa showed an average canopy interception for the total monitored period varying from 4.3% in E. urophylla, 2 years, in an area with high potential evapotranspiration and sandy soil (Souza et al., 2019) to 29% in *E. saligna*, 8 years-old, during a very rainy year (Reichert et al., 2017) (Table 3). Only Consensa (2012) compared eucalyptus species and no other study of canopy interception for E. benthamii was found in the Pampa biome. Because of the importance of this species for locations with higher frost risk, this is an important contribution of our study.

The study of Reichert et al. (2017) was the only one that indicated the litter interception: 1.6% of the incident precipitation in the first monitored year and 1.1% in the second. We observed higher values (3.5%, 4.5%, and 4.6% for E. benthamii, E. dunnii, and E.saligna) for a younger forest stand. The differences and the uncertainties in the methods used to calculate the litter interception can explain the difference. However, our study included the period before self-thinning and forest canopy changes that can also influence the results. Reichert et al. (2017) observed a strong influence of rainfall in rainfall partitioning. The more extended period of analysis of the present study reduces the effect of the climatic variability in the monitored values, but it is still dependent on the plantation age. The small number of samples collected is a limiting factor for determining rainfall partitioning since the spatial variability of these processes can be significant (Consensa et al., 2012).

Average values observed in our study for throughfall (Tf) and stemflow (Sf) are, respectively, within the ranges 67–98% and 0.8–11.1% of the incident precipitation (see data Table 3). Throughfall was the component of the rainfall partitioning with the greatest relationship with P, as also observed for Sari et al. (2016), while Momolli et al. (2019) obtained the lowest correlation between INT and P. Most studies were conducted in natural forests (e.g., Arcova et al., 2003; Lima et al., 2018; Sari et al., 2016), and few conducted in planted forests in the subtropics. For *E. grandis*, Sari et al. (2016) obtained a similar correlation between Tf and P, while Momolli et al. (2019), for E. dunnii, and Souza et al. (2019), for E. urophylla plantations, observed higher correlation possibly because of different ages of the plantations and weather conditions.

Stemflow in E. dunnii and E. benthamii increased with increasing DBH, similarly to the observed by Martins Filho (2014) in young *E. grandis*. However, *E. saligna*, species with the largest Sf, had the lowest correlation between P and DBH. This result may be due to the greater LAI and lower leaf inclination of this species (Mattos, 2015). Since the species analyzed have smooth bark and the plantations are young, variation in bark storage was not determinant for the results obtained, contrary to the observed in studies with other species (Levia & Germer, 2015).

In the present study, we focused on the differences in rainfall partitioning between different eucalyptus species under the same meteorological conditions. The empirical regression equations between interception and rainfall calculated have the disadvantage of

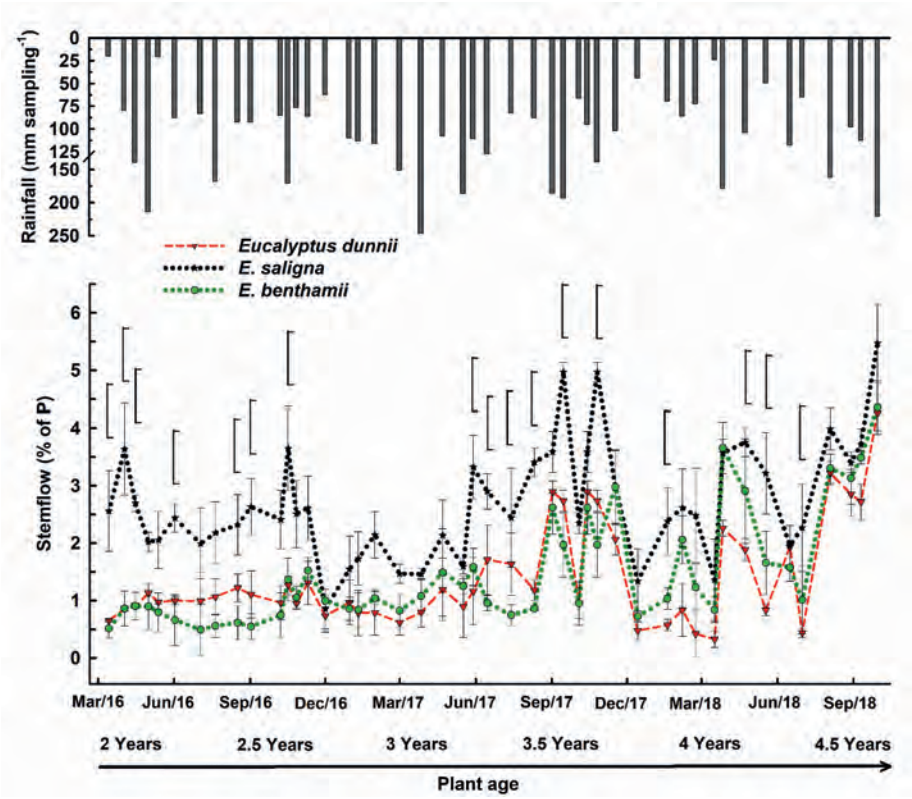

Fig. 7. Rainfall (P) and stemflow (Sf) from March 2016 to September 2018. On the stemflow plot, vertical bars on data represent standard, and on top of plot indicate the minimum significant difference ($p < 0.05$) and, when absent, insignificant ($p > 0.05$) by Tukey test.

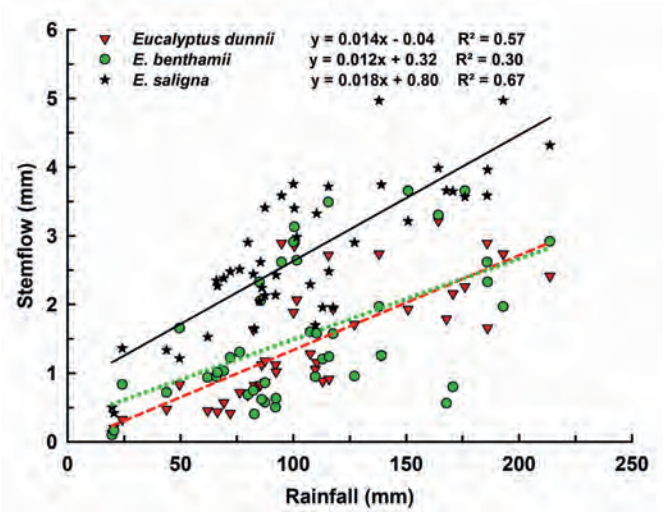

Fig. 8. Regression of stemflow (Sf) in as a function of rainfall (P) in área with Eucalyptus dunnii, E. benthamii, and *E. saligna*.

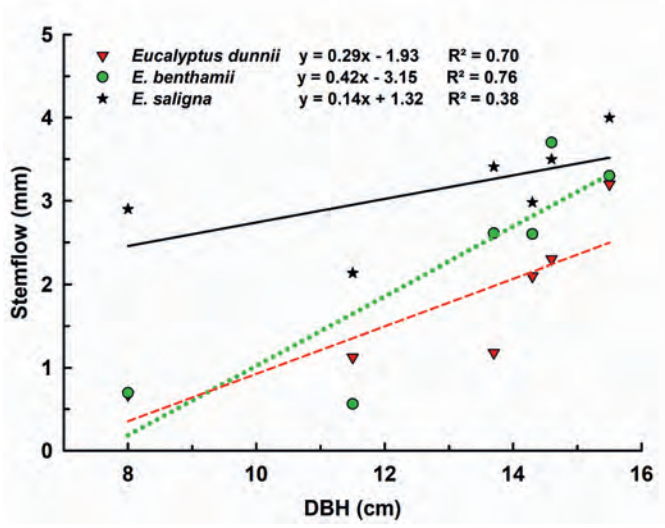

Fig. 9. Regression of stemflow (Sf) as a function of diameter at breast height (DBH) in the area with Eucalyptus dunnii, E. benthamii, and *E. saligna*.

not taking meteorological variables into account and, therefore, that they can be extrapolated only to similar forests in the same climate (Hörmann et al., 1996). Meteorological conditions (e.g., amount and intensity of rainfall and speed of wind) impact the canopy storage capacity (Rowe, 1983) and, therefore, the rainfall partitioning (Levia et al., 2010; Van Stan et al., 2011). However, the importance of their contribution depends on the vegetation types (Zhang et al., 2016; Ida et al., 2017). For low rainfall intensity (<0.3 mm), Viessman Júnior et al. (1977) observed the entire volume of rain is retained, while only about 10–40% may be retained by canopy for more than 1 mm of rainfall. Our study showed, among the three eucalyptus species, total interception by vegetation varied, on average for the whole series, from 26 to 33% (slopes of Fig. 12), which fall within the range previsouly reported. Furthermore, accumulated throughfall close to trunks may often exceeded rainfall, especially for long-duration rainfall >5 mm, because of a 'funnel effect', where high throughfall concentration

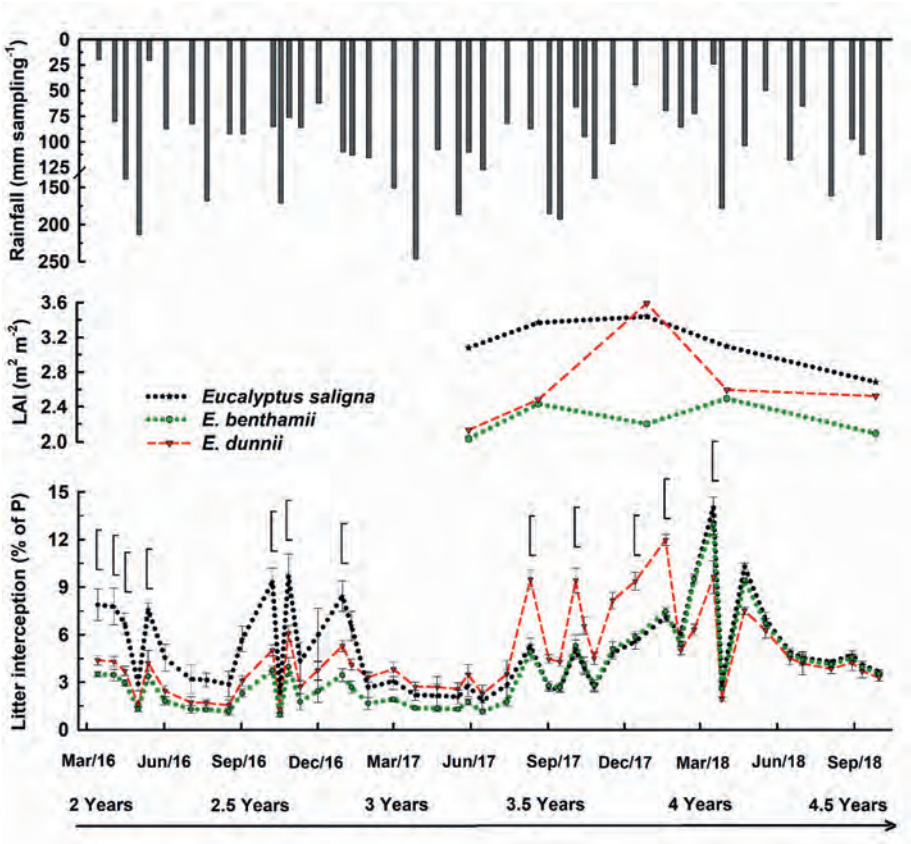

Fig. 10. Rainfall (P), leaf area index (LAI) and litter interception (IL) in Eucalyptus saligna, E. benthamii, and E. dunnii species from March 2016 to September 2018. On the litter interception plot, vertical bars on data represent standard deviation, and on top of plot indicate the minimum significant difference ($p < 0.05$) and, when absent, insignificant ($p > 0.05$) by Tukey test.

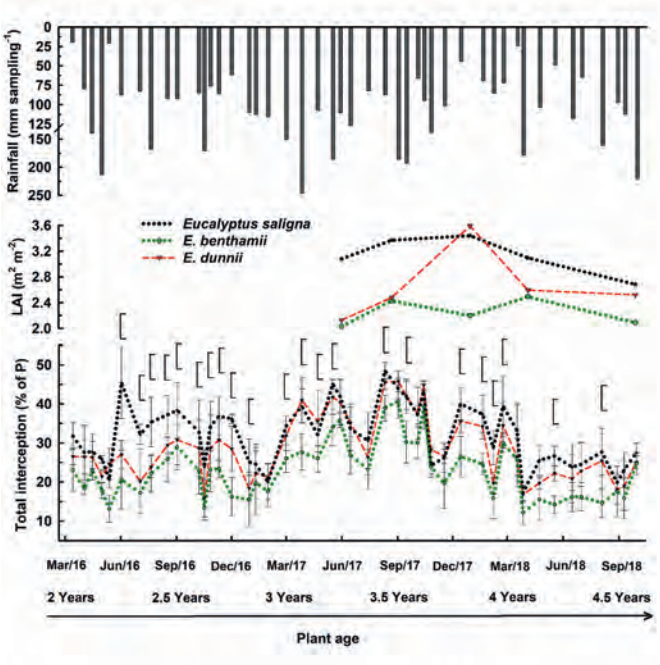

Fig. 11. Rainfall (P), leaf area index (LAI) and total interception (INT) by collect in Eucalyptus saligna, E. benthamii, and E. dunnii species from March 2016 to September 2018.

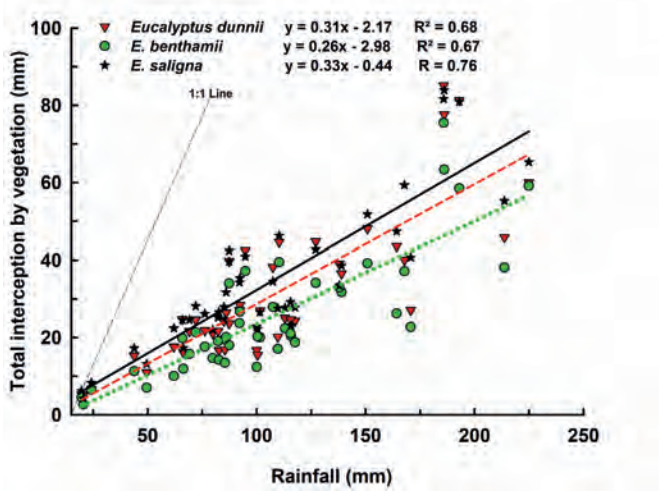

Fig. 12. Relationship between total interception by vegetation (INT) and rainfall (P) in the area with Eucalyptus dunnii, E. benthamii, and *E. saligna*. Vertical bars on data represent standard deviation, and on top of plot indicate the minimum significant difference ($p < 0.05$) and, when absent, insignificant ($p > 0.05$) by Tukey test.

and temporal stability are possibly related to canopy structure (Sato et al., 2011). Thus, size and arrangement of pluviometers to capture throughfall in eucalyptus crop are of practical importance.

Table 3
Canopy interception (cINT), throughfall (Tf) and stemflow (Sf), as percentage of the total precipitation (P) in the monitored period, for the present and previous studies in the Brazilian Pampa biome.

Reference	Monitored period	Species	Age (years)	cINT (%)	Tf (%)	Sf (%)	Total P (mm)
Present study	2.5 years	E. benthamii	2–4.5	19.4%	79.0%	1.5%	5010
Present study	2.5 years	E. dunnii	2–4.5	25.1%	73.5%	1.4%	5010
Present study	2.5 years	*E. saligna*	2–4.5	27.4%	69.9%	2.7%	5010
Momolli et al. (2019)	1 year	E. dunnii	8	8.9%	90.3%	0.8%	1903
Dick et al. (2018)	2 years	E. dunnii	4–6	7.5%	91.3%	1.1%	2771
Correa et al. (2019)	1 year	E. dunnii	1–2	7%	98%	2%	1586
Sari et al. (2016)	8 months	*E. grandis*	3	14.6%	78.1%	11.1%	958
Consensa et al. (2012)	1 year	E. dunnii	6	10%	84.9%	5.1%	1297
Consensa et al. (2012)	1 year	E. urograndis	5	26.8%	67.6%	5.6%	1297
Santos et al. (2014)	1 year	*E. saligna*	5	15.9%	81.0%	3.1%	1225
Souza et al. (2019)[1]	1 year	E. urophylla	2	4.3%	95.3%	1.3%	2050
Souza et al. (2019)[2]	1 year	E. urophylla	2	6.2%	91.7%	3.2%	2050
Valente et al. (2016)	2 years	E. urophylla x globulus	5–6	–	78%	–	1705
Reichert et al. (2017)[3]	1 year	*E. saligna*	7–8	14.8%	81.3%	5.6%	1577
Reichert et al. (2017)4	1 year	*E. saligna*	8–9	29.0%	67.5%	4.5%	2599
Baumhardt (2014)	1 year	E. dunnii and E. urograndis	1–2	25.5%	–	–	1299

1,2 The study included two treatments: one with a smaller fertilization (1), and one with a greater fertilization (2).
3,4 We chose to maintain the division of the monitored period as indicated by the authors in order to analyze a year with normal precipitation (3) and a high-rainfall year (4).

4.2. Implications for water and forest management

Total interception of rainfall (INT) was frequently greater than 30% of P, which highlights the importance of studies that consider this component separately from plant transpiration, since INT does not indicate water consumption by plants, and total evapotranspiration, including INT, can be greater than potential evaporation (David et al., 2005). The INT in E. benthamii was 10.7% lower than in *E. saligna* in the first year of our study, of the 2210 mm of P that occurred in this first year, 1742 mm reached the soil in E. benthamii, but only 1512 mm in *E. saligna*. Thus, in soils with adequate water infiltration, as usually observed in forest plantations (Melloni et al., 2008), there is a higher water supply to the soil in E. benthamii. This water can either favor tree growth during dry periods or percolate for aquifer recharge and stream base flow (Reichert et al., 2017). In the first hypothesis, E. benthamii would have greater water availability during drought periods, whereas in the second the plantations of this species could be used preferably in areas with water use conflicts where *E. saligna* would not be a preferable choice for these conditions. Furthermore, E. benthamii has leaves with a greater tilt angle toward the soil than the other species (Mattos, 2015), possibly contributing to the lower canopy interception observed for this species.

Weather conditions also contributed to lower INT (in % of P), especially in E. benthamii, namely reduction in P in the second year between November 2017 and February 2018. This reduction in P caused water deficit in the soil that decreased the growth rate of plants (Almeida et al., 2007), mainly in DBH, increased defoliation of plants in response to water deficit (Bourne et al., 2015; Paiva, 2009), and as already discussed increased bronze bug infestation and consequent tree defoliation. On the other hand, the reduced INT was beneficial for replenishing soil water storage with rainfall, because of the higher amount of water reaching the soil. Whitehead and Breadle (2004) indicate several mechanisms of Eucalyptus genus to avoid drought, among which the variation in the leaf area index and the leaf arrangement close to the vertical.

Stemflow is governed by canopy conditions, e.g., the density and slope of the branches, and climate, such as the intensity of rainfall and wind speed (Levia et al., 2010; Van Stan et al., 2011). Furthermore, the canopy state is generally a good estimator of Sf (Mużylo et al., 2012; Staelens et al., 2008). Because of the difficulty in measuring Sf in periods of greater plant diameter growth, the Sf in E. dunnii and E. benthamii can be neglected in the annual water balance evaluation in watersheds with young eucalyptus plantations, since the maximum value monthly of Sf observed in this study was 3.6% of P. However, the Sf may have greater importance related to nutrient flow and water flow in areas of greater root concentration (Laclau et al., 2003; Levia & Germer, 2015).

Rainfall and eucalyptus species and leaf area index affected stemflow, throughfall, and total interception (by litter plus canopy), whereas eucalyptus tree diameter at breast height affected throughfall. Total interception ranged from 11 to 47%, and it was greatest for *E. saligna* and during the rainiest analyzed periods. The highest CWS in the *E. saligna* contributed to greater water losses by INT. Evaporation of the intercepted water is a nonproductive share (i.e., not used in biomass production) of the green-water flow in terrestrial ecosystems (Falkenmark & Rockström, 2006). On the other hand, stemflow and throughfall will recharge soil moisture (unsaturated water storage) to be consumed by the evapotranspiration flux (green water flow), and excess becomes surface and groundwater storage and fluxes (blue water flow) (Falkenmark & Rockström, 2006). Hence, eucalyptus species and age are important components in green-blue water partitioning. A significant challenge of commercial forestry, thus, is planning and managing forestry to decrease evaporation and increase the efficiency of green-water use, while generating runoff for ecological flows and draining to recharge groundwater (Ferreto et al., 2020), seeking catchment ecological elasticity and ecosystem function (Falkenmark & Rockström, 2010).

6. Conclusion

Eucalyptus trees, aged of 2–4.5 years, had rainfall interception varying between 22 mm (for 178 mm of rainfall) and 42 mm (for 87 mm of rainfall), throughfall between 106 mm (for 186 mm of rainfall) and 44 mm (for 74 mm of rainfall), and stemflow between 0.5 mm (for 92 mm of rainfall) and 1.4 mm (for 24 mm of rainfall). The relationship between interception and rainfall was not high ($R2 < 0.76$), indicating interception depends on other variables, possibly including antecedent rainfall, rainfall intensity, and seasonality. Interception decreased with reduction in leaf area index caused by eucalyptus defoliation.

Throughfall decreased with tree growth until the age of 3.5 years, and then increased because of drought and associated insect attack, which caused defoliation and thus decreased the leaf area index. With the lowest leaf area, E. benthamii reached the greatest

throughfall, whereas *E. saligna* with the greatest leaf area showed the lowest throughfall most of the time. Regression equations show E. benthamii had 0.75 mm of throughfall per mm of rainfall, whereas the latter two species had 0.71 mm and 0.68 mm for E. dunnii and *E. saligna*. Stemflow was higher in *E. saligna* than in E. dunnii and E. benthamii in most of the study period. Stemflow in E. benthamii and E. dunnii had a higher positive correlation with DBH, whereas in *E. saligna* the highest correlation was with rainfall.

These results contribute to bridging forest management with ecosystem processes, such as choosing the most fit eucalyptus species to the local climate, to improve the synchronization crop-demand versus soil-water-supply, while maintaining streamflow to fulfill other ecological and production needs, considering watershed ecological resilience and ecosystem functions. While eucalyptus monoculture will still be under scrutiny due to its water use, choosing least-consuming species is a forest managing practice to minimize the green-water share with no productive function, and provide blue-water to satisfy the surface and subsurface pools and flows.

Funding

Fapergs, CNPq, Capes (Finance code 001), and Celulose Riograndense Company, all from Brazil.

Availability of data and material

Data will be made available upon request.

Authors' contributions

The authors Décio Oscar Cardoso Ferreto, José Miguel Reichert, and Rosane Barbosa Lopes Cavalcante contributed to the study conception and design. Material preparation, data collection, and analysis were performed by Décio Oscar Cardoso Ferreto and Rosane Barbosa Lopes Cavalcante. The first draft of the manuscript was written by Décio Oscar Cardoso Ferreto, and all authors commented on previous versions of the manuscript. All authors read and approved the final manuscript.

Declaration of competing interest

The authors declare that they have no known competing financial interests or personal relationships that could have appeared to influence the work reported in this paper.

Acknowledgments

We thank the Foundation for Research Support of the State of Rio Grande do Sul (Fapergs), the Coordination for the Improvement of Higher Education Personnel (Capes) – Finance code 001, and the National Council for Scientific and Technological Development (CNPq). We also thank the Celulose Riograndense Company (CMPC) for the financial support and study area.

Appendix A. Supplementary data

Supplementary data to this article can be found online at https://doi.org/10.1016/j.iswcr.2021.01.002.

References

Almeida, A. C., Soares, J. V., Landsberg, J. J., & Rezende, G. D. (2007). Growth and water balance of Eucalyptus grandis hybrids plantations in Brazil during a rotation for pulp production. *Forest Ecology and Management, 25*, 10–21. https://doi.org/10.1016/j.foreco.2007.06.009

Alvares, C. A., Stape, J. L., Sentelhas, P. C., Gonçalves, J. L. M., & Sparovek, G. (2013). Köppen's climate classification map for Brazil. *Meteorologische Zeitschrift, 22*, 711–728. https://doi.org/10.1127/0941-2948/2013/0507

Arcova, F. C. S., Cicco, V., & Rocha, P. A. B. (2003). Precipitação efetiva e interceptação das chuvas por floresta de Mata Atlântica em uma microbacia experimental em Cunha - São Paulo. *Revista Árvore, 27*, 257–262. https://doi.org/10.1590/S0100-67622003000200014

Baumhardt, E. (2014). *Hidrologia de bacia de cabeceira com eucaliptocultura e campo nativo da região da campanha gaúcha (Doctorate dissertation)*. Santa Maria, RS, Brazil: Universidade Federal de Santa Maria.

Bourne, A. E., Haigh, A. M., & Ellsworth, D. S. (2015). Stomatal sensitivity to vapour pressure deficit relates to climate of origin in Eucalyptus species. *Tree Physiology, 35*, 266–278. https://doi.org/10.1093/treephys/tpv014

Cavalli, J. P., Reichert, J. M., Rodrigues, M. F., & de Araújo, E. F. (2020). Composition and functional soil properties of arenosols and acrisols: Effects on eucalyptus growth and productivity. *Soil and Tillage Research, 196*, Article e104439. https://doi.org/10.1016/j.still.2019.104439

Chang, M. (2012). *Forest hydrology: An introduction to water and forests*. United States: Taylor & Francis.

Consensa, B. C. (2012). *Precipitação pluviométrica e interna em povoamentos de Eucalyptus spp. em Rosário do Sul, RS (Masters dissertation)*. Santa Maria, RS, Brazil: Universidade Federal de Santa Maria.

Correa, R. S., Schumacher, M. V., Momolli, D. R., & Berger, C. (2019). Aspectos da precipitação pluviométrica em um povoamento jovem de Eucalyptus dunnii no bioma Pampa. *Advances in Forestry Science, 6*(3), 717–721. https://doi.org/10.34062/afs.v6i3.7617

Crockford, R. H., & Richardson, D. P. (2000). Partitioning of rainfall into throughfall, stemflow and interception: Effect of forest type, ground cover and climate. *Hydrological Processes, 14*, 2903–2920. https://doi.org/10.1002/1099-1085(200011/12)14:16/17<2903::AID-HYP126>3.0.CO, 2-6.

David, J. S., Valente, F., & Gash, J. H. C. (2005). Evaporation of intercepted rainfall. In M. G. Anderson (Ed.), *Encyclopedia of hydrological sciences*. United States: John Wiley and Sons Ltd. https://doi.org/10.1002/0470848944.hsa046.

Dick, G., Schumacher, M. V., Momolli, D. R., & Viera, M. (2018). Nutrient input via incident rainfall in a Eucalyptus dunnii stand in the Pampa biome. *Floresta e Ambiente, 25*(3), Article e20160559. https://doi.org/10.1590/2179-8087.055916

Ebling, E. D., Reichert, J. M., Peláez, J. J. Z., Rodrigues, M. F., Valente, M. L., Cavalcante, R. B. L., Reggiani, P., & Srinivasan, R. (2020). Event-based hydrology and sedimentation in paired watersheds under commercial eucalyptus and grasslands in the Brazilian Pampa biome. *International soil and water conservation Research*. https://doi.org/10.1016/j.iswcr.2020.10.008

Falkenmark, M., & Rockström, J. (2004). *Balancing water for humans and nature: The new approach in ecohydrology*. London: Earthscan.

Falkenmark, M., & Rockström, J. (2006). The new blue and green water paradigm: Breaking new ground for water resources planning and management. *Journal of Water Resources Planning and Management, 132*, 129–132. https://doi.org/10.1061/(ASCE)0733-9496, 2006)132:3(129.

Falkenmark, M., & Rockström, J. (2010). Building water resilience in the face of global change: From a blue-only to a green-blue water approach to land-water management. *Journal of Water Resources Planning and Management, 136*, 606–610. https://doi.org/10.1061/(ASCE)WR.1943-5452.0000118

Ferraz, S. F. B., Lima, W. P., & Rodrigues, C. B. (2013). Managing forest plantation landscapes for water conservation. *Forest Ecology and Management, 301*, 58–66. https://doi.org/10.1016/j.foreco.2012.10.015

Ferreto, D. O. C., Reichert, J. M., Lopes Cavalcante, R. B., & Srinivasan, R. (2020). Water budget fluxes in catchments under grassland and Eucalyptus plantations of different ages. *Canadian Journal of Forest Research*. cjfr-2020-0156, 2020, e-First.

Giglio, J. N., & Kobiyama, M. (2013). Interceptação da chuva: Uma revisão com ênfase no monitoramento em florestas brasileiras. *Revista Brasileira de Recursos Hídricos, 18*, 297–317. https://doi.org/10.21168/rbrh.v18n2.p297-317

Hörmann, G., Branding, A., Clemen, T., Herbst, M., Hinrichs, A., & Thamm, F. (1996). Calculation and simulation of wind controlled canopy interception of a beech forest in Northern Germany. *Agricultural and Forest Meteorology, 79*, 131–148.

IBÁ – Indústria Brasileira de Árvores. (2017). Relatório anual IBÁ 2017. Retrieved from http://iba.org/pt/biblioteca-iba/publicacoes Accessed 5 December 2018.

INMET - Instituto Nacional de Meteorologia. (2009). Normais climatológicas do brasil 1961-1990, 2009. Retrieved from http://www.inmet.gov.br/portal/index.php?r=clima/normaisClimatologicas Accessed 20 October 2017.

Laclau, J. P., Ranger, J., Nzila, J. D., Bouillet, J. P., & Deleporte, P. (2003). Nutrient cycling in a clonal stand of Eucalyptus and an adjacent savanna ecosystem in Congo: 2. Chemical composition of soil solutions. *Forest Ecology and Management, 180*, 527–544. https://doi.org/10.1016/S0378-1127(02)00645-X

Levia, D. F., & Germer, S. A. (2015). Review of stemflow generation dynamics and stemflow-environment interactions in forests and shrublands. *Reviews of Geophysics, 53*, 673–714. https://doi.org/10.1002/2015RG000479

Levia, D. F., Keim, R. F., Carlyle-Moses, D. E., & Frost, E. E. (2011). Throughfall and stemflow in wooded ecosystems. In D. Levia, D. Carlyle-Moses, & T. Tanaka (Eds.), *Forest hydrology and biogeochemistry: Ecological studies (analysis and synthesis)*. Dordrech: Springer. https://doi.org/10.1007/978-94-007-1363-5_21.

Levia, D. F., Van Stan, J. T., Mage, S. M., & Kelley-Hauske, P. W. (2010). Temporal variability of stemflow volume in a beech-yellow poplar forest in relation to tree species and size. *Journal of Hydrology, 380*, 112–120. https://doi.org/10.1016/j.jhydrol.2009.10.028

Lida, S., Levia, D. F., Nanko, K., Sun, X., Shimizu, T., Tamai, K., & Shinohara, Y. (2018). Correction of canopy interception loss measurements in temperate forests: A comparison of necessary adjustments among three different rain gauges based on a dynamic calibration procedure. *Journal of Hydrometeorology, 19*, 547–553. https://doi.org/10.1175/JHM-D-17-0124.1

Lima, S. R., Bourscheidt, V., & Tanaka, M. O. (2018). Relationships between rainfall and throughfall in a secondary forest in southeastern Brazil: An evaluation of different statistical models. *Revista Brasileira de Recursos Hídricos, 23*, 1–14. https://doi.org/10.1590/2318-0331.231820170155

Lleyton, L., Reynolds, E. R. C., & Thompson, F. B. (1965). Rainfall interception in forest and moorland. In W. E. Sopper, & H. W. Lull (Eds.), *Vol. 1967. Forest hydrology. Proceedings of the international symposium on forest hydrology* (pp. 163–178). Pennsylvania: Pergamon.

Martins Filho, F. M. (2014). *Balanço hídrico e erosão do solo em uma plantação de eucaliptos novos (Doctoral dissertation)*. São Carlos, SP, Brazil: Escola de Engenharia de São Carlos, USP.

Mattos, E. M. (2015). *Caracterização da sazonalidade do crescimento do lenho, da copa e da eficiência do uso da luz em clones do gênero Eucalyptus (Masters dissertation)*. Piracicaba, SP, Brazil: Escola Superior de Agricultura Luiz de Queiroz, USP.

Momolli, D. R., Schumacher, M. V., Viera, M., Ludvichak, A. A., Guimarães, C. C., & Souza, H. P. (2019). Incident precipitation partitioning: Throughfall, stemflow and canopy interception in Eucalyptus dunnii stand. *Journal of Agricultural Science, 11*, 372–380. https://doi.org/10.5539/jas.v11n5p372

Mużylo, A., Liorens, P., & Domingo, F. (2012). Rainfall partitioning in a deciduous forest plot in leafed and leafless periods. *Ecohydrology, 5*, 759–767. https://doi.org/10.1002/eco.266

Nosetto, M. D., Jobbágy, E. G., Brizuela, A. B., & Jackson, R. B. (2012). The hydrologic consequences of land cover change in central Argentina. *Agriculture, Ecosystems & Environment, 154*, 2–11. https://doi.org/10.1016/j.agee.2011.01.008

Oliveira, T. A., Freitas, D. A., Gianezini, M., Ruviaro, C. F., Zago, D., Mércio, T. Z., Dias, E. D., Lampert, V. N., & Barcellos, J. O. J. (2017). Agricultural land use change in the Brazilian Pampa Biome: The reduction of natural grasslands. *Land Use Policy, 63*, 394–400. https://doi.org/10.1016/j.landusepol.2017.02.010

Paiva, Y. G. (2009). *Estimativa do índice de área foliar por métodos óticos e sensoriamento remoto para calibrar modelo ecofisiológico em plantios de eucalipto em áreas de relevo ondulado (Masters dissertation)*. Viçosa, MG, Brazil: Universidade Federal de Viçosa.

Reichert, J. M., Rodrigues, M. F., Peláez, J. J. Z., Lanza, R., Minella, J. P. G., Arnold, J. G., & Cavalcante, R. B. L. (2017). Water balance in paired watersheds with Eucalyptus and degraded grassland in Pampa biome. *Agricultural and Forest Meteorology, 237*, 282–295. https://doi.org/10.1016/j.agrformet.2017.02.014

Rodrigues, M. F., Reichert, J. M., Burrow, R. A., Flores, E. M. M., Minella, J. P. G., Rodrigues, L. A., Oliveira, J. S. S., & Cavalcante, R. B. L. (2018). Coarse and fine sediment sources in nested watersheds with eucalyptus forest. *Land Degradation & Development, 29*, 2237–2253. https://doi.org/10.1002/ldr.2977

Rodrigues, M. F., Reichert, J. M., Minella, J. P. G., Dalbianco, L., Ludwig, R. L., Ramon, R., Rodrigues, L. A., & Borges Júnior, N. (2014). Hydrosedimentology of nested subtropical watersheds with native and eucalyptus forests. *Journal of Soils and Sediments, 14*, 1311–1324. https://doi.org/10.1007/s11368-014-0885-5

Rohatyn, S., Rotenberg, E., Ramati, E., Tatarinov, F., Tas, E., & Yakir, D. (2018). Differential impacts of land use and precipitation on "ecosystem water yield. *Water Resources Research, 54*, 5457–5470. https://doi.org/10.1029/2017WR022267

Rowe, L. K. (1983). Rainfall interception by an evergreen beech forest, Nelson, New Zealand. *Journal of Hydrology, 66*, 143–158.

Santos, H. G., Jacomine, P. K. T., Anjos, L. H. C., Oliveira, V. A., Oliveira, J. B., Coelho, M. R., Lumbreras, J. F., & Cunha, T. J. F. (2013a). *Sistema brasileiro de classifcação de solos*. Rio de Janeiro: Embrapa Solos.

Santos, G. A., Resende, M. D. V., Silva, L. D., Higa, A., & Assis, T. F. (2013b). Adaptabilidade de híbridos multiespécies de Eucalyptus ao estado do Rio Grande do Sul. *Revista Árvore, 37*, 759–769. https://doi.org/10.1590/S0100-67622013000400019, 2013.

Santos, G. A., Resende, M. D. V., Silva, L. D., Higa, A., & Assis, T. F. (2015). Interação genótipos x ambientes para produtividade de clones de Eucalyptus L'Hér. no estado do Rio Grande do Sul. *Revista Árvore, 39*, 81–91. https://doi.org/10.1590/0100-67622015000100008

Santos, J. C., Schumacher, M. V., & Araújo, E. F. (2014). *Distribuição da precipitação em um povoamento de Eucalyptus saligna Smith em São Gabriel – RS (Boletim Técnico 44)*. Santa Maria: CCR, UFSM.

Sari, V., Paiva, E. M. C. D., & Paiva, J. B. D. (2016). Interceptação da chuva em diferentes formações florestais na região sul do Brasil. *Revista Brasileira de Recursos Hídricos, 21*, 65–79. https://doi.org/10.21168/rbrh.v21n1.p65-79

Sato, A. M., Avelar, A. S., & Netto, A. L. C. (2011). Spatial variability and temporal stability of throughfall in a eucalyptus plantation in the hilly lowlands of southeastern Brazil. *Hydrological Processes, 25*, 1910–1923. https://doi.org/10.1002/hyp.7947

Savenije, H. H. G. (2004). The importance of interception and why we should delete the term evapotranspiration from our vocabulary. *Hydrological Processes, 18*, 1507–1511. https://doi.org/10.1002/hyp.5563

Shi, Z., Xu, D., Yang, X., Jia, Z., Guo, H., & Zhang, N. (2012). Ecohydrological impacts of eucalypt plantations: A review. *Journal of Food Agriculture and Environment, 10*, 1419–1426.

Souza, H. P., Momolli, D. R., Ludvichak, A. A., Schumacher, M. V., & Malheiros, A. C. (2019). Linear regression of incident precipitation explains the throughfall, stemflow and interception by the eucalyptus canopy under different fertilization management. *Journal of Experimental Agriculture International, 33*(4), 1–11. https://doi.org/10.9734/jeai/2019/v33i430147

Staelens, J., De Schrijver, A., Verheyen, K., & Verhoest, N. E. C. (2008). Rainfall partitioning into throughfall, stemflow, and interception within a single beech (fagus sylvatica L.) canopy: Influence of foliation, rain event characteristics, and meteorology. *Hydrological Processes, 22*, 33–45. https://doi.org/10.1002/hyp.6610

Stape, J. L., Binkley, D., Ryan, M. G., Fonseca, S., Loos, R. A., Takahashi, E. N., Silva, C. R., Silva, S. R., Hakamada, R. E., Ferreira, J. M. A., Lima, A. M. N., Gava, J. L., Leite, F. P., Andrade, H. B., Alves, J. M., Silva, G. G. C., & Azevedo, M. R. (2010). The Brazil eucalyptus potential productivity project: Influence of water, nutrients and stand uniformity on wood production. *Forest Ecology and Management, 259*, 1684–1694. https://doi.org/10.1016/j.foreco.2010.01.012

USDA – Soil Survey Staff. (1999). *Soil Taxonomy – a basic system of soil classification for marking and interpreting soil survey*. Washington: USDA.

Valente, M. L., Schumacher, M. V., Correa, R. S., Araújo, E. F., & Trüby, P. (2016). Quantificação de nutrientes na precipitação em um plantio de *Eucalyptus urophylla* x *Eucalyptus globulus* subsp. *maidenii*, Eldorado do Sul, RS. *Scientia Forestalis, 44*, 249–259. https://doi.org/10.18671/scifor.v44n109.24

Valente, M. L., Reichert, J. M., Legout, C., Tiecher, T., Cavalcante, R. B. L., & Evrard, O. (2020). Quantification of sediment source contributions in two paired catchments of the Brazilian Pampa using conventional and alternative fingerprinting approaches. *Hydrological Processes, 34*, 2965–2986. https://doi.org/10.1002/hyp.13768

Van Stan, J. T., Siegert, C. M., Levia, D. F., Jr., & Scheick, C. E. (2011). Effects of wind-driven rainfall on stemflow generation between codominant tree species with differing crown characteristics. *Agricultural and Forest Meteorology, 151*, 1277–1286. https://doi.org/10.1016/j.agrformet.2011.05.008

Viessman Júnior, W., Knapp, J. W., Lewis, G. L., & Harbaugh, T. E. (1977). *Introduction to hydrology* (2nd ed.). New York: Harper and Row.

Whitehead, D., & Breadle, C. L. (2004). Physiological regulation of productivity and water use in Eucalyptus: A review. *Forest Ecology and Management, 193*, 113–140. https://doi.org/10.1016/j.foreco.2004.01.026

Zhang, Z., Zhao, Y., Li, X., Huang, L., & Tan, H. (2016). Gross rainfall amount and maximum rainfall intensity in 60-minute influence on interception loss of shrubs: A 10-year observation in the tengger desert. *Scientific Reports, 6*, 26030. https://doi.org/10.1038/srep26030

GUIDE FOR AUTHORS

INTRODUCTION

Types of paper

Contributions falling into the following categories will be considered for publication: Original research papers, reviews, letters to the editor.

Please ensure that you select the appropriate article type from the list of options when making your submission. Authors contributing to special issues should ensure that they select the special issue article type from this list.

BEFORE YOU BEGIN

Ethics in Publishing

For information on Ethics in Publishing and Ethical guidelines for journal publication see http://www.elsevier.com/publishingethics and http://www.elsevier.com/ethicalguidelines.

Conflict of interest

All authors are requested to disclose any actual or potential conf ict of interest including any f nancial, personal or other relationships with other people or organizations within three years of beginning the submitted work that could inappropriately inf uence, or be perceived to inf uence, their work. See also http://www.elsevier.com/conf ictsof nterest.

Submission declaration

Submission of an article implies that the work described has not been published previously (except in the form of an abstract or as part of a published lecture or academic thesis), that it is not under consideration for publication elsewhere, that its publication is approved by all authors and tacitly or explicitly by the responsible authorities where the work was carried out, and that, if accepted, it will not be published elsewhere including electronically in the same form, in English or in any other language, without the written consent of the copyright-holder.

Changes to authorship

This policy concerns the addition, deletion, or rearrangement of author names in the authorship of accepted manuscripts:

Before the accepted manuscript is published in an online issue: Requests to add or remove an author, or to rearrange the author names, must be sent to the Journal Manager from the corresponding author of the accepted manuscript and must include: (a) the reason the name should be added or removed, or the author names rearranged and (b) written conf rmation (e-mail, fax, letter) from all authors that they agree with the addition, removal or rearrangement. In the case of addition or removal of authors, this includes conf rmation from the author being added or removed. Requests that are not sent by the corresponding author will be forwarded by the Journal Manager to the corresponding author, who must follow the procedure as described above. Note that: (1) Journal Managers will inform the Journal Editors of any such requests and (2) publication of the accepted manuscript in an online issue is suspended until authorship has been agreed.

After the accepted manuscript is published in an online issue: Any requests to add, delete, or rearrange author names in an article published in an online issue will follow the same policies as noted above and result in a corrigendum.

Copyright

[example: Upon acceptance of an article, authors will be asked to complete a 'Journal Publishing Agreement'. Acceptance of the agreement will ensure the widest possible dissemination of information. An e-mail will be sent to the corresponding author conf rming receipt of the manuscript together with a 'Journal Publishing Agreement' form or a link to the online version of this agreement.

Permission of the International Research and Training Center on Erosion and Sedimentation or the China Water and Power Press is required for resale or distribution outside the institution and for all other derivative works, including compilations and translations (please consult paige.chyu@gmail.com or iswcr@foxmail.com). If excerpts from other copyrighted works are included, the author(s) must obtain written permission from the copyright owners and credit the source(s) in the article.]

Role of the funding source

You are requested to identify who provided f nancial support for the conduct of the research and/or preparation of the article and to brief y describe the role of the sponsor(s), if any, in study design; in the collection, analysis and interpretation of data; in the writing of the report; and in the decision to submit the paper for publication. If the funding source(s) had no such involvement then this should be stated. Please see http://www.elsevier.com/funding.

Language and language services

Please write your text in good English (American or British usage is accepted, but not a mixture of these). Authors who require information about language editing and copyediting services pre- and post-submission please visit http://webshop.elsevier.com/languageediting or our customer support site at http://support.elsevier.com for more information.

Submission

Submission to this journal proceeds totally online. Use the following guidelines to prepare your article. Via the homepage of this journal (http://www.evise.com/evise/faces/pages/navigation/NavController.jspx?JRNL_ACR=ISWCR) you will be guided stepwise through the creation and uploading of the various f les. The system automatically converts source f les to a single Adobe Acrobat PDF version of the article, which is used in the peer-review process. Please note that even though manuscript source f les are converted to PDF at submission for the review process, these source f les are needed for further processing after acceptance. All correspondence, including notif cation of the Editor's decision and requests for revision, takes place by e-mail and via the author's homepage, removing the need for a hard-copy paper trail. If you are unable to provide an electronic version, please contact the editorial off ce prior to submission [example: e-mail: paige.chyu@gmail.com or iswcr@foxmail.com; telephone: +86 10 68786416; or fax: 86 10 68411174].

Additional Information

Tables and f gures may be presented with captions within the main body of the manuscript; if so, f gures should additionally be uploaded as high resolution f les.

PREPARATION

Use of wordprocessing software

It is important that the f le be saved in the native format of the wordprocessor used. The text should be in single-column format. Keep the layout of the text as simple as possible. Most formatting codes will be removed and replaced on processing the article. In particular, do not use the wordprocessor's options to justify text or to hyphenate words. However, do use bold face, italics, subscripts, superscripts etc. When preparing tables, if you are using a table grid, use only one grid for each individual table and not a grid for each row. If no grid is used, use tabs, not spaces, to align columns. The electronic text should be prepared in a way very similar to that of conventional manuscripts (see also the Guide to Publishing with Elsevier: http://www.elsevier.com/guidepublication). Note that source f les of f gures, tables and text graphics will be required whether or not you embed your f gures in the text. See also the section on Electronic illustrations.

To avoid unnecessary errors you are strongly advised to use the "spell-check" and "grammar-check" functions of your wordprocessor.

LaTeX

If the LaTeX f le is suitable, proofs will be produced without rekeying the text. The article should preferably be written using Elsevier's document class "elsarticle", or alternatively any of the other recognized classes and formats supported in Elsevier's electronic submissions system, for further information see http://www.elsevier.com/wps/f nd/authorsview.authors/latex-ees-supported.

The Elsevier "elsarticle" LaTeX style f le package (including detailed instructions for LaTeX preparation) can be obtained from the Quickguide: http://www.elsevier.com/latex. It consists of the f le: elsarticle.cls, complete user documentation for the class f le, bibliographic style f les in various styles, and template f les for a quick start.

Article structure

Subdivision - numbered sections

Divide your article into clearly def ned and numbered sections. Subsections should be numbered 1.1 (then 1.1.1, 1.1.2, ...), 1.2, etc. (the abstract is not included in section numbering). Use this numbering also for internal cross-referencing: do not just refer to "the text". Any subsection may be given a brief heading. Each heading should appear on its own separate line.

Introduction

State the objectives of the work and provide an adequate background, avoiding a detailed literature survey or a summary of the results.

Material and methods

Provide suff cient detail to allow the work to be reproduced. Methods already published should be indicated by a reference: only relevant modif cations should be described.

Theory/calculation

A Theory section should extend, not repeat, the background to the article already dealt with in the Introduction and lay the foundation for further work. In contrast, a Calculation section represents a practical development from a theoretical basis.

Results

Results should be clear and concise.

Discussion

This should explore the signif cance of the results of the work, not repeat them. A combined Results and Discussion section is often appropriate. Avoid extensive citations and discussion of published literature.

Conclusions

The main conclusions of the study may be presented in a short Conclusions section, which may stand alone or form a subsection of a Discussion or Results and Discussion section.

Appendices

If there is more than one appendix, they should be identif ed as A, B, etc. Formulae and equations in appendices should be given separate numbering: Eq. (A.1), Eq. (A.2), etc.; in a subsequent appendix, Eq. (B.1) and so on. Similarly for tables and f gures: Table A.1; Fig. A.1, etc.

Essential title page information

- ***Title.*** Concise and informative. Titles are often used in information-retrieval systems. Avoid abbreviations and formulae where possible.
- ***Author names and affiliations.*** Where the family name may be ambiguous (e.g., a double name), please indicate this clearly. Present the authors' aff liation addresses (where the actual work was done) below the names. Indicate all aff liations with a lower-case superscript letter immediately after the author's name and in front of the appropriate address. Provide the full postal address of each aff liation, including the country name, and, if available, the e-mail address of each author.
- ***Corresponding author.*** Clearly indicate who will handle correspondence at all stages of refereeing and publication, also post-publication. **Ensure that telephone and fax numbers (with country and area code) are provided in addition to the e-mail address and the complete postal address. Contact details must be kept up to date by the corresponding author.**
- ***Present/permanent address.*** If an author has moved since the work described in the article was done, or was visiting at the time, a "Present address" (or "Permanent address") may be indicated as a footnote to that author's name. The address at which the author actually did the work must be retained as the main, aff liation address. Superscript Arabic numerals are used for such footnotes.

Abstract

A concise and factual abstract is required. The abstract should state brief y the purpose of the research, the principal results and major conclusions. An abstract is often presented separately from the article, so it must be able to stand alone. For this reason, References should be avoided, but if essential, then cite the author(s) and year(s). Also, non-standard or uncommon abbreviations should be avoided, but if essential they must be def ned at their f rst mention in the abstract itself.

Keywords

Authors are invited to submit keywords associated with their paper.

Abbreviations

Def ne abbreviations that are not standard in this f eld in a footnote to be placed on the f rst page of the article. Such abbreviations that are unavoidable in the abstract must be def ned at their f rst mention there, as well as in the footnote. Ensure consistency of abbreviations throughout the article.

Acknowledgements

Collate acknowledgements in a separate section at the end of the article before the references and do not, therefore, include them on the title page, as a footnote to the title or otherwise. List here those individuals who provided help during the research (e.g., providing language help, writing assistance or proof reading the article, etc.).

Nomenclature and units

Follow internationally accepted rules and conventions: use the international system of units (SI). If other quantities are mentioned, give their equivalent in SI. Authors wishing to present a table of nomenclature should do so on the second page of their manuscript.

Math formulae

Present simple formulae in the line of normal text where possible and use the solidus (/) instead of a horizontal line for small fractional terms, e.g., X/Y. In principle, variables are to be presented in italics. Powers of e are often more conveniently denoted by exp. Number consecutively any equations that have to be displayed separately from the text (if referred to explicitly in the text).

Footnotes

Footnotes should be used sparingly. Number them consecutively throughout the article, using superscript Arabic numbers. Many wordprocessors build footnotes into the text, and this feature may be used. Should this not be the case, indicate the position of footnotes in the text and present the footnotes themselves separately at the end of the article. Do not include footnotes in the Reference list.

Table footnotes

Indicate each footnote in a table with a superscript lowercase letter.

Artwork

Electronic artwork

General points

- Make sure you use uniform lettering and sizing of your original artwork.
- Save text in illustrations as "graphics" or enclose the font.
- Only use the following fonts in your illustrations: Arial, Courier, Times, Symbol.
- Number the illustrations according to their sequence in the text.
- Use a logical naming convention for your artwork f les.
- Provide captions to illustrations separately.
- Produce images near to the desired size of the printed version.
- Submit each f gure as a separate f le.

A detailed guide on electronic artwork is available on our website: http://www.elsevier.com/artworkinstructions

You are urged to visit this site; some excerpts from the detailed information are given here.

Formats

Regardless of the application used, when your electronic artwork is f nalised, please "save as" or convert the images to one of the following formats (note the resolution requirements for line drawings, halftones, and line/halftone combinations given below):

EPS: Vector drawings. Embed the font or save the text as "graphics".
TIFF: color or grayscale photographs (halftones): always use a minimum of 300 dpi.
TIFF: Bitmapped line drawings: use a minimum of 1000 dpi.
TIFF: Combinations bitmapped line/half-tone (color or grayscale): a minimum of 500 dpi is required.

If your electronic artwork is created in a Microsoft Off ce application (Word, PowerPoint, Excel) then please supply "as is".

Please do not:

- Supply f les that are optimised for screen use (like GIF, BMP, PICT, WPG); the resolution is too low;
- Supply f les that are too low in resolution;
- Submit graphics that are disproportionately large for the content.

Color artwork

Please make sure that artwork f les are in an acceptable format (TIFF, EPS or MS Off ce f les) and with the correct resolution. If, together with your accepted article, you submit usable color f gures then Elsevier will ensure, at no additional charge, that these f gures will appear in color on the Web (e.g., ScienceDirect and other sites) regardless of whether or not these illustrations are reproduced in color in the printed version.

Figure captions

Ensure that each illustration has a caption. Supply captions separately, not attached to the f gure. A caption should comprise a brief title (**not** on the f gure itself) and a description of the illustration. Keep text in the illustrations themselves to a minimum but explain all symbols and abbreviations used.

Tables

Number tables consecutively in accordance with their appearance in the text. Place footnotes to tables below the table body and indicate them with superscript lowercase letters. Avoid vertical rules. Be sparing in the use of tables and ensure that the data presented in tables do not duplicate results described elsewhere in the article.

References

Citation in text

Please ensure that every reference cited in the text is also present in the reference list (and vice versa). Any references cited in the abstract must be given in full. Unpublished results and personal communications are not recommended in the reference list, but may be mentioned in the text. If these references are included in the reference list they should follow the standard reference style of the journal and should include a substitution of the publication date with either "Unpublished results" or "Personal communication" Citation of a reference as "in press" implies that the item has been accepted for publication.

Web references

As a minimum, the full URL should be given and the date when the reference was last accessed. Any further information, if known (DOI, author names, dates, reference to a source publication, etc.), should also be given. Web references can be listed separately (e.g., after the reference list) under a different heading if desired, or can be included in the reference list.

References in a special issue

Please ensure that the words 'this issue' are added to any references in the list (and any citations in the text) to other articles in the same Special Issue.

Reference management software

This journal has standard templates available in key reference management packages EndNote (http://www.endnote.com/support/enstyles.asp) and Reference Manager (http://refman.com/support/rmstyles.asp). Using plug-ins to wordprocessing packages, authors only need to select the appropriate journal template when preparing their article and the list of references and citations to these will be formatted according to the journal style which is described below.

Reference style

The International Soil and Water Conservation Research (ISWCR) follows the Publication Manual of the American Psychological Association (APA) 6th for reference lists and text citation. The author are referred to the Publication Manual of the American Psychological Association, Fifth Edition, ISBN 1-55798-790-4, copies of which may be ordered from http://www.apa.org/books/4200061.html *or* APA Order Dept., P.O.B. 2710, Hyattsville, MD 20784, USA. *or* APA, 3 Henrietta Street, London, WC3E 8LU, UK. Details concerning this referencing style can also be found at http://humanities.byu.edu/linguistics/Henrichsen/APA/APA01.html.

Examples:
Text: All citations in the text should refer to:

One author
–Smith (2002) found…
–(Smith, 2002).

Two Authors:
–Smith and Jones (2003) found…
–(Smith & Jones, 2003).

Three or More Authors
–Smith et al. (2001) found…
- (Phelps et al., 2004)
–Smith et al. (2002) found…

Groups as Authors:
–1st Citation:
(American Psychological Association [APA], 2000).
–Subsequent Citations:
(APA, 2000).

Anonymous or No Author
–Use first few words of reference list entry (usually title):
(—Study Finds, 1995)
(TEA, 2007)

Authors with Same Surname
–Include initials: S. T. Smith (2000) and J. D. Smith (1999)

Two of more works within the same parentheses
–In order alphabetically, as they would appear in references, separated by semi-colons
(Jones, 2003; Thomas, 2010)
–If by same author, then by date
(Jones, 2003, 2007)

References should be arranged first alphabetically and then further sorted chronologically if necessary. More than one reference from the same author(s) in the same year must be identified by the letters "a", "b", "c", etc., placed after the year of publication

Reference to a journal publication
Carlson, L. A. (2003). Existential theory: Helping school counselors attend to youth at risk for violence. *Professional School Counseling, 6*(5), 10-15.

Sagarin, B. J., & Lawler-Sagarin, K. A. (2005). Critically evaluating competing theories: An exercise based on the Kitty Genovese murder. *Teaching of Psychology, 32*(3), 167–169.

Hughes, J. C., Brestan, E. V., & Valle, L. A. (2004). Problem-solving interactions between mothers and children. *Child and Family Behavior Therapy, 26*(1), 1-16.

Journal with more than seven authors
Gilbert, D. G., McCleron, J. F., Rabinovich, N. E., Sugai, C., Plath, L. C., Asgaard, G., Botros, N. (2004). Effects of quitting smoking on EEG activation and attendtionlast for more than 31 days and are more severe with stress. *Nicotine and Tobacco Research, 6*, 249-267.

Herbst-Damm, K.L., & Kulik, J.A. (2005). Volunteer support, marital status, and the survival times of terminally ill patients. *Health Psychology, 24,* 225-229. doi: 10.1037/0278-6133.24.2.225

Silick, T.J., & Schutte, N.S. (2006). Emotional intelligence and self-esteem mediate between perceived early parental love and adult happiness. *E-Journal of Applied Psychology, 2(2),* 38-48. Retrieved from http://ojs.lib.swin.edu.au/index.php/ejap.

Reference to a book
Beck, C. A. J., & Sales, B. D. (2001). *Family mediation: Facts, myths, and future prospects.* Washington, DC: American Psychological Association.

Johnson, R. A. (1989). Retrieval inhibition as an adaptive mechanism in human memory. In H. L. RoedigerIII & F. I. M. Craik(Eds.), *Varieties of memory & consciousness* (pp. 309-330). Hillsdale, NJ: Erlbaum.

English translation of a book:
Lang, P. S. (1951). *A philosophical essay on probabilities* (F. W. Truscott & F. L. Emory, Trans.). New York, NY: Dover. (Original work published 1814)

*In text, cite original date and translation date: (Lang, 1814/1951).

Dissertations and Theses
Caprette, C. L. (2005). *Conquering the cold shudder: The origin and evolution of snake eyes* (Doctoral dissertation). Ohio State University, Columbus, OH.

Pecore, J. T. (2004). *Sounding the spirit of Cambodia: The living tradition of Khmer music and dance-drama in a Washington, DC community* (Doctoral dissertation). Retrieved from Dissertations and Theses database. (UMI No. 3114720)

Caprette, C. L. (2005). *Conquering the cold shudder: The origin and evolution of snake eyes* (Doctoral dissertation). Retrieved from http://www.ohiolink.edu/etd/send-pdf.cgi?acc_num=osu1111184984

Online resource from group/government
U.S. Department of Health and Human Services. (2003). Managing asthma: A guide for schools. Retrieved from http://www.nhibi.nih.gov/health/prof/lung/asthma/asth_sch.pdf

Reference in other Language
Hughes, J. C., Brestan, E. V., & Valle, L. A. (2004). Problem-solving interactions between mothers and children. *Child and Family Behavior Therapy, 26*(1), 1-16. (*In Chinese*)

Journal abbreviations source
Journal names should be abbreviated according to
Index Medicus journal abbreviations: http://www.nlm.nih.gov/tsd/serials/lji.html;
List of title word abbreviations: http://www.issn.org/2-22661-LTWA-online.php;
CAS (Chemical Abstracts Service): http://www.cas.org/sent.html.

Submission checklist
The following list will be useful during the final checking of an article prior to sending it to the journal for review. Please consult this Guide for Authors for further details of any item.

Ensure that the following items are present:
One Author designated as corresponding Author:
- E-mail address
- Full postal address
- Telephone and fax numbers

All necessary files have been uploaded
- Keywords
- All figure captions
- All tables (including title, description, footnotes)

Further considerations
- Manuscript has been "spellchecked" and "grammar-checked"
- References are in the correct format for this journal
- All references mentioned in the Reference list are cited in the text, and vice versa
- Permission has been obtained for use of copyrighted material from other sources (including the Web)
- Color figures are clearly marked as being intended for color reproduction on the Web (free of charge) and in print or to be reproduced in color on the Web (free of charge) and in black-and-white in print
- If only color on the Web is required, black and white versions of the figures are also supplied for printing purposes

For any further information please visit our customer support site at http://support.elsevier.com.

AFTER ACCEPTANCE

Use of the Digital Object Identifier
The Digital Object Identifier (DOI) may be used to cite and link to electronic documents. The DOI consists of a unique alpha-numeric character string which is assigned to a document by the publisher upon the initial electronic publication. The assigned DOI never changes. Therefore, it is an ideal medium for citing a document, particularly 'Articles in press' because they have not yet received their full bibliographic information. The correct format for citing a DOI is shown as follows (example taken from a document in the journal *Physics Letters B*): doi:10.1016/j.physletb.2010.09.059 When you use the DOI to create URL hyperlinks to documents on the web, they are guaranteed never to change.

Proofs
One set of page proofs (as PDF files) will be sent by e-mail to the corresponding author (if we do not have an e-mail address then paper

proofs will be sent by post) or, a link will be provided in the e-mail so that authors can download the f les themselves. Elsevier now provides authors with PDF proofs which can be annotated; for this you will need to download Adobe Reader version 7 (or higher) available free from http://get.adobe.com/reader. Instructions on how to annotate PDF f les will accompany the proofs (also given online). The exact system requirements are given at the Adobe site: http://www.adobe.com/products/reader/systemreqs.

If you do not wish to use the PDF annotations function, you may list the corrections (including replies to the Query Form) and return them to Elsevier in an e-mail. Please list your corrections quoting line number. If, for any reason, this is not possible, then mark the corrections and any other comments (including replies to the Query Form) on a printout of your proof and return by fax, or scan the pages and e-mail, or by post. Please use this proof only for checking the typesetting, editing, completeness and correctness of the text, tables and f gures. Signif cant changes to the article as accepted for publication will only be considered at this stage with permission from the Editor. We will do everything possible to get your article published quickly and accurately – please let us have all your corrections within 72 hours. It is important to ensure that all corrections are sent back to us in one communication: please check carefully before replying, as inclusion of any subsequent corrections cannot be guaranteed. Proofreading is solely your responsibility. Note that Elsevier may proceed with the publication of your article if no response is received.

Offprints

The corresponding author, at no cost, will be provided with a PDF f le of the article via e-mail. For an extra charge, paper offprints can be ordered via the offprint order form which is sent once the article is accepted for publication. The PDF f le is a watermarked version of the published article and includes a cover sheet with the journal cover image and a disclaimer outlining the terms and conditions of use.

More information about article offprint is available here: http://webshop.elsevier.com/

AUTHOR INQUIRIES

For inquiries relating to the submission of articles (including electronic submission) please visit this journal's homepage. Contact details for questions arising after acceptance of an article, especially those relating to proofs, will be provided by the publisher. You can track accepted articles at http://www.elsevier.com/trackarticle. You can also check our Author FAQs (http://www.elsevier.com/authorFAQ) and/or contact Customer Support via http://support.elsevier.com.